THE COMPUTER SIMULATION OF MOLECULAR LIQUIDS

A thesis submitted to the University of Manchester for the degree of PhD in the Faculty of Technology

by

David Brown B.Sc.

U.M.I.S.T

Department of Chemistry

April 1985.

In memory of my father

James Brown (1925-1977).

DECLARATION

No portion of the work referred to in this thesis has been submitted in support of an application for another degree or qualification of this or any other university or other institution of learning.

ABSTRACT

The rheological properties of a number of liquids composed of model molecules have been characterized in detail using the technique of Molecular Dynamics (MD). The models consisted of molecules composed of 2, 3 and 6 interaction centres including, in the latter case, internal degrees of freedom. It has been shown that of the available methods of determinining the viscosity by MD, (the Green-Kubo formula, perturbation experiment and homogeneous shear non-equilibrium molecular dynamics (HSNEMD)), HSNEMD is the most accurate and efficient.

HSNEMD calculations on fluids composed of diatomic molecules have been performed at various densities and for different molecular anisotropies. For these models a simple correlation has been established between the pressure coefficient of the viscosity and the compressibility. Comparisons of diatomic and triatomic models representing ethane and propane under the same conditions of temperature and pressure show that the difference in rheological behaviour has its origins primarily in the different effective temperatures of the two liquids. Similar experiments performed on a model n-hexane fluid with and without barriers to internal rotation have shown that the degree of flexibility of a molecule has a strong influence on its temperature

coefficient of viscosity. For the first time the ability of shear flow to extend molecules has been demonstrated convincingly.

ACKNOWLEDGEMENTS

I would like to express my thanks to my supervisor, Julian Clarke, for his continued support and encouragement and also to Martin Whittle both of whom I have enjoyed working with and with whom I have had many thought provoking and stimulating discussions. For their help with various technical aspects of the work I would like to thank Bill Smith, David Heyes, David Fincham and Jean-Paul Ryckaert and also many other members of CCP5 too numerous to mention.

I would like to express my gratitude to Shell for their financial assistance throughout this work and to Mr.J.F.Hutton of Shell's Thornton Research Centre for his support for and continued interest in the project.

The UMRCC and the SERC are thanked for the provision of generous allocations of computer time and I would also like to thank the staff of the Control Systems Centre at UMIST for their friendly assistance in using the PRIME computer.

Finally, I would like to express my gratitude to my brother, Alan, for providing a certain amount of the inspiration to undertake research and for his help in obtaining this opportunity.

LIST OF CONTENTS

LIST OF FIGURES

(The number in parentheses indicates the numbered page preceding the figure)

CHAPTER 1

INTRODUCTION

1.1 The Aims of this Work

Relating the properties of liquids to the structure of the molecules of which they are composed has been the aim of much experimental and theoretical research. The identification of specific molecular characteristics which are responsible for certain behaviour would obviously be of great importance. The main difficulty, however, in this type of research lies in distinguishing the effect of one molecular characteristic on the properties of a liquid from all the rest. Ideally we would like to observe the interdependence between a particular macroscopic property and just one molecular variable. In reality this is in general impossible to realise due to the coupling between the molecular variables. In practice it is possible to observe trends within certain groups of compounds for many properties but this does not necessarily lead to the determination of the relative importance to a particular bulk quantity of the characteristics which constitute the molecule in question.

The specific purpose of this work is to investigate how the details of molecular interactions affect the rheological properties of fluids, i.e. the properties of materials undergoing deformation or flow. This has a particular bearing on the lubrication industry where there is a constant need for

new lubricants capable of working in more extreme conditions of, for instance, high and low temperatures, high pressures and high shear rates. Experimentally the measurement of the molecular properties of fluids subjected to the extreme conditions mentioned is extremely difficult using the conventional techniques employed at equilibrium. Indeed, investigations within this field of research are traditionally carried out using either disc machines to model the lubrication situation, or high frequency oscillating shear equipment. These techniques have been mainly used to obtain data concerning the pressure, shear rate and frequency dependence of the viscosity of a wide range of fluids. Little if anything, however, can be determined about the effects of the applied conditions at a molecular level.

To try and obtain detailed molecular information computer simulations using molecular dynamics (MD) have been carried out [1]. In this method the classical N-body problem of a particle moving in the fluctuating force field of its neighbours is solved numerically with the aid of a computer. This is achieved by integrating the equations of motion over a small time interval ($\sim 10^{-14}$s) for a small number of particles, N (typically N<1000), which interact through a known force law and which are subject to specified boundary conditions. Repeating this procedure produces a complete history of the N-particle system's trajectory through phase space. Flow situations have been modelled previously using MD by imposing

velocity gradients and it has been shown that even systems consisting of simple spherical particles show qualitatively similar rheological behaviour to that of much more complex real molecules [2]. The main objective of this research has been to extend these model studies to more elaborate types of molecules with the intention of obtaining some insight into the effect of changes in the molecular variables on the macroscopic rheological properties of the liquids.

1.2 Experimental Studies

The need to acquire molecular information concerning the rheological behaviour of liquids subject to extreme conditions is the direct result of observations from studies carried out on disc machines [3-5]. In these experiments two rotating discs are loaded together in line contact with their axes parallel. The surface of the cylinders are continuously lubricated and the variation in the lubricant film thickness and the traction between the cylinders are measured as a function of the mean and relative circumferential speeds of the cylinders and as a function of the normal load. Originally [3] this form of equipment was designed to model the lubrication situation found in gears and roller bearings. This is generally termed elasto-hydrodynamic lubrication as the hydrodynamic pressures generated between opposing surfaces

can be large enough to induce appreciable elastic deformation of the materials being lubricated. The initial results of these studies [3] proved by resistivity measurements that a film of lubricant did exist between the cylinders so that there was no significant solid contact. Clearly the magnitude of the film thickness is of great practical importance as this will determine the rate at which the surfaces wear and thus eventually fail. Consequently much of the effort in these initial studies was spent in attempts to correlate experimental findings with available theories of film thickness [6]. The results of these studies have been adequately reviewed in the literature [7,8] and the general conclusion reached was that the film thickness could be adequately predicted assuming that the liquid is Newtonian and that the viscosity is a known function of pressure.

For the frictional traction these basic assumptions lead to predictions far from the experimental results. The high shear rates, $\rightarrow 10^{7}s^{-1}$ and the high pressures , ~1GPa, involved and the actual duration of the transit, $1 \rightarrow 10^{-6}s$, make the situation difficult to treat theoretically [9]. This is because the material parameters and functions required to give a reasonable model description of the problem cannot usually be obtained even from more controllable rheological experiments. It was realised at an early stage [5] that the behaviour of the lubricant differed markedly from the assumed behaviour of $\eta = \sigma/\dot{\gamma}$, where σ is the stress, which is related

to the frictional traction, and η and $\dot{\gamma}$ are the viscosity and shear rate respectively, $\eta(t) \propto \exp(-1/T)$ and $\eta(P) \propto \exp(P)$. It was noted that the viscosity depended upon the relative motion of the cylinders i.e. sliding speed, which is proportional to the shear rate, suggesting a non-Newtonian relation between the stress and the shear rate i.e. $\eta(\dot{\gamma})$. In particular it was found that [5] the apparent viscosity decreased as a function of increasing shear rate, behaviour known as shear thinning, to such an extent that it could not be caused entirely by the viscous heating.

Since the early results of Crook [3] there have been further reports of experiments performed using various kinds of disc machines [7,8,10-16]. These have extended the range of conditions over which the material properties have been calculated and also varied the geometry of the contact zone as well as increasing the number of different lubricants that have been studied. Furthermore Johnson and coworkers [17,18] have concluded that the behaviour of a fluid in an elasto-hydrodynamic (EHD) contact can be adequately parametrised using empirical relationships and data obtained from sample trials on a simple two disc machine. For most practical purposes a reasonable prediction of the behaviour of a lubricant is all that is required but this provides us with little or no understanding of the effects at a molecular level.

To try and obtain information from a different source use has been made of the connection between the behaviour of fluids in oscillating and continuous shear. In theory a knowledge of the frequency dependence of the viscosity can be used to predict the time dependence of the viscosity in response to a shear rate, applied as a step function, by Fourier transformation. This is only strictly true, however, in the limit of small shear rates. Some models of visco-elastic relaxation [19] predict a connection between the viscosity in oscillatory shear and continuous shear at all shear rates but if non-Newtonian effects begin to prevail the connection becomes less certain. Nevertheless these forms of measurements have produced interesting results.

Until the introduction of piezo-electric transducers [20,21] alternating shear methods of viscosity measurement were restricted to frequencies of less than $2*10^4$ Hz [22] using mechanical or electro-magnetic devices for wave generation. To observe any elastic behaviour the reciprocal frequency has to be of the same order as the characteristic shear relaxation time of the fluid, τ_m, given by the Maxwellian relation $\tau_m=\eta/G_\infty$. Typically G_∞ , the infinite frequency shear modulus, is of the order of 10^9Pa for many liquids [23] so only liquids of viscosities greater than 10^4Pa s, e.g. polymeric liquids, could previously be studied. This effectively excluded all simple liquids as their viscosities tend to be less than 10^{-2} Pa s. However, the

increased frequency range accessible using piezo-electric transducers, up to 10^9Hz, allows the investigation of liquids with viscosities ~1Pa s. This is still higher than the viscosities of many liquids but by increasing the viscosity either by supercooling [22] or by increasing the pressure [24] it has been demonstrated that the technique can be used even for single component relatively simple fluids [25]. The restriction being that the material does not crystallise as the temperature is lowered or as the pressure is raised.

Measurements using this technique are generally made by observing the change in phase and amplitude of shear waves repeatedly reflected from the interface between a fused quartz bar and the sample liquid as compared to that between a fused quartz bar/air interface. This allows the calculation of the shear mechanical impedance of the liquid and indirectly the components of the complex shear modulus, $G^*(i\omega)$, and the complex viscosity, $\eta^*(i\omega)$. In theory it is possible by varying the value of ω , the frequency, to obtain the shear modulus and the viscosity over the entire frequency range. However, in general experiments are performed at certain fixed frequencies and the results obtained at different temperatures and/or pressures are compared using the principle of time-frequency reducibility [23]. This involves the use of a reduced frequency $\omega_r=\omega\tau_m$ which is varied not by changing the actual frequency ω but by varying τ_m which is a function of temperature and pressure. Dyson [19] has compared the results

obtained from both oscillatory and continuous shear experiments. At low shear rates or frequencies the agreement is good as is expected theoretically ($\eta(\omega)_{\omega \to 0} = \eta(\dot{\gamma})_{\dot{\gamma} \to 0} = \eta_0$) but as the frequency and shear rate are increased there is less agreement. This makes it difficult to relate the results from the two forms of experiments.

One interesting aspect of Barlow and Lamb's early work [22] using oscillating shear techniques was their attempts to relate the results for $G^*(i\omega)$ to the components making up the oil used. They arrived at assignations of broad frequency regimes as major contributions to $G^*(i\omega)$ arising from certain components of the oil. This was, however, later shown to be an over simplification by Hutton [26] who performed experiments on some of the individual fractions. Much more effort, however, has been put into explaining the results in terms of models of visco-elastic relaxation.

There are several models which incorporate both elastic and viscous responses to applied strain rates. These models use as an analogy the response of a Hookean spring and a 'dashpot', i.e. piston, to an extension to represent the elastic and Newtonian viscous behaviour. The simplest of these models is the Maxwell element which corresponds to a spring and dashpot connected in series. This element will thus exhibit viscous behaviour if it is extended slowly ,elastic behaviour when it is quickly extended and a

combination of both in between. Although this model is intuitively appealing and the response to both oscillatory and steady shear rates can be readily calculated few liquids actually behave in this manner. More complicated models can be readily generated by adding further elements in parallel or series to obtain more realistic responses but this procedure is purely arbitrary and does not reveal any of the fundamental processes governing viscoelastic relaxation.

A much more successful description of the viscoelastic behaviour of real fluids has been found to be given by the BEL model of Barlow, Erginsav and Lamb [27]. This model does not have an analogy in terms of springs and dashpots but it was originally arrived at by adding the reciprocal impedances, $1/Z_1$ = particle velocity/-shear stress, for a purely elastic element and a purely viscous element to obtain that of a viscoelastic fluid. This model has been shown [28] to fit accurately the results obtained for the shear mechanical impedance from high frequency oscillating shear experiments. The same equation has also been derived by Phillips et al [29] using a defect diffusion model. Although this approach does offer some understanding at a molecular level it is based on the rather unphysical idea that molecular relaxation can only occur when a defect or 'hole' diffuses to a neighbouring site.

In its original form the BEL model can describe quite well the behaviour of many single component systems there are,

however, several deficiencies. For mixtures it has been found necessary to include one [30] or even two [31] adjustable parameters to adequately describe the response of these multi-component systems. Secondly, it has been pointed out [25,32] that there can be systematic deviations of the predictions of the BEL model from the experimental results, especially at low frequencies. Lastly, it has also been shown that the BEL model predicts unphysical behaviour as the frequency tends to zero for the first normal stress difference [25] and for recoverable strain [33]. Consequentially the failure of the BEL model at low frequencies is attributed to its theoretical shortcomings.

One other equation which has been successfully applied to model viscoelastic relaxation is that of Davidson and Cole [34]. Originally used as an empirical equation to model the results for dielectric relaxation it has been employed by Davies et al [32] to describe their results obtained for a number of pure fluids from high frequency shear experiments. Although similar in some respects to the BEL model it does contain three adjustable, though theoretically interdependent, variables which have to some extent been correlated with molecular sphericity and flexibility in a series of organic molecules. In general the tendency towards sphericity has been associated with a narrower distribution of relaxation times whereas increased flexibility has been shown to some extent to have the opposite effect of increasing the spread of

relaxation times. More specifically Kim [35] has discussed the Davidson-Cole model in terms of the translational and rotational relaxation times of molecules but reaches a similar conclusion.

Interpretation of these models in terms of molecular behaviour remains speculative as in general the dynamical properties of the molecules comprising the fluid in question are not known. Furthermore, even less is known about the effect of applied conditions of high pressure and high shear rate on the structural and dynamical properties of the fluid and how this alters the rheological behaviour. For this reason comparisons made between experiments performed using oscillating shear, where the fluid is assumed to be close to equilibrium, and continuous shear, where the fluid can be far from equilibrium, can only give qualitative information as the experiments are performed on effectively different liquids.

1.3 Simulation Studies

An alternative to the methods already discussed for determining rheological behaviour is that of molecular dynamics (MD). Although few studies [1,2] have specifically set out to correlate the rheology of real and model liquids there has been a good deal of effort put into the evaluation of the viscosity of model liquids which has indirectly produced results of interest concerning the visco-elastic and non-linear effects which are of primary importance to the problem in question.

Originally MD calculations were performed on systems consisting of spherical particles which interacted through discontinuous potentials [36]. Later techniques were developed for employing realistic continuous potentials [37] and eventually methods were devised for modelling molecules with rotational degrees of freedom [38,39,40] and ultimately molecules containing internal modes [41]. The advantage of MD over other computer techniques, e.g. Monte-Carlo [42], is that it provides not only static equilibrium properties but also a complete record of the dynamical evolution of the system. The dynamics of the system are directly responsible for the fundamental processes of mass, momentum, and energy transport which can be described as processes which strive to make the intrinsic state variables independent of position. On a macroscopic scale when averages of state variables are

functions of position gradients will exist. If the system is close to equilibrium any gradient, G, of a state variable will be related to its conjugate flux, Q, by a linear relationship of the form Q=CG. C, the constant of proportionality, determines the rate at which the system approaches equilibrium and is called the transport coefficient. In the case of momentum transport the gradient is the shear rate, $\dot{\gamma}$, the conjugate flux is the stress, σ, and the transport coefficient is the shear viscosity, η, $\sigma=\eta\dot{\gamma}$.

In equilibrium molecular dynamics (EMD) the state variables are not on average functions of position so consequently gradients do not exist and the viscosity cannot be calculated from the simple relation given. However, in a system fluctuating about its equilibrium state fluxes will be spontaneous and short lived. The theoretical treatment of such fluctuations has been accomplished notably by Green [43] and Kubo [44] with the result that a transport coefficient can be written as the integral under the appropriate correlation function [45]. In the case of shear viscosity

$$\eta = \frac{V}{kT}\int_0^\infty \langle\sigma_{\alpha\beta}(0)\sigma_{\alpha\beta}(t)\rangle\, dt \qquad (1.3.1)$$

where V is the volume of the system, T is the temperature and $\langle\sigma_{\alpha\beta}(0)\sigma_{\alpha\beta}(t)\rangle$ is the stress correlation function. $\sigma_{\alpha\beta}$ is an off-diagonal component of the microscopic stress tensor defined as

$$\underline{\underline{\sigma}} = \frac{-1}{V}\left[\sum_{i=1}^{N}\frac{1}{m_i}\underline{p}_i\underline{p}_i + \sum_{i=1}^{N}\sum_{j>i}^{N}\underline{R}_{ij}\underline{F}_{ij}\right] \qquad (1.3.2)$$

where m_i, $\underline{p}_i$ and $\underline{R}_i$ are the mass, momentum and position of the centre of mass of molecule i , $\underline{R}_{ij} = \underline{R}_i - \underline{R}_j$ and $\underline{F}_{ij}$ is the force on molecule i due to molecule j.

The first attempt at calculating the shear viscosity from EMD simulations was made by Alder, Gass and Wainwright [46] on a system of hard spheres. They did not use the Green-Kubo expression, eqn.1.3.1 ,but the equivalent Einstein expression [47] which relates the viscosity to a mean squared centre of momentum displacement

$$\eta = \lim_{t\to\infty} \frac{1}{2VkTt}\left\langle\left[\sum_{i=1}^{N} p_{\alpha_i}(t)R_{\beta_i}(t) - p_{\alpha_i}(0)R_{\beta_i}(0)\right]\right\rangle$$

where $\underline{p}_i$ is the momentum of particle i and α,β = x,y,z.

The first calculations for systems interacting through continuous potentials were made by Levesque et al [48] on model liquid argon. Their results and those of subsequent studies [49,50] have gone to underline the difficulty of obtaining the stress correlation function to sufficient accuracy for the length of time required to obtain a limiting value for the Green-Kubo integrand. As the stress is an N-particle property there is only a limited amount of averaging available from a MD simulation as compared to a

single particle property. The only way of obtaining better results is to either increase N or to integrate the equations of motion for a longer amount of time. However, even runs of 100,000 time steps have proved insufficient [48] due to the apparent correlations which persist for long times, the so called `long time tail' to the stress correlation function. The resulting viscosities obtained from these calculations have been found to give [48-50] qualitative agreement with the viscosities of the real fluid the potentials used are modelling, even though the potentials used are invariably fitted to the static properties of the liquid rather than the dynamic properties.

Although this method is impractical for producing precise values of the viscosity it does give good results for the short time behaviour of the stress correlation function. As it is the integral of the stress correlation function which determines the response of a liquid to a step function increase in shear rate it is of fundamental importance as it provides a direct test of models of visco-elastic relaxation which can usually only be tested in frequency space as the stress response function is generally unobtainable directly from experiments on real fluids. Furthermore, the zero time value of the stress correlation function is related to the infinite frequency shear modulus through the equation [51]

$$G_\infty = \frac{V}{kT} \langle \sigma^2_{\alpha\beta}(0) \rangle \quad .$$

G_∞ is an important viscoelastic parameter as combined with the viscosity it determines the characteristic, or Maxwell, relaxation time of the fluid $\tau_m = \eta/G_\infty$. In real liquids it is determined from data obtained in oscillating shear experiments [23]. As already described these experiments are limited in the range of conditions at which they can be performed thus the variation of G_∞ with temperature and pressure etc. is not generally known. In contrast to this it is theoretically possible to evaluate G_∞ of a model liquid at any state point.

The problem of obtaining results of reasonable precision for the viscosity led to the development of different techniques for evaluating transport coefficients. The general idea behind this new approach was artificially to perturb the MD system and then to use the Navier-Stokes equations of macroscopic hydrodynamics [52] to determine the viscosity. The perturbation that is applied also prevents the system from attaining equilibrium and thus these methods are generally referred to as non-equilibrium molecular dynamics (NEMD).

One of the first successful applications of NEMD was that of Gosling et al [49] who devised a method to measure the shear viscosity of argon modelled by a Lennard-Jones 12-6 potential. In their method the particles are subject to an additional external force which acts in the x-direction but

depends upon the particle's z-coordinate,

$$F_x(Z) = F_o \sin(2\pi nZ/L)$$

where L is the length of the MD cell, F_o is a constant and n is an integer. This type of force is consistent with the periodic boundary conditions as $F_x(L) = F_x(0) = 0$. The solution of the Navier-Stokes equation involving an external force indicates that a sinusoidal drift velocity,

$$U_x(Z) = U_o \sin(2\pi nZ/L) \ ,$$

is set up. Determination of the amplitude, U_o, after steady state has been achieved, allows the determination of the viscosity from

$$\eta = \frac{\rho L^2 F_o}{4\pi^2 n^2 m}$$

where m is the mass of an atom. Reasonable agreement was achieved with experimental studies over a range of state points for which the viscosity varies by a factor of 8. Difficulties arose , however, from the need to use a value for F_o large enough to produce a measurable response in such a small system. It was found that F_o had to be of the order of 1/10 of the root mean square intermolecular force before an acceptable signal-to-noise ratio was achieved unfortunately this resulted in the temperature of the system rising rapidly

by 1Ø's of degrees K within times of $\sim 10^{-10}$s . Higher values of F_o were found to produce more precise results for the drift velocity but also caused the system to heat up more rapidly due to the greater amount of work being done. One other factor that had to be taken into account was the fact that the equations used are strictly true only in the long wavelength limit i.e. as $k \rightarrow Ø$, where $k=2\pi n/L$. Indeed it was found by Gosling et al [49] that their results for η were significantly reduced by increasing the wave vector, k, by a factor of two. Nevertheless, the results obtained were considered to be as precise as those obtained from the Green-Kubo formulae which used ten to twenty times the amount of computing time.

At about the same time alternative methods of NEMD were being pioneered by Ashurst and Hoover [53]. They decided to abandon the usual periodic boundary condition in an attempt to simulate planar Couette flow, i.e. the flow of a fluid between parallel plates moving relative to each other at a set distance apart. They first experimented with hard and repulsive walls in the positive and negative z-directions but unacceptable density gradients were imposed on the system. Eventually they used a system which was periodic in the $\pm$x and $\pm$y directions but which was bounded in the $\pm$z-directions by extra layers of particles of thickness dz. dz and the number of particles in the `fluid walls', N_w , was chosen so as to maintain the same density as the bulk. Any particle attempting to leave either of the three regions through a z

face was reflected back into the same region simply by reversing its z component of velocity. To impose a velocity gradient on the bulk the velocities of the particles in the wall regions are scaled continuously to maintain a constant wall velocity of opposite sign in the two regions. At steady state a linear velocity profile should be set up between the walls through the bulk and the sum of the forces on the particles making up the walls due to those in the bulk is equal to the wall shear stress times the area of the xy plane, $\sigma_{xz}L^2$. The shear viscosity can then be calculated from the mean velocity gradient, $\langle \frac{dU_x}{dZ} \rangle = \langle \dot{\gamma} \rangle$, and the mean shear stress as

$$\eta = \langle \sigma_{xz} \rangle / \langle \dot{\gamma} \rangle \quad .$$

This method alleviated the problem of viscous heating as the particle velocities in the fluid wall could be scaled to maintain a constant temperature in these regions with the effect that heat is removed from the bulk. Result for η obtained using this method for LJ argon and the soft sphere fluid ($\Phi(r) \propto r^{-12}$) were found to depend upon the shear rates used and also the system size. However, using simple relationships to correct for infinite size, i.e. k=Ø, and zero shear rate they achieved good agreement with experimental data for argon. It was further noted that shear rates in excess of $10^{10} s^{-1}$, far beyond the range of real experiments, were required to separate the responses of the system to the shear flow from the natural fluctuations inherent in small

sample sizes.

The main disadvantage of the 'fluid' wall method is the dependence upon the width of the system, which is effectively a number dependence. Hoover and Ashurst found that [53] the viscosity of LJ argon, close to the triple point, determined with N=108,216 and 324 particles i.e. widths of L, 2L and 3L, differed from each other, systematically decreasing with increasing width. To avoid extrapolations to zero k most subsequent NEMD calculations of the shear viscosity have used the boundary conditions first suggested by Lees and Edwards (LE) [54]. There innovation was to apply a linear velocity profile to the primary MD cell whilst maintaining consistency with the usual periodic boundary conditions. For a shear in the xz plane it involves the translation of periodic images above (below) the primary cell in the positive (negative) x-direction a distance $\dot{\gamma}$Lt , where L is the length of the MD cell and t is the time into the simulation. This effectively reduces the width dependence as the velocity profile stretches to infinity in both the +z and -z directions. In the $\pm$x and $\pm$y directions normal periodic boundaries are retained. Particles crossing the $\pm$z boundaries are displaced a distance $\mp\dot{\gamma}$Lt in the x-direction on re-entering through the $\mp$z faces. The actual shearing of the particles can be achieved in two ways. Firstly, a displacement $\dot{\gamma}(Z-L/2)\Delta t$ can be added to each particle at every time step or alternatively allowing the z-axis to vary as a function of time such that the angle θ

between the z-axis at time t=Ø and some later time t=t is given by [55]

$$\theta = \tan^{-1}(\dot{\gamma}t) .$$

This type of homogeneous shear NEMD (HSNEMD) has been used since by Naitoh and Ono [56] to obtain the viscosity of a system of hard spheres and by Heyes et al [1,2] who made a detailed study of the changes in the structural, thermodynamic and dynamic properties of the LJ argon system subjected to high shear rates at high densities. A refinement of the basic HSNEMD algorithm has been developed by Evans [55]. This takes into account the fact that the shear rate, as determined from the particle velocities, fluctuates spontaneously in small systems. Whereas the method previously described assumes that these fluctuations average to zero Evans method suppresses them by altering the velocity of each particle in such a way that a linear least squares fit to the shear rate,

$$\dot{\gamma} = \sum_{i=1}^{N} v_{x_i} Z_i \Big/ \sum_{i=1}^{N} Z_i^2 \quad ,$$

returns the required value for $\dot{\gamma}$. The viscous heat generated is also removed by simulated contact with an ideal heat bath, i.e. scaling of the momenta. Using this method Evans has determined the rheological behaviour of soft sphere mixtures [57] ,LJ argon [58], soft discs [59], and various polyatomic fluids [55,6Ø,61]. Strict control of the shear rate also allows it to be made a function of time and Evans [55] has

also demonstrated the practicability of evaluating the frequency dependence of the shear viscosity by applying an oscillating shear rate.

More recently Hoover et al [62] have proposed modifications to Hamiltons equations of motion based on the Doll's tensor, $\Sigma \underline{qp}$, formulation to produce a shear flow driven by a fictitious external tensor field. This method still requires the use of translating image cells or time dependent axes and not surprisingly results obtained using this and the other homogeneous shear variants compare well [62]. Evans [63] and Hoover [64] have also discussed further modifications to Hamilton's equations of motion which allow certain ensemble properties to be exact constants of the time evolution of the system. So far these 'damped force ' equations have been used in MD by Hoover, Ladd and Moran [65] and Brown and Clarke [66] to constrain the temperature and by Evans [63] to constrain the internal energy in HSNEMD calculations.

In the non-equilibrium techniques so far outlined the gradients that have had to be applied are so large that the measurements made are inevitably in the non-linear regime. This is evident from the often pronounced $\dot{\gamma}$ dependence of the shear viscosity, the pressure and the energy that has been found in all HSNEMD calculations so far. This in itself is of considerable importance but the main reason for developing

NEMD was to obtain the zero shear viscosity. To avoid the use of large gradients Singer, Singer and Fincham [67] adapted the perturbation method of Ciccotti et al [68] to be used in conjunction with the Lees-Edwards boundary conditions. The basic idea of this method is to obtain the difference in stress between two trajectories in phase space starting from the same point, one unperturbed and one slightly perturbed by a small shear rate, $\Delta\dot{\gamma} \sim 1s^{-1}$. This can be achieved either by actually computing both trajectories in two separate MD runs or more efficiently by using a Taylor expansion, truncated after the linear terms, of the Hamiltonian in terms of the perturbed coordinates. The response obtained has been shown [68] to be equivalent to, at least in theory, the usual Green-Kubo stress correlation function and as such can be used to calculate the viscosity. This method relies upon the cancellation of correlated noise due to the proximity of the two trajectories in phase space. Eventually these paths must diverge exponentially and the response becomes swamped in noise. This means that averages have to be taken over a number of different starting points to obtain reasonable results. Unfortunately the perturbation approach has proved only to be successful in the case of LJ argon [67,69]. For molecular fluids, except at low densities, the long stress relaxation times cause the response to become lost in noise long before the 'plateau' region can be observed [70]. Some improvement can be made by applying delta function rather than step function [71] perturbations but in general the cost in

terms of computer time make it no more efficient than the usual Green-Kubo method. Where comparisons have been made between the two [71] the short time behaviour of the correlation functions are in reasonable agreement with the difference between the two being either statistical or possibly due to the fact that in the perturbation approach the correlation function evaluated is at zero k whereas in the G-K method the lowest k value is determined by the dimensions of the MD cell.

1.4 Results from and Conclusions of Simulation Studies.

The application of MD to the study of the flow properties of liquids has produced information in areas where previously little, if any, had existed. Single component liquids of low molecular weight have often been considered as 'simple' liquids which to all intent and purpose behave as Newtonian liquids. Experimentally this is generally the case as the time scales involved are much longer than the Maxwell relaxation time and thus the frequencies and shear rates available to real experiments are much lower than the reciprocal characteristic relaxation time. What MD has predicted is that phenomena such as viscoelasticity, shear dilatancy, shear thinning and normal pressure differences are common to all, even the 'simplest', of liquids. Furthermore, information not generally available from conventional rheological experiments, such as shear reorientation and the

structure of liquids under shear, has also become available through the use of MD.

The property which has received most attention in NEMD calculations is the shear rate dependent viscosity, $\eta(\dot{\gamma})$. This is not surprising as the determination of the zero shear rate viscosity has been the primary aim of most studies of this kind and the shear rates used have ensured its non-linearity. Consequently interest has centred on the form of $\eta(\dot{\gamma})$ and the best way to extrapolate back to $\dot{\gamma}=0$. Ashurst and Hoover [72] used the Ree-Eyring (RE) theory of rate activated processes [73] prediction

$$\eta(\dot{\gamma}) = \eta(0)\sinh^{-1}(\dot{\gamma}\tau)/(\dot{\gamma}\tau) \qquad (1.4.1)$$

to fit their data for argon. Later Naitoh and Ono preferred to use an asymptotic relation

$$\lim_{\dot{\gamma}\to 0} \eta(\dot{\gamma}) = \eta(0) - A\dot{\gamma}^{1/2} \qquad (1.4.2)$$

, due originally to the mode coupling theory of Kawasaki and Gunton (KG) [74], for their calculations on hard sphere systems. Ashurst and Hoover later pointed out [75] that Naitoh and Ono's data could equally well be fitted using the RE inverse sinh curve. Evans [58] repeated and extended the measurements made previously [72] on the LJ argon system, close to the Triple point , to much higher shear rates. The

results appeared to indicate a clear vindication of the $\dot{\gamma}^{1/2}$ dependence (KG) despite its non-analytic nature, i.e.

$$\lim_{\dot{\gamma}\to 0} \frac{d\eta(\dot{\gamma})}{d\dot{\gamma}} = -\infty \quad .$$

Further supportive evidence has also been found in the shear rate dependence of the viscosity of soft spheres [76] and for LJ argon at a different state point [77] and in two dimensions for soft disks [59] where KG theory predicts a logarithmic dependence of η upon $\dot{\gamma}$. For molecular systems the square root dependence has only been shown to fit for low density systems where there is little shear thinning [60,70]. For a dense model fluorine system [70] a systematic departure from the $\dot{\gamma}^{1/2}$ dependence was noted at the higher shear rates used.

For all the results mentioned measurements have only been made in the region of $\dot{\gamma} = 10^{10} \to 10^{12} s^{-1}$, due to the loss of response at the lower shear rates and the excessive temperature increases at the highest shear rates, which is only a small part of the available range. This casts an appreciable amount of doubt on the validity of extrapolating back to $\dot{\gamma}=0$ using the square root law, or any other proposed functional form. Furthermore, the non-analytic nature of the KG theory means that as $\dot{\gamma}\to 0$ $\frac{d\eta}{d\dot{\gamma}} \to -\infty$. This behaviour has never been observed experimentally in real systems though in general the magnitude of the viscosity change involved may be less than can be measured.

For real shear thinning fluids many empirical expressions have been used to correlate $\eta(\dot{\gamma})$ data [78] but there are relatively few which have been derived from molecular type theories. In a series of papers [79,80,81] Hess has developed a theory to describe the non-equilibrium behaviour of the alignment of molecular liquids. By considering the energy and entropy contributions due to alignment and by formulating constitutive laws Hess derives two coupled inhomogeneous relaxation equations for the pressure and alignment tensors. Their subsequent solution for the case of Couette flow results in a prediction for the non-linear dependence of η upon $\dot{\gamma}$ of the form

$$\eta(\dot{\gamma}) = \eta(0)\left[1 - k(\dot{\gamma}\tau)^2/(R^2 + (\dot{\gamma}\tau)^2)\right] \qquad (1.4.3)$$

where τ is a relaxation time and k and R are combinations of unknown coefficients but for fluids where there is no transition to a liquid crystal phase R=1 [80]. Unfortunately this theory does not apply for molecules which cannot align and as such cannot be tested against the simulation data for argon. Hess has, however, considered the case of spherical particles [82] by examining the dynamics of the pair correlation function under the influence of a velocity field. The analysis again leads to an expression governing the rate of change of the pressure tensor and its solution for the case of Couette flow implies that

$$\eta(\dot{\gamma}) = \eta(0) / (1+(\dot{\gamma}\tau)^2) \qquad (1.4.4)$$

where τ is the Maxwell relaxation time. Hess's predictions remain to be tested thoroughly against either real or computer generated results but the indications are that for monatomic fluids Hess's curve is at odds with the apparent $\dot{\gamma}^{\frac{1}{2}}$ dependence.

More recently two papers have appeared [83,84] which have presented a theory of non-newtonian fluid behaviour, derived an expression for $\eta(\dot{\gamma})$ and then compared it with the NEMD results of Heyes et al [1], Ashurst and Hoover [75] and Evans [58]. Quentrec [83] uses linearized local order theory to derive an expression for $\eta(\dot{\gamma})$ which is very similar to that obtained by Hess [80]

$$\eta(\dot{\gamma}) = \eta(0)\left[1 - k_q(\dot{\gamma}\tau_q)^2/(1 + (\dot{\gamma}\tau_q)^2\right] \quad . \qquad (1.4.5)$$

Quentrec further derives expressions for k_q and τ_q in terms of measurable equilibrium properties . Eu [84] uses the Boltzmann equation, and its generalization to dense fluid systems, as a starting point for his treatment but obtains an expression identical to that previously due to Ree-Eyring [73]

$$\eta(\dot{\gamma}) = \eta(0)\sinh^{-1}(\dot{\gamma}\tau_e)/(\dot{\gamma}\tau_e) \quad . \qquad (1.4.6)$$

Eu's expression differs from Ree-Eyring in that the value of

τ_e is defined absolutely from known parameters whereas τ is generally treated as an adjustable parameter in the RE formulation. In comparing their expressions with the simulation data both find satisfactory agreement despite the fact that neither has realised that the results of Evans are quoted as a function of the irreducible strain rate

$$\bar{\dot{\gamma}} = \frac{1}{2}\left[\frac{dU_x}{dy} + \frac{dU_y}{dx}\right]$$

($= \frac{1}{2}\frac{dU_x}{dy}$ for flow in the XY plane) whereas Heyes et al [1] and Hoover and Ashurst [75] quote results in terms of $\dot{\gamma} = \frac{dU_x}{dy}$.

The rather confusing state of affairs concerning eqns.1.4.3 and 1.4.5 where one theory, only applicable to alignable molecules, predicts the same result as another theory ,only applicable to spherical molecules, is further complicated by considering the Cross equation [85]

$$\eta(\dot{\gamma}) = \eta(0) + (\eta(0) - \eta(\infty))/(1 + (\dot{\gamma}\tau)^M)$$

substituting $\eta(\infty) = \eta(0)(1 - k)$ and rearranging gives for M=2

$$\eta(\infty) = \eta(0)\left[1 - k(\dot{\gamma}\tau)^2/(1 + (\dot{\gamma}\tau)^2)\right] \qquad (1.4.6)$$

Once again the same curve is recovered. The Cross equation is theoretically based on [86] the assumption that shear thinning

is a result of deflocculation in polydisperse systems and it is found to be quite successful at describing the $\eta(\dot{\gamma})$ behaviour of many complex systems [86,87]. For monodisperse systems the exponent M is generally taken to be equal to 1 not 2 so although it is interesting to note the equivalence of the mathematical formulae it would be unwise to use any apparent fit to this form of equation to vindicate any of the assumptions or methods used in the formulation of these various theories.

Apart from the changes induced in the off-diagonal elements of the pressure tensor by shear a common observation made in many HSNEMD simulations has been the increase in the hydrostatic pressure, $P = \frac{1}{3}(P_{xx} + P_{yy} + P_{zz})$, with also $\langle P_{xx} \rangle \neq \langle P_{yy} \rangle \neq \langle P_{zz} \rangle$. These normal pressure (or stress) effects are of interest as they are known of in real fluids [88] but have not been characterized at a molecular level. The increase in hydrostatic pressure in HSNEMD simulations is associated with the behaviour known as shear dilatancy. Technically shear dilatancy refers to the increase in volume which occurs when a material is sheared but as most HSNEMD calculations performed to date have been at fixed density the effect manifests itself through an increase in the pressure. In rheology there has been some confusion over the term 'dilatant' [89] as it has often been used to describe fluids whose viscosity increases with increasing rate of shear , shear thickening. What MD has shown is that shear thickening

and shear dilatancy are separate phenomena as simple fluids ,like LJ argon, exhibit both shear thinning and shear dilatancy if sheared at high enough rates.

In a series of papers Evans and Hanley [90,91,92] have attempted to rationalise the behaviour of shear induced pressure increases, and the related effect of internal energy increase, within the framework of thermodynamics. They postulate a change to the first law which allows for the shear rate to become an extra state variable. In this formulation it is assumed that $P(\dot{\gamma})$ is a known function at constant temperature and density. Specifically

$$\lim_{\dot{\gamma}\to 0} P(\dot{\gamma}) = P(0) + P_1|\dot{\gamma}|^{\frac{3}{2}} \qquad (1.4.7)$$

where P_1 is a state dependent constant. This equation is originally due to the same theory of Kawasaki and Gunton [74] which predicts a $\dot{\gamma}^{\frac{1}{2}}$ dependence of $\eta(\dot{\gamma})$. As for the case of $\eta(\dot{\gamma})$ the actual predicted values of the coefficients P_1 and A in eqns.1.4.2 and 1.4.7 are not in agreement, by two orders of magnitude, with the results of NEMD calculations [93] although at least in the case of LJ argon the predicted dependence has apparently been observed [94].

The main consequences of the generalized first law and the results of consistency checks have been reviewed previously [93,94]. Numerical tests on LJ argon [90] have

provided qualitative agreement with experimental findings that imposition of Couette flow can alter the position of phase boundaries.

Apart from being able to provide information on the shear dependence of bulk properties MD has the unique ability to also allow a detailed and direct analysis of the microscopic consequences of the previously described macroscopic effects. At equilibrium the structure of the fluid is characterized by the radial distribution function, g(r), where r is the scalar separation of two particles. In a system under shear g(r) is no longer a simple scalar function due to the distortion set up by the flow and instead becomes $g(\underline{r})$, where $\underline{r}$ is the vector separation. Various methods of representing $g(\underline{r})$ have been discussed in terms of expansions about the equilibrium g(r) [1,56,95,96] and have been accompanied by the results of NEMD calculations of the relevant functions for monatomic fluids. There is a consensus between the three studies as each shows that in the plane of the shear there is a net reduction of the number of particles on the inside of each coordination shell, with a corresponding increase on the outside, for the positive first and third quadrants. For the other two quadrants the opposite occurs. Heyes et al [1] have gone on further to discuss the time dependence of $g(\underline{r})$ following a step function increase in shear rate. They conclude that the structural reorganization having the symmetry of the plane of shear, xz say, is faster than that

having x^2, y^2 or z^2 symmetry. Furthermore, the reorganization having x^2 or z^2 symmetry attains steady state faster than that having y^2 symmetry. This is obviously of importance as the time dependence of $g(\underline{r})$ is closely linked to that of the pressure tensor. It is also interesting to note that measurements of the directional number densities under shear [1] show some tendency for atoms to form layers normal to the plane of shear in monatomic fluids.

Associated with the anisotropic structural rearrangements under shear are the consequent effects on the single particle dynamics of the system. Naitoh and Ono [56] computed the shear rate dependent self-diffusion coefficient in the directions perpendicular to the direction of flow and detected a systematic decrease in magnitude with increasing shear rate. However, as their calculations were not isothermal the diffusion coefficients had to be corrected for the temperature difference. Heyes et al [1] calculated the diffusion coefficients, excluding the shear component, in all three directions for LJ argon at a number of densities and shear rates. Isothermal conditions were maintained throughout so the diffusion coefficients obtained were not subject to errors in extrapolation. At equilibrium all three were found to be equal, as must obviously be the case, but under shear the two in the plane of shear increased more than that normal to the plane. This result is more in agreement with the intuitive argument that a decrease in viscosity is accompanied by an

increase in fluidity.

Although most NEMD simulations to date have concentrated on atomic systems there is increasing interest in the effect of shear flow on molecular fluids. Unlike atomic fluids molecular fluids have extra degrees of freedom which allow orientations and, in flexible molecules, conformations to couple to the velocity gradient. The first of these, shear induced realignment, is well known in real fluids as it gives rise to the optical property of first order shear birefringence. Less well understood is the ability of shear fields to induce conformational changes in the structure of the constituent molecules. This is an important consideration as shear flows are often used to measure the viscosity of polymers and it is often assumed in the analysis of the data [97,98] that these large molecules do not undergo conformational changes in the presence of a velocity gradient.

These effects have been studied in several NEMD studies. Evans [6Ø] has subjected a model diatomic chlorine fluid to homogeneous shear and has noted the preferred alignment of molecules in the positive first and third quadrants of the plane of shear. As for the monatomic fluids chlorine also exhibits shear thinning and shear dilatancy but as the simulations were carried out at a relatively low density there extent was not as pronounced. Allen and Kivelson [7Ø] have also applied the HSNEMD algorithm to fluorine and carbon

dioxide modelled by two centre LJ models. They also used the perturbation technique as refined by Singer et al [67] to measure the stress and aligment response functions and to attempt to obtain the zero shear rate viscosity. Their main interest was, however, in evaluating the parameters which appear in and testing the predictions for the time dependence of the stress and orientation of their generalized hydrodynamic theory of transverse motion in molecular fluids. They conclude that the theory provides a semi-quantitative description of the time resolved responses examined. They further conclude that the evaluation of the zero shear viscosity from the perturbation technique becomes impractical as the density is increased as the relaxation times for the stress and reorientation become longer than the time for the trajectories to diverge to such an extent as to swamp the response in noise. At lower densities this is less of a problem but then the steady state method is even more efficient as there is less shear thinning so extrapolation to $\dot{\gamma}=0$ is not as problematic as at higher densities. Interestingly the stress and the orientation evolve on a similar time scale for these model fluids of small anisotropy although initially the stress responds rapidly to the step in shear rate before tending to the long time limit whereas the orientation responds more gradually.

NEMD calculations on molecules with internal degrees of freedom have been limited to one study of small alkane like

molecules by Weber and Annan [99]. They have applied the sinusoidal force method [49] to two and three LJ centre models of ethane and propane. The propane model additionally included a bond angle potential with minima at 109° and 180° to allow a small degree of flexibility. Not surprisingly the application of a sinusoidal shearing force to the propane fluid did not produce any change in the proportions of conformers since their equilibrium run of 25ps had only produced one transition. They did note significant alignment in both the ethane and propane simulations with the direction of flow and between molecules. Overall their results are fairly inconclusive, as far as the response of flexible molecules to shear is concerned, as they are based on short runs, 5ps, with unrealistic flow fields on a not particularly flexible molecule.

These simulation studies have provided much of the essential ground work for what follows. The methods used in this work have already been introduced in this section and their exact details are given in chapter 2. Some of the issues raised in this section will form a recurring theme throughout. What is novel in this work, however, is the approach used whereby the effect of certain parameters has been investigated by way of comparisons between similar molecules. Thus, in chapter 3 results of simulations on

chlorine type diatomic molecules of differing anisotropy are given. In chapter 4 the effect of going from two to three site models is investigated and in chapters 5,6 and 7. the question of how important is the flexibility of a polyatomic molecule with respect to its rheological properties is addressed.

CHAPTER 2

METHODS

2.1 Molecular Dynamics

All the methods to be used throughout this work fall under the general heading of Molecular Dynamics (MD). In MD the classical equations of motion for a small number of particles (N), typically $10^2 < N < 10^4$, are solved numerically subject to specific boundary conditions. Interactions between particles are specified by well defined potentials which generally take the form of effective pair potentials which do not necessarily represent the interactions of isolated pairs but at fluid densities incorporate the effects of the three, four, five etc. body terms. This simplification reduces the number of interactions to be computed to manageable proportions. Without it the cost of computing all significant contributions to the potential energy would make MD impracticable. At least in the case of argon an effective potential of the familiar Lennard-Jones (LJ) 12-6 form

$$\Phi(r) = 4\epsilon\left[\left[\frac{\sigma}{r}\right]^{12} - \left[\frac{\sigma}{r}\right]^{6}\right] \qquad (2.1.1)$$

,including short range repulsive and long range attractive terms, has been found to give a good representation of the Noble gas fluid at a wide range of temperatures and densities [100] with an appropriate choice of the well depth, ϵ, and collision diameter, σ. The LJ 12-6 potential is certainly not

the only one to be used in MD calculations but its simplicity and flexibility make it a natural choice when only bulk properties are trying to be reproduced rather than the form of the individual interactions.

Conventionally equilibrium molecular dynamics calculations are carried out at constant volume, V, which means that, as N is fixed, the number density, $\rho=N/V$, is also constant. If the potential is conservative then the total energy of the system, kinetic plus potential, must also be conserved. To obviate a large surface area to volume ratio what are known as periodic boundaries are generally used. This in effect means that the primary cell is reproduced to infinity in three spacial dimensions so that it is surrounded by 26 images of itself , in three dimensions, generated simply by translation of the coordinates a cell length distance orthogonal to the edges of the cell. To maintain constant N particles leaving the primary cell are replaced by the appropriate incoming image particle.

With the constraints of constant N,V and energy, E, the MD cell would correspond to the microcanonical ensemble of statistical mechanics but the periodic boundaries force a fourth constraint on the system that of conservation of linear momentum. Thus this ensemble is sometimes referred to as the MD ensemble. Usually the sum of the momenta is set to zero initially in a MD calculation and its constancy, and that of

the total energy, is used as a measure of the accuracy to which the equations are being integrated.

2.2 MD for Atomic Systems with Continuous Potentials

The method of molecular dynamics originally described by Alder and Wainwright [36] for use on systems of hard spheres differs in the integration of the equations of motion quite markedly from that for systems where continuous potentials are used. In hard sphere systems the forces are impulsive and act instantaneously when a collision occurs. Between collisions particles move in straight lines so the problem of solving the equations of motion reduces to one of obtaining the shortest time interval to the next collision. Once this has been found all the particle positions can be updated by the same time interval. This makes hard sphere calculations particularly efficient at traversing phase space and also very accurate as there are no errors in the trajectories calculated. Rahman [37] was the first to demonstrate the use of continuous potentials in MD. As the particles are subject to forces, hence accelerate, at all times the problem becomes one of how best to approximate the trajectories of the particles or in other words how to solve numerically the classical equations of motion of the N particles. The usual way of solving differential equations numerically is by finite difference techniques which involve the use of a fixed timestep, Δt. Many such schemes have been suggested, e.g. [101], for

integrating Newton's classical second order differential equation of motion

$$\underline{F}_i = m_i \ddot{\underline{r}}_i$$

where $\underline{F}_i$, m_i and $\underline{r}_i$ are the force on, mass and position of particle i and the two dots refer to the second differential w.r.t. time , $\ddot{\underline{r}} = \frac{d^2\underline{r}}{dt^2}$. One such scheme which has become very popular is that first used by Verlet [1Ø2] and results from Taylor series expansions of $\underline{r}_i(t\pm\Delta t)$ forwards and backwards in time about $\underline{r}_i(t)$.

$$\underline{r}_i(t+\Delta t) = \underline{r}_i(t) + \dot{\underline{r}}_i(t)\Delta t + \ddot{\underline{r}}_i(t)\frac{\Delta t^2}{2!} + \dddot{\underline{r}}_i(t)\frac{\Delta t^3}{3!} + \cdots \qquad (2.2.1)$$

$$\underline{r}_i(t-\Delta t) = \underline{r}_i(t) - \dot{\underline{r}}_i(t)\Delta t + \ddot{\underline{r}}_i(t)\frac{\Delta t^2}{2!} - \dddot{\underline{r}}_i(t)\frac{\Delta t^3}{3!} + \cdots \qquad (2.2.2)$$

Summing eqns.2.2.1 and 2.2.2 gives on rearrangement

$$\underline{r}_i(t+\Delta t) = 2\underline{r}_i(t) - \underline{r}_i(t-\Delta t) + \ddot{\underline{r}}_i(t)\Delta t^2 + O(\Delta t^4) \qquad (2.2.3)$$

and ignoring terms of order Δt^4 for Δt small and substituting for $\ddot{\underline{r}}$ gives

$$\underline{r}_i(t+\Delta t) = 2\underline{r}_i(t) - \underline{r}_i(t-\Delta t) + \frac{\underline{F}_i(t)}{m_i}\Delta t^2 \qquad (2.2.4)$$

This simple algorithm, often termed Verlet's algorithm, is particularly useful as it requires the storage of only three vectors $\underline{r}_i(t)$, $\underline{r}_i(t-\Delta t)$ and $\underline{F}_i(t)$ which is an important consideration as available computer memory is invariably

limited. The accuracy of the algorithm is third order in positions but for the velocities subtracting eqn.2.2.2 from eqn.2.2.1 and rearranging gives

$$\dot{\underline{r}}_i(t) = (\underline{r}_i(t+\Delta t) - \underline{r}_i(t-\Delta t))/2\Delta t + O(\Delta t^3)$$

This means that the velocities are only accurate to second order but as they do not appear in the integration procedure the trajectories remain accurate to third order. For implementation in MD programs it is useful to define a half step velocity $\underline{v}(t-\Delta t/2)$ where

$$\underline{v}_i(t-\Delta t/2) = [\,\underline{r}_i(t) - \underline{r}_i(t-\Delta t)]/\Delta t \qquad (2.2.5)$$

so as to avoid having to reset two vectors when a particle crosses a periodic boundary and to allow a crude form of temperature adjustment by scaling these half step velocities. The integration steps, once the forces have been determined at time t, can now be written as

$$\underline{v}_i(t+\Delta t/2) = \underline{v}_i(t-\Delta t/2) + \frac{\underline{F}_i(t)\Delta t}{m_i} \qquad (2.2.6)$$

$$\underline{r}_i(t+\Delta t) = \underline{r}_i(t) + \underline{v}_i(t+\Delta t/2)\Delta t \qquad (2.2.7)$$

$$\underline{v}_i(t) = [\underline{v}_i(t-\Delta t/2) + \underline{v}_i(t+\Delta t/2)]/2 \qquad (2.2.8)$$

This slightly different form of algorithm, often referred to

as the 'leapfrog' algorithm, is algebraically equivalent to the Verlet algorithm but is computationally more desirable for the points mentioned. Once again only three vectors have to be stored, $\underline{r}_i(t)$, $\underline{v}_i(t-\Delta t/2)$ and $\underline{F}_i(t)$.

The main job of the computer in MD is the calculation of all the N(N-1)/2 possible pair separations from which the forces can be calculated. These separations must also be subject to the minimum image convention which is the problem of finding out if, say, particle i interacts with particle j in the primary cell or with one of its images in the surrounding periodic images. This is illustrated in fig.2.1 for the case of two dimensions. To find the nearest image we have to find which of the vectors $\underline{r}_{ij}$, $\underline{r}'_{ij}$, $\underline{r}''_{ij}$ etc. has the smallest modulus. This is equivalent to asking the question if the primary cell was centred on particle i which image of j would also be in this cell. It then follows that $|r_{ij_\alpha}| < L/2 \quad \alpha = x,y$ where L is the length of the cell. The procedure is then to obtain initially $\underline{r}_{ij}$ the vector separation of the primary positions from

$$\underline{r}_{ij} = \underline{r}_i - \underline{r}_j$$

and then the following transformations are applied

$$\text{if } r_{ij_\alpha} < -L/2 \text{ , } r_{ij_\alpha} = r_{ij_\alpha} + L$$

$$\text{if } r_{ij_\alpha} > L/2 \text{ , } r_{ij_\alpha} = r_{ij_\alpha} - L$$

Figure 2.1 Periodic images in 2-dimensions.

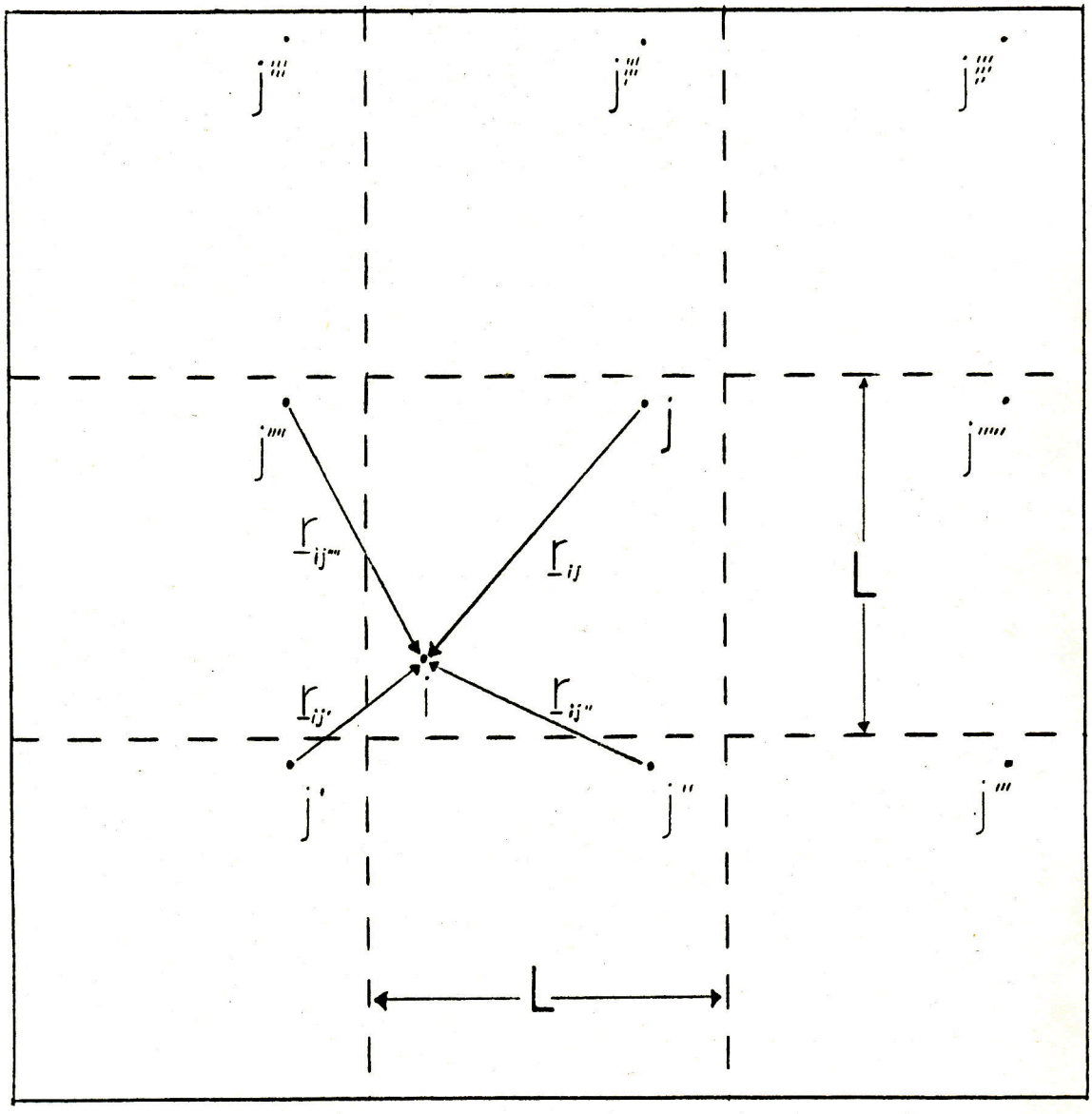

for all α=x,y,z. The scalar separation is simply $|\underline{r}_{ij}|$ after these transformations have been performed. On the computer there are various ways of making this transformation more efficient than using 'IF' statements. One of these depends on having a coordinate system with the origin at the centre of the cell and then defining the length of the cubic cell to be two units so that all coordinates lie between $\pm$1. A simple double loop to evaluate all pair separations incorporating periodic imaging can then be written in FORTRAN as :-

```
      N1=N-1
      DO 1ØØ I=1,N1
      I1=I+1
      XI=X(I)
      YI=Y(I)
      ZI=Z(I)
      DO 1ØØ J=I1,N
      XD=XI-X(J)
      YD=YI-Y(J)
      ZD=ZI-Z(J)
      XD=XD-2.Ø*INT(XD)
      YD=YD-2.Ø*INT(YD)
      ZD=ZD-2.Ø*INT(ZD)
      R2=XD**2+YD**2+ZD**2
      :
  1ØØ CONTINUE
```

In this way the transformations are accomplished efficiently in three lines using the INT function, which returns the integer part of a real number, rather than in six lines using 'IF' statements. Many other schemes are possible and the most efficient will certainly be machine dependent to a large extent depending on the relative speeds of intrinsic functions, 'IF' statements and integer/real arithmetic.

Once the separation has been obtained it then remains to

find the force acting between the particles. For a spherically symmetric potential such as the inverse power LJ 12-6 type, fig.2.2, the forces must be equal in magnitude and opposite in direction and are simply derived from differentiation w.r.t. r. So if

$$\Phi(r) = 4\epsilon\left[\left[\frac{\sigma}{r}\right]^{12} - \left[\frac{\sigma}{r}\right]^{6}\right]$$

differentiating w.r.t. r gives the magnitude of the force, f, to be

$$f = \frac{d\Phi(r)}{dr} = \frac{48\epsilon}{r}\left[-\left[\frac{\sigma}{r}\right]^{12} + \frac{1}{2}\left[\frac{\sigma}{r}\right]^{6}\right]$$

and the vector force, $\underline{F}_{ij}$, as

$$\underline{F}_{ij} = -f\hat{\underline{r}}_{ij} = \frac{48\epsilon}{\sigma^2}\left[\left[\frac{\sigma}{r}\right]^{14} - \frac{1}{2}\left[\frac{\sigma}{r}\right]^{8}\right]\underline{r}_{ij} \qquad (2.2.9)$$

Thus the LJ 12-6 potential, or any even powered LJ potential, is computationally advantageous in that we do not have to use the slow SQRT function to obtain r from r^2 as odd powers of r do not appear in eqn.2.2.9. The use of periodic boundaries restricts the direct sphere of influence of a particle to the largest sphere that can be inscribed in the MD cell thus interactions are customarily truncated at distances greater than a cutoff radius r_c where $r_c < L/2$.

To perform the dynamics all that is further required to

Figure 2.2 Lennard-Jones 12-6 potential.

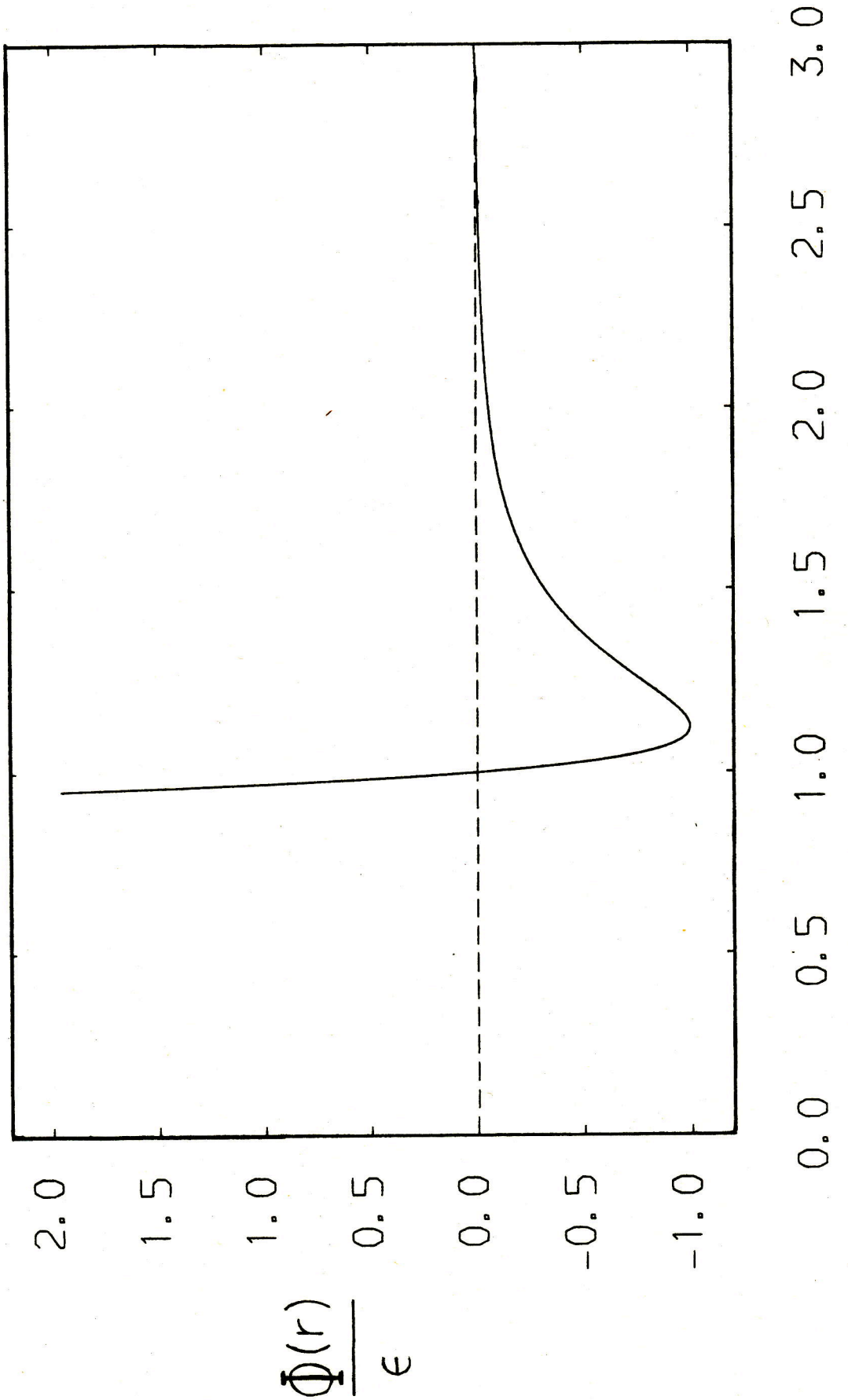

specify are the initial conditions, i.e. a set of coordinates and velocities. Generally these are taken from a previous simulation but if none exist coordinates can be generated by reference to some form of crystal lattice. A favourite among molecular dynamicists has been the face-centred cubic lattice which requires $4n^3$ atoms to fill a cubic cell and thus explains the widespread use of sample sizes of N=32(n=2), N=1Ø8 (n=3), N=256 (n=4) etc. Although it is not particularly important how the N particles are initially set out a face centred cubic arrangement does have the advantage of allowing very efficient packing so that high densities can be chosen initially without the danger of severe overlap of particles.

The choice of particle velocities is usually determined by the temperature required , the constraint of zero total linear momentum and that if the initial configuration is ordered then there exists some degree of randomness to aid equilibration. For these reasons the procedure generally adopted is to assign random velocities from a Maxwell-Boltzmann distribution having a zero mean and a root mean square velocity corresponding to the temperature required. On many mainframe computer systems access is possible to the NAG library which contains many routines one of which, GØ5DDF, is specifically designed for this purpose. Of the various criteria given for the choice of velocities the least important is the distribution as this will quickly attain the Maxwell-Boltzmann form during equilibration. It is

more important to ensure that total linear momentum is zero and that either the configuration or the velocities are random otherwise the system can remain trapped in a small region of phase space.

With the initial conditions specified it is possible then to solve the equations of motion in a stepwise fashion over a set number of time steps to produce a complete history of the evolution of the system through phase space. This provides a record of the positions , velocities and forces of all the particles for all the time investigated and from these it is possible to evaluate the primary static and dynamic properties of the system.

2.3 Evaluation of Equilibrium Properties

The primary equilibrium thermodynamic properties of the system kinetic energy (KE), potential energy (Φ), pressure (P) and temperature (T) can be readily calculated for the N-particles each step in the MD calculation from the following formulae :-

$$\Phi = \sum_{i=1}^{N} \sum_{j>i}^{N} \Phi(r_{ij}) \qquad (2.3.1)$$

$$KE = \frac{1}{2} \sum_{i=1}^{N} m_i \underline{v}_i^2 \qquad (2.3.2)$$

$$T = \frac{1}{3(N-1)k} \sum_{i=1}^{N} m_i \underline{v}_i^2 = \frac{2KE}{3(N-1)k} \qquad (2.3.3)$$

$$P = \frac{1}{3V}\left[\sum_{i=1}^{N} m_i \underline{v}_i \cdot \underline{v}_i + \sum_{i=1}^{N}\sum_{j>i}^{N} \underline{r}_{ij} \cdot \underline{F}_{ij}\right] \qquad (2.3.4)$$

which as $\underline{F}_{ij} = -\frac{d\Phi(r_{ij})}{dr}\,\hat{\underline{r}}_{ij}$ means that

$$P = \frac{1}{3V}\left[\sum_{i=1}^{N} m_i \underline{v}_i \cdot \underline{v}_i - \sum_{i=1}^{N}\sum_{j>i}^{N} \frac{d\Phi(r_{ij})}{dr}\, r_{ij}\right]$$

or

$$P = \frac{1}{3V}\left[\sum_{i=1}^{N} m \underline{v}_i \cdot \underline{v}_i - \Psi\right] \qquad (2.3.5)$$

where the virial, Ψ, is given by

$$\Psi = \sum_{i=1}^{N}\sum_{j>i}^{N} \frac{d\Phi(r_{ij})}{dr}\, r_{ij} \qquad (2.3.6)$$

In eqn. 2.3.3 the factor N-1 occurs rather than N as strictly speaking the constraint of constant total linear momentum reduces the number of degrees of freedom by three, i.e. as

$$\sum_{i=1}^{N} m_i \underline{v}_i = 0$$

$$m_j \underline{v}_j = -\sum_{i=1, i\neq j}^{N} m_i \underline{v}_i$$

thus knowing the momenta of N-1 particles and the sum of the momenta of all N particles means we can always determine the momenta of the Nth particle. This fact has generally been ignored in MD simulations and its importance depends largely

on the size of the system as the percentage difference between temperatures calculated with a factor N rather than N-1 is 100/N. So for a N=108 system the error is ~1% which is less than the inherent error in the mean temperature, <T>, due to spontaneous fluctuations [66]. Therefore, the approximation $T=2KE/3Nk$ is a good one for systems where N is of order 10^2 or greater.

As MD attempts to model a system of infinite size corrections generally have to be made to the N-particle potential energy and the virial, as given by eqns.2.3.1 and 2.3.6, due to the truncation of the potential at the cutoff radius r_c. To obtain these long-range corrections it is necessary to introduce the radial distribution function (r.d.f) g(r).

In words g(r) is a function of r , the scalar separation of two particles, which is equal to the mean number of particles in a thin spherical shell between r and $r+\delta r$ divided by the number of particles in the same shell assuming a completely random distribution of particles. The denominator in this equation is simply found by multiplying the volume of the thin shell by the number density

$$\frac{N}{V}\left[\frac{4\pi}{3}(r+\delta r)^3 - \frac{4\pi}{3}r^3\right]$$

which on ignoring terms of δr^2 gives the denominator as

$\frac{N}{V} 4\pi r^2 \delta r$.

In MD calculations g(r) has to be calculated as a discrete function by accumulating in a histogram, usually in the forces double loop, the number of particles at a separation between r and $r+\delta r$. The resolution required determines the size of δr and as $\delta r \to 0$ the discrete function will tend to the actual g(r). As the averaging procedure is carried out over all N atoms per configuration g(r) can be obtained to within a precision of 1→2% within a few thousand time steps depending upon the length of the time step and the state point. In fluid systems which interact through short range largely repulsive potentials g(r) has the limiting values of $g(r) \to 0$ for $r < \sigma$ and $g(r) \to 1$ as $r \to \infty$ indicating little penetration of the hard core of atoms and a decay of correlations between atoms as r increases. In practice the use of short range potentials in MD, such as the LJ 12-6 form where the potential energy at 2.5σ is only ~1% of that at the minimum, ensures that correlations in the positions of atoms decay within a few σ . This is important as otherwise much larger sample sizes would have to be used to avoid correlations due to the periodic boundaries.

Knowledge of g(r) allows us to calculate the mean potential energy and virial for the N particle system from the following integral expressions :-

$$\langle \Phi \rangle = \frac{N}{2} \int_0^\infty \Phi(r) g(r) 4\pi r^2 \frac{N}{V} \, dr$$

$$\langle \Psi \rangle = \frac{N}{2} \int_0^\infty r \frac{d\Phi(r)}{dr} g(r) 4\pi r^2 \frac{N}{V} \, dr$$

These integrals are simply the limiting cases, $\delta r \to 0$, of summing up the average contribution to either the potential energy or the virial from successive thin spherical shells of thickness δr containing $g(r)4\pi r^2 \delta r N/V$ particles per shell at a distance r from the reference atom. The factor N accounts for all N particles and the factor of 1/2 avoids counting the contributions of the interaction twice. In practice the energy and the virial in the range $0<r<r_c$ are calculated directly as this is simpler and because the time dependence of these properties allows the calculation of the fluctuations in the system. Beyond the cutoff the expressions are used to calculate the long range corrections to the virial (VIRLRC) and the potential energy (PELRC)

$$\text{PELRC} = \frac{N}{2} \int_{r_c}^\infty \Phi(r) g(r) 4\pi r^2 \frac{N}{V} \, dr \qquad (2.3.7)$$

$$\text{VIRLRC} = \frac{N}{2} \int_{r_c}^\infty r \frac{d\Phi(r)}{dr} g(r) 4\pi r^2 \frac{N}{V} \, dr \qquad (2.3.8)$$

For the LJ 12-6 potential the expressions reduce to

$$\text{PELRC} = \frac{8\pi\epsilon N^2 \sigma^3}{3V} \left[\frac{1}{3} \left[\frac{\sigma}{r_c} \right]^9 - \left[\frac{\sigma}{r_c} \right]^3 \right]$$

$$VIRLRC = \frac{16\pi\epsilon N^2\sigma^3}{V}\left[\left[\frac{\sigma}{r_c}\right]^3 - \frac{2}{3}\left[\frac{\sigma}{r_c}\right]^9\right]$$

where it has been assumed that g(r)=1 for $r>r_c$. For $r_c=2.5\sigma$ the assumption that g(r)=1 is usually well founded and if we take for example the case where σ=3.405Å, ϵ/k=119.8K and the molar volume =28.48cm^3 the actual molar values for PELRC and VIRLRC are -445J and 267ØJ respectively. Furthermore from eqn.2.3.5 it follows that the long range correction to the pressure is -94Ø Bar (1Bar = $10^5 N/m^2$). The use of these long range corrections thus allows us to make good estimates of the large N limit.

Molecular dynamics is then a particularly useful method of investigating the equilibrium and structural properties of model systems and has been used on many occasions for various atomic systems, e.g.[37,48,1Ø2]. There are in theory any number of equilibrium functions that can be calculated given that the positions, forces and velocities are known at all times. What makes MD unique, however, is its ability to provide information on dynamical properties.

2.4 Evaluation of Dynamical Properties

Although it is possible to obtain a complete record of the dynamical evolution of a collection of particles by molecular dynamics this in itself is not particularly informative. We require some means to interpret the wealth of data in some coherent consistent fashion. In MD great use has been made of the method of time correlation functions [1Ø3]. In general the time correlation function, C(t), of two dynamical variables A(t) and B(t) is defined as

$$C(t) = \langle A(s)B(t+s) \rangle$$

where the angle brackets denote an average over the ensemble and time origins, s. If the system is isolated then the correlation function is independent of the time origin in which case s is set equal to zero

$$C(t) = \langle A(\emptyset)B(t) \rangle .$$

It also follows from this [1Ø3] that C(t)=C(-t) and $\frac{dC(0)}{dt} = 0$. The short time limit of C(t) is obviously <AB> whereas at long times the limit becomes <A><B> thus it is always possible to define a function which decays to zero by rewriting eqn.2.4.1 as

$$C(t) = \langle (A(\emptyset)-\langle A \rangle)(B(t)-\langle B \rangle) \rangle .$$

If A and B are the same function C(t) is then known as the auto-correlation function and although the actual dynamical variables can be scalars, vectors, tensors etc. the correlation function itself is always scalar.

These functions can be used to provide a measurement of the amount of correlation between two dynamical variables and the way in which the correlation develops through time. For an auto-correlation function perfect correlation must exist at t=Ø and can, therefore, only persist or decay as time progresses whereas for correlation functions involving separate variables it is possible for the correlation to be greater at some time other than t=Ø. Obviously there are many possible correlation functions which can be calculated but some are of particular importance as they are related to transport coefficients through the Green-Kubo expressions [45]. One of the most readily calculable and useful correlation functions of this type that can be obtained from MD experiments is the velocity auto-correlation function (VACF), $C_v(t)$,

$$C_v(t) = \langle \underline{v}_i(0).\underline{v}_i(t) \rangle . \qquad (2.4.3)$$

It is related to the diffusion coefficient by the well known Green-Kubo equation

$$D = \frac{1}{3} \int_0^\infty C_v(t)\, dt . \qquad (2.4.4)$$

This can be substantiated by reference to the corresponding Einstein relation for the diffusion coefficient

$$D = \lim_{t\to\infty} \langle (\underline{r}_i(t) - \underline{r}_i(0))^2 \rangle / 6t \qquad (2.4.5)$$

which on substituting for

$$\underline{r}_i(t) - \underline{r}_i(0) = \int_0^t \underline{v}_i(s)\, ds$$

and performing some algebra and integration returns the aforementioned result. So from eqns.2.4.5 and 2.4.4 the diffusion coefficient is related to the mean squared displacement of particles and the integral over the VACF. Thus in a MD calculation there are two possible ways of calculating D and as it is a single particle property results of a high precision can be expected through averaging over all N particles.

The existence of two expressions for the diffusion coefficient is also true for other transport properties. In the case of the shear viscosity η can either be related to a mean squared centre of momentum displacement or to the integral over the stress auto-correlation function (SACF), $C_s(t) = \langle \sigma_{\alpha\beta}(0)\sigma_{\alpha\beta}(t) \rangle$, where $\sigma_{\alpha\beta}$ is an off-diagonal component of the stress tensor,

$$\eta = \frac{V}{kT} \int_0^\infty C_s(t)\, dt \,. \qquad (2.4.6)$$

As already stated the stress is a collective property so the amount of averaging is limited when compared to the VACF consequently the determination of η from eqn.2.4.6 is subject to large statistical errors [48,49,50].

The actual numerical calculation of correlation functions does not usually present any problems. The functions have to be discretised, of course, and can consume an appreciable amount of computer time when they are being calculated. Their usefulness in the understanding of correlated dynamics has been repeatedly underlined by many simulations particularly in molecular systems where extra degrees of freedom permit coupling between rotations and translations [104].

2.5 MD for Polyatomic Systems

As many aspects of MD are common for all systems the general method has been explained for the simplest case of monatomic particles so as to avoid introducing complications at an early stage. For polyatomic systems the major problem is dealing with the rotational part of the motion. For the centre of mass there is no problem as once the total force on the molecule has been evaluated the equation of motion is the same as for monatomics. There are at present two general approaches to modelling polyatomic molecules. Firstly, the atoms within a molecule can be held together and given the correct geometry by the use of bond and bond angle potentials. These potentials have to have deep wells to keep bond lengths and bond angles close to their required equilibrium values. This in turn means that the forces from these potentials change rapidly and thus require short time steps to be integrated successfully [105,106].

The assumption that the vibrations decouple from other motions has been used in the second method of modelling polyatomic molecules. In this case the atoms are fixed together by rigid bonds and bond angles are also fixed at specific values. Depending on the particular molecule internal modes may or may not be present. If the molecule is entirely rigid then the problem reduces to solving the rigid body equations of motion. For the first approach to modelling polyatomic molecules the procedure differs very little from the monatomic case as the system is effectively a collection of separate particles.

Studies on fluid systems composed of polyatomic molecules modelled by the second approach began with the work of Barojas, Levesque and Quentrec on diatomic nitrogen [38]. They used a two centre LJ model consisting of two LJ 12-6 interaction sites joined by a rigid bond of length l to represent nitrogen. They used Euler angles [107] to specify the orientations of molecules and numerically integrated Euler's equations of rigid body motion. This was fairly successful but suffered from the drawback that two of the Euler angles become indistinguishable if the azimuthal angle tends to 0° or 180°. This meant that the angle for a particular molecule had to be redefined from a different origin if its azimuthal angle became too close to 0° or 180°, otherwise the solution of the equation of motion became unstable and the total energy drifted. In their simulations of nitrogen Cheung

and Powles [108] used the special geometry of the homonuclear diatomic to reduce the normal second order differential equation for rotational motion to a first order one. To integrate the equations of motion they used a fourth order predictor-corrector method [109] to solve for angular velocity and a fifth order predictor-corrector for the centre of mass motion.

To avoid the problems associated with Euler angles and to generalise to any rigid polyatomic system Evans [110,40] has developed an algorithm which uses quaternion parameters. These four variables, defined in terms of the usual Euler angles, map the orientation of a rigid body onto a point on the surface of a four dimensional sphere. As this space is Euclidean the equations of motion in terms of the quaternions are free of singularities and results in two sets of coupled first order differential equations which can be solved numerically.

In the work of Singer et al [39,111] on linear molecules yet another algorithm was used for the rotational motion. This involved the use of a 'free flight' phase which allowed the constituent atoms to first move as if unrestricted and then this movement was converted into an equivalent path due to the restriction of the constant bond length. This form of algorithm which allows a 'free flight' phase has been treated formally and generalised to treating any complex molecule by

Ryckaert, Ciccotti and Berendsen [41]. This method involves the solution of the equations of motion subject to a number of predefined Lagrangian constraints which have to be satisfied at each step by solving for undetermined multipliers. Fincham [112] has shown that for any linear rigid molecule, where there is only the one constraint of constant bond length, the method of constraints is particularly suited as the equation for the undetermined multiplier reduces to a simple quadratic. For more complicated molecules the undetermined multipliers have to be found either by matrix inversion or by iteration [41].

The choice of algorithm to use depends to some extent upon the molecule to be modelled. Obviously the constraints method could be used for all molecules of ths type but for rigid molecules the method of quaternions [11Ø] is particularly elegant and more efficient than constraints because it does not require any iterative procedures or matrix inversions [41]. As previously stated one exception to this is the diatomic case. The advantage of freezing out entirely the vibrational degrees of freedom is that larger time steps can be used so for an equivalent amount of computer time we can sample more of phase space. This is one of the most important considerations in MD. In order to obtain meaningful results for time averaged quantities the actual duration of the experiment must be chosen to be longer than the relaxation times of all relevant processes in the system. This becomes

particularly important as the molecules become more complex, which causes the spectrum of relaxation times to broaden. As the aim of this work is to investigate the rheological behaviour of several different molecules, rigid and constrained models of molecules have been used throughout to allow systems to be studied under a wider range of applied conditions. The algorithms used, constraints and quaternions, require further detailed explanation as they constitute a fundamental part in the efficient simulation of polyatomic molecular fluids. One way to approach this is to treat increasingly more complicated molecules starting from the two centre molecule then progressing to the general n-centred rigid molecule and ultimately to molecules subject to a known number of constraints but capable of intramolecular rearrangement.

2.6 Diatomic Molecules

Here we consider the case of a two centre molecule where the positions of the atoms of molecule i and the centre of mass (COM) are specified by the vectors $\underline{r}_{i1}$, $\underline{r}_{i2}$ and $\underline{R}_i$ respectively. If the masses of atoms 1 and 2 are m_{i1} and m_{i2} then $\underline{R}_i$ can be calculated from

$$\underline{R}_i = (\underline{r}_{i1}m_{i1} + \underline{r}_{i2}m_{i2})/M_i \qquad (2.6.1)$$

where $M_i=m_{i1}+m_{i2}$ is the mass of molecule i. The equations of

motion [41] for the atoms and the COM can be written as

$$\ddot{\underline{r}}_{ik} = (\underline{F}_{ik} + \underline{G}_{ik})/m_{ik} \qquad (2.6.2)$$

$$\ddot{\underline{R}}_i = \sum_{k=1}^{2} \underline{F}_{ik}/M_i \qquad (2.6.3)$$

where $\underline{F}_{ik}$ is the force on atom k of molecule i due to all the other molecules and $\underline{G}_{ik}$ is the force along the bond joining the two atoms. From Newton's first law it follows that

$$\underline{G}_{i1} = -\underline{G}_{i2} \; . \qquad (2.6.4)$$

The equation of motion for the COM is of the same form as for a monatomic particle and as such can be integrated without difficulty using the 'leapfrog' algorithm. If we apply the 'leapfrog' algorithm to the equations of motion for the atoms we obtain [112]

$$\underline{r}_{i1}(t+\Delta t) = \underline{r}_{i1}(t) + \dot{\underline{r}}_{i1}(t-\Delta t/2)\Delta t + \frac{\underline{F}_{i1}}{m_{i1}}\Delta t^2 + \frac{\underline{G}_{i1}}{m_{i1}}\Delta t^2 \qquad (2.6.5)$$

$$\underline{r}_{i2}(t+\Delta t) = \underline{r}_{i2}(t) + \dot{\underline{r}}_{i2}(t-\Delta t/2)\Delta t + \frac{\underline{F}_{i2}}{m_{i2}}\Delta t^2 - \frac{\underline{G}_{i1}}{m_{i2}}\Delta t^2 \qquad (2.6.6)$$

Subtracting eqn.2.6.6 from 2.6.5 and introducing the bond vector

$$\underline{l}_i = \underline{r}_{i1} - \underline{r}_{i2} \qquad (2.6.7)$$

gives

$$\underline{l}_i(t+\Delta t) = \underline{l}_i(t) + \dot{\underline{l}}_i(t-\Delta t/2)\Delta t + \left[\frac{\underline{F}_{i1}}{m_{i1}} - \frac{\underline{F}_{i2}}{m_{i2}}\right]\Delta t^2 + \underline{G}_{i1}\left[\frac{\underline{l}}{m_{i1}} + \frac{\underline{l}}{m_{i2}}\right]\Delta t^2 . \qquad (2.6.8)$$

Now as $\underline{G}_{i1}$ must act along the bond vector the final term in eqn.2.6.8 can be written as

$$\underline{G}_{i1}\left[\frac{\underline{l}}{m_{i1}} + \frac{\underline{l}}{m_{i2}}\right]\Delta t^2 = h\underline{l}_i(t) \qquad (2.6.9)$$

where h is an undetermined multiplier. If we also allow

$$\tilde{\underline{l}}_i = \underline{l}_i(t) + \dot{\underline{l}}_i(t-\Delta t/2)\Delta t + \left[\frac{\underline{F}_{i1}}{m_{i1}} - \frac{\underline{F}_{i2}}{m_{i2}}\right]\Delta t^2$$

i.e. $\tilde{\underline{l}}_i$ is the bond vector after 'free flight' of the atoms then

$$\underline{l}_i(t+\Delta t) = \tilde{\underline{l}}_i + h\underline{l}_i(t) \; . \qquad (2.6.10)$$

To determine h the constraint that the bond length is a fixed length, l, is used. This means that

$$\underline{l}_i^2(t+\Delta t) - l^2 = 0$$

$$(\tilde{\underline{l}}_i + h\underline{l}_i(t))^2 - l^2 = 0$$

$$\Rightarrow \quad h^2l^2 + 2h\underline{l}_i(t)\cdot\tilde{\underline{l}}_i + \tilde{\underline{l}}_i^2 - l^2 = 0 \qquad (2.6.11)$$

Eqn.2.6.11 is quadratic in h and the solution is found simply from

$$h = -\,\tilde{\underline{l}}_i\cdot\underline{l}_i(t) + \frac{\sqrt{(\underline{l}_i(t)\cdot\tilde{\underline{l}}_i)^2 - l^2(\tilde{\underline{l}}_i^2 - l^2)}}{l^2}$$

and then $\underline{l}_i(t+\Delta t)$ can be calculated from eqn.2.6.1Ø. Having obtained $\underline{l}_i(t+\Delta t)$ the half step bond vector velocity can be found from

$$\dot{\underline{l}}_i(t+\Delta t/2) = (\underline{l}_i(t+\Delta t) - \underline{l}_i(t))/\Delta t$$

and the on step velocity from

$$\dot{\underline{l}}_i(t) = (\dot{\underline{l}}_i(t-\Delta t/2) + \dot{\underline{l}}_i(t+\Delta t/2))/2 \quad .$$

The new atomic positions are then calculated from the updated COM position and the new bond vector

$$\underline{r}_{i1}(t+\Delta t) = \underline{R}_i(t+\Delta t) + \left[\frac{m_{i2}}{m_{i1}+m_{i2}}\right]\underline{l}_i(t+\Delta t)$$

$$\underline{r}_{i2}(t+\Delta t) = \underline{R}_i(t+\Delta t) - \left[\frac{m_{i1}}{m_{i1}+m_{i2}}\right]\underline{l}_i(t+\Delta t)$$

Thus in this way the equations of motion of a diatomic can be integrated by a relatively simple algorithm which requires the storage of eight vectors per molecule $\underline{R}(t)$, $\underline{R}(t-\Delta t/2)$, $\underline{r}_1(t)$, $\underline{r}_2(t)$, $\underline{l}(t)$, $\underline{l}(t-\Delta t/2)$, $\underline{F}_1(t)$ and $\underline{F}_2(t)$ or just one more vector per atom than for a monatomic simulation.

The introduction of the rotational degrees of freedom means that the kinetic energy can be separated into two components. The translational kinetic energy (TRKE) can be readily calculated from

$$\text{TRKE} = \frac{1}{2}\sum_{i=1}^{N} M_i \dot{\underline{R}}_i^{\,2}$$

but the usual expression for the rotational kinetic energy (RTKE) is

$$RTKE = \frac{1}{2}\sum_{i=1}^{N} I\underline{\omega}_i^2$$

where I is the moment of inertia and ω is the angular velocity. As this algorithm does not use angular velocities an alternative approach is to use the fact that the total kinetic energy (TKE) is equal to the sum of the rotational and translational kinetic energies

$$TKE = \frac{1}{2}\sum_{i=1}^{N} m_{i1}\dot{\underline{r}}_{i1}^2 + m_{i2}\dot{\underline{r}}_{i2}^2 = TRKE + RTKE$$

$$\Rightarrow \quad RTKE = \frac{1}{2}\sum_{i=1}^{N} m_{i1}\dot{\underline{r}}_{i1}^2 + m_{i2}\dot{\underline{r}}_{i2}^2 - M_i\dot{\underline{R}}_i^2 \qquad (2.6.12)$$

Now differentiating eqn.2.6.1 w.r.t. time gives

$$\dot{\underline{R}}_i = (m_{i1}\dot{\underline{r}}_{i1} + m_{i2}\dot{\underline{r}}_{i2})/M_i$$

then substituting for $\dot{\underline{R}}_i$ in eqn.2.6.12 and simplifying gives

$$RTKE = \frac{1}{2}\sum \frac{m_{i1}m_{i2}}{m_{i1}+m_{i2}}\left[\dot{\underline{r}}_{i1}^2 - 2\dot{\underline{r}}_{i1}\dot{\underline{r}}_{i2} + \dot{\underline{r}}_{i2}^2\right]$$

Differentiation of eqn.2.6.7 w.r.t. time means that

$$\dot{\underline{l}}_i = \dot{\underline{r}}_{i1} - \dot{\underline{r}}_{i2}$$

and squaring gives

$$\dot{\underline{l}}_i^2 = \dot{\underline{r}}_{i1}^2 - 2\dot{\underline{r}}_{i1}\dot{\underline{r}}_{i2} + \dot{\underline{r}}_{i2}^2$$

so from eqn.2.6.12

$$RTKE = \frac{1}{2}\sum_{i=1}^{N} \mu_i \dot{\underline{l}}_i^2 \quad ,$$

where $\mu_i = m_{i1}m_{i2}/M_i$ is the reduced mass of molecule i. For a classical diatomic molecule there are five degrees of freedom three translations and two rotations. By equipartition of energy it is possible to define three temperatures for this system :-

Translational temperature, $TTEMP = 2TRKE/3(N-1)k$

Rotational temperature , $RTEMP = RTKE/Nk$

Overall temperature , $TEMP = 2TKE/(5N-3)k$

In the equation for the rotational temperature the factor N rather than N-1 occurs because the intrinsic angular momentum is not a conserved property. Therefore, there is not the reduction in the number of degrees of freedom that occurs in the case of linear momentum. It is, however, important to ensure that on average the sum of the angular momenta is zero otherwise the temperature calculation has to take into account the net spin of the molecules.

2.7 Rigid Molecules

In this case a rigid body consisting of n mass points at the positions $\underline{r}_1$, $\underline{r}_2$, ... $\underline{r}_n$ is considered. The COM is again given by

$$\underline{R} = \frac{\sum_{j=1}^{N} m_j \underline{r}_j}{\sum_{i=1}^{N} m_j} \qquad (2.7.1)$$

For a rigid molecule the positions of the atoms relative to the COM can be defined by fixed vectors which have the unit principal axis vectors as their basis. So for a particular atom its position is always defined by a vector $\underline{r}_{pj} = (x_{pj}, y_{pj}, z_{pj})$ where x_{pj}, y_{pj} and z_{pj} are constants and the basis vectors $\hat{\underline{X}}$, $\hat{\underline{Y}}$ and $\hat{\underline{Z}}$ are the unit principal axis vectors which form an orthogonal set and are defined w.r.t. the fixed laboratory coordinate system. In time $\hat{\underline{X}}$, $\hat{\underline{Y}}$ and $\hat{\underline{Z}}$ will change as the molecule rotates but $\underline{r}_{pj}$ remains the same. The transformation from a principal to laboratory frame of reference is simply

$$\underline{r}_j - \underline{R} = \underline{r1}_j = x_{pj}\,\hat{\underline{X}} + y_{pj}\,\hat{\underline{Y}} + z_{pj}\,\hat{\underline{Z}} \qquad (2.7.2)$$

or

$$\underline{r1}_j = \underline{\underline{A}}^T \underline{r}_{pj} \qquad (2.7.3)$$

where $\underline{\underline{A}}^T$ is the transpose of the rotation matrix $\underline{\underline{A}}$ and is constructed from the principal axis vectors [11Ø]

$$\underline{\underline{A}}^T = (\hat{\underline{X}}, \hat{\underline{Y}}, \hat{\underline{Z}}) \,. \qquad (2.7.4)$$

As $\underline{\underline{A}}^T$ is formed from an orthogonal basis it follows that [113]

$$\underline{\underline{A}}^T = \underline{\underline{A}}^{-1}$$

so therefore, multiplying each side of eqn.2.7.3 by $\underline{\underline{A}}$ gives

$$\underline{\underline{A}}\underline{r}_{1_j} = \underline{r}_{p_j} . \qquad (2.7.5)$$

The choice of principal axes is governed by the condition that the moment of inertia tensor $\underline{\underline{I}}$ is diagonal i.e. the $I_{\alpha\alpha}$ terms are the only non-zero ones. $\underline{\underline{I}}$ is given by the equation [107]

$$\underline{\underline{I}} = \sum_{j=1}^{n} m_j(\underline{r}_{p_j}^2 \underline{\underline{1}} - \underline{r}_{p_j}\underline{r}_{p_j}) \qquad (2.7.6)$$

where $\underline{\underline{1}}$ is the identity matrix. In practice some or all of the principal axes can be found from the symmetry of the molecule but if necessary standard methods [113] can be used to find the principal axes which diagonalise $\underline{\underline{I}}$.

Once the principal axes have been obtained the orientation of the molecule can be specified with respect to laboratory reference frame in terms of the three Euler angles (ψ, θ, ϕ).

The angles ψ, θ and ϕ are defined as the angles of rotation about the axes shown in operations 1, 2 and 3 respectively of fig.2.3. Using these Euler angles the orientation can also be represented by the four quaternions [11Ø] :-

$$q_1 = \cos(\theta/2)\cos((\psi+\phi)/2)$$

$$q_2 = \sin(\theta/2)\cos((\psi-\phi)/2)$$

$$q_3 = \sin(\theta/2)\sin((\psi-\phi)/2)$$

$$q_4 = \cos(\theta/2)\sin((\psi+\phi)/2)$$

These four variables are not linearly independent as it can be easily shown that they satisfy the constraint relationship

$$\sum_{i=1}^{4} q_i^2 = 1 \quad . \qquad (2.7.7)$$

The Euler angles can be also be used to calculate the principal axis vectors from

$$\hat{\underline{X}} = (\cos\phi\cos\psi - \sin\phi\sin\psi\cos\theta \; , \; \cos\phi\sin\psi + \sin\phi\cos\psi\cos\theta \; , \; \sin\theta\sin\phi)$$

$$\hat{\underline{Y}} = (-\sin\phi\cos\psi - \cos\phi\sin\psi\cos\theta \; , \; \cos\phi\cos\psi\cos\theta - \sin\phi\sin\psi \; , \; \cos\phi\sin\theta)$$

$$\hat{\underline{Z}} = (\sin\psi\sin\theta \; , \; -\sin\theta\cos\psi \; , \; \cos\theta)$$

Figure 2.3 Euler angles.

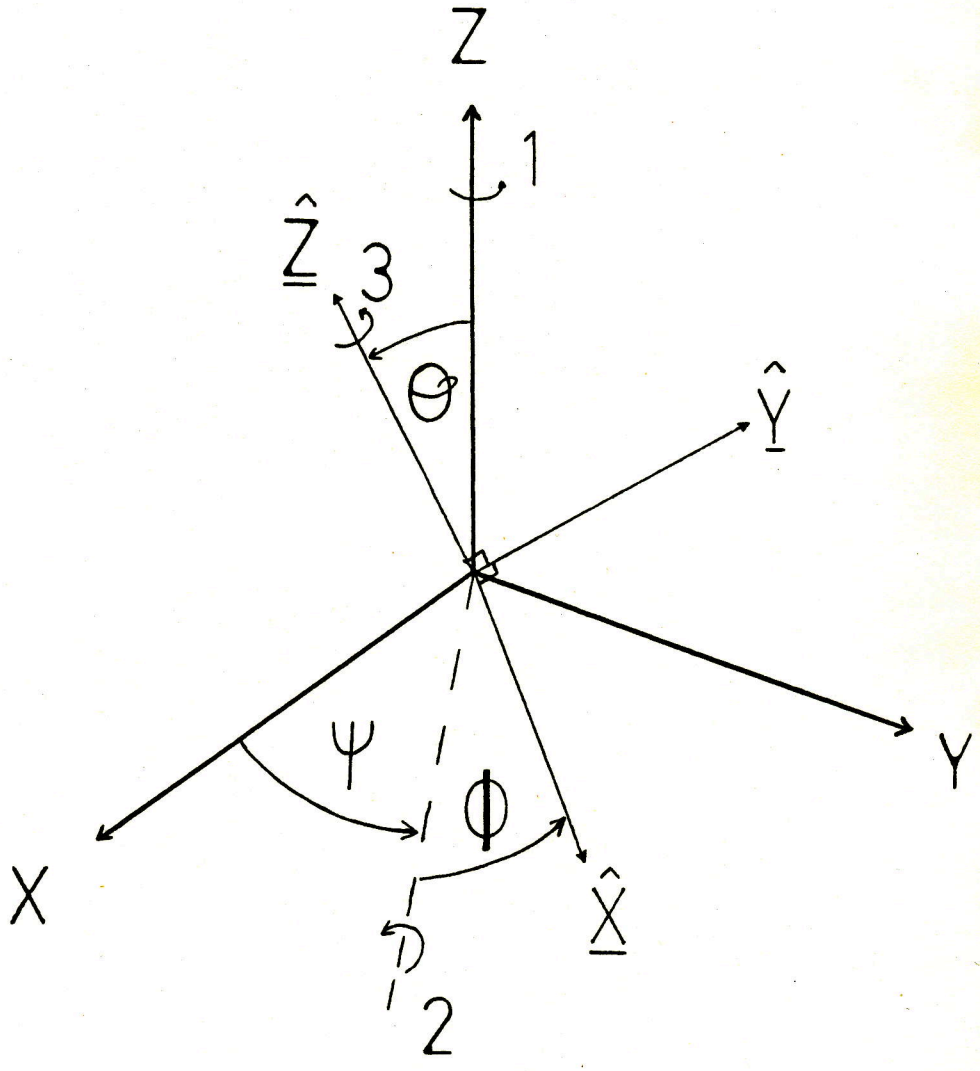

and thus the rotation matrix $\underline{\underline{A}}$ from eqn.2.7.4. The principal axes can just as easily be written in terms of the quaternions and the rotation matrix then becomes [110]

$$\underline{\underline{A}} = \begin{bmatrix} -q_3^2 + q_2^2 - q_4^2 + q_1^2 , & 2(q_4q_1 - q_3q_2) , & 2(q_2q_4 + q_3q_1) \\ -2(q_3q_2 + q_4q_1) , & q_3^2 - q_2^2 - q_4^2 + q_1^2 , & 2(q_2q_1 - q_3q_4) \\ 2(q_2q_4 - q_3q_1) , & -2(q_3q_4 + q_2q_1) , & -q_3^2 - q_2^2 + q_4^2 + q_1^2 \end{bmatrix} \quad (2.7.8)$$

The basic equations used in the rotational motion of rigid bodies involving quaternions are [110,114]

$$\dot{\underline{J}} = \underline{T} \quad (2.7.9)$$

$$\underline{J}_p = \underline{\underline{A}}\underline{J} \quad (2.7.10)$$

$$\omega_{p\alpha} = J_p/I_{\alpha\alpha} \quad (2.7.11)$$

$$\begin{bmatrix} \dot{q}_3 \\ \dot{q}_2 \\ \dot{q}_4 \\ \dot{q}_1 \end{bmatrix} = \frac{1}{2} \begin{bmatrix} -q_4 & -q_1 & q_2 & q_3 \\ q_1 & -q_4 & -q_3 & q_2 \\ q_3 & q_2 & q_1 & q_4 \\ -q_2 & q_3 & -q_4 & q_1 \end{bmatrix} \begin{bmatrix} \omega_{p_x} \\ \omega_{p_y} \\ \omega_{p_z} \\ 0 \end{bmatrix}$$

or

$$\dot{\underline{q}} = \underline{\underline{Q}}\underline{\omega}_p \quad (2.7.12)$$

where $\underline{J}$ is the angular momentum and $\underline{T}$ is the torque. The angular momentum can be calculated in the principal frame of reference from

$$\underline{J}_p = \sum_{j=1}^{n} \underline{r}_{p_j} \times m_j \underline{v}_{p_j} \qquad (2.7.13)$$

which as

$$\underline{v}_{p_j} = \underline{\omega}_{p_j} \times \underline{r}_{p_j} \qquad (2.7.14)$$

gives

$$\underline{J}_p = \sum_{j=1}^{n} \underline{r}_{p_j} \times m_j (\underline{\omega}_{p_j} \times \underline{r}_{p_j}) \qquad (2.7.15)$$

and can be transformed into the laboratory reference frame using the rotation matrix

$$\underline{J} = \underline{\underline{A}}^T \underline{J}_p . \qquad (2.7.16)$$

Once the forces on all the atoms of a molecule have been computed in cartesian space the total torque can be calculated from

$$\underline{T} = \sum_{j=1}^{n} \underline{r}_{1_j} \times \underline{F}_j . \qquad (2.7.17)$$

Having established which quantities are required for handling rigid body rotations and how they can be calculated all that remains is to integrate the equations of motion. This immediately poses a problem as the form of the equations of motion, coupled first order differential equations, does not permit the straightforward implementation of a Verlet or 'leapfrog' type algorithm. It is possible to use higher order

predictor-corrector algorithms [109] but Fincham [114] has pointed out that the numerical errors introduced by these higher order algorithms become significantly larger than those obtained using the simple 'leapfrog' scheme as the time step is increased [69,114]. To obviate the problem of having to use high order algorithms Fincham [114] has developed a scheme capable of integrating eqns.2.7.9 and 2.7.12 using a 'leapfrog' type formulation.

2.8 Algorithm for Rotational Motion using Quaternions [114]

Using Taylor expansions forwards and backwards in time an amount $\Delta t/2$ about t for $\underline{J}$ gives

$$\underline{J}(t-\Delta t/2) = \underline{J}(t) - \dot{\underline{J}}(t)\Delta t/2 + \ddot{\underline{J}}(t)(\Delta t/2)^2/2! - \ldots \qquad (2.8.1)$$

$$\underline{J}(t+\Delta t/2) = \underline{J}(t) + \dot{\underline{J}}(t)\Delta t/2 + \ddot{\underline{J}}(t)(\Delta t/2)^2/2! + \ldots \qquad (2.8.2)$$

Subtracting eqn.2.8.1 from 2.8.2 gives

$$\underline{J}(t+\Delta t/2) = \underline{J}(t-\Delta t/2) + \dot{\underline{J}}(t)\Delta t + O(\Delta t^3) \qquad (2.8.3)$$

which from eqn.2.7.9 gives

$$\underline{J}(t+\Delta t/2) = \underline{J}(t-\Delta t/2) + \underline{T}(t)\Delta t + O(\Delta t^3) \qquad (2.8.4)$$

For the equation of motion involving quaternions applying the

same form of algorithm at time t rather than $t-\Delta t/2$ gives

$$\underline{q}(t+\Delta t) = \underline{q}(t) + \dot{\underline{q}}(t+\Delta t/2)\Delta t + O(\Delta t^2) \qquad (2.8.5)$$

but

$$\dot{\underline{q}}(t+\Delta t/2) = \underline{\underline{Q}}(t+\Delta t/2)\underline{\omega}_p(t+\Delta t/2)$$

so as $\underline{\underline{Q}}(t+\Delta t/2)$ involves $\underline{q}(t+\Delta t/2)$ the algorithm cannot be implemented directly. In order to approximate a value for $\underline{q}(t+\Delta t/2)$ Fincham [114] uses a truncated Taylor expansion

$$\underline{q}(t+\Delta t/2) = \underline{q}(t) + \dot{\underline{q}}(t)\Delta t/2 + O(\Delta t^2) \qquad (2.8.6)$$

$$\Rightarrow \quad \underline{q}(t+\Delta t/2) = \underline{q}(t) + \underline{\underline{Q}}(t)\underline{\omega}_p(t)\Delta t/2 \qquad (2.8.7)$$

The overall sequence of steps in the rotational algorithm then takes the form [114] :-

1) Begin calculation with $\underline{J}(t-\Delta t/2)$, $\underline{q}(t)$ and $\underline{T}(t)$.

2) Calculate on step angular momentum from eqn.2.8.4

$$\underline{J}(t) = \underline{J}(t-\Delta t/2) + \underline{T}(t)\Delta t/2 \,.$$

3) Transform lab. angular momentum to principal angular momentum using the rotation matrix formed from $\underline{q}(t)$

$$\underline{J}_p(t) = \underline{\underline{A}}(t)\underline{J}(t) \,.$$

4) Use eqn.2.7.11 to calculate on-step angular velocities

$$\omega_{p\alpha}(t) = J_{p\alpha}(t)/I_{\alpha\alpha} \qquad \alpha=x,y,z \,.$$

5) Approximate $\underline{q}(t+\Delta t/2)$ using eqn.2.8.7

$$\underline{q}(t+\Delta t/2) = \underline{q}(t) + \underline{\underline{Q}}(t)\underline{\omega}_p(t)\Delta t/2$$

6) Use $\underline{q}(t+\Delta t/2)$ to calculate $\underline{\underline{A}}(t+\Delta t/2)$ and $\underline{\underline{Q}}(t+\Delta t/2)$.

7) Calculate new half step angular momentum

$$\underline{J}(t+\Delta t/2) = \underline{J}(t-\Delta t/2) + \underline{T}(t)\Delta t$$

8) Transform to principal coordinate frame

$$\underline{J}_p(t+\Delta t/2) = \underline{\underline{A}}(t+\Delta t/2)\underline{J}(t+\Delta t/2)$$

9) Calculate half step angular velocities

$$\underline{\omega}_{p\alpha}(t+\Delta t/2) = \underline{J}_{p\alpha}(t+\Delta t/2)/I_{\alpha\alpha} \qquad \alpha=x,y,z$$

10) Obtain new quaternions from eqn.2.8.5

$$\underline{q}(t+\Delta t) = \underline{q}(t) + \underline{\underline{Q}}(t+\Delta t/2)\underline{\omega}_p(t+\Delta t/2)\Delta t$$

11) Using the constraint relation, eqn.2.7.7, normalize the quaternions

$$\underline{q}'(t+\Delta t) = a\underline{q}(t+\Delta t)$$

where

$$a = \left[\frac{1}{\underline{q}^2(t+\Delta t)}\right]^{\frac{1}{2}}$$

The purpose of step 11) is to prevent any numerical errors accumulating which might lead to inaccuracies in the trajectory. Once the quaternions have been obtained it is a simple matter to generate the new atom positions from the updated COM and the position vectors $\{\underline{r}_{pj}\}$

$$\underline{r}_j(t+\Delta t) = \underline{R}(t+\Delta t) + \underline{\underline{A}}^T(t+\Delta t)\underline{r}_{pj}$$

As can be seen the algorithm requires minimal store since

only the three vectors $\underline{J}(t-\Delta t/2)$, $\underline{q}(t)$ and $\underline{T}(t)$ need to be retained at each step. The algorithm as a whole is only second order accurate but tests on a three centre model for cyclopropane [114] have shown it to be more stable than either a fourth order predictor-corrector or a constraints algorithm.

In contrast to the diatomic algorithm angular velocities are required so the total rotational kinetic energy can be calculated directly from

$$RTKE = \sum_{j=1}^{N} \frac{1}{2} \left(I_{xx}\omega_{pxj}^2 + I_{yy}\omega_{pyj}^2 + I_{zz}\omega_{pzj}^2 \right)$$

2.9 The Method of Constraints

In this case we consider the dynamics of a molecule consisting of n mass points at the positions $\underline{r}_1$, $\underline{r}_2$, ... $\underline{r}_n$ in cartesian space and of mass m_1 , m_2 , ... m_n . We further assume that the molecule is subject to n_c rigid length constraints of the form $|\underline{r}_{ij}| = d_{ij}$. Thus a bond length is preserved by constraining the distance between nearest neighbours and a bond angle by constraining the distances between three nearest neighbours. At each step the total force on each atom, $\underline{F}_i$, due to all intra- and intermolecular potentials can be calculated from the positions leaving the unknown $\underline{G}_i$, the force due to the constraints imposed.

As for the diatomic the equation of motion is

$$\ddot{\underline{r}}_i = (\underline{F}_i + \underline{G}_i)/m_i \quad . \qquad (2.9.1)$$

Implementing the 'leapfrog' algorithm to this equation we obtain

$$\underline{r}_i(t+\Delta t) = \underline{r}_i(t) + \dot{\underline{r}}_i(t-\Delta t/2) + (\underline{F}_i + \underline{G}_i)\Delta t^2/m_i \qquad (2.9.2)$$

which can be written as

$$\underline{r}_i(t+\Delta t) = \underline{r}'_i + \delta\underline{r}_i \qquad (2.9.3)$$

where $\underline{r}'_i$ is the position after 'free flight' and

$$\delta\underline{r}_i = \underline{G}_i\Delta t^2/m_i \quad . \qquad (2.9.4)$$

As the forces constituting $\underline{G}_i$ can only act along the direction of the constrained lengths it is possible to rewrite $\delta\underline{r}_i$ as

$$\delta\underline{r}_i = \sum_j h_{ij}\underline{r}_{ij}(t)$$

where the sum over j extends to those atoms that form a constrained pair with i. The problem then is to determine once again the set of multipliers $\{h_{ij}\}$. The methods by which this can be achieved have been discussed previously [41]. The particular version used throughout this work does not explicitly calculate the $\{h_{ij}\}$ but achieves the same result by

an iterative procedure [41].

2.1Ø The Constraints Algorithm

After 'free flight' it is possible to write down for any pair of constrained atoms an equation of the form

$$\left[(\underline{r}'_i + g_i\underline{r}_{ij}(t)) - (\underline{r}'_j + g_j\underline{r}_{ij}(t))\right]^2 = d_{ij}^2$$

or

$$(\underline{r}'_{ij} + g_{ij}\underline{r}_{ij}(t))^2 = d_{ij}^2 \qquad (2.10.1)$$

where $g_{ij} = g_i - g_j$ is the multiplier which ignoring all the other constraints produces new positions

$$\underline{r}''_i = (\underline{r}'_i + g_i\underline{r}_{ij}(t)) \qquad (2.10.2)$$

and

$$\underline{r}''_j = (\underline{r}'_j + g_j\underline{r}_{ij}(t)) \qquad (2.10.3)$$

which satisfy the constraint relation between atoms i and j. Equation 2.1Ø.1 is quadratic in g_{ij} and can be solved exactly to give

$$g_{ij} = \frac{-\underline{r}_{ij}(t)\cdot\underline{r}'_{ij} + \sqrt{(\underline{r}_{ij}(t)\cdot\underline{r}'_{ij})^2 - \underline{r}_{ij}^2(t)(\underline{r}'^2_{ij} - d_{ij}^2)}}{\underline{r}_{ij}^2(t)} \qquad (2.10.4)$$

It follows from the fact that the forces of constraint on particles i and j must be equal and opposite that

$$g_i = g_{ij}(m_j/(m_i + m_j)) \qquad (2.10.5)$$

$$g_j = - g_{ij}(m_i/(m_i + m_j)) \qquad (2.10.6)$$

So it is then possible to determine $\underline{r}_i''$ and $\underline{r}_j''$ from eqns.2.1Ø.2 and 2.1Ø.3. The next step then is to redefine $\underline{r}_i'=\underline{r}_i''$ and $\underline{r}_j'=\underline{r}_j''$ and then to pass to the next pair of constrained atoms and repeat the procedure. Of course the satisfaction of the constraint between the next pair will destroy that of the previous two so the process has to be repeated. The procedure is terminated when all the constraints are satisfied to a specified tolerance, TOL, i.e. when

$$\left|\,|\underline{r}_{ij}'| - d_{ij}\right|/d_{ij} < \mathrm{TOL} \; . \qquad (2.10.7)$$

The total number of iterations required per molecule is largely determined by the tolerance. In molecules where many constraints have to be satisfied the evaluation of a large number of square roots, eqn.2.1Ø.4, can cause the time spent in the iterative procedure to become a significant contributor to the overall duration of the MD simulation. It is then important to maximise the efficiency of this procedure and one way to do this [115] is by using the following approximation.

The quadratic equation for the multiplier, eqn.2.1Ø.1, can be written as

$$g_{ij}^2 \underline{r}_{ij}^2(t) + 2g_{ij}\underline{r}_{ij}' \cdot \underline{r}_{ij}(t) + \underline{r}_{ij}'^2 - d_{ij}^2 = 0$$

Ignoring the quadratic term gives an approximation to g_{ij}

$$g_{ij} \approx (d_{ij}^2 - \underline{r}_{ij}'^2)/2(\underline{r}_{ij}' \cdot \underline{r}_{ij}(t)) \qquad (2.10.8)$$

It turns out that although this method requires more iterations it is in fact faster in terms of computing time. The satisfaction of the constraint relationship step can also be accomplished efficiently with this procedure by rewriting the tolerance condition, eqn.2.10.7. Since we require

$$\left| |\underline{r}_{ij}'| - d_{ij} \right| < TOL*d_{ij}$$

it follows that

$$\left| |\underline{r}_{ij}'| + d_{ij} \right| < TOL*d_{ij} + 2d_{ij}$$

so multiplying these two conditions together gives

$$\left| \underline{r}_{ij}'^2 - d_{ij}^2 \right| < TOL^2 d_{ij}^2 + 2*TOL*d_{ij}^2 .$$

For small TOL the term involving TOL^2 is negligible so the condition can be written as

$$\left| \underline{r}_{ij}'^2 - d_{ij}^2 \right| < 2*TOL*d_{ij}^2$$

which as can be seen requires nothing extra to be calculated.

Having satisfied all the constraints to within the specified tolerance all that remains is to update the atomic positions

$$\underline{r}_i(t+\Delta t) = \underline{r}_i'$$

and the half step velocities

$$\dot{\underline{r}}_i(t+\Delta t/2) = (\underline{r}_i(t+\Delta t) - \underline{r}_i(t))/\Delta t \quad .$$

The full step velocities are then calculated in the usual way

from

$$\underline{\dot{r}}_i(t) = (\underline{\dot{r}}_i(t-\Delta t/2) + \underline{\dot{r}}_i(t+\Delta t/2))/2 \quad .$$

The COM velocity can be simply calculated from differentiating the equation for the COM position

$$\underline{R} = \frac{\sum_{i=1}^{n} m_i \underline{r}_i}{\sum_{i=1}^{n} m_i}$$

w.r.t. time

$$\dot{\underline{R}} = \sum_{i=1}^{n} m_i \dot{\underline{r}}_i / M \quad .$$

For a system of such molecules the total translational kinetic energy is then simply

$$TRKE = \sum_{i=1}^{N} \frac{1}{2} M_i \dot{\underline{R}}_i^2$$

but as angular velocities and principal moments of inertia are not used the rotational kinetic energy is calculated from

$$RTKE = TKE - TRKE = \left[\sum_{i=1}^{N} \left[\sum_{j=1}^{n_i} \frac{1}{2} m_{ij} \dot{\underline{r}}_{ij} \right] \right] - TRKE \quad .$$

The corresponding temperatures can be calculated from the number of degrees of freedom, N_f, which for molecule i of this kind is given by

$$N_{f_i} = 3n_i - n_{c_i}$$

, n_i and n_{c_i} being the number of atoms and the number of constraints, respectively, in molecule i. In three dimensions

the number of translational degrees of freedom per molecule is always three so the remainder will be rotations.

2.11 Polyatomics : General Considerations

So far an outline has been given of how the equations of motion for polyatomic systems can be numerically integrated given the forces acting on the molecule and the constraints imposed upon it. The calculation of the kinetic energy has also been dealt with for each of the specific cases. Most of the other properties are calculated in the same manner as for monatomics but there are some points to bear in mind.

For the total intermolecular energy the equation for an N particle system of n_i atoms per molecule is

$$\Phi = \sum_{i=1}^{N} \sum_{j>i}^{N} \sum_{k=1}^{n_i} \sum_{l=1}^{n_j} \Phi(|\underline{r}_{i_k j_l}|) \qquad (2.11.1)$$

The contribution to which within the cutoff radius, r_c, can be calculated directly. The equation for the long range correction then becomes

$$PELRC = \frac{1}{2} \frac{n_a^2}{V} \int_{r_c}^{\infty} \Phi(r)\, 4\pi r^2\, dr \qquad (2.11.2)$$

where n_a is the total number of atoms in the system

$$n_a = \sum_{i=1}^{N} n_i$$

For this equation to be correct it is necessary for the cutoff radius to be greater than the largest possible distance between two atoms of the same molecule otherwise some fraction of the volume from $r=r_c \to \infty$ will be occupied by sites which do not contribute to the intermolecular energy. For consistency it is also necessary to ensure that half the box length is also greater than the largest possible distance between atoms of the same molecule as otherwise a molecule could interact with the image of itself.

For the pressure tensor the usual equation is

$$\underline{\underline{P}} = \frac{1}{V}\left[\sum_{i=1}^{N} M_i \dot{\underline{R}}_i \dot{\underline{R}}_i + \sum_{i=1}^{N}\sum_{j>i}^{N} \underline{R}_{ij}\underline{F}_{ij}\right]. \qquad (2.11.3)$$

For polyatomic systems where the intermolecular forces are non-central i.e. do not act along the COM separation vector, and the COM does not correspond to any of the interaction sites the evaluation of the potential contribution,

$$\underline{\underline{P}}^{\Phi} = \frac{1}{V}\sum_{i=1}^{N}\sum_{j>i}^{N} \underline{R}_{ij}\underline{F}_{ij}, \qquad (2.11.4)$$

can present a slight problem. It is always possible to evaluate $\underline{\underline{P}}^{\Phi}$ as it stands but this means evaluating at least one extra vector in the forces double loop at some point and storing all the forces on molecule i due to molecule j. It also means that the molecules must be looped over

systematically where it might be more efficient to loop over certain atoms. This problem can be avoided through recourse to the following rearrangement [116].

Firstly, if we define a tensor $\underline{\underline{P}}^{\Phi}_{aa}$ as

$$\underline{\underline{P}}^{\Phi}_{aa} = \frac{1}{V} \sum_{i=1}^{N} \sum_{j>i}^{N} \sum_{k=1}^{n_i} \sum_{l=1}^{n_j} \underline{r}_{i_k j_l} \underline{f}_{i_k j_l} \qquad (2.11.5)$$

where

$$\underline{r}_{i_k j_l} = \underline{r}_{i_k} - \underline{r}_{j_l}$$

and $\underline{f}_{i_k j_l}$ is the force on atom k of molecule i due to atom l of molecule j. Now writing the vector joining the COM of molecule i to atom k of molecule i as

$$\underline{r}_{ic_k} = \underline{r}_{i_k} - \underline{R}_i$$

$$\Rightarrow \underline{r}_{i_k} = \underline{r}_{ic_k} + \underline{R}_i$$

and then substituting for both $\underline{r}_{i_k}$ and $\underline{r}_{j_l}$ in eqn.2.11.5 gives

$$\underline{\underline{P}}^{\Phi}_{aa} = \frac{1}{V} \sum_{i=1}^{N} \sum_{j>i}^{N} \sum_{k=1}^{n_i} \sum_{l=1}^{n_j} \left[(\underline{r}_{ic_k} + \underline{R}_i) - (\underline{r}_{jc_l} + \underline{R}_j) \right] \underline{f}_{i_k j_l}$$

$$= \frac{1}{V} \sum_{i=1}^{N} \sum_{j>i}^{N} \sum_{k=1}^{n_i} \sum_{l=1}^{n_j} \left[\underline{R}_{ij} \underline{f}_{i_k j_l} + \underline{r}_{ic_k} \underline{f}_{i_k j_l} + \underline{r}_{jc_l} \underline{f}_{j_l i_k} \right]$$

since $\underline{f}_{i_k j_l} = - \underline{f}_{j_l i_k}$. It then follows from the fact that

$$\sum_{i=1}^{N} \sum_{j>i}^{N} \sum_{k=1}^{n_i} \sum_{l=1}^{n_j} \underline{R}_{ij} \underline{f}_{i_k j_l} = \sum_{i=1}^{N} \sum_{j>i}^{N} \underline{R}_{ij} \sum_{k=1}^{n_i} \sum_{l=1}^{n_j} \underline{f}_{i_k j_l}$$

$$= \sum_{i=1}^{N} \sum_{j>i}^{N} \underline{R}_{ij}\underline{F}_{ij}$$

and

$$\sum_{i=1}^{N} \sum_{j>i}^{N} \sum_{k=1}^{n_i} \sum_{l=1}^{n_j} \underline{r}_{ic_k}\underline{f}_{i_k j_l} + \underline{r}_{jc_l}\underline{f}_{j_l i_k} = \sum_{i=1}^{N} \sum_{k=1}^{n_i} \underline{r}_{ic_k}\underline{f}_{i_k}$$

that

$$\underline{\underline{P}}^{\Phi}_{aa} = \underline{\underline{P}}^{\Phi} + \frac{1}{V} \sum_{i=1}^{N} \sum_{k=1}^{n_i} \underline{r}_{ic_k}\underline{f}_{i_k}$$

or

$$\underline{\underline{P}}^{\Phi} = \underline{\underline{P}}^{\Phi}_{aa} - \frac{1}{V} \sum_{i=1}^{N} \sum_{k=1}^{n_i} \underline{r}_{ic_k}\underline{f}_{i_k} \qquad (2.11.6)$$

Thus the pressure tensor can be evaluated efficiently by summing up the atom-atom contributions in the usual way in the forces double loop and then all that is required is a simple loop over all molecules to calculate the additional term. For the normal pressure components there is, as before, a long range correction to be made which has to be adjusted in the same way as the potential energy long range correction for polyatomics.

2.12 Homogeneous Shear NEMD

The methods described so far give a basic outline of the procedures used to perform equilibrium molecular dynamics of monatomic and polyatomic fluids. As already discussed it is possible to obtain information of a rheological nature from either equilibrium MD (EMD) or non-equilibrium MD (NEMD). The limitations of and the difficulties encountered in determining the stress correlation function from EMD [48,49,5Ø] suggested that the more fruitful approach to the problem of elucidating the shear flow behaviour of molecules would probably be NEMD. Of the available NEMD methods for measuring rheological properties those described by Evans [55] and Singer et al [67] appeared to be worthy of particular attention. As already discussed both methods employ the Lees-Edwards (LE) [54] boundary conditions to simulate shear flow but whereas Evans' method [55] employs a large velocity gradient to produce a steady state stress response Singer et al [67] use a perturbation technique [68] to obtain the integral of the stress relaxation function. The actual algorithms employed here differ slightly from those given in the appropriate references [55,67] so it is necessary to describe the algorithms used in detail.

Figure 2.4 Lees-Edwards boundary conditions.

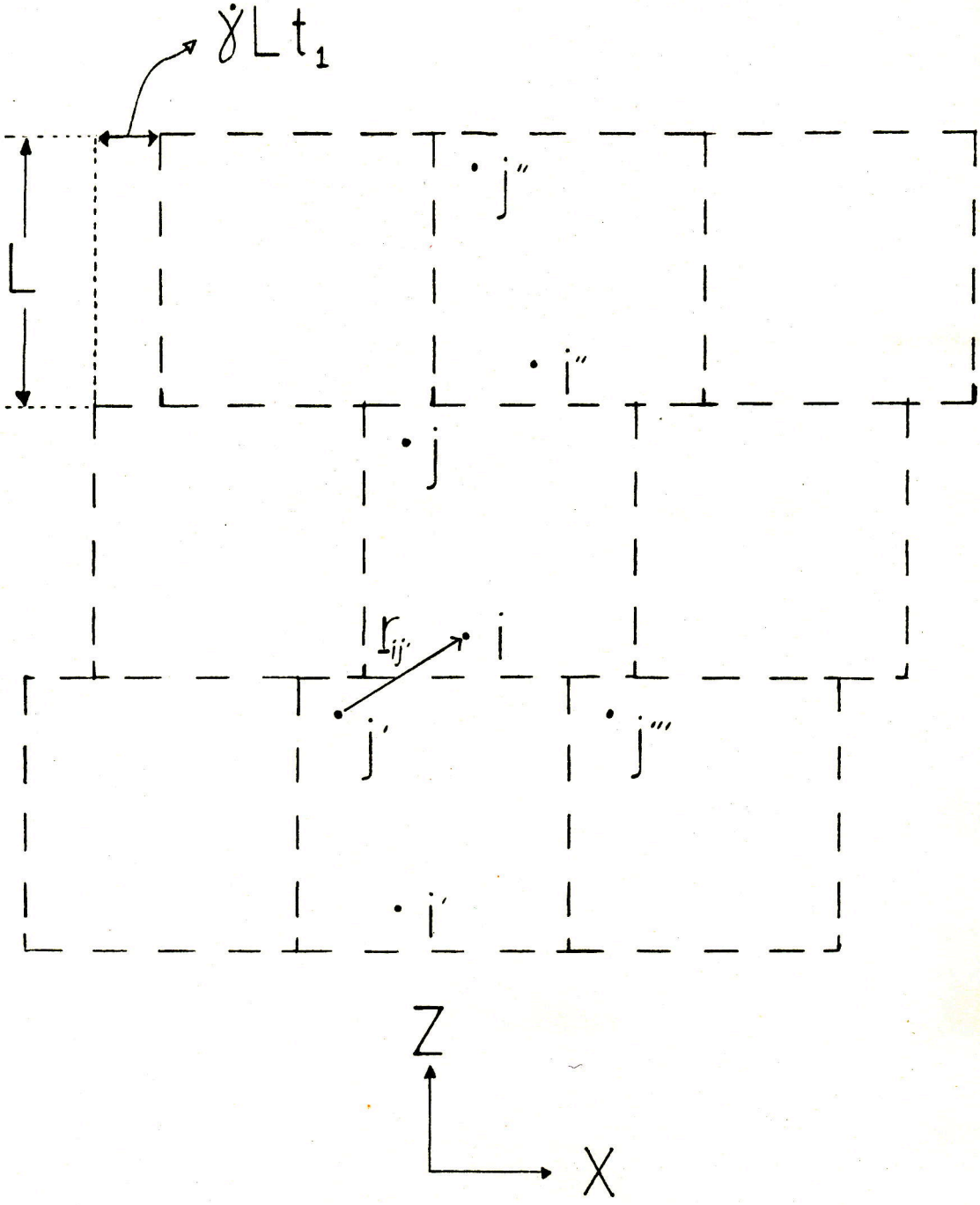

2.13 Lees-Edwards Boundary Conditions

For both the direct and perturbation methods LE boundary conditions were used throughout. These have already been described in general terms in chap.1 and the situation is illustrated in fig.2.4.

Initially the simulation begins as an equilibrium simulation with normal periodic boundaries. To be consistent with the imposition of a constant shear rate, $\dot{\gamma}$, the position of the periodic boundaries at some later time, t_1, must be displaced a distance $\dot{\gamma}Lt_1$, where L is the length of the cell. In a numerical simulation t_1 can be written as $n_1\Delta t$ where Δt is the time step. In a homogeneous shear NEMD simulation these moving periodic boundaries have to be used both in the forces double loop for calculating the nearest image and for determining where the image of a particle leaving the box enters. The transformations that were required to achieve the first of these in an equilibrium simulation have already been given. For the non-equilibrium case where the shear is applied in the XZ-plane they change to :-

$$\text{if } r_{z_{ij}} < -L/2 \;,\quad r_{x_{ij}} = r_{x_{ij}} + \dot{\gamma}Ln_1\Delta t$$

$$\text{if } r_{z_{ij}} > L/2 \;,\quad r_{x_{ij}} = r_{x_{ij}} - \dot{\gamma}Ln_1\Delta t$$

$$\text{if } r_{x_{ij}} < -L \;,\quad r_{x_{ij}} = r_{x_{ij}} + L$$

$$\text{if } r_{x_{ij}} > L \;,\quad r_{x_{ij}} = r_{x_{ij}} - L$$

$$\text{if } r_{\alpha_{ij}} < -L/2 \;,\quad r_{\alpha_{ij}} = r_{\alpha_{ij}} + L$$

$$\text{if } r_{\alpha_{ij}} > L/2 \;,\quad r_{\alpha_{ij}} = r_{\alpha_{ij}} - L$$

for α=x,y,z. As before these transformations can be carried out efficiently in FORTRAN using the INT function. To determine the position of incoming particles a similar procedure is adopted :-

$$\text{if } r_{z_i} < -L/2 \;,\quad r_{x_i} = r_{x_i} + \dot{\gamma} L n_1 \Delta t$$
$$\text{if } r_{z_i} > L/2 \;,\quad r_{x_i} = r_{x_i} - \dot{\gamma} L n_1 \Delta t$$
$$\text{if } r_{\alpha_i} < -L/2 \;,\quad r_{\alpha_i} = r_{\alpha_i} + L$$
$$\text{if } r_{\alpha_i} > L/2 \;,\quad r_{\alpha_i} = r_{\alpha_i} - L$$

for α=x,y,z.

These then are the essential features of LE boundary conditions which are common to all simulations which have used them [1,2,56]. Where simulations differ is in the actual details of how the fluid is sheared. In Lees and Edwards' original paper [54] the actual imposition of the boundary conditions alone was used to drive the system to steady state. Naitoh and Ono [56] and Heyes [1,2] changed the position of the COM of a particle an amount $\dot{\gamma} r_z \Delta t$ in the X-direction at each step whereas Evans [55] altered the velocities of particles so that a least squares fit to the velocity gradient returned the correct shear rate.

2.14 Shear Algorithm for the Perturbation Method

In each of the methods used here the basic procedure of shearing the fluid has followed a similar format. If we take the simplest example of a monatomic fluid where the positions $\{\underline{r}(t)\}$ and half step velocities $\{\underline{v}(t-\Delta t/2)\}$ are known initially and let GLT = $\dot{\gamma}Lt$ and GLTC = Ø then the procedure for the perturbation technique was as follows :-

1) Evaluate the total force on each molecule, $\underline{f}_i(t)$, in the usual way w.r.t. the LE boundary conditions.

2) Move the periodic boundaries

$$GLTC = GLTC + GLT$$

$$\text{and if } GLTC > L/2, \quad GLTC = GLTC - L$$

3) Integrate the equations of motion.

4) Add shear displacements in the X-direction using

$$r'_x(t+\Delta t) = r_x(t+\Delta t) + \dot{\gamma} r_z \Delta t .$$

5) Apply LE boundary conditions for particles leaving primary cell.

6) Return to 1)

Those thermodynamic functions which are normally calculated in equilibrium simulations, temperature, pressure, energy etc., can be evaluated in the usual way using this scheme. In applying the perturbation technique the approach employed was to obtain the stress tensor, $\underline{\underline{\sigma}} = -\underline{\underline{P}}$, as a function of time at one shear rate , $\dot{\gamma}_1$, using the algorithm

as described, and then, starting from the same initial configuration, obtaining $\underline{\underline{\sigma}}(t)$ at a slightly different shear rate $\dot{\gamma}_1+\Delta\dot{\gamma}$. In general $\dot{\gamma}_1$ was set equal to zero and $\Delta\dot{\gamma}\sim 10^2 s^{-1}$ which is a very low shear rate for these simple fluids. The symmetrized XZ component of the stress difference between two runs, $\Delta\underline{\underline{\sigma}}(t)$, has been shown in theory [68] to be proportional to the integral over the stress auto-correlation function and hence the viscosity through the equation

$$\eta = \frac{\Delta\sigma_{xz}(\infty)}{\Delta\dot{\gamma}}.$$

The extension of this method to polyatomic systems is straightforward as all that is required is to substitute for the coordinates of the COM of the molecule at step 4). This in effect means that the shear displacement of all the atoms of a molecule is that of their COM.

2.15 Shear Algorithm for the Direct Method

In the direct method the idea is to produce a measurable steady state stress response which differs significantly from the inherent stress fluctuations. To do this it is neccessary to use large velocity gradients which have the unfortunate effect of causing the temperature of the system to rise. It has been shown that it is possible [1,2,56] to apply a large gradient using the algorithm as described for the perturbation method but this algorithm ignores the fact that there are spontaneous fluctuations of the measured shear rate of a

system even at equilibrium. In a steady state NEMD experiment using this method the hope is that these random fluctuations will average to zero leaving just the applied shear rate as being responsible for the measured mean stress. For the perturbation technique this is less of a problem as the random fluctuations will be well correlated between the two runs and thus cancel out so that the measured response is due to $\Delta\dot{\gamma}$ only.

An alternative method due to Evans [55] maintains a strict control of the measured shear rate . The steps involved are, taking again the simplest case of a monatomic fluid, :-

1), 2) and 3) as before

4) Apply the LE boundary conditions to particles leaving the primary cell with the additional conditions that:-

$$\text{if } r_{z_i} > L/2 \ , \quad v'_{x_i} = v_{x_i} - \dot{\gamma}L$$

$$\text{if } r_{z_i} < -L/2 \ , \quad v'_{x_i} = v_{x_i} + \dot{\gamma}L$$

5) Reset the velocities by using the following procedure :-

i) Calculate a least squares fit to the velocity gradient, $\dot{\gamma}'$, from

$$\dot{\gamma}' = \frac{\sum_{i=1}^{N} v_{x_i} r_{z_i}}{\sum_{i=1}^{N} r_{z_i}^2}$$

ii) Calculate the mean linear momentum in the X-direction, $\bar{p}_x$,

$$\bar{p}_x = \frac{1}{N}\sum_{i=1}^{N} m_i v_{x_i}$$

iii) Reset the velocities of the particles such that repeating i) and ii) would return $\dot{\gamma}' = \dot{\gamma}$ and $\bar{p}_x = 0$ by

$$v'_{x_i} = v_{x_i} - \bar{p}_x/m_i + (\dot{\gamma} - \dot{\gamma}')r_{z_i}$$

6) Calculate the temperature of the system, T_{cal}.

7) Rescale the temperature to the required value, T_{req}, by altering the velocities in the following manner

$$v'_{x_i} = (v_{x_i} - \dot{\gamma}r_{z_i})*b + \dot{\gamma}r_{z_i}$$
$$v'_{\alpha_i} = v_{\alpha_i}*b \quad , \quad \alpha=y,z$$

where $b = (T_{req}/T_{cal})^{1/2}$

8) Return to 1)

It is apparent from steps 4) and 7) that the shear velocity of a particle is assumed to be consistent with its position. Thus in step 4) if a particle has an x-direction velocity of v_{x_i} then it is assumed that its x-direction thermal velocity, $v^{th}_{x_i}$, is defined by

$$v^{th}_{x_i} = v_{x_i} - \dot{\gamma}r_{z_i} \quad . \qquad (2.15.1)$$

Now if this particle crosses the +z face then

$$v'_{x_i} = v^{th}_{x_i} + \dot{\gamma}(r_{z_i} - L) = v_{x_i} - \dot{\gamma}L \quad .$$

In steps 6) and 7) eqn.2.15.1 is also required to find $v^{th}_{x_i}$ so that the temperature can be calculated and rescaled. It should also be noted that $v^{th}_{x_i}$ must also be used in the calculation of the stress/pressure tensor.

The extension of this method to polyatomic systems is reasonably straightforward. For integration algorithms which define the positions and velocities of the atoms relative to the COM, e.g. quaternions, there is in general no problem and the positions and velocities used throughout the scheme become those of the COM. If a molecule does happen to straddle a Z face such that some atoms have +ve Z coordinates and others have -ve Z coordinates then there are no inconsistencies since one set of atoms will have their velocities specified relative to the actual COM while the others will be relative to an image COM outside the primary cell. Where difficulties do arise is when the actual positions and velocities of the atoms define the motion of the COM. For example in the constraints algorithm for flexible molecules the motion of the COM is determined by that of the constituent atoms rather than by its own equation of motion. Although the paths obtained from either approach should be equivalent numerical errors arising from the constraints being satisfied to a certain tolerance can allow them to diverge slightly. As step 5) attempts to zero the momentum of the system the question arises as to whether to zero the momentum as defined by the COM or as defined by the velocities of the atoms. It is possible for the sum of COM momenta to be different from the sum of the atomic momenta because if a molecule straddles a Z face then the shear velocity of some of the atoms will not be the same as the rest if the molecule is forced to be 'dissociated' by the periodic boundaries. To maintain consistency throughout

these calculations step 5) has been applied to the COM at all cases where at all times the COM remains within the primary cell. For the constraints method the simplest way to do this is to retain two sets of atomic coordinates. The primary set are for the 'undissociated' molecule and at all times the COM is given by

$$\underline{R}_i = \sum_{j=1}^{n_i} m_{ij}\underline{r}_{ij} / M_i \quad .$$

where $\underline{R}_i$ must lie within the MD cell. The second set $\{\underline{r}'\}$ result from applying the LE periodic boundary conditions to the first set $\{\underline{r}\}$ thus $\{\underline{r}'\}$ must always be confined to be within the boundaries of the primary cell whereas some of the $\{\underline{r}\}$ may not. If a molecule lies across a boundary then

$$\underline{R}_i \neq \sum_{j=1}^{n_i} m_{ij}\underline{r}'_{ij}/M_i \quad .$$

When the COM crosses a boundary then the coordinates , and the velocities if it is a Z-face , of all the atoms of the molecule and the COM are reset in the way described. The second set of coordinates is required in the forces double loop where it is essential that all the coordinates lie within the MD cell for the LE periodic boundary conditions to work as described.

CHAPTER 3

DIATOMIC RESULTS

3.1 Introduction

The objective of this work was to use the technique of molecular dynamics to obtain information concerning the effect of molecular characteristics upon the rheological properties of model liquids. It had to be recognized , however, that from the very nature of the method that there are more possible approaches to the problem than could be physically realised. For instance in principle it would be possible to vary all the molecular parameters, e.g. mass, bond lengths, interaction potentials etc., at will giving an immense range of model fluids that could be studied. With such a plethora of choices a strategy had to be developed which would produce some relevant results. One approach would be to evaluate and compare the rheological properties of tried and tested models of liquids but this would be of little use as the number of variables that have to be changed would render any comparisons worthless in terms of extracting information on the effect of the molecular characteristics. It is exactly this situation that the experimentalists find themselves in and by using MD was hoped could be avoided. A second approach would be to use purely hypothetical molecules, hard cubes or triangles perhaps, which although they are more likely to lend themselves to an exact theoretical treatment bear little resemblance to any real molecule. The fact that a model

molecule does not resemble any real one is not particularly important in this case as we are looking at the way changes in the molecule effect its flow properties. It could well be that to gain some understanding of the phenomena of shear thinning, say, we first of all have to find a system which does not shear thin and then to find out what changes have to be made to allow shear thinning to occur. As it has already been shown that LJ argon [1] and even hard spheres [56] shear thin we are at once looking for simpler systems. However, on the other hand it may be better to keep some degree of reality and look at the differences in the rheological properties of two or more very similar molecules. In general it has been this final approach which has been used in the hope of maintaining a modicum of contact with the real world but without the restrictions thereof.

As there already had been several studies of monatomic fluids under shear [1,2,49,53,56,57,58,59] it was originally intended to extend these kind of studies to more complex molecules consequently it was decided for several reasons to start by looking at the next simplest molecule, the two centre model of a diatomic. Firstly, there already existed interaction potentials which had been used to model adequately the equilibrium properties of such molecules as N_2 [108], F_2, Cl_2 and Br_2 [39] and thus the data existed with which the performance of a diatomic MD program could be compared. Secondly, Evans [60] had already applied a steady state shear

method to chlorine at a low density in order to evaluate its shear viscosity. This would allow a comparison between the direct and perturbation methods of viscosity determination as outlined in the previous chapter and that of an external source. Thirdly, the diatomic model can easily be altered to give a different molecule most simply by changing the bond length to either increase or decrease the anisotropy.

3.2 Chlorine Model and Computational Details

A program was developed to model the single component homonuclear diatomic fluid chlorine. The model for the interaction potential has previously been used by Singer et al [39] and is shown in diagrammatical form in fig.3.1. As can be seen the model consists of two sites a distance l (the bond length) apart which interact with sites of other molecules through the LJ 12-6 potential

$$\Phi(r) = 4\epsilon\left[\left[\frac{\sigma}{r}\right]^{12} - \left[\frac{\sigma}{r}\right]^{6}\right]$$

where ϵ/k=173.5K and σ=3.353Å. Initially the reduced bond length, l^*, was set equal to Ø.6Ø841 and the mass of a molecule was in all cases $1.178*10^{-25}$kg. The use of these parameters has been shown [39] to give a good fit to the experimental equation of state of chlorine along the zero pressure isobar. The equations of motion were integrated using the constraints algorithm as described for linear

Figure 3.1 Model diatomic.

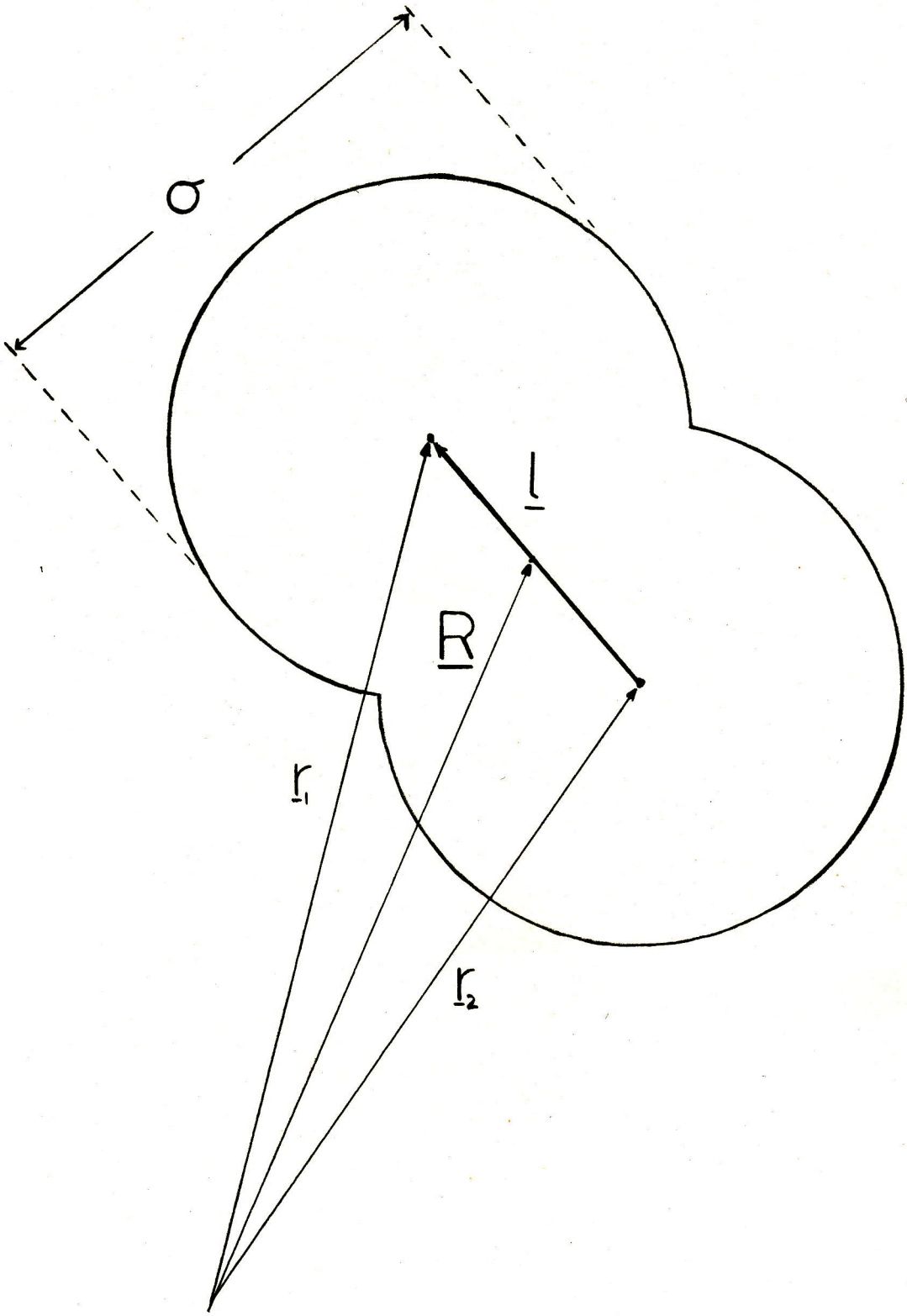

molecules, sec.2.6, with a time step of, unless stated otherwise, $0.8 * 10^{-14}$ s . The potential was truncated at a distance of 2.5σ and the appropriate long range corrections to the energy and the virial were made.

3.3 Chlorine Results at T~260K, P~0, l^*=0.608 and l^*=1.0

The program was tested by monitoring the total linear momentum and the total energy. No perceptible drift was found in either quantity and the energy was conserved to within ±0.05%. A point was then chosen close to the MD calculated [39] zero pressure isobar at T^* (= Tk/ϵ) ~ 1.5 and $\rho^*(=N\sigma^3/V)$ = 0.48243 and equilibrium simulations were performed. Parametrised equations already exist [39] for calculating the total energy, U, the pressure , P, and the diffusion coefficient, D, for this system as a function of temperature and density. The results of two simulations for N=256 and N=2048 molecules, the latter using a link cell version of the program (see Appendix 1.), are shown in table 3.1 together with the predictions of the parametrised equations [39] in parentheses.

Table 3.1 A comparison of the total energy, pressure and diffusion coefficient as determined by EMD simulations on model chlorine with the parametrised equations of Singer et al [39] at a reduced number density of Ø.48243.

T/K	U/J mol^{-1}	P/bar	D/10^5 cm^2 s^{-1}	Length of run /ps	N
261.1	~-12ØØØ	16±63	4.7±Ø.3	24.Ø	256
	(-12Ø5Ø±7Ø)	(29±64)	(4.3±Ø.4)		
261.4	-12Ø46±25	4Ø±2Ø	4.7±Ø.2	1Ø.8	2Ø48
	(-12Ø4Ø±7Ø)	(34±64)	(4.3±Ø.4)		

The comparisons in table 3.1 are quite favourable and establish the reliability of the basic program. It was then adapted for determining rheological properties by NEMD using the two techniques discussed in sec.2.12. Previously Evans [6Ø] had determined the shear dependent viscosity of a slightly different chlorine model [39] (σ=3.332Å, l^*=Ø.63, ϵ/k=178.3K) at a similar state point (P~Ø, ρ^*=Ø.461, T^*=1.532) using his homogeneous shear method. The differences between the model and the state point used here and that of Evans were considered to be small enough to allow at least a qualitative comparison between the methods used.

Starting from equilibrated configurations of chlorine at

the state point (ρ^*=Ø.48243, T^* ~1.5) the perturbation and direct methods were applied to systems of 256 molecules. The procedure for the perturbation method was to obtain the stress as a function of time for an equilibrium run of 15Ø time steps (≡1.2ps) and then for the same amount of time having applied a step function in shear rate, $\Delta\dot{\gamma}$, to the same initial configuration. The response $\Delta\underline{\underline{\sigma}}(t)$ was then averaged over twenty of these 'segments'. At the same time the difference in the alignment tensor $\Delta\underline{\underline{D}}(t)$, where $\underline{\underline{D}}$ is given by

$$\underline{\underline{D}} = \frac{1}{N}\sum_{i=1}^{N} \hat{\underline{i}}_i \hat{\underline{i}}_i \quad ,$$

was obtained also to monitor the response of the collective orientation to the shear flow. With an actual mechanical perturbation it was found that for a $\Delta\dot{\gamma}$ of less than ~$10s^{-1}$ the stress response became subject to truncation errors because of the small differences between the stress in each run as compared to the magnitude. In this case a value of $\Delta\dot{\gamma}=125s^{-1}$ was used throughout to avoid this problem.

For the direct method a step function in shear rate was applied to an equilibrium configuration in the manner described in sec.2.15 and sufficient time was allowed for the system to achieve steady state (~1ØØØΔt). The properties of interest were then averaged over an amount of time ajudged to give reasonable statistical precision. For the stress the problem is one of producing in the system a response

significantly different from the inherent uncertainty, $\sim 10^{7}$ Pa. This immediately imposes a restriction on the lower limit of the shear rates that can be used as the viscosities of these materials is generally $\sim 10^{-3}$ Pa s so typically the lower limit on the shear rate is, from $\eta=\sigma/\dot{\gamma}$, $\sim 10^{10}\,s^{-1}$. For these calculations two shear rates were employed $\dot{\gamma}=5*10^{10}\,s^{-1}$ and $\dot{\gamma}=10^{12}\,s^{-1}$ which are in the same range as those used by Evans [60]. As in the case of the perturbation method the alignment tensor can be calculated but this time the property of interest is its mean value, $\langle \underline{\underline{D}} \rangle$. Unlike the stress tensor $\underline{\underline{D}}$ is always symmetric and at equilibrium the average values of the elements of the alignment tensor are $\langle D_{\alpha\beta} \rangle = 0$ and $\langle D_{\alpha\alpha} \rangle = 1/3$, for $\alpha,\beta = x,y,z$, showing no preffered alignment of the molecules. Under shear it is likely that the off-diagonal component that couples most to the flow will be that in the same plane as the flow i.e. D_{xz}. The effect on the on-diagonal elements is less predictable but at all times $D_{xx}+D_{yy}+D_{zz}=1$.

The significant components of $\underline{\underline{\sigma}}$ and $\underline{\underline{D}}$ from the results of these steady state calculations are given in table 3.2. The shear rate dependent viscosities, $\eta(\dot{\gamma}) = \langle \sigma_{xz} \rangle / \langle \dot{\gamma} \rangle$, and orientation coefficients, $\chi_d(\dot{\gamma}) = \langle D_{xz} \rangle / \langle \dot{\gamma} \rangle$, obtained from the simulations are given in table 3.3.

Table 3.2 The mean significant components of the stress and alignment tensors obtained from the steady state calculations on chlorine at ~260K.

$\dot{\gamma}/10^{10}s^{-1}$	$\langle\sigma_{xz}\rangle$ /bar	$\langle\sigma_{xx}\rangle$ /bar	$\langle\sigma_{yy}\rangle$ /bar	$\langle\sigma_{zz}\rangle$ /bar	Length of run/ps
4.992	112±22	1±61	-45±61	-8±49	44.0
99.96	2126±49	-889±75	-636±80	-1219±80	40.0

$\dot{\gamma}/10^{10}s^{-1}$	$\langle D_{xz}\rangle$	$\langle D_{xx}\rangle-1/3$	$\langle D_{yy}\rangle-1/3$	$\langle D_{zz}\rangle-1/3$
4.992	0.014±0.007	0.003±0.009	-0.004±0.008	0.001±0.010
99.96	0.133±0.004	0.102±0.004	-0.040±0.008	-0.062±0.008

Table 3.3 The resultant shear viscosities and orientation coefficients obtained from the steady state calculations on chlorine at ~260K.

$\dot{\gamma}/10^{10}s^{-1}$	$\eta(\dot{\gamma})$/mPa s	$\chi_d(\dot{\gamma})/10^{-12}s$
4.992	0.225±0.045	0.280±0.150
99.96	0.213±0.005	0.133±0.004

The results obtained by Evans [60] for the viscosity of a slightly different chlorine system are plotted, along with the results given in table 3.3, in fig.3.2 as a function of the square root of the shear rate. As can be seen their is good agreement between the two sets of data when one takes into account the errors and the different model parameters used. Evans [60] estimates the zero shear viscosity to be 0.2423mPa s whereas a reasonable estimate of $\eta(0)$ from the two

Figure 3.2 $\eta(\dot{\gamma})$ vs. $\dot{\gamma}^{\frac{1}{2}}$ Chlorine, l^*=0.608, T~260K, P~0, (- - - □ - - -).
Evan's results (—— Δ ——).

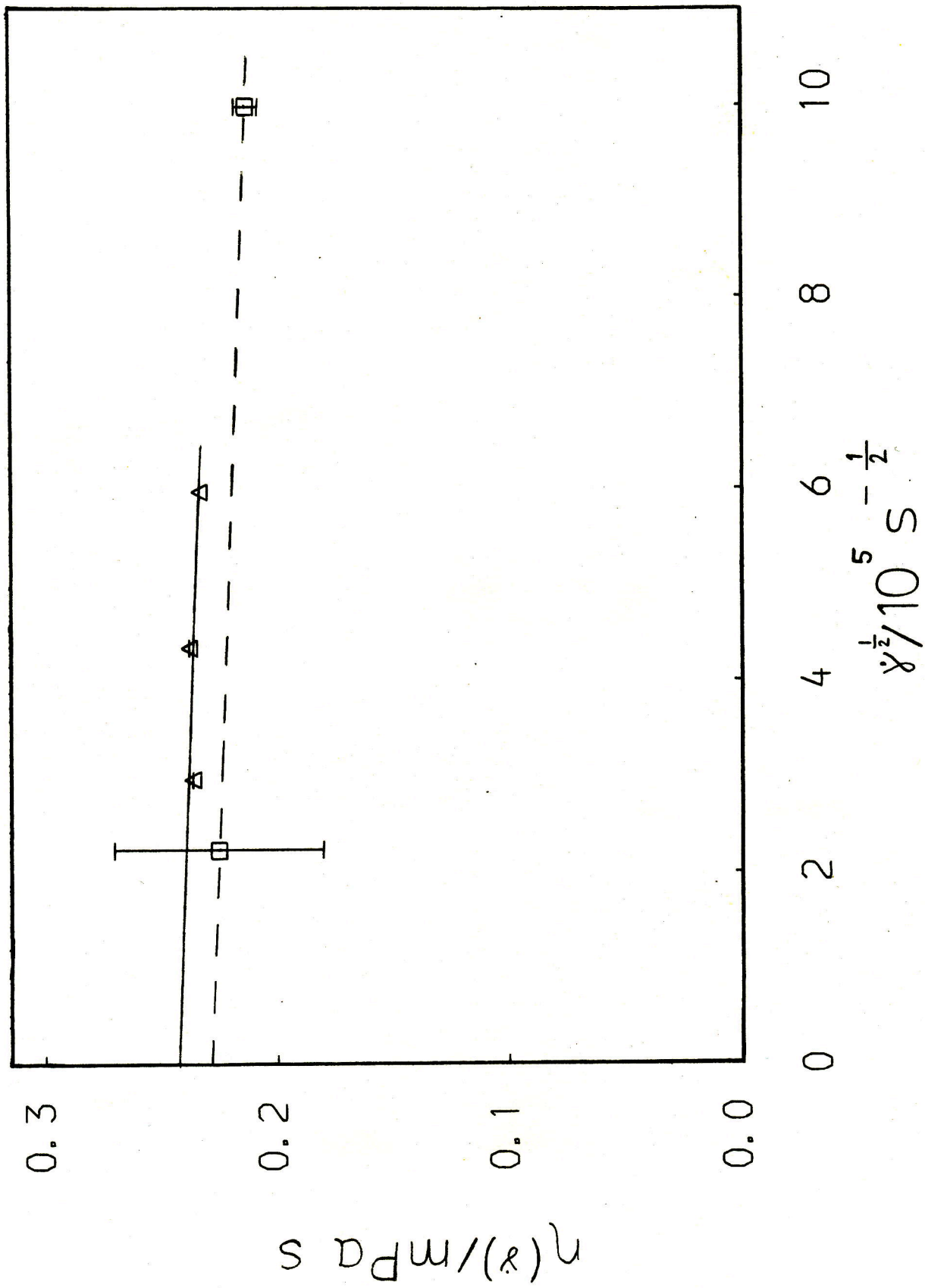

points calculated here is Ø.23±Ø.Ø2mPa s. Both curves show little shear thinning behaviour, as would be expected at this high temperature, low density point, so the extrapolations involved in estimating $\eta(Ø)$ are quite valid and probably not in error by more than 1Ø%.

The point of using two methods of NEMD was to evaluate their comparative usefulness. To do this for the alignment and the viscosity the responses $\Delta\sigma_{\alpha\beta}(t)$ and $\Delta D_{\alpha\beta}(t)$ are plotted in fig.3.3. From the steady state calculations the expected plateau value for the stress is $\eta\Delta\dot{\gamma}=(Ø.23\pm Ø.Ø2)*10^{-3}*125 = Ø.Ø288\pm Ø.ØØ25$Pa and this is marked on fig.3.3 as a dotted line. The best statistical fit of this response to a single exponential of the form

$$\frac{\Delta\sigma_{xz}(t)}{\Delta\dot{\gamma}} = \eta(1 - \exp(-t/\tau))$$

gives the values η = Ø.224mPa s and τ = Ø.12ps. One further piece of information that can be estimated from the response is the infinite frequency shear modulus, G_∞. As $\Delta\sigma_{xz}(t)$ is related to the integral over the stress auto-correlation function through

$$\Delta\sigma_{xz}(t) = \Delta\dot{\gamma}\,\frac{V}{kT}\int_0^t C_s(t')\,dt'$$

and $C_s(t)$ can be written as

$$C_s(t) = \frac{kT}{V}\,G_\infty\,\hat{C}_s(t)$$

Figure 3.3 $\Delta\sigma_{\alpha\beta}(t)$ and $\Delta D_{\alpha\beta}(t)$ vs. t, chlorine, l^*=0.608, T~260K, P~0.

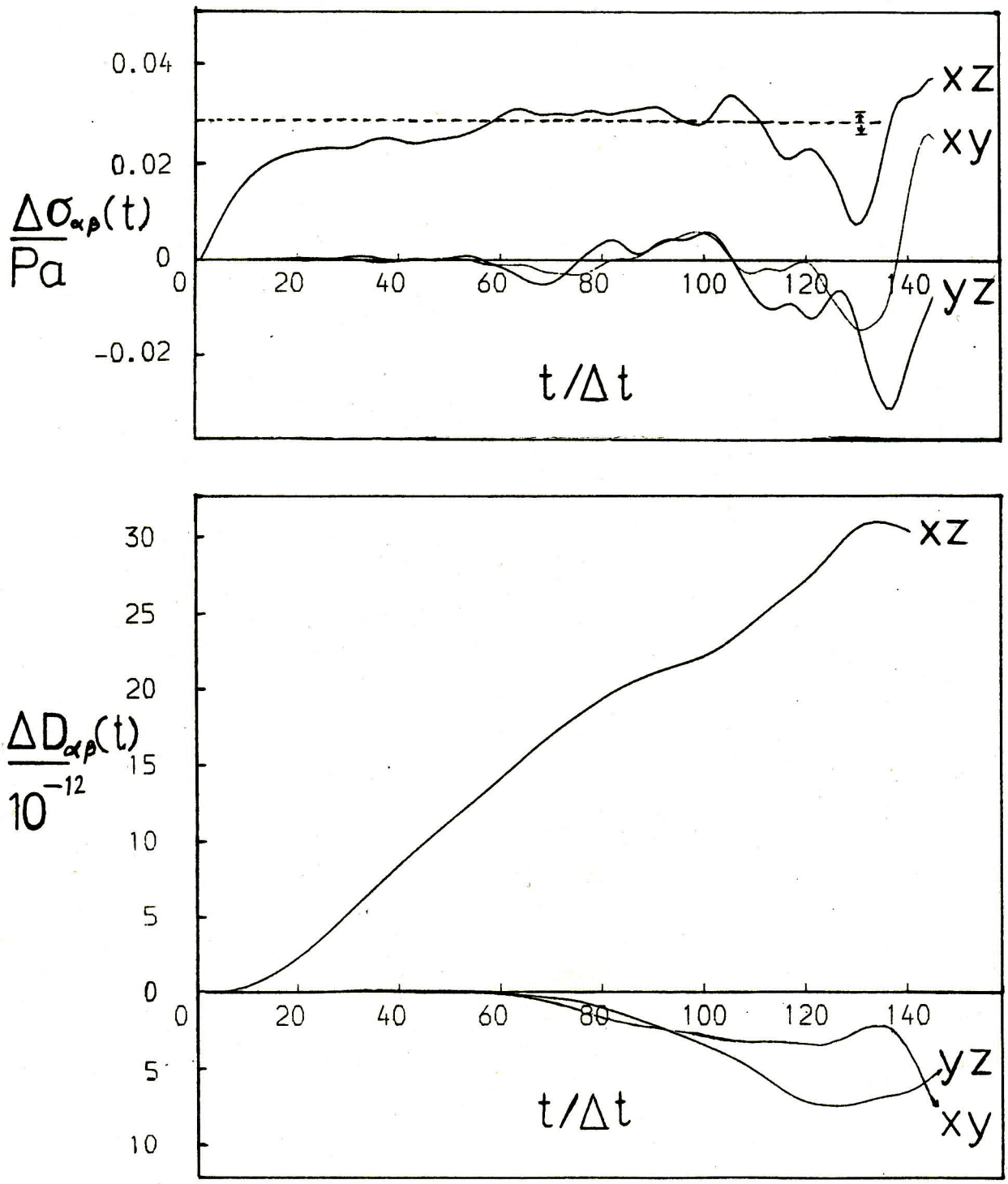

then substituting for $C_s(t)$ and differentiating w.r.t. time gives

$$\frac{d\Delta\sigma_{xz}(t)}{dt} = \Delta\dot{\gamma}\, G_\infty\, \hat{C}_s(t) \quad .$$

Now as $\hat{C}_s(0)=1$ G_∞ can be simply estimated from the initial slope of the stress response. In this case a value of G_∞ of 1.9GPa was obtained which is the same order as that found for many liquids experimentally [23].

The information gleaned from the perturbation technique is also theoretically obtainable from equilibrium MD by way of evaluating the stress correlation function. From the chlorine equilibrium simulation at this state point for N=2048 the stress was stored and correlated. As the length of the simulation was only 10.8ps (1350Δt) the amount of averaging was small but as there are six possible off-diagonal components of the stress tensor $(\sigma_{xz}+\sigma_{zx})/2$, $(\sigma_{xy}+\sigma_{yx})/2$, $(\sigma_{yz}+\sigma_{zy})/2$, $(\sigma_{xx}-\sigma_{yy})/2$, $(\sigma_{xx}-\sigma_{zz})/2$ and $(\sigma_{yy}-\sigma_{zz})/2$, the last three obtained by rotation of the stress tensor by 45° about the x,y and z axes [77], and as each time step is a possible time origin compared to the perturbation technique there is much more averaging possible. The resulting normalised correlation function $\hat{C}_s(t)$ is shown in fig.3.4. The shear modulus obtained from the mean squared stress,

$$G_\infty = V\langle\sigma^2_{\alpha\beta}(0)\rangle/kT \quad ,$$

was 2.4GPa and although the integral over the correlation

Figure 3.4 The normalized stress correlation function $\hat{C}_s(t)$ vs. t, l^*=0.608, T~260K, P~0, N=2048.

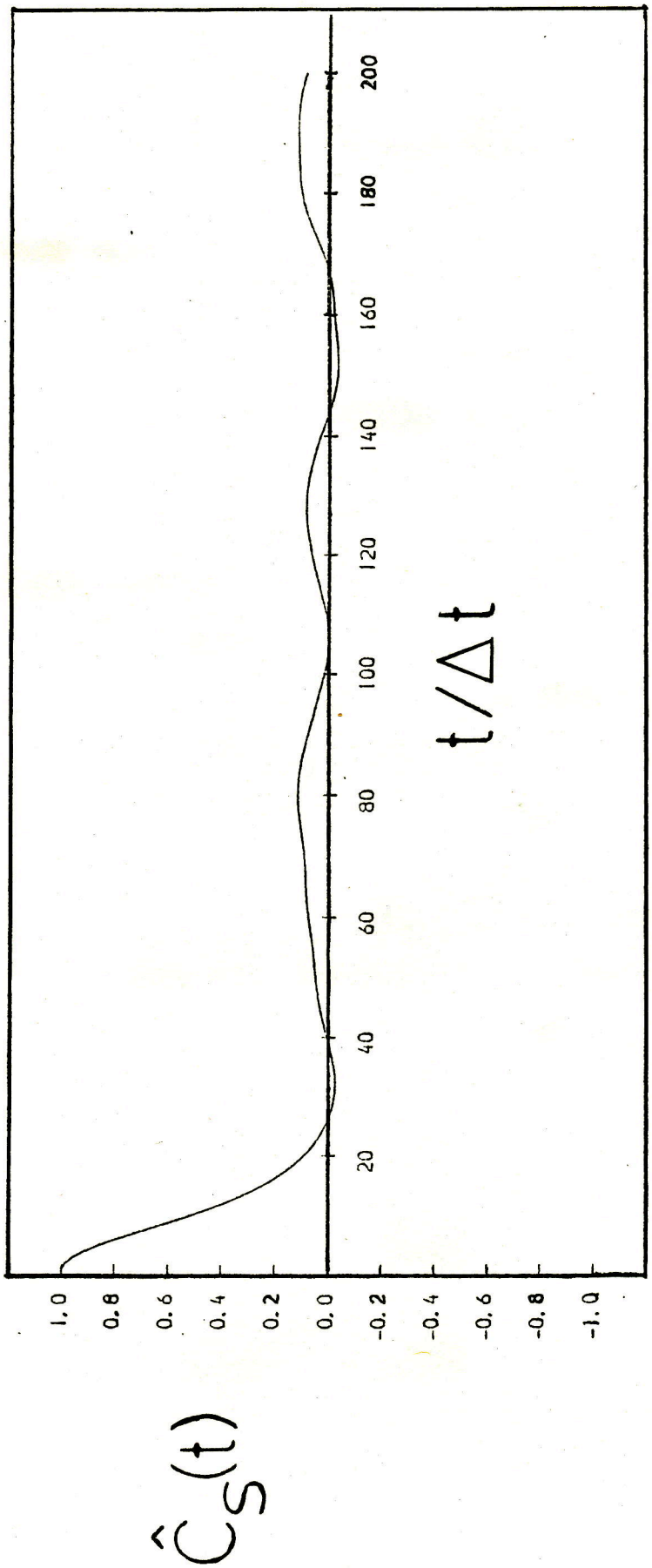

function is subject to large errors estimates of the viscosity in the region 60→100Δt, which is the plateau region from the perturbation result, give values of around 0.23→0.24mPa s in good agreement with the NEMD methods.

For $\Delta D_{xz}(t)$, fig.3.3, it is difficult to tell whether the response has reached a plateau value or not as the noise begins to swamp the signal at around 100Δt. However, if we assume a relation of the form $\langle D_{xz} \rangle = \chi_d(\dot{\gamma})\langle \dot{\gamma} \rangle$, which is analogous to the Newtonian stress/viscosity relation, then using the same extrapolation procedure for $\eta(\dot{\gamma})$ an approximate value of $\chi_d(0)=0.3*10^{-12}$s was obtained. This then gives a $\Delta D_{xz}(\infty)$ of $125*0.3*10^{-12}=0.38*10^{-10}$ which, considering the approximations involved, suggests that $\Delta D_{xz}(t)$ is approaching close to its infinite time value.

The results obtained from these initial studies have a number of possible implications. Firstly, both the NEMD methods used here and that employed by Evans [60] give results which are in good agreement. This is an important result as it implies that the viscosity measured is that of the actual system and is, therefore, method independent. Secondly, it appears that for a similar expenditure of computer time the steady state method is a more efficient and more precise way of calculating $\eta(0)$. This is a tentative conclusion as it is based only on the results at one state point. At higher densities the degree of shear thinning will no doubt increase

making extrapolations to $\dot{\gamma}=0$ difficult but as has already been seen there are the problems in the perturbation technique of deciding whether the stress has reached its plateau value and determining what it is. This is further borne out by the response for the alignment which even for this low density point shows little signs of reaching a steady state value before the noise becomes too great. The effect of increasing the density can only compound these problems.

Thirdly, comparisons between the perturbation technique and the Green-Kubo method suggest that, although in this case there is a large difference in system size, both can produce at least the short time behaviour of the stress relaxation function with possibly the correlation function approach being more efficient because of the greater averaging possible. For the viscosity it turns out that both give similar values at about the same time but without the steady state results it would be difficult with either to put any degree of certainty on the viscosities obtained. Where the two methods do apparently disagree is in the value for G_∞ ,1.9GPa from the perturbation response and 2.4GPa from the mean squared stress, without determining the actual error bars on these results it is in fact difficult say whether they do disagree at all. However, it is likely that the value obtained from the mean squared stress is the more accurate as it is an equilibrium property and probably in error by at most 10% from the spread of results obtained from the various off-diagonal components.

A possible explanation of the disparity is that the G_∞ determined from the perturbation response is calculated from the difference in stress one time step after the perturbation has been applied and is thus only an approximation to the initial slope

$$\frac{d\Delta\sigma_{xz}(t)}{dt} \simeq \frac{\Delta\sigma_{xz}(\Delta t)}{\Delta t}$$

which will if anything underestimate the limiting slope. A test of this would be to perform perturbation calculations with progressively shorter time steps but as G_∞ is only of minor interest it was not thought worthwhile to do this.

From these conclusions it was apparent that one of the next steps would be to test these methods under less favourable conditions at more interesting points i.e. where the equilibrium viscosity is much higher and where shear thinning is more pronounced. This would establish, for instance, whether the perturbation method was of any general use in these systems.

In a systematic attempt to evaluate the effect of changing the molecular characteristics on the rheological properties, a second model liquid was generated by extending the bond length from l^*=Ø.6Ø841 to l^*=1.Ø whilst retaining ϵ and σ constant with the intention of comparing results with those obtained for model chlorine. This immediately poses a

problem as the actual extension of the bond length causes a drastic change in the equilibrium properties. As we are trying to isolate the effect of increasing the bond length alone on the rheological properties the problem is to separate this from the changes induced by the different equilibrium conditions. Ideally experiments would be performed at equivalent states. For example certain monatomics modelled with a L-J 12-6 potential with differing equilibrium properties in real terms can be brought to corresponding states by use of reduced variables [1ØØ]. However, for diatomics the introduction of the extra variable, l, makes this far more complicated even for models of the same σ and ϵ. In the absence of any obvious corresponding states prescription it was decided to perform the calculations at states of approximately equal temperature and pressure. The only justification for this being that this would be the case in experiments on actual fluids.

To find the density which corresponds to P~Ø for the l^*=1.Ø model a number of short simulations (5ØØΔt) were performed on a system of N=256 molecules at varying densities at 26ØK. By a process of extrapolation and interpolation a figure of ρ^*=Ø.32157 was arrived at as being close enough to the zero pressure isobar to allow the desired comparisons. In the same way as for the l^*=Ø.6Ø8 Cl_2 a series of perturbation experiments were then performed starting from an equilibrated configuration. Averages were this time taken over ten

segments of 150Δt and the mean equilibrium properties from the unperturbed system are compared with those obtained from the equivalent runs for the shorter bond length model.

Table 3.4 A comparison of the equilibrium properties obtained for l^*=1.0 and l^*=0.608 Cl_2 from 10 and 20 runs of 1.2ps respectively. U=total energy, Φ=total potential energy, T_t=translational temperature and T_r=rotational temperature.

l^*	U /Jmol	Φ /Jmol	T /K	T_t /K	T_r /K	P /bar
1.0	-5830±80	-11240±40	259.9±2.9	258.8±2.2	261.6±5.6	61±51
0.608	~-12000	~-17500	261.1±1.0	261.6±2.3	260.4±2.4	16±63

The combined effect of increasing the bond length and reducing ρ^* from 0.48243 to 0.32157 to produce systems at about the same temperature and pressure can be seen to decrease by more than a third the potential energy of the fluid. The reason for this is quite simply the decrease in the density of interaction sites.

The off-diagonal stress and alignment responses obtained from these perturbation experiments on the l^*=1.0 system are shown in fig.3.5. From the initial slope of the stress response and the best fit of a single exponential of the same form as used for the l^*=0.608 case the following values were obtained G_∞=1.2GPa, η=0.092mPa s and τ=0.077ps. A single steady state shear simulation at $\dot{\gamma}$=12.5*10^{10} s^{-1} of length 40ps

Figure 3.5 $\Delta\sigma_{\alpha\beta}(t)$ and $\Delta D_{\alpha\beta}(t)$ vs. t, chlorine, $l^*=1.0$, T~260K, P~0.

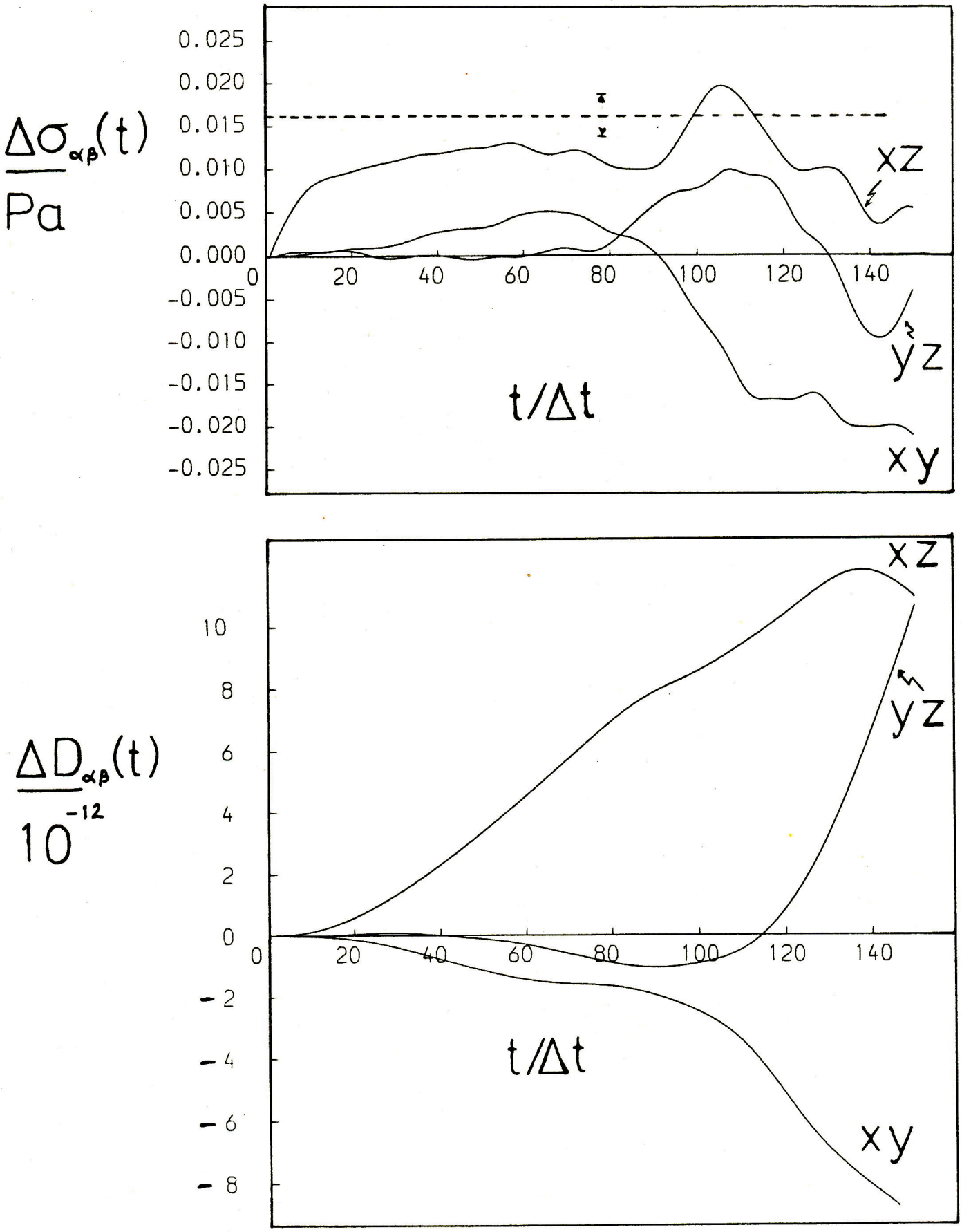

(=5000Δt) produced the values of $\eta(\dot{\gamma})$=0.131+0.02mPa s and $\chi_d(\dot{\gamma})$=(0.21+0.07)*10^{-12}s. Using the steady state viscosity to predict the long time value of the stress response gave $\Delta\sigma_{xz}(\infty)$=0.0164+0.0025Pa which is shown as the dotted line on fig.3.5. For the alignment the steady state figure for $\chi_d(\dot{\gamma})$ predicts a $\Delta D_{xz}(\infty)$=2.6+0.8. As the values of η and χ_d used to predict the limiting stress and alignment responses are likely to be, if anything, underestimations of the actual zero shear quantities it appears that neither has quite attained its long time limit.

Comparisons between the two systems reveal that the viscosity , shear modulus, and best fit relaxation time are all ~40% less in the l^*=1.0 case. This is very similar to the difference in the potential energies. There is also a clear tendency for the l^*=0.608 system to realign to a greater degree and at a faster rate than the l^*=1.0 system. This too is probably a result of the density being lower in the l^*=1.0 case allowing the molecules more opportunity to randomise their orientations and thus reducing the degree of alignment. Some justification of this hypothesis can be given by comparing the relative free volume of the molecules. Assuming that the effective 'volume', V_e, of a molecule is given by that of a spherocylinder

$$V_e = \frac{4\pi}{3}\left[\frac{\sigma}{2}\right]^3 + l^*\sigma\pi\left[\frac{\sigma}{2}\right]^2$$

or $$V_e^* = \frac{V_e}{\sigma^3} = \frac{\pi}{2}(1/3 + l^*/2)$$

which for l^*=1.Ø gives V_e^* =1.3Ø9 and for l^*=Ø.6Ø8 gives V_e^*=1.ØØ1. Now the mean reduced volume available for one molecule, V_m^*, is simply given by $1/\rho^*$ and so from the densities V_m^*=3.11Ø for l^*=1.Ø and V_m^* =2.Ø73 for l^*=Ø.6Ø8. The percentage free volume, $((V_m^* - V_e^*)/V_m^*)*100$ are then 58% for l^*=1.Ø and 52% for l^*=Ø.6Ø8. Alternatively V_e can be defined as that of two overlapping spheres in which case

$$V_e = \frac{\pi\sigma^3}{6}(1 + 1.5l^* - 0.5l^{*3})$$

the percentage free volumes then become 66% and 55% respectively. This is a very simplistic approach and the difference may not appear large but to change the percentage free volume from 52% to 58% implies a change in ρ^* from Ø.48243 to Ø.41958. This in turn implies, from the equation of state [39], an increase in temperature of ~9ØK if zero pressure is to be maintained.

These preliminary comparisons establish a basis from which it will be possible to qualify comparisons at a different state. Intuitively it might be expected that a longer molecule would produce a more viscous system what has been shown here is that this is clearly dependent upon the choice of conditions at which to make the comparisons. To obtain further information from this approach it is necessary

to change the applied conditions. To increase the density and maintain contact with the initial studies there are two possibilities either keeping P constant and decreasing T or increasing P and keeping T constant. The increased density in either case would probably lead to an increase in the degree of shear thinning and shear induced alignment. As there is some practical interest in the effect of high pressure on liquids in the field of lubrication it was decided that experiments would be performed at an elevated pressure.

3.4 Chlorine results at T~260K, P~1GPa, l^*=0.608 and l^*=1.0

To make the experiments at different conditions worthwhile it was important that there was a substantial increase in the viscosity to enhance the non-Newtonian behaviour and to emphasise the differences between the two model systems. It is known that many fluids show an exponential dependence of viscosity on pressure [117],

$$\eta(P) = \eta(0)\exp(\alpha P) ,$$

where α is the pressure coefficient of viscosity and is typically of order $10^{8} \rightarrow 10^{9} Pa^{-1}$ [117]. Thus for an increase in the viscosity by a factor of ten pressures of ~1GPa are required. This is also the kind of pressure that can be generated in an EHD contact so this situation would also be of practical interest.

To generate a high pressure equilibrium configuration, in

the l^*=Ø.6Ø8 case, without any knowledge of the P vs ρ isotherm the following procedure was adopted. A sample of 256 molecules at equilibrium at the original state point (T=26ØK, P~Ø, ρ^*=Ø.48243) was compressed over a period of 6ØØΔt by reducing the volume intermittently (~1ØΔt) by about Ø.5% whilst maintaining the temperature constant by velocity scaling. From the resultant pressure increase a value of the reduced number density of Ø.66 was deduced as being of the correct magnitude to give a pressure of ~1GPa. An equilibrium configuration was then obtained at this density in the usual manner and the perturbation technique was applied to determine the stress and alignment responses. Averages were taken over ten segments of 1.2ps each and from which the mean pressure in the non-perturbed runs was calculated to be 11300±1ØØ bar.

To equilibrate a sample of l^*=1.Ø Cl_2 at the same temperature and pressure use was made of a program developed to perform MD in the (N,P,H) ensemble using the method described by Andersen [118] and others [119,12Ø,121]. In contrast to the usual MD ensemble (N,V,E), where the volume remains constant and the pressure fluctuates, in this method the volume is allowed to change in accordance to the imbalance between the calculated pressure, P_c, of the system and the required pressure, P_r, such that

$$\ddot{V} = (P_c - P_r)/M ,$$

where M is a constant. This enables the mean value of the pressure , <P>, to be set to any prescribed value P_r.

The procedure was then simply to start from an equilibrium configuration of l^*=1.Ø Cl_2 at T=26ØK, P~Ø and then to run the 'constant' pressure program with P_r=11ØØbar whilst maintaining the temperature at 26ØK by periodically rescaling the momenta. After approximately 1ØØØΔt the volume was deemed to have relaxed to the value corresponding to the required pressure. This gave a reduced number density of Ø.55124. Once again an equilibrium configuration was generated and the perturbation technique was applied with averages being taken over ten segments. The mean thermodynamic properties resulting from the unperturbed runs for both versions of Cl_2 are shown in table 3.5.

Table 3.5 A comparison of the equilibrium properties obtained for l^*=1.Ø and l^*=Ø.6Ø8 Cl_2 from 1Ø runs of 1.2ps each.

l^*	U /J mol^{-1}	Φ /J mol^{-1}	T /K	P /bar
1.Ø	-1Ø15Ø±8Ø	-1564Ø±4Ø	264.5±2.2	1153Ø±8Ø
Ø.6Ø8	-1567Ø±1ØØ	-23Ø3Ø±6Ø	258.8±2.8	1131Ø±1ØØ

The densification of the two systems, apart from increasing the pressure, leads to a more negative potential energy as the number of molecules residing in the sphere of interest of a particular molecule is increased. Comparisons with the results at the lower pressure (Table 3.4) show that the difference in potential energies between the systems has

dropped by ~1000 $J\ mol^{-1}$ i.e. between 15% and 20% the difference at P~0. The discrepancy in the pressure is probably caused by the rather high temperature in the l^*=1.0 case. The likely cause of this is the thermalisation procedure used at the start of each new segment which calculates the temperature of the initial configuration and then rescales it to the required value before the dynamics are performed. With averages being taken over ten segments only there is the possibility that the thermalisation procedure adds energy to the system more times than it takes it out. Thus causing the temperature to be higher than required for these runs. Over a large number of segments, however, this must produce an average temperature close to that specified.

In an attempt to improve the signal to noise ratio , in these perturbation experiments, a delta function strain rate was applied for one step as this has been shown to be numerically superior to the step function approach [71]. In this case the response is proportional to the actual stress correlation function rather than to its integrand. The off-diagonal stress and alignment responses are shown in fig.3.6. These were obtained by numerically integrating , using the trapezium rule, the curves which result from the delta function perturbation. The significant stress response, $\Delta\sigma_{xz}(t)$, has been fitted to the two exponential form suggested by Kivelson and Allen [70]

Figure 3.6 $\Delta\sigma_{\alpha\beta}(t)$ and $\Delta D_{\alpha\beta}(t)$ vs. t, chlorine, l^*=0.608, T 260K, P 1GPa.

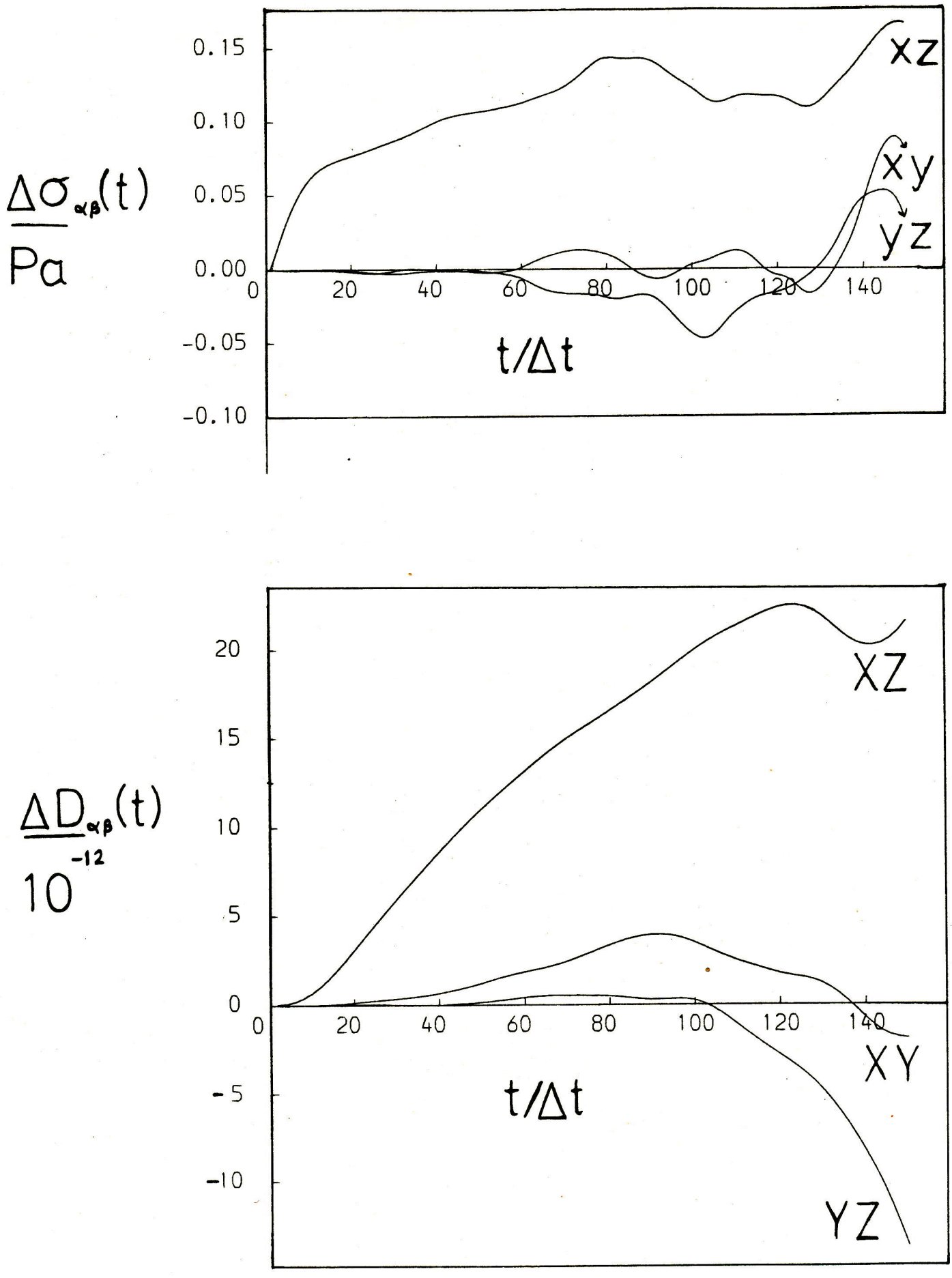

Figure 3.7 $\Delta\sigma_{\alpha\beta}(t)$ and $\Delta D_{\alpha\beta}(t)$ vs. t, chlorine, $l^*=1.0$, T~260K, P~1GPa.

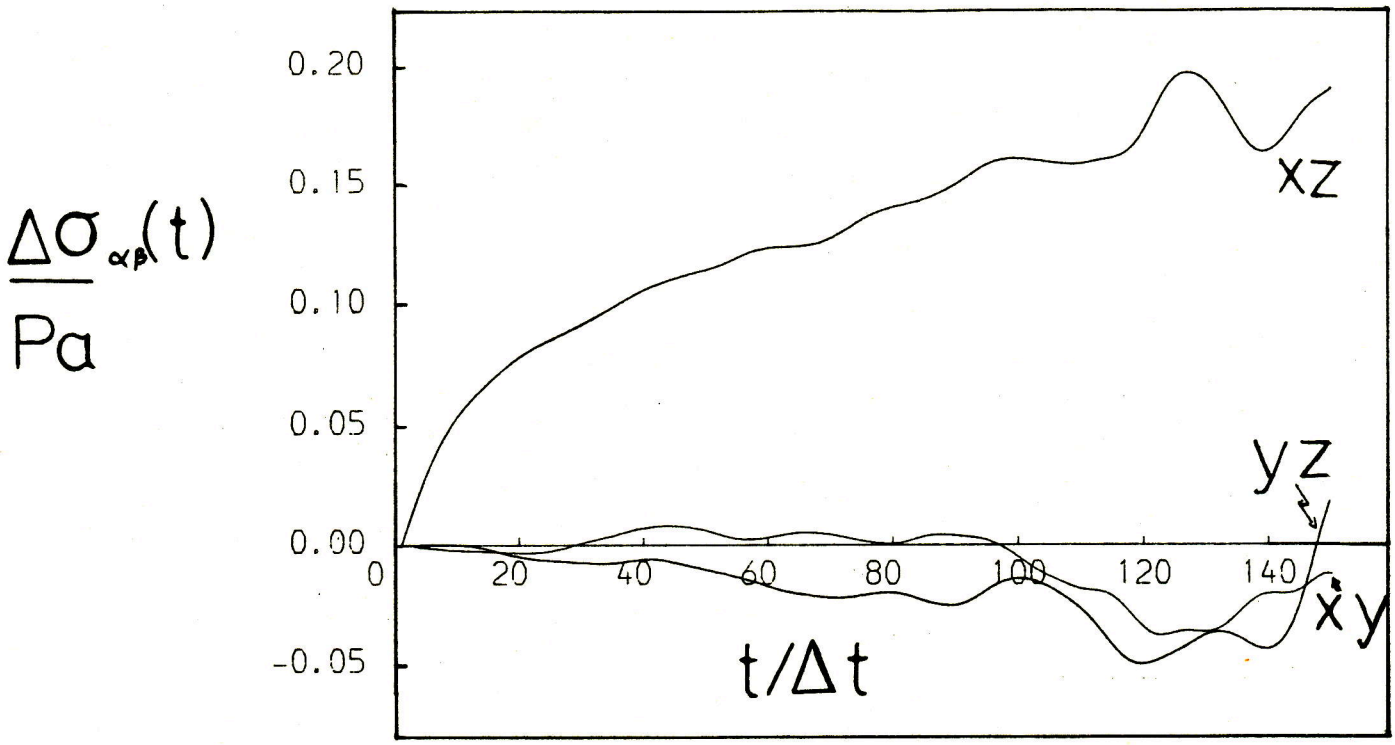

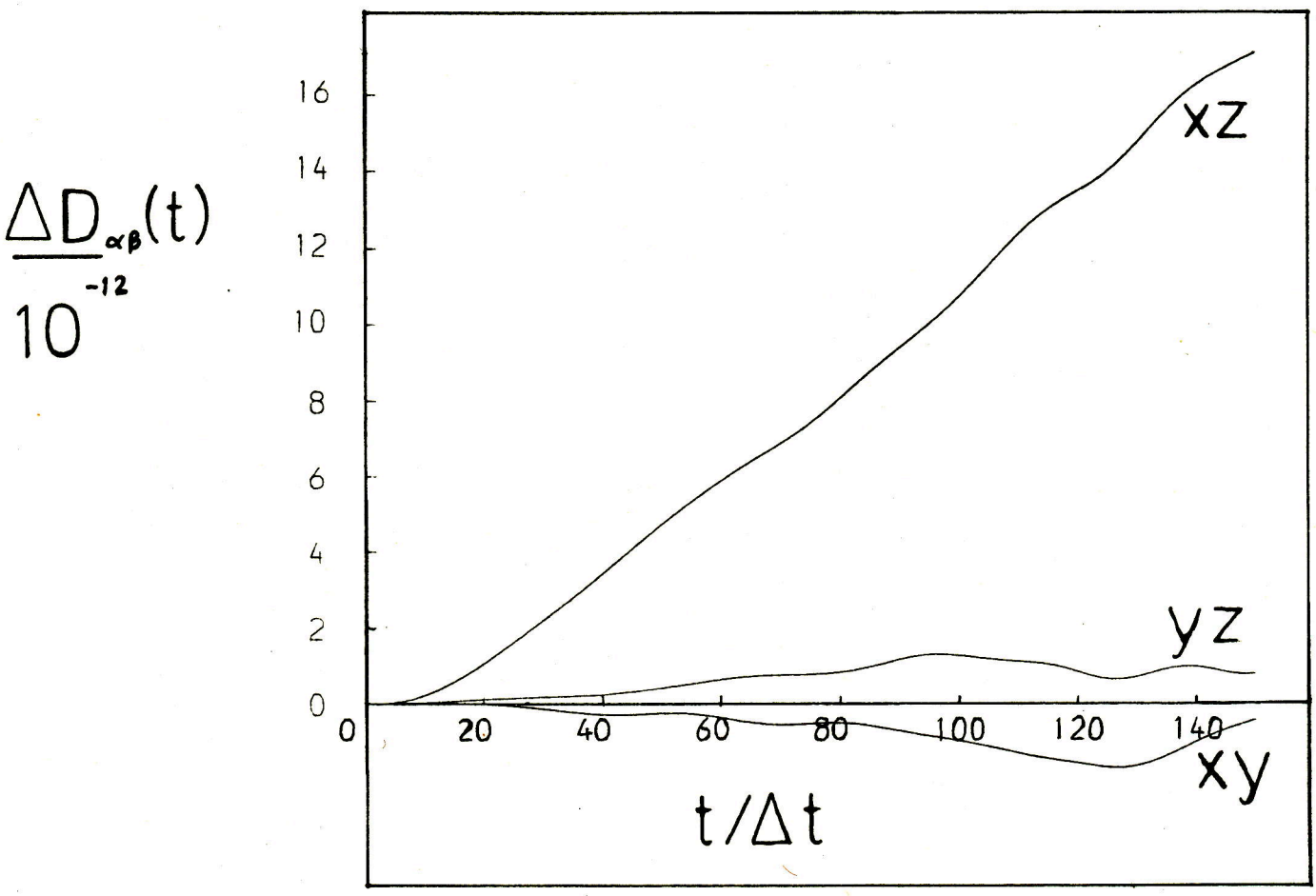

$$\frac{\Delta\sigma_{xz}}{\Delta\dot{\gamma}} = \eta(t) = \eta_1(1 - \exp(-t/\tau_1)) + \eta_2(1 - \exp(-t/\tau_2))$$

for both cases. As before the initial slope, $\frac{d\eta(0)}{dt} \simeq \frac{\Delta\sigma_{xz}(\Delta t)}{\Delta t\, \Delta\dot{\gamma}}$, gives an approximation to G_∞ which in this case is given by

$$G_\infty = \eta_1/\tau_1 + \eta_2/\tau_2 \quad .$$

The parameters for the best fit and the predicted viscosities, $\eta=\eta_1+\eta_2$, are given in table 3.6.

Table 3.6 The best fit parameters to the form of two exponentials for the stress responses obtained from the perturbation experiments on l^*=1.Ø and l^*=Ø.6Ø8 at T~26ØK, P~1.1GPa.

l^*	τ_1 /ps	τ_2 /ps	η_1 /mPa s	η_2 /mPa s	G_∞ /GPa	η /mPa s
1.Ø	Ø.85	Ø.Ø8	1.21	Ø.52	8.Ø	1.74
Ø.6Ø8	Ø.24	Ø.Ø8	Ø.59	Ø.44	8.2	1.Ø3

From figs.3.6 and 3.7 and table 3.6 the indications are that the situation at P~Ø has been reversed to some extent. The larger stress response in the l^*=1.Ø case suggests that it is now the more viscous fluid. The shear moduli of both fluids have increased, as might be expected, with the l^*=1.Ø Cl_2 again increasing a larger amount such that the G_∞'s are almost equal. There is also a close similarity between the form of the responses themselves, at least initially, where, from the fit to two exponentials, the relaxation times are the

same. For the l^*=Ø.6Ø8 case it is not clear whether $\Delta\sigma_{xz}(t)$ has reached its limiting value but for l^*=1.Ø it appears the stress is still rising at the end of the 15ØΔt that the responses were followed for. This casts doubt on the values given for the viscosities in table 3.6 which will almost certainly be underestimations of the actual viscosity.

For the alignment there is no doubt that, in either case, ΔD_{xz} is far from its long time value. The alignment response for the l^*=Ø.6Ø8 is again faster than the l^*=1.Ø Cl_2 but comparisons with the results at P~Ø show that whereas for l^*=Ø.6Ø8 ΔD_{xz} responds more slowly at the higher pressure for l^*=1.Ø the response of ΔD_{xz} to the perturbation is, if anything, slightly faster. The reasons for this are not clear but it is possibly a density effect. At the low density limit the scarcity of interactions will probably cause the rate of realignment to be very slow and at high densities the hinderance to rotations will have the same effect. In the intermediate density region the rate of alignment will first increase with density , as interactions between molecules become more frequent, and then decrease as rotations become hindered. This could possibly explain , to some extent, the results for the rates of realignment.

Having applied the perturbation technique results were then obtained at a number of shear rates using the steady state method. The mean thermodynamic properties and the

length of the simulations are given in table 3.7, the mean stress, resultant viscosity and normal pressure components ($P_{\alpha\alpha}=-\sigma_{\alpha\alpha}$) are given in table 3.8. and in table 3.9. the significant components of the alignment tensor are shown.

Table 3.7 The mean thermodynamic properties obtained from steady state shear calculations on the l^*=1.0 and l^*=0.608 Cl_2 systems at T~260K and P~1GPa.

(l^*=1.0)

$\dot{\gamma}/10^{10}s^{-1}$	U/J mol^{-1}	Φ/J mol^{-1}	T/K	P/bar	Length of run /ps
0.0	-10380±40	-15780±40	259.9±0.1	11360±80	64
0.502	-10420±40	-15820±40	260.0±0.1	11320±50	64
0.754	-10350±40	-15760±40	260.0±0.1	11400±60	136
1.247	-10350±40	-15750±40	260.0±0.1	11350±70	112
2.490	-10240±40	-15650±40	260.0±0.1	11450±70	72
4.990	-10090±40	-15490±40	260.1±0.2	11610±40	72
12.50	-9640±50	-15050±50	260.5±0.4	12060±50	32

(l^*=0.608)

$\dot{\gamma}/10^{10}s^{-1}$	U/J mol^{-1}	Φ/J mol^{-1}	T/K	P/bar	Length of run /ps
0.824	-15600±40	-21010±40	260.1±0.1	11340±70	188
1.243	-15590±40	-20990±40	260.1±0.1	11370±50	112
5.0	-15420±30	-20820±30	260.1±0.1	11600±40	88
12.5	-15060±40	-20480±50	260.3±0.1	12070±70	72
24.98	-14400±30	-19860±30	262.8±0.1	12930±30	40

Table 3.8 The mean shear stress, resultant shear rate dependent viscosity and mean normal pressure components from the steady state shear calculations on l^*=1.0 and l^*=0.608 Cl_2 at T~260K and P~1GPa.

(l^*=1.0)

$\dot{\gamma}/10^{10}s^{-1}$	σ_{xz}/bar	$\eta(\dot{\gamma})$/mPa s	P_{xx}/bar	P_{yy}/bar	P_{zz}/bar
0.502	242±23	4.81±0.47	11330±80	11370±140	11250±70
0.754	302±47	4.01±0.62	11390±100	11460±110	11360±80
1.247	503±84	4.04±0.68	11280±120	11380±130	11400±80
2.490	776±53	3.12±0.21	11290±60	11570±70	11480±70
4.990	1016±41	2.03±0.08	11390±90	11690±80	11750±110
12.50	1870±36	1.50±0.03	11670±110	12050±60	12460±100

(l^*=0.608)

$\dot{\gamma}/10^{10}s^{-1}$	σ_{xz}/bar	$\eta(\dot{\gamma})$/mPa s	P_{xx}/bar	P_{yy}/bar	P_{zz}/bar
0.824	261±70	3.17±0.85	11390±92	11280±100	11370±100
1.243	368±62	2.96±0.50	11340±100	11400±70	11380±100
5.0	1200±58	2.40±0.12	11430±140	11590±130	11780±110
12.5	2057±42	1.65±0.03	11650±120	12010±130	12550±120
24.98	3247±86	1.30±0.03	12200±70	12920±80	13680±50

Table 3.9 The mean significant components of the alignment tensor obtained from the steady state shear calculations on the l^*=1.0 and l^*=0.608 Cl_2 systems at T~260K and P~1GPa.

(l^*=1.0)

$\dot{\gamma}/10^{10}s^{-1}$	D_{xz}	$D_{xx}-1/3$	$D_{yy}-1/3$	$D_{zz}-1/3$
0.502	0.030±0.012	0.005±0.008	-0.007±0.009	0.002±0.009
0.754	0.045±0.007	0.010±0.013	-0.011±0.007	0.001±0.012
1.247	0.066±0.008	0.028±0.007	-0.016±0.006	-0.012±0.007
2.49	0.080±0.006	0.035±0.010	-0.003±0.010	-0.033±0.010
4.99	0.097±0.006	0.070±0.012	-0.018±0.010	-0.051±0.014
12.50	0.201±0.007	0.095±0.007	-0.029±0.006	-0.068±0.009

(l^*=0.608)

$\dot{\gamma}/10^{10}s^{-1}$	D_{xz}	$D_{xx}-1/3$	$D_{yy}-1/3$	$D_{zz}-1/3$
0.824	0.027±0.009	-0.002±0.009	0.007±0.009	-0.004±0.006
1.243	0.043±0.005	0.001±0.010	-0.009±0.006	0.007±0.012
5.0	0.107±0.006	0.036±0.011	-0.020±0.008	-0.016±0.009
12.5	0.141±0.004	0.068±0.008	-0.032±0.006	-0.036±0.008
24.98	0.176±0.005	0.119±0.007	-0.069±0.007	-0.051±0.007

The shear viscosities are plotted as a function of $\dot{\gamma}^{1/2}$ in fig.3.8 for both systems. As predicted by the perturbation result the l^*=1.0 Cl_2 is now more viscous than its shorter bond length counterpart. The perturbation results apparently underestimate $\eta(0)$ by a factor of, at least, five in each case. This underestimation of the zero shear rate viscosity

Figure 3.8 $\eta(\dot{\gamma})$ vs. $\dot{\gamma}^{1/2}$, l^*=1.0 (□) and l^*= 0.608 (Δ)
T 260K, P 1GPa.

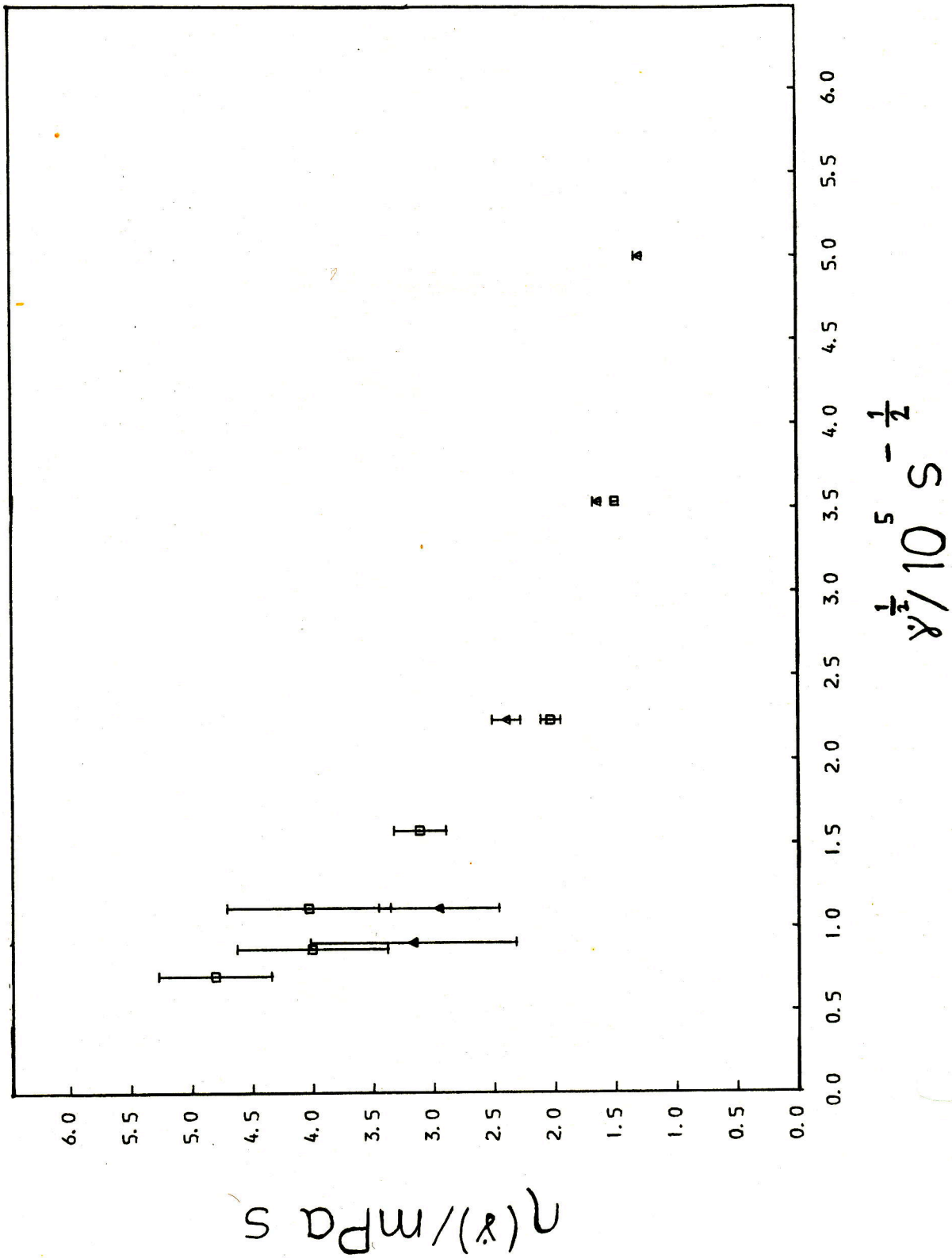

is a result of not being able to determine accurately the form of the response due to its slow relaxation compared to the time before which statistical noise dominates. Clearly the rise of $\Delta\sigma_{xz}(t)$ to its long time limit must be particularly slow compared to the initial relaxation and to compute the full response using the perturbation method is, at present, uneconomic.

3.5 The Shear Rate Dependence of the Viscosity

There is a marked degree of shear thinning in both systems with the 1^*=1.Ø case showing the noticeably greater effect. The eventual result of this is that at the higher shear rates the viscosities tend to similar limiting values in each case. No fully satisfactory theory has ever been produced which correctly predicts the shear rate dependence of the viscosity although many have been proposed [73,74,78,79,82,83,84,86]. Some of these theories are empirical in their approach [86] to the problem but others specifically take into account molecular considerations. The theories of Ree-Eyring (RE) [73] , Kawasaki and Gunton (KG) [74] and Hess [79,8Ø,81] are examples of these more fundamental treatments. The RE and KG theories are particularly interesting as RE theory is favoured by experimentalists [18] whereas what data that has been produced by NEMD has been interpreted in terms of KG theory. Hess's theory is more recent and has largely remained untested but it

does specifically take into account the alignability of molecules. In an attempt to evaluate these theories and to try and estimate $\eta(0)$ the curves predicted by these theories were fitted to the $\eta(\dot{\gamma})$ data obtained for the chlorine systems studied here.

The predicted form of the shear rate dependent viscosity is in each case :-

RE $$\eta(\dot{\gamma}) = \eta(0)\ \sinh^{-1}(\dot{\gamma}\tau_r)/(\dot{\gamma}\tau_r) \qquad (3.5.1)$$

KG $$\eta(\dot{\gamma}) = \eta(0) - A\dot{\gamma}^{1/2} \qquad (3.5.2)$$

Hess $$\eta(\dot{\gamma}) = \eta(0)\left[1 - k(\dot{\gamma}\tau_h)^2/(R^2 + (\dot{\gamma}\tau_h)^2)\right] \qquad (3.5.3)$$

In Hess's equation R is a function of $\dot{\gamma}\tau_h$ but to first approximations R=1 [80] so this has been used throughout. For eqns.3.5.1 and 3.5.3 best fit curves were obtained by varying the adjustable parameters, $\eta(0)$ and τ_r for eqn.3.5.1 and $\eta(0)$, k and τ_h for eqn.3.5.3, to minimise the root mean square difference (RMSD) between the predicted curves, $\eta'(\dot{\gamma})$, and the actual data, $\eta(\dot{\gamma})$. The RMSD is defined as

$$RMSD = \left[\frac{1}{N_p}\sum_{i=1}^{N_p}(\eta(\dot{\gamma}_i) - \eta'(\dot{\gamma}_i))^2\right]^{1/2} \qquad (3.5.4)$$

where N_p is the number of experimental points. As the curve in the KG prediction is of the form y=mx+c the best fit was

simply found by the method of least squares where the slope, -A, is given by

$$-A = \frac{N_p \sum_{i=1}^{N_p} \eta(\dot{\gamma}_i)\dot{\gamma}_i^{1/2} - \left[\sum_{i=1}^{N_p} \dot{\gamma}_i^{1/2}\right]\left[\sum_{i=1}^{N_p} \eta(\dot{\gamma}_i)\right]}{N_p \sum_{i=1}^{N_p}\left[\dot{\gamma}_i^{1/2}\right]^2 - \left[\sum_{i=1}^{N_p} \dot{\gamma}_i^{1/2}\right]^2} \qquad (3.5.5)$$

and the intercept, $\eta(0)$, by

$$\eta(0) = \frac{\left[\sum_{i=1}^{N_p} \eta(\dot{\gamma}_i)\right]\left[\sum_{i=1}^{N_p}\left[\dot{\gamma}_i^{1/2}\right]^2\right] - \left[\sum_{i=1}^{N_p} \dot{\gamma}_i^{1/2}\right]\left[\sum_{i=1}^{N_p} \eta(\dot{\gamma}_i)\dot{\gamma}^{1/2}\right]}{N_p \sum_{i=1}^{N_p}\left[\dot{\gamma}_i^{1/2}\right]^2 - \left[\sum_{i=1}^{N_p} \dot{\gamma}_i^{1/2}\right]^2} \qquad (3.5.6)$$

The best fit curves are shown for both systems in figs.3.9 and 3.10 and the parameters used are shown in table 3.10 along with the RMSD's.

Figure 3.9 $\eta(\dot{\gamma})$ vs. $\dot{\gamma}^{1/2}$, l^*=1.0, T~260K, P~1GPa, (Δ). Fit to the predictions of the theories of Hess (——), Ree-Eyring (- - -) and Kawasaki-Gunton (—·—·—).

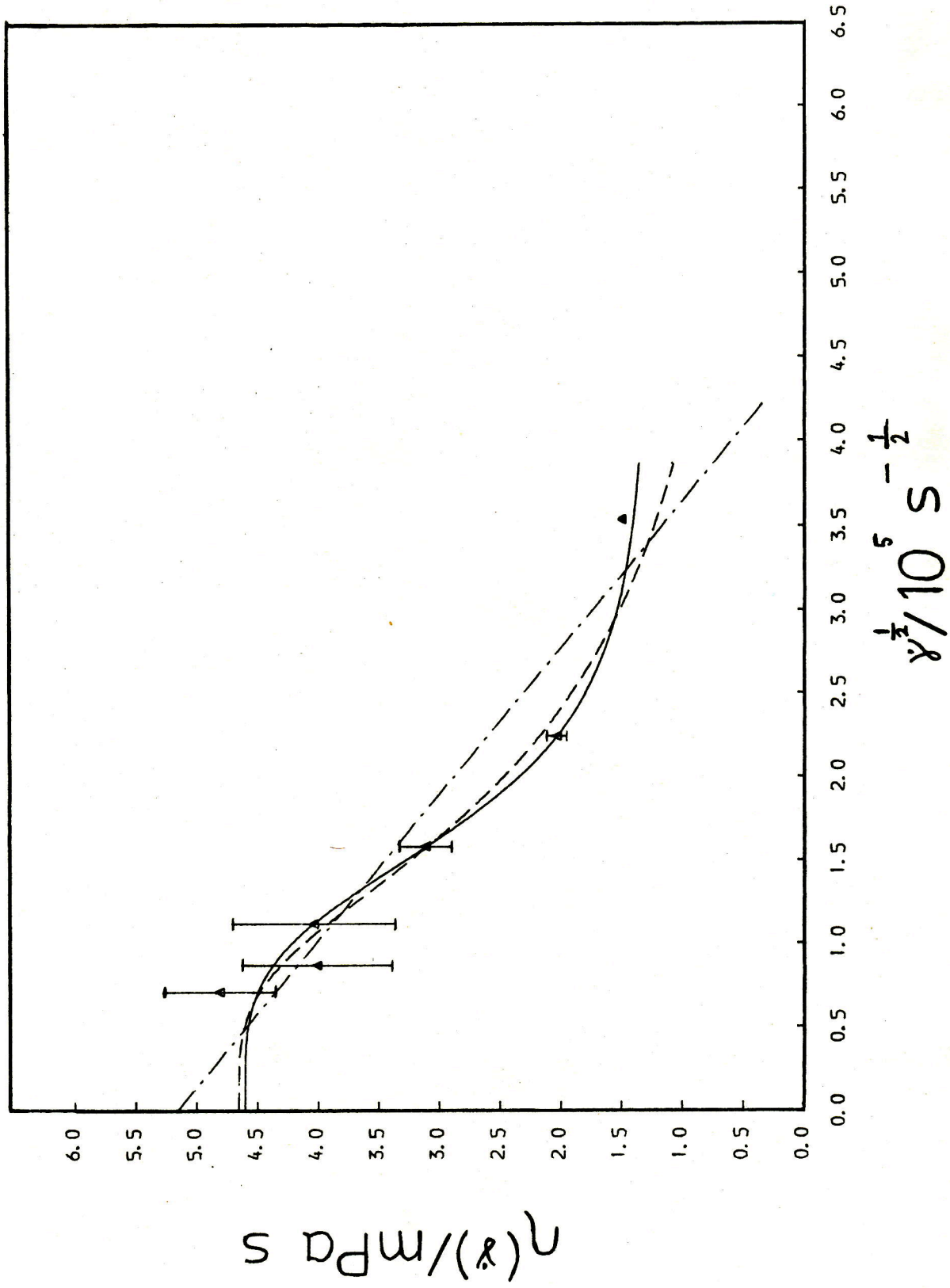

Figure 3.10 $\eta(\dot{\gamma})$ vs. $\dot{\gamma}^{1/2}$, l^{*}=0.608, T~260K, P~1GPa, (Δ). Fit to the predictions of the theories of Hess (——), Ree-Eyring (- - -) and Kawasaki-Gunton (—·—·—).

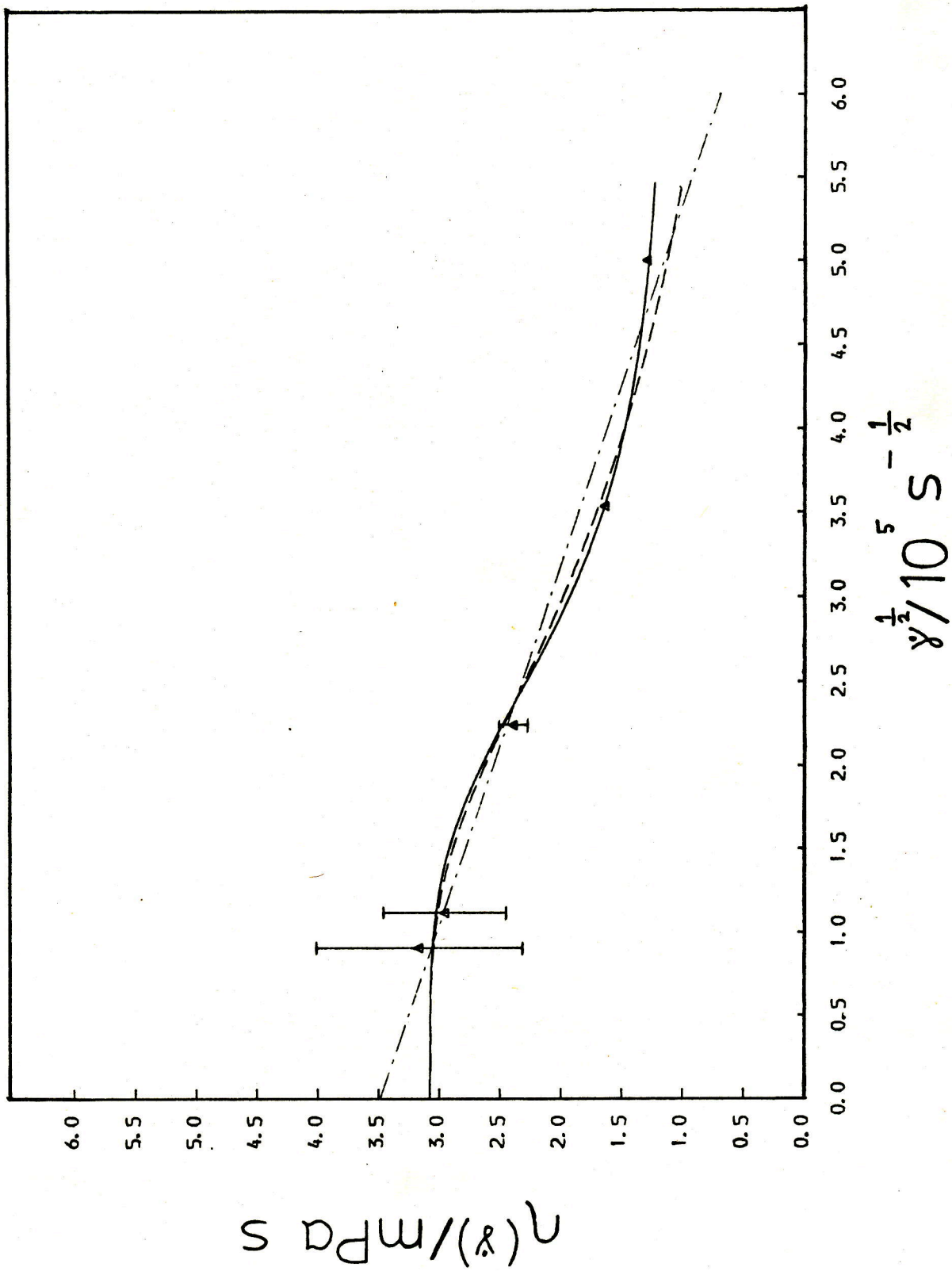

Table 3.1Ø Best fit parameters and root mean square differences for various predicted curves for chlorine viscosity data at T~26ØK, P~1GPa, a) for all shear rates b)for all except the highest shear rate.

		(a)		(b)	
		l^*=1.Ø	l^*=Ø.6Ø8	l^*=1.Ø	l^*=Ø.6Ø8
Hess	η(Ø)/mPa s	4.6Ø	3.Ø8	4.5Ø	3.Ø4
	τ_h/ps	35.9	13.2	27.5	13.8
	k	Ø.73	Ø.64	Ø.88	Ø.57
	RMSD/mPa s	Ø.2Ø	Ø.Ø7	Ø.24	Ø.1Ø
KG	η(Ø)/mPa s	5.16	3.49	5.8Ø	3.65
	$A/10^{-5}$mPa $s^{\frac{3}{2}}$	1.14	Ø.47	1.69	Ø.56
	RMSD/mPa s	Ø.36	Ø.12	Ø.18	Ø.Ø3
RE	η(Ø)/mPa s	4.67	3.Ø9	4.67	3.Ø9
	τ_r/ps	97.2	29.Ø	1Ø4.Ø	31.6
	RMSD/mPa s	Ø.22	Ø.1Ø	Ø.21	Ø.Ø7

A comparison of the root mean square differences reveals that their is little to choose between the curves on a statistical basis. Qualitatively the Hess and RE curves correctly predict the apparent lessening in the rate at which the viscosity decreases at high shear rates whereas the KG line does not. This is not surprising as the curve quoted is only the asymptotic limit which should fit the behaviour of $\eta(\dot{\gamma})$ as $\dot{\gamma}\rightarrow Ø$ and not as $\dot{\gamma}\rightarrow\infty$. The infinite shear limits of

the Hess and RE curves are $\eta(\infty)=\eta(0)(1-k)$ and $\eta(\infty)=0$ respectively so Hess theory predicts a second Newtonian region which there is some evidence for in polymer solutions [78]. In the low shear region there are again differences. As $\dot{\gamma}\rightarrow 0$ the slope $\frac{d\eta(\dot{\gamma})}{d\dot{\gamma}}$ tends to zero in both the RE and Hess curves but for KG $\frac{d\eta(\dot{\gamma})}{d\dot{\gamma}}=-A\dot{\gamma}^{-\frac{1}{2}}$ which means that the slope is infinite at the zero shear rate limit. On a practical basis this is probably beyond experimental detection as the changes in the viscosity involved are very small. A similar argument holds for the apparent lack of any Newtonian region for all the $\eta(\dot{\gamma})$ functions discussed. For Hess and RE theory $\eta(\dot{\gamma})$ only significantly differs (~5%) from $\eta(0)$ if $\dot{\gamma}\tau\ 10^{-1}\rightarrow 1$ so for τ in the region of 10^{-10}s there is a large region up to $\dot{\gamma}=10^{9}s^{-1}$ where the viscosity is apparently $\eta(0)$. Even for the KG expression an A value of $\sim 10^{-5}$mPa $s^{\frac{3}{2}}$, typical of the fluids studied here, means that shear rates up to $10^{8}s^{-1}$ will only alter the viscosity by ~0.1mPa s which is certainly undetectable using MD and, as the highest shear rates achievable using experimental techniques are $\sim 10^{6}s^{-1}$, also by real experiments.

Also given in table 3.10 are the best fits to all but the highest shear rate points, the actual curves are shown in figs.3.11 and 3.12. As has been found previously [70] this procedure certainly produces a better fit to the KG prediction. This is borne out by the RMSD's which are reduced markedly for the square root formula when the highest shear

Figure 3.11 As fig.3.9 but excluding highest shear rate point.

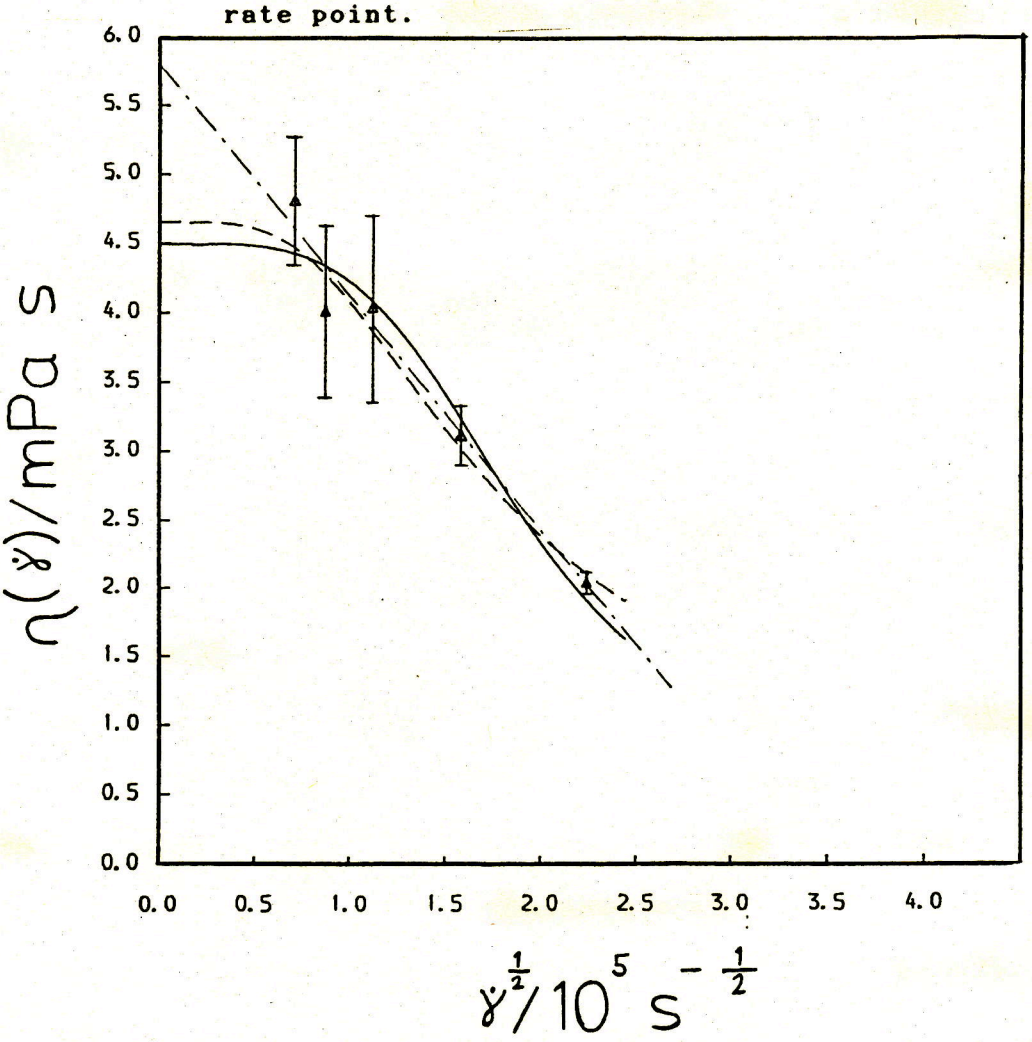

Figure 3.12 As fig.3.10 but excluding highest shear rate point.

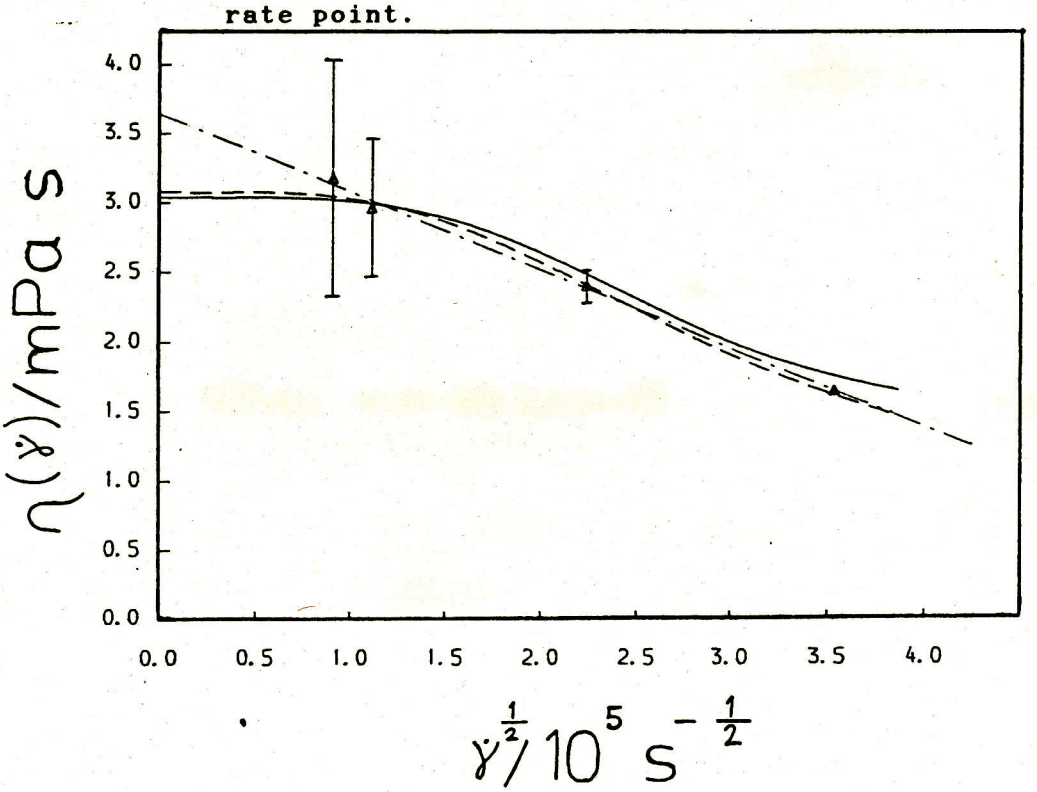

rates in each case are omitted whereas for the other two functions there is little change. This approach to estimating the $\dot{\gamma}=0$ viscosity is justified to some extent in that the KG prediction is valid only as $\dot{\gamma}\rightarrow 0$.

These various attempts at fitting the $\eta(\dot{\gamma})$ data do not lead to any firm conclusions. It is clear that more accurate data is required over a larger range of shear rates for a number of different systems to say if any of these three predictions accurately represents the data. As far as determining $\eta(0)$ is concerned this rather inconclusive result means that there is a range of estimates for $\eta(0)$. The zero shear viscosities are consequently quoted as $\eta(0)=5.2\pm0.7$mPa s for $l^*=1.0$ Cl_2 and $\eta(0)=3.3\pm0.4$mPa s for $l^*=0.608$ Cl_2.

3.6 The Pressure/Density Dependence of the Viscosity

Even with these rather large error bars it is still clear that the effect on the viscosity of the increase in pressure is markedly different between the two systems. The effect of pressure on the viscosity is usually quantified in terms of the pressure coefficient of viscosity, α, defined by

$$\eta(P_2) = \eta(P_1)\exp(\alpha(P_2 - P_1)). \qquad (3.6.1)$$

This coefficient was calculated for both systems and the values obtained are given in table 3.11 together with the

pressures and viscosities used to determine it.

Table 3.11 The pressure coefficients of viscosity obtained from the data given for chlorine at T~260K.

l^*	P_1/bar	P_2/bar	$\eta(P_1)$/mPa s	$\eta(P_2)$/mPa s	α/GPa^{-1}
1.0	61	11360	0.13	5.2	3.3
0.608	16	11310	0.23	3.3	2.4

On the basis of the differing a values it might be concluded that the response of the viscosity of two very similar systems to a change in a state parameter is unrelated. How significant this is depends whether the viscosity is directly or only indirectly dependent upon the state parameter in question. In the case of pressure it could be equally well argued that it is the change in density, caused by the increase in pressure, which is the more important factor. The change in density/volume with pressure is generally given by the compressibility, β, defined as

$$\beta = -\frac{1}{V}\frac{dV}{dP} \qquad (3.6.2)$$

which as $V \propto 1/\rho$ is also given by

$$\beta = \frac{1}{\rho}\frac{d\rho}{dP} \; . \qquad (3.6.3)$$

As only two widely separated state points have been studied and as the compressibility is not a constant at a particular

temperature mean compressibilities have been estimated from

$$\bar{\beta} = \frac{1}{\bar{\rho}} \frac{\Delta\rho}{\Delta P} \qquad (3.6.4)$$

where $\Delta\rho=\rho_1-\rho_2$, $\Delta P=P_1-P_2$ and $\bar{\rho}=(\rho_1+\rho_2)/2$. The resultant mean compressibilities, given in table 3.12 along with the values of the densities and pressures used, indicate the $l^*=1.0$ Cl_2 system is certainly the more compressible of the two. This is a reasonable result as the compressibility is an inverse measure of the ability of molecules to pack efficiently and it would be expected that the compressibility decreases as $l^* \rightarrow 0$ i.e. the sphere.

Table 3.12 The mean compressibilities obtained from the data given for chlorine at T~260K.

l^*	ρ_1	ρ_2	P_1/bar	P_2/bar	$\bar{\beta}$/GPa^{-1}
1.0	0.32157	0.55124	61	11360	0.47
0.608	0.48243	0.66	16	11310	0.28

Having established the difference in compressibilities it remains to be shown whether the viscosity is more a function of density than pressure. To do this it has been assumed that as $P \propto \rho$ a relationship similar to that given by eqn.3.6.1 might also hold for the density

$$\eta(\rho_2) = \eta(\rho_1)\exp(\alpha_\rho(\rho_2 - \rho_1)) . \qquad (3.6.5)$$

With only two points it is not possible to test this hypothesis but as for the pressure it is useful to calculate and compare the two coefficients. These are given in table 3.13. along with the various quantities required for their calculation.

Table 3.13 The density coefficients of viscosity obtained from the data given for chlorine at T~260K.

l^*	ρ_1	ρ_2	$\eta(P_1)$/mPa s	$\eta(P_2)$/mPa s	α_ρ
1.0	0.31577	0.55124	0.13	5.2	16.1
0.608	0.48243	0.66	0.23	3.3	15.0

Compared to the pressure coefficients of viscosity the α_ρ's show good agreement considering the errors in determining the viscosity. It could be that this is purely a coincidence of the conditions studied and does not stand up to the test of a more thorough examination. The implication if it is correct though is that it is the densification that occurs under increasing pressure, at constant temperature, that is the important factor in relation to the viscosity rather than the pressure change itself.

3.7 Shear Induced Alignment

The effect of shear on the alignment tensor is given in table 3.9 and is shown graphically in figs.3.13 to 3.16. At these higher densities there is an increased amount of realignment of the molecules as might be expected. Quite clearly the overall trend is the same in both cases with molecules having preferred alignment in the +ve XZ quadrant which principally affects the value of D_{xz} and D_{xx}. As D_{xx} increases the constraint relationship $D_{xx}+D_{yy}+D_{zz}=1$ means that the values of D_{yy} and D_{zz} must also change. It is found that these two other components tend to decrease roughly by the same amount for the l^*=Ø.6Ø8 case but with D_{zz} decreasing noticeably more than D_{yy} in the l^*=1.Ø case.

The one significant off-diagonal component of $\underline{\underline{D}}$ is D_{xz} as D_{xy} and D_{yz} are effectively zero because of the symmetry of the shear. In both cases D_{xz} increases continuously with shear rate though at the lower shear rates D_{xz} is greater for the l^*=1.Ø system but at the higher shear rates the opposite is true. Intuitively it might be expected that a longer molecule would align to a larger extent than a shorter one. This would not necessarily manifest itself in a larger value of D_{xz}. This is so because D_{xz} can pass through a maximum and decrease to zero again as D_{xz}=Ø if all the molecules are aligned parallel to the x-axis. The maximum value of D_{xz} possible is Ø.5 which only occurs if all the molecule are

Figure 3.13 $D_{xz}(\dot{\gamma})$ vs. $\dot{\gamma}^{1/2}$, l^*=1.0 (□) and l^*=0.608 (Δ), T~260K, P~1GPa.

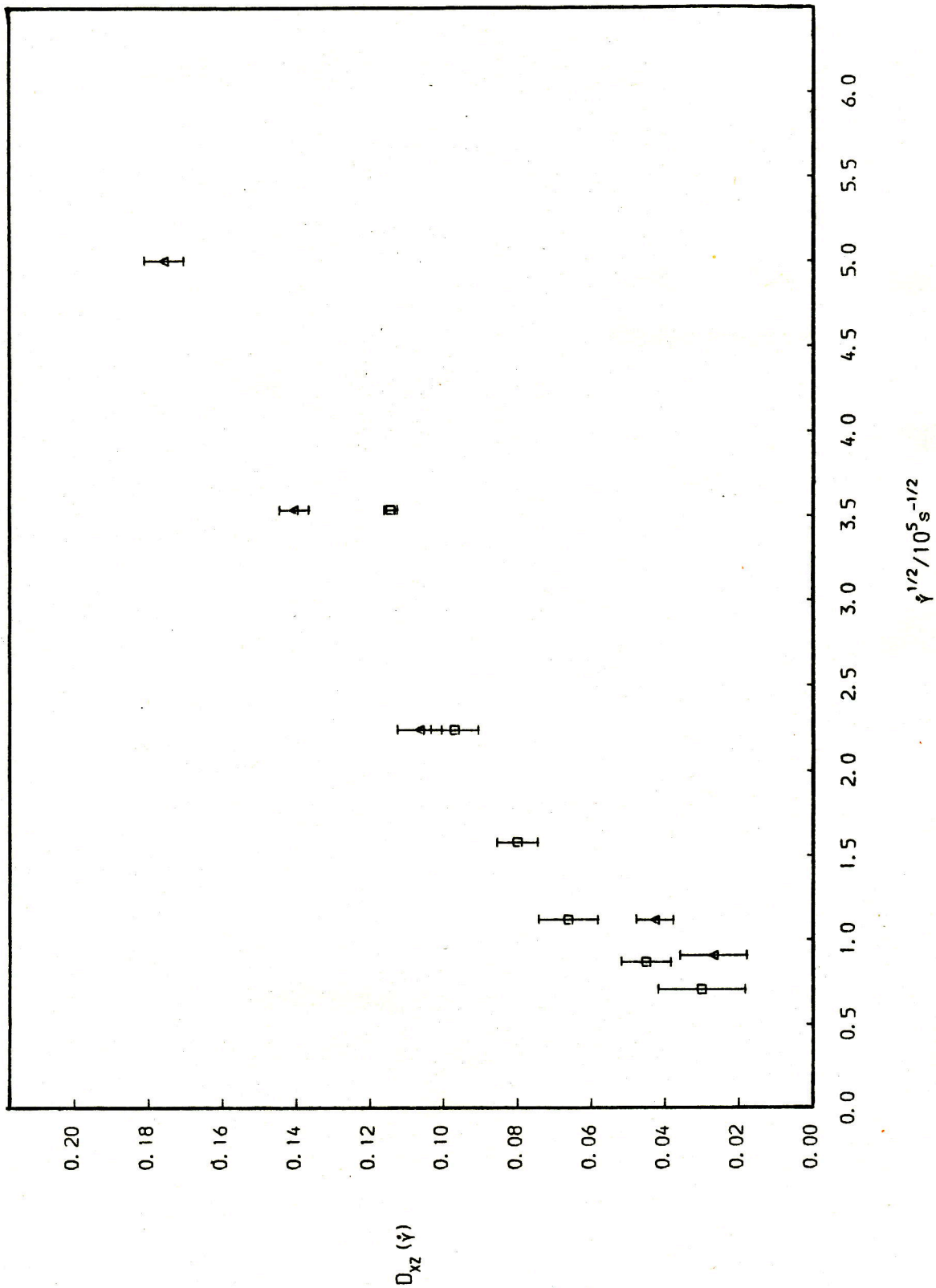

Figure 3.14 $D_{xx}(\dot{\gamma})-1/3$ vs. $\dot{\gamma}^{1/2}$, $l^*=1.0$ (□) and $l^*=0.608$ (Δ), T~260K, P~1GPa.

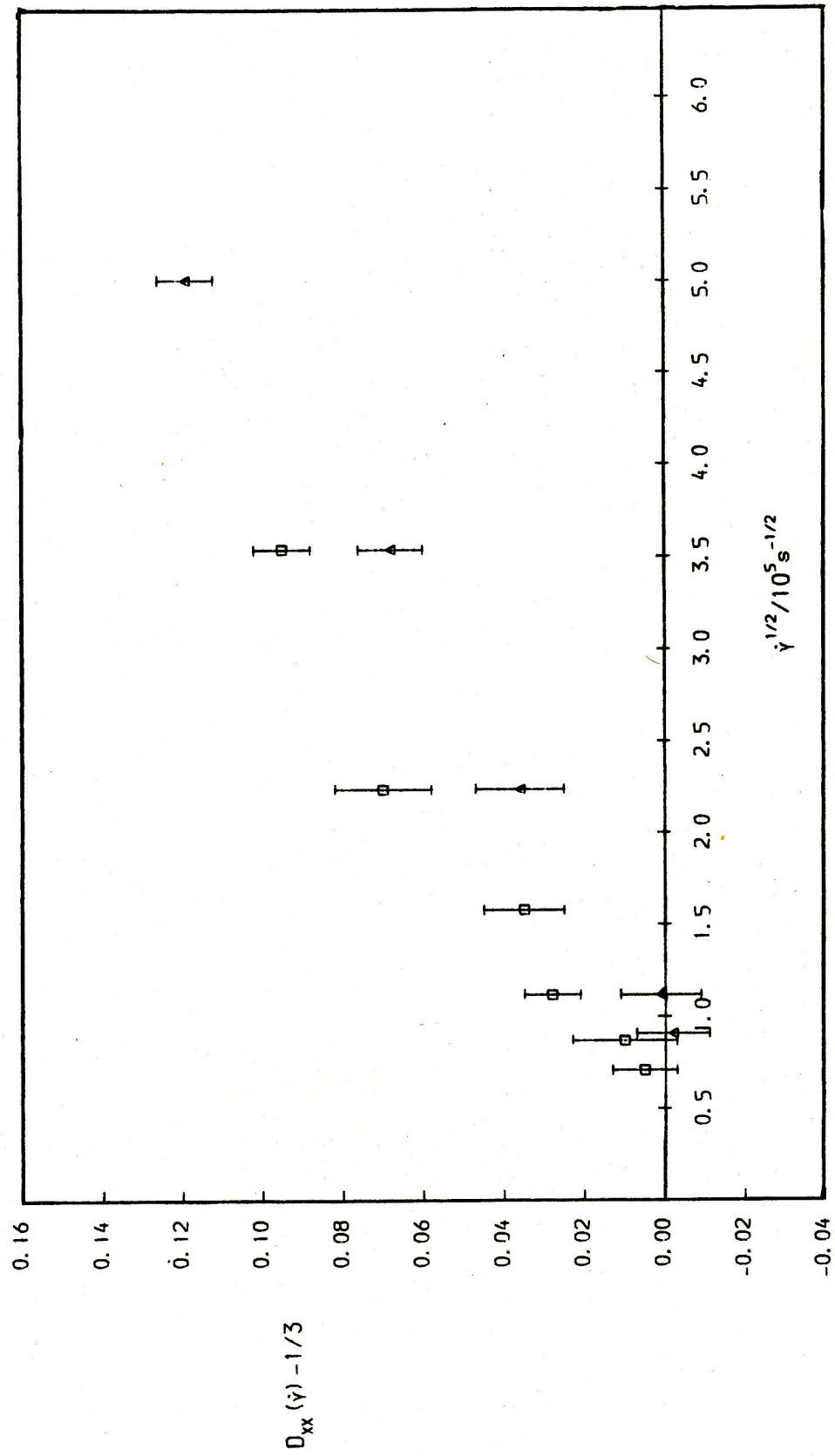

Figure 3.15 $D_{yy}(\dot{\gamma})-1/3$ vs. $\dot{\gamma}^{1/2}$, $l^*=1.0$ (□) and $l^*=0.608$ (Δ), T~260K, P~1GPa.

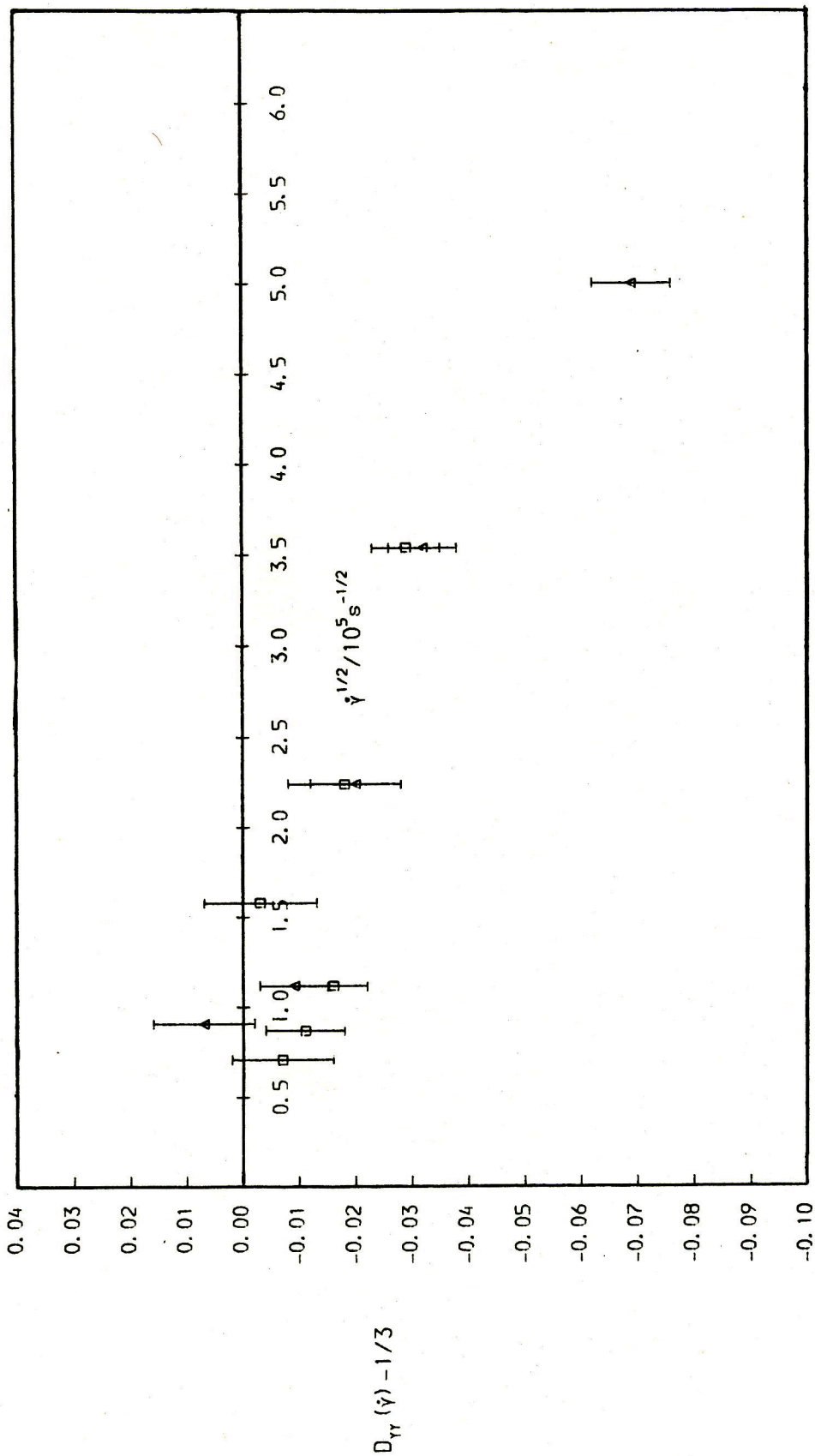

Figure 3.16 $D_{zz}(\dot{\gamma})-1/3$ vs. $\dot{\gamma}^{1/2}$, $l^*=1.0$ (□) and $l^*=0.608$ (Δ), T~260K, P~1GPa.

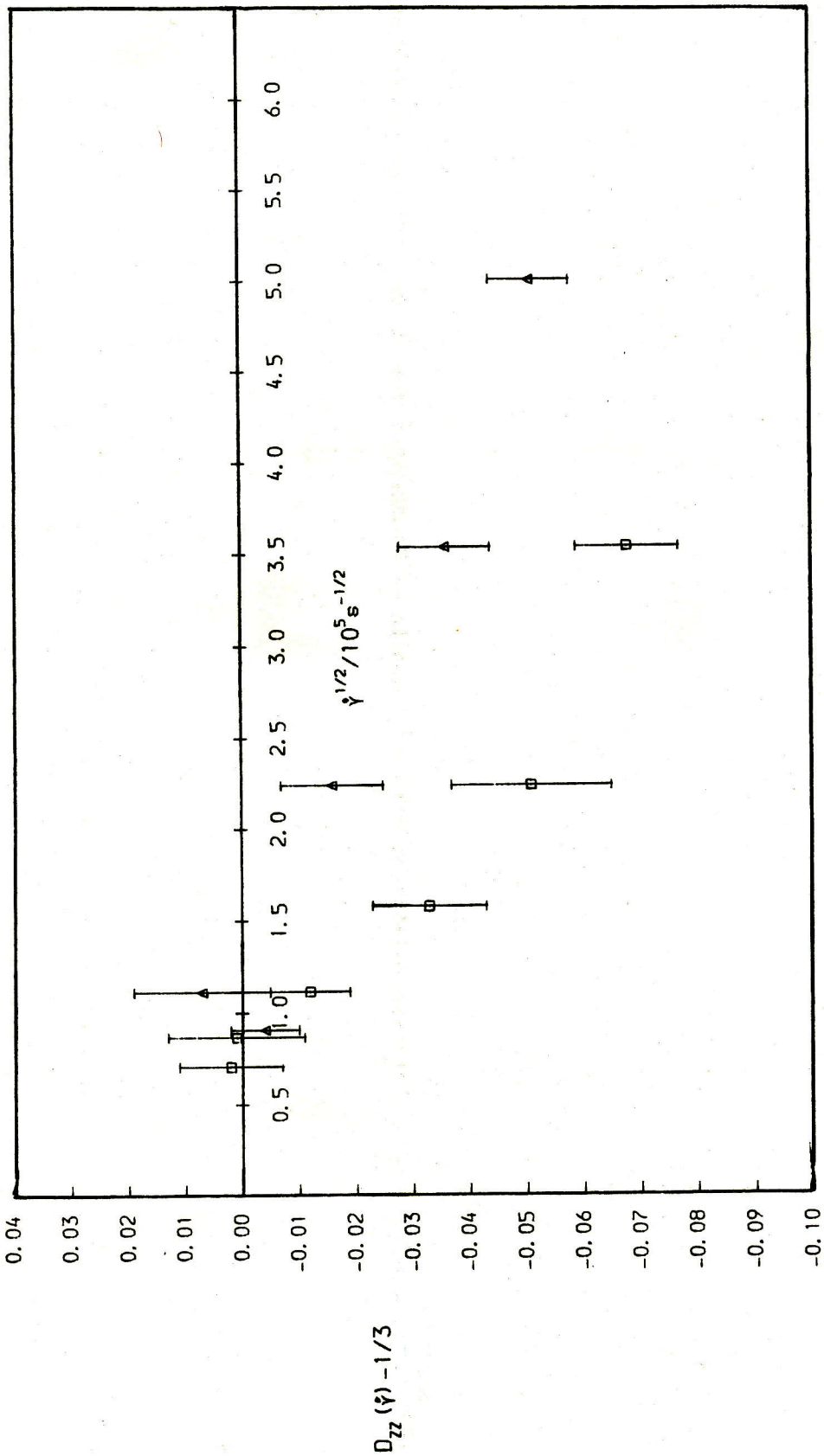

aligned at 45° to the x-axis in the XZ plane. As this situation is highly unlikely and there is bound to be a distribution in the y direction any observable maximum will almost certainly be somewhat lower than Ø.5. This is not the case for D_{xx}, however, which for all the shear rates that are comparable is greater in the l^*=1.Ø case indicating alignment more parallel to the x-axis.

Two other orientation functions which have also been calculated are the shear orientation coefficient, χ_d, defined as [7Ø]

$$\chi_d(\dot{\gamma}) = \langle D_{xz} \rangle / \langle \dot{\gamma} \rangle \qquad (3.7.1)$$

and an extinction angle, θ_e, defined previously [122] as

$$\theta_e = \frac{1}{2} \tan^{-1} \frac{2\langle D_{xz} \rangle}{\langle D_{xx} - D_{zz} \rangle}, \qquad (3.7.2)$$

which is of the type measured in flow birefringence experiments. The values of these two quantities are given as a function of shear rate in table 3.14 for both the systems studied and are shown as a function of $\dot{\gamma}^{1/2}$ in figs.3.17 and 3.18.

Table 3.14 The shear orientation coefficients and extinction angles obtained from the steady state shear calculations on the l^*=1.Ø and l^*=Ø.6Ø8 Cl_2 systems at T~26ØK and P~1GPa.

(l^*=1.Ø)

$\dot{\gamma}/10^{10}s^{-1}$	$\chi_d(\dot{\gamma})$/ps	$\theta_e(\dot{\gamma})$/deg
Ø.5Ø2	6.Ø2±2.33	-
Ø.754	5.99±Ø.89	-
1.247	5.32±Ø.64	36.6±3.Ø
2.49	3.22±Ø.22	33.5±2.7
4.99	1.96±Ø.13	29.Ø±2.4
12.5	Ø.92±Ø.Ø3	27.3±1.1

(l^*=Ø.6Ø8)

$\dot{\gamma}/10^{10}s^{-1}$	$\chi_d(\dot{\gamma})$/ps	$\theta_e(\dot{\gamma})$/deg
Ø.824	3.28±1.Ø8	-
1.243	3.44±Ø.4Ø	-
5.Ø	2.13±Ø.12	38.2±2.4
12.5	1.13±Ø.Ø3	34.8±1.2
24.98	Ø.7Ø±Ø.Ø2	32.1±Ø.8

As found by Kivelson and Allen [7Ø] for fluorine $\chi_d(\dot{\gamma})$ becomes distinctly non-linear in $\dot{\gamma}^{\frac{1}{2}}$ when the density is increased. Indeed $\chi_d(\dot{\gamma})$ behaves in much the same way as $\eta(\dot{\gamma})$ for both systems, fig.3.8, implying some connection between $\sigma_{xz}(\dot{\gamma})$ and $D_{xz}(\dot{\gamma})$ although the nature of D_{xz} tends to suggest that this may be coincidental.

Figure 3.17 $x_d(\dot{\gamma})$ vs. $\dot{\gamma}^{1/2}$, l^*=1.0 (□) and l^*=0.608 (Δ), T~260K, P~1GPa.

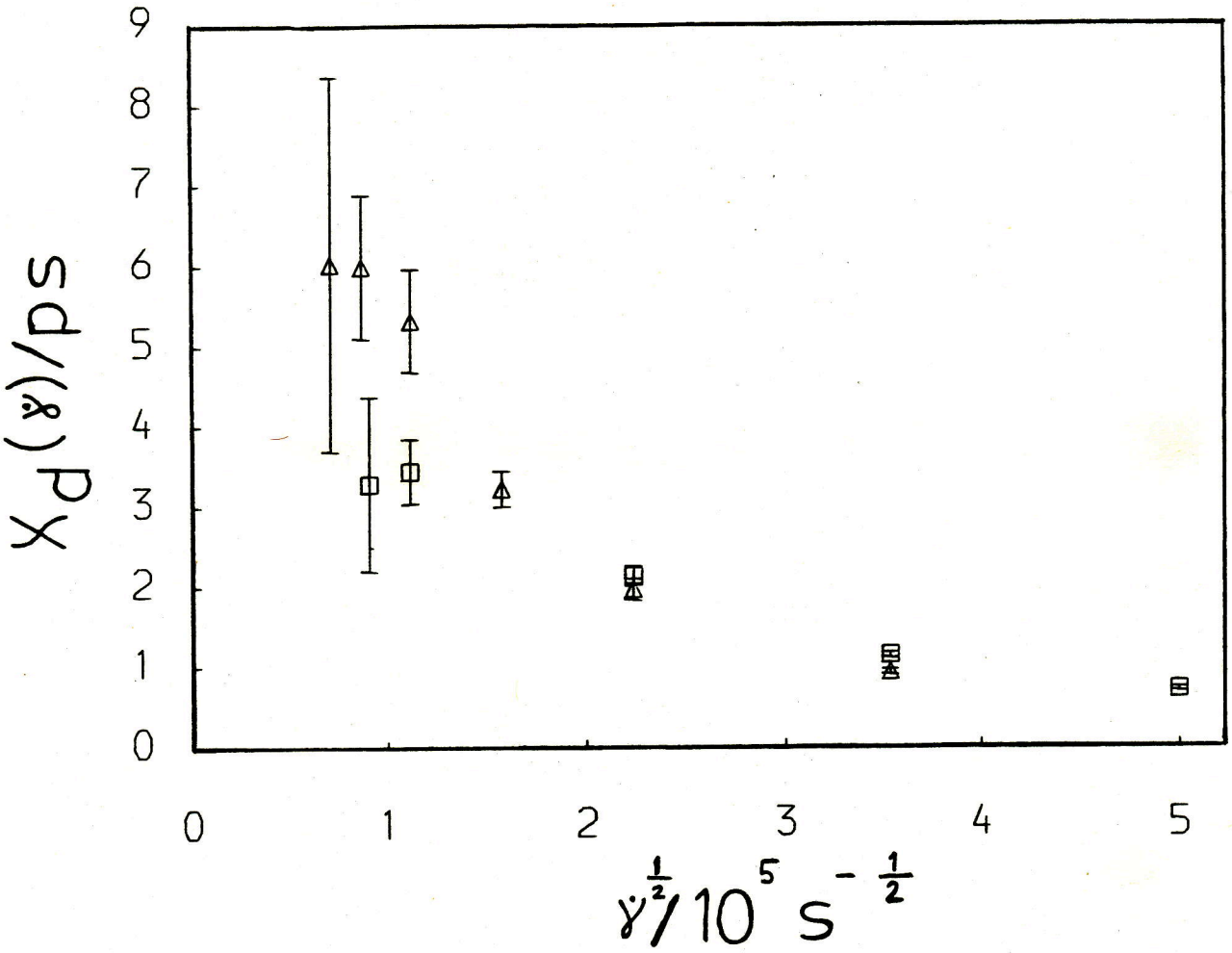

Figure 3.18 $\theta_e(\dot{\gamma})$ vs. $\dot{\gamma}^{\frac{1}{2}}$, $l^*=1.0$ (□) and $l^*=0.608$ (Δ), T~260K, P~1GPa.
Comparisons with the predictions of Hess's theory, $l^*=1.0$ (——) and $l^*=0.608$ (- - -)

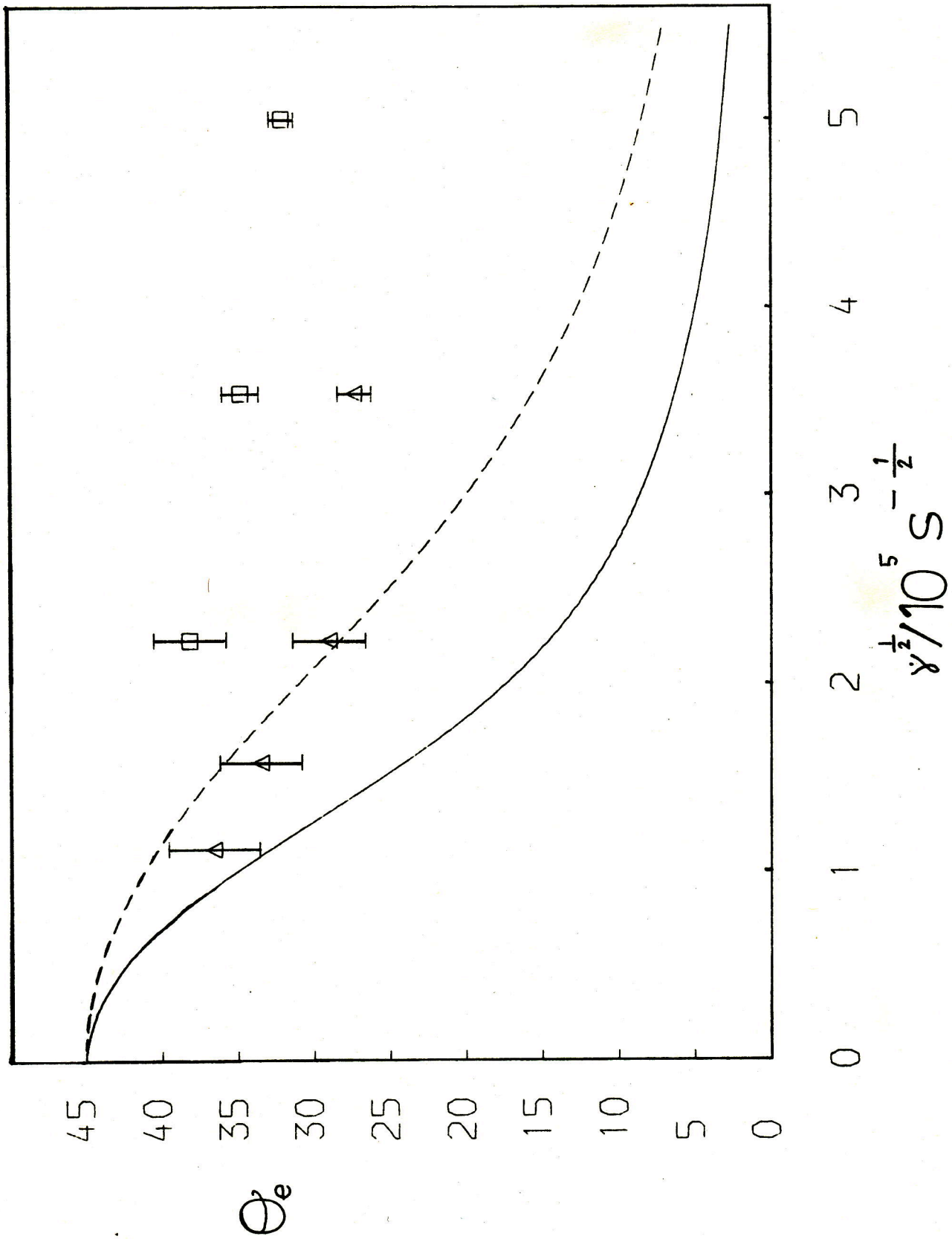

The second function, θ_e, is subject to more errors than χ_d because of the combination of three quantities. At the lower shear rates the actual value of $\langle D_{xx} - D_{zz} \rangle$ was less than the calculated error and thus gave indeterminate results for θ_e. At the higher shear rates the l^*=1.Ø Cl_2 has a consistently lower value of θ_e than the l^*=Ø.6Ø8 Cl_2 which is probably indicative of the greater amount of alignment in the longer bond length system. Also included in fig.3.18 are the predictions for θ_e as determined from the Hess theory. Hess theory in fact gives predictions for all the components of $\underline{\underline{D}}$ but these curves include undetermined constants. When combined as in eqn.3.7.2 the constants cancel out to leave, in the first approximation,

$$\theta_e(\dot{\gamma}) = \frac{1}{2} \tan^{-1}(1/\dot{\gamma}\tau_h). \qquad (3.7.3)$$

Unfortunately first approximation Hess theory, which is stated to be valid for those systems which do not undergo a transition to a liquid crystalline phase [8Ø], predicts that $D_{yy}(\dot{\gamma})=0$ for all $\dot{\gamma}$. This is obviously not the case and thus not surprisingly the curves produced using eqn.3.7.3 and the values of τ_h from table 3.1Ø are not in agreement with the experimental data.

To give a clearer picture of what the alignment due to shear involves probability densities involving the direction cosines of molecules have been calculated. The starting point

is the bond vector associated with each molecule $\underline{l}_i=\underline{r}_{i1}-\underline{r}_{i2}$. For a homonuclear diatomic the individual atoms are indistinguishable so that a bond vector $\underline{l}_i$ has an equivalent alignment to one with a value of $-\underline{l}_i$. To avoid this degeneracy for a shear gradient in the XZ plane the following direction cosines can be defined :-

$$D_x = \hat{l}_x|\hat{l}_z|/\hat{l}_z$$
$$D_y = \hat{l}_y|\hat{l}_x|/\hat{l}_x$$
$$D_z = \hat{l}_z|\hat{l}_x|/\hat{l}_x$$

where $\hat{l}_x$, $\hat{l}_y$ and $\hat{l}_z$ are the components of the unit bond vector. This normalization ensures that equivalent alignments with respect to the direction of shear give the same value of D_x, D_y and D_z. Probability densities were then obtained by dividing the region between -1 and +1 into small equally sized intervals of ΔD_α and accumulating in a histogram the number of times a particular value of D_α occurs. It can be easily shown that by dividing into regions of equal ΔD_α, effectively $\Delta\cos\theta$, the resultant probability densities are flat for a completely random distribution of bond vectors. Accordingly probability densities, $\rho(D_\alpha)$, have been normalized such that $\rho(D_\alpha)=1$ for all values of D_α when the distribution is random.

The results obtained for all three direction cosines at two different shear rates for both systems are shown in figs.3.19 to 3.22. The averages have been taken over an interval of 8ps in all cases for systems considered to be at a steady state at the particular shear rate. At the lower shear

Figure 3.19 The normalised probability densities for the direction cosines $\rho(D_\alpha)$ vs. D_α
$l^*=0.608$, $\dot{\gamma}=1.25*10^{10}s^{-1}$, T~260K, P~1GPa.

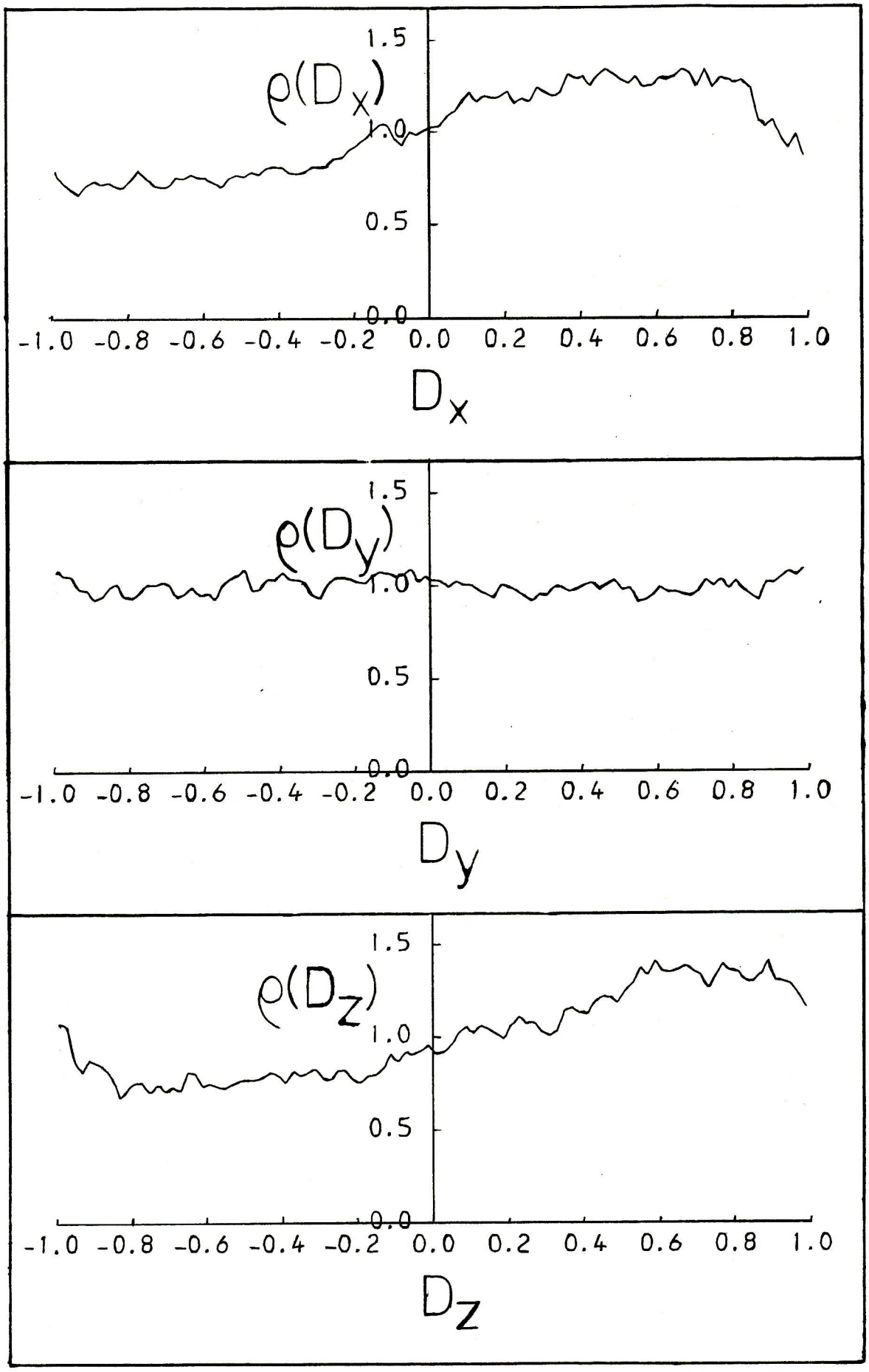

Figure 3.20 As fig.3.19 $l^{*}=1.0$.

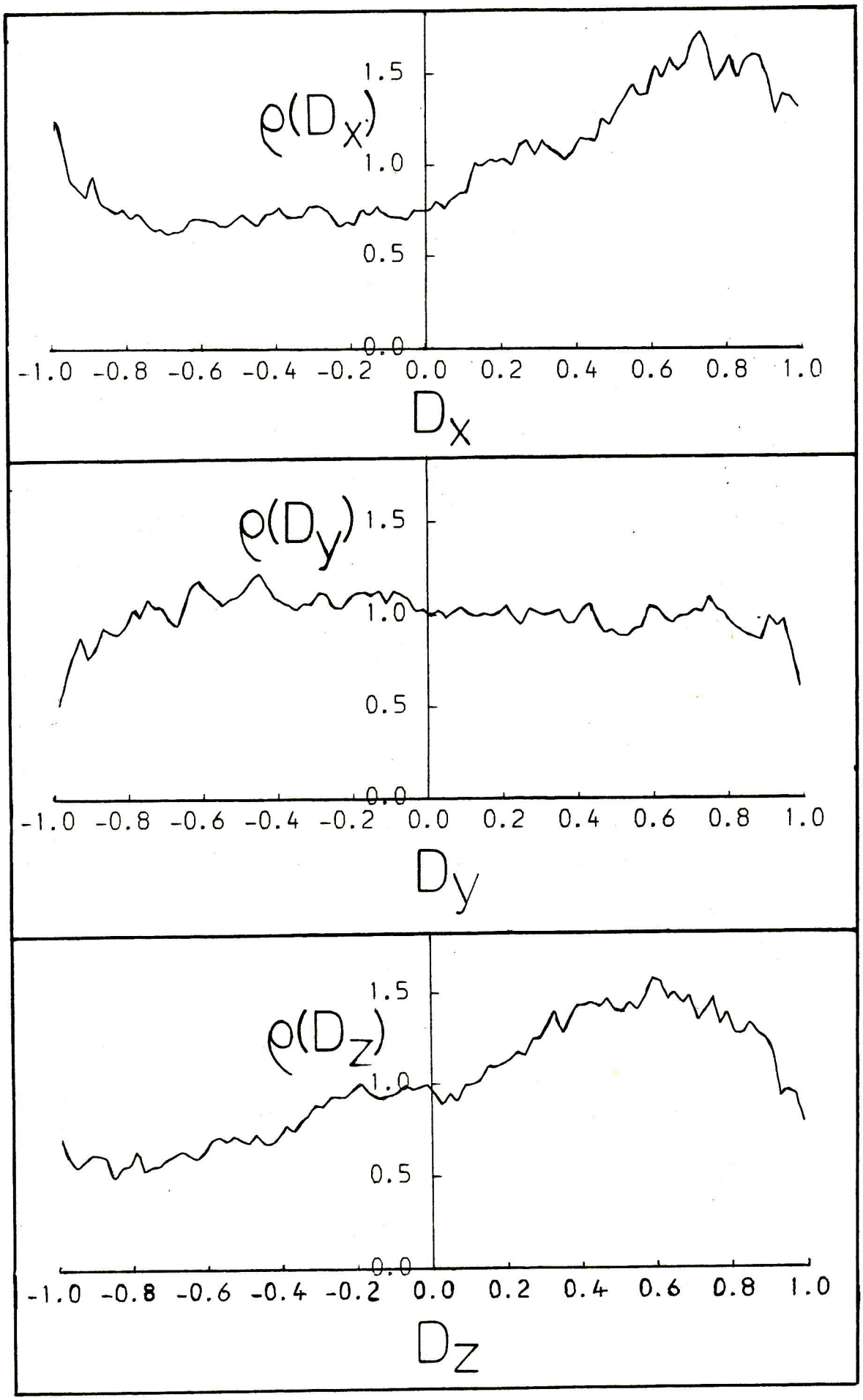

Figure 3.21 As fig.3.19 $l^{*}=0.608$, $\dot{\gamma}=25*10^{10}s^{-1}$.

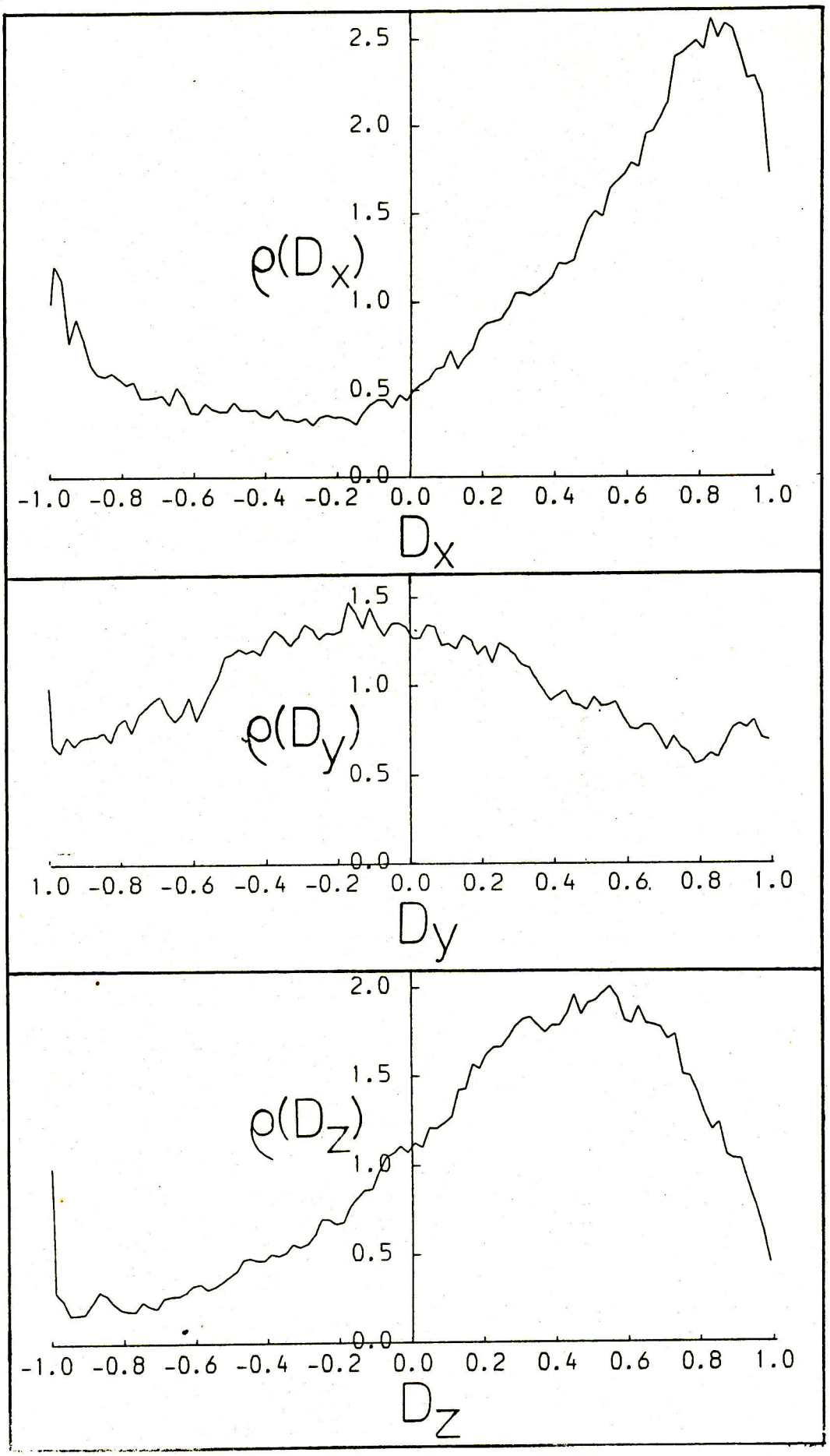

Figure 3.22 As fig.3.19 $l^{*}=1.0$, $\dot{\gamma}=12.5*10^{10}s^{-1}$.

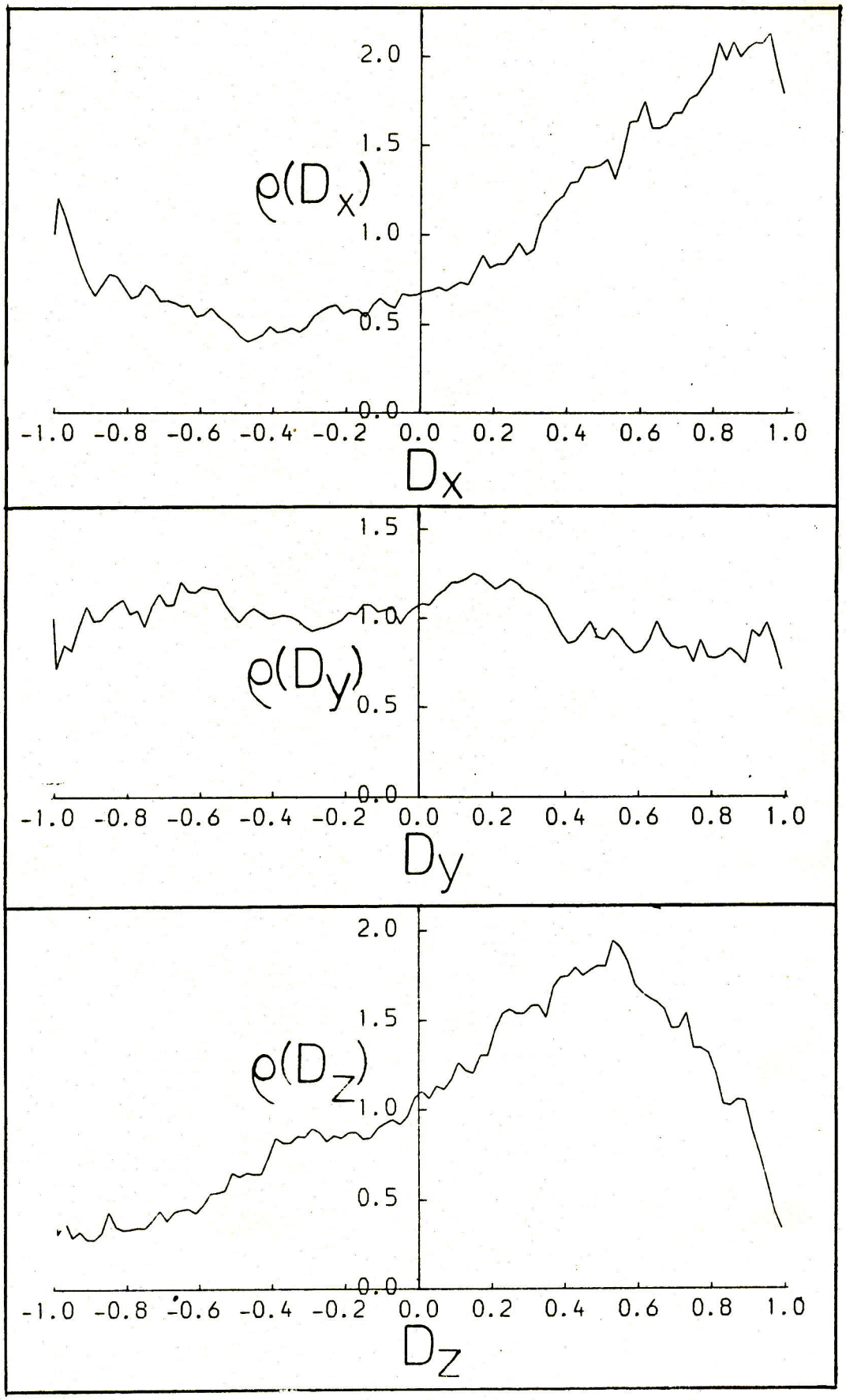

rate, $\dot{\gamma}=1.25*10^{10}s^{-1}$ in each case, there is some deviation from a flat distribution for $\rho(D_x)$ and $\rho(D_z)$ whereas $\rho(D_y)$ is not significantly altered for either $l^*=1.0$ or $l^*=0.608$ Cl_2. For $\rho(D_x)$ and $\rho(D_y)$ there is a tendency for a symmetric distribution to be set up with an excess of molecules aligned in the +ve quadrant with a minimum in $\rho(D_\alpha)$ at ~-0.5 and a maximum at $\sim+0.5$. Comparisons between the two sets of distributions at this lower shear rate show that there is little difference in them in keeping with the results for the alignment tensor.

At the highest shear rates used the distributions become more asymmetric for D_x and D_z. For $\rho(D_x)$ there is a large peak at $D_x\sim0.8$ showing that the most preferred orientation of molecules is in the +ve XZ quadrant almost parallel to the x-axis. $\rho(D_z)$ shows a different distribution with an almost complete lack of molecules aligned parallel to the z-axis, $D_z=\pm1.0$. The majority of molecules have +ve values of D_z which again shows alignment in the +ve XZ quadrant. The peak in $\rho(D_z)$ is at $D_z\sim0.5$ which is equivalent to a bond vector making an angle of 60^o with the z-axis. These observations hold for both systems even though the shear rates are different. For $\rho(D_y)$ there is a tendency, certainly in the $l^*=0.608$ case, for alignment parallel to the y-axis, $D_y=\pm1.0$, to become unfavourable. As the y-axis is orthogonal to the plane of shear this shows up as a roughly symmetric distribution for $\rho(D_y)$ with a broad peak centred at $D_y\sim0$ which

is in agreement with the demonstrated tendency for molecules to align parallel to the x-axis.

3.8 Non-equilibrium thermodynamics

As discussed in sec.1.4 there has been some interest shown in the thermodynamics of systems undergoing steady state planar couette flow [90,91,92]. Hanley and Evans [90] have argued the case for the modification of the first and second laws of thermodynamics for such systems to explain such phenomena as shear induced melting, shear dilation and the change in internal energy. Moreover, their HSNEMD simulations on the monatomic L-J fluid [90] produced results for the shear rate dependent pressure and internal energy that obeyed the following functional forms :-

$$P(\dot{\gamma}) = P(0) + P_1 \dot{\gamma}^{\frac{3}{2}} \qquad (3.8.1)$$

$$U(\dot{\gamma}) = U(0) + U_1 \dot{\gamma}^{\frac{3}{2}} \qquad (3.8.2)$$

where $P(0)$ and $U(0)$ are the equilibrium pressure and internal energy and P_1 and U_1 are state dependent constants. The origin of the $\dot{\gamma}^{\frac{3}{2}}$ dependence is the same theory which predicts a $\dot{\gamma}^{\frac{1}{2}}$ dependence for the shear viscosity [74].

To compare the changes induced in the systems studied here and to test the validity of eqns.3.8.1 and 3.8.2 the

functions $\Delta P(\dot{\gamma})(=P(\dot{\gamma})-P(0))$ and $\Delta U(\dot{\gamma})(=U(\dot{\gamma})-U(0))$ are given in table 3.15 and in figs.3.23 and 3.24 $\log_{10}\Delta P(\dot{\gamma})$ and $\log_{10}\Delta U(\dot{\gamma})$ are plotted as a function of $\log_{10}\dot{\gamma}$. From eqns.3.8.1 and 3.8.2 plotting these functions implies that a straight line should be observed of slope 3/2. At the lower shear rates the estimated errors in ΔP and ΔU are larger than the actual values so only the highest three shear rate points are plotted in figs.3.23 and 3.24.

Table 3.15 The functions $\Delta P(\dot{\gamma})$ and $\Delta U(\dot{\gamma})$, as defined in the text, obtained from the steady state shear calculations on the l^*=1.0 and l^*=0.608 Cl_2 systems at T~260K and P~1GPa.

l^*=1.0

$\dot{\gamma}/10^{10}s^{-1}$	$\log_{10}(\dot{\gamma}/10^{10}s^{-1})$	$\Delta P(\dot{\gamma})$/bar	$\Delta U(\dot{\gamma})$/J mol^{-1}
0.502	-0.299	-40±90	-40±60
0.754	-0.123	40±100	20±60
1.247	0.096	-10±100	20±60
2.49	0.396	90±100	140±60
4.99	0.698	250±80	290±60
12.50	1.097	700±90	740±60

l^*=0.608

$\dot{\gamma}/10^{10}s^{-1}$	$\log_{10}(\dot{\gamma}/10^{10}s^{-1})$	$\Delta P(\dot{\gamma})$/bar	$\Delta U(\dot{\gamma})$/J mol^{-1}
0.824	-0.084	30±120	70±110
1.243	0.095	60±110	80±110
5.0	0.699	290±110	250±100
12.5	1.097	760±120	610±110
24.98	1.398	1620±100	1270±100

It can be seen from table 3.15 and the graphs that both the energy and the pressure increase with shear rate as has been found in all previous HSNEMD simulations. The latter of these effects is also known as positive shear dilatancy and is well documented for real systems [89] where it can be observed in the more usual form as an increase in volume upon shearing. In these simulations the fixed volume causes the pressure to

Figure 3.23 $Log_{10}\Delta P(\dot{\gamma})$ vs. $log_{10}\dot{\gamma}$, l^*=1.0 (—Δ—) and l^*=0.608 (- -□- -), T~260K, P~1GPa.

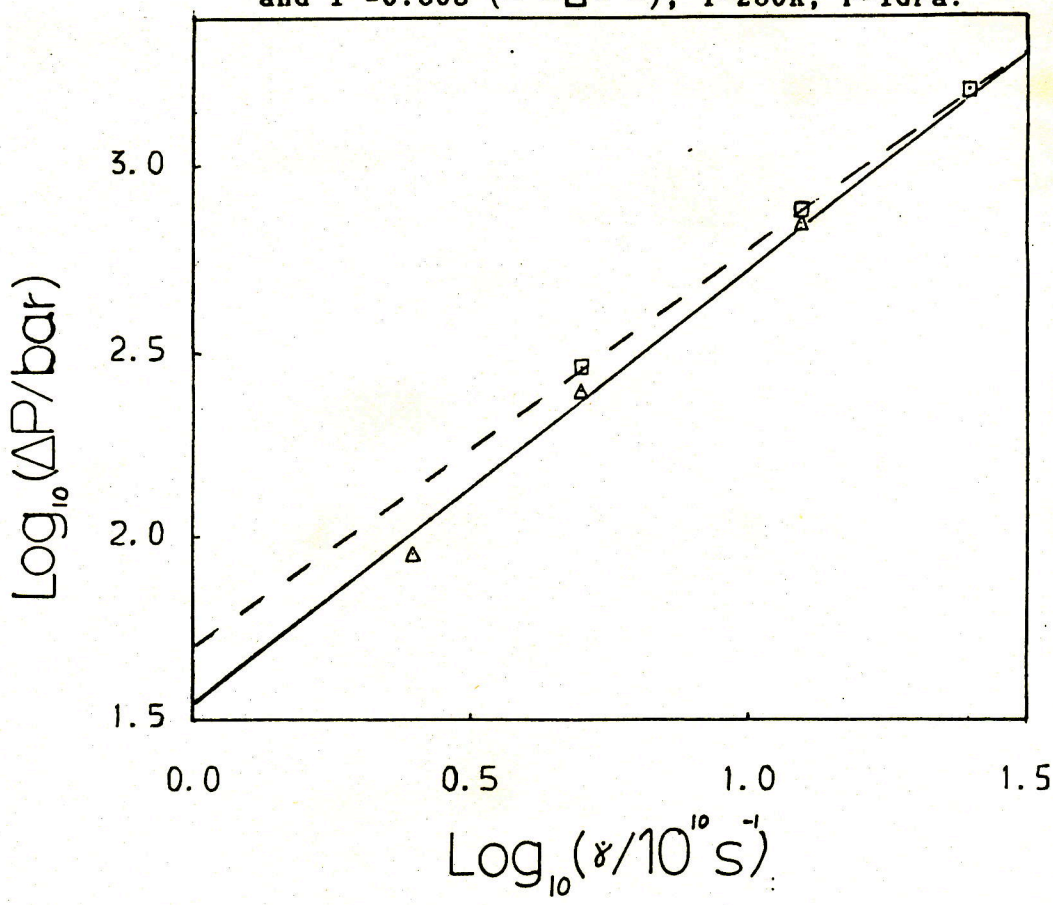

Figure 3.24 $Log_{10}\Delta u(\dot{\gamma})$ vs. $log_{10}\dot{\gamma}$, l^*=1.0 (—Δ—) and l^*=0.608 (- -□- -), T~260K, P~1GPa.

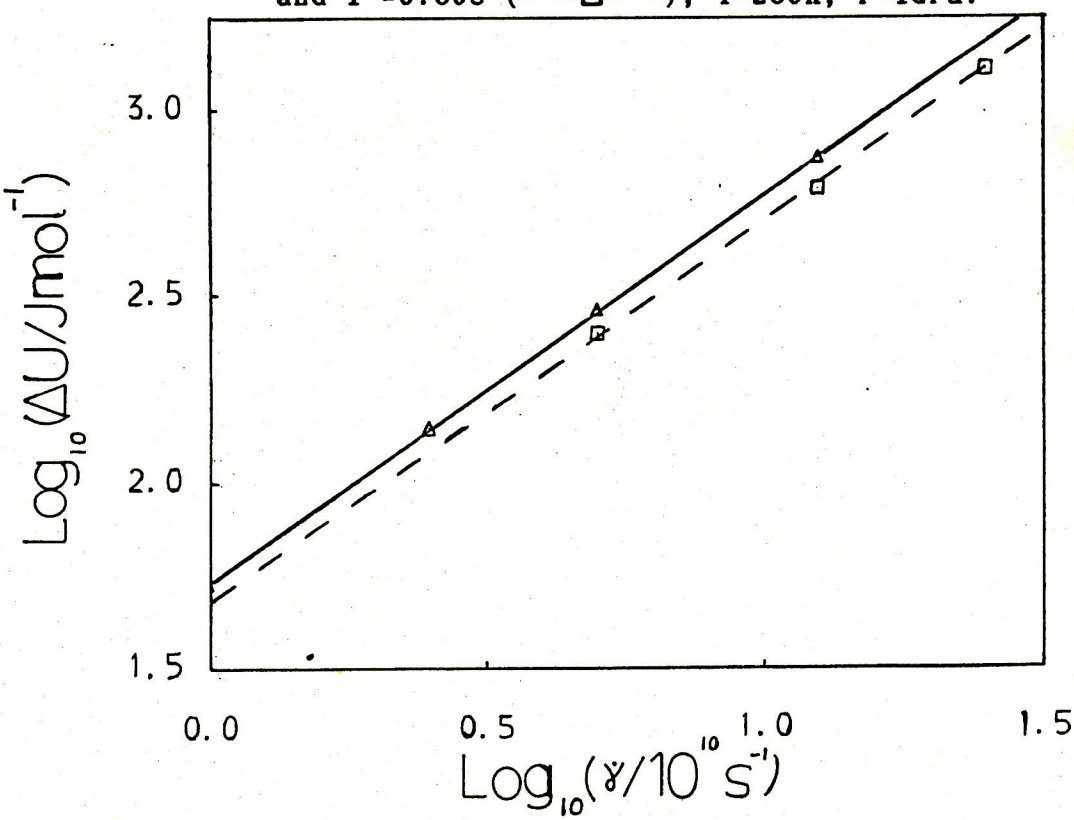

rise instead.

For the limited amount of data available $\Delta P(\dot{\gamma})$ and $\Delta U(\dot{\gamma})$ show an apparent power dependence in $\dot{\gamma}$. However, the slope in all cases is ~1.Ø significantly lower than the 1.5 observed for L-J argon [9Ø]. The data was consequently fitted to the forms

$$\Delta P(\dot{\gamma}) = P_1(\dot{\gamma}/10^{10}s^{-1})^a \qquad (3.8.3)$$

and

$$\Delta U(\dot{\gamma}) = U_1(\dot{\gamma}/10^{10}s^{-1})^b \qquad (3.8.4)$$

and reasonable results were obtained using the parameters given in table 3.16.

Table 3.16 Best fit parameters for the data obtained for the shear rate dependent pressure and energy to the forms given in eqns.3.8.3 and 3.8.4.

l^*	P_1/bar	a	U_1/J mol^{-1}	b
1.Ø	35.2	1.18	51.2	1.Ø6
Ø.6Ø8	5Ø.1	1.Ø8	48.1	1.Ø3

As well as the slope there is also a close similarity in the magnitudes of $\Delta P(\dot{\gamma})$ and $\Delta U(\dot{\gamma})$ for the l^*=1.Ø and l^*=Ø.6Ø8 Cl_2 systems in the rather narrow range that can be compared. The similarity in these static properties contrasts markedly with the differences found between the systems for such dynamic properties as the viscosity and the alignment.

As shown in table 3.8 the pressure increase that occurs upon shearing is not uniformly distributed in the three cartesian directions. To clarify this the set of functions

$$\Delta P_{\alpha\alpha}(\dot{\gamma}) = P_{\alpha\alpha}(\dot{\gamma}) - P(\dot{\gamma}) \qquad \alpha=x,y,z. \qquad (3.8.5)$$

have been calculated and are given in table 3.17.

Table 3.17 The functions $\Delta P_{\alpha\alpha}(\dot{\gamma})$, as defined in the text, (eqn.3.8.5), obtained from the steady state shear calculations on the l^*=1.0 and l^*=0.608 Cl_2 systems at T~260K and P~1GPa.

l^*=1.0

$\dot{\gamma}/10^{10}s^{-1}$	$P(\dot{\gamma})$/bar	$\Delta P_{xx}(\dot{\gamma})$/bar	$\Delta P_{yy}(\dot{\gamma})$/bar	$\Delta P_{zz}(\dot{\gamma})$/bar
0.502	11320±50	10±100	50±150	-70±80
0.754	11400±60	-10±120	50±120	-40±100
1.247	11350±70	-70±130	30±150	50±100
2.49	11450±70	-160±90	120±100	30±100
4.99	11610±40	-220±100	80±90	140±120
12.50	12060±50	-390±120	-10±70	400±110

l^*=0.608

$\dot{\gamma}/10^{10}s^{-1}$	$P(\dot{\gamma})$/bar	$\Delta P_{xx}(\dot{\gamma})$/bar	$\Delta P_{yy}(\dot{\gamma})$/bar	$\Delta P_{zz}(\dot{\gamma})$/bar
0.824	11340±70	50±110	-70±120	30±120
1.243	11370±50	-30±110	30±90	10±110
5.0	11600±40	-170±150	-10±140	180±110
12.5	12070±70	-420±130	-60±150	480±140
24.98	12930±30	-730±80	-10±80	750±60

At the lower shear rates the error bars are once again too large to determine any clear trend but at the higher shear

rates it can be seen that $P_{xx}(\dot{\gamma}) < P(\dot{\gamma})$, $P_{yy}(\dot{\gamma}) \simeq P(\dot{\gamma})$ and $P_{zz}(\dot{\gamma}) > P(\dot{\gamma})$. These normal pressure effects are well known in real systems and lead to a number of flow phenomena such as the Weissenberg effect and extrudate swell [98]. As the pressure is largely determined by the configuration of the molecules changes induced in it by the shear are the macroscopic manifestations of the underlying microscopic structural rearrangements.

3.9 Shear Induced Structural Changes

In MD the structure of fluid systems are generally characterised in terms of radial distribution functions (rdf's). For a diatomic molecule the most readily accessible are the site-site rdf, g(r), and the COM-COM rdf, G(R). At equilibrium these functions adequately describe the structure of a diatomic fluid because of its isotropic nature but under shear the strucure becomes neccessarily directional dependent so these rdf's tend to average out the structural changes. This is particularly true for the site-site rdfs, which are shown, along with the COM-COM rdfs, at a range of shear rates in figs.3.25 to 3.26. For the shear rates studied here there is no significant change in g(r) for either the l^*=1.Ø or the l^*=Ø.6Ø8 Cl_2. The peaks at r=1σ and 2σ are those due to nearest and next nearest neighbours in both cases but whereas the l^*=Ø.6Ø8 has an intermediate peak at ~1.6σ, corresponding to the second atom of a molecule whose other atom is in the

Figure 3.25 The radial distribution functions (rdf) for the COM, G(R), and the sites, g(r), l^*=0.608, (a) $\dot{\gamma}$=0.824*$10^{10}s^{-1}$, (b) $\dot{\gamma}$=1.25*$10^{10}s^{-1}$, (c) $\dot{\gamma}$=25*$10^{10}s^{-1}$, T~260K, P~1GPa.

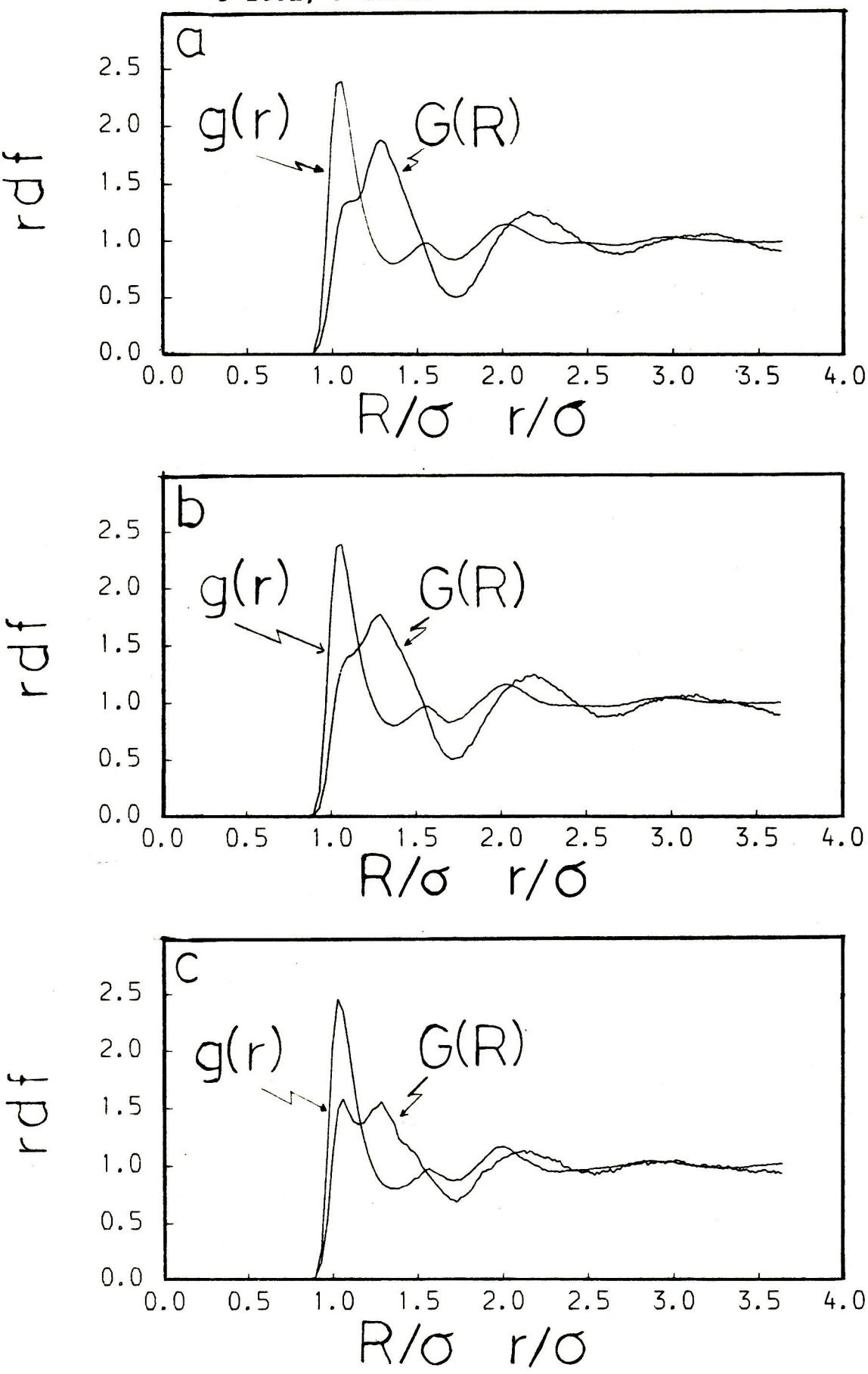

Figure 3.26 As fig.3.25 $l^{*}=1.0$, (a) $\dot{\gamma}=0.75*10^{10}s^{-1}$, (b) $\dot{\gamma}=5*10^{10}s^{-1}$, (c) $\dot{\gamma}=12.5*10^{10}s^{-1}$.

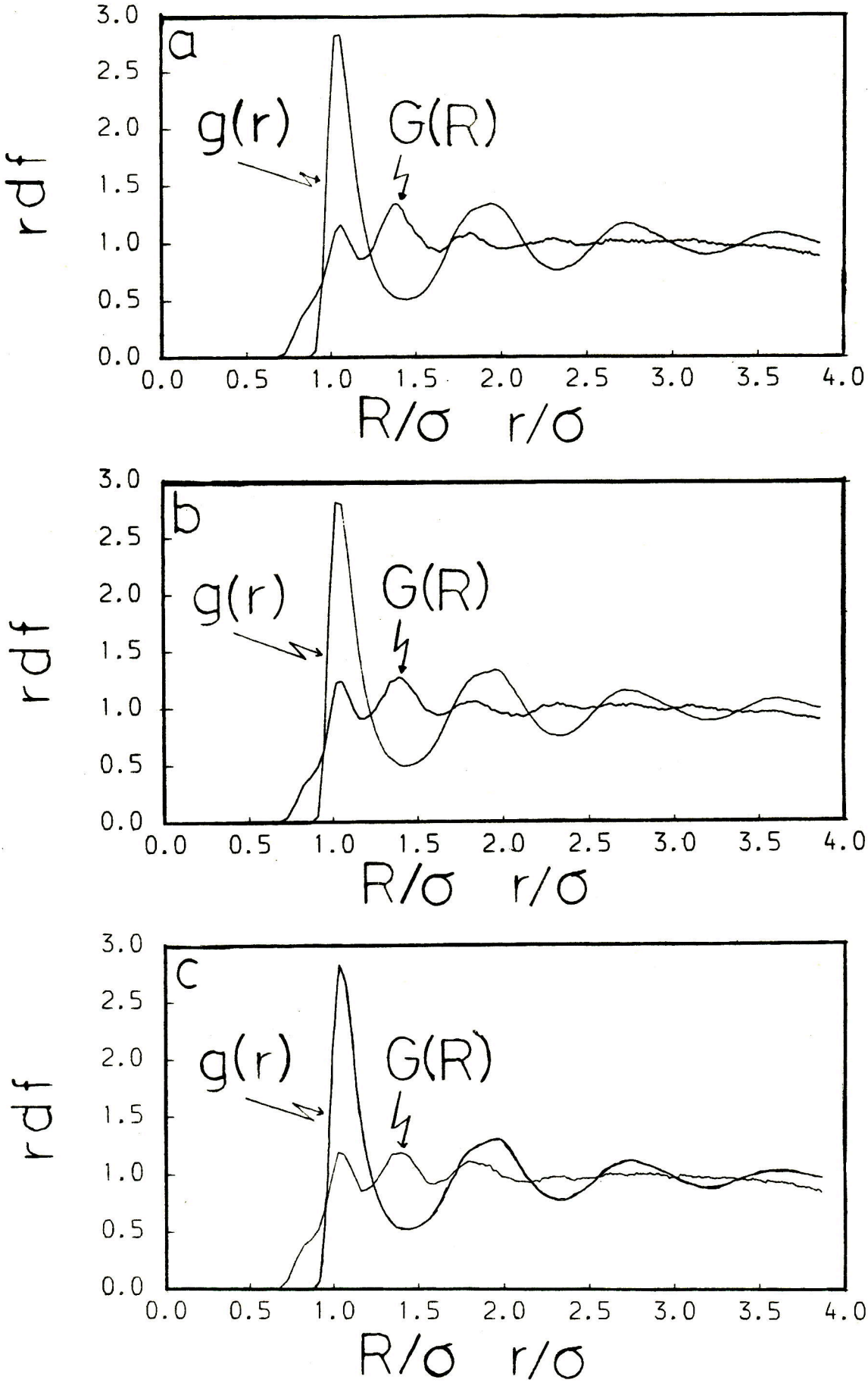

nearest neighbour shell, in the l^*=1.Ø case the bond length also corresponds to the next nearest neighbour distance so only one peak is observed.

For the COM rdf, G(R), noticeable changes do occur, as the shear rate is increased, in the nearest neighbour shell. The peaks in G(R) at ~1.3σ for l^*=Ø.6Ø8 and ~1.4σ for l^*=1.Ø and the first and second peaks in g(r) are consistent with pairs of molecules forming a 'T' configuration. It appears that this 'T' configuration becomes less preferred at higher shear rates, as is shown by its decreasing height in both systems, and is replaced by the parallel configuration which gives rise to a peak at ~1σ. This is particularly clearly shown in the l^*=Ø.6Ø8 case where at the lowest shear rate there is only a shoulder which develops into a peak at the highest shear rate. These changes are consistent with the observed increase in alignment and the increase in internal energy which occurs as the lower energy 'T' configurations are replaced by the higher energy parallel configurations.

3.10 Conclusions

From these initial studies a number of significant points have arisen concerning the methods implemented and the results observed. Firstly, it is clear that as a technique for elucidating the behaviour of fluids undergoing shear steady state HSNEMD is particularly useful providing us with detailed information at a molecular level regarding some well known laboratory observed phenomena. It is less successful at determining the zero shear rate viscosity as the degree of shear thinning increases making extrapolations difficult. Under favourable conditions, i.e. low density, it is still more efficient at determining $\eta(0)$ than either of the alternative Green-Kubo or perturbation methods.

It has been further shown that the perturbation technique is of very limited use. It does provide an alternative , if more expensive, route to the stress response function, which is a useful internal check, but neither it nor the EMD Green-Kubo method can economically provide a value for $\eta(0)$.

The results obtained for the diatomic fluids qualitatively reaffirm those found previously for other diatomic systems [60,70]. Shear thinning is found to be common even for these 'simple' liquids although it remains to be explained satisfactorily by an actual molecular theory. Of the available theories none can be said to be wholly

consistent with the available data. Observations of the behaviour of the internal energy and the pressure under shear confirm the previous findings [90] that in 'simple' liquids the pressure and the energy increase with shear rate apparently obeying a power law dependence in $\dot{\gamma}$ though, in the cases studied here, not the $\dot{\gamma}^{\frac{3}{2}}$ dependence of Kawasaki-Gunton theory reported previously. The reorientation of molecules that occurs under shear has been characterised by several different functions all of which give results which are consistent with a preferred alignment tending to be parallel to the axis of shear.

These initial efforts to investigate the effects of molecular anisotropy upon the rheological properties of fluids have produced some interesting, if not totally conclusive, results. Originally it was intended that by looking at two similar molecules of different lengths it could be established if a larger molecule was more or less viscous than a shorter one. In real liquids it is impossible to do this important experiment unambiguously as to study molecules of different anisotropy inevitably means studying molecules which differ in other respects also. However, because of the drastic effect of the increased bond length on the equation of state, and the known dependence of the viscosity thereupon, it is still not possible to do the desired experiment completely unambiguously even for these model liquids. Without any corresponding states prescription comparisons were carried out at the same

temperature and pressures. At a pressure close to atmospheric the initially unexpected result was obtained that a diatomic fluid comprising molecules of l^*=1.Ø was less viscous than one comprised of molecules of l^*=Ø.6Ø8. This drew attention to the importance of the density in relation to the viscosity. This was further substantiated by comparing the same two systems at an elevated pressure which revealed that their pressure dependences of viscosity were not comparable but, because of the differing compressibilities, their density dependences of viscosity were very similar. At the higher pressure it was also found that the two systems showed very similar shear induced changes in the pressure and the internal energy. This contrasted with the quite different $\eta(\dot{\gamma})$ behaviour which clearly showed the tendency for the more anisotropic system to shear thin to a larger extent. It could be that this difference in the degree of shear thinning could be correlated in the same way as the zero shear rate viscosity in that if the dependence of the degree of shear thinning was known as a function of density then it would be interesting to compare the respective coefficients for the two systems. Putting aside the fact that at present there is no universally accepted way of measuring the degree of shear thinning its variation with density, at constant temperature, remains largely unknown even for real systems. If such coefficients could be evaluated and turned out to be very similar for the molecules studied here it would suggest that the density was the overriding factor in determining the shear thinning

behaviour and not the anisotropy. One point to bear in mind is that at the higher shear rates the viscosity tends to a similar limit in each case. This suggests that the viscosity is to some extent dependent on the profile that the molecules present to the shear flow as this will, for the molecules used here, become more similar as the molecules align parallel to the axis of flow.

CHAPTER 4

ETHANE AND PROPANE RESULTS

4.1 Introduction

The method used so far, of changing the bond length of a diatomic molecule, to investigate the effect of anisotropy on the rheological properties of fluids has limited scope for development. To broaden comparison with experiment it was decided to study a series of molecules built up from different numbers of equivalent interaction sites. It has previously been shown by Ryckaert and Bellemans [123,124] that the n-alkane fluids butane and decane can be adequately simulated by representing CH_2 and CH_3 groups as one equivalent interaction site of equal mass, the n sites being held together by rigid C-C bonds and C-C-C bond angles. As hydrogen atoms were not specifically taken into account their main effect of hindering internal rotations was modelled by employing a dihedral angle potential. To prevent overlap sites separated by three or more intervening ones interacted through the same LJ 12-6 potential as used for the intermolecular interactions.

It was thus proposed that a study be made of a series of molecules resembling n-alkanes constructed in the fashion set out by Ryckaert and Bellemans [123]. It was not intended at the outset that any one of these model molecules would

reproduce accurately any of the properties of its real counterpart. To do this would involve much parameter fitting for each molecule which would be costly and self-defeating in that it would result in the loss of the basic similarity between the molecules.

To make some general comparisons with the work already done on diatomics it was decided the first two, non-spherical, rigid members of the series be studied initially with a view to extending the calculations to molecules with internal flexibility at a later stage. These first two members are the two centre model , or rigid diatomic, and three centre model, or rigid triatomic, which correspond to 'ethane' and 'propane'. In the next chapter results will be given for a six centre model incorporating internal degrees of freedom.

4.2 Ethane and Propane Models and Computational Details

To model 'propane' and 'ethane' the interaction potential, bond lengths, bond angles and masses were those used previously for n-alkanes [123]. The intermolecular site-site interaction potential takes the familiar Lennard-Jones 12-6 form with ϵ/k=84K and σ=3.92Å. The C-C bond length was in all cases 1.53Å and C-C-C bond angle was fixed at the tetrahedral angle of 109° 28' in propane. The mass of all sites was set to 14.15134 g/mol.

As ethane is modelled as a rigid diatomic the same methods , and hence the same programs, were used as for chlorine. For propane the addition of an extra site means that a different algorithm has to be used to integrate the equations of motion. In this case the method of quaternions [40] was used to integrate the rotational equations of motion using an algorithm due to Fincham [114], as described in section 2.8. A program was then written incorporating this algorithm to perform equilibrium molecular dynamics on a system of rigid triatomic molecules. The program was tested in the usual way on a sample of 108 propane molecules, initially arranged on a crystal lattice, modelled using the parameters given. In all the simulations reported here on propane the potential was truncated at half the box length and appropriate corrections were added to the virial and the potential energy. The timestep used was $0.4*10^{-14}s$ in all cases unless stated otherwise. For ethane a sample of 256 molecules was used throughout and the potential cutoff and timestep were as for the diatomics , namely 2.5σ and $0.8*10^{-14}s$ respectively.

4.3 Results at T~200K, P~0

To compare the two fluids equilibrium configurations were generated at a temperature of 200K close to the zero pressure isobar. The temperature chosen was fairly arbitrary but as it was intended to look at a series of molecules it was neccessary to use a temperature which would ensure that all the liquids were in the fluid regime yet not be too low that the relaxation times of the more complex fluids became too much of a problem. In the case of propane the desired state was achieved by interpolating and extrapolating from the pressure obtained at various densities. For ethane the constant pressure MD technique [120] was used to equilibrate a sample, initially in a crystal configuration, by setting the required pressure to zero and allowing the density to relax to a constant value. The reduced number densities resulting from these procedures were ρ^*=0.51846 and ρ^*=0.50052 for ethane and propane respectively. These densities were used in all subsequent calculations.

Having obtained equilibrium configurations the perturbation method was applied to determine the response of each system to a shear flow. The procedure was the same as that used on chlorine. Equilibrium trajectories were first obtained for a period of 0.8ps then the same initial configuration was mechanically perturbed using a delta function in shear rate with the trajectories then being

followed for the same amount of time. The initial configurations were thermalised at the start of each new segment by rescaling the momenta. In each case a total of ten segments were averaged together. The results for the equilibrium properties are given in table 4.1.

Table 4.1 The equilibrium properties of ethane and propane determined from the averages of ten runs of Ø.8ps at T~2ØØK.

	ρ^*	U/J mol^{-1}	Φ/J mol^{-1}	T/K	P/bar
Ethane	Ø.51846	-5Ø4Ø±8Ø	-917Ø±2Ø	198.9±3.1	-3Ø±4Ø
Propane	Ø.5ØØ52	-1434Ø±9Ø	-193ØØ±5Ø	199.Ø±2.4	12Ø±5Ø

From the table it can be seen that the addition of an extra interaction site effects the potential energy markedly. As the number of interactions per molecular pair is equal to n^2, where n is the number of sites per molecule, then empirically it would be expected that the ratio of the potential energies would be of order 9:4 or 2.25:1. This neglects the excluded volume effect from adding on the extra site, and the resultant structural changes, and any differences in number density. The actual ratio is ~2.1:1 which is remarkably close. The explanation for this is that with a bond length of 1.53Å and σ=3.92Å, effectively l^*=Ø.39, there is a large amount of overlap in these molecules between neighbouring sites so the increase in excluded volume going from ethane to propane is small, compared to the case of the

different bond length chlorine molecules. This effect must also account for the small differences in the zero pressure densities.

In figs.4.1→4.5 the equilibrium radial distribution functions are shown. In the case of ethane the COM G(R) and the site-site g(r) are given. For propane the site-site g(r) has been resolved into three components g_{AA}, g_{BB} and g_{AB} where A denotes an end site and B denotes a central site. In ethane the short bond length, $\emptyset.39\sigma$, results in a broad first peak in g(r) extending from $r\sim1.\emptyset\sigma$, the nearest neighbour separation, to 1.4σ which covers the range of possible values for r of the second atom of a molecule whose first atom is in the nearest neighbour shell. In chlorine this first peak was split indicating preferred orientations of molecules at close quarters. In ethane the shorter bond length and also the different conditions appear to result in no preferred alignment. This is also indicated by the G(R) which peaks at $\sim1.2\sigma$ the mid-point of the range $1.\emptyset\sigma$ to 1.4σ which corresponds to the minimum and maximum separation of the centres of mass of two molecules which have site-site interaction distances of 1σ.

In propane the overall site-site g(r) is very similar to that of ethane with peaks at $r=1.2\sigma$ and $r\sim2.3\sigma$ of heights ~1.4 and ~1.1 respectively. The resolution of g(r) into three components reveals that contributions to the first peak are

Figure 4.1 The radial distribution functions (rdf) for the COM, G(R), and the sites, g(r), ethane, T~200K.

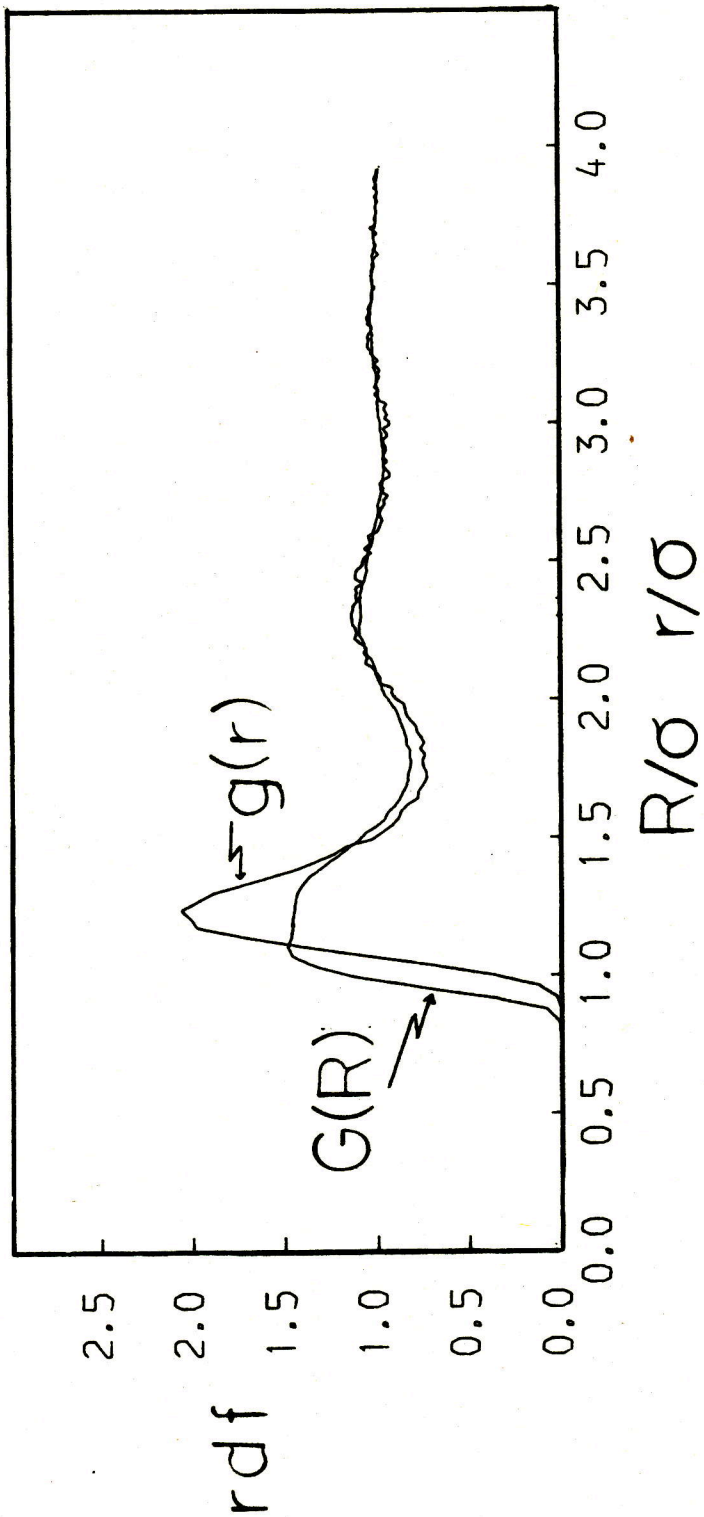

Figure 4.2 The site-site rdf, g(r), propane, T~200K.

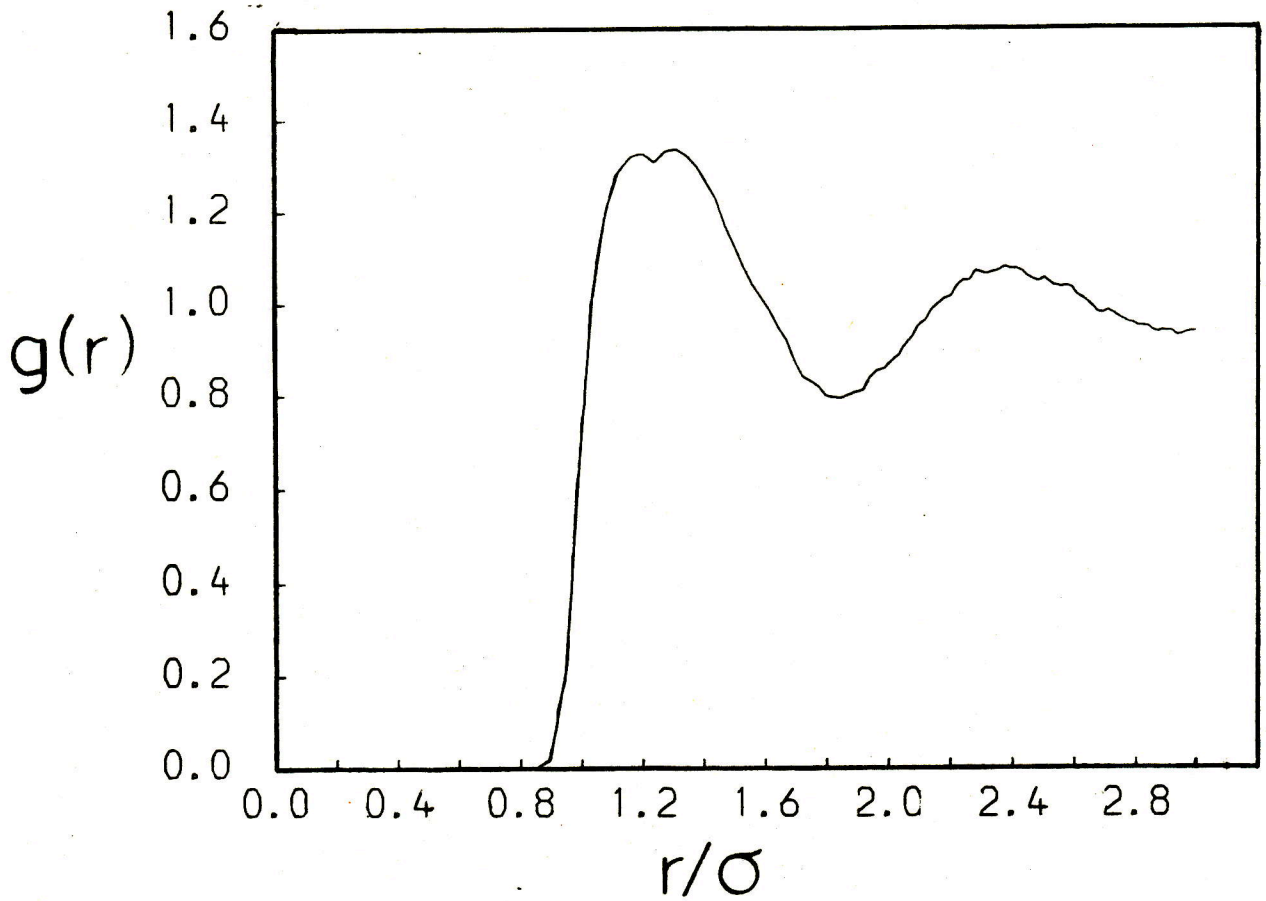

Figure 4.3 The end site-end site rdf, $g_{AA}(r)$, propane

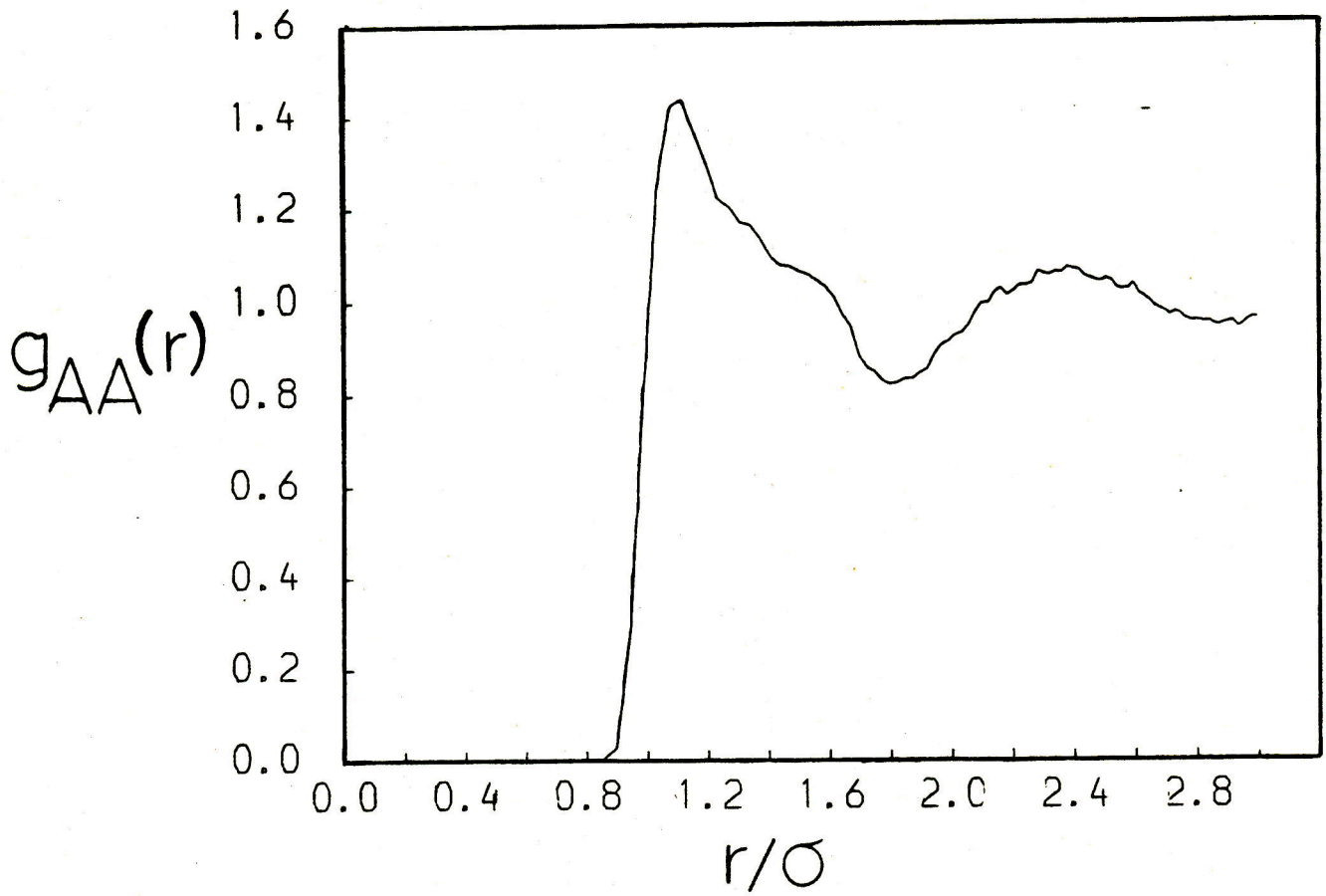

Figure 4.4 The end site-centre site rdf, $g_{AB}(r)$, propane.

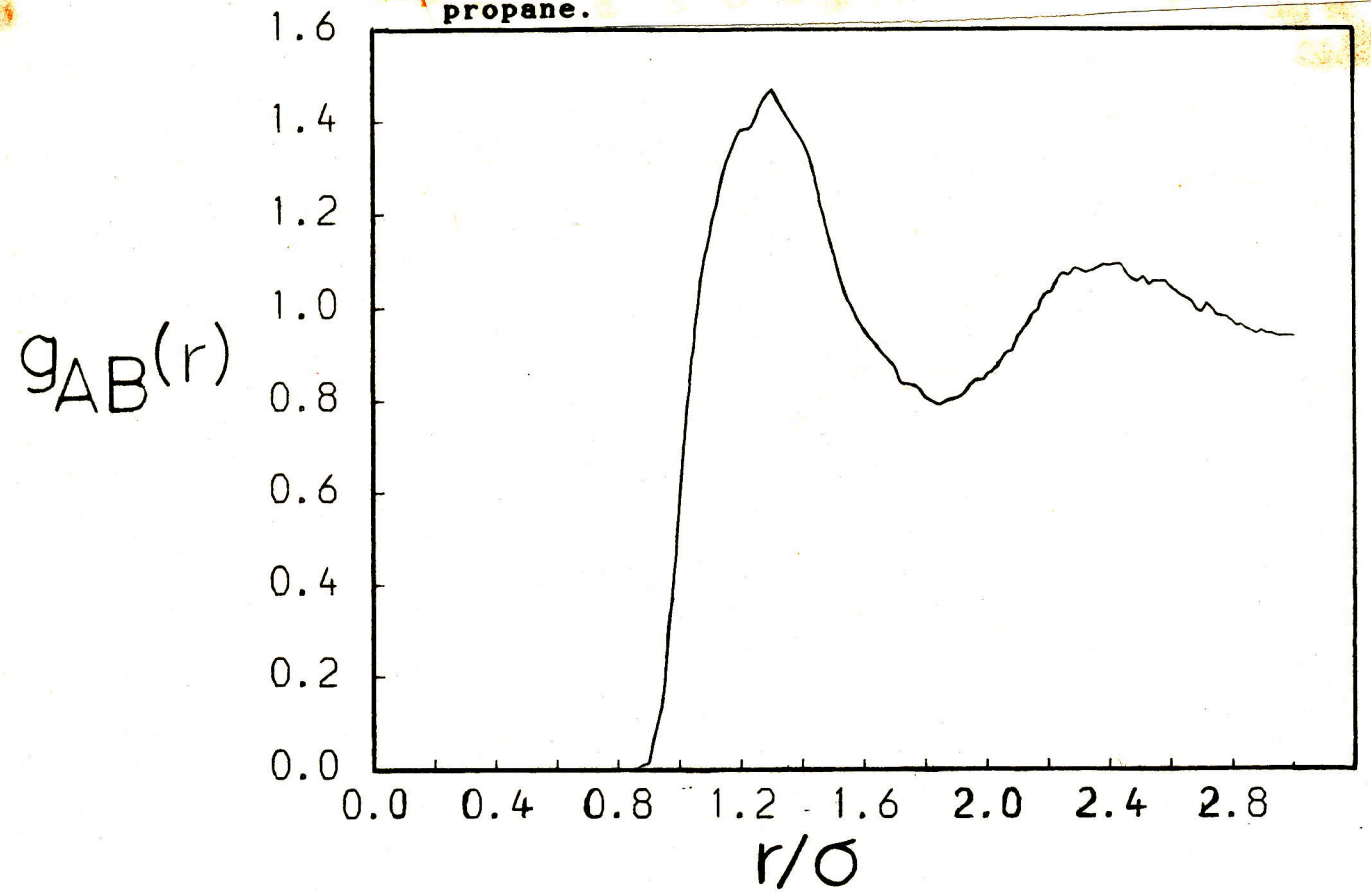

Figure 4.5 The centre site-centre site rdf, $g_{BB}(r)$, propane.

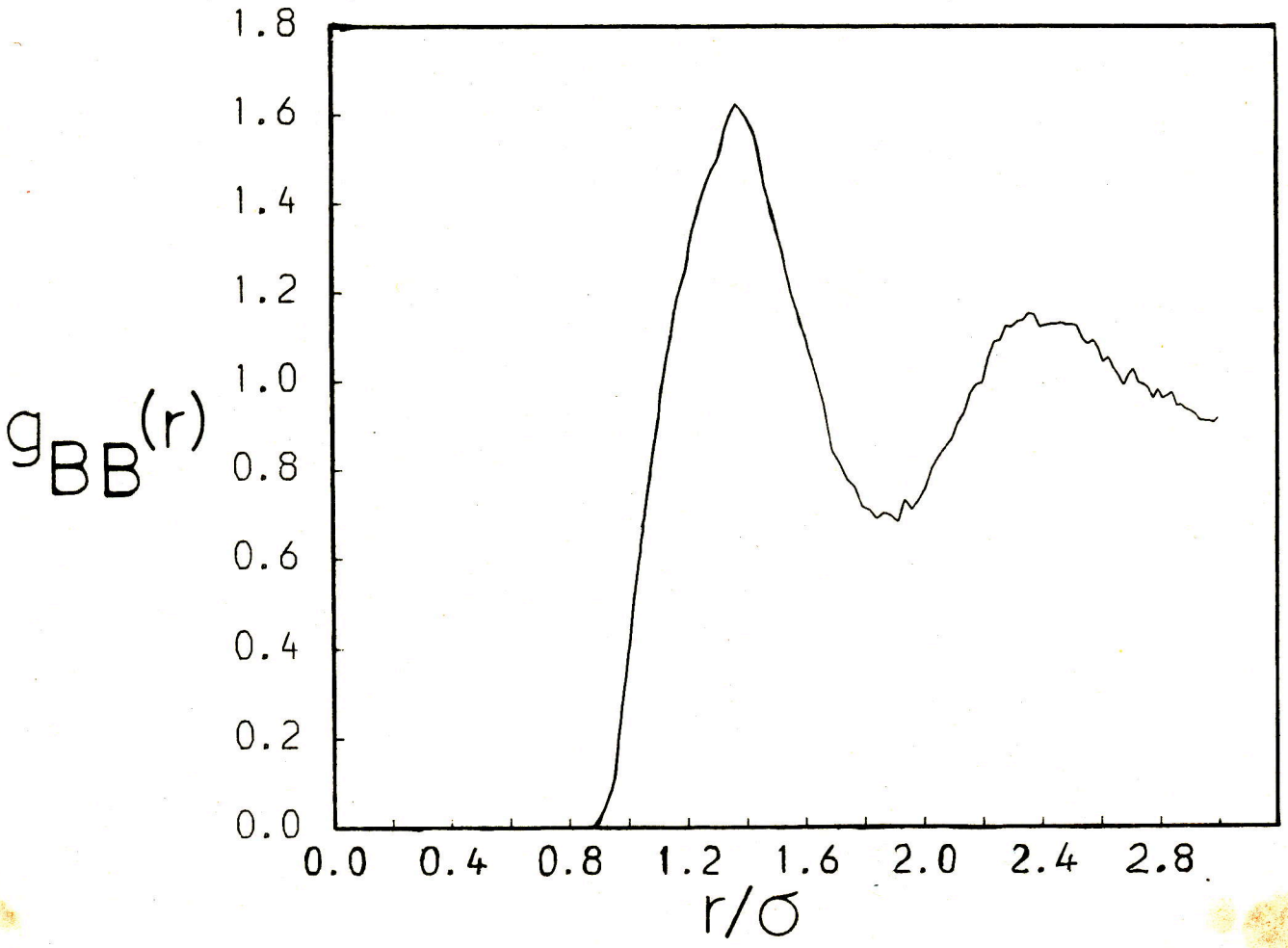

not the same from the various interactions. As there are four end-end interactions, type AA, and four end-centre interactions, type AB, and only one centre-centre interaction, type BB, per molecular pair

$$g(r) = (4g_{AA}(r) + g_{BB}(r) + 4g_{AB}(r))/9. \qquad (4.3.1)$$

As can be seen from figs.4.3 and 4.4 g_{AA} and g_{AB} differ in the region of the first peak, $g_{AA}(r)$ has a maximum at $r \sim 1.1\sigma$ whereas $g_{AB}(r)$ peaks at 1.3σ. This is a reasonable result because the large amount of overlap of the sites in a molecule means that the central site is 'shielded' from the sites of other molecules by the end atoms which are conversely more exposed. This is also shown by $g_{BB}(r)$ which is qualitatively similar to $g_{AB}(r)$ but has higher peaks and lower troughs indicating more order in the structure of central sites.

During the course of these equilibrium runs the mean squared displacements of the centres of mass were calculated and from these the diffusion coefficients were estimated to be $(9.7 \pm 1.0) * 10^{-9} m^2 s^{-1}$ and $(3.6 \pm 0.4) * 10^{-9} m^2 s^{-1}$ for ethane and propane respectively. Clearly the indication from this result is that, as the viscosity is generally considered to be inversely proportional to the diffusion coefficient, the added interaction centre will, as expected, increase the viscosity.

From the perturbation experiments the stress responses

were obtained and the off-diagonal components are shown , in their integrated form, in figs.4.6 and 4.7 for ethane and propane respectively. The significant components, $\Delta\sigma_{xz}(t)$, were fitted to the form

$$\frac{\Delta\sigma_{xz}(t)}{\Delta\dot{\gamma}} = \eta(1 - \exp(-t/\tau)) \qquad (4.3.2)$$

, where $\Delta\dot{\gamma}$ was the perturbation in shear rate and was equal to $125s^{-1}$ in both cases. The constants from these best fits, η, τ and $G_\infty=\eta/\tau$, are given in table 4.2.

Table 4.2 The best fit parameters for $\Delta\sigma_{xz}(t)/\Delta\dot{\gamma}$ fitted to the form given in eqn.4.3.2 for the results obtained from 10 perturbation runs of length 0.8ps on ethane and propane T~200K.

	η/mPa s	τ/ps	G_∞/GPa
ethane	0.08	0.11	0.74
propane	0.38	0.22	1.71

As before the noise that begins to affect the response , at ~0.4ps and beyond, makes the estimation of the viscosity from the curves themselves subject to large errors. The viscosities are accordingly quoted as 0.07±0.02mPa s and 0.32±0.06mPa s for ethane and propane respectively. These viscosities differ from those quoted in table 4.2. for which the viscosities and relaxation times have been treated as adjustable parameters to optimise the fit to a single

Figure 4.6 $\Delta\sigma_{\alpha\beta}(t)$ vs. t, ethane, T~200K.

Estimates of $\Delta\sigma_{xz}(\infty)$ $(=\eta(0)\Delta\dot{\gamma})$ are from the fits of the non-equilibrium data to the theories of Kawasaki-Gunton (- - - -) and RE and Hess (—·—·—).

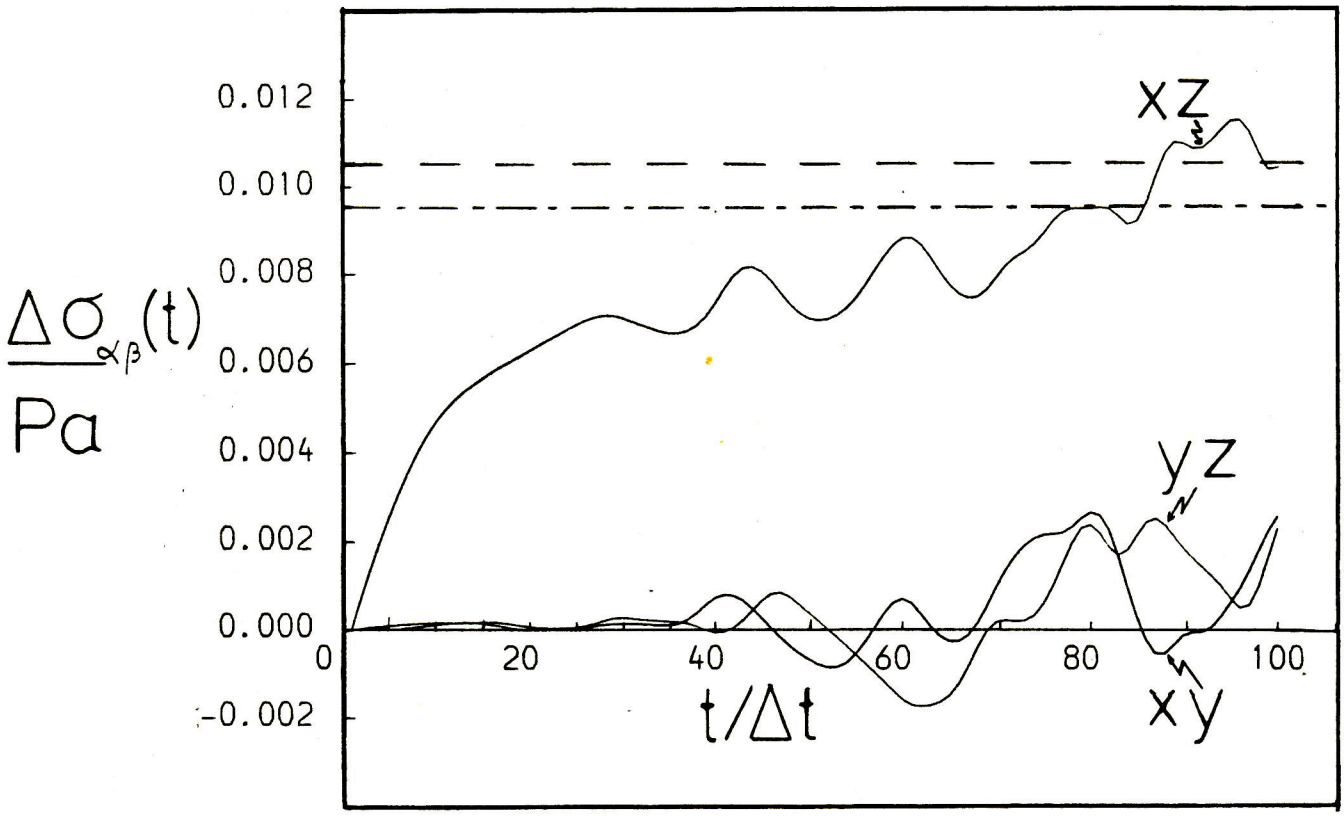

Figure 4.7 As fig.4.6 propane, T~200K.

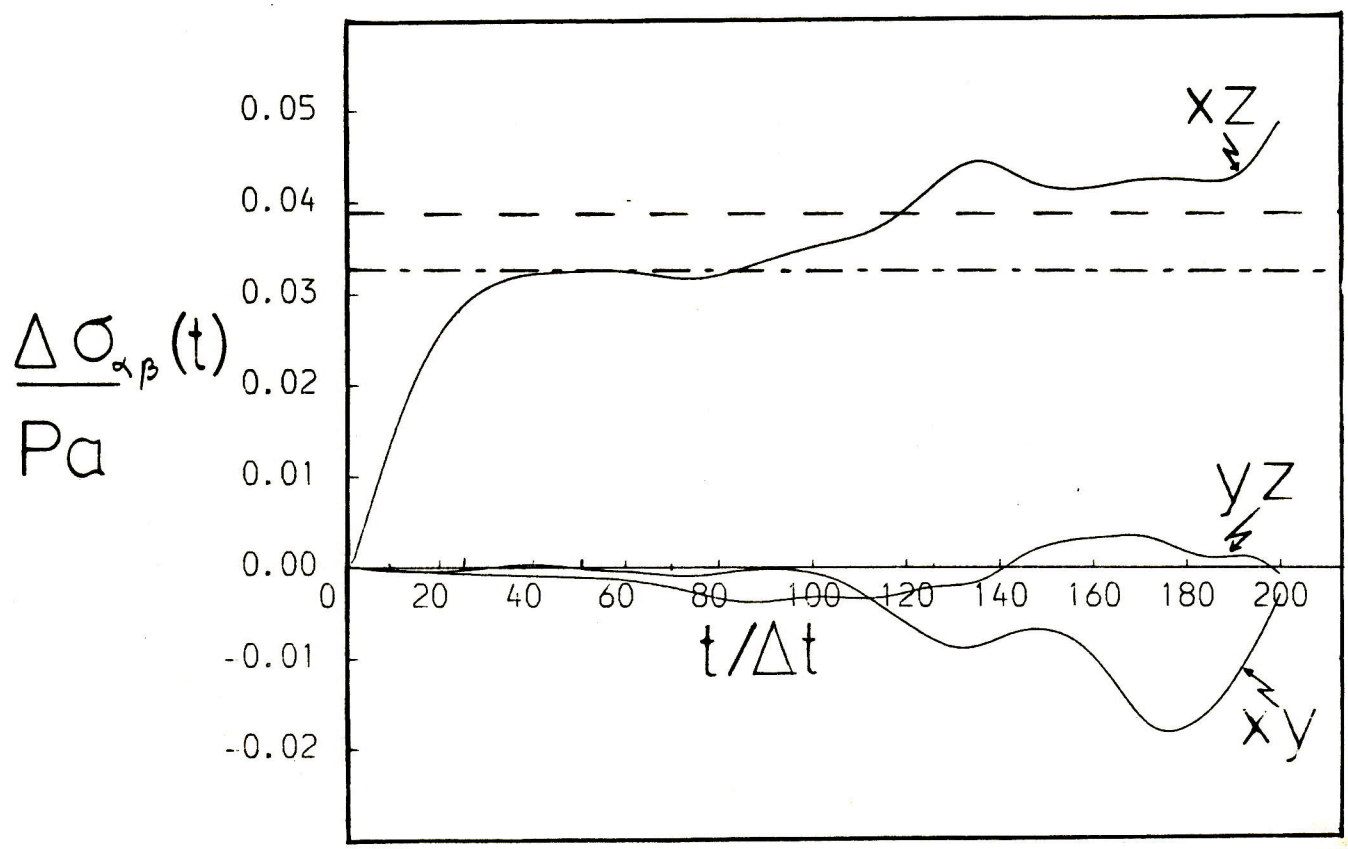

exponential. In fact these cannot be varied independently as their ratio, $\eta/\tau=G_\infty$, is fixed by the initial slope. As can be seen from figs.4.8 and 4.9 the single exponential is not a particular good fit to either response. It is significant, however, that the viscosity is substantially higher, G_∞ is larger and the relaxation time, τ, is longer for propane than for ethane.

In the case of propane the stress evaluated from the equilibrium runs was used to obtain the correlation function, $C_s(t)=\langle\sigma_{\alpha\beta}(0)\sigma_{\alpha\beta}(t)\rangle$, averages being taken over all three off-diagonal components. The correlation function and its integrand are shown in a normalised form in fig.4.10. The infinite frequency shear modulus, G_∞, evaluated from the mean squared stress, $G_\infty = V\langle\sigma^2_{\alpha\beta}(0)\rangle/kT$, was 1.74GPa which compares well with that calculated from the perturbation result. In theory the curves shown in figs.4.7 and 4.10, the integrated correlation function and the integrated response to a delta function, should be equivalent. The viscosity estimated from the integrand of the correlation function,

$$\eta(t) = \frac{V}{kT}\int_0^t C_s(t')\,dt' \quad ,$$

in the same time range as that estimated from the perturbation result, is 0.15 ± 0.03mPa s. This does not compare well with the previous result of $\eta=0.32\pm0.06$mPa s but in view of the known number dependence [77] of the viscosity evaluated from

Figure 4.8 Fit of $\Delta\sigma_{xz}(t)$ to single a exponential (- - -), ethane.

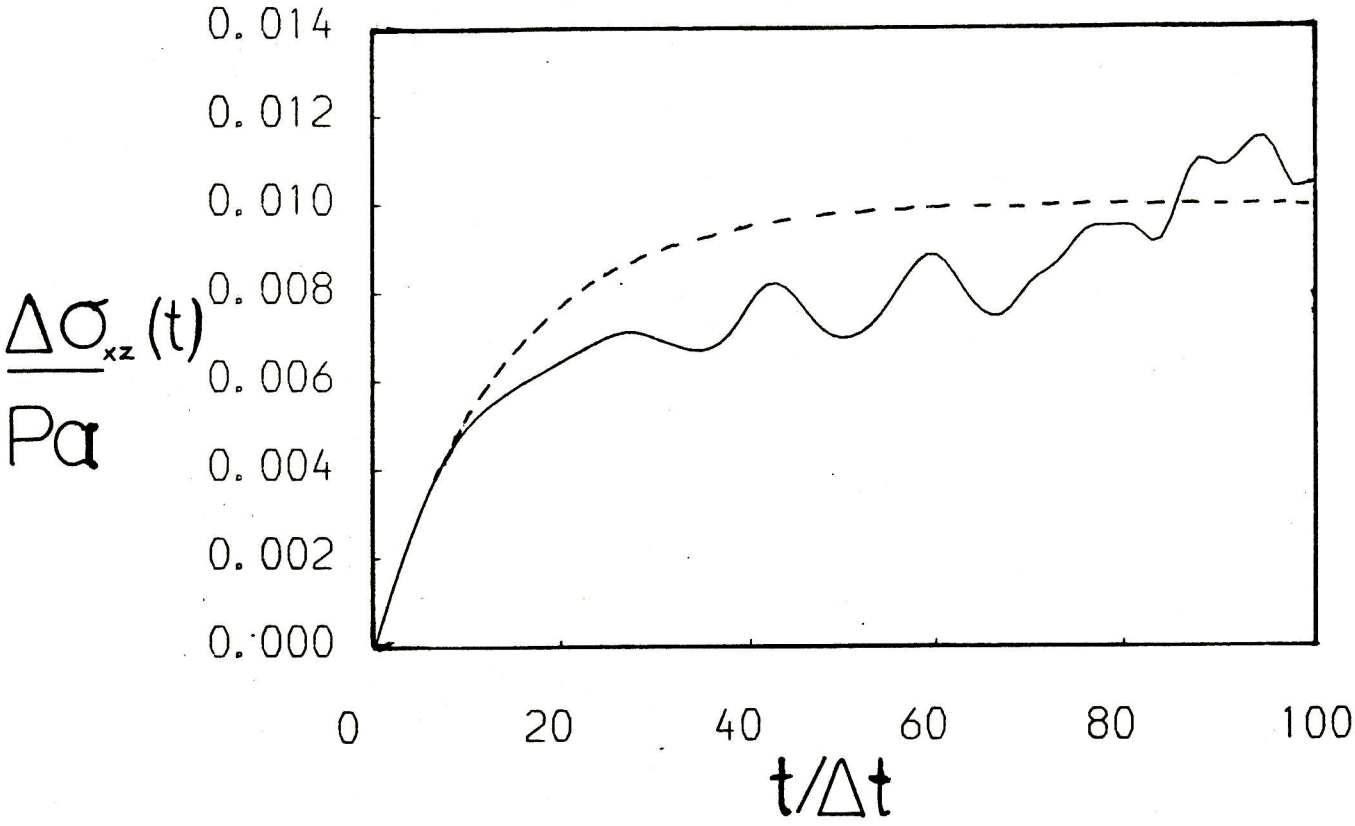

Figure 4.9 Fit of $\Delta\sigma_{xz}(t)$ to a single exponential (—+—), propane.

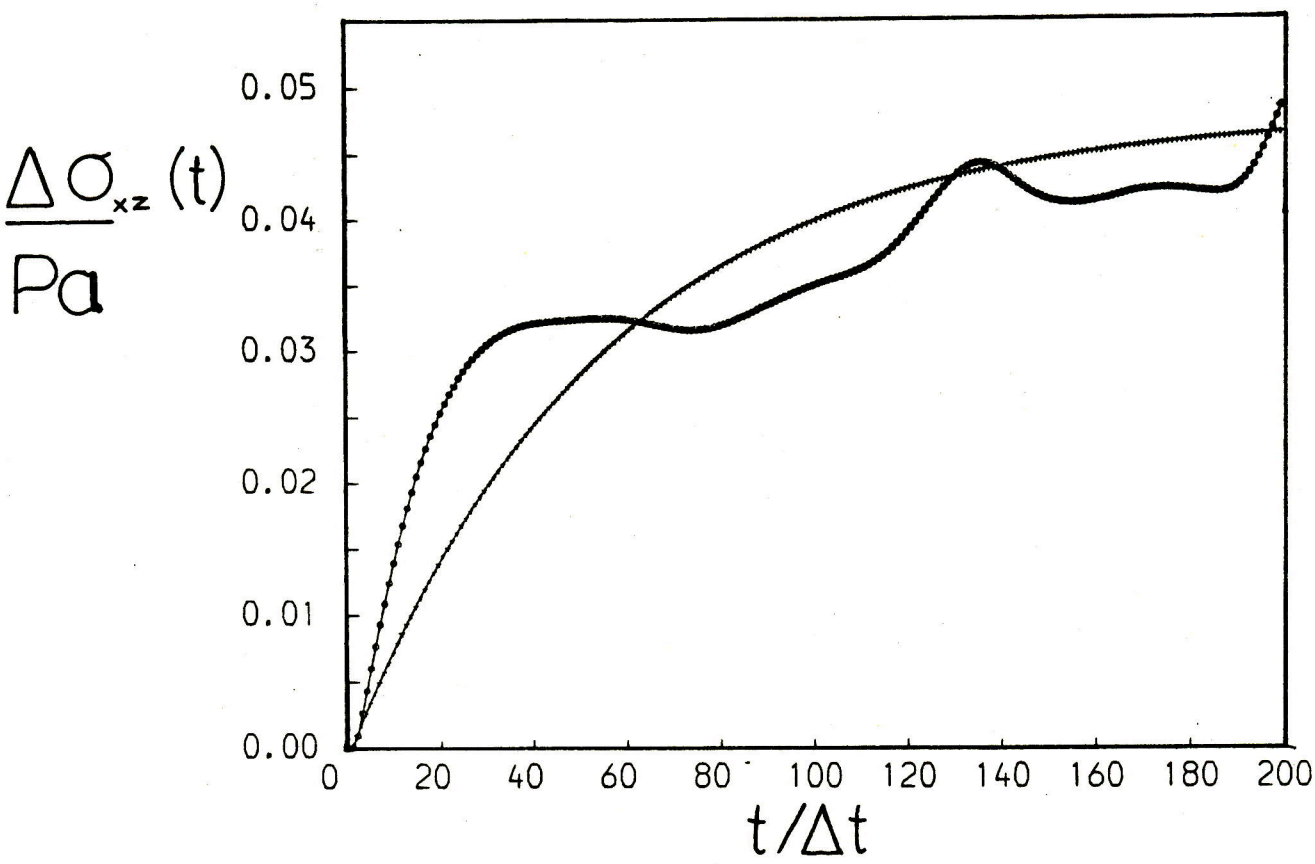

Figure 4.10 The normalized stress correlation function $\hat{C}_s(t)$ vs. t and its integrand, propane.

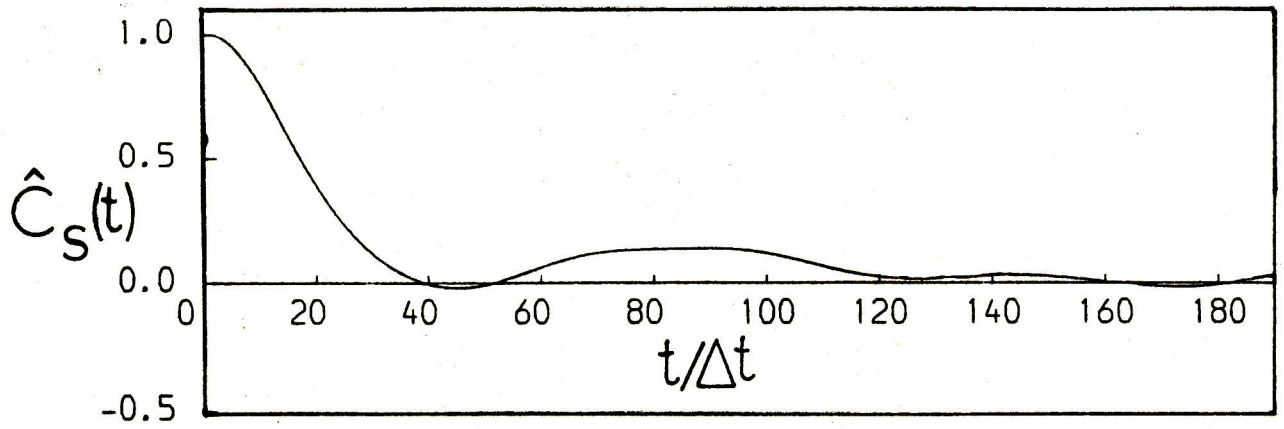

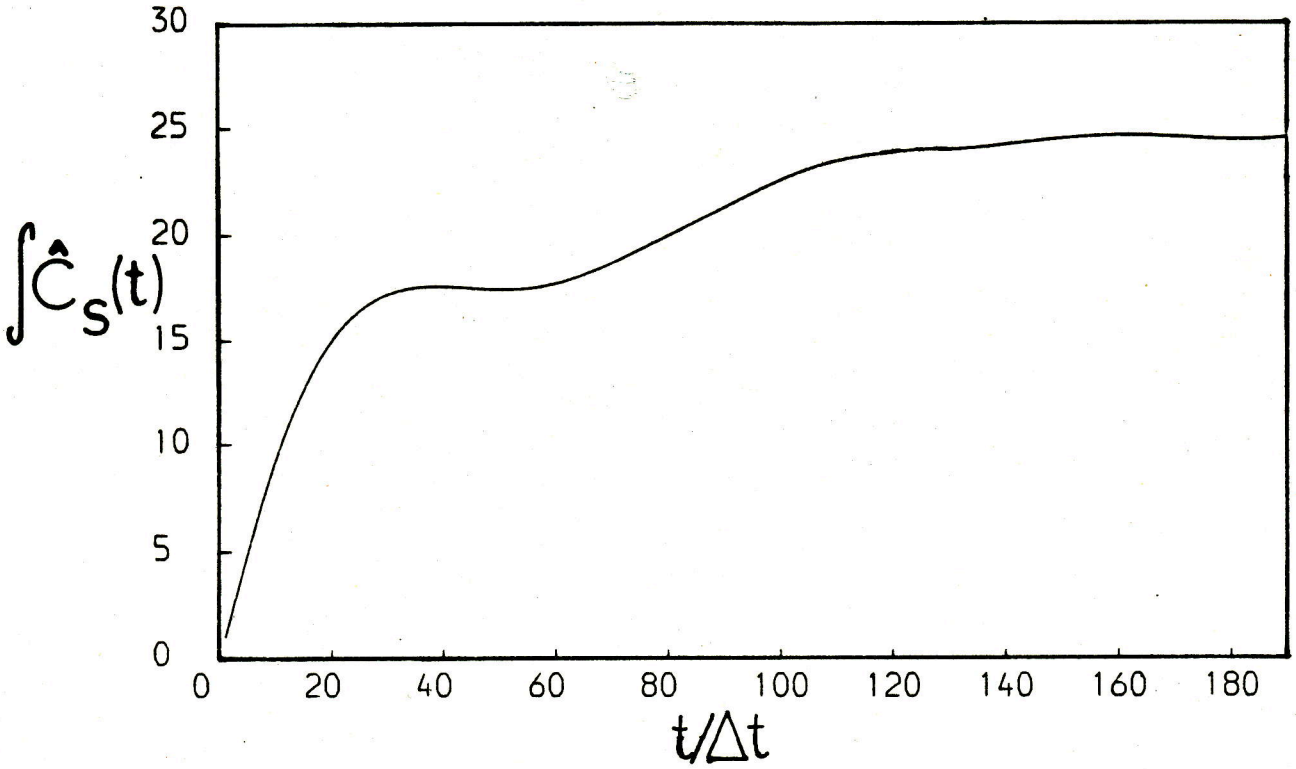

the correlation function approach this disparity is not unexpected.

As for the diatomics the response of the collective orientation tensor, $\underline{\underline{D}}$, to a perturbation in shear rate was also followed.

As ethane is modelled as a diatomic the response of the off-diagonal components, shown in their integrated form in fig.4.11, are qualitatively and quantitatively very similar to those found for the chlorine systems at T~260K, P~0.

Unlike ethane propane has three distinct axes of symmetry which are termed $\hat{\underline{X}}_p$, $\hat{\underline{Y}}_p$ and $\hat{\underline{Z}}_p$ and are illustrated in fig.4.12. These axes ensure that the moment of inertia tensor is diagonal and are used in the quaternion algorithm to specify the position of the constituent atoms relative to the COM, as in these body fixed axes the coordinates of the atoms remain the same. It is thus possible to specify three different collective orientation tensors of the form

$$\underline{\underline{D}}^{\alpha} = \frac{1}{N}\sum_{i=1}^{N} \underline{\alpha}_p\underline{\alpha}_p \qquad \text{for } \alpha=X,Y,Z \qquad (4.3.3)$$

and in turn observe their response, $\Delta\underline{\underline{D}}^{\alpha}(t)$, to a perturbation. It must be noted that these three tensors are not independent as at all times the following expression must be true

Figure 4.11 $\Delta D_{\alpha\beta}(t)$ vs. t, ethane.

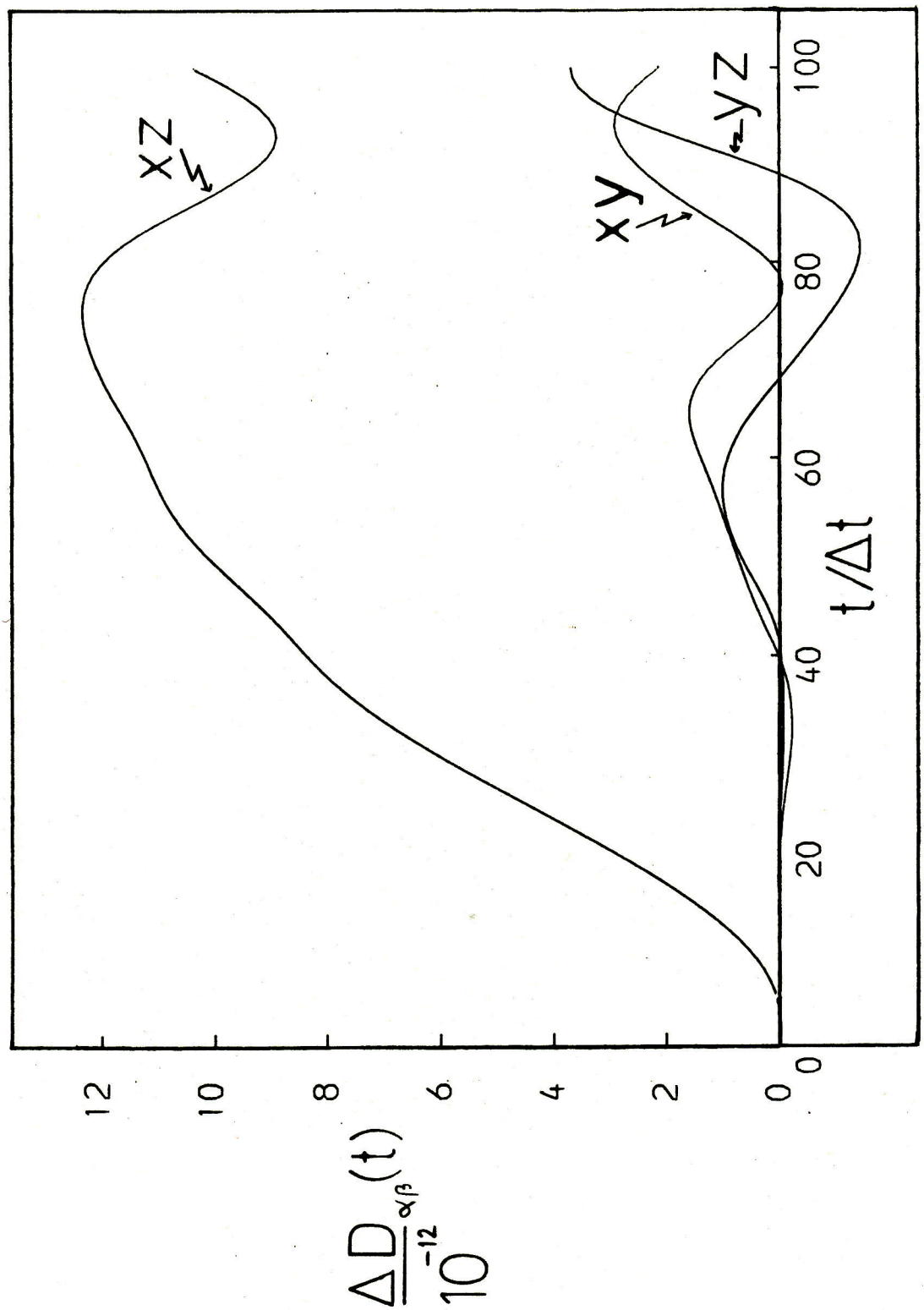

Figure 4.12 The principal axis vectors in the propane model.

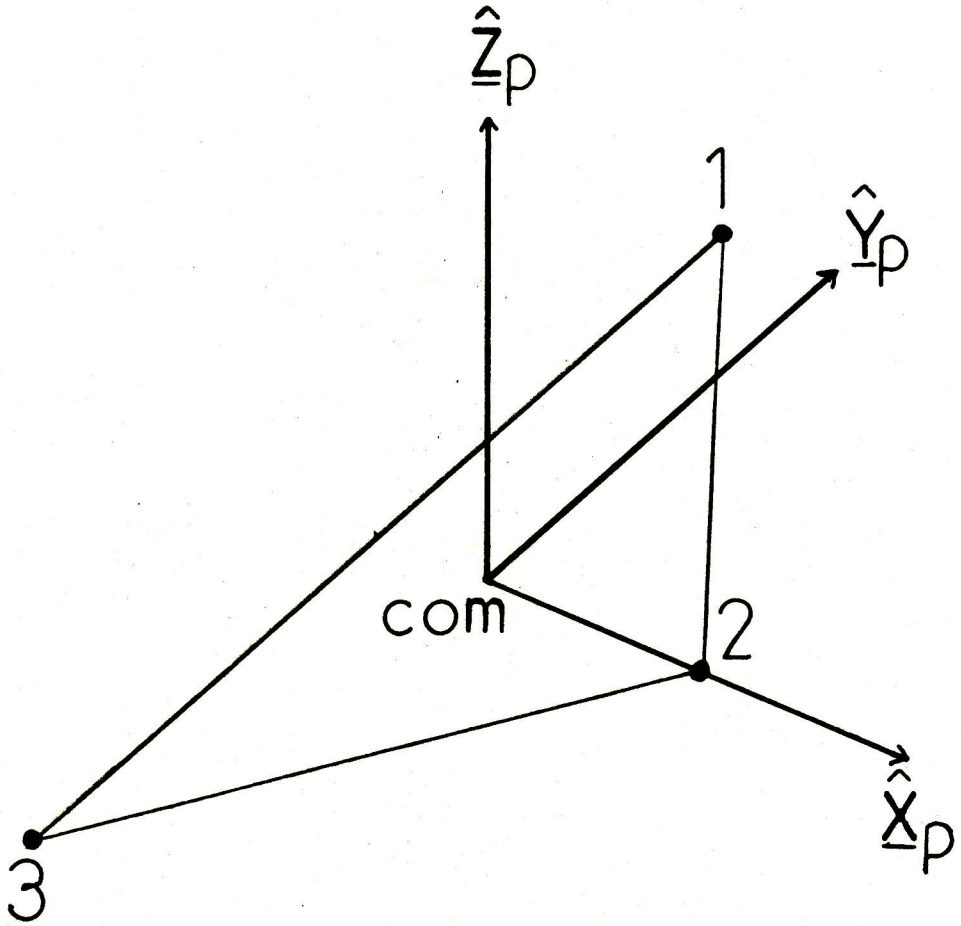

Figure. 4.13 $\Delta D_{\alpha\beta}(t)$ vs. t, for the three principal axes vectors of propane.

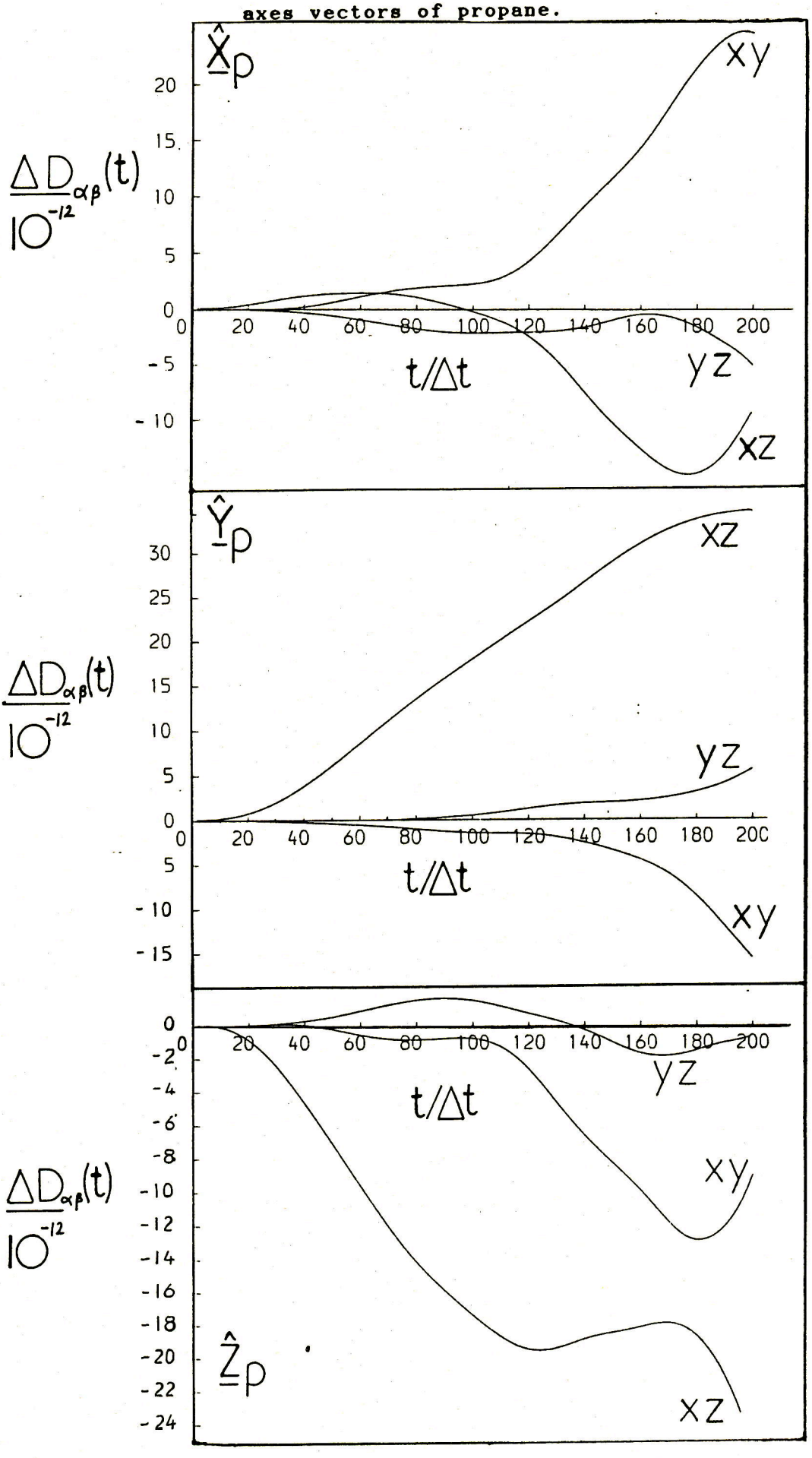

$$\underline{\underline{D}}^X + \underline{\underline{D}}^Y + \underline{\underline{D}}^Z - \underline{\underline{1}} = 0 \qquad (4.3.4)$$

The off-diagonal components of the $\Delta\underline{\underline{D}}^{\alpha}(t)$ are shown in fig.4.13.

For the $\Delta D^X_{\alpha\beta}(t)$ it is not clear whether there is any response at all. $\Delta D^X_{xz}(t)$ changes slightly initially but it is likely that the changes occuring beyond ~100Δt are due to noise. For the second axis, $\hat{\underline{Y}}_p$, $\Delta D^Y_{xz}(t)$ shows a similar change as the long axis of a diatomic. This is understandable as $\hat{\underline{Y}}_p$ is effectively the long axis of the molecule. In contrast $\Delta D^Z_{xz}(t)$ shows a negative change indicating alignment in the -ve quadrant of the plane of shear. Clearly if one of the principal axes is realigning in the shear plane then it follows that at least one of the other axes must also be changing. What is interesting is that it is mainly $\hat{\underline{Z}}_p$ which is realigning which indicates that the preferred orientation of the plane of the molecule is perpendicular to the plane of shear. Of the two axes, $\hat{\underline{X}}_p$ and $\hat{\underline{Z}}_p$, $\hat{\underline{X}}_p$ is the 'longer' so it might be expected that it would align in the XZ plane to minimise the profile the molecule presents to the direction of shear flow. These results suggest this is not the case.

As for the diatomics steady state homogeneous shear simulations were performed at a number of shear rates and the main results are given in tables 4.3, 4.4 and 4.5.

Table 4.3 The mean thermodynamic properties obtained from steady state shear calculations on the ethane and propane systems at T~200K.

Ethane

$\dot{\gamma}/10^{10}s^{-1}$	$U/J\ mol^{-1}$	$\Phi/J\ mol^{-1}$	T/K	P/bar	Length of run /ps
12.5	-4970±10	-9130±10	200.1±0.1	6±8	72
25.0	-4970±10	-9130±10	200.1±0.1	13±7	88
50.0	-4880±20	-9060±10	201.2±0.3	64±6	48
100.0	-4720±10	-8910±10	201.7±0.1	214±4	24

Propane

$\dot{\gamma}/10^{10}s^{-1}$	$U/J\ mol^{-1}$	$\Phi/J\ mol^{-1}$	T/K	P/bar	Length of run /ps
10.0	-14270±20	-19260±20	200.1±0.1	150±27	128
15.0	-14240±20	-19230±20	200.2±0.1	184±18	136
25.0	-14140±10	-19140±10	200.4±0.2	291±7	40
50.0	-13890±30	-18930±30	202.4±0.1	513±36	56
100.0	-13200±50	-18300±40	204.5±0.1	1061±43	64

Table 4.4 The mean shear stress, resultant shear rate dependent viscosity and mean normal pressure components from the steady state calculations on ethane and propane at T~200K.

Ethane

$\dot{\gamma}/10^{10}s^{-1}$	σ_{xz}/bar	$\eta(\dot{\gamma})$/mPa s	P_{xx}/bar	P_{yy}/bar	P_{zz}/bar
12.5	95±9	0.076±0.007	3±19	8±11	6±10
25.0	194±4	0.078±0.002	11±11	2±10	28±12
50.0	366±9	0.073±0.002	95±12	19±13	78±13
100.0	646±5	0.065±0.001	261±7	114±8	271±10

Propane

$\dot{\gamma}/10^{10}s^{-1}$	σ_{xz}/bar	$\eta(\dot{\gamma})$/mPa s	P_{xx}/bar	P_{yy}/bar	P_{zz}/bar
10.0	269±33	0.269±0.033	146±36	146±45	158±34
15.0	373±25	0.249±0.017	172±34	169±31	212±36
25.0	570±10	0.228±0.004	303±39	227±19	341±15
50.0	979±29	0.196±0.006	636±26	286±60	616±57
100.0	1593±38	0.159±0.004	1033±43	808±59	1342±69

Table 4.5 The mean significant components of the alignment tensor obtained from the steady state shear calculations on ethane and propane at T~200K.

Ethane

$\dot{\gamma}/10^{10}s^{-1}$	D_{xz}	$D_{xx}-1/3$	$D_{yy}-1/3$	$D_{zz}-1/3$
12.5	0.012±0.003	0.002±0.003	-0.003±0.004	0.001±0.002
25.0	0.024±0.002	0.002±0.003	-0.000±0.004	-0.001±0.003
50.0	0.043±0.001	0.007±0.003	-0.006±0.003	-0.001±0.004
100.0	0.068±0.001	0.018±0.001	-0.012±0.002	-0.006±0.002

Propane

X-axis

$\dot{\gamma}/10^{10}s^{-1}$	D_{xz}	$D_{xx}-1/3$	$D_{yy}-1/3$	$D_{zz}-1/3$
10.0	-0.013±0.006	-0.002±0.004	0.003±0.005	-0.001±0.005
15.0	-0.017±0.004	-0.004±0.004	0.008±0.005	-0.004±0.005
25.0	-0.024±0.005	-0.016±0.007	0.015±0.006	0.001±0.003
50.0	-0.025±0.004	-0.028±0.005	0.031±0.005	-0.002±0.005
100.0	-0.026±0.005	-0.048±0.003	0.048±0.004	0.000±0.003

Y-axis

$\dot{\gamma}/10^{10}s^{-1}$	D_{xz}	$D_{xx}-1/3$	$D_{yy}-1/3$	$D_{zz}-1/3$
10.0	0.056±0.007	0.004±0.006	-0.004±0.011	-0.001±0.008
15.0	0.071±0.006	0.010±0.007	-0.011±0.009	0.000±0.008
25.0	0.105±0.005	0.030±0.010	-0.014±0.008	-0.016±0.004
50.0	0.140±0.007	0.046±0.009	-0.014±0.006	-0.032±0.006
100.0	0.150±0.006	0.078±0.007	-0.033±0.008	-0.045±0.007

Z-axis

$\dot{\gamma}/10^{10}s^{-1}$	D_{xz}	$D_{xx}-1/3$	$D_{yy}-1/3$	$D_{zz}-1/3$
10.0	-0.043±0.005	-0.002±0.005	0.000±0.007	0.002±0.006
15.0	-0.054±0.005	-0.006±0.005	0.002±0.006	0.004±0.006
25.0	-0.081±0.006	-0.014±0.004	-0.001±0.005	0.016±0.005
50.0	-0.115±0.004	-0.017±0.007	-0.017±0.007	0.034±0.005
100.0	-0.124±0.004	-0.029±0.006	-0.015±0.006	0.044±0.006

4.4 The Shear Rate Dependence of the Viscosity

The shear rate dependent viscosities, plotted in figs.4.14 as a function of $\dot{\gamma}^{\frac{1}{2}}$, obtained are of the same order as those estimated from the perturbation technique. This indicates that the stress relaxes rapidly in these two systems at the state points used. It is also clear that propane is at least three times more viscous than ethane and also shear thins to a larger extent. Indeed ethane only noticeably shows non-linear behaviour at the highest shear rate, $10^{12}s^{-1}$. The $\eta(\dot{\gamma})$ data has again been fitted to the three functional forms predicted by the theories of Ree-Eyring(RE), Hess and Kawasaki-Gunton (KG) as described in section 3.5. The best fit parameters and root mean square differences are given in table 4.6 and the curves are shown in figs.4.15 and 4.16.

Figure 4.14 $\eta(\dot{\gamma})$ vs. $\dot{\gamma}^{1/2}$, ethane (□) and propane (Δ).

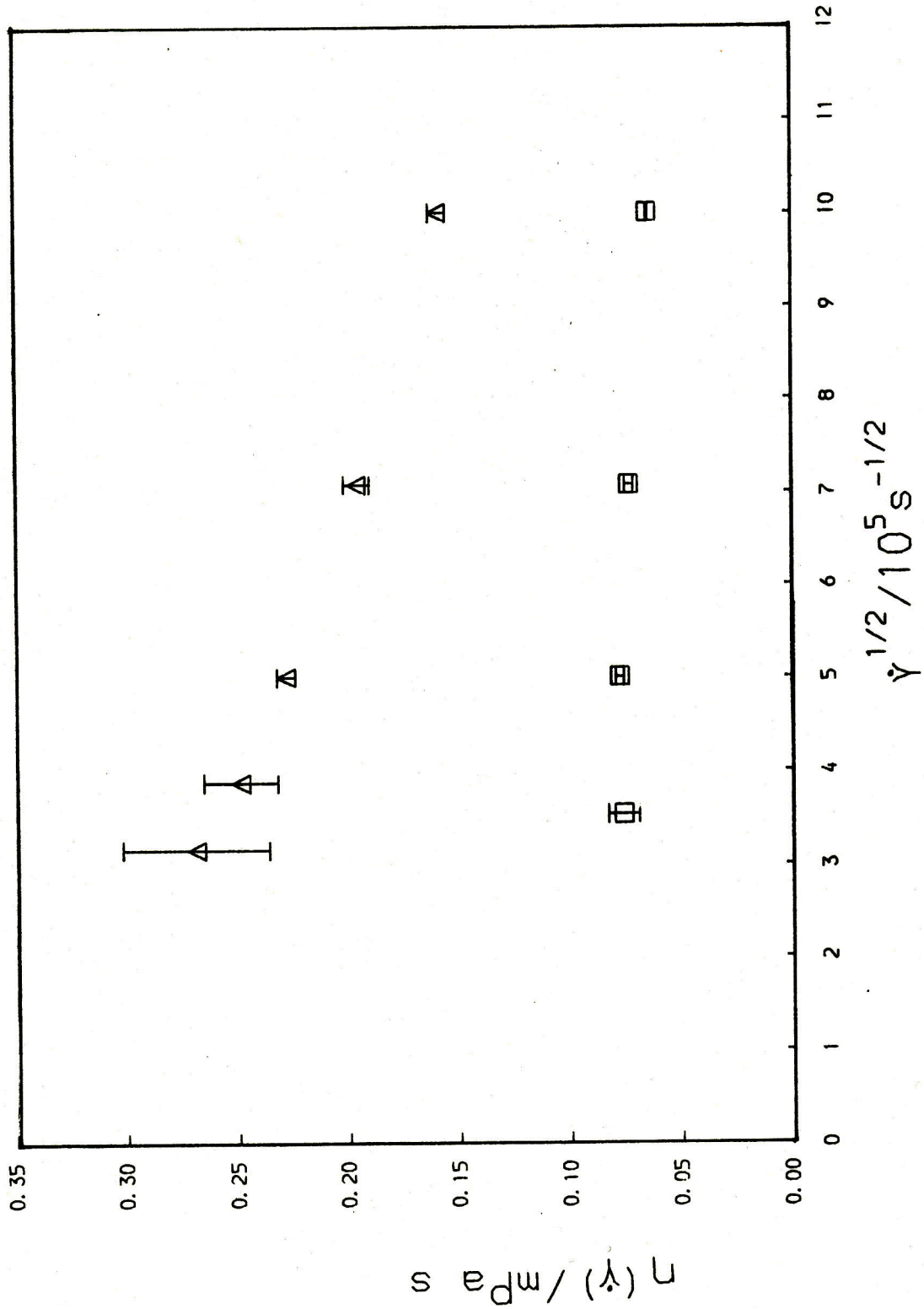

Figure 4.15 $\eta(\dot{\gamma})$ vs. $\dot{\gamma}^{1/2}$, ethane (Δ). Fit to the predictions of the theories of Hess (——), Ree-Eyring (- - -) and Kawasaki-Gunton (—·—·—).

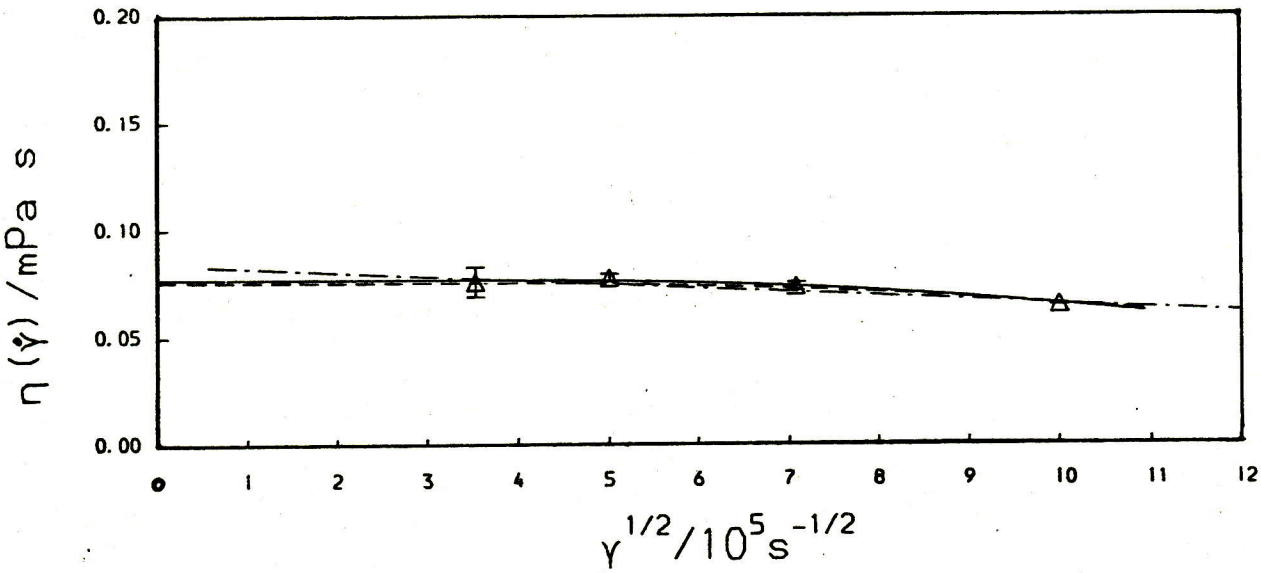

Figure 4.16 As fig 4.15 for propane.

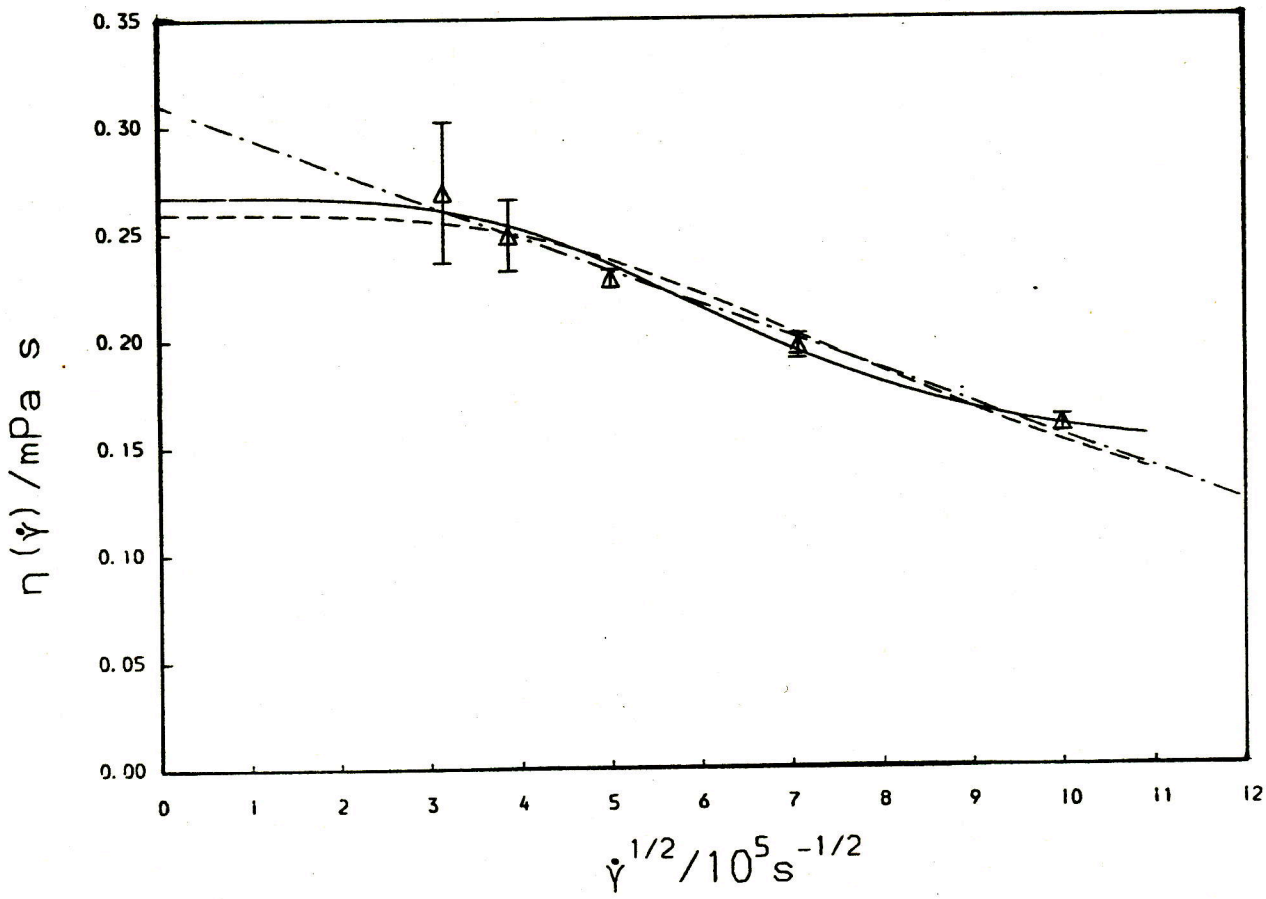

Table 4.6 The best fit parameters and root mean square differences (RMSD) for various predicted $\eta(\dot{\gamma})$ dependences for ethane and propane at T~200K.

		Ethane	Propane
Hess	$\eta(0)$/mPa s	0.077	0.267
	τ_h/ps	0.603	2.307
	k	0.600	0.482
	RMSD/mPa s	0.001	0.005
KG	$\eta(0)$/mPa s	0.085	0.311
	A/10^{-5}mPa $s^{\frac{3}{2}}$	0.192	1.562
	RMSD/mPa s	0.002	0.005
RE	$\eta(0)$/mPa s	0.077	0.260
	τ_r/ps	1.115	3.241
	RMSD/mPa s	0.001	0.009

For ethane the lack of shear thinning means that all the forms give reasonable fits and the zero shear rate viscosity can be quoted, with some confidence, as $\eta(0)=0.081\pm0.004$mPa s compared to the rather uncertain value of $\eta(0)=0.07\pm0.02$mPa s obtained from the perturbation experiments. Propane shows significant shear thinning and consequentially a notable difference in the estimates for $\eta(0)$. The RE and Hess curves give $\eta(0)$'s in the range 0.26→0.27mPa s, the KG fit gives a

higher $\eta(0)$ of ~0.31mPa s. These also compare well with the estimation from the perturbation method of $\eta(0)=0.32\pm0.06$mPa s although an $\eta(0)$ of 0.26mPa s would imply that there is no long time relaxation in the stress response function as it means that the plateau value, $\Delta\sigma_{xz}(\infty) = \eta(0)\Delta\dot{\gamma}$, in the perturbation experiment should be ~0.0325Pa which corresponds to the apparent plateau reached by $\Delta\sigma_{xz}(t)$ in ~0.2ps, see fig.4.7. As for chlorine none of the functional forms does outstandingly well at predicting the shape of the $\eta(\dot{\gamma})$ vs. $\dot{\gamma}$ curve in that there appears to be a systematic, rather than random, deviation of the data points from all the curves. In terms of the root mean square differences the KG and Hess fits are statistically better than the RE fit.

The apparent underestimation of the viscosity by the RE and Hess functions is probably a result of the range of shear rates used. Further data at lower shear rates would probably bring all three estimates for $\eta(0)$ closer but as lowering the shear rate inevitably causes more uncertainty in the results for $\eta(\dot{\gamma})$ it was not considered profitable to obtain this information.

4.5 Shear Induced Alignment

As ethane is modelled as a diatomic it is not surprising that qualitatively the behaviour of the orientation tensor under shear is the same as for chlorine. The magnitude is somewhat less reflecting the effect of the shorter bond length and the lower density. The values of the shear orientation parameter, $\chi_d(\dot{\gamma}) = D_{xz}(\dot{\gamma})/\dot{\gamma}$, are given together with those for propane in table 4.7.

Table 4.7 The shear orientation parameters determined from the steady state shear calculations on ethane and propane at T~200K.

Ethane

$\dot{\gamma}/10^{10}s^{-1}$	$\chi_d(\dot{\gamma})$ /ps
12.5	0.095±0.022
25.0	0.094±0.007
50.0	0.086±0.002
100.0	0.068±0.001

Propane

	X-axis	Y-axis	Z-axis
$\dot{\gamma}/10^{10}s^{-1}$	$\chi_d(\dot{\gamma})$ /ps	$\chi_d(\dot{\gamma})$ /ps	$\chi_d(\dot{\gamma})$ /ps
10.0	-0.131±0.056	0.558±0.073	-0.427±0.047
15.0	-0.115±0.023	0.474±0.039	-0.358±0.031
25.0	-0.096±0.020	0.418±0.018	-0.323±0.024
50.0	-0.051±0.009	0.280±0.013	-0.230±0.008
100.0	-0.026±0.005	0.150±0.006	-0.124±0.004

$x_d(\dot{\gamma})$ is plotted in fig.4.17 as a function of $\dot{\gamma}^{\frac{1}{2}}$ and a linear extrapolation to $\dot{\gamma}=0$ gives a value for $x_d(0)$ of ~0.11ps. Multiplying $x_d(0)$ by the magnitude of the shear rate ($125s^{-1}$) used in the perturbation experiments gives as an estimate for the plateau value of $D_{xz}(t)$, i.e. $D_{xz}(\infty)$, of ~$0.138*10^{-10}$ which compares well with the highest value obtained by $D_{xz}(t)$ of ~$0.12*10^{-10}$ which indicates that the for ethane the orientation relaxes within the duration of the perturbation experiment.

For propane the results from the perturbation runs are confirmed by the steady state values of the alignment tensors. The $\hat{Y}_p$ axis is found to behave in the same way as the long axis of a diatomic in that upon shearing D^Y_{xz} and D^Y_{xx} increase in magnitude whereas D^Y_{yy} and D^Y_{zz} decrease showing a tendency for alignment to occur in the positive quadrant of the XZ plane. Through the interdependence of the three tensors, eqn.4.3.4, counterbalancing changes must occur in the other orientation tensors. The perturbation results suggested that the majority of the change would occur for the $\hat{Z}_p$ axis and this is indeed what the steady state results show as D^Z_{xz} decreases more than, by up to five times at the highest shear rate, D^X_{xz}. Correspondingly D^Z_{xx} decreases and D^Z_{zz} increases emphasising the tendency for the $\hat{Z}_p$ axis to align in the negative XZ quadrant. Furthermore D^Z_{yy} shows, at the higher shear rates, a slight negative trend which, as for the diatomics and the $\hat{Y}_p$ axis, accompanies the realignment of the

Figure 4.17 $\chi_d(\dot{\gamma})$ vs. $\dot{\gamma}^{1/2}$, ethane (□).

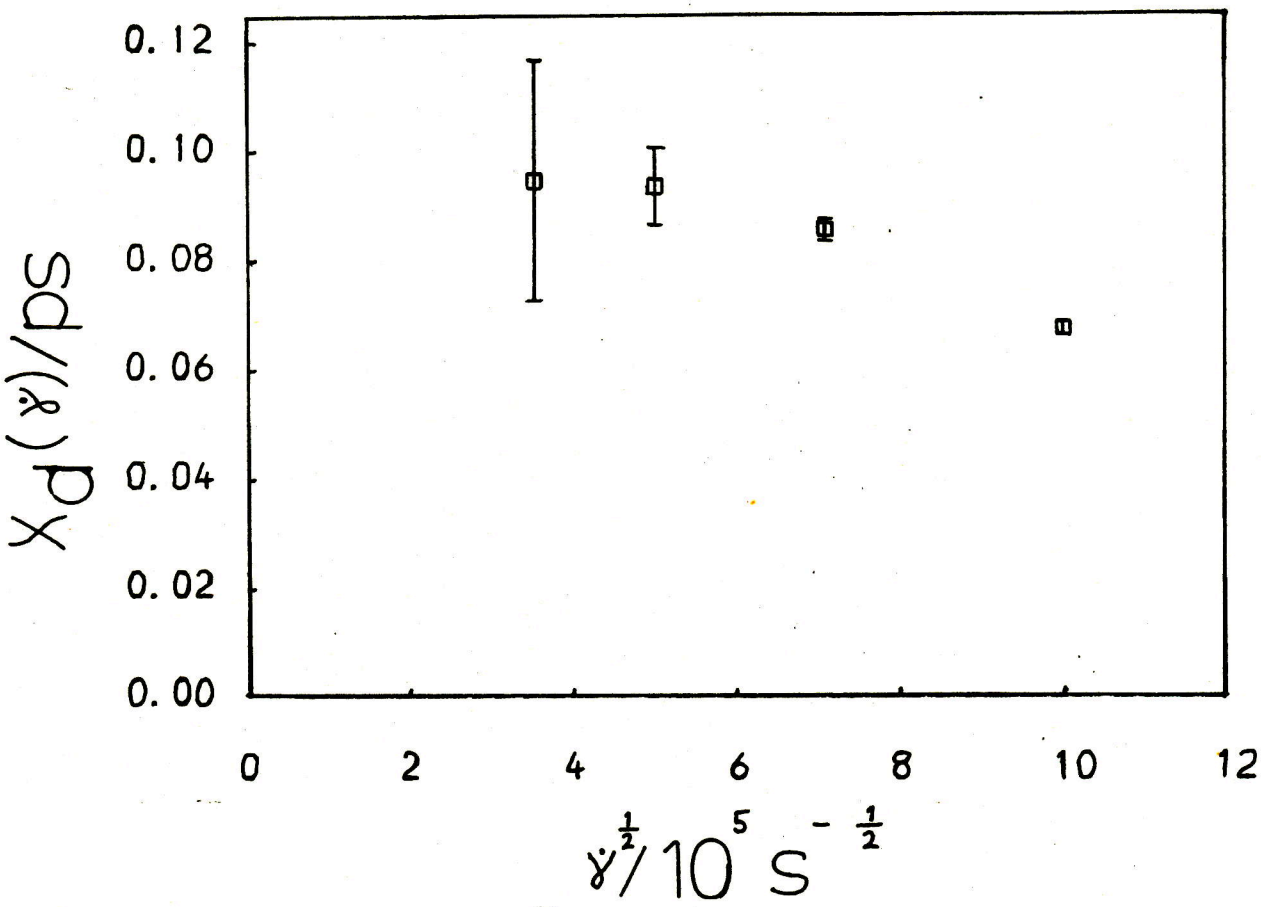

Figure 4.18 $\chi_d(\dot{\gamma})$ vs. $\dot{\gamma}^{1/2}$, propane,
$\hat{\underline{X}}_p$(□), $\hat{\underline{Y}}_p$ axis (Δ), $\hat{\underline{Z}}_p$ axis (▽).

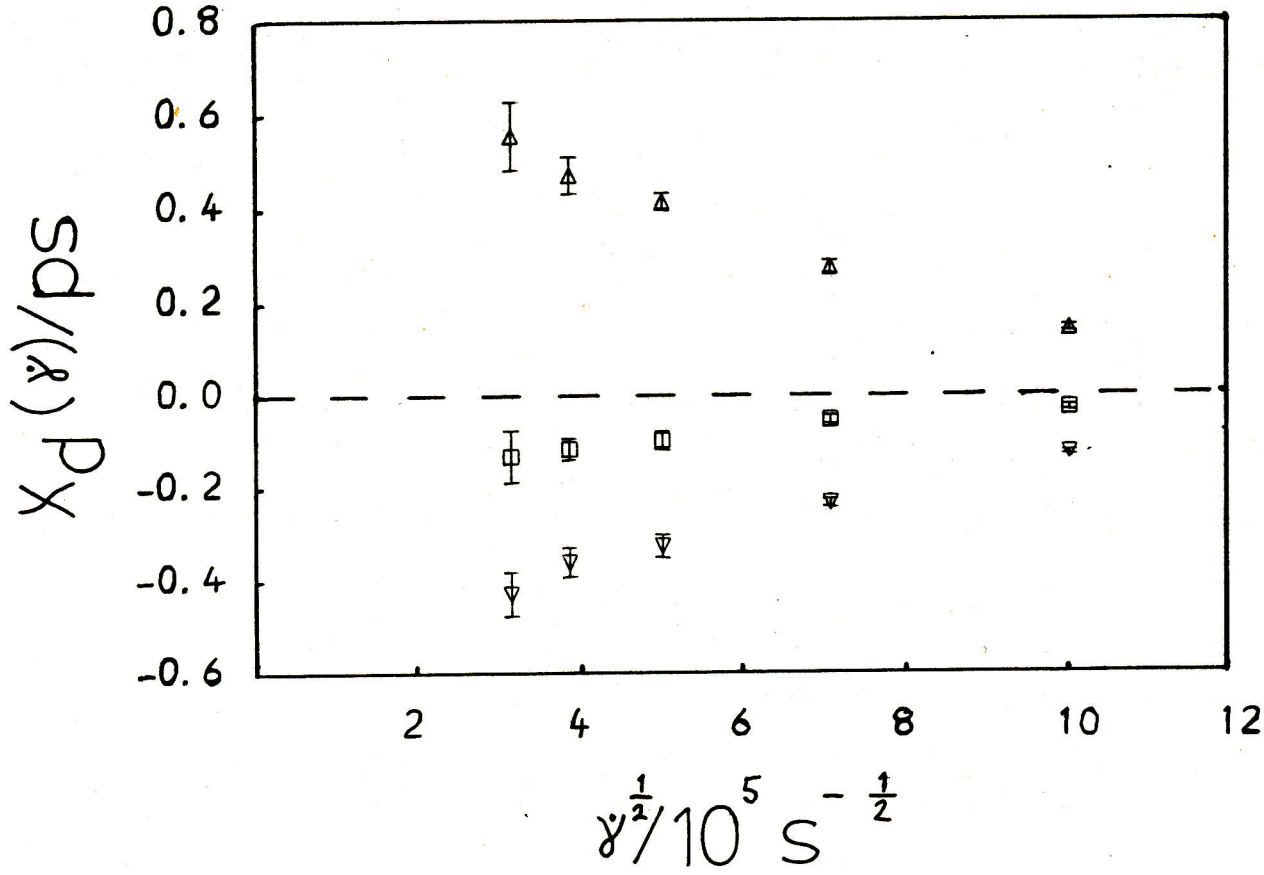

axis in the plane of shear.

The general picture that emerges for liquid propane is that the molecules tend to align with the plane of the molecule perpendicular to the plane of shear. This simple picture is complicated by the fact that D^{X}_{xz} does change, which would not occur if the proposed alignment were exactly true. Why the molecules should align in this way rather than with the plane of shear is not clear. One possible explanation is that it is a consequence of the molecules forming into layers in the XY plane to assist easier flow. This is thought to happen in monatomic fluids [1,2] but is difficult to quantify as it is a collective dynamic property.

The shear orientation parameters for each of the tensors are given in table 4.7. and are shown in fig.4.18 plotted as a function of $\dot{\gamma}^{\frac{1}{2}}$. Estimates of the $\chi_d(\emptyset)$ were made using a linear fit to the lowest four shear rates and the following results were obtained -Ø.2ps, Ø.75ps and -Ø.56ps for $\hat{\underline{X}}_p$, $\hat{\underline{Y}}_p$ and $\hat{\underline{Z}}_p$ respectively. Unlike ethane these estimates of $\chi_d(\emptyset)$ give values for the long time limit of $\Delta D_{xz}(t)$, in the perturbation experiments, of at least three times in excess of the highest value of $\Delta D_{xz}(t)$ attained within the time span of the experiment. This is an interesting result as estimates of the zero shear rate viscosity tended to suggest that the shear stress relaxation was complete within this same time interval. Now as the response of the collective orientation to a change

in the shear rate is a measure of the rate at which the configuration comes to equilibrium after such a perturbation it follows that the stress, as it is largely a function of the configuration, must also take at least the same amount of time to come to equilibrium. What this result implies is that the long time relaxation of the stress contributes very little to the eventual resultant viscosity.

4.6 Non-equilibrium thermodynamics

From table 4.3. it is clear that both the energy and the pressure are again functions of the shear rate. To correlate this behaviour the same procedure has been adopted as for the diatomics. In table 4.8. the functions $\Delta P(\dot{\gamma})$ and $\Delta U(\dot{\gamma})$, as defined in sec.3.8, are given and in figs.4.19 and 4.20 $\log_{10}\Delta P(\dot{\gamma})$ and $\log_{10}\Delta U(\dot{\gamma})$ are plotted against $\log_{10}\dot{\gamma}$. At the lower shear rates the data suffers through the imprecision in the results and the small differences between the pressure and the energy in the sheared and unsheared states. At the higher shear rates the difference increases so the uncertainty in the results becomes less. For this reason only the highest three shear rates have been considered in fitting the data to the forms given in eqns.3.8.3 and 3.8.4. From figs.4.19 and 4.20 it can be seen that for these higher shear rates the data gives a good fit to the linear forms of these equations. The resultant best fit slopes (a and b) and constants (P_1 and U_1) are given in table 4.9.

Table 4.8 The functions $\Delta P(\dot{\gamma})$ and $\Delta U(\dot{\gamma})$ obtained from the steady state shear calculations on ethane and propane at T~200K.

Ethane

$\dot{\gamma}/10^{10}s^{-1}$	$\log_{10}(\dot{\gamma}/10^{10}s^{-1})$	$\Delta P(\dot{\gamma})$/bar	$\Delta U(\dot{\gamma})$/J mol^{-1}
12.5	1.097	33±36	66±82
25.0	1.398	39±36	74±82
50.0	1.699	89±36	163±83
100.0	2.0	240±35	321±82

Propane

$\dot{\gamma}/10^{10}s^{-1}$	$\log_{10}(\dot{\gamma}/10^{10}s^{-1})$	$\Delta P(\dot{\gamma})$/bar	$\Delta U(\dot{\gamma})$/J mol^{-1}
10.0	1.0	31±55	72±90
15.0	1.176	65±51	106±89
25.0	1.398	171±48	196±88
50.0	1.699	393±59	454±91
100.0	2.0	942±64	1140±100

Table 4.9 The best fit parameters to the forms given in eqns.3.8.3 and 3.8.4 for the data obtained for $\Delta P(\dot{\gamma})$ and $\Delta U(\dot{\gamma})$ from the steady state calculations on ethane and propane at T~200K.

	P_1/bar	a	U_1/jmol	b
Ethane	0.49	1.35	2.80	1.03
Propane	3.34	1.23	3.08	1.29

In comparison to the chlorine results the dependence on the shear rate of the pressure and the energy is found to be

Figure 4.19 $Log_{10}\Delta P(\dot{\gamma})$ vs. $log_{10}\dot{\gamma}$, ethane (- - □ - -) and propane (——△——).

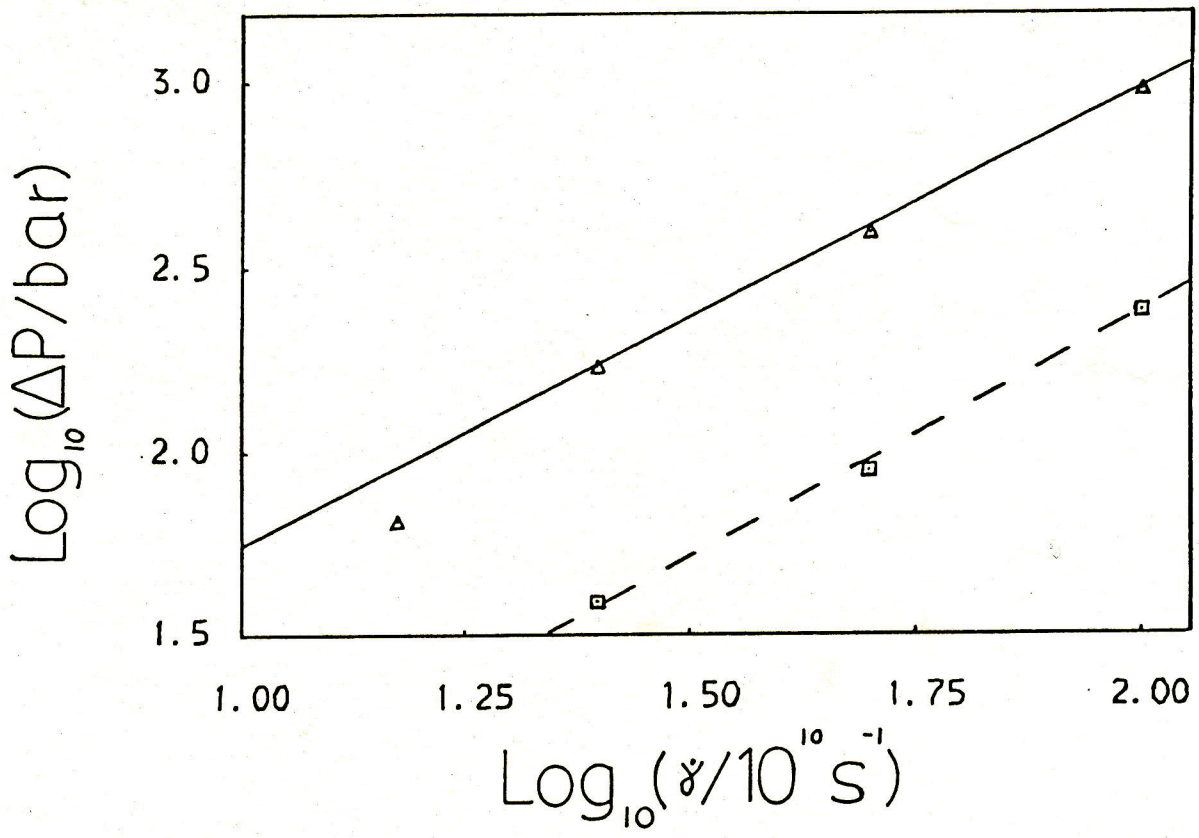

Figure 4.20 $Log_{10}\Delta U(\dot{\gamma})$ vs. $log_{10}\dot{\gamma}$, ethane (- - □ - -) and propane (——△——).

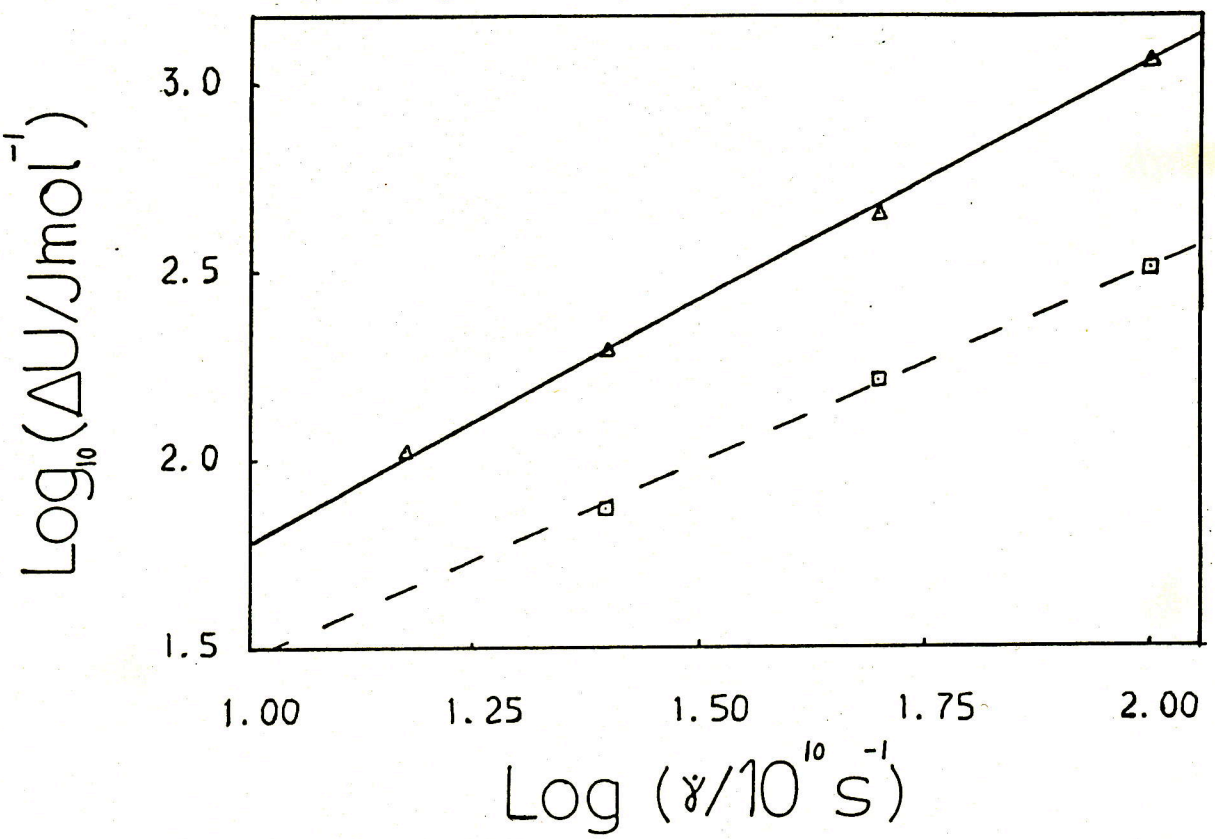

$\sim \dot{y}^{1.2} \rightarrow \dot{y}^{1.4}$, which is closer to the predicted dependence of $\dot{y}^{\frac{3}{2}}$ [90], except in the case of the energy in the ethane system. For ethane the energy is found to vary approximately as $\dot{y}$ which is similar to that found in chlorine but anomalous in the context of the other three dependences shown in figs.4.19 and 4.20. There is a greater difference between the chlorine and the alkane systems for the constants , U_1 and P_1, of at least an order of magnitude. This is understandable given the large difference in the conditions and the models used. There is also a significant difference between ethane and propane in the magnitude of $\Delta P(\dot{y})$ and $\Delta U(\dot{y})$ with propane showing the larger change in both cases. It is not obvious why this should be the case since in chapter 3 it was shown that two diatomics with the same interaction site potential and at the same state point but with differing anisotropies showed very similar changes in the pressure and energy under shearing. Here we have two molecules made up of two and three identical sites at roughly the same state point which show a noticeable difference in the magnitude of the effects. It has already been noted that these two molecules differ in their equilibrium potential energies by a factor of ~2 which is largely a result of the extra interactions involved in a three site as compared to a two site molecule. This means that the average potential between two molecules has a deeper well in the case of propane and thus any similar change in the structure of the fluid caused by the shear flow will cause a larger change in the potential energy and also in its first

derivative, which at constant temperature effectively determines the change in pressure, than in ethane.

A further resolution of the shear induced pressure changes is given by the three normal pressure components. Their change relative to $P(\dot{\gamma})$ are given by the functions $\Delta P_{\alpha\alpha\alpha}(\dot{\gamma})$, as defined in eqn.3.8.5, and are shown for ethane and propane in table 4.1Ø.

Table 4.1Ø The functions $\Delta P_{\alpha\alpha\alpha}(\dot{\gamma})$ as determined from the steady state calculations on ethane and propane at T~2ØØK.

Ethane

$\dot{\gamma}/10^{10}s^{-1}$	$\Delta P_{xx}(\dot{\gamma})$/bar	$\Delta P_{yy}(\dot{\gamma})$/bar	$\Delta P_{zz}(\dot{\gamma})$/bar
12.5	-3±2Ø	2±14	Ø±13
25.Ø	-2±13	-11±12	15±14
5Ø.Ø	32±18	-45±18	15±14
1ØØ.Ø	47±8	-1ØØ±9	56±11

Propane

$\dot{\gamma}/10^{10}s^{-1}$	$\Delta P_{xx}(\dot{\gamma})$/bar	$\Delta P_{yy}(\dot{\gamma})$/bar	$\Delta P_{zz}(\dot{\gamma})$/bar
1Ø.Ø	-3±45	-4±52	8±43
15.Ø	-12±38	-15±36	27±4Ø
25.Ø	13±4Ø	-63±2Ø	51±17
5Ø.Ø	124±44	-227±7Ø	1Ø3±68
1ØØ.Ø	-28±55	-253±53	281±56

There is a clear trend in both ethane and propane for $P_{yy}(\dot{\gamma})$ to decrease relative to $P(\dot{\gamma})$ as the shear rate is

increased and for $P_{zz}(\dot{\gamma})$ to increase relative to $P(\dot{\gamma})$. $\Delta P_{xx}(\dot{\gamma})$ shows less certain behaviour. In ethane it appears to increase like $\Delta P_{zz}(\dot{\gamma})$ whereas in propane $\Delta P_{xx}(\dot{\gamma})$ is small at the lower three shear rates, becomes significantly positive at $\dot{\gamma} = 5*10^{10} s^{-1}$ but then decreases at the highest shear rate, $\dot{\gamma} = 10^{12} s^{-1}$. This general behaviour of $P_{xx}(\dot{\gamma}) > P(\dot{\gamma})$ and $P_{yy}(\dot{\gamma}) < P(\dot{\gamma})$ differs from that found for the diatomics where $P_{xx}(\dot{\gamma}) < P(\dot{\gamma})$ and $P_{yy}(\dot{\gamma}) \approx P(\dot{\gamma})$. It is not possible to make any firm conclusions as to why this might be so because of the large disparity in the state points used but as ethane itself is modelled as a pseudo-diatomic it is unlikely that the difference in the behaviour of the normal pressures is due to the way in which the molecules are modelled. It is likely that simulations performed on ethane and propane at conditions comparable to those used in the chlorine system would produce similar trends for the normal pressures.

4.7 Shear Induced Structural Changes

The changes in fluid structure which give rise to the increased energy and pressure have been monitored by calculating radial distribution functions. For ethane the only noticeable differences between the r.d.fs at equilibrium and at a shear rate of $10^{12} s^{-1}$ are a slight movement of the first peak of the site-site g(r) to a lower r value and an increase in the height of the COM-COM G(R) from ~1.9 to ~2.1.

These findings are consistent with an increase in energy and pressure, as the sites penetrate further into the repulsive part of the potential , and with the alignment that occurs under shear producing more structure in the COM G(R).

For propane the g(r)s from simulations at the highest shear rate, $10^{12}s^{-1}$, have been superimposed over the equilibrium g(r)s in fig.4.21→4.24. The largest change occurs in $g_{BB}(r)$ but as this only contributes 1/9 to g(r) its effect upon g(r) is small. The general trend for g(r) and its resolved parts , $g_{AA}(r)$, $g_{AB}(r)$ and $g_{BB}(r)$, is the same with the first peak becoming larger, the first trough becoming shallower and a consequent decrease in the height of the second peak. As already noted the one extra site in the propane model makes interpretation of the r.d.fs difficult. The behaviour of the overall g(r) is similar to the cases of ethane and the diatomics but as the COM G(R) has not been calculated the ordering of the molecules cannot be discerned in the same way as before. Qualitatively it might be expected that $g_{BB}(r)$ resembles G(R) as the separation of the central site and the COM is only $\emptyset.15\sigma$. Assuming this is so propane shows similar behaviour as the diatomics with the greater changes being more apparent for the COM structure.

Figure 4.21 g(r) vs. r, propane $\dot{\gamma}=10^{12}s^{-1}$ (——), $\dot{\gamma}=0$ (- - -).

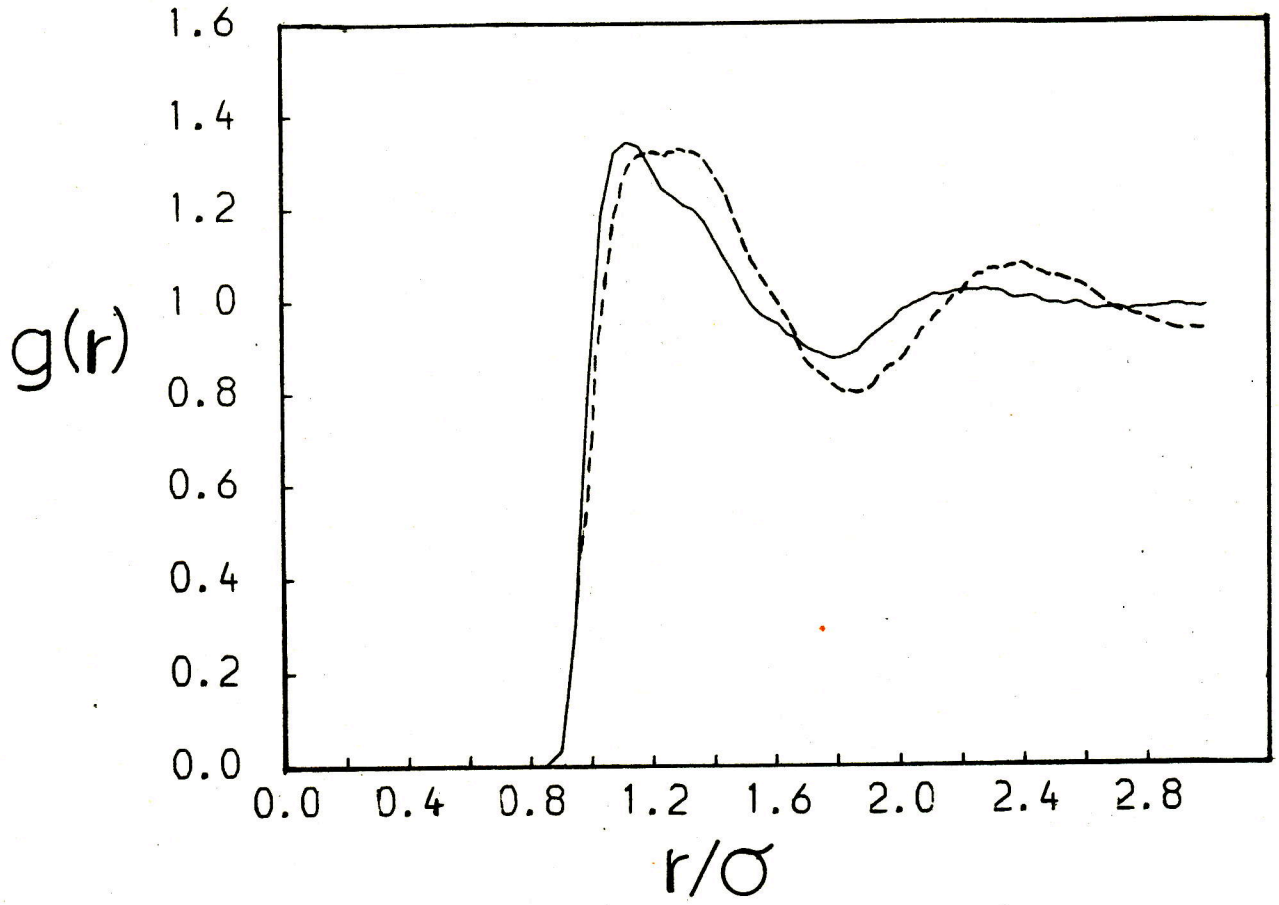

Figure 4.22 $g_{AA}(r)$ vs. r, propane $\dot{\gamma}=10^{12}s^{-1}$ (——), $\dot{\gamma}=0$ (- - -).

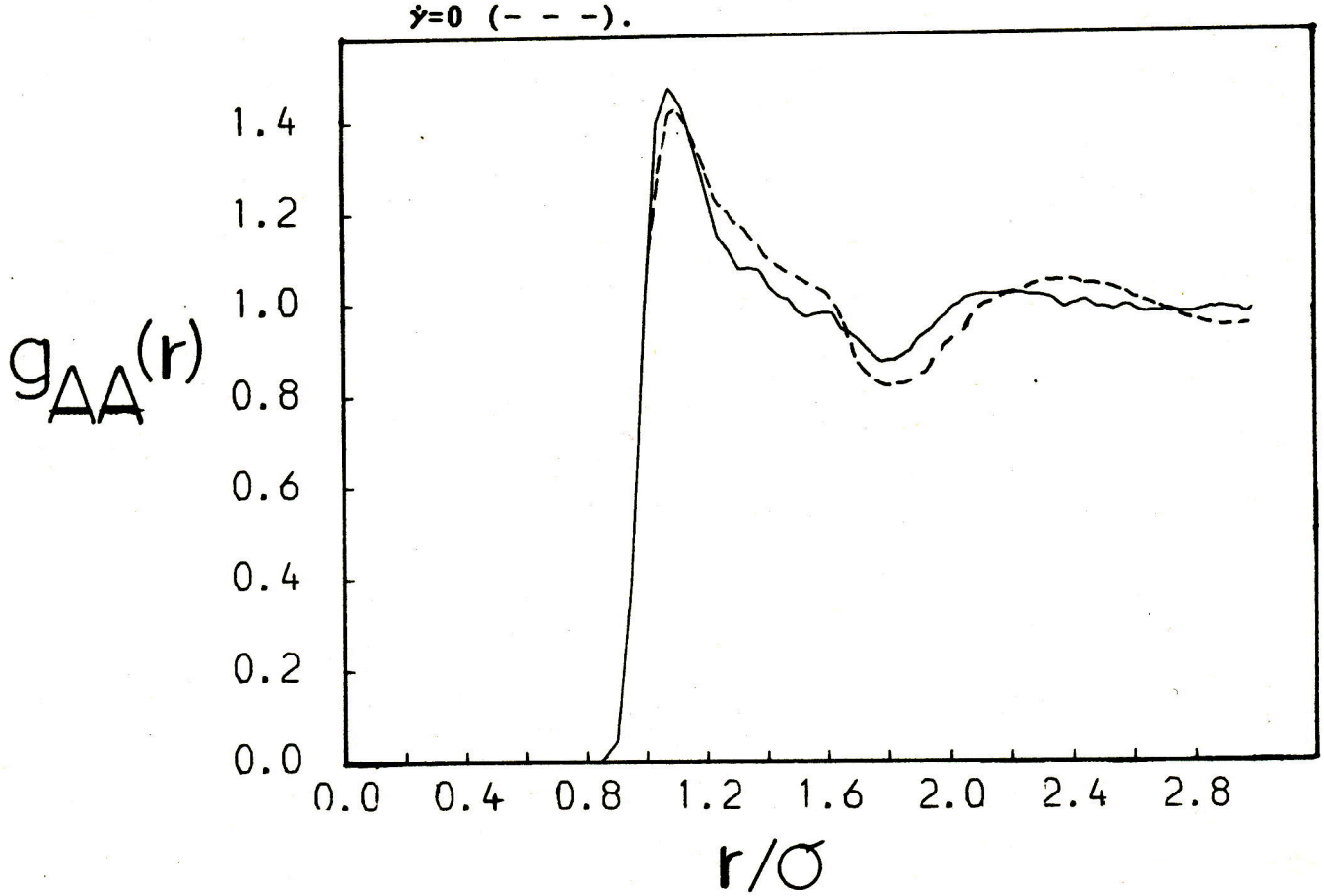

Figure 4.23 $g_{AB}(r)$ vs. r, propane $\dot{\gamma}=10^{12}s^{-1}$ (——), $\dot{\gamma}=0$ (- - -).

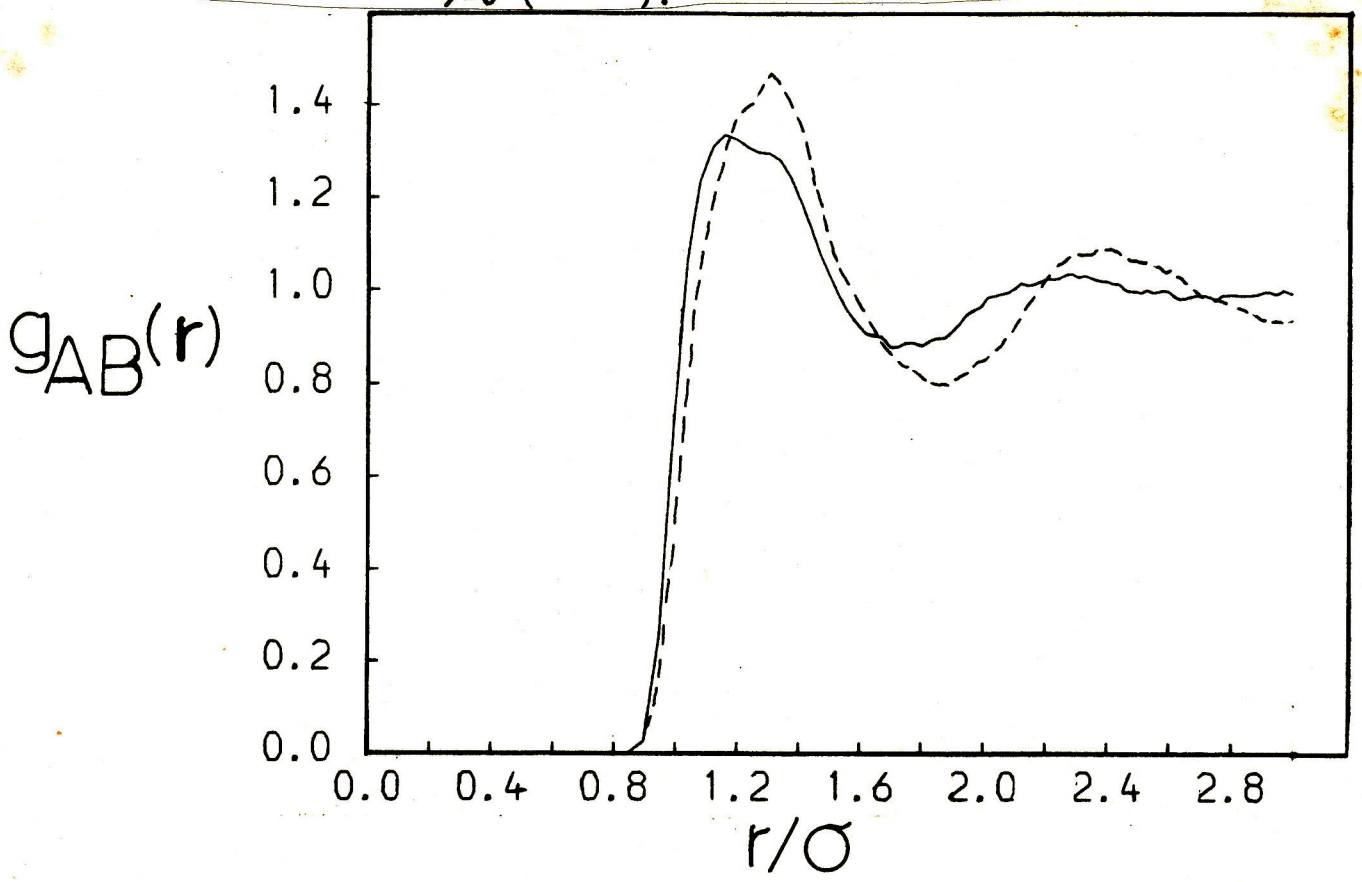

Figure 4.24 $g_{BB}(r)$ vs. r, propane $\dot{\gamma}=10^{12}s^{-1}$ (——), $\dot{\gamma}=0$ (- - -).

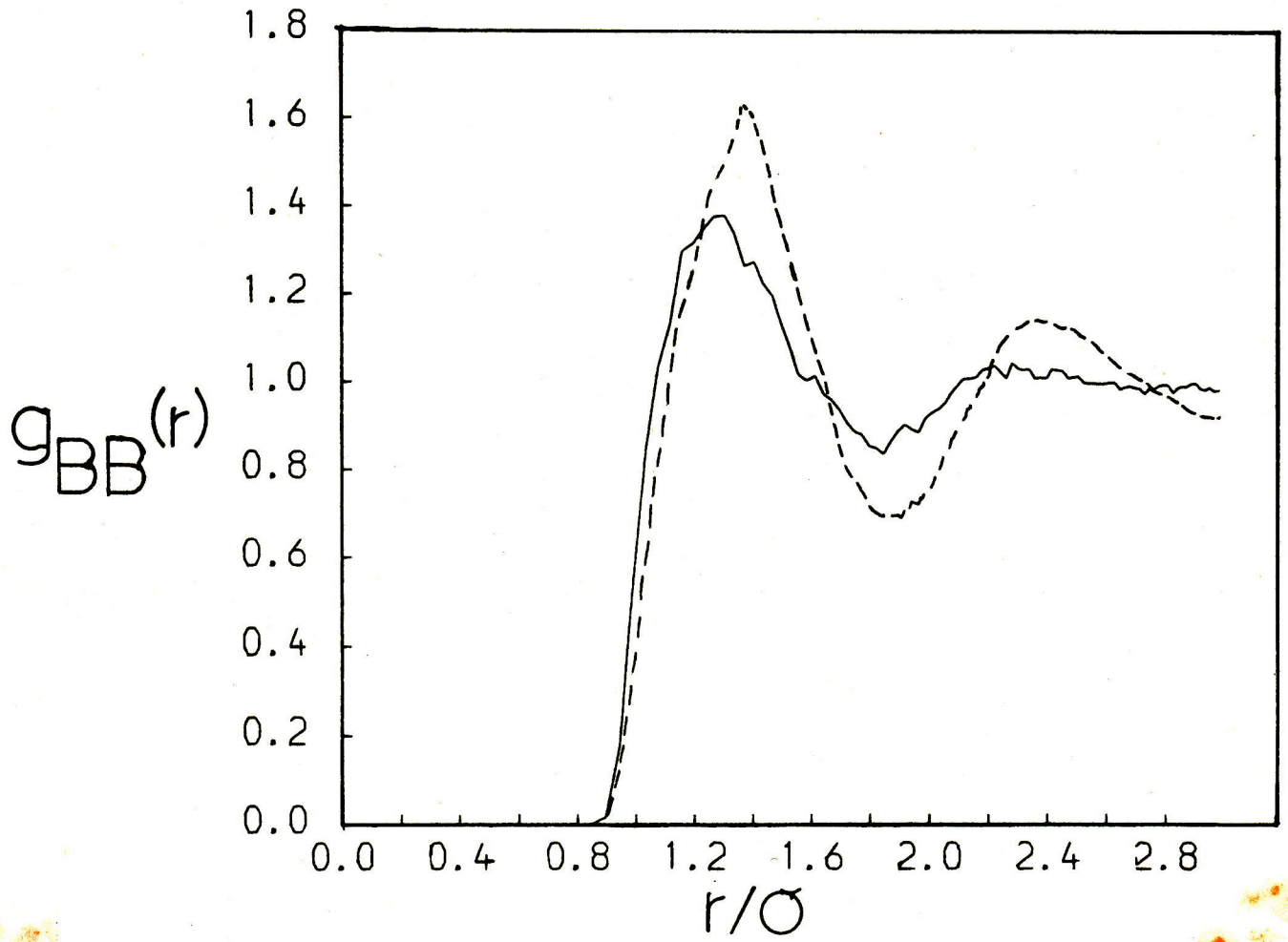

4.8 Conclusions

Clearly the addition of an extra site to the diatomic model produces quite drastic changes in virtually all the properties measured. This can be rationalised as being caused by an effective halving of the reduced temperature on going from ethane to propane as the interaction potential energy more than doubles. So to evaluate the effect of the change in the geometry between a diatomic and a triatomic it would probably be better to compare propane at 200K with ethane ~100K. This again raises the problem of corresponding states if one is trying to answer questions about the relative rheological properties of molecules of different 'shape'. However, in a crude, but probably more realistic, way molecules can be said to vary not because of their different shapes so much but because the numbers and/or intensities of their constituent 'sites' are different. The comparison between 'ethane' and 'propane' is a particularly dramatic example of this.

CHAPTER 5

HEXANE AND FLEXANE : EQUILIBRIUM RESULTS AT 200K

5.1 Introduction

Up to now the simulations reported here have been limited to entirely rigid molecules. Although interesting results have been obtained it has proved difficult to perform the totally unambiguous experiments desired because of the problem of finding corresponding states. Even though systems have been looked at with differing bond lengths and numbers of interaction centres it has not been possible to prove that, for instance, larger molecules are inherently more viscous, say, than smaller ones because of the arbitrariness in choosing the conditions at which to make the comparisons. Studying molecules which possess internal degrees of freedom has the advantages of allowing much closer comparisons between molecules to be carried out, as the changes induced in the state functions by altering the barriers to internal rotations are likely to be small, and it also means that a property of particular relevance, i.e. flexibility, is being probed as it exists in all real liquid lubricant molecules.

It was, thus, proposed that two similar model molecules be studied, using molecular dynamics, differing only in their 'flexibility'. In this way it was hoped that an unbiased view of the effect of hindered internal rotation upon the rheological properties of a fluid might be obtained which

although not directly relatable to any one particular molecule might give some insight into the comparative behaviour of different molecules. The six centre n-alkane model was chosen as a compromise, being a molecule of sufficient complexity for which it would be possible to simulate a representative sample for long enough times within the limitations of computer resources.

5.2 Details of the Models

MODEL 1 : HEXANE

As described in sec.4.2 the model of a n-alkane originally used by Ryckaert and Bellemans [123] has been adopted. N-hexane is modelled as six centres of equal mass (14.5134 $gmol^{-1}$) which represent the CH_2 and CH_3 groups. Carbon-Carbon bond lengths are rigidly fixed at 1.53Å and CCC bond angles at 109° 28′. Each centre is the site of a Lennard-Jones 12-6 potential with parameters σ = 3.92Å and ϵ/k= 84K which determines intermolecular interactions between sites of different molecules and intramolecular interactions between sites separated by three or more centres within a molecule. Furthermore, a dihedral angle potential , $\Phi(\alpha)$, defined as

Figure 5.1 **The dihedral angle potential $\Phi(\alpha)$ vs. α, Hexane, T=200K.**

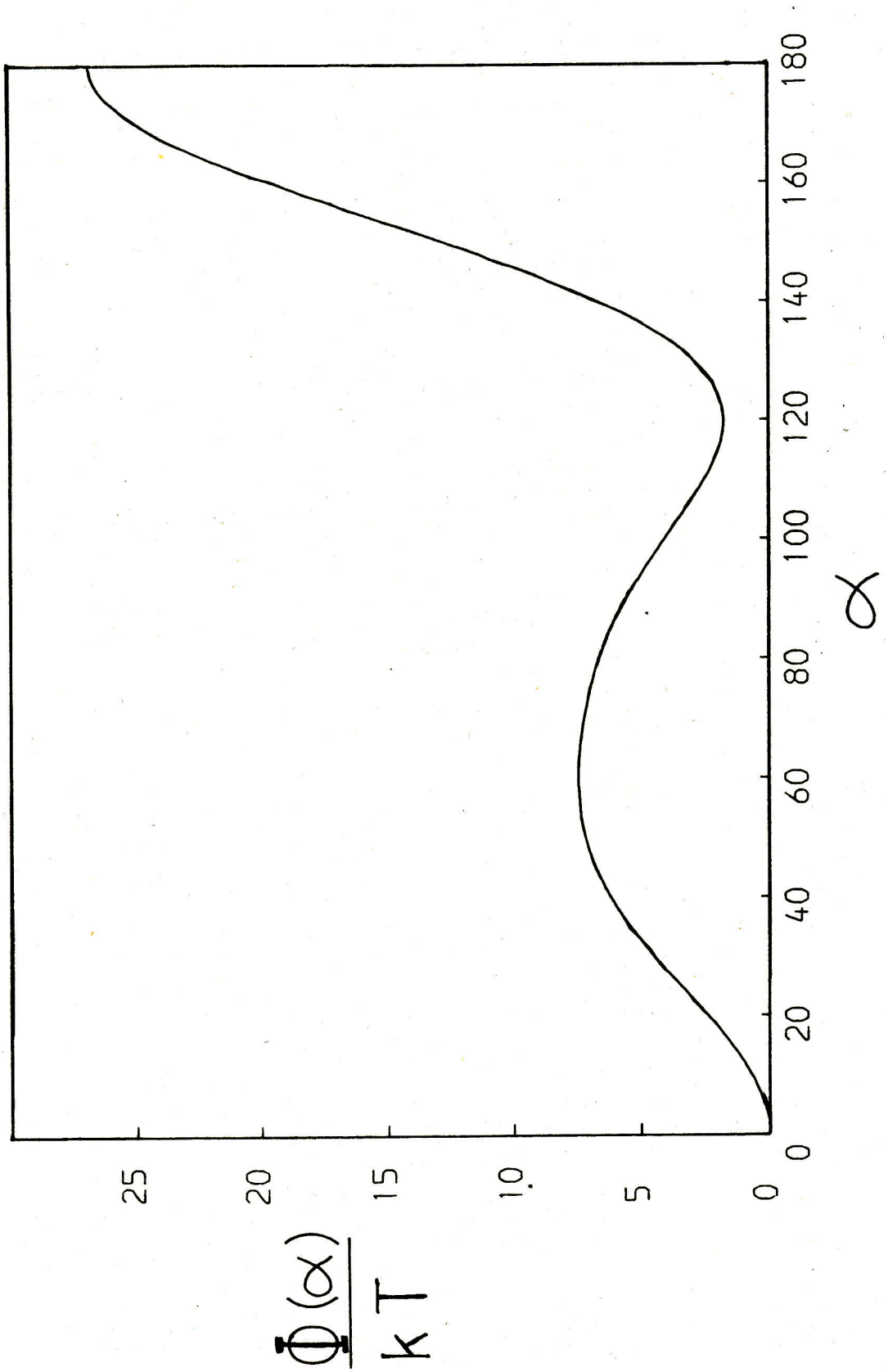

$$\Phi(\alpha)/k = (1.116 + 1.462\cos\alpha - 1.578\cos^2\alpha - 0.368\cos^3\alpha + 3.156\cos^4\alpha - 3.788\cos^5\alpha)/10^3 K \qquad (5.2.1)$$

is used to restrict the rotation around all three dihedral angles per molecule. $\Phi(\alpha)$ is illustrated in fig.5.1 and the method used to evaluate the forces on the sites due to $\Phi(\alpha)$ is given in Appendix 2.

MODEL 2 : FLEXANE

Is as model 1 in all respects except that forces arising from the dihedral angle potential, $\Phi(\alpha)$, are set to zero. This is equivalent to setting $\Phi(\alpha) = 0$ but it was found useful to accumulate $\Phi(\alpha)$ as in eqn.5.2.1 to provide information on the changes in distribution of dihedral angles. As this is a more flexible form of hexane it is called FLEXANE for convenience.

5.3 Details of the Simulations

All simulations were performed with N=108 molecules in a cubic cell at temperatures of 200K and 300K. The equations of motion were solved using the 'leapfrog' form of the Verlet algorithm in conjunction with the 'constraints' scheme as described in sec.2.9. The time step used was of length $0.4*10^{-14}$s and the constraints of fixed bond lengths and bond angles were maintained to a tolerance of 10^{-5} for most of the

simulations. The number of iterations required to satisfy these constraints per molecule per time step was ~18 for hexane and ~12 for flexane at 200K. For each time step a vectorised version of the program required ~0.6s of CPU time on a Cray-1 machine whereas the scalar program required ~1.6s of CPU time on a CDC-7600. The latter used a method of nearest neighbour tables to reduce the amount of time needed to evaluate the forces (see Appendix 3).

It was subsequently found that the modifications to the constraints procedure outlined in sec.2.10 meant that the tolerance could be reduced to 10^{-6} without seriously affecting the amount of CPU time required per time step. The number of iterations required per molecule per time step to satisfy the higher tolerance increased to ~33 for hexane and ~27 for flexane at the same temperature as before. Although the number of iterations has roughly doubled there is no significant increase in the CPU time consumed because the modified procedure requires no SQRT functions to be evaluated.

It was intended that in all calculations the L-J 12-6 potential be truncated at $r_c=2.5\sigma$ and long range corrections were added to the energy and the virial assuming this and that the site-site g(r)=1 for $r>r_c$. However, having completed all the simulations it was subsequently discovered that in employing a cut-off the square of the separation of two interacting sites had been compared erroneously with r_c

instead of r_c^2. As distances were measured in box units, i.e. all coordinates lie between -1 and +1, the difference between r_c and r_c^2 in these units was small but effectively meant that the cut-off used was in fact 2.924σ. This meant that the pressure and energy as calculated were in error by a small but constant amount which has had to be corrected for. This is not a serious problem as the conditions chosen at which to compare the two models were largely arbitrary but as the results for the smaller alkanes were obtained at the state point (T~200K, P~0) this point was initially chosen for these calculations. Therefore, in the process of equilibrating a sample of flexane at the desired temperature the volume was adjusted to give an apparent pressure of ~0. With the discovery of the error in the cut-off the actual pressure is somewhat away from zero.

The method of preparation of equilibrated configurations of hexane and flexane was to allow an initially cubic lattice of all Trans , i.e α=0, conformers of flexane to equilibrate at 200K for ~50ps. In the absence of a dihedral angle potential rotations around the dihedral angle were rapid and the sample quickly established an equilibrium state.To produce a sample of hexane the dihedral potential was then gradually introduced and the system then allowed a further 70ps to relax.As can be seen from fig.5.1 the barriers to transitions are high compared to kT (T=200K) indeed no $G_+ \rightarrow G_-$ transitions were observed and the frequency of G-T transitions was only ~1

per ps for 1Ø8 molecules, which implies a mean time between transitions for one dihedral angle in excess of 1ØØps. This means we cannot be certain then that the distribution of conformers in hexane has completely reached equilibrium.

5.4 Results at 2ØØK

Having obtained configurations for hexane and flexane further simulations were performed at equilibrium and at shear rates in the range $10^{10} \rightarrow 2*10^{11} s^{-1}$, the results of the latter will be given in the next chapter. In all these simulations the reduced number density, ρ^*, was fixed at Ø.33749. As the HSNEMD calculations are carried out isothermally the equilibrium simulations were performed using the same procedure for maintaining constant temperature (see sec.2.15) so as to obtain the best comparisons between the results at equilibrium and under shear. To check the stability of the numerical integration scheme and to allow comparisons with the constant temperature simulations results were also obtained at constant energy.

In table 5.1 a comparison is given between the thermodynamic data obtained for hexane and flexane from simulations at both constant temperature and constant energy.

Table 5.1 The mean thermodynamic functions obtained from simulations at constant temperature (N,V,T) and constant energy (N,V,E) for hexane and flexane at T~200K, ρ^*=0.33749. U=total energy, Φ=total LJ 12-6 potential energy, Φ_i=intramolecular contribution to Φ and Φ_α=total dihedral angle potential energy (* indicates calculated for comparison only).

	Hexane		Flexane	
	(N,V,T)	(N,V,E)	(N,V,T)	(N,V,E)
U/J mol^{-1}	-37330±70	-37580±0	-42330±60	-42300±0
Φ/J mol^{-1}	-50270±40	-50290±60	-49810±60	-49750±80
Φ_i/J mol^{-1}	-	-1480±10	-1370±10	-1370±10
Φ_α/J mol^{-1}	5460±60	5210±60	*30420±480	*30500±250
T/K	200.0±0.0	200.4±1.5	200.0±0.0	200.0±1.6
P/bar	550±30	570±70	280±50	300±40
Length of run /ps	48.0	62.4	97.6	21.6

To the number of significant figures quoted in table 5.1 the error in the total energy is zero for the constant energy simulations. The actual constancy of the energy was monitored by calculating the root mean squared deviation in U and was found to be no more than 0.005% of the mean total energy for either hexane or flexane.

As found previously for simpler systems [66] (N,V,T) and (N,V,E) MD simulations produce results for the thermodynamic

properties which are in good agreement. Apart from the dihedral angle potential energy in hexane, which in turn affects the total energy, all other properties agree to within the estimated errors for both systems. This disparity in the Φ_α for hexane is almost certainly a result of the, previously mentioned, long relaxation times involved in the conformational changes and the fact that the respective simulations did not start from the same initial configuration, consequentially they represent different time periods in the evolution of the system. Comparisons between hexane and flexane reveal that energetically the systems are very similar. The total energies differ by ~5000J mol^{-1}, largely due to the contribution from Φ_α which does not exist in flexane. The Φ_α's given in table 5.1 for flexane have been calculated for comparison only and they show the large difference in the internal structure of the molecules. There is a smaller difference, ~450J mol^{-1}, in the total LJ 12-6 potential energies of which ~100J mol^{-1} is accounted for by the intramolecular contribution, further reflecting the different internal structure. The remaining small difference implies that the intermolecular structure is affected by the introduction of the dihedral angle potential. This is also borne out by the higher pressure in the hexane system.

To determine the significance of this pressure disparity, ~270bar, a sample of flexane was compressed and equilibrated at a slightly higher density of ρ^*=0.34197 for a period of

~60ps. Averages were then taken over a further period of 20ps at constant temperature. The densification caused an increase in the pressure to 650±40bar and a decrease in the total energy to -42840±80J mol^{-1}. This was wholly due to a change in the intermolecular LJ potential energy as the intramolecular contribution remained constant, to within the errors of the calculation, upon densification and the temperature was the same as before. From the pressure and volume changes an approximate compressibility has been determined using the following equation

$$\beta = -\frac{1}{\bar{V}}\frac{\Delta V}{\Delta P} \quad ,$$

where $\bar{V}=(V_1+V_2)/2$, $\Delta V=V_1-V_2$ and $\Delta P=P_1-P_2$, The value of β obtained of $(3.6\pm0.6)*10^{-5}bar^{-1}$, is in the range found for many real liquids [125]. It was further estimated that a volume decrease of only ~1% would be required to bring the pressure of the flexane system up to that of hexane.

These results show that thermodynamically these two fluids are very simiar, especially when compared to the previous cases of the diatomics and the shorter alkanes. Clearly the conformations of the molecules are likely to be radically altered by the introduction of a dihedral angle potential so it is important to compare the fluids at a more fundamental level to establish the possible causes of any differences in their rheological behaviour.

5.5 Radial Distribution Functions

Fig.5.2 shows the site-site pair distribution function, g(r), for sites of different molecules. The slight difference between the two is consistent with the pressure and energy disparities. Although the potential is truncated the oscillations around g(r)=1 continue out at least to half a box length, 3.42σ. The error introduced by calculating the long range correction to the potential energy with g(r)=1 for $r>r_c$ was calculated by numerically integrating the relevant function over g(r). This error was found to be ~Ø.1% of the total potential energy which is of the same order as the inherent error due to fluctuations in the system.

Fig.5.3 shows the radial distribution function for the centres of mass G(R). The reduction in the amount of averaging on going from sites to COM results in poorer statistics but there are significant differences between the two. Hexane exhibits a split first peak indicating preferred alignments within the nearest neighbour shell. This has also been seen in rigid diatomics modelled by a two centre LJ 12-6 potential [39] where for moderate anisotropies the splitting is caused by molecules being aligned with their axes either parallel or perpendicular, the parallel alignment being that of minimum COM separation. Flexane shows a broader less aligned distribution with a noticeable tendency for the COMs

Figure 5.2 g(r) vs. r, hexane (——) and flexane (—·—·—), T~200K.

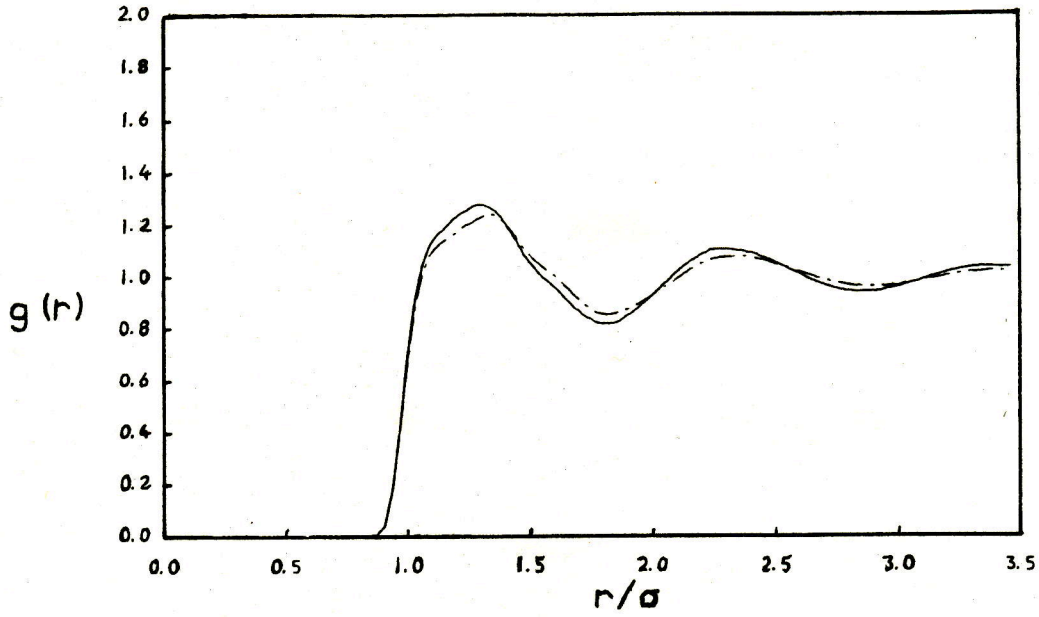

Figure 5.3 G(R) vs. R, hexane (——) and flexane (—·—·—), T~200K.

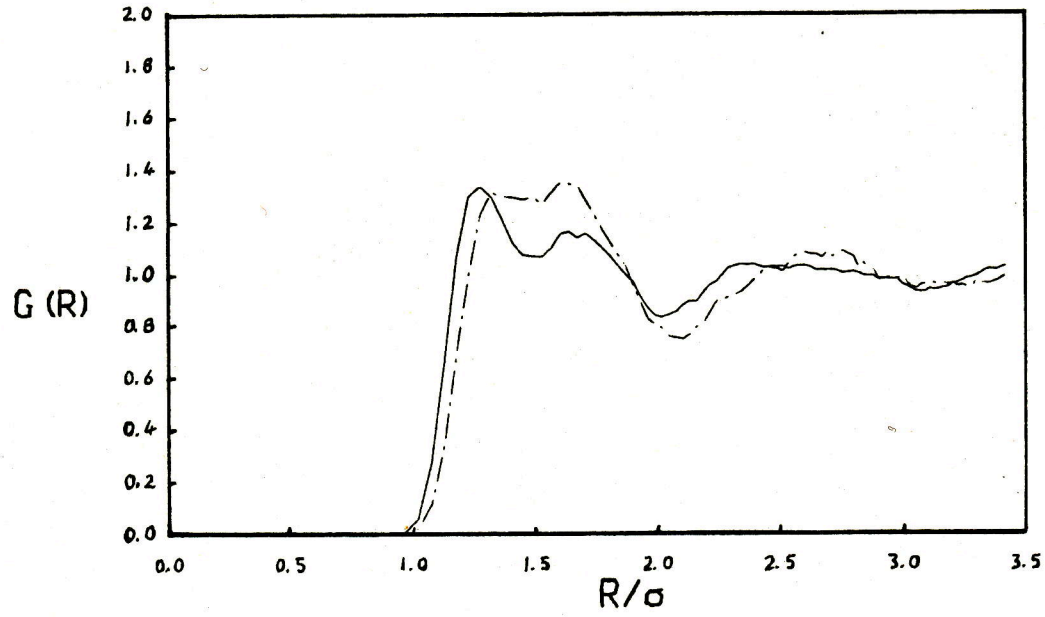

to be further apart within the range 1.Ø→1.3σ than in hexane.

5.6 Orientational Cross Correlation Function

To further determine the degree of alignment between molecules as a function of COM separation a cross correlation function has been calculated, $P_1(R)$, defined as

$$P_1(R) = \frac{\sum_{i=1}^{N} \sum_{j>i}^{N} (\hat{r}_{1\mathfrak{G}_i} \cdot \hat{r}_{1\mathfrak{G}_j})^2 \, \delta(|\underline{R}_{ij}| - R)}{\sum_{i=1}^{N} \sum_{j>i}^{N} \delta(|\underline{R}_{ij}| - R)} \qquad (5.6.1)$$

,where $\underline{R}_i$ is the position of the COM of molecule i. For no preferred orientation the average value of $P_1(R)$ will be 1/3, for parallel alignment $P_1(R) > 1/3$ and for perpendicular alignment $P_1(R) < 1/3$. In fig.5.4 $P_1(R)$ is plotted as a function of R for hexane and flexane. The function is similar for both fluids beyond ~2σ as it quickly decays to the expected large R value of 1/3. In the region between 1σ and 2σ there are noticeable differences between the two with hexane becoming aligned at slightly smaller separations than flexane and to a greater extent. This is consistent with the previous interpretation of the G(R).

Figure 5.4 The orientational cross-correlation function $P_1(R)$ vs. R, hexane (——) and flexane (—·—·—), T~200K.

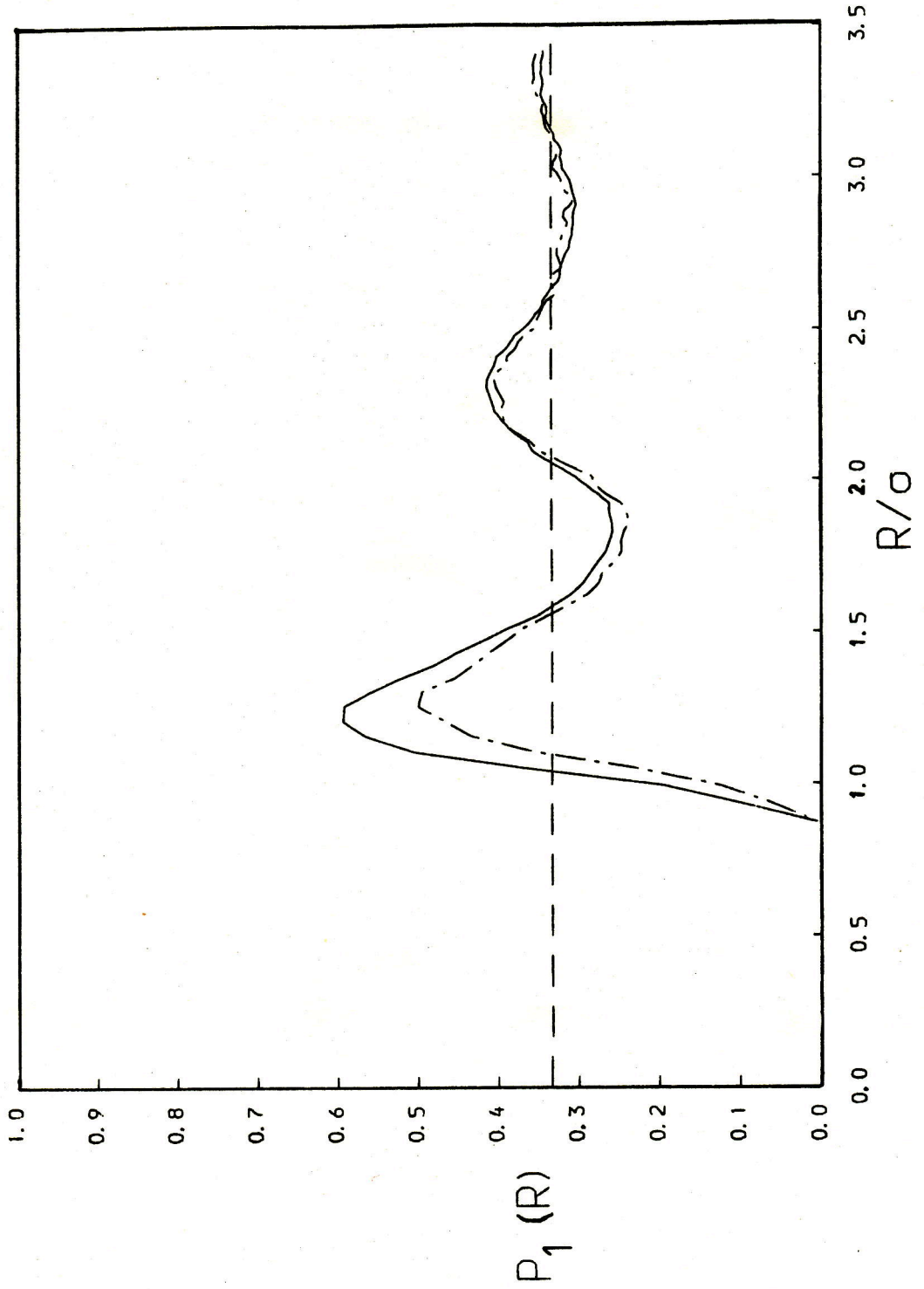

5.7 Intramolecular Structure

Figs.5.5, 5.6 and 5.7 give the probability densities for the separation of sites within a molecule that are separated by two, three and four others, respectively. All possible contributions are taken in these distributions so fig.5.5 is the average of $r_{14}(=|\underline{r}_{14}|)$, r_{25} and r_{36}, where the indices refer to the six sites of a molecule and $\underline{r}_{ij} = \underline{r}_i - \underline{r}_j$. There is a marked difference between the distributions for hexane and flexane caused by the inclusion of the dihedral angle potential. Hexane shows prominent peaks at points which correspond to the minima in $\Phi(\alpha)$, G_- (α=-120°), T (α= 0°) and G_+ (α =120°). For sites separated by two others the effect of $\Phi(\alpha)$ is most pronounced producing a sharp peak for the Trans conformer and a broader smaller peak for the Gauche conformers. For sites separated by three others there are peaks corresponding to TT and TG conformers but GG states are not present because they lead to separations less than σ and are therefore less likely as these sites interact through the LJ 12-6 potential. This results in only a few of the otherwise 27 possible conformers being in evidence for the end-to-end separation, r_{16}. The main conformers being TTT (r_{16} =6.308Å), TGT (r_{16} =5.793Å), G_+TG_- and GTT (r_{16}=5.226Å for both).

In flexane the distributions are much broader but not entirely featureless. There is some indication that all sites

Figure 5.5 The probability density for the distance between sites separated by two others $\rho(r_{14})$ vs. r_{14}, hexane (——) and flexane (—·—·—), T~200K.

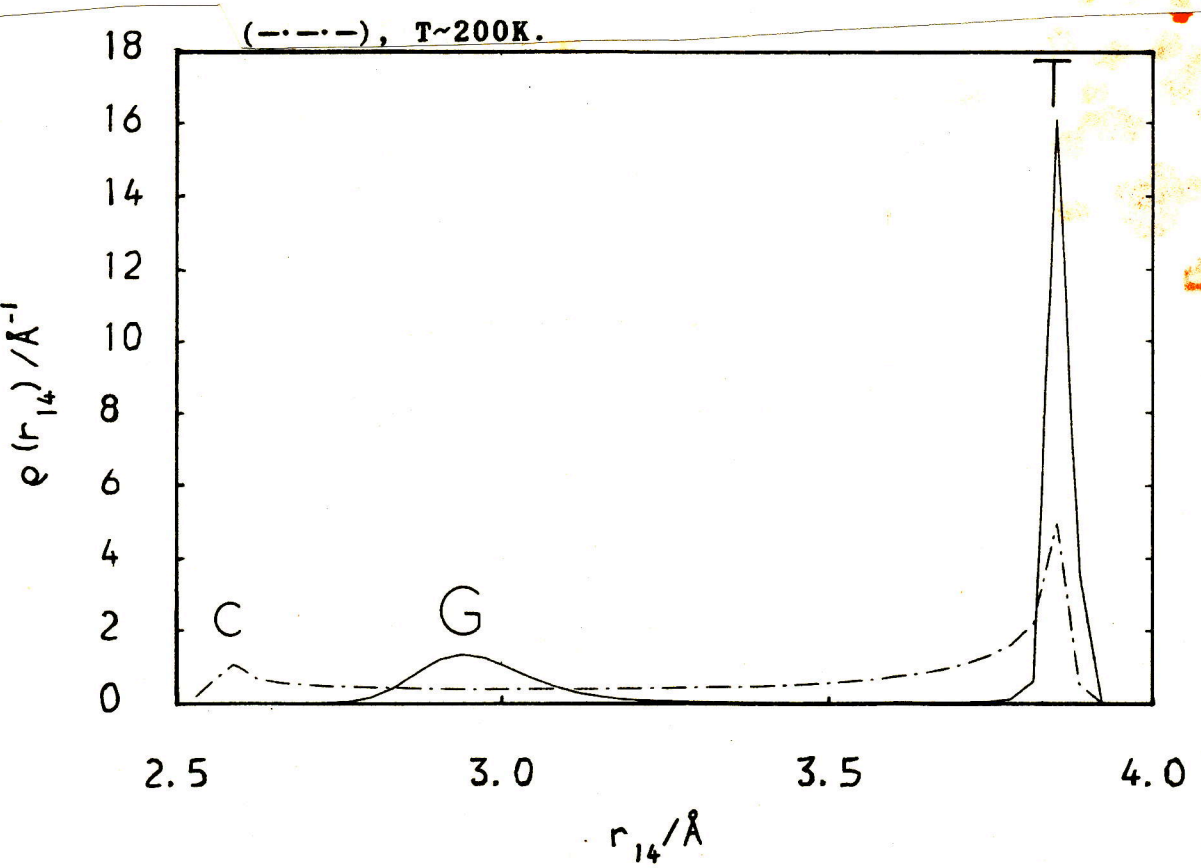

Figure 5.6 The probability density for the distance between sites separated by three others $\rho(r_{15})$ vs. r_{15}, hexane (——) and flexane (—·—·—), T~200K.

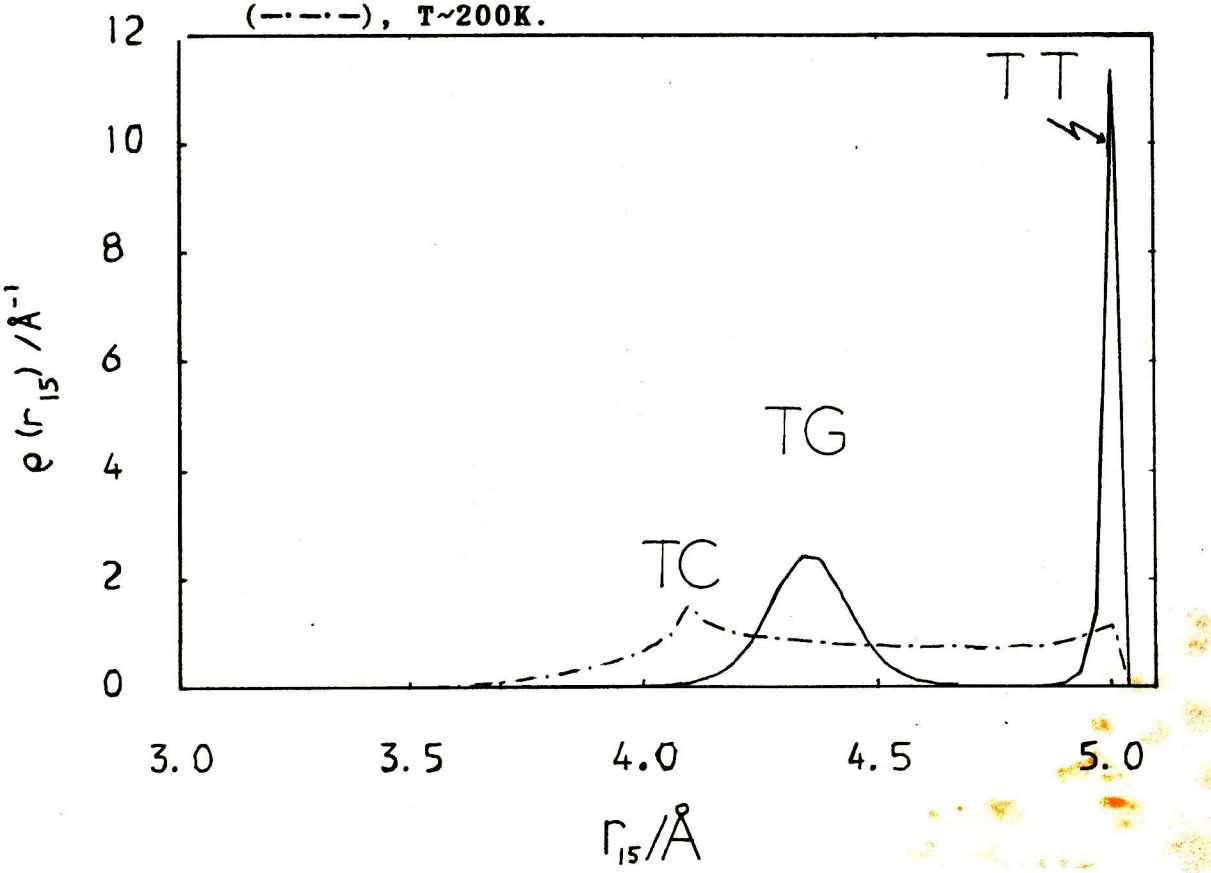

Figure 5.7 The probability density for the end-to-end separation of sites, $\rho(r_{16})$ vs. r_{16}, hexane (——) and flexane (—·—·—), T~200K.

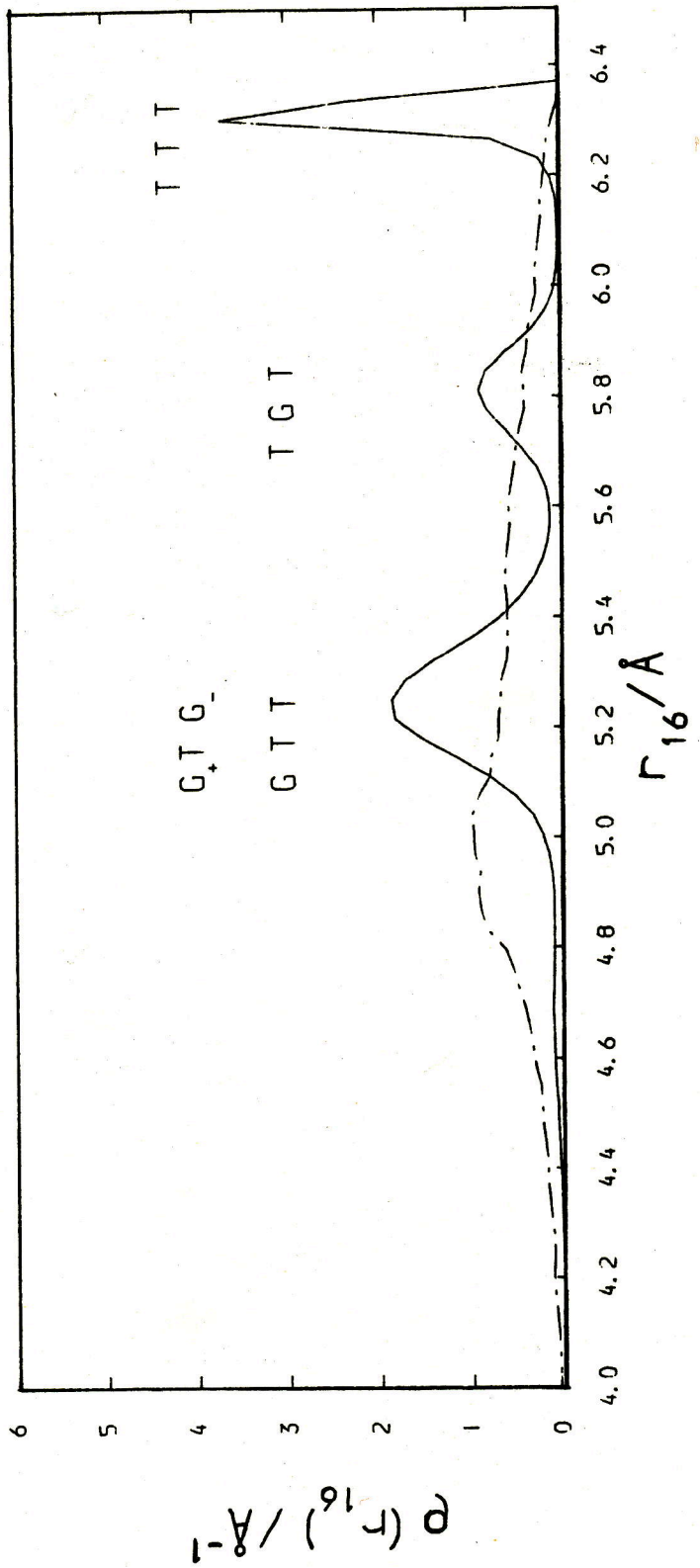

align in the same plane, i.e. with $\{\alpha\} = 0^\circ$ (Trans) or 180° (Cis). For sites separated by three others there are discernible peaks for the TT and TC conformations. For r_{16} this is less pronounced but there is a broad peak between 4.8Å and 5.0Å which corresponds to the TTC and CTC conformers.

The distribution of dihedral angles which give rise to the various conformers have also been calculated. In the models used here the two outer dihedral angles, α_1 and α_3, are equivalent and so the distributions obtained from these two have been averaged together and are shown in fig.5.8 whereas the distribution for the central angle, α_2, are shown in fig.5.9. Once again the effect of $\Phi(\alpha)$ is very marked in the hexane case producing peaks corresponding to the minima in the potential.

To further compare the internal structures the percentages of G_+, T and G_- dihedral angles, and hence the percentage conformers, has been calculated using the following criteria for assigning a label to a dihedral angle, α :-

G_- if $-180^\circ < \alpha < -60^\circ$

T if $-60^\circ < \alpha < 60^\circ$

G_+ if $60^\circ < \alpha < 180^\circ$

The average percentages of dihedral angles and the various conformers from the equilibrium simulations on hexane and flexane are given in table 5.2.

Figure 5.8 The probability density for the outer dihedral angle $\rho(\alpha_{1,3})$ vs. $\alpha_{1,3}$, hexane (1) and flexane (2), T~200K.

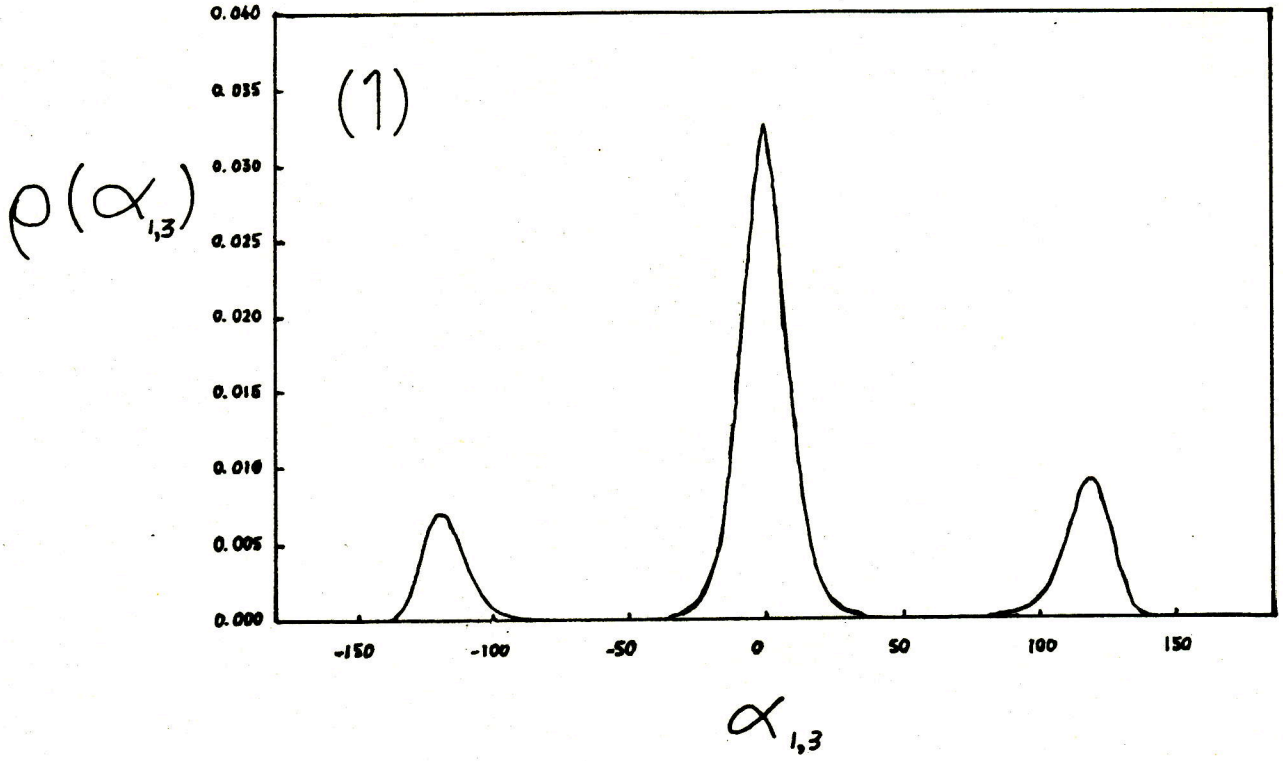

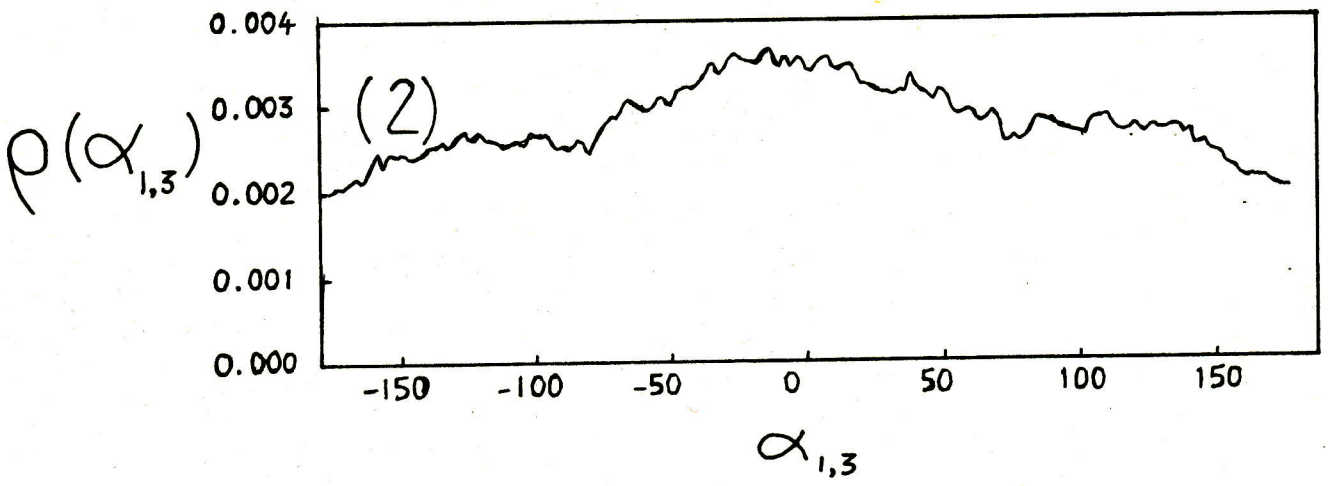

Figure 5.9 The probability density for the central dihedral angle $\rho(\alpha_2)$ vs. α_2 , hexane (1) and flexane (2), T~200K.

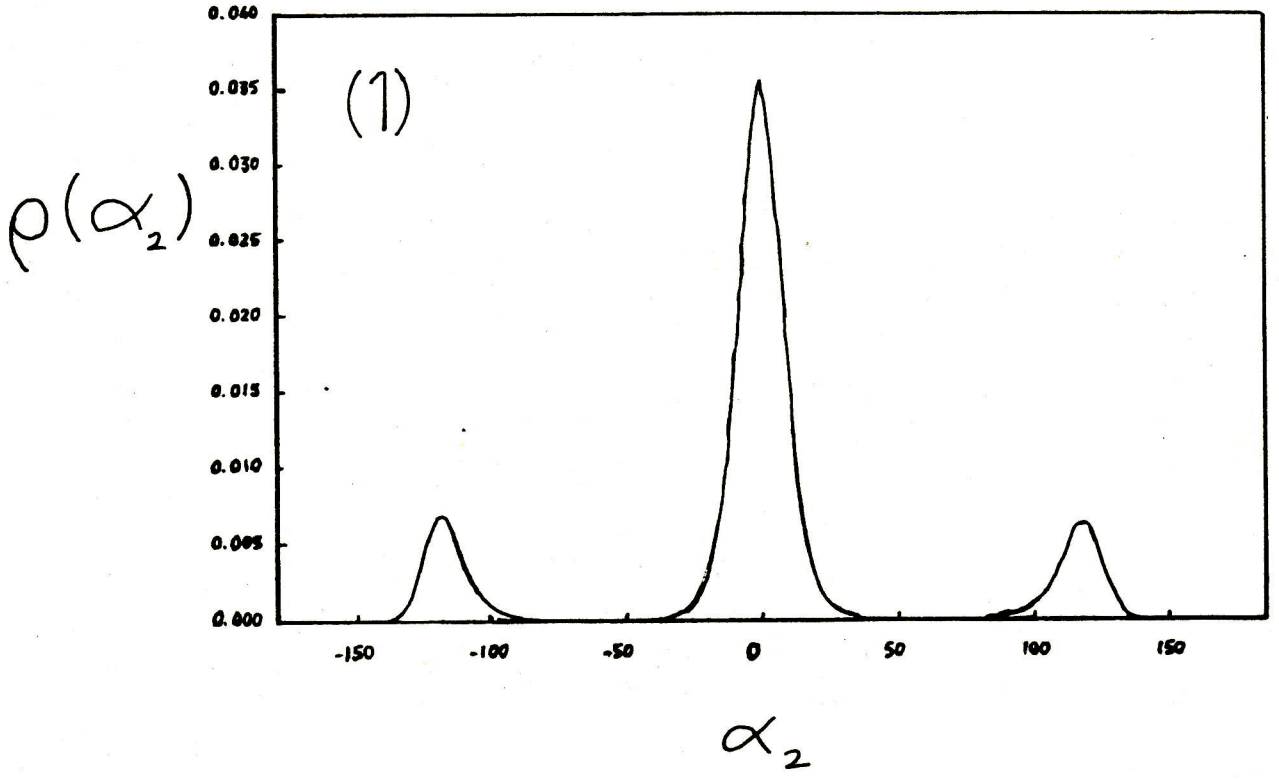

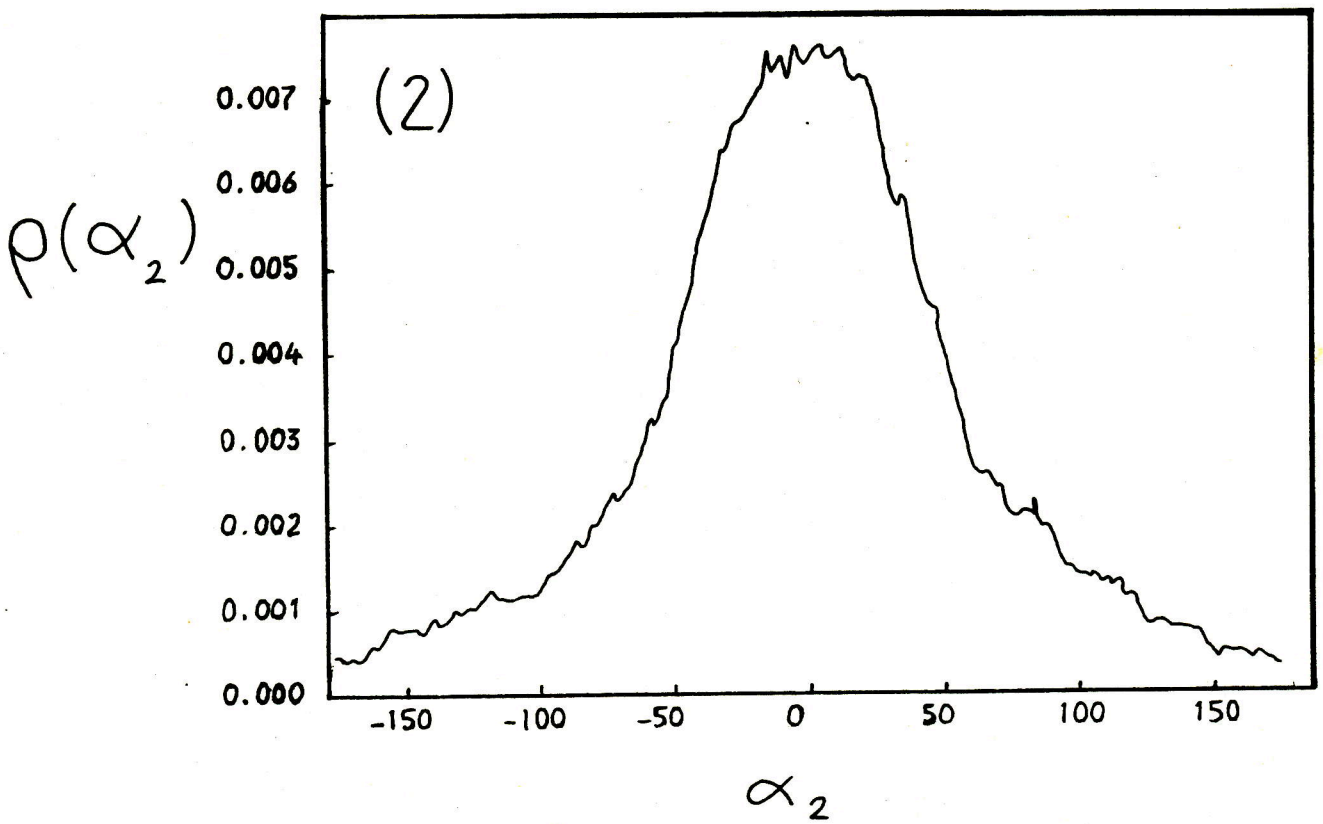

Table 5.2 The mean percentage of dihedral angles and conformers from the equilibrium calculations on hexane and flexane at T~200K.

% of dihedral angles

	Hexane		Flexane	
	$\alpha_{1,3}$	α_2	$\alpha_{1,3}$	α_2
G_-	13.0±1.5	12.3±0.8	30.4±1.5	14.7±1.5
T	73.2±2.2	74.8±1.9	39.1±1.8	70.6±1.7
G_+	13.9±1.7	12.8±1.1	30.5±1.4	14.7±1.2

% of conformers

	Hexane	Flexane
TTT	32.0±2.5	6.0±0.6
TTG	33.2±1.7	30.0±1.2
TGT	24.2±1.6	11.7±1.0
TGG	0.6±0.4	12.0±0.8
TG_+G_-	0.0±0.0	0.9±0.1
GTG	5.4±0.7	17.3±1.0
G_+TG_-	4.5±0.4	17.3±0.9
GGG	0.0±0.1	4.1±0.4
Others	0.0±0.0	0.8±0.1

The percentage of dihedral angles and the distribution functions indicate that there is a balance in the number of G_+ and G_- states for both hexane and flexane. In flexane this is to be expected because of the lack of barriers to rotation but in hexane it is possible that the slow relaxation of the

internal modes could result in the system being trapped in a non-equilibrium state on the time scale of these experiments. The fact that there is near equality in the number of G_+ and G_- angles maybe a fortuitous result of the equilibration procedure or it could indicate that the system is close to equilibrium.

Apart from the clear differences in the distribution of dihedral angles between hexane and flexane there is also a contrast in the distribution for ther outer angles, α_1 and α_3, and the central angle, α_2. In hexane the distribution for both types of angle are very similar but in flexane there is a striking contrast with a large proportion ~70% of α_2's being in the T state compared to ~40% for the outer angles. Without any dihedral angle potential this must be entirely due to the intramolecular interactions between sites 1, 2, 5 and 6 and the intermolecular interactions. To determine the degree to which the bulk fluid effects the conformations of these molecules probability densities were generated for a molecule in isolation. This was achieved by measuring the total intramolecular energy, Φ_{int}, for a particular configuration generated by rotating the dihedral angles through 360° in 5° steps. Permutating over all the combinations of dihedral angles in this way accounts for the inherent degeneracy of states. The probability for a particular configuration, p_i, was then calculated using

$$p_i = \exp(-\Phi_{int_i}/kT) / \sum_j \exp(-\Phi_{int_j}/kT)$$

, where the sum is over all the 373248 configurations sampled. The p_i's were then used to calculate probability densities for the dihedral angles $\rho(\alpha_{1,3})$ and $\rho(\alpha_2)$ and for the end-to-end separation $\rho(r_{16})$. These gas phase probability densities are shown in figs.5.10, 5.11 and 5.12 together with the experimental ones determined from the equilibrium simulations.

In flexane the distribution of dihedral angles agrees quite well with that predicted for a single molecule in isolation. There is a slight tendency for there to be an excess in the region of $\alpha_2 = 0^\circ$ and $\alpha_{1,3} = \pm 180^\circ$ which is consistent with the excess in $\rho(r_{16})$ in the region of 5Å indicating that in the bulk fluid the TTC and CTC conformers are preferred to some extent.

In hexane there are significantly higher proportions of gauche angles than predicted from the boltzmann factors. This has been quantified in terms of the observed and 'theoretical' percentages of the respective angles in table 5.3.

Figure 5.10 $\rho(\alpha_{1,3})$ and $\rho(\alpha_2)$, hexane, comparison with 'gas phase' distribution (- - -), T~200K.

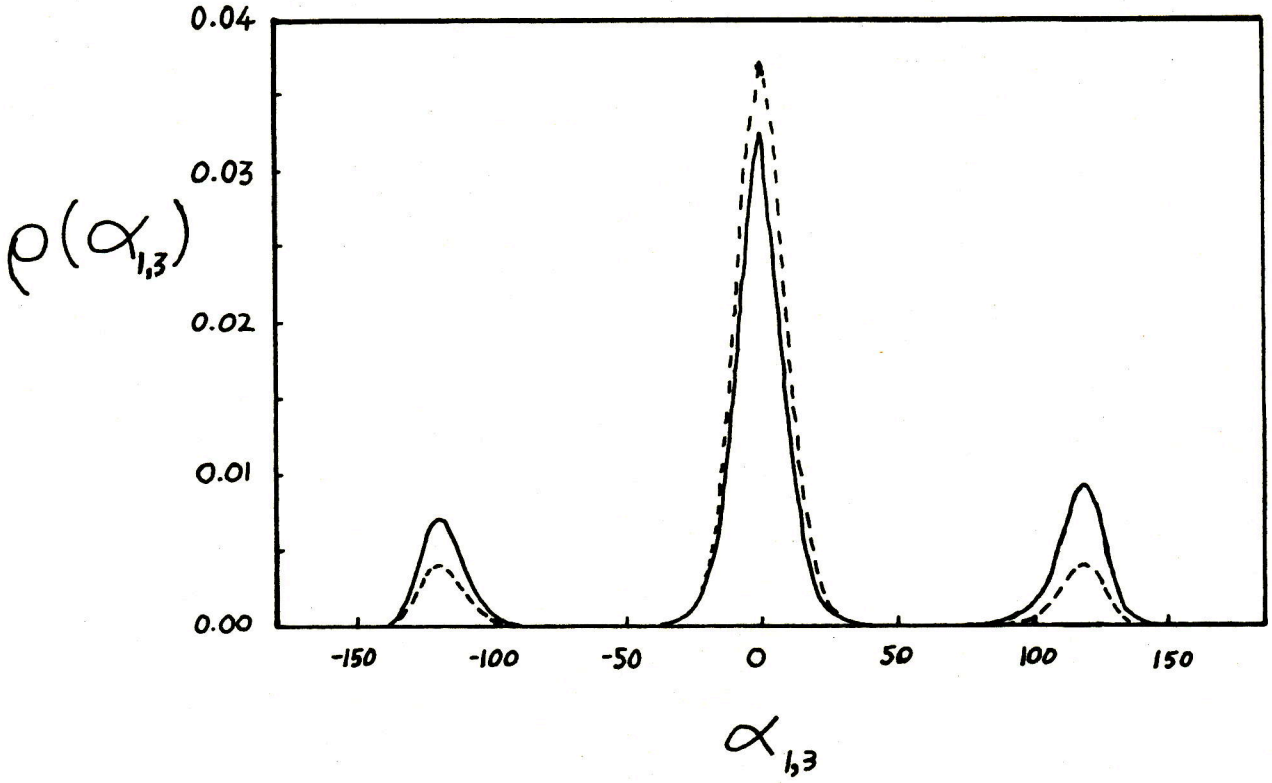

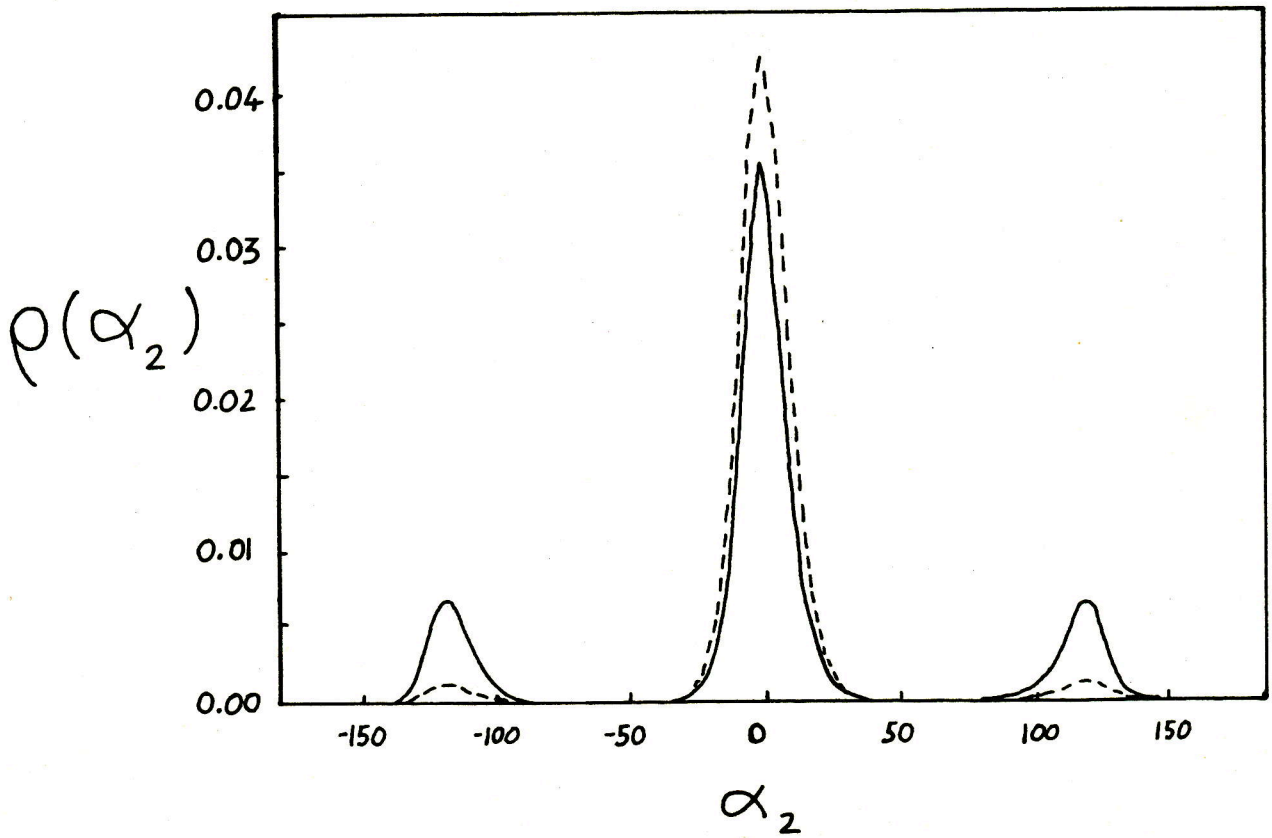

Figure 5.11 As fig.5.10 for flexane, T~200K.

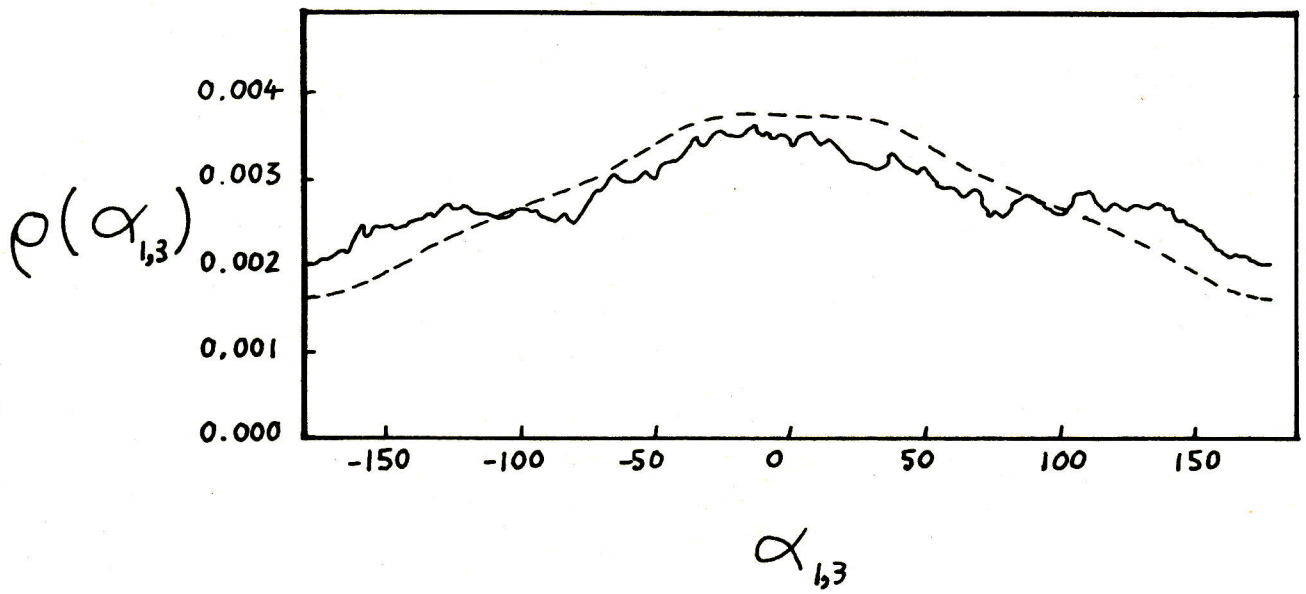

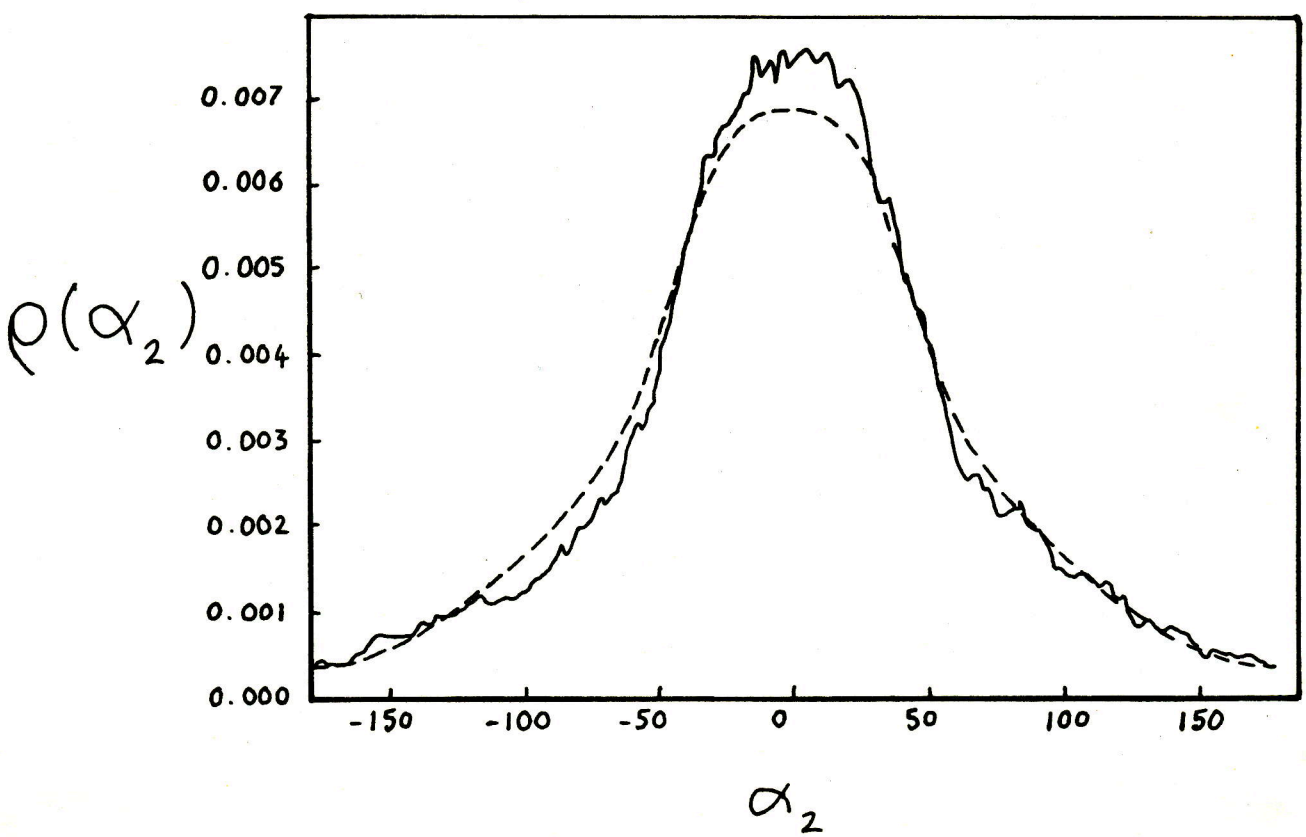

Figure 5.12 $\rho(r_{16})$, comparison with the 'gas phase' distribution (- - -), hexane (1) and flexane (2), T~200K.

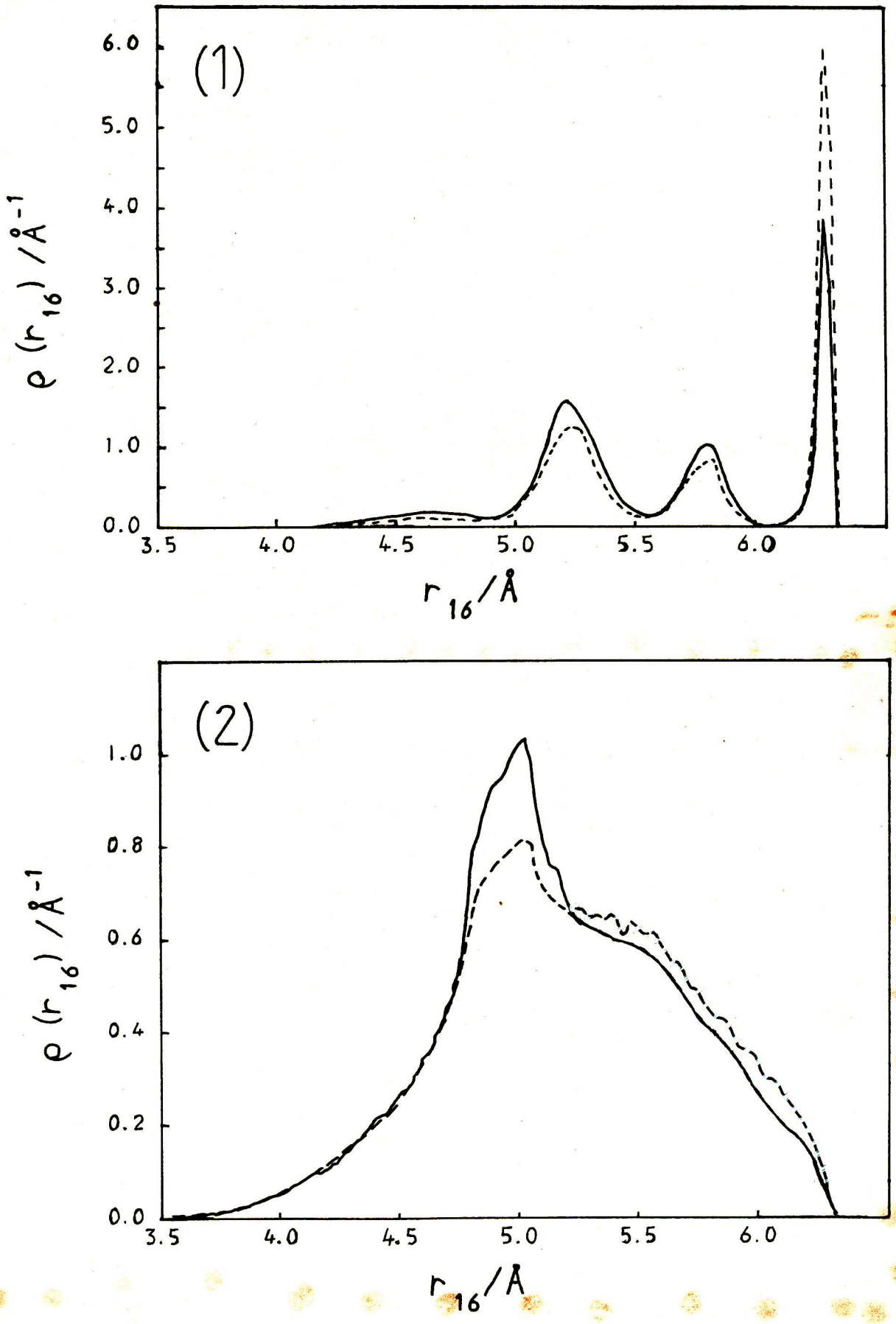

Table 5.3. The observed (obs) and expected (exp) percentages of dihedral angles for hexane and flexane at T~200K.

		$\alpha_{1,3}$		α_2	
		G	T	G	T
Hexane	Obs	27	73	25	75
	Exp	16	84	5	95
Flexane	Obs	61	39	29	71
	Exp	57	43	32	68

Qualitatively the same effect is seen in the $\rho(r_{16})$ with significantly less all trans conformers than is predicted and a correspondingly larger probability of conformers containing a gauche angle.

From the flexane case it is clear that the bulk fluid does exert some slight influence on the internal structure of molecules. In hexane there is an apparently much greater effect which is not unfeasible as it is likely that a fluid of more rigid molecules will influence the intramolecular arrangement of a molecule more than a fluid made up of flexible ones. It could be equally well argued that a rigid molecule is more capable of resisting the efforts of the bulk fluid to alter its structure. This again brings into question the equilibration procedure and the possibility that the

hexane system is to some extent 'frozen' in a non-equilibrium state.

5.8 Intramolecular Dynamics

To establish whether the system is in equilibrium requires a knowledge of the rates of transition over the internal barriers for the competing G→T and T→G processes. Parity between these rates would be indicative of equilibrium but their actual determination in a MD experiment is not always straightforward because of the ambiguity in defining what constitutes a 'transition' and the possible poor statistics which will occur when slow transition rates are combined with the fact that there are relatively few dihedral angles to be sampled over. As an attempt at determining these transition rates the changes in the dihedral angles were followed closely in equilibrium runs for hexane and flexane. Transitions were deemed to have occurred when the angle passed through any of the three maxima in the potential at $\alpha = \pm 60^{\circ}$ and $\alpha = 180^{\circ}$, with the direction of crossing determining whether it is a G→T or a T→G transition in the case of $\alpha = \pm 60^{\circ}$. It is then a simple matter to count up the number of each type in a certain time span and arrive at an estimate for the frequency of a transition. The definition of a transition used here is a simple one and does not take into account the possibility that an angle may temporarily just cross one of the 'barriers' only to return to the same potential well causing two

transitions to be registered using the accounting scheme described whereas, in fact, no complete transitions took place. Other definitions have similar problems and thus the ambiguity.

In table 5.4 the numbers of the various transitions from a period of ~62ps of an equilibrium simulation of 108 hexane molecules is given along with those for the same count performed over a much shorter time ~22ps on a flexane system.

Table 5.4 The number of transitions observed in equilibrium simulations at T~200K on hexane and flexane in a period of 62ps and 22ps respectively.

	$\alpha_1+\alpha_3$			α_2		
	G→T	T→G	G→G	G→T	T→G	G→G
Hexane	69	60	0	31	25	0
Flexane	2559	2550	2793	1234	1233	190

The flexane data is included for comparison only as their are no barriers to rotation arising from a dihedral angle potential but it is interesting to note that for α_2 G→G transitions are much less frequent than the rest. The probability densities in fig.5.9 reveal that in flexane α_2 values in the region of $\pm 180^\circ$ are particularly unfavourable because of the intramolecular LJ interactions consequentially there is a low rate of G→G transitions. For the other transitions there are no appreciable barriers and the rates of

crossing are high with virtual equality in the numbers of G→T and T→G movements. Rates of G⟷T transitions are only slightly less for α_2 as the total number counted less than half the figure for the total for α_1 and α_3.

In hexane a period of almost three times that sampled for flexane produces relatively few transitions. As expected there are no G→G transitions as this barrier is of order 10kT at 200K. There is an imbalance in the numbers of G→T and T→G transitions but with such poor statistics it is impossible to say whether this is systematic or not. As for flexane there is no indication that the rates of T⟷G movements is significantly larger for the end dihedral angles. From the total number of transitions (N_t), the length of the sampling time (t_s) and the total number of dihedral angles (N_a) the mean time between transitions (τ_m) in a dihedral angle has been estimated from

$$\tau_m = N_a t_s / N_t \quad . \qquad (5.8.1)$$

For hexane τ_m~110ps but for flexane τ_m~0.7ps which gives a measure of the contrasting timescales for the internal modes in these two models.

To examine in more detail the dynamics of the internal degrees of freedom two other types of functions were calculated. Firstly, the time correlation function for the dihedral angles, $C_\alpha(t)$, defined as

$$C_\alpha(t) = \langle \alpha_i(0)\alpha_j(t) \rangle \quad , \qquad (5.8.2)$$

where j=i for the auto-correlation function (acf) and j≠i for the cross correlation functions, and secondly the mean squared displacement of the dihedral angles

$$\bar{\alpha}_i^2 = \langle (\alpha_i(t) - \alpha_i(0))^2 \rangle \quad . \qquad (5.8.3)$$

The acf's for α are shown for hexane and flexane in figs.5.13 and 5.14. Once again the different time scales for the relaxation are apparent with hexane showing a decrease of only 20% in correlation in 35ps whereas in flexane the angles have totally decorrelated in one tenth of that time. It is possible to discern in flexane a different relaxation curve for α_2 whereas in hexane the time over which correlations were carried out is not long enough to establish a similar trend. Fitting the functions to the form $C_\alpha(t)=\exp(-t/\tau)$ gives relaxation times of ~0.33ps for $\alpha_{1,3}$ and ~0.54ps for α_2 in flexane and relaxation times in excess of 100ps for hexane.

The dihedral angle cross correlation functions are shown in fig.5.15 for flexane. The functions $\langle \alpha_1(0)\alpha_2(t) \rangle$ and $\langle \alpha_2(0)\alpha_3(t) \rangle$ have significant zero time values and show similar relaxation behaviour as the self correlation functions but $\langle \alpha_1(0)\alpha_3(t) \rangle$ has a much smaller zero time value and is a particularly noisy function. The existence of correlation

Figure 5.13 The normalised dihedral angle correlation function $\hat{C}_\alpha(t)$ vs. t, hexane, T~200K.

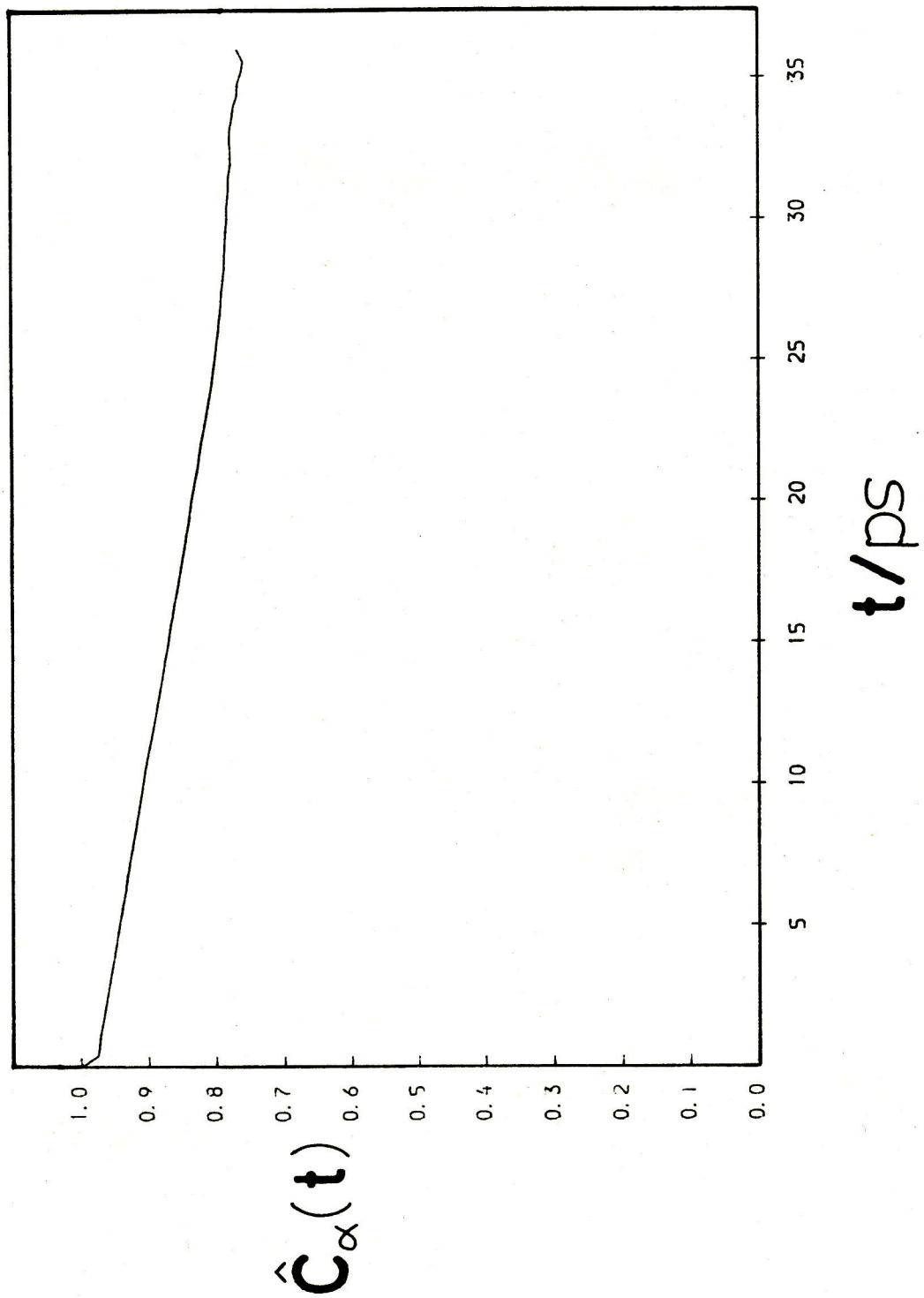

Figure 5.14 As fig.5.13 for flexane, T~200K.

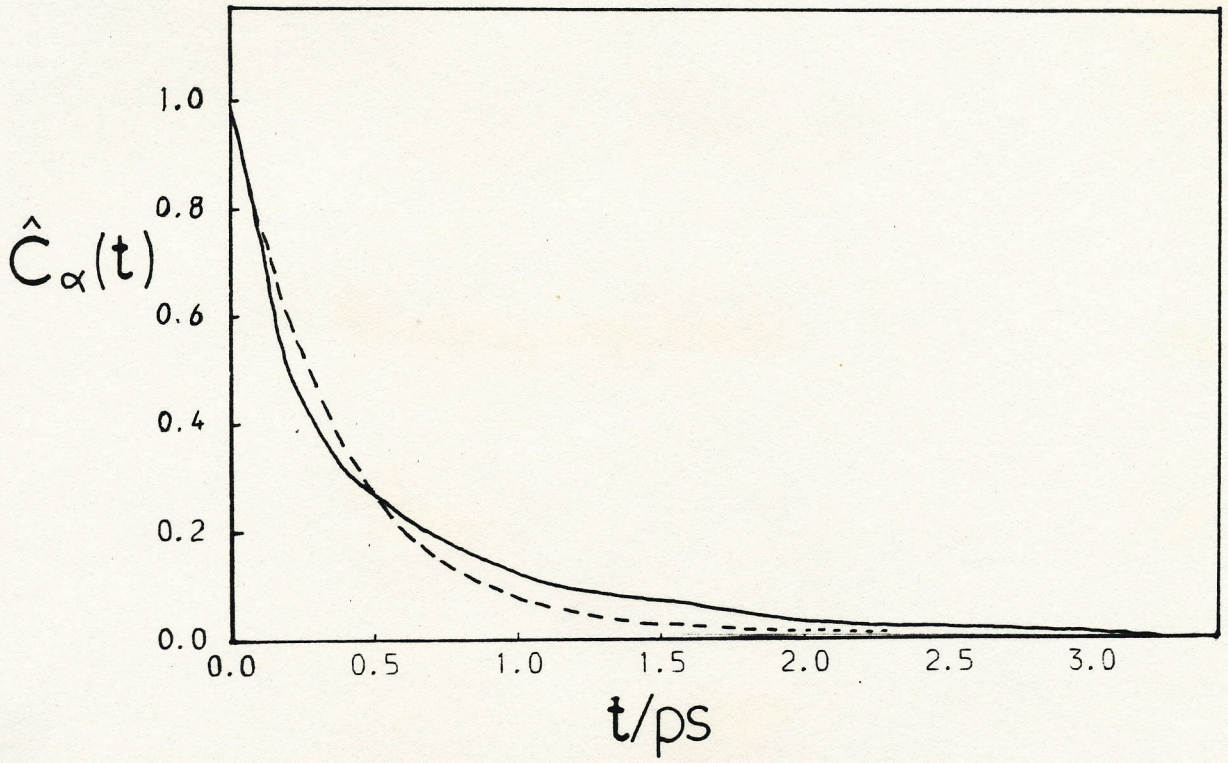

Figure 5.15 The normalised dihedral angle cross-correlation function $\hat{C}_{\alpha_{ij}}(t)$ vs. t flexane, T~200K.

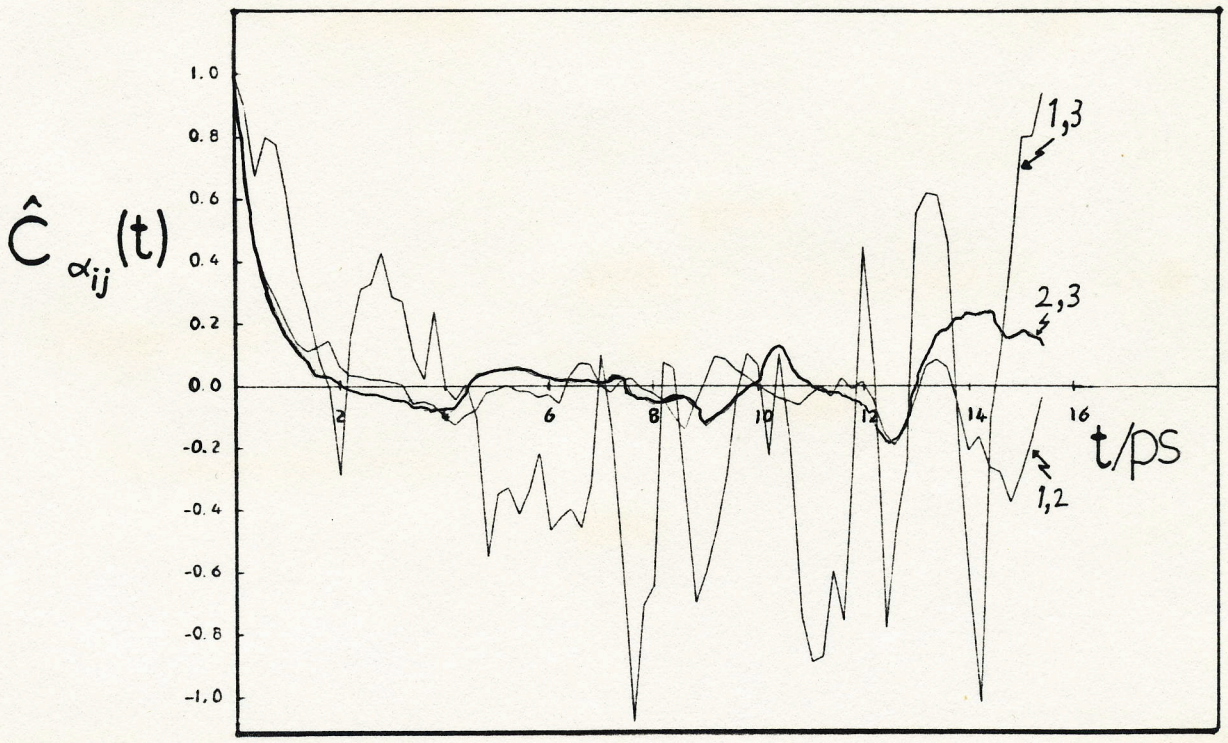

between nearest neighbour angles points to a degree of cooperative motion even in this highly flexible molecule. For hexane the length of correlation times is such that it is impossible to see this effect in the systems used here without sampling considerably more of phase space.

The second function, $\bar{\alpha}^2(t)$, is shown for hexane and flexane at short times in fig.5.16 and at long times in fig.5.17. At all times there is a considerable difference in the magnitude of $\bar{\alpha}^2(t)$ between hexane and flexane as would be expected. The interesting differences lie in the qualitative behaviour at short times. Flexane shows a smooth transition from an initial quadratic rise of $\bar{\alpha}^2(t)$ with time to a linear rise very similar to that seen in the mean squared displacement of particles. In hexane $\bar{\alpha}^2(t)$ shows the effect of the dihedral angle potential particularly well as the function is highly oscillatory at short times. For $\bar{\alpha}_2^2(t)$ there are at least nine discernible oscillations in a period of 1.8ps. For $\bar{\alpha}_{1,3}^2(t)$ in hexane the behaviour is slightly different at short times as the oscillations are damped out by the tendency for angles to undergo transitions which gives rise to a more linear increase in $\bar{\alpha}^2(t)$. Flexane shows a factor of two difference in $\bar{\alpha}^2(t)$ between the end angles, α_1 and α_3, and the central angle, α_2, even at short times whereas in hexane only the long time values of $\bar{\alpha}^2(t)$ show the divergence of the functions for the different types of angle. From the long time slope of $\bar{\alpha}^2(t)$ it is possible to define an

Figure 5.16 The mean squared displacement of the dihedral angles $\alpha^2(t)$ vs. t at short times, hexane (1) and flexane (2), T~200K.

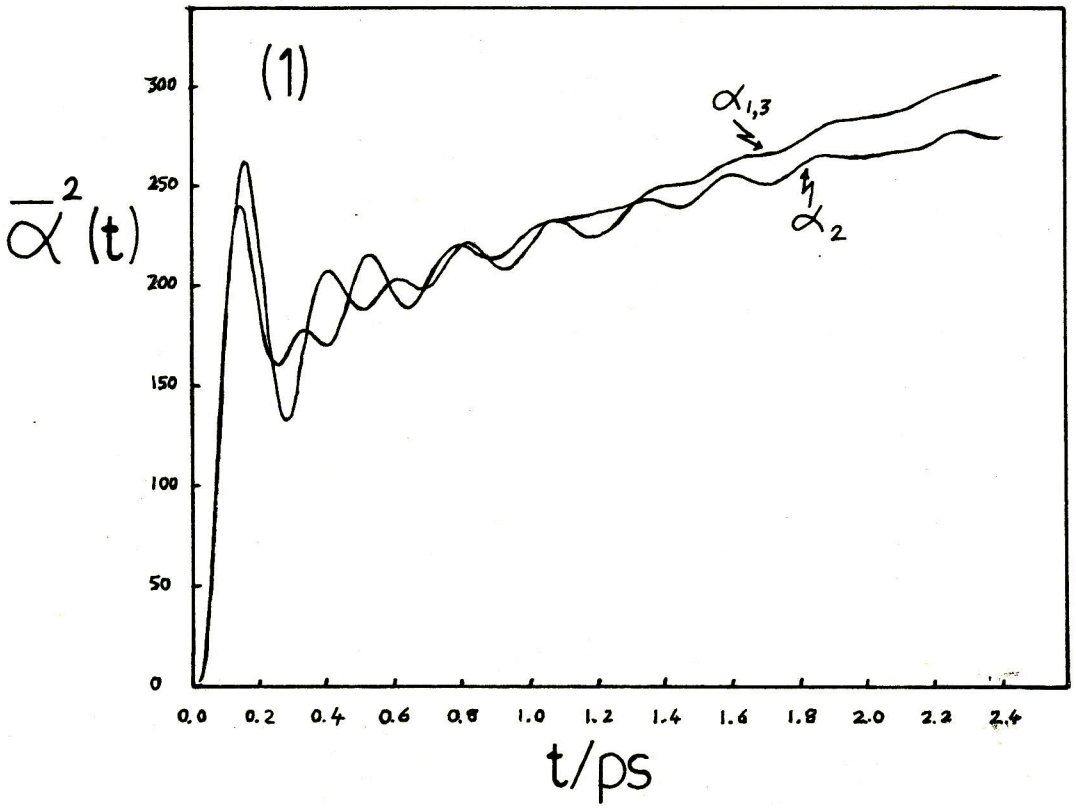

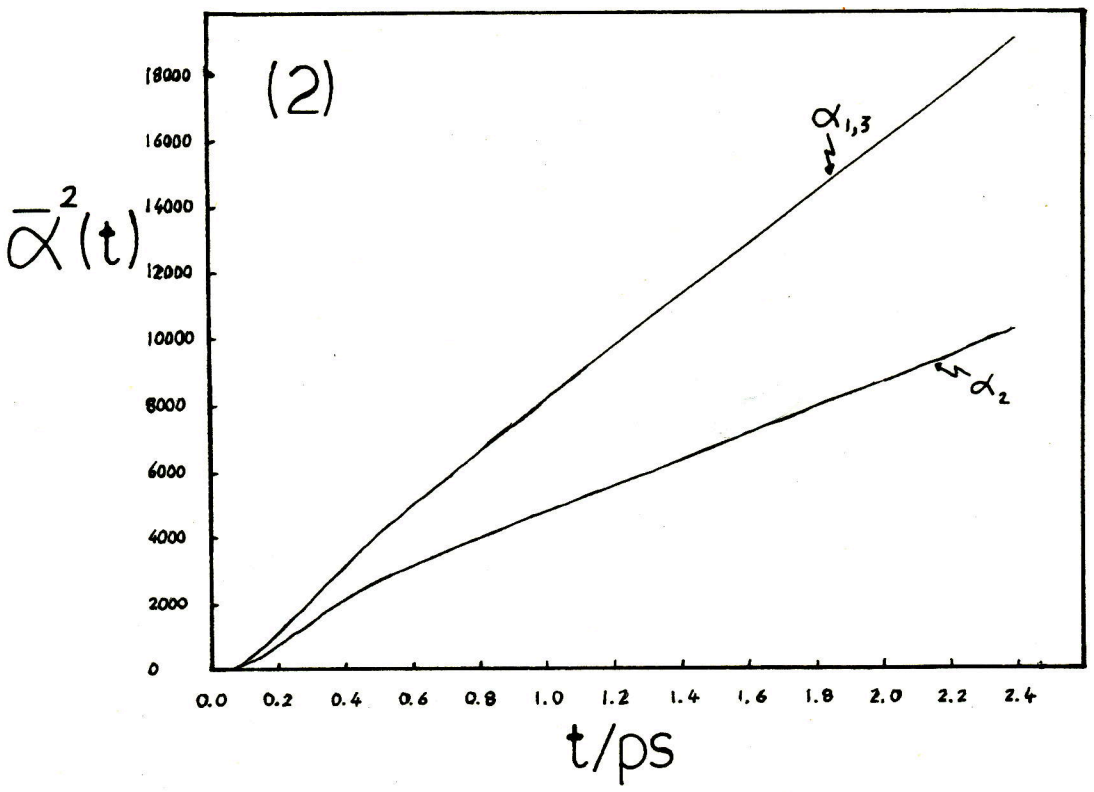

Figure 5.17 $\bar{\alpha}^2(t)$ vs. t at longer times, hexane (1) and flexane (2), T~200K.

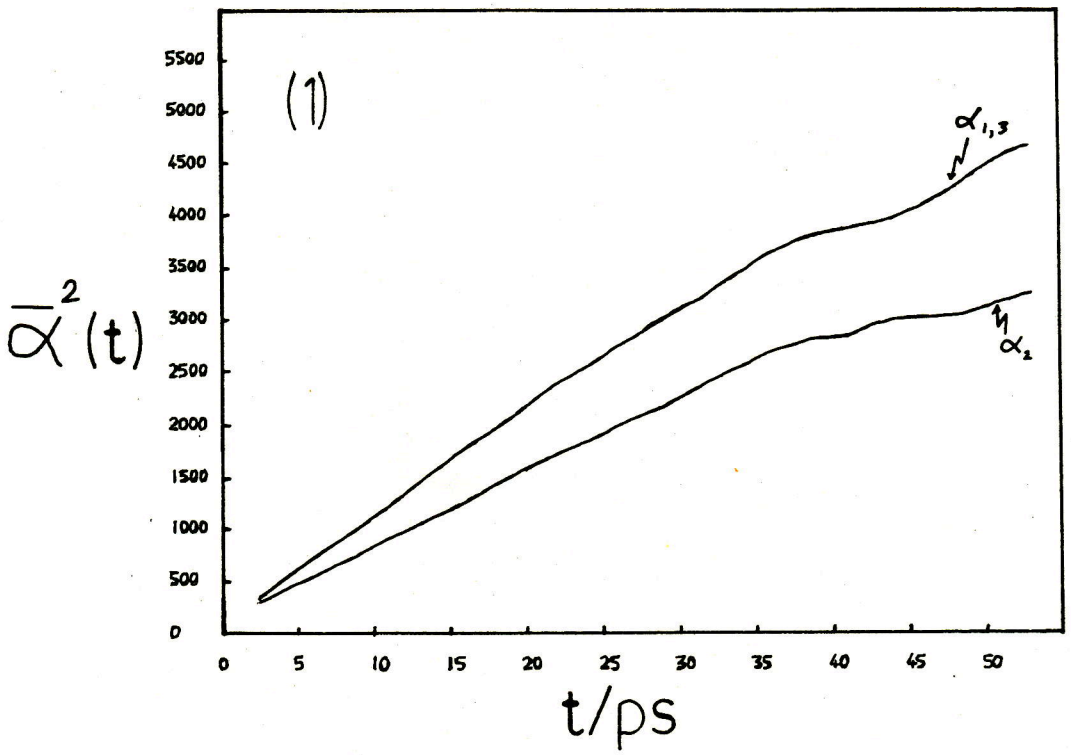

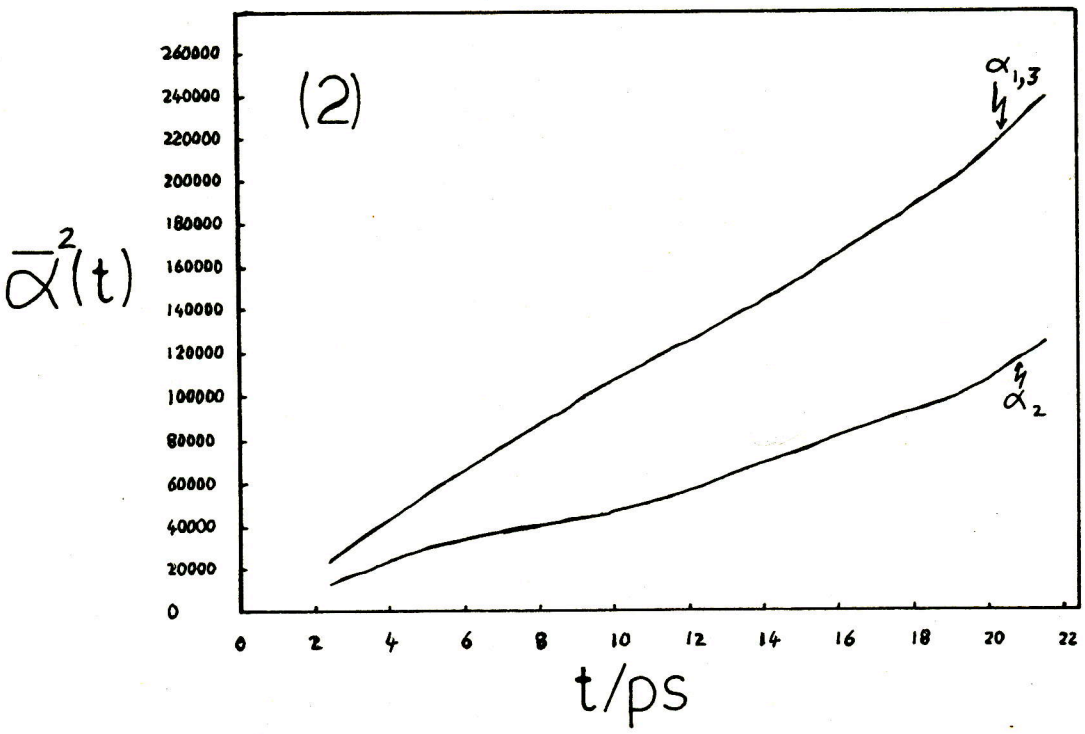

angular diffusion coefficient D_{α_i} given by

$$D_{\alpha_i} = \lim_{t\to\infty} \frac{d\bar{\alpha}^2(t)}{dt} . \qquad (5.8.4)$$

Furthermore, if one assumes that two transitions, one forward and one backward, are possible for each 120 degrees that the angle diffuses through then it is also possible to define another mean time between transitions, τ_m, as

$$\tau_m = 120^2/2D_\alpha . \qquad (5.8.5)$$

The results for D_α and τ_m are given in table 5.5. for hexane and flexane.

Table 5.5 The angular diffusion coefficient, D_α, and the mean transition time, τ_m, as defined in eqns.5.8.4 and 5.8.5, determined from equilibrium simulations of hexane and flexane at T~200K.

	D_{α_1}/ps^{-1}	D_{α_2}/ps^{-1}	τ_{m_1}/ps	τ_{m_2}/ps
Hexane	100±10	70±10	72±8	99±10
Flexane	10960±530	5530±500	0.66±0.03	1.03±0.12

It can be seen from table 5.5 that the mean transition times evaluated using eqn.5.8.5 are in reasonable agreement with those obtained using eqn.5.8.1.

So far it has been established that the two molecules

have very similar gross thermodynamical properties some small differences in static intermolecular correlations and completely different internal structure and dynamics. The torsional modes in these fluids have already been shown to be on a time scale comparable to that of intermolecular motions so it is more than likely that there will be significant coupling between the two. The possibility is then that there will be differences in the diffusive motion of the two molecules, and thus presumably in their viscosity.

5.9 Self Diffusion

The diffusive motion of these molecules has been monitored in the usual way through the velocity auto-correlation function (VACF) given by

$$C_v(t) = \langle \underline{v}_i(0) \cdot \underline{v}_i(t) \rangle \quad , \qquad (5.9.1)$$

and the mean squared displacement

$$\bar{R}^2(t) = \langle (\underline{R}_i(t) - \underline{R}_i(0))^2 \rangle = \langle \left(\int_0^t \underline{v}_i(s)\, ds \right)^2 \rangle \qquad (5.9.2)$$

where $\underline{R}_i$ and $\underline{v}_i$ are the position and velocity of the COM of molecule i. In addition a number of resolutions have been performed to try and probe the motions of these molecules more deeply and these will be discussed in turn.

In theory it is possible to determine the diffusion coefficient from either $C_v(t)$ or $\bar{R}^2(t)$ from the following eqns.

$$D = \frac{1}{3}\int_0^\infty C_v(t)\,dt \qquad (5.9.3)$$

and

$$D = \lim_{t\to\infty} \bar{R}^2(t)/6t \qquad (5.9.4)$$

In practice it is simpler and more efficient to calculate D from eqn.5.9.4 as all that is required is a knowledge of the position of the COM relative to its original position at a number of time intervals. This quantity squared, averaged and plotted as a function of time allows a slope to be determined graphically , or otherwise, from which D can be obtained. Eqn.5.9.3, however, requires a detailed accurate knowledge of $C_v(t)$ which requires the storage of much more information, in the form of velocity vectors, and a large amount of correlating. For systems in which diffusive relaxation times are short it has been shown previously that reliable estimates can be obtained from both methods [66].

For the reasons stated above the VACF has only been determined for short times, ~2ps, whereas the the mean squared displacement has been followed for much longer periods. $C_v(t)$

and $\bar{R}^2(t)$ are shown in figs.5.18 and 5.19. From fig.5.19 it can be seen that flexane clearly diffuses more rapidly than hexane and this is quantified by the diffusion coefficients obtained from the slopes of these graphs given in table 5.6. Also given in table 5.6. is the value for D obtained by numerically integrating the VACFs shown in fig.5.18.

Table 5.6. The diffusion coefficients for hexane and flexane obtained from :-

(a) the mean squared displacements and

(b) the integral over the velocity auto-correlation function.

	(a)	(b)
	$D/10^{-9}m^2s^{-1}$	$D/10^{-9}m^2s^{-1}$
Hexane	Ø.35±Ø.Ø2	Ø.49±Ø.Ø8
Flexane	Ø.53±Ø.1Ø	Ø.96±Ø.Ø6

There is a large disparity in the values obtained from the different expressions but this is not unlikely considering the fact that the VACF for both fluids shows a tendency to remain negative out to at least 2ps and it is known for other fluids that this long time tail can persist for much longer [126]. Truncation of $C_v(t)$ in this case will, thus, result in the observed overestimation of D.

The general form of the VACFs is the same, an initial rapid decay is followed by a long negative region out to about t=2ps beyond which $C_v(t)\sim Ø$. In the case of hexane the

Figure 5.18 The normalised velocity auto-correlation function $\hat{C}_v(t)$ vs. t, hexane (——) and flexane (—·—·—), T~200K.

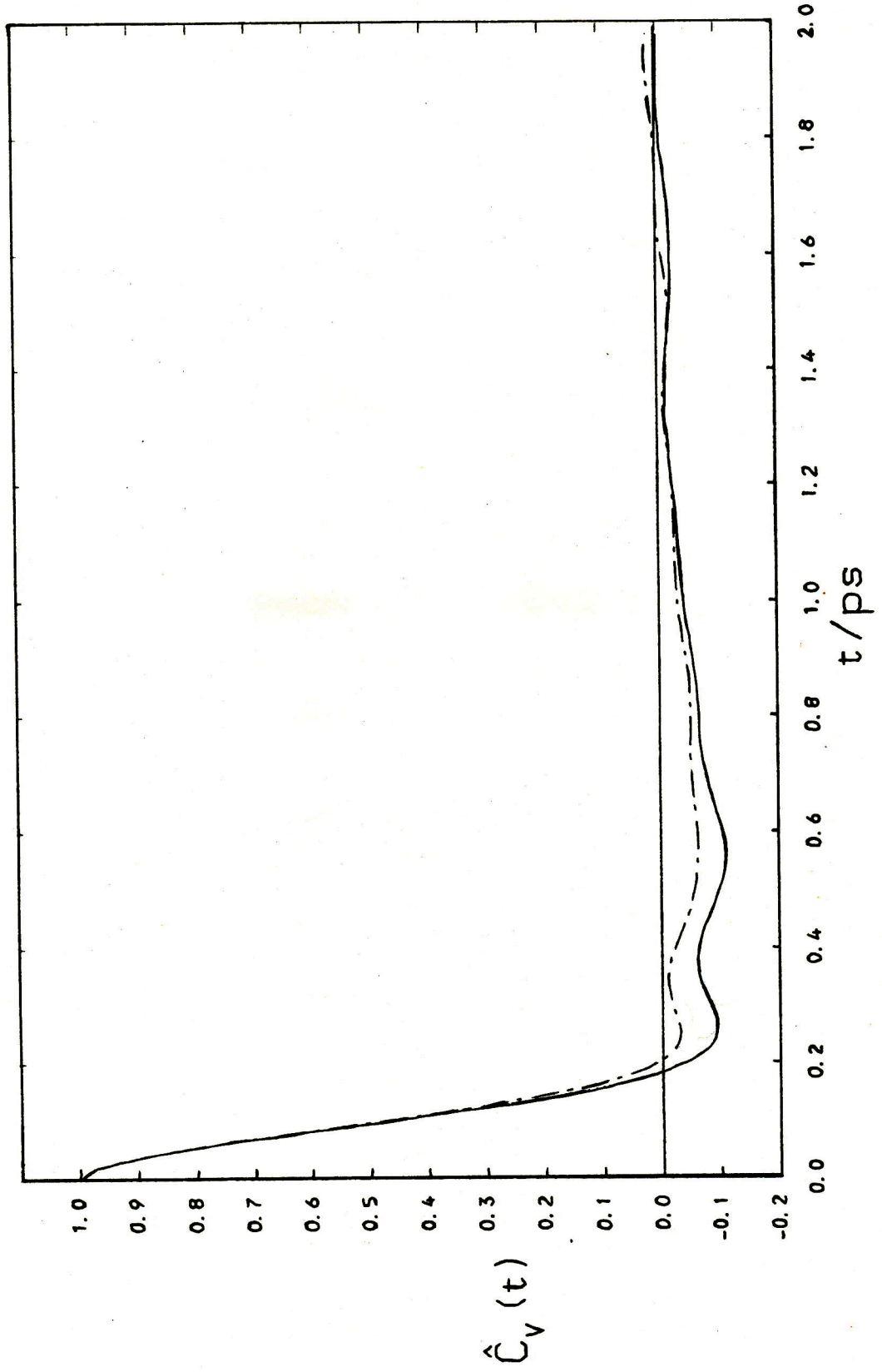

Figure 5.19 The mean squared displacement of the centres of mass $\overline{R}^2(t)$ vs. t, hexane (1) and flexane (2), T~200K.

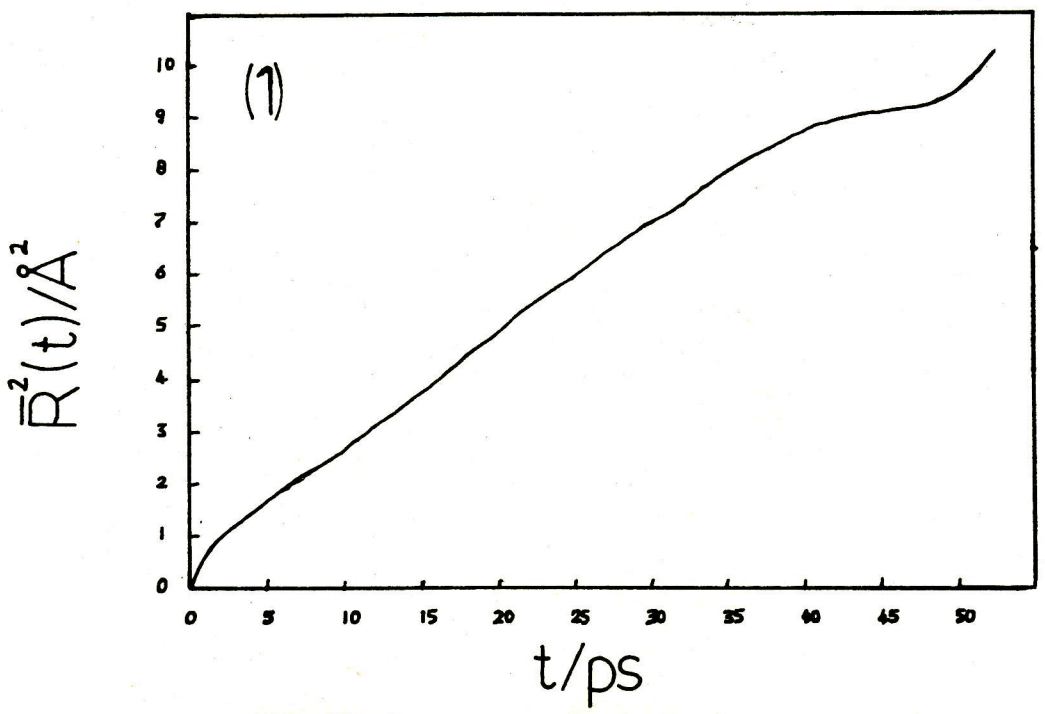

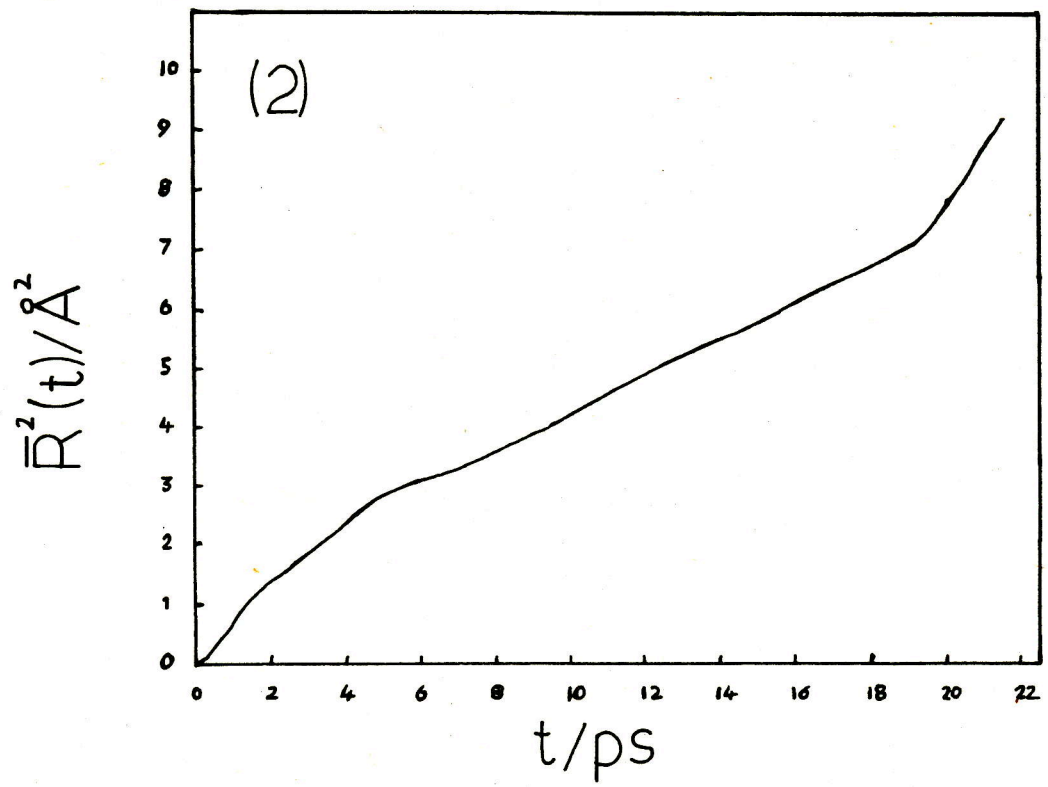

negative part of the function is much more pronounced than in flexane with the result that the integral over $C_v(t)$, and, therefore, D, is less for hexane than for flexane.

The two minima that appear in both functions, at t~Ø.25ps and t~Ø.55ps, are characteristic of molecular fluids [111]. Resolution of the VACF into directions parallel and perpendicular to the end-to-end vector, $\underline{r}_{16}$, are shown in figs.5.2Ø and 5.21 for hexane and flexane where

$$\hat{C}_{v_{\parallel}}(t) = \langle \underline{v}_{\parallel}(0)\cdot\underline{v}_{\parallel}(t)\rangle / \langle \underline{v}_{\parallel}^2(0)\rangle \,, \qquad (5.9.5)$$

$$\hat{C}_{v_{\perp}}(t) = \langle \underline{v}_{\perp}(0)\cdot\underline{v}_{\perp}(t)\rangle / \langle \underline{v}_{\perp}^2(0)\rangle, \qquad (5.9.6)$$

$$\underline{v}_{\parallel} = (\underline{v}\cdot\hat{\underline{r}}_{16})\hat{\underline{r}}_{16}$$

and

$$\underline{v}_{\perp} = \underline{v} - \underline{v}_{\parallel} \,.$$

These clearly show that the double minima originates from the motion perpendicular to $\underline{r}_{16}$. This has previously been interpreted for diatomics [111] as being caused by successive collisions of either end of the molecule. The results here suggest that it is a feature of elongated molecules in general. It can also be seen from figs.5.2Ø and 5.21 that there is a less pronounced negative dip in flexane for both $C_{v_{\parallel}}(t)$ and $C_{v_{\perp}}(t)$, as was the case for $C_v(t)$, which shows that the enhanced diffusion does not occur specifically in

Figure 5.20 The normalised auto-correlation function for the velocity parallel to $\underline{r}_{16}$ $C_{v_{\parallel}}(t)$ vs. t, hexane (——) and flexane (—·—·—), T~200K.

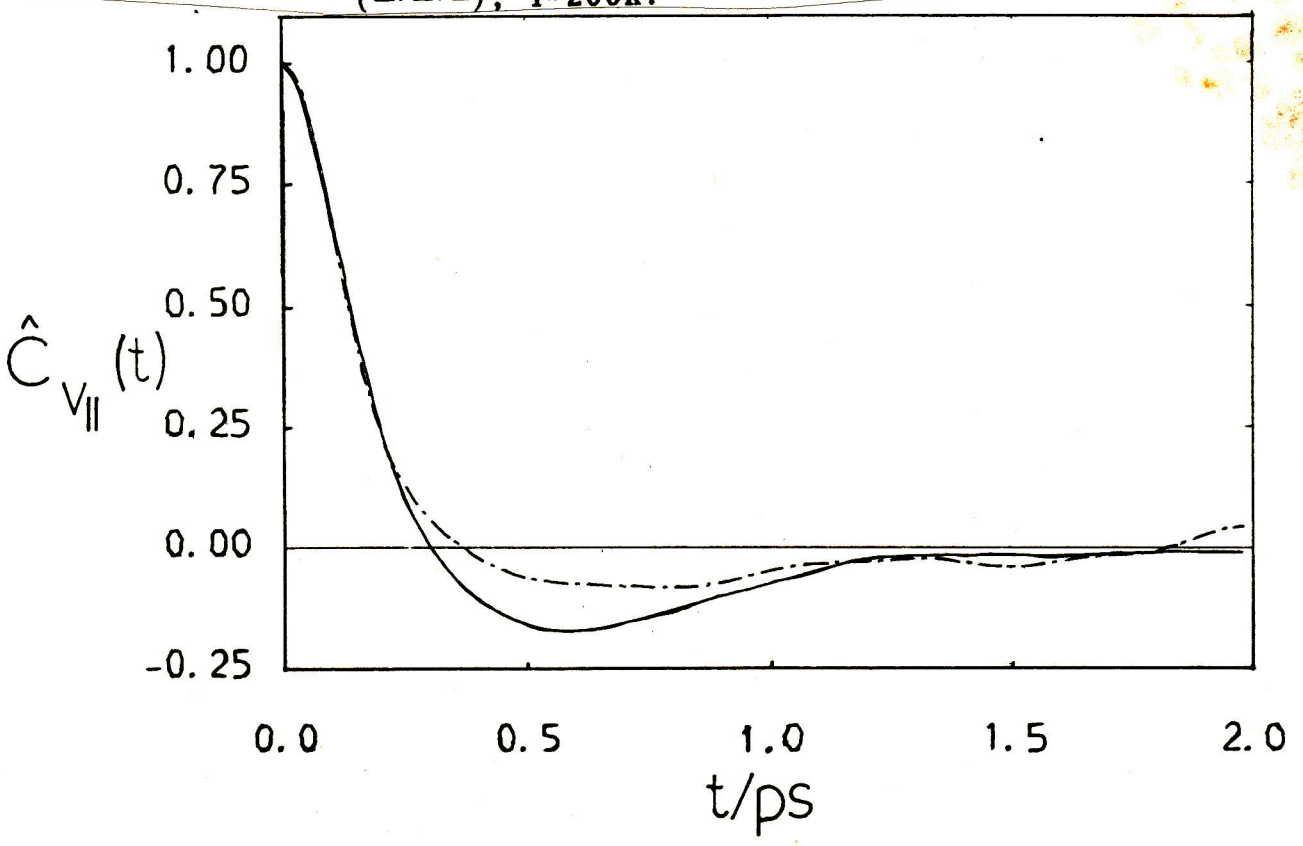

Figure 5.21 The normalised auto-correlation function for the velocity perpendicular to $\underline{r}_{16}$ $C_{v_{\perp}}(t)$ vs. t, hexane (——) and flexane (—·—·—), T~200K.

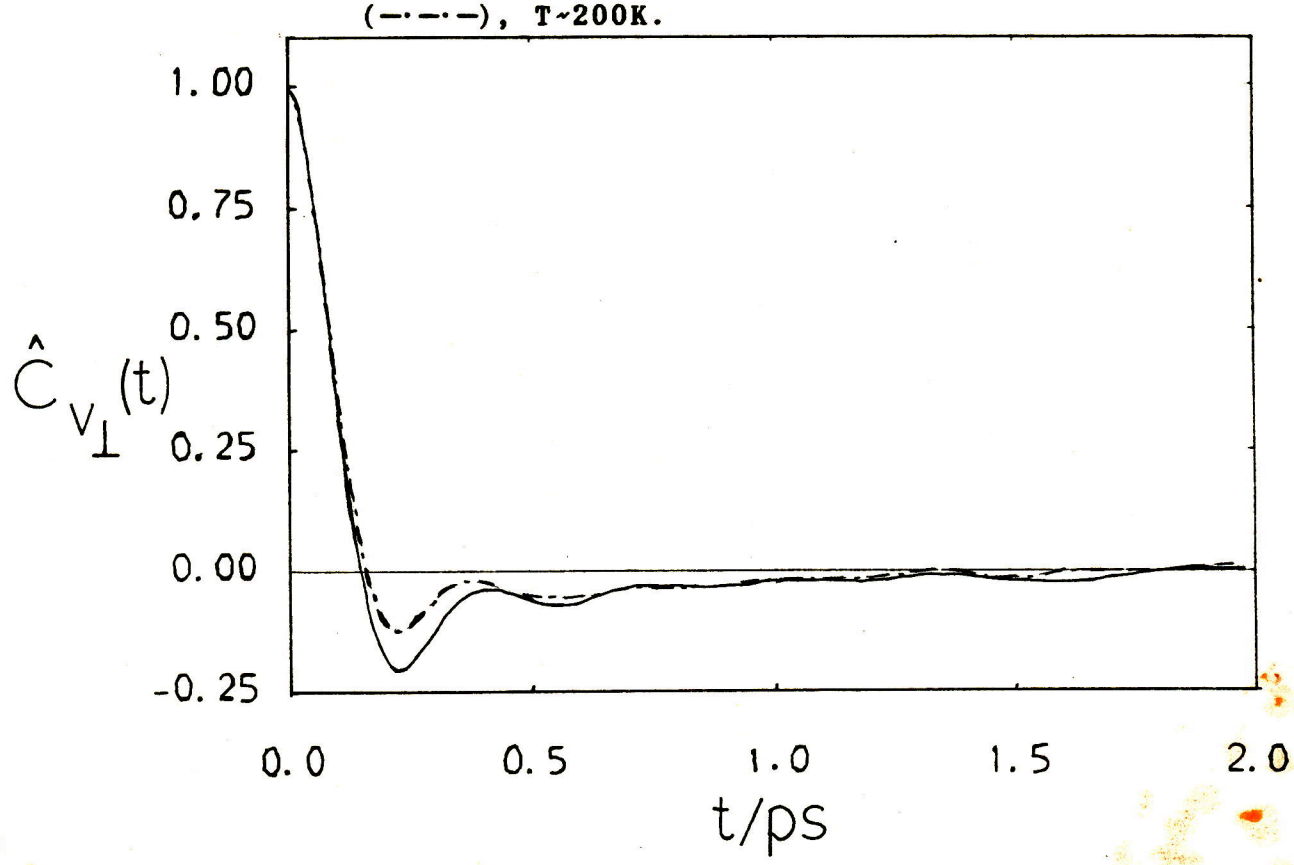

either of the directions but is an isotropic effect.

The integrals of these functions would give values for the diffusion coefficients parallel, $D_{\parallel}$, and perpendicular, $D_{\perp}$, to $\underline{r}_{16}$ but as these are subject to the same problems as evaluating D from $C_v(t)$ the ratio $D_{\parallel}/D_{\perp}$ has been calculated and is given, along with the zero time values, in table 5.7.

Table 5.7 The mean squared velocities and the relative diffusion coefficients parallel and perpendicular to $\underline{r}_{16}$ in hexane and flexane at T~200K.

	$\langle \underline{v}_{\parallel}^2(0) \rangle / m^2 s^{-2}$	$\langle \underline{v}_{\perp}^2(0) \rangle / m^2 s^{-2}$	$D_{\parallel}/D_{\perp}$
Hexane	18900±410	38020±500	1.32±0.23
Flexane	18790±460	37540±420	1.04±0.09

The factor of two difference between $C_{v_{\parallel}}(0)$ and $C_{v_{\perp}}(0)$ is simply caused by the fact that there is only one degree of freedom associated with the velocity parallel to $\underline{r}_{16}$ whereas the remaining two degrees of freedom are associated with the velocity perpendicular to $\underline{r}_{16}$. What is significant is that $D_{\parallel}/D_{\perp}$ is in both cases greater than one which shows that the molecules diffuse twice as fast in a direction parallel to $\underline{r}_{16}$ than they do in any possible perpendicular direction.

To corroborate this finding the mean squared displacements perpendicular and parallel to $\underline{r}_{16}$ were calculated using the equations

$$\bar{R}_{\parallel}^2(t) = \langle \left(\int_0^t \underline{v}_{\parallel}(s)\, ds \right)^2 \rangle \qquad (5.9.7)$$

and

$$\bar{R}_{\perp}^2(t) = \langle \left(\int_0^t \underline{v}_{\perp}(s)\, ds \right)^2 \rangle \qquad (5.9.8)$$

, where the definitions of $\underline{v}_{\parallel}$ and $\underline{v}_{\perp}$ are as in eqns.5.9.5 and 5.9.6. The results are shown in figs.5.22 and 5.23 and the close similarity of the curves for $\bar{R}_{\parallel}^2(t)$ and $\bar{R}_{\perp}^2(t)$ in both cases bears out the previous observation of enhanced diffusion parallel to $\underline{r}_{16}$.

Qualitatively the larger diffusion coefficient of flexane can be explained by the less negative dip in the VACF. This shows that in flexane there is less of a tendency for the COM velocity to reverse its direction so it doesn't return as close to its starting position after each 'collision' and, thus, diffuses further at each collision. This is reasonable as the relaxation of the internal modes of flexane is fast enough to cushion the impact of the impact of two colliding molecules whereas in hexane the dihedral angle potential prevents this occuring to a large extent.

Figure 5.22 The mean squared displacement (MSD) of the COM, $\bar{R}^2(t)$, and its resolution parallel, $\bar{R}^2_{\parallel}(t)$, and perpendicular, $\bar{R}^2_{\perp}(t)$, to $\underline{r}_{16}$, hexane, T~200K.

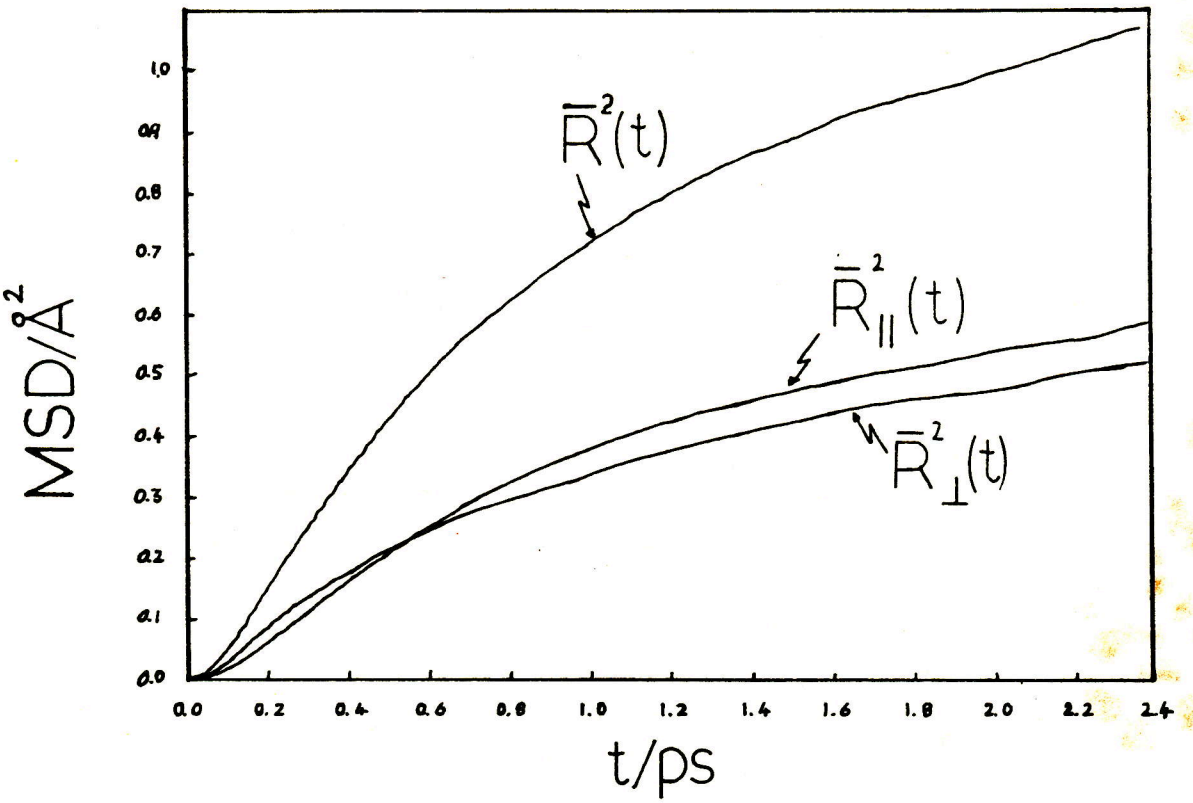

Figure 5.23 As fig.5.22 flexane, T~200K.

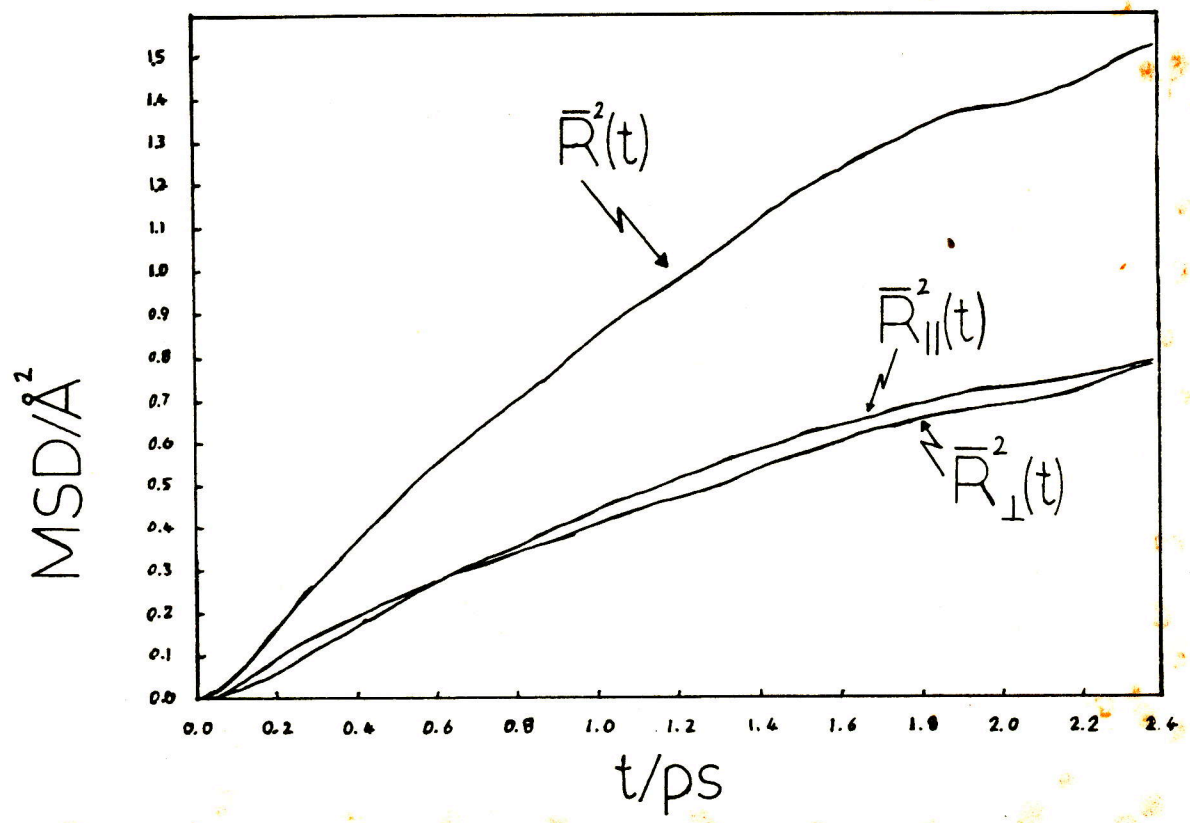

5.10 Correlation Functions for Force, Torque, Reorientation and Stress

One piece of evidence which supports the case for harder collisions in hexane is the mean squared force, $\langle \underline{F}_i^2(0) \rangle$, given together with the mean squared torque, $\langle \underline{T}_i^2(0) \rangle$, in table 5.8.

Table 5.8 The mean squared force and torque for hexane and flexane from equilibrium simulations at T~200K.

	Hexane	Flexane
$\langle \underline{F}_i^2(0) \rangle / 10^{-18} N^2$	0.186±0.002	0.177±0.004
$\langle \underline{T}_i^2(0) \rangle / 10^{-38} N^2 m^2$	0.642±0.012	0.538±0.012

As can be seen the mean squared force in the hexane system is greater than that in the flexane system.

The normalized correlation functions for the force and the torque are shown in figs.5.24 and 5.25 respectively. The only discernible difference is one of slightly less damped oscillations for hexane. One other point to note is that the normalized correlation functions for torque and force coincide. This result indicates that the reorientation of these molecules is largely decoupled from the fluctuations in the forces. To check this the correlation function for the normalized end-to-end vector, $\hat{C}_1(t)$, has been calculated from

Figure 5.24 The normalised force auto-correlation function $\hat{C}_F(t)$ vs. t, hexane (——) and flexane (—·—·—), T~200K.

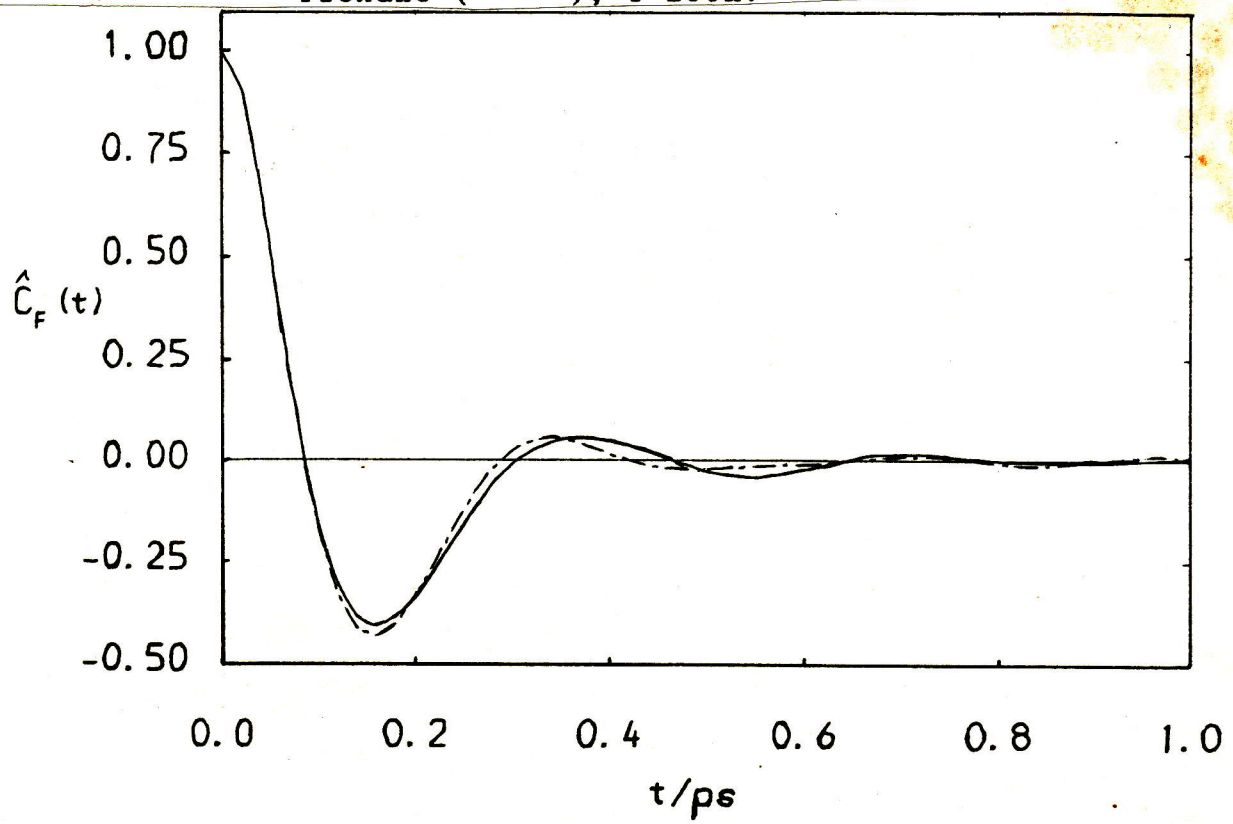

Figure 5.25 The normalised torque auto-correlation function $\hat{C}_T(t)$ vs. t, hexane (——) and flexane (—·—·—), T~200K.

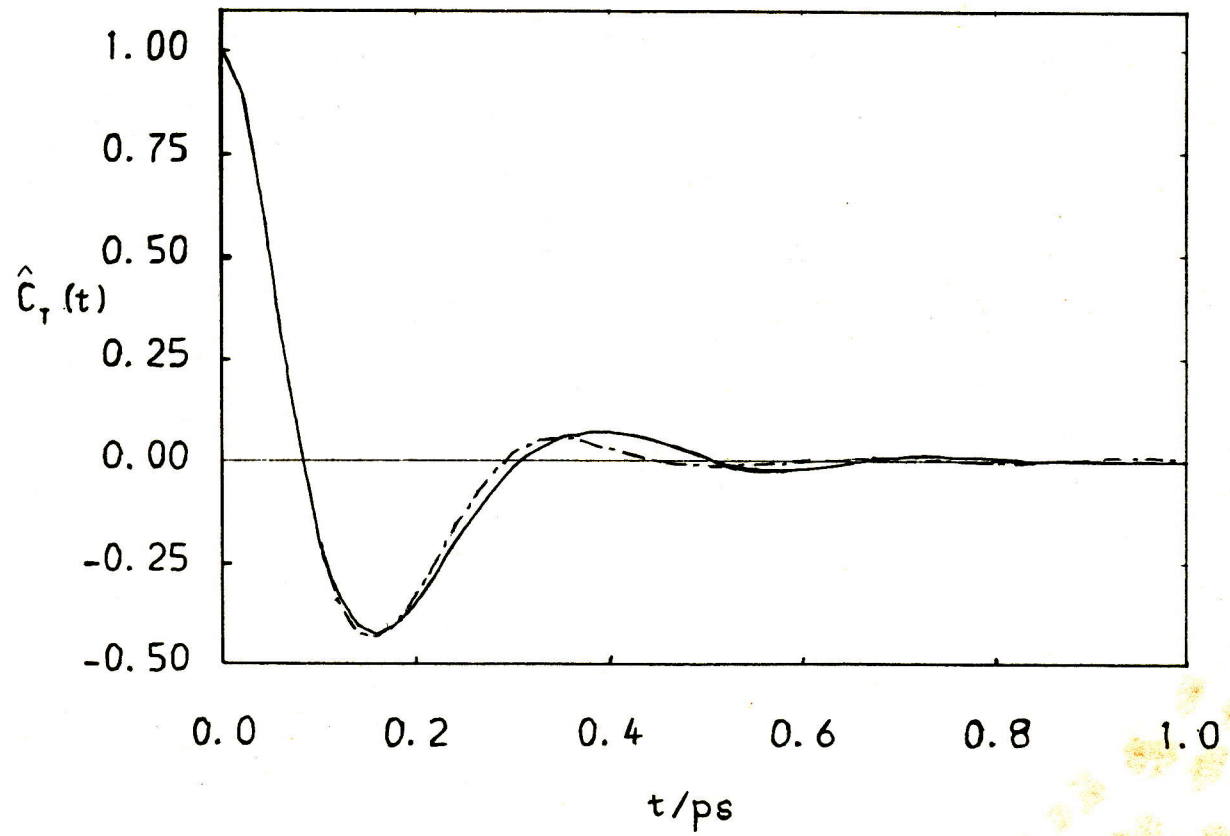

$$C_1(t) = \langle \hat{\underline{r}}_{16}(0) \cdot \hat{\underline{r}}_{16}(t) \rangle \qquad (5.10.1)$$

Although $\underline{r}_{16}$ is a crude measure of the orientation of a molecule its relaxation can only be the same as or faster than that of the 'true' orientation as the internal modes can only aid decorrelation. The function $C_1(t)$ is shown for hexane and flexane in fig.5.26. It can be seen from this figure that in the time it takes for the forces to relax, ~1ps, there is only a small change in $C_1(t)$ confirming the decoupling of reorientation from the force fluctuations. $C_1(t)$ for flexane decays more rapidly than for hexane, indeed the best fits to the form

$$C_1(t) = \exp(-t/\tau)$$

give estimates for the relaxation time, τ, to be ~30ps and ~70ps for flexane and hexane respectively. How much of this difference in the relaxation times is accounted for by the ease of internal rotations in flexane and how much is caused by a 'true' difference in the rate of reorientation is not obvious from these results. To obtain this information would require the calculation of a more meaningful orientational correlation function, possibly based on the vectors which diagonalise the moment of inertia tensor. For flexible molecules these vectors also change with time, like $\underline{r}_{16}$, but the actual process of having to diagonalise N matrices at each step the orientation is needed would be quite time consuming

Figure 5.26 The normalised auto-correlation function for the end-to-end vector $\hat{C}_1(t)$ vs. t, hexane (1) and flexane (2), T~200K.

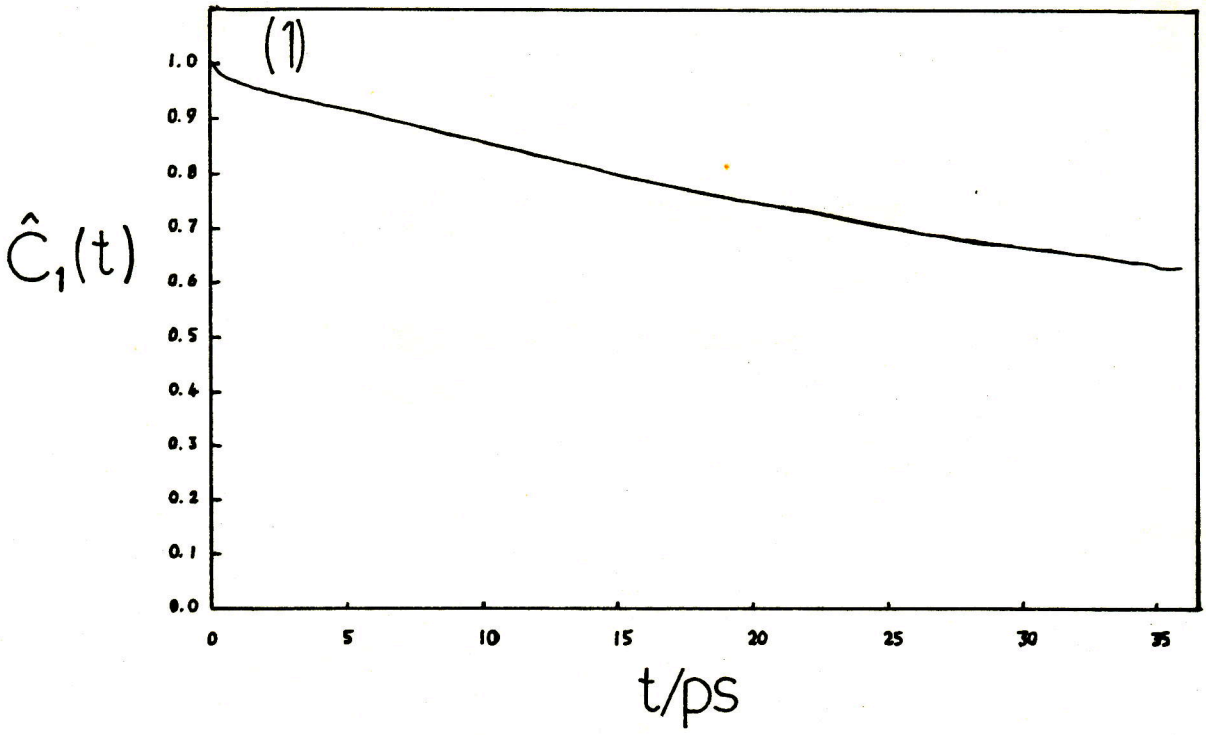

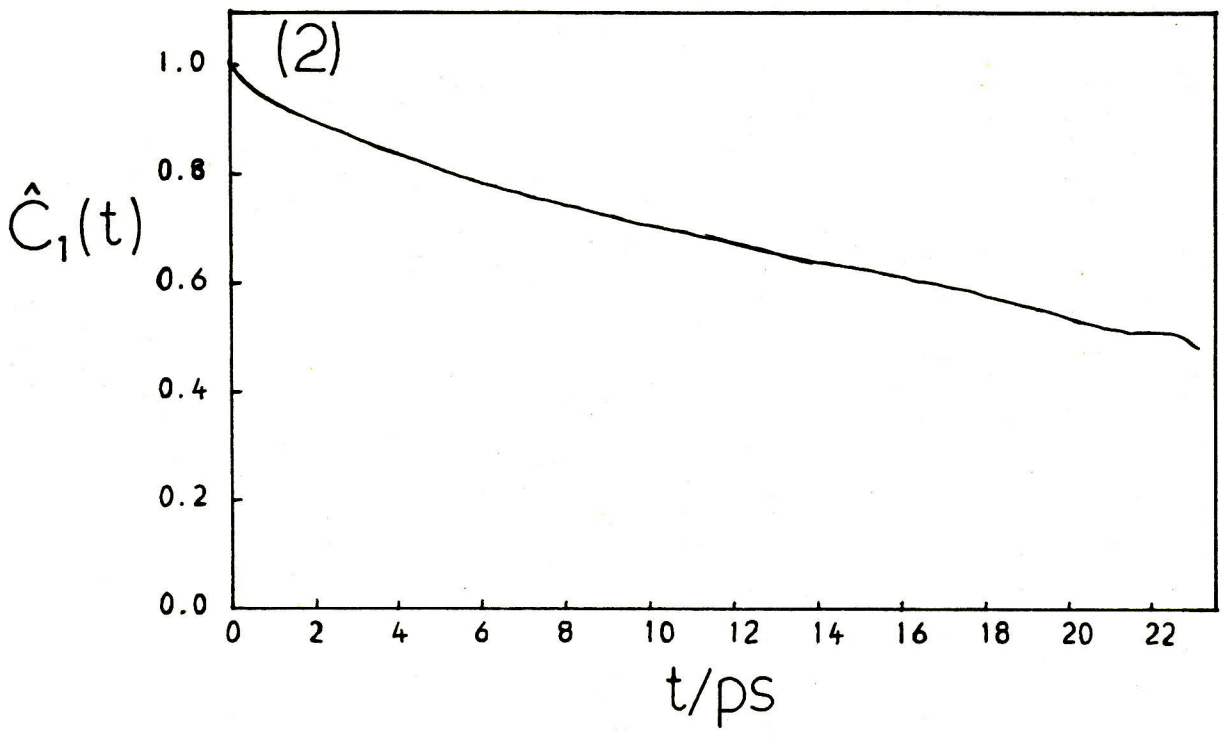

and was not considered worthwhile for the purposes for which the orientation was required here.

To complete the characterisation of these fluids at equilibrium one other correlation function has been evaluated. This is the stress correlation function, $C_s(t)$, defined as

$$C_s(t) = \langle \sigma_{\alpha\beta}(0)\sigma_{\alpha\beta}(t) \rangle$$

, where $\sigma_{\alpha\beta}$ is an off-diagonal element of the stress tensor. In theory it is possible to determine the viscosity from $C_s(t)$ but because of the problems already discussed of poor statistics, stemming from its collective nature, and long time correlations, it is impractical for this purpose within present day limitations. It does produce two useful pieces of information though , the infinite frequency shear modulus, G_∞ $(=\langle \sigma^2_{\alpha\beta}(0) \rangle V/kT)$, and the form of the stress relaxation, at least at short times. The normalized stress correlation functions, $\hat{C}_s(t)$, are shown in figs.5.27 and 5.28 for hexane and flexane. $C_s(t)$ was averaged over all possible off-diagonal elements of the stress tensor, the total length of the averaging period being ~38ps for hexane and 26ps for flexane. The mean squared stress, resultant G_∞ and viscosity, obtained from numerically integrating $C_s(t)$ are given in table 5.9.

Figure 5.27 The normalised stress correlation function $\hat{C}_s(t)$ vs. t, (i) at short times, (ii) at longer times and (iii) the integral of $\hat{C}_s(t)$ vs. t, hexane, T~200K.

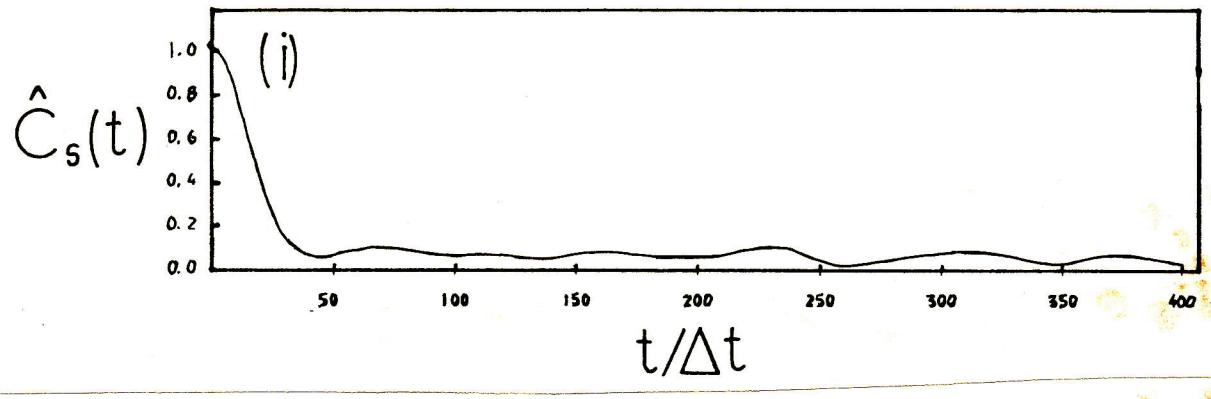

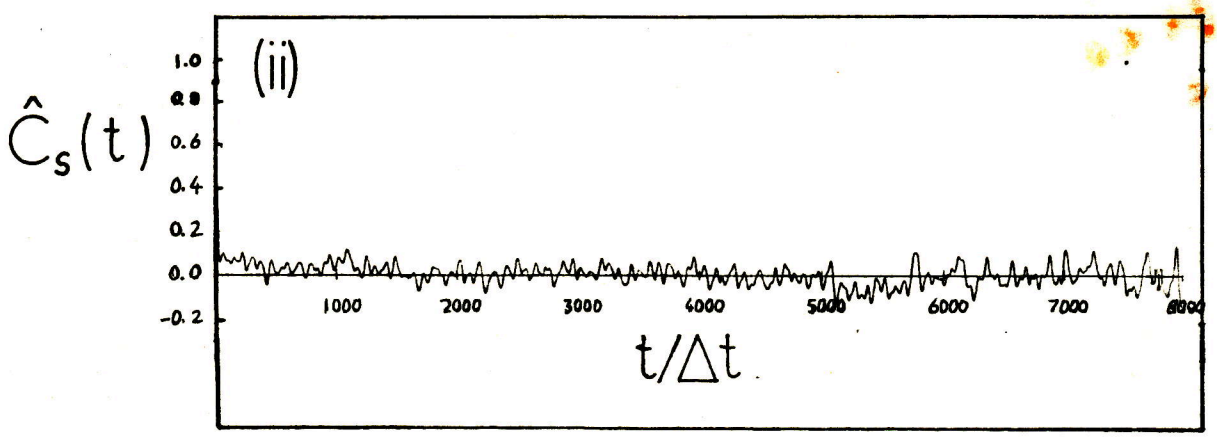

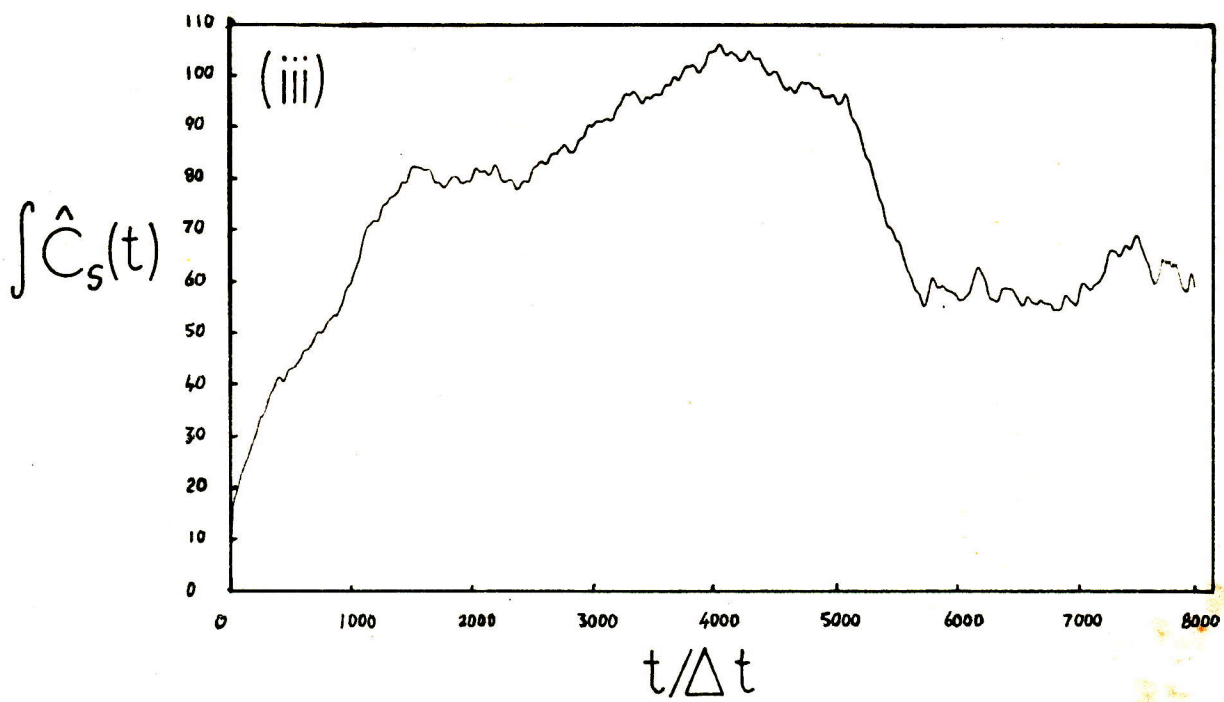

Figure 5.28 As fig.5.27 for flexane, T~200K.

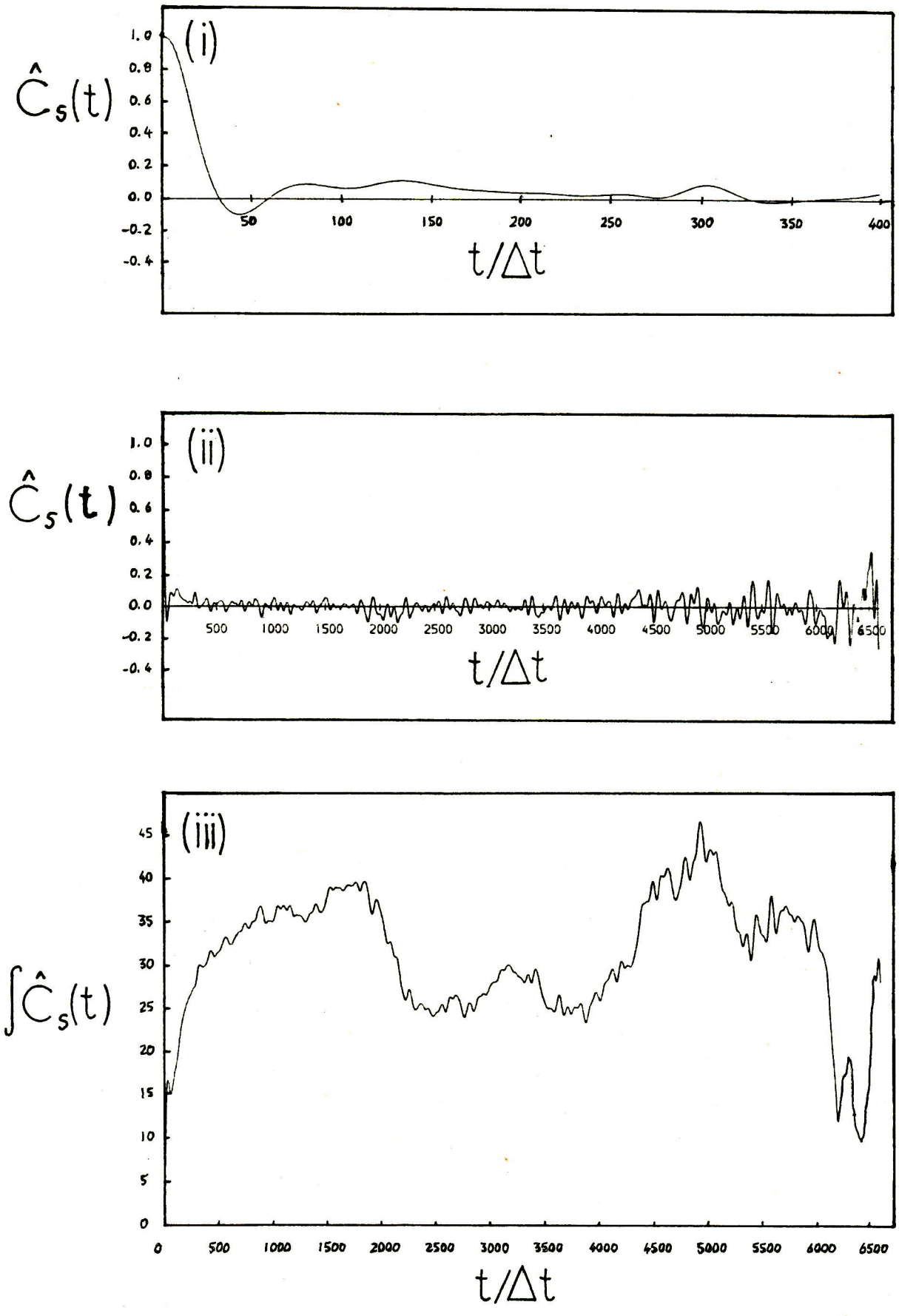

Table 5.9 The mean squared stress , infinite frequency shear modulus and viscosity determined from the stress correlation function for hexane and flexane at T~200K.

	$\langle\sigma^2_{\alpha\beta}(0)\rangle/10^{15}Pa^2$	G_∞/GPa	η/mPa s
Hexane	0.62	4.3	1.3±0.4
Flexane	0.59	4.1	0.5±0.2

From the figures it can be seen that the initial relaxation is complete within ~0.2ps which, understandably, coincides with that of the intermolecular forces which largely determine the stress. In flexane $C_s(t)$ exhibits a pronounced negative dip in this early part of the relaxation which appears to be dampened out in hexane. Beyond about 0.4ps it becomes difficult to distinguish the actual form of $C_s(t)$ from the noise but from the integrals, not shown here, it is clear that $C_s(t)$ has a long positive tail which causes the integrand to, on average rise, out to at least 5ps.

Like many of the other static intermolecular properties of these two systems the mean squared stress, and hence G_∞, are very similar. The viscosities evaluated from $C_s(t)$ are not, however, differing by a factor of about two despite the large error bars. How much credence is to be placed in these values for the viscosity must be tempered by the previous poor comparisons made already between η determined from $C_s(t)$ and η determined by non-equilibrium methods.

5.11 Conclusions

The principal aim in this study is to determine the extent to which flexibility affects the rheological , i.e. flow, properties of molecular fluids. So far it has been shown that the equilibrium static intermolecular properties of these fluids are very similar but the intramolecular structure and dynamics are quite different. Furthermore, the internal structure and dynamics has been found to affect the diffusive motion of the molecules to a significant extent. This, and the results for the stress correlation function, raise the possibility of different flow behaviour particularly as the most important rheological property η, the viscosity, can be related to the inverse of the diffusion coefficient [127]. To determine whether this was the case HSNEMD simulations were performed, the results of which are given in the next section.

CHAPTER 6

HEXANE AND FLEXANE : NON-EQUILIBRIUM RESULTS AT 200K

6.1 Introduction

To measure the rheological properties of these systems the method of HSNEMD was used as described already in sec.2.15. The general procedure was to apply a step function shear rate, $\dot{\gamma}$, to a configuration which was either at equilibrium or at a steady state at the next lowest shear rate. For the shear rates less than $1*10^{11}\ s^{-1}$ the former approach was used, so that the relaxation to a steady state could be observed, whereas for the higher shear rates the latter method was employed, so as to reduce the amount of time required to attain a steady state.

Shear rates of 1,2,5,10 and $20*10^{10}\ s^{-1}$ and 2,5,10 and $20*10^{10}\ s^{-1}$ were applied to the hexane and flexane systems respectively. To monitor the relaxation to a steady state the components of the stress/pressure tensor, eqn.2.11.3, and a collective orientation tensor, $\underline{\underline{D}}$, defined as

$$\underline{\underline{D}} = \sum_{i=1}^{N} \hat{\underline{r}}_{i6} \hat{\underline{r}}_{i6} \quad ,$$

have been followed as a function of time after the imposition of a step function change in shear rate. The most important components of these tensors are the off-diagonal elements σ_{xz}

and D_{xz} which directly couple to the shear for the geometry of the flow imposed here, $\dot{\gamma}=\frac{dV_x}{dZ}$. The other off-diagonal components are small for this flow symmetry. The on-diagonal components of the tensors are also important , especially those of the stress tensor with regard to the normal pressure effects.

6.2 Results at 200K

In the previous simulations, on simple diatomic and triatomic molecules, relaxation to a steady state presented no problems as it occurred rapidly within a few picoseconds of applying the step function in shear rate. In these much more complex systems it was found that the relaxation of the alignment was particularly slow requiring of order 50ps to approach close to its long time value. The stress, however, apparently relaxed much faster. This is demonstrated in fig.6.1 where the development of $\sigma_{xz}(t)$ and $D_{xz}(t)$ are shown, normalized by their estimated long time values, for the case of a shear rate of $1*10^{10}s^{-1}$ applied as a step function to an equilibrium sample of hexane. The stress correlation function, discussed previously and shown in fig.5.27, indicates that the initial relaxation of the stress will be rapid but will then be followed by a period of slower relaxation to its final long time value. In an experiment such as this it is difficult to see any long time relaxation in the stress because of the large and rapid fluctuations in

Figure 6.1 The shear stress, $\sigma_{xz}(t)$, (Δ), and the alignment, $D_{xz}(t)$, (□), expressed as fractions of the limiting long time (70-120ps) values and plotted as a function of time elapsed from the imposition of a steady strain rate of $10^{10}s^{-1}$. The full and broken lines are best fits to the form $f(t)=1-\exp(-t/\tau)$, (- - - τ=2.8ps, —— τ=25ps).

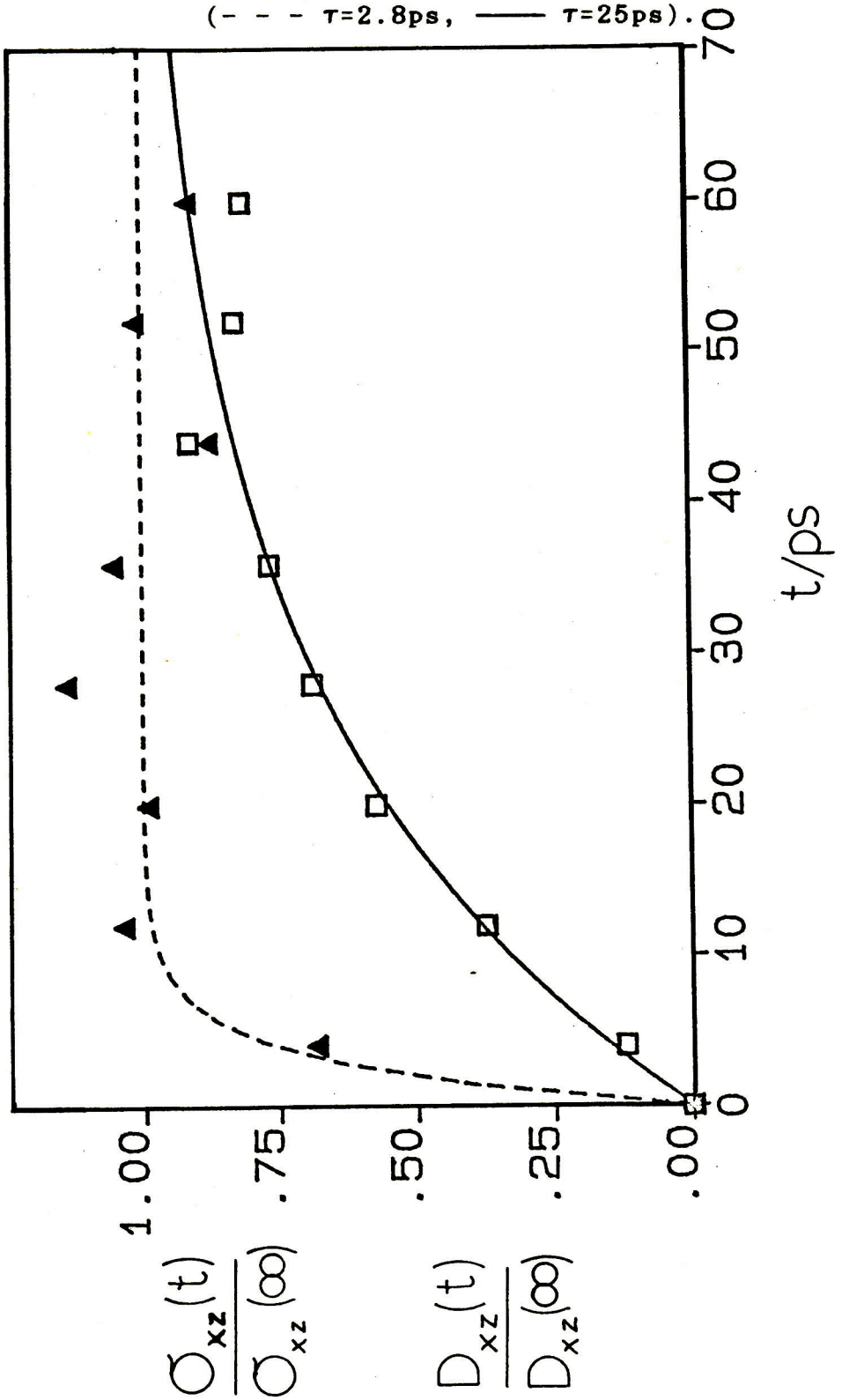

this property. Indeed, from table 5.9 it can be seen that the root mean square value of the stress is of order 250bar.

This is not the case for the alignment which varies much more slowly and fluctuates much less. It is clear from fig.6.1 that the collective orientation requires a long time to reach a steady state. This is to be expected as the rate of collective reorientation must be determined to a large extent by that of the single molecule reorientation. As has been shown in sec.5.10 single molecule relaxation times are in the tens of picoseconds range which is consistent with the relaxation time of τ=25ps for the best fit of $D_{xz}(t)$ to the form

$$D_{xz}(t)/D_{xz}(\infty) = 1 - \exp(-t/\tau) \quad . \qquad (6.2.1)$$

A corresponding fit to $\sigma_{xz}(t)$ gives a value of τ~3ps which means that the stress relaxation is complete within ~10ps which agrees with the result from the stress correlation function shown in sec.5.10. The conclusion from this must be that although the non-attainance of a steady state in the collective orientational order implies a similar state of affairs for the intermolecular structure, and hence the stress, this long time relaxation of the stress provides a negligible contribution to the viscosity at least for the large perturbation applied here for which a highly non-linear response would be expected.

The relaxation times for the best fits to the form of eqn.6.2.1 are given in table 6.1 for hexane and flexane at all the shear rates in which an equilibrium fluid was perturbed.

Table 6.1 The best fit τ values for the form of $D_{xz}(t)$ as given in eqn.6.2.1, following a step function application of a shear rate, $\dot{\gamma}$, to a sample of hexane and flexane at T~200K. $D_{xz}(\infty)$ is the estimated long time value of $D_{xz}(t)$.

	$\dot{\gamma}/10^{10-1}$ s	τ/ps	$D_{xz}(\infty)$
Hexane	1	25.0	0.150
Hexane	2	20.0	0.174
Flexane	2	10.0	0.128
Hexane	5	9.5	0.202
Flexane	5	6.5	0.175

Two points to note are that the τ values decrease with increasing $\dot{\gamma}$ showing the non-linearity of the responses and that τ for hexane is larger than that for flexane. The difference between the rates of collective reorientation in hexane and flexane is roughly a factor of two, which corresponds with the difference between the rates for single particle reorientation, discussed in sec.5.10 This is consistent with the supposition that the rate of collective realignment due to shear is closely connected with the rate of reorientation of individual molecules at equilibrium.

Steady state averages of some thermodynamic properties and the significant components of the stress/pressure tensor and alignment tensor are given in tables 6.2, 6.3 and 6.4.

Table 6.2 The mean thermodynamic functions obtained from the steady state shear calculations on hexane and flexane, T~200K, (* indicates calculated for comparison only). The figures in parentheses are the total time of the simulation.

Hexane

$\dot{\gamma}/10^{10}s^{-1}$	U /J mol^{-1}	Φ /Jmol^{-1}	Φ_α /Jmol^{-1}	T/K	P/bar	Length of run /ps
1	-37480 ±120	-50120 ±120	5150 ±20	200.00 ±0.00	730 ±80	48 (108)
2	-37550 ±50	-50060 ±60	5040 ±70	200.01 ±0.01	800 ±50	60 (108)
5	-37540 ±80	-49730 ±30	4700 ±60	200.04 ±0.01	1130 ±20	60 (108)
10	-37400 ±120	-49430 ±50	4550 ±70	200.10 ±0.00	1370 ±10	48 (48)
20	-37290 ±120	-48850 ±90	4070 ±100	200.26 ±0.02	1850 ±60	48 (48)

Flexane

$\dot{\gamma}/10^{10}s^{-1}$	U /J mol^{-1}	Φ /Jmol^{-1}	Φ_α /Jmol^{-1}	T/K	P/bar	Length of run /ps
2	-42320 ±70	-49810 ±70	30100 ±360	200.00 ±0.02	370 ±50	122 (150)
5	-42240 ±80	-49720 ±80	29870 ±450	200.02 ±0.01	460 ±50	82 (117)
10	-42030 ±60	-49510 ±60	28620 ±360	200.08 ±0.01	690 ±50	42 (106)
20	-41660 ±130	-49150 ±130	28660 ±600	200.27 ±0.02	990 ±110	46 (104)

Table 6.3 The mean shear stress, resultant shear viscosity and mean normal presssure components from the steady state calculation on hexane and flexane, T~200K.

Hexane

$\dot{\gamma}/10^{10}\,s^{-1}$	σ_{xz}/bar	η/mPa s	P_{xx}/bar	P_{yy}/bar	P_{zz}/bar
1	292±43	2.919±0.434	702±77	615±87	741±62
2	495±22	2.477±0.110	721±65	737±46	931±66
5	751±50	1.501±0.100	898±60	969±10	1520±30
10	897±12	0.897±0.012	1004±92	1318±58	1791±66
20	1135±55	0.568±0.028	1231±44	1810±107	2501±88

Flexane

$\dot{\gamma}/10^{10}\,s^{-1}$	σ_{xz}/bar	η/mPa s	P_{xx}/bar	P_{yy}/bar	P_{zz}/bar
2	287±69	1.437±0.346	300±85	354±77	436±74
5	532±63	1.065±0.127	350±69	405±109	618±79
10	759±66	0.759±0.066	342±100	544±95	884±112
20	1117±92	0.558±0.046	485±110	786±162	1323±187

Table 6.4 The mean significant components of the alignment tensor obtained from the steady state shear calculations on hexane and flexane, T~200K.

Hexane

$\dot{\gamma}/10^{10}s^{-1}$	D_{xz}	$D_{xx}-1/3$	$D_{yy}-1/3$	$D_{zz}-1/3$
1	0.150±0.011	0.053±0.013	-0.009±0.017	-0.040±0.008
2	0.174±0.007	0.099±0.013	-0.053±0.008	-0.045±0.012
5	0.202±0.008	0.188±0.018	-0.076±0.012	-0.113±0.012
10	0.216±0.007	0.265±0.014	-0.132±0.005	-0.131±0.012
20	0.189±0.019	0.316±0.017	-0.149±0.020	-0.166±0.014

Flexane

$\dot{\gamma}/10^{10}s^{-1}$	D_{xz}	$D_{xx}-1/3$	$D_{yy}-1/3$	$D_{zz}-1/3$
2	0.128±0.016	0.084±0.021	-0.038±0.018	-0.045±0.012
5	0.175±0.012	0.168±0.011	-0.108±0.007	-0.059±0.011
10	0.194±0.015	0.189±0.013	-0.098±0.012	-0.090±0.012
20	0.186±0.015	0.242±0.015	-0.110±0.017	-0.131±0.015

6.3 The Shear Rate Dependence of the Viscosity

In fig.6.2 the shear rate dependent viscosities, given in table 6.3, are plotted as a function of the square root of the shear rate for both hexane and flexane. The curves show characteristic shear thinning behaviour but to differing extents. At the lowest shear rate the viscosities differ by at least a factor of two but hexane shear thins much more than

flexane so that at the highest shear rates there is virtually no difference in the viscosities.

As for the other fluids the $\eta(\dot{\gamma})$ data has been fitted to the three different theories discussed in sec.3.5. The parameters for the best fits to these theories are given in table 6.5 together with the root mean squared difference (RMSD) between the data points and the fitted curves. Figs.6.3 and 6.4 show the actual best fit curves for all three predictions for hexane and flexane respectively.

Table 6.5 The best fit parameters and root mean square differences (RMSD) for the predictions of the shear rate dependence of the viscosity from the theories of Hess, Ree-Eyring(RE) and Kawasaki-Gunton(KG) , (see sec.3.5), for the $\eta(\dot{\gamma})$ vs. $\dot{\gamma}$ data for hexane and flexane, T~200K.

		Hexane	Flexane
RE	$\eta(0)$/mPa s	3.47	1.58
	τ_e /ps	112.2	44.8
	RMSD/mPa s	0.056	0.030
Hess	$\eta(0)$/mPa s	2.95	1.52
	τ_h /ps	21.6	16.2
	k	0.868	0.699
	RMSD/mPa s	0.060	0.020
KG	$\eta(0)$/mPa s	3.37	1.76
	A /10^{-5} mPa $s^{3/2}$	0.690	0.284
	RMSD/mPa s	0.259	0.079

From figs.6.3 and 6.4 and the RMSD's it is clear that the

Figure 6.2 $\eta(\dot{\gamma})$ vs. $\dot{\gamma}^{1/2}$, hexane (Δ) and flexane (□), T~200K.

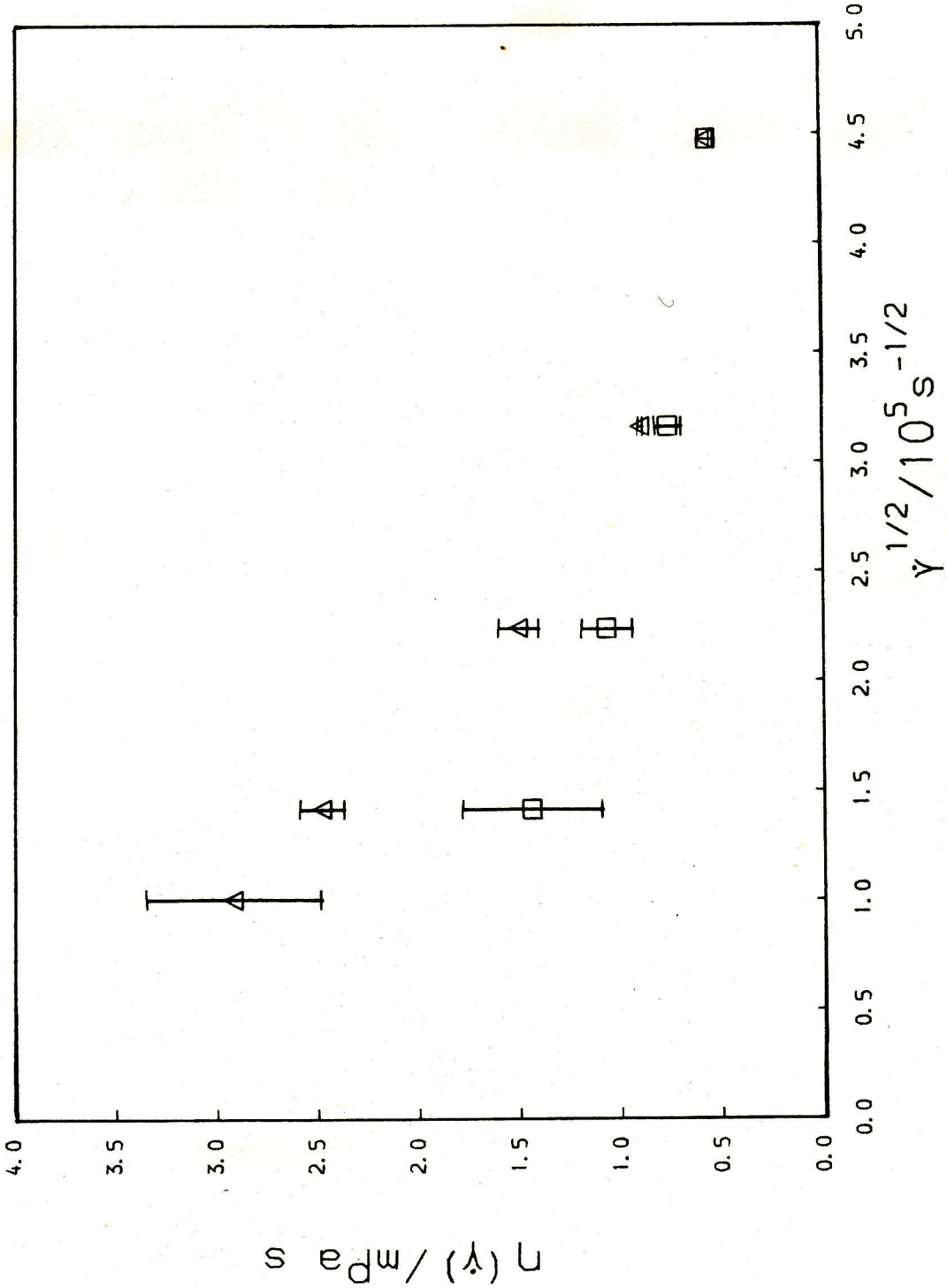

Figure 6.3 $\eta(\dot{\gamma})$ vs. $\dot{\gamma}^{1/2}$, hexane (Δ). Fits to the predictions of the theories of Hess (——), Ree-Eyring (- - -) and Kawasaki-Gunton (—·—·—).

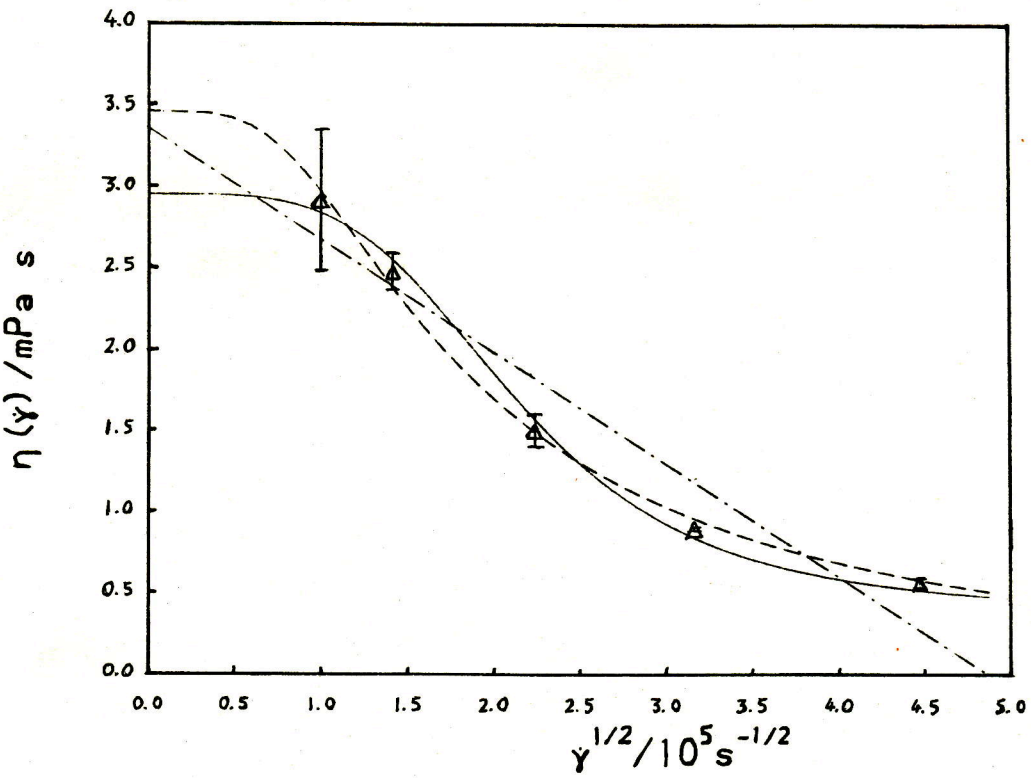

Figure 6.4 As fig.6.3 for flexane, T~200K.

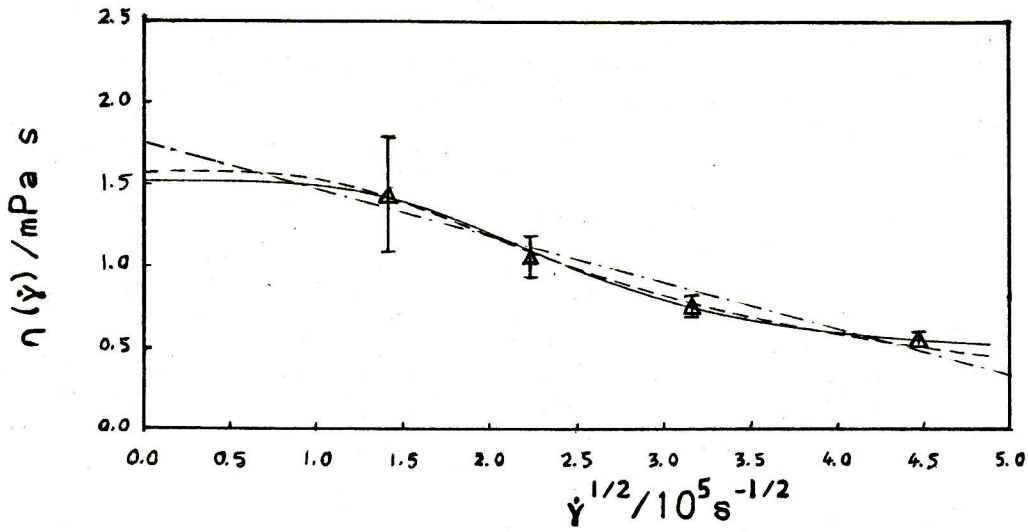

KG square root law is particularly poor at predicting the $\eta(\dot{\gamma})$ behaviour. In hexane the KG curve shows a systematic and large deviation from the computed points. In flexane the deviation is not as large because of the smaller amount of shear thinning but there is still a tendency for the data to lie systematically above and below the line. Indeed, the shape of the $\eta(\dot{\gamma})$ vs. $\dot{\gamma}$ curves is much better represented by the Hess and RE fits. In terms of the RMSD's there is little to choose between these two in either case although it has to be said that there is one additional adjustable parameter in the Hess prediction. In flexane both give similar estimates for $\eta(0)$ but in hexane there is a substantial difference of ~0.5mPa s. There is then a good deal of imprecision in any result quoted for the $\eta(0)$ of hexane. This is compounded if we use the criterion of Allen and Kivelson [70] who choose those data points which fit to the $\dot{\gamma}^{1/2}$ law to estimate the $\dot{\gamma}=0$ viscosity, reasoning that at high shear rates a 'saturation effect' causes the viscosity to diverge from the square root dependence. If this same criterion is applied to the lowest three shear rates for hexane and flexane further estimates of the zero shear rate viscosity can be obtained of ~4.1mPa s and 2.0mPa s respectively. Consequently the $\eta(0)$'s of these two fluids are quoted as 3.5 ± 0.6mPa s and 1.7 ± 0.3mPa s for hexane and flexane respectively.

Despite the uncertainty in the estimates of the equilibrium viscosities there is still a relatively large

difference between the values for the two systems. It must be concluded that the flexibility of a molecule is a significant factor in determining this the most fundamental of rheological properties.

6.4 Shear Induced Alignment

In figs.6.5→6.8 the data given in table 6.4 is plotted as a function of the square root of the shear rate. Qualitatively the same behaviour is found in hexane and flexane as in all the other models previously studied with D_{xz} and D_{xx} increasing whilst D_{yy} and D_{zz} decrease with $D_{yy} \simeq D_{zz}$. This shows the expected alignment, for the type of shear applied, of the 'long' axis of these molecules in the XZ plane. For all the the components of $\underline{\underline{D}}$ there is a tendency for the greater change to occur in hexane implying more alignment of the $\underline{r}_{16}$ vectors in hexane than in flexane. Significantly the magnitudes of the changes in these components are larger for these molecules than for the diatomics and triatomics. A likely result considering the greater anisotropy of these polyatomic models but not an obvious result because of the demonstrated density dependence of $\underline{\underline{D}}(\dot{\gamma})$. One further interesting point is that $D_{xz}(\dot{\gamma})$ passes through a maximum in both cases at a shear rate of about $10^{11} s^{-1}$. This has not been observed before but the possibility of it happening has already been discussed in sec.3.7.

Figure 6.5 $D_{xz}(\dot{\gamma})$ vs. $\dot{\gamma}^{1/2}$, hexane (□) and flexane (Δ) T~200K.

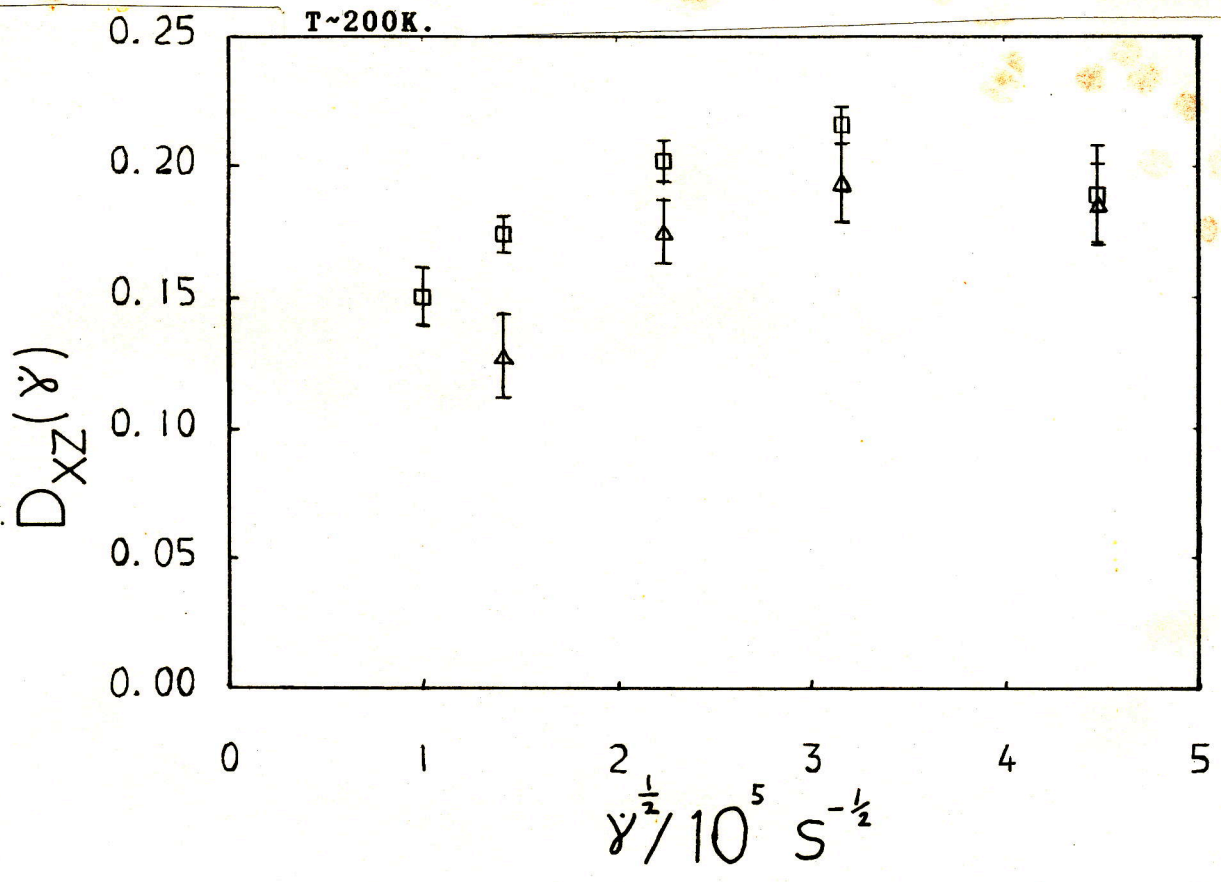

Figure 6.6 $D_{xx}(\dot{\gamma})-1/3$ vs. $\dot{\gamma}^{1/2}$, hexane (□) and flexane (Δ), T~200K.

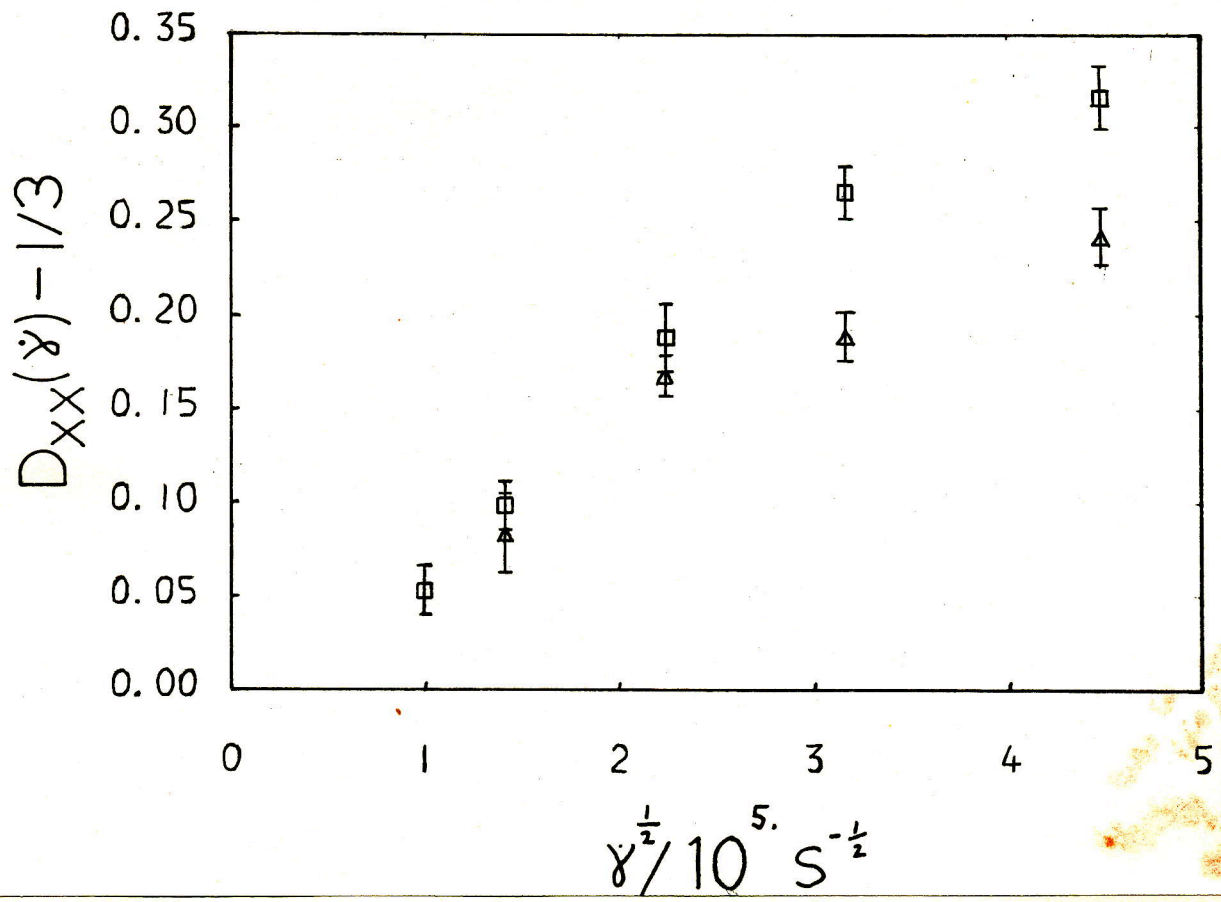

Figure 6.7 $D_{yy}(\dot{\gamma})-1/3$ vs. $\dot{\gamma}^{1/2}$, hexane (□) and flexane (Δ), T~200K.

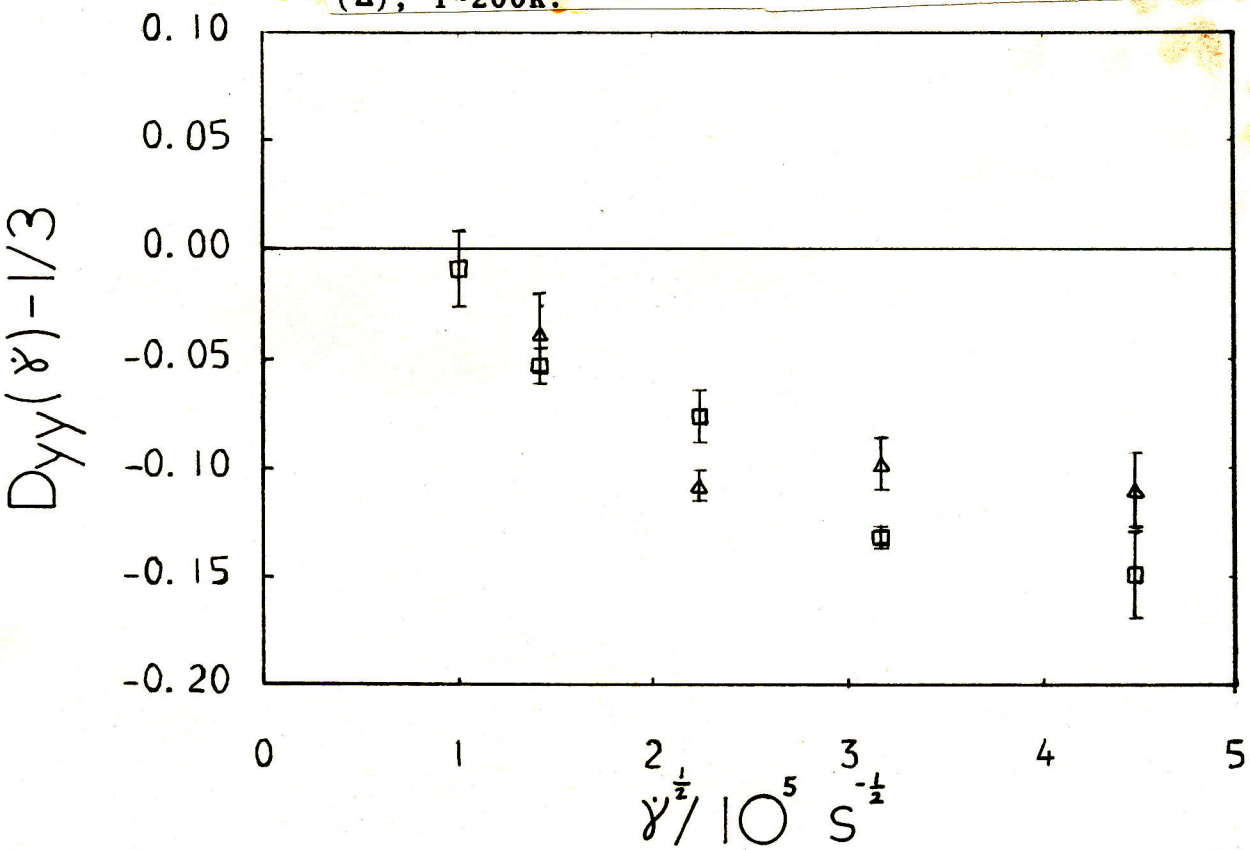

Figure 6.8 $D_{zz}(\dot{\gamma})-1/3$ vs. $\dot{\gamma}^{1/2}$, hexane (□) and flexane (Δ), T~200K.

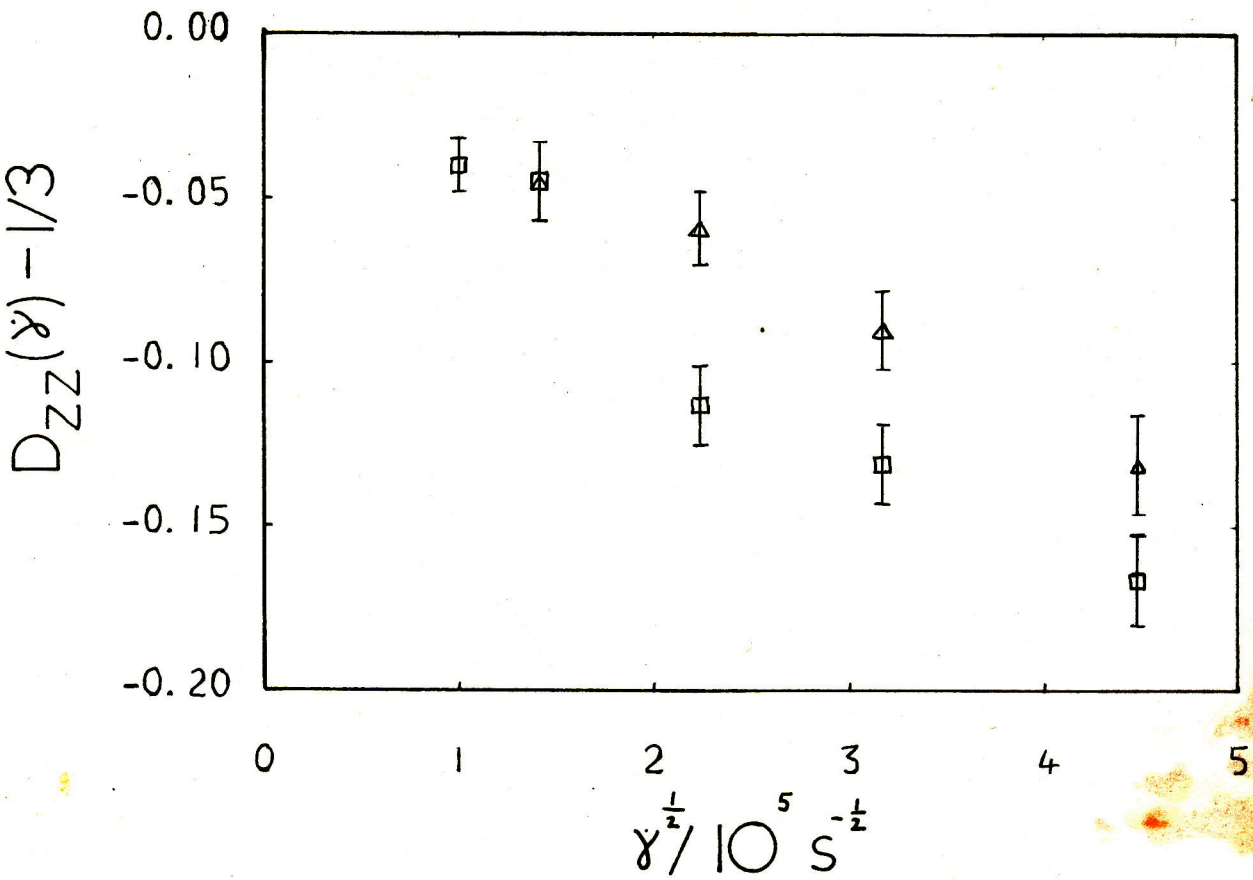

The ability of D_{xz} to pass through a maximum does not make it the best indicator of the amount of alignment in the system. A possibly better, and more experimentally relevant, measurement is afforded by the extinction angle, θ_e, which is a function of the off and on diagonal elements of $\underline{\underline{D}}$, as defined in eqn.3.7.2. The shear rate dependent values of the extinction angle, $\theta_e(\dot{\gamma})$, are given in table 6.6.

Table 6.6 The extinction angle obtained from the steady state shear calculations on hexane and flexane at T~2ØØK.

	Hexane	Flexane
$\dot{\gamma}/10^{10}s^{-1}$	θ_e/deg	θ_e/deg
1	36.4±1.7	-
2	33.8±1.5	31.6±3.1
5	26.6±1.2	28.5±1.4
1Ø	23.7±1.1	27.1±1.5
2Ø	19.6±1.6	22.5±1.5

In fig.6.9 $\theta_e(\dot{\gamma})$ is plotted as a function of the square root of the shear rate along with the predictions of Hess's theory for this property which is given by eqn.3.7.3 in the first approximation. The values of τ being taken from the best fits to the viscosity data given in table 6.5. To first approximations Hess's theory fails to predict any change in D_{yy} under shear and so not surprisingly does not do well at predicting the form of $\theta_e(\dot{\gamma})$, as was the case with diatomics. In comparison hexane and flexane show very similar behaviour

Figure 6.9 The extinction angle $\theta_e(\dot{\gamma})$ vs. $\dot{\gamma}^{1/2}$, hexane (□) and flexane (Δ), T~200K. Comparison with the prediction of Hess's theory, hexane (——) and flexane (- - -).

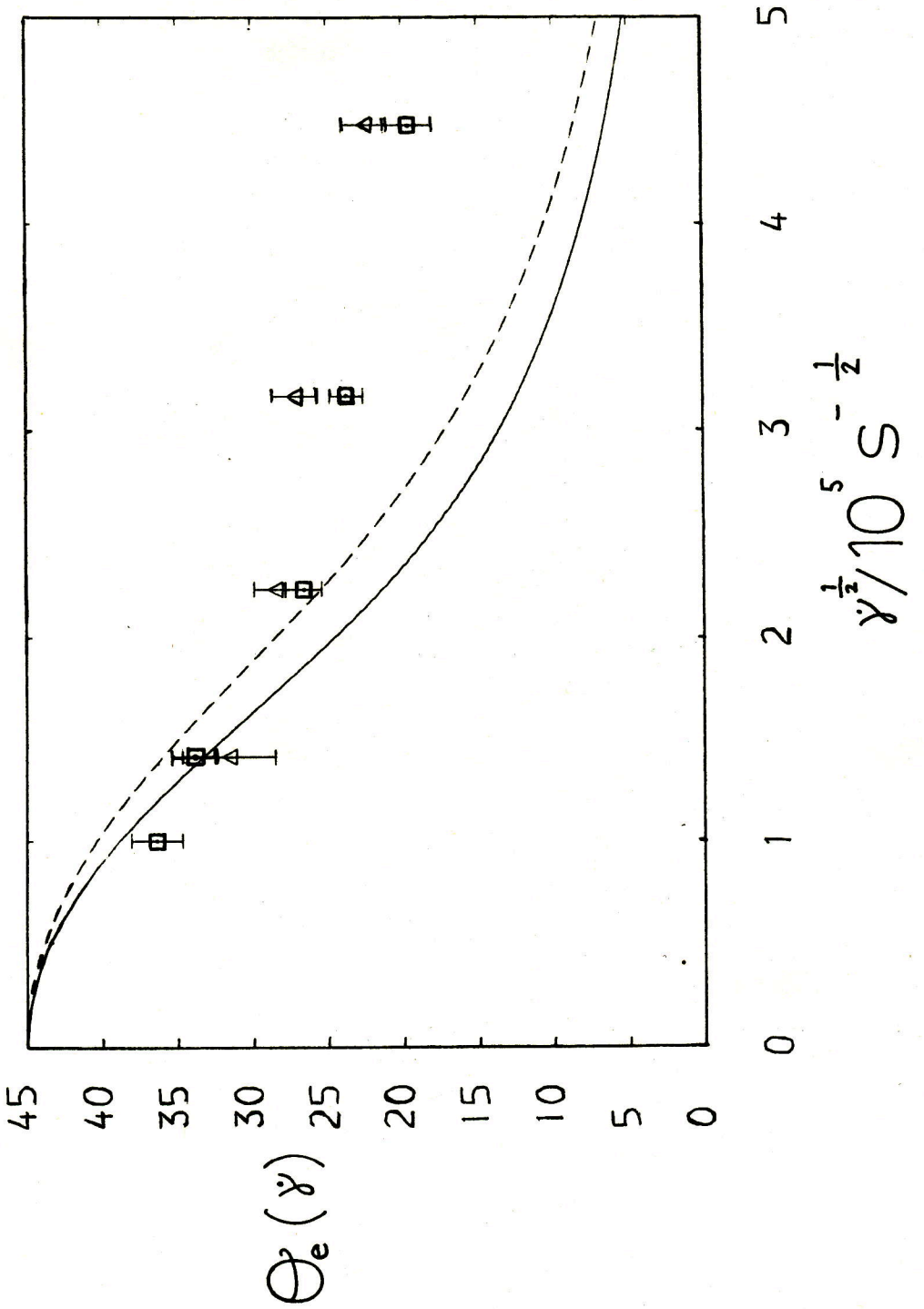

for $\theta_e(\dot{\gamma})$ with hexane having slightly lower values at the higher shear rates, again pointing to slightly more alignment in hexane. This similarity in $\theta_e(\dot{\gamma})$ contrasts sharply with the behaviour of $\eta(\dot{\gamma})$ which shows significant differences in both magnitude and variation with $\dot{\gamma}$ between hexane and flexane. This again could be construed as an indication of the looseness of the coupling between stress and molecular reorientation under shear.

As with the diatomics the probability densities for the direction cosines, $\{D_\alpha\}$ $\alpha=x,y,z$, have been calculated using the definitions and methods described in sec.3.7, except that for these molecules $\hat{\underline{r}}_{i6_i}$ has been substituted for $\hat{\underline{l}}_i$. Figs.6.1Ø to 6.11 show these functions at the highest shear rate used of $2*10^{11}s^{-1}$. There is considerable distortion of the probability densities away from the equilibrium distribution of $\rho(D_\alpha)=1$ for all values of D_α, especially in the case of D_x which shows a very strong tendency for alignment to occur along the x-axis. The $\rho(D_y)$ and $\rho(D_z)$ are consistent with this streaming of molecules in this direction, as discussed in sec.3.7. These functions also underline the similarity in the behaviour of the orientation under shear of hexane and flexane as the difference in the $\rho(D_\alpha)$'s are small.

Figure 6.10 The normalised probability density for the x direction cosine $\rho(D_x)$ vs. D_x, hexane (a) and flexane (b), $\dot{\gamma}=2*10^{11}s^{-1}$, T~200K.

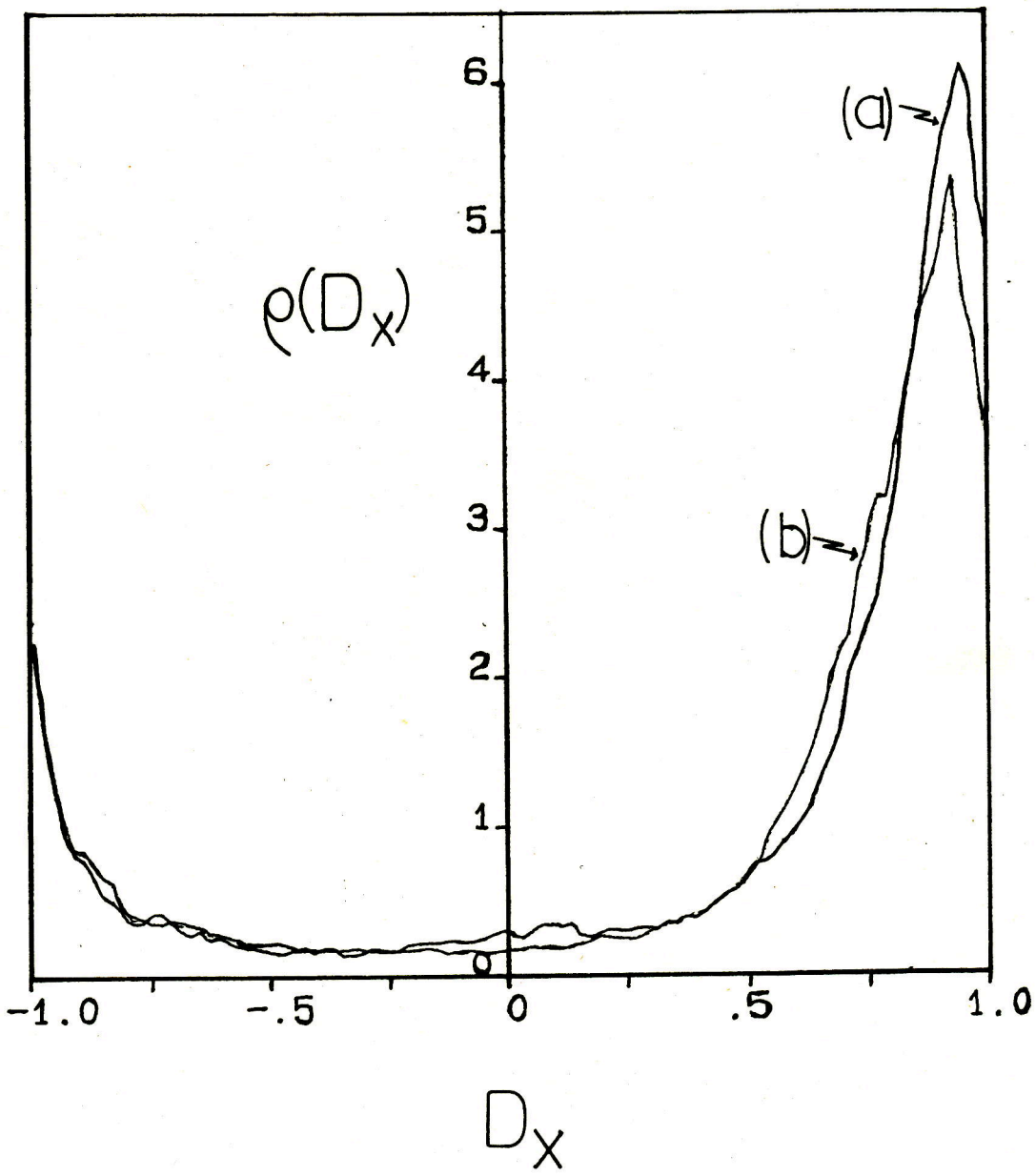

Figure 6.11 The normalised probability densities for the y direction cosines $\rho(D_y)$ vs. D_y, (1) and the z direction cosines $\rho(D_z)$ vs. D_z, (2), hexane (——) and flexane (- - -), $\dot{\gamma}=2*10^{11}s^{-1}$, T~200K.

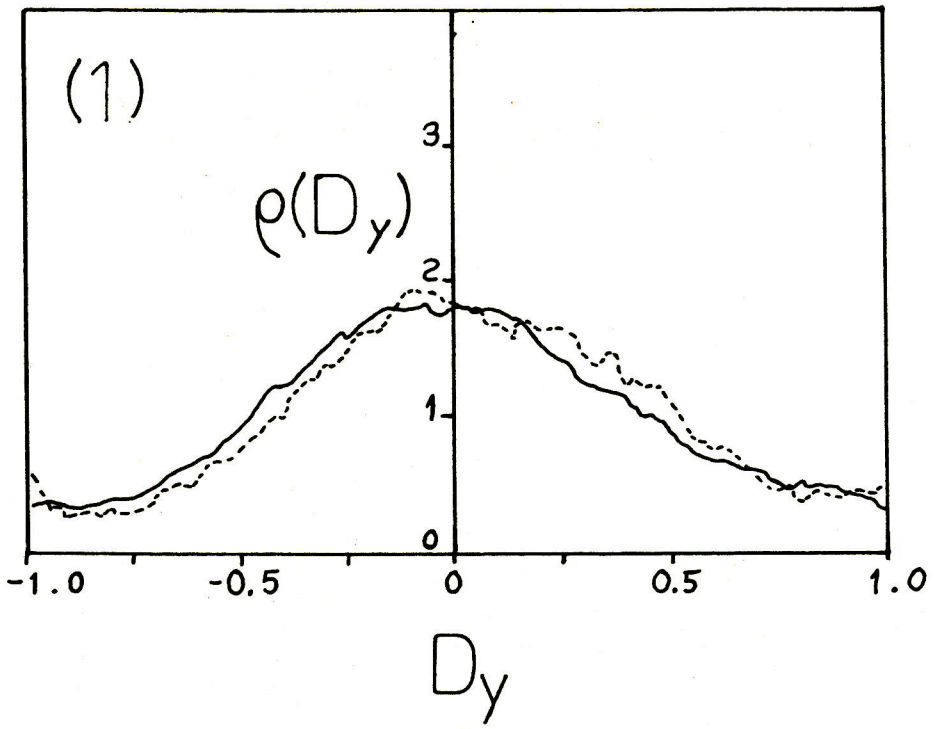

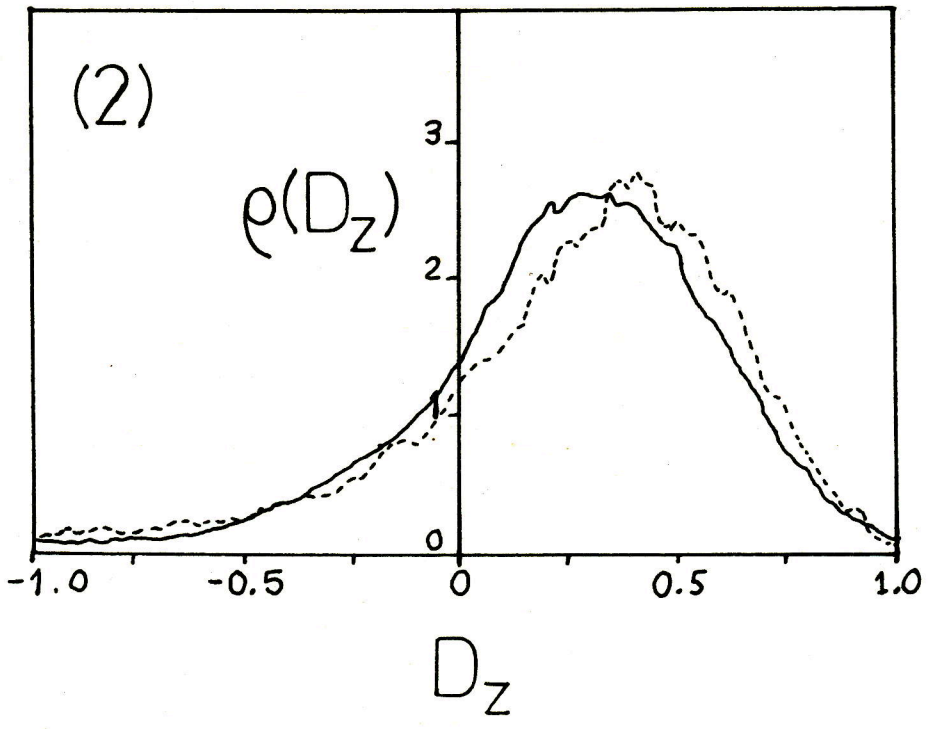

6.5 Non-equilibrium thermodynamics

With the rigid model molecules previously studied it has been seen that the pressure and total energy are functions of the shear rate. Although the findings for diatomics and triatomics have confirmed a power law dependence of these variables upon shear rate the actual exponent has tended to fall below the value of 1.5 expected by theory [74,90]. The introduction of flexibility into the model molecules means that the change in total energy under shear at constant temperature is no longer caused by the change in the intermolecular potential energy alone. Internal rearrangements of the molecules will cause changes in the dihedral angle potential energy and the intramolecular contribution to the LJ 12-6 potential energy. For this reason two other functions, $\Delta\Phi(\dot{y})$ and $\Delta\Phi_\alpha(\dot{y})$ defined as

$$\Delta\Phi(\dot{y}) = \Phi(\dot{y}) - \Phi(0) \qquad (6.5.1)$$

$$\Delta\Phi_\alpha(\dot{y}) = \Phi_\alpha(\dot{y}) - \Phi_\alpha(0) \qquad (6.5.2)$$

where Φ is the total (inter + intra) LJ 12-6 potential energy and Φ_α is the dihedral angle potential potential energy, have been calculated as well as $\Delta U(\dot{y})$ and $\Delta P(\dot{y})$. Although Φ_α does not contribute to the total energy in flexane $\Delta\Phi_\alpha$ has been calculated for comparison with $\Delta\Phi_\alpha$ for hexane. These functions are given in table 6.7.

Table 6.7 The functions $\Delta U(\dot{\gamma})$, $\Delta\Phi(\dot{\gamma})$, $\Delta\Phi_\alpha(\dot{\gamma})$ and $\Delta P(\dot{\gamma})$ obtained from the steady state shear calculations on hexane and flexane at T~200K. (* indicates calculated for comparison only.)

Hexane

$\dot{\gamma}/10^{10}s^{-1}$	$\Delta U(\dot{\gamma})/Jmol^{-1}$	$\Delta\Phi(\dot{\gamma})/Jmol^{-1}$	$\Delta\Phi_\alpha(\dot{\gamma})/Jmol^{-1}$	$\Delta P(\dot{\gamma})$/bar
1	-150±140	150±130	-300±60	180±90
2	-220±80	210±70	-420±90	250±60
5	-210±110	550±50	-760±80	580±30
10	-60±140	840±70	-910±90	820±30
20	40±140	1420±90	-1510±60	1300±70

Flexane

$\dot{\gamma}/10^{10}s^{-1}$	$\Delta U(\dot{\gamma})/Jmol^{-1}$	$\Delta\Phi(\dot{\gamma})/Jmol^{-1}$	$\Delta\Phi_\alpha(\dot{\gamma})/Jmol^{-1}$	$\Delta P(\dot{\gamma})$/bar
2	5±90	5±90	-320±600	90±70
5	90±100	90±100	-550±660	180±70
10	300±90	300±90	-1800±600	410±70
20	670±140	610±140	-1760±770	720±120

It can be seen from the table that the inclusion of the dihedral angle potential has a marked effect. In flexane, and the previous models used, $\Delta U(\dot{\gamma})$ is effectively the same as $\Delta\Phi(\dot{\gamma})$ because of the constraint of constant temperature. The difference between the two at high shear rates being caused by the slight temperature rise that occurs when the constant temperature algorithm cannot remove all of the heat generated by the flow. So as $\Delta\Phi(\dot{\gamma})$ increases $\Delta U(\dot{\gamma})$ must increase in flexane. In hexane Φ_α gives U an extra degree of energetic

freedom so even though $\Delta\Phi(\dot{\gamma})$ increases it turns out that $\Delta U(\dot{\gamma})$ does not increase because of the counterbalancing effect of the decrease in $\Delta\Phi_\alpha(\dot{\gamma})$. For this reason $\log_{10}(\Delta\Phi(\dot{\gamma})/\mathrm{Jmol}^{-1})$ has been plotted against $\log_{10}(\dot{\gamma}/10^{10}\mathrm{s}^{-1})$ in fig.6.12 rather than $\log_{10}(\Delta U(\dot{\gamma})/\mathrm{Jmol}^{-1})$. In fig.6.13 $\log_{10}(\Delta P(\dot{\gamma})/\mathrm{bar})$ has been plotted in the same way. The points at higher shear rates are once again more precise because of the larger differences from the equilibrium value of the energy and the pressure. From the figures it can be seen that the points fit reasonably well to the straight line form , at least at the higher shear rates, expected for an algebraic dependence upon shear rate of the type given in eqn.3.8.3 for the pressure and by

$$\log_{10}(\Delta\Phi(\dot{\gamma})/\mathrm{Jmol}^{-1}) = c*\log_{10}(\dot{\gamma}/10^{10}\mathrm{s}^{-1}) + \log_{10}(\Phi_1/\mathrm{Jmol}^{-1})$$

or alternatively

$$\Delta\Phi(\dot{\gamma}) = \Phi_1(\dot{\gamma}/10^{10}\mathrm{s}^{-1})^c \qquad (6.5.3)$$

,where Φ_1 is a state dependent constant, for the total LJ 12-6 potential energy. The values obtained for the slopes from the straight lines shown in figs.6.12 and 6.13 are given in table 6.8 along with the values estimated for the constants of proportionality.

Figure 6.12 $Log_{10}\Delta\Phi(\dot{\gamma})$ vs. $log_{10}\dot{\gamma}$, hexane (—⊡—) and flexane (- - Δ - -), T~200K.

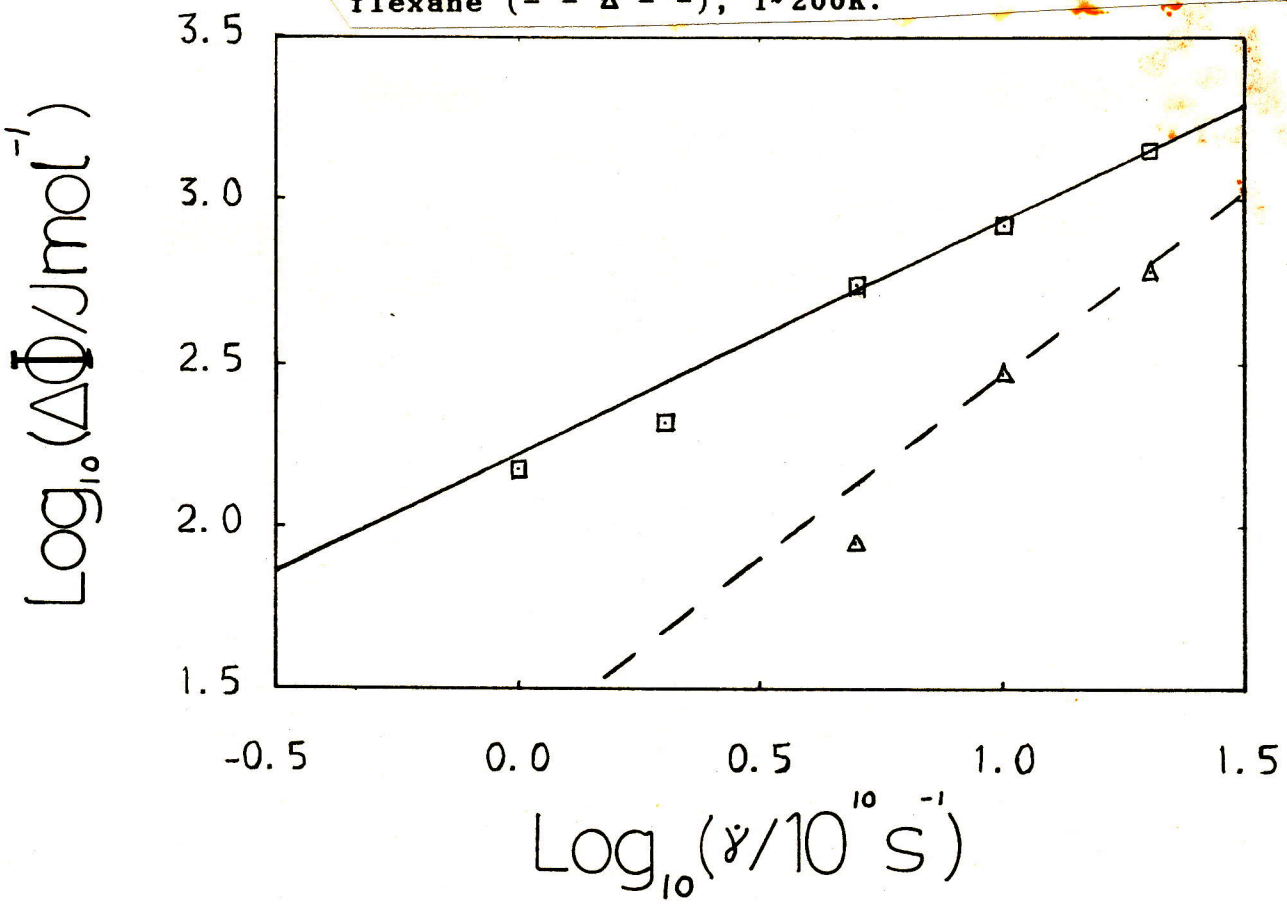

Figure 6.13 $Log_{10}\Delta P(\dot{\gamma})$ vs. $log_{10}\dot{\gamma}$, hexane (—⊡—) and flexane (- - Δ - -), T~200K.

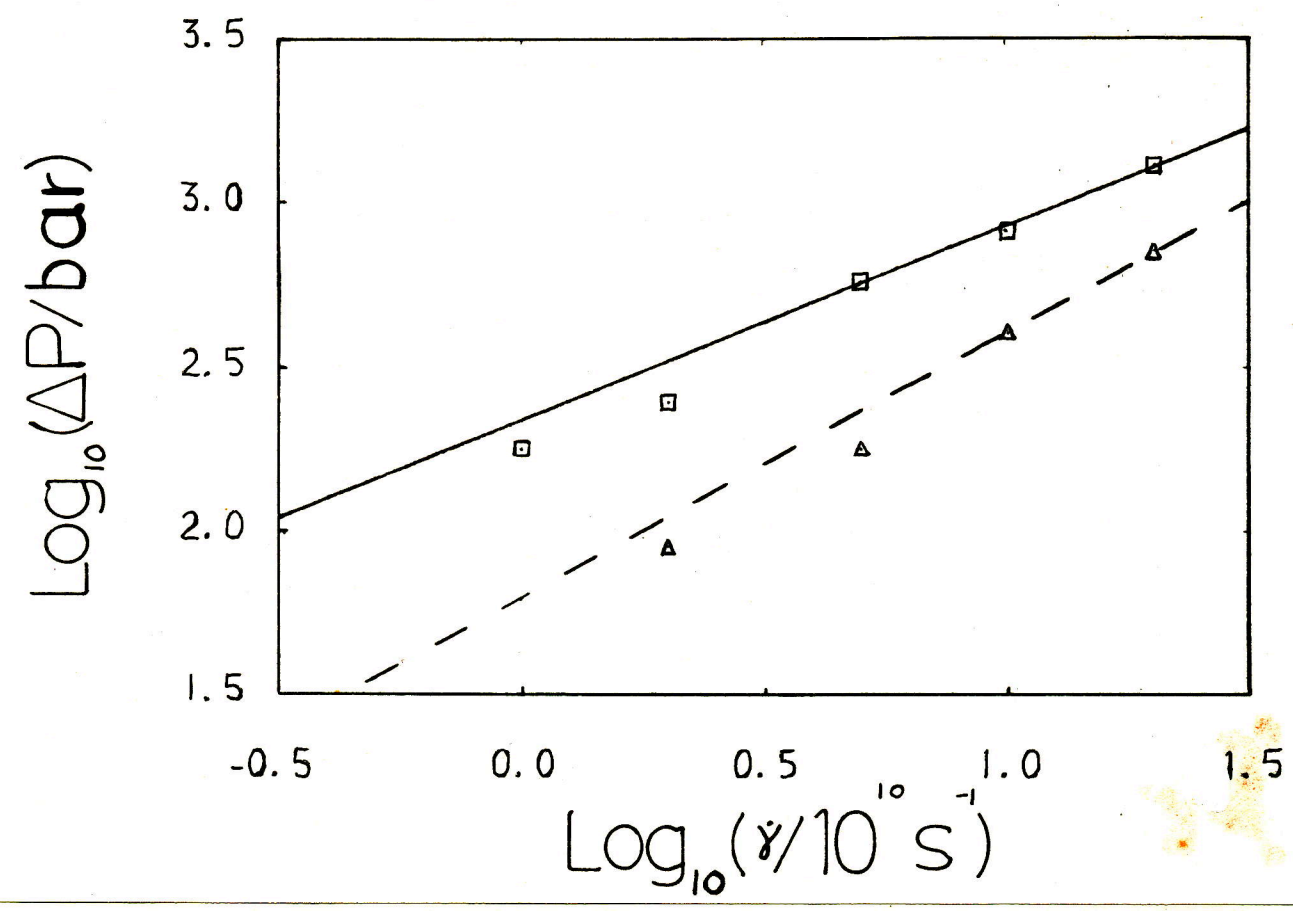

Table 6.8 The slopes (a and c) and proportionality constants (P_1 and Φ_1) for the fits of $\Delta\Phi(\dot{\gamma})$ and $\Delta P(\dot{\gamma})$ to the forms given in eqns.3.8.3 and 6.5.3 from the steady state calculations on hexane and flexane at T~200K.

	P_1/bar	a	Φ_1/Jmol^{-1}	c
Hexane	224	0.59	165	0.72
Flexane	62	0.81	22	1.13

For both the pressure and the LJ potential energy hexane shows the greater actual change in these properties under shear but also a slower rate of increase. This behaviour leads to the situation given in table 6.8 where P_1 and Φ_1 are greater in hexane but a and c are less. All the slopes fall well below the value of 1.5 demanded by theory even allowing for the large uncertainties there is in the data. It appears that from this, and the earlier data on diatomics and triatomics, that although an algebraic dependence of the pressure and potential energy upon shear rate is a reasonable approximation the actual exponent is certainly molecule dependent and probably state dependent also.

The interesting finding that the dihedral angle potential energy changes under shear in hexane is made more credible by the fact that $\Delta\Phi_\alpha(\dot{\gamma})$ also decreases in flexane which, as no forces derive from Φ_α in flexane, indicates that even in a model free of hindered internal rotation the shear flow does impart a different influence on the structure of the molecules

than at equilibrium. The conformational changes underlying this phenomenon will be discussed in sec.6.7.

As with the previous models the pressure increase has been resolved into its component parts. This has been achieved in this case by calculating the functions $\Delta P_{\alpha\alpha x}(\dot{\gamma})$ defined as

$$\Delta P_{\alpha\alpha x}(\dot{\gamma}) = P_{\alpha\alpha x}(\dot{\gamma}) - P(\dot{\gamma}) \qquad \alpha = x,y,z \qquad (6.5.4)$$

where

$$P(\dot{\gamma}) = (P_{xx}(\dot{\gamma}) + P_{yy}(\dot{\gamma}) + P_{zz}(\dot{\gamma}))/3 \quad . \qquad (6.5.5)$$

This differs from the definition given previously, eqn.3.8.5, as in the hexane and flexane calculations $P(\dot{\gamma})$ derives from the stress tensor which is averaged over the period for which σ_{xz} appears to be at steady state whereas $P(\dot{\gamma})$ is averaged over the period shown in table 6.2 The functions $\Delta P_{\alpha\alpha x}(\dot{\gamma})$ are given in table 6.9.

Table 6.9 The functions $\{\Delta P_{\alpha\alpha}(\dot{\gamma})\}$ as defined in eqn.6.5.4 from the steady state shear calculations on hexane and flexane at T~200K.

Hexane

$\dot{\gamma}/10^{10}s^{-1}$	$P(\dot{\gamma})$/bar	$\Delta P_{xx}(\dot{\gamma})$/bar	$\Delta P_{yy}(\dot{\gamma})$/bar	$\Delta P_{zz}(\dot{\gamma})$/bar
1	690±80	20±110	-70±110	50±100
2	800±30	-80±70	-60±40	130±40
5	1130±30	-230±90	-160±70	390±80
10	1370±70	-370±120	-50±90	420±100
20	1850±80	-620±90	-40±130	650±120

Flexane

$\dot{\gamma}/10^{10}s^{-1}$	$P(\dot{\gamma})$/bar	$\Delta P_{xx}(\dot{\gamma})$/bar	$\Delta P_{yy}(\dot{\gamma})$/bar	$\Delta P_{zz}(\dot{\gamma})$/bar
2	360±80	-60±120	-10±110	70±110
5	460±90	-110±110	-50±140	160±120
10	590±100	-250±140	-50±140	290±150
20	860±150	-380±190	-80±190	460±210

These functions show a clear trend in the normal pressure components which is in general $P_{xx}(\dot{\gamma})<P(\dot{\gamma})$, $P_{yy}(\dot{\gamma})\simeq P(\dot{\gamma})$ and $P_{zz}(\dot{\gamma})>P(\dot{\gamma})$. This is the same behaviour found in the chlorine systems at high density which implies that this is the more typical reaction of dense fluids to this kind of flow whereas the different trends found in the ethane and propane case are probably characteristic of a low density high temperature fluid.

6.6 Shear Induced Intermolecular Structural Changes

The modified fluid structure which underlies the changes in pressure and intermolecular energy have been probed in the usual way by calculating distributiion functions. Apart from the normal r.d.fs g(r) and G(R), for the individual sites and the centres of mass respectively, a directional distribution function for COM separation has been calculated and also the orientational cross correlation function $P_1(R)$ defined in sec.5.6.

In figs.6.14 and 6.15 the g(r)s and G(R)s are given for hexane and flexane at the highest shear rate of $\dot{\gamma}=2*10^{11}s^{-1}$ together with the same functions at equilibrium. These functions are scalar so are not ideal for probing this highly oriented structure which is obviously present from the results for the alignment tensor. Nevertheless, there are some changes in the r.d.fs. g(r) shows a slight tendency for the height of the first peak to increase in both cases but is in general very similar to the equilibrium g(r). However, the G(R)s show a much greater change as the first peak is reduced in width, increased in height and is moved slightly to smaller values of R.The second peak for hexane, which is difficult to discern at equilibrium, is made more distinct by the shear flow. These findings are consistent with the previously noted changes in the energy and the pressure and also the alignment.

Figure 6.14 g(r) vs. r, hexane (1) and flexane (2), $\dot{\gamma}=2*10^{11}s^{-1}$ (——) and $\dot{\gamma}=0$ (—·—), T~200K.

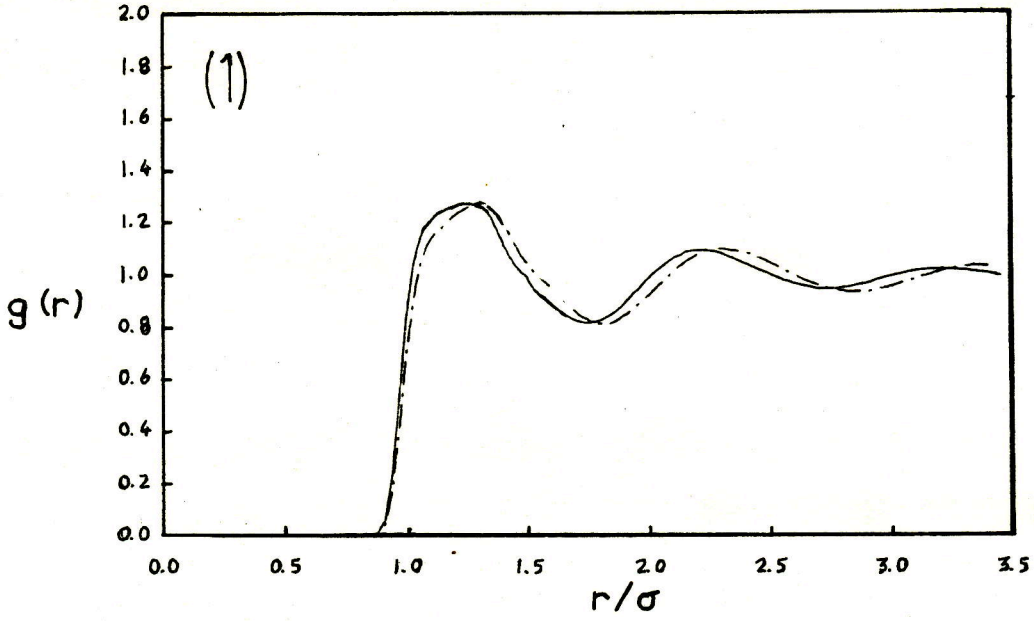

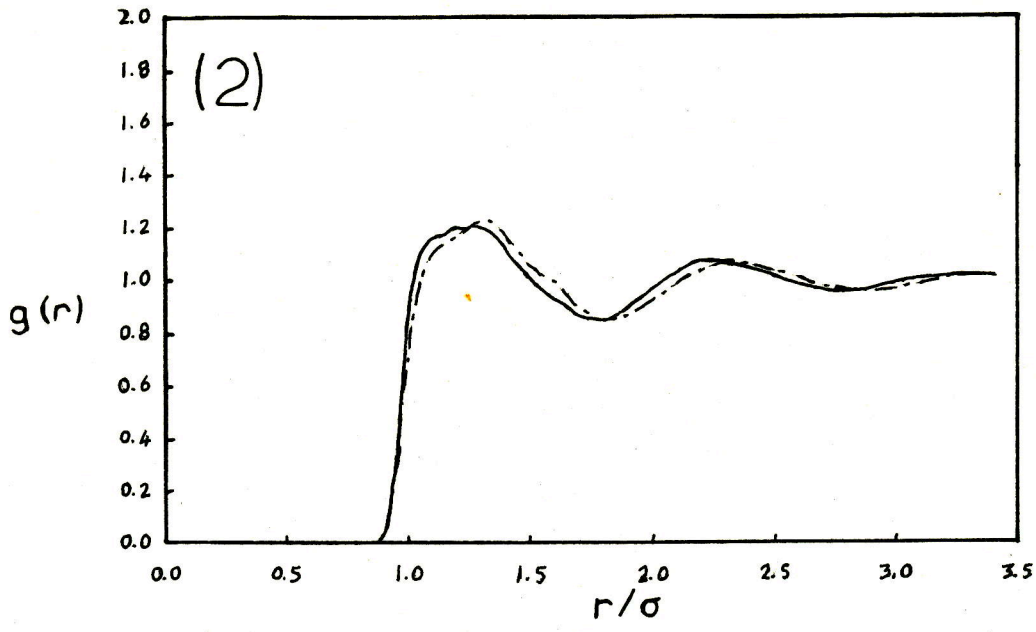

Figure 6.15 G(R) vs. R, hexane (1) and flexane (2), $\dot{\gamma}=2*10^{11}s^{-1}$ (——) and $\dot{\gamma}=0$ (—·—), T~200K.

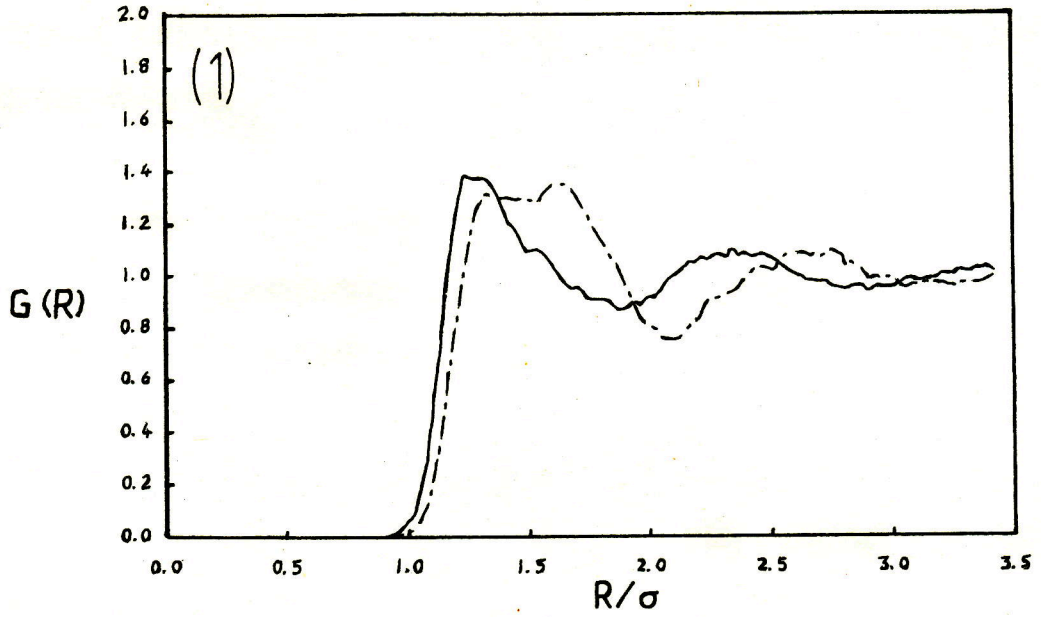

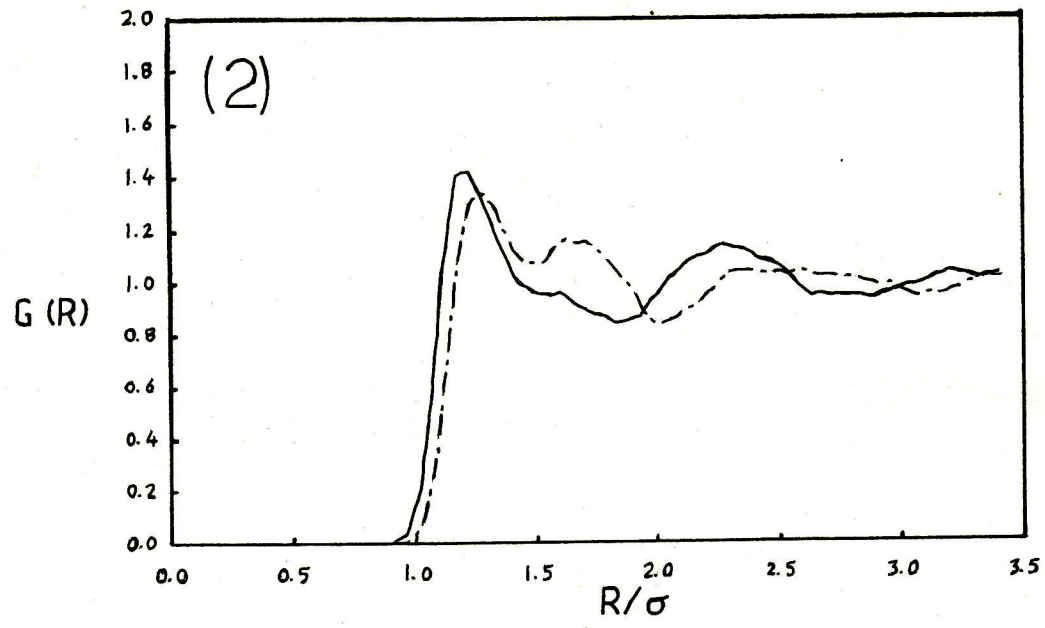

To try and understand more about the intermolecular rearrangements under shear directional distribution functions, $\{G(\alpha)\}$, have been calculated. In the x direction G(X) is defined as the mean number of molecules which satisfy the following three conditions for the COM separation vector $\underline{R}_{ij}=(X_{ij},Y_{ij},Z_{ij})$:-

i) $X < |X_{ij}| < X+\Delta X$

ii) $|Y_{ij}| < S/2$

iii) $|Z_{ij}| < S/2$

divided by the expected number of molecules in this region if the structure was entirely random i.e. $2S^2\Delta X\, N/V$. This gives a measure of the relative probability of finding another molecule, j, at a separation X in the x direction in a column of cross-sectional area S*S centred on the COM of molecule i. The dimension S is arbitrary but if S is large, say, compared to the size of a molecule then molecules are counted which may have a small x separation but are in fact quite a distant apart and, therefore, uncorrelated. On the other hand if S is too small then the statistics become poor because of the small numbers of molecules. To try and avoid these pitfalls a value of S=5.0Å was chosen as a compromise. Even so the results shown in figs.6.16 and 6.17 for all three directions, for hexane and flexane at the highest shear rate of $\dot{\gamma}=2*10^{11}\,s^{-1}$, are still prone to a significant amount of statistical noise even after being averaged over the entire time the system was

Figure 6.16 The directional distribution functions for the separations of the COM in the three orthogonal directions G(α) vs. α, for α=X (——), α=Y (—·—) and α=Z (- -), hexane $\dot{\gamma}=2*10^{11}s^{-1}$, T~200K.

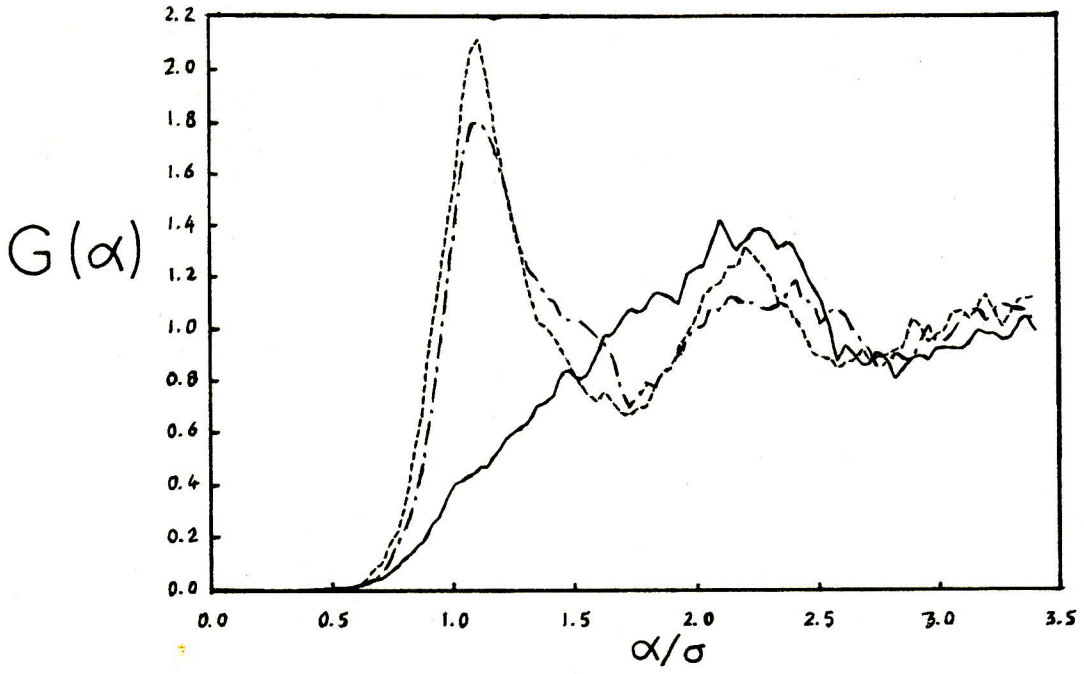

Figure 6.17 As fig.6.16 for flexane.

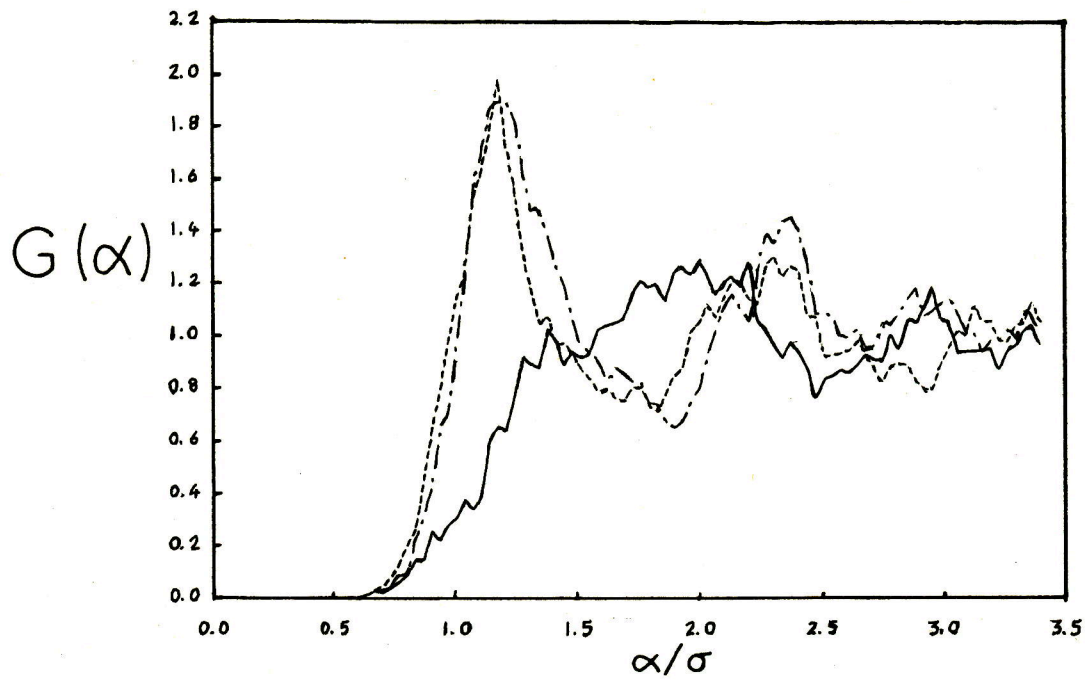

adjudged to be at a steady state. Nevertheless these functions reveal some interesting features about the distribution of the centres of mass. From the figures it can be seen that G(Y) and G(Z) have the 'usual' r.d.f. type structure with the main peak at a separation of around 1σ and subsequent peaks diminishing in height at 2σ and 3σ. G(X) shows a very different form with no peak at all at lo just a gradual rise to a broad peak around 2σ. This is consistent with the result from the alignment tensor since as these molecules align along the x-axis much of the columnal region in front, or behind, of the COM of a molecule in the x direction is taken up by sites of its own chain forcing the COM of other molecules to be more distant. In the y and z directions molecules lie parallel to one another to a large extent, thus, the relatively narrow peaks at 1σ. These observations also explain the changes in G(R) which occur under shear. The narrowing of the first peak in G(R) results from contributions in the y and z directions and the more pronounced second peak results not only from G(X) but also the distinct structure seen in G(Y) and G(Z).

The results for $P_1(R)$ are shown in figs.6.18 and 6.19 once again for the highest shear rate used along with the same functions at equilibrium, for hexane and flexane respectively. With a preferred orientation in the system the large R value of $P_1(R)$ increases from that of 1/3 for a random distribution of orientations as found at equilibrium. The tendency is for molecules to be parallel in a sheared fluid so the angle

Figure 6.18 $P_1(R)$ vs. R, hexane,
$\dot{\gamma}=2*10^{11}s^{-1}$ (——) and $\dot{\gamma}=0$ (—·—), T~200K.

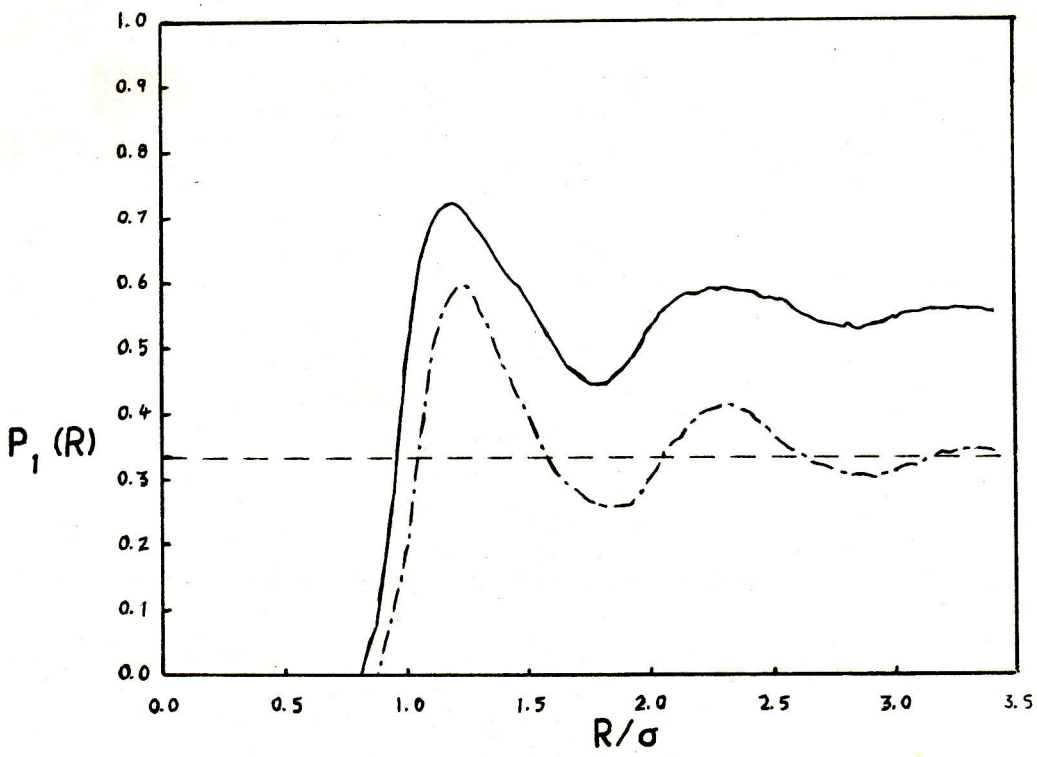

Figure 6.19 $P_1(R)$ vs. R, flexane,
$\dot{\gamma}=2*10^{11}s^{-1}$ (——) and $\dot{\gamma}=0$ (—·—), T~200K.

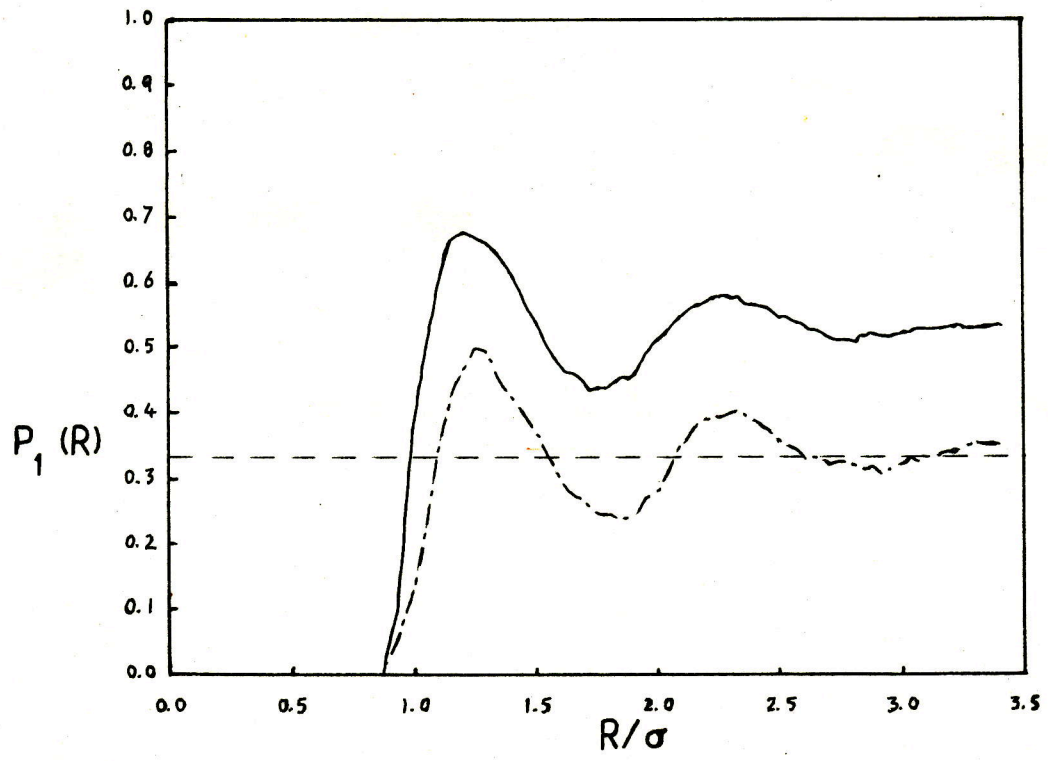

between the $\underline{r}_{16}$ vectors of different molecules, e_{ij}, tends to zero and thus $P_1(R)$, which is a function of $\cos e_{ij}$ increases. It can also be seen that there is some movement of the peaks in $P_1(R)$ to smaller R consistent with the results for the G(R) and the $G(\alpha)$s.

6.7 Shear Induced Intramolecular Structural Changes

It has been generally assumed that shear flow will tend to increase the average length of flexible molecules [128] but it has never been directly observed in real systems. One previous paper [99] discussed the results of NEMD experiments on a model of flexible propane but no significant change in internal structure was observed. With the longer molecules used here noticeable changes have been found to occur in the mean intramolecular separations of sites, $d_{\alpha\beta} = \langle|\underline{r}_{\alpha\beta}|\rangle$, and the root mean square radii of gyration, $s_\alpha = \langle(\underline{r}_{\alpha_i}-\underline{R}_i)^2\rangle^{\frac{1}{2}}$, which must ultimately stem from the effect of the shear flow upon the distribution of conformers and dihedral angles.

In the models of hexane and flexane used here the distances between neighbours and next neighbours are rigidly fixed so the mean separations which can vary are $d_{14}(=\langle|\underline{r}_{14}|\rangle$, d_{15}, d_{16}, d_{25}, d_{26} and d_{36}. Only computationally is site 1 distinguishable from site 6 etc. so the actual quantities quoted are calculated from :-

$$d_{14} = (d_{14} + d_{25} + d_{36})/3 \qquad (6.7.1)$$

$$d_{15} = (d_{15} + d_{26})/2 \quad (6.7.2)$$
$$d_{16} = d_{16} \quad (6.7.3)$$
$$s_1 = (s_1 + s_6)/2 \quad (6.7.4)$$
$$s_2 = (s_2 + s_5)/2 \quad (6.7.5)$$
$$s_3 = (s_3 + s_4)/2 \quad (6.7.6)$$

These functions are given as a function of shear rate in tables 6.10 and 6.11

Table 6.10 The shear rate dependent mean intramolecular separation of sites, $d_{\alpha\beta}(\dot{\gamma})$ as defined in eqns.6.7.1→6.7.3, from the equilibrium and steady state shear calculations on hexane and flexane at T~200K.

Hexane

$\dot{\gamma}/10^{10}s^{-1}$	$d_{14}(\dot{\gamma})$/Å	$d_{15}(\dot{\gamma})$/Å	$d_{16}(\dot{\gamma})$/Å
0	3.582±0.004	4.635±0.004	5.569±0.007
1	3.614±0.002	4.668±0.003	5.663±0.011
2	3.628±0.006	4.687±0.008	5.701±0.014
5	3.654±0.006	4.712±0.007	5.790±0.015
10	3.671±0.003	4.731±0.005	5.843±0.009
20	3.701±0.001	4.778±0.001	5.913±0.001

Flexane

$\dot{\gamma}/10^{10}s^{-1}$	$d_{14}(\dot{\gamma})$/Å	$d_{15}(\dot{\gamma})$/Å	$d_{16}(\dot{\gamma})$/Å
0	3.392±0.010	4.409±0.008	5.197±0.024
2	3.404±0.007	4.426±0.008	5.225±0.021
5	3.421±0.010	4.444±0.011	5.270±0.024
10	3.430±0.008	4.459±0.009	5.302±0.021
20	3.442±0.012	4.473±0.014	5.340±0.026

Table 6.11 The shear rate dependent root mean square radii of gyration, $s_\alpha(\dot{\gamma})$ as defined in eqns. 6.7.4→6.7.6, from the equilibrium and steady state shear calculations on hexane and flexane at T~200K.

Hexane

$\dot{\gamma}/10^{10}s^{-1}$	$s_1(\dot{\gamma})$/Å	$s_2(\dot{\gamma})$/Å	$s_3(\dot{\gamma})$/Å
0	2.862±0.003	1.873±0.002	0.900±0.013
1	2.901±0.004	1.867±0.002	0.898±0.005
2	2.916±0.006	1.870±0.003	0.890±0.005
5	2.950±0.006	1.862±0.002	0.888±0.004
10	2.971±0.005	1.861±0.002	0.883±0.003
20	3.000±0.002	1.876±0.001	0.861±0.003

Flexane

$\dot{\gamma}/10^{10}s^{-1}$	$s_1(\dot{\gamma})$/Å	$s_2(\dot{\gamma})$/Å	$s_3(\dot{\gamma})$/Å
0	2.690±0.012	1.847±0.009	0.931±0.009
2	2.703±0.009	1.848±0.007	0.928±0.007
5	2.723±0.011	1.843±0.007	0.929±0.009
10	2.737±0.010	1.845±0.009	0.924±0.011
20	2.752±0.013	1.841±0.006	0.924±0.009

As a measure of the elongation of a molecule the mean separation of sites is a better indicator than the root mean square radii of gyration as in all cases $d_{\alpha\beta}$ is a maximum for the all trans conformer whereas this is not so for the $\{s_\alpha\}$. The reason for this is that the COM does not necessarily, and in general will not, lie on the molecule. If, for example, we consider the case of an all trans conformer with $\alpha=0$ for all

the three dihedral angles the COM lies midway between sites 3 and 4 and so s_3 will be equal to half the bond length i.e. Ø.765Å. So this case represents the minimum possible value for s_3. This explains the data in tables 6.1Ø and 6.11 where it can be seen that $d_{\alpha\beta}$ increases with shear rate in all cases but only s_1 consistently increases and s_3 in hexane noticeably decreases. All these results can be interpreted as deriving from an overall elongation of these molecules under shear.

To compare this effect in hexane and flexane a percentage extension in d_{16} has been calculated as

$$\Delta d_{16}(\dot{\gamma}) = 100*(d_{16}(\dot{\gamma}) - d_{16}(0))/d_{16}(0) \qquad (6.7.7)$$

and the results are given in table 6.12.

Table 6.12 The function $\Delta d_{16}(\dot{\gamma})$, as defined in eqn. 6.7.7, from the steady state shear calculations on hexane and flexane at T~2ØØK.

	Hexane	Flexane
$\dot{\gamma}/10^{10}s^{-1}$	$\Delta d_{16}(\dot{\gamma})$	$\Delta d_{16}(\dot{\gamma})$
1	1.69+Ø.23	-
2	2.37+Ø.28	Ø.55+Ø.61
5	3.97+Ø.3Ø	1.41+Ø.65
1Ø	4.92+Ø.21	2.Ø3+Ø.61
2Ø	6.18+Ø.13	2.74+Ø.68

Figure 6.20 The percentage change in the mean end-to-end separation $\Delta d_{16}(\dot{\gamma})$ vs. $\dot{\gamma}^{1/2}$, hexane (□) and flexane (Δ), T~200K.

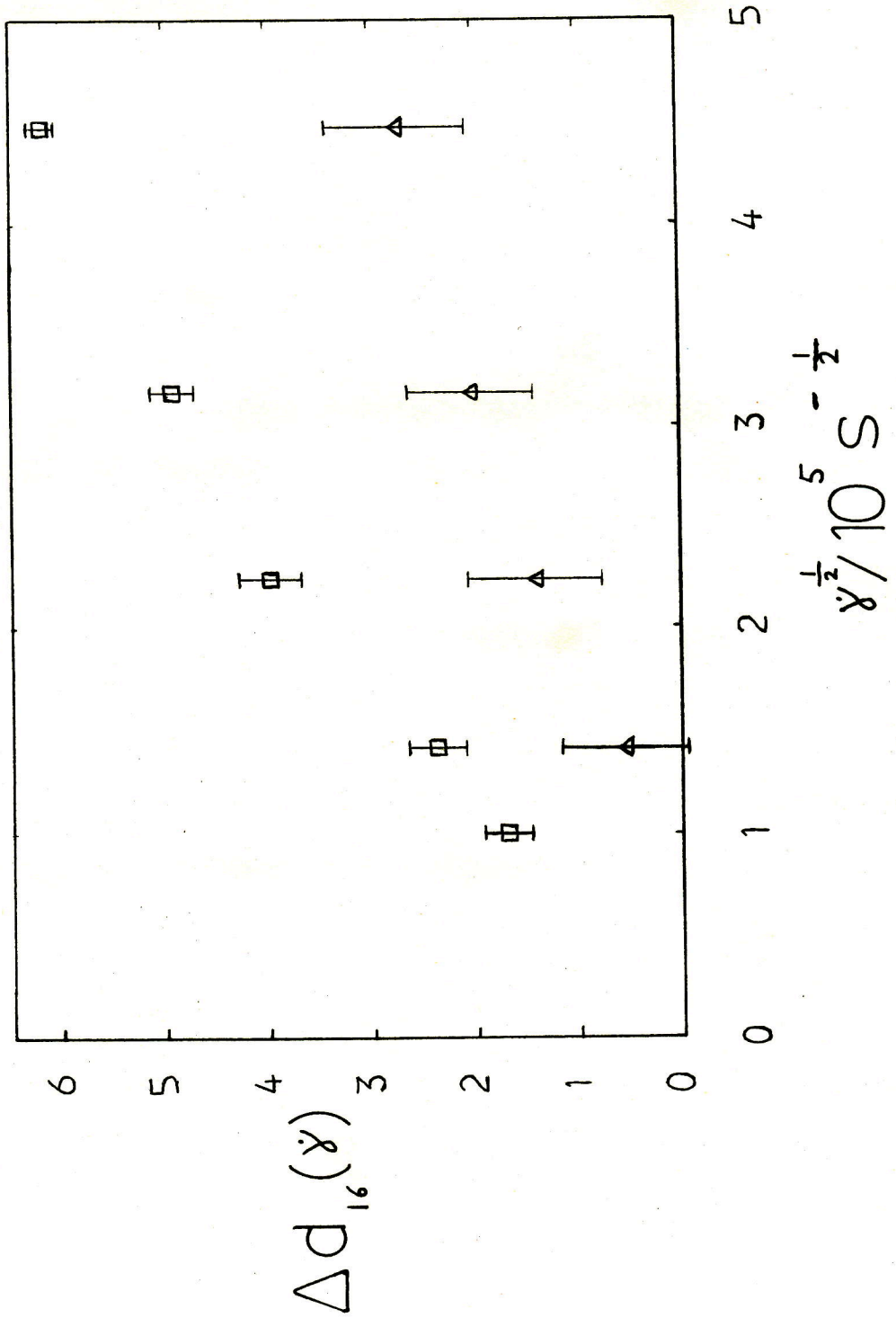

In fig.6.2Ø $\Delta d_{16}(\dot{\gamma})$ is plotted against the square root of the shear rate. At first sight there appears to be a paradox in that the more flexible molecule is extended less than the more rigid molecule under shear. Indeed the ~6% extension of hexane over its equilibrium length is well over twice that of flexane.This can be explained by considering the energies of the various configurations of the molecules. In hexane the all trans conformer is by far the most energetically favourable because of the overwhelming influence of the dihedral angle potential. Moreover, once in the TTT state it is kept closer to its maximum length by the steepness of the potential thus in turn maximising d_{16}. In flexane the all trans conformer does not coincide with that of lowest energy, as can be seen from fig.5.12 in sec.5.7. This is caused by a combination of the intramolecular LJ interactions which mean that the minimum energy conformer in flexane has an r_{16} of about 5.ØÅ. Thus, an increase in d_{16} in flexane causes an increase in the intramolecular energy. This increase in energy is small, because of the nature of the potential, compared to the large decrease in intramolecular energy that occurs when a hexane molecule undergoes a transition from one of the conformers containing a gauche state to an all trans conformer.

To see this in more detail the probability densities for the distribution of r_{16}'s and dihedral angles have been calculated and are shown in figs.6.21 and 6.22 for the highest

Figure 6.21 The probability density for the end-to-end separation $\rho(r_{16})$ vs. r_{16}, hexane (1) and flexane (2), $\dot{\gamma}=2*10^{11}s^{-1}$ (——) and $\dot{\gamma}=0$ (—·—), T~200K.

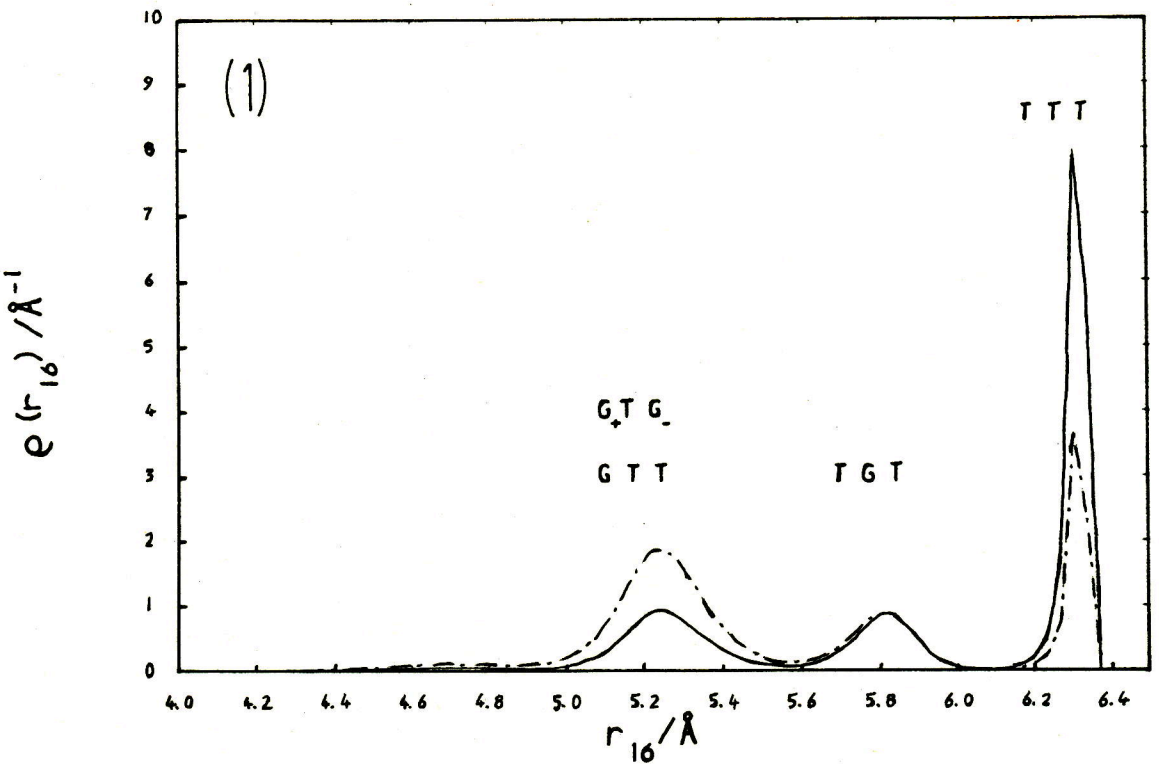

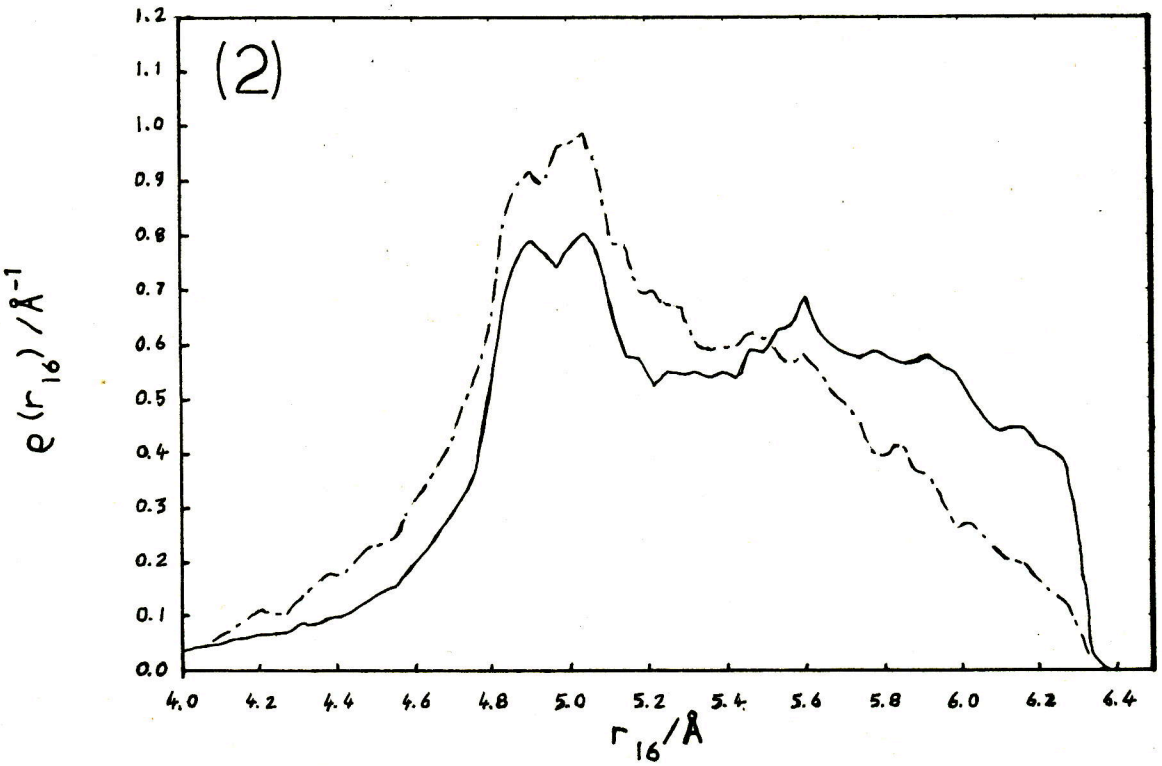

Figure 6.22 The probability density for the dihedral angle $\rho(\alpha)$ vs. α, hexane (1) and flexane (2), $\dot{\gamma}=2*10^{11}s^{-1}$ (——) and $\dot{\gamma}=0$ (—·—), T~200K.

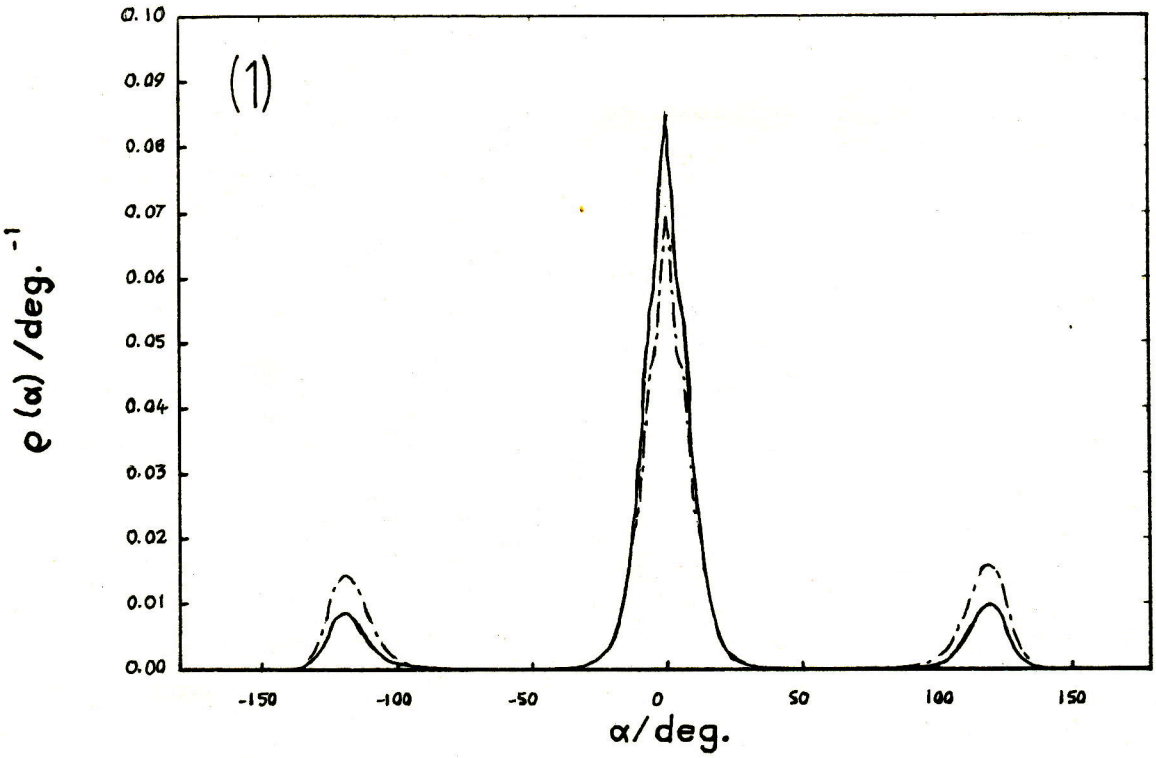

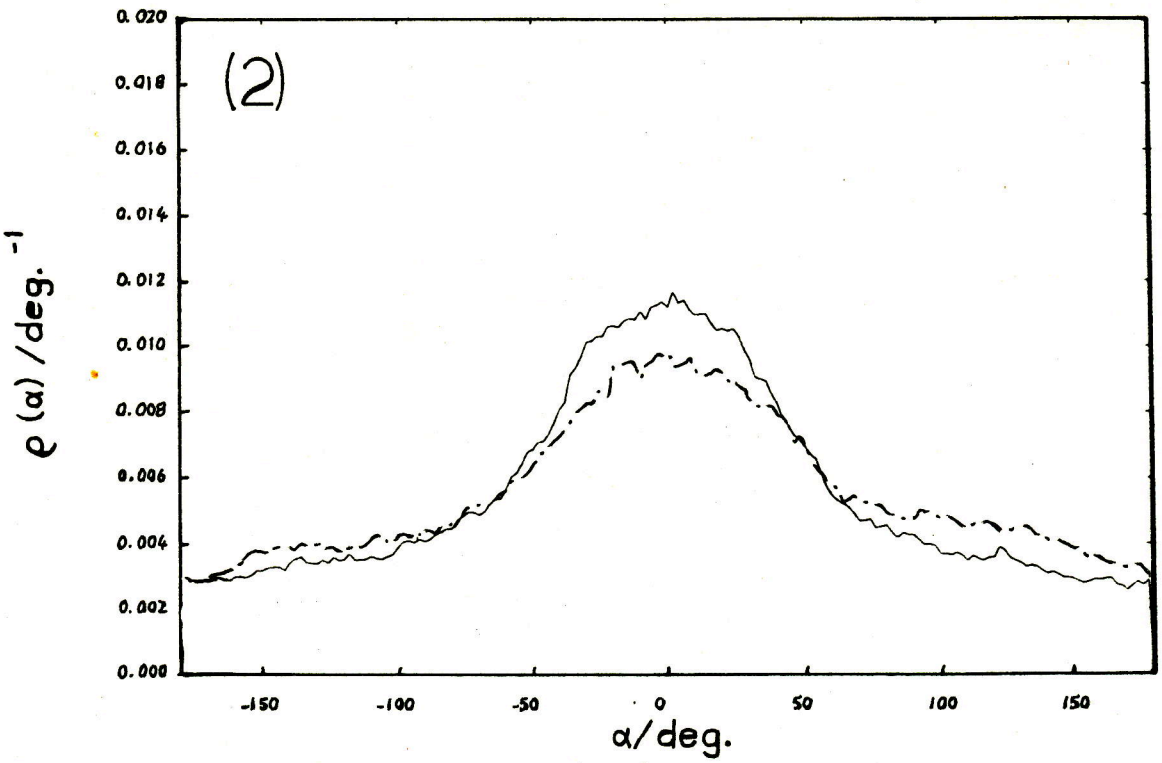

shear rate along with the same functions at equilbrium. For the dihedral angles the probability densities show a clear trend towards more trans states in both hexane and flexane. To compare these changes further the difference between the probability densities at $\dot{\gamma}=0$ and $\dot{\gamma}=2*10^{11}s^{-1}$, $\Delta\rho(\alpha)$, has been plotted in fig.6.23 for both hexane and flexane. The function clearly shows the greater changes which occur in hexane as the numbers of angles in the trans state increases at the expense of those in the G_+ and G_- state. Flexane shows a less well defined change but there is still a discernible tendency for the dihedral angles to take up values around the trans and cis angles $\alpha=0^\circ$ and 180° which gives rise to more 'flattened' molecules. This is confirmed by the general trend to larger values of r_{16} shown in fig.6.21 for flexane with the retention of a peak at r_{16}~5.0Å corresponding to the CTC and TTC conformers. For hexane fig.6.21 shows an approximately 30% increase in the number of TTT conformers largely at the expense of the G_+TG_- and GTT conformers. The numbers of TGT conformers remains almost unaltered by the shear. Why this is so is not clear but from the equilibrium results it is known that transitions in α_2, the central dihedral angle , are if anything slightly less frequent than those in the outer angles. It could be then that it is easier for the outer gauche angles in the G_+TG_- and GTT conformers to undergo transitions to form TTT molecules than it is for the central angle of a TGT conformer to do the same.

Figure 6.23 The difference between the probability densities for the dihedral angle $\Delta\rho(\alpha)$ vs. α, at $\dot{\gamma}=2*10^{11}s^{-1}$ and $\dot{\gamma}=0$, (a) hexane and (b) flexane, T=200K.

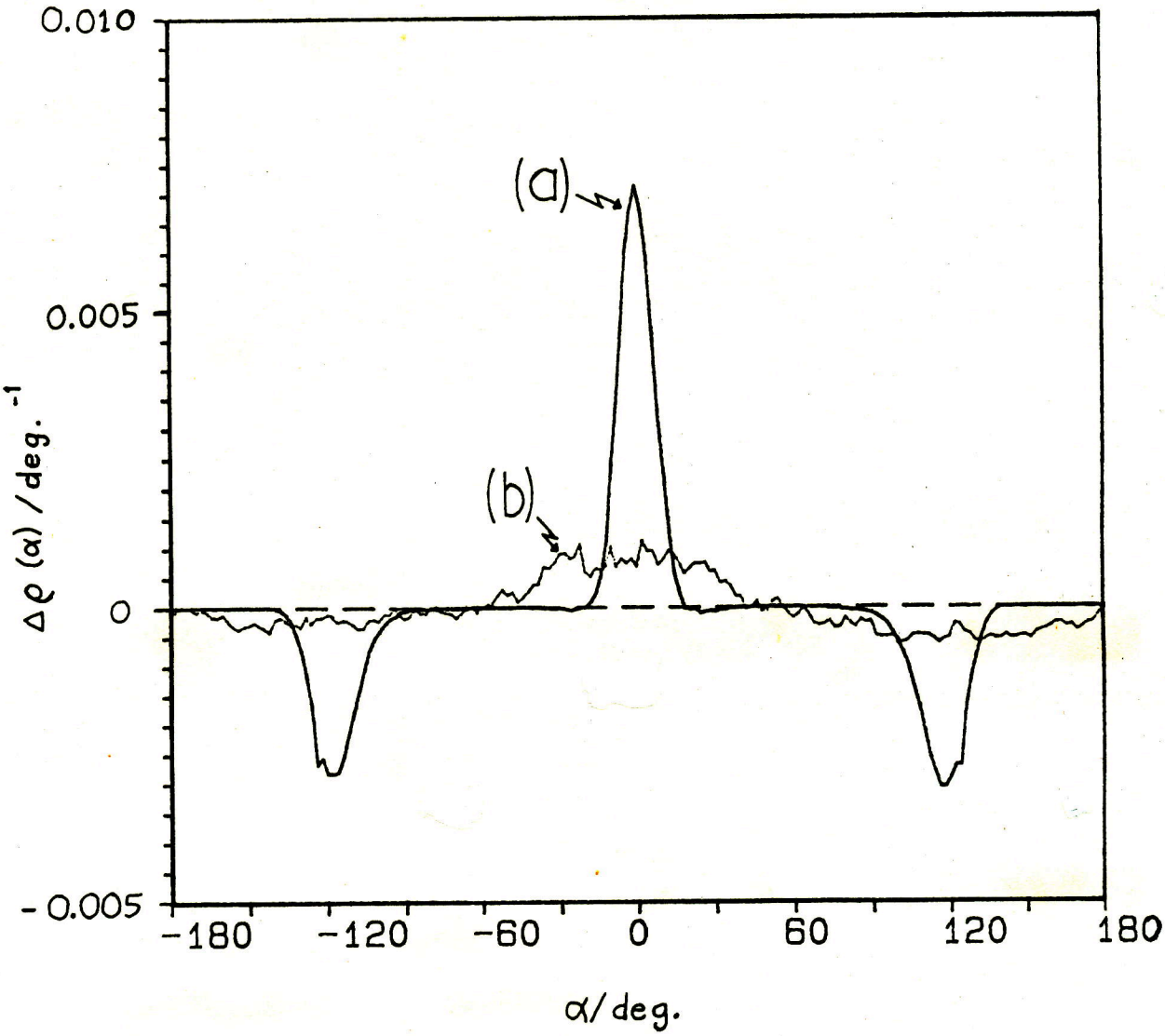

6.8 Self Diffusion

The one dynamic property most likely to be affected by the shear flow is the self-diffusion through its connection with the viscosity which has been shown to be a strong function of $\dot{\gamma}$. It would be expected that as the viscosity fell the diffusion would increase and this has been found to occur in monatomic fluids [1]. With the shear flow directionality imposed upon the system it is by no means certain that diffusion will change isotropically especially with the already observed high degree of alignment in the system.

To monitor any changes in the diffusion and to see how anisotropic they are the diffusion coefficients in the three orthogonal directions of the laboratory frame have been calculated from

$$D_x = \lim_{t\to\infty} < \left[\int_0^t (V_x(s) - \dot{\gamma}Z(s))\, ds\right]^2 >/6t \qquad (6.8.1)$$

and

$$D_\alpha = \lim_{t\to\infty} < \left[\int_0^t (V_\alpha(s)\, ds\right]^2 >/6t \qquad \alpha=y,z \qquad (6.8.2)$$

where $\underline{V}=(V_x,V_y,V_z)$ and $\underline{R}=(X,Y,Z)$ are the velocity and position of the COM of a molecule. The definition in eqn.6.8.1 accounts for the fact that V_x contains a contribution from the

net shear flow in the system which must be subtracted before calculating the diffusion. As in sec.5.9 the diffusion coefficients perpendicular and parallel to $\underline{r}_{i6}$ have also been calculated from the integrals over the correlation functions given in eqns. 5.9.5 and 5.9.6. Once again making the same adjustment to V_x as in eqn.6.8.1. In table 6.13 the self-diffusion coefficient, D, which from eqns.6.8.1, 6.8.2 and 5.9.3 is given by the sum of D_x, D_y and D_z, is given along with its resolution in to the laboratory frame, the ratio of $D_{\parallel}/D_{\perp}$ and also the product of the diffusion coefficient and the viscosity at the particular shear rate.

Table 6.13 The diffusion coefficients D, D_x, D_y, D_z, as defined in the text, the ratio $D_{\parallel}/D_{\perp}$ and the product $D(\dot{\gamma})\eta(\dot{\gamma})$ for hexane and flexane from the equilibrium and steady state shear calculations at T~200K.

Hexane

$\dot{\gamma}/10^{10}s^{-1}$	D	D_x	D_y	D_z	$D_{\parallel}/D_{\perp}$	$D\eta/pN$
	←		$/10^{-9}m^2s^{-1}$		→	
0	0.35 ±0.02	0.12 ±0.01	0.12 ±0.01	0.12 ±0.01	1.32 ±0.23	1.23 ±0.22
1	0.43 ±0.03	0.15 ±0.03	0.15 ±0.03	0.15 ±0.03	1.33 ±0.25	1.26 ±0.21
2	0.60 ±0.09	0.22 ±0.04	0.18 ±0.04	0.18 ±0.04	1.61 ±0.19	1.49 ±0.23
5	1.06 ±0.07	0.45 ±0.07	0.29 ±0.03	0.29 ±0.03	1.40 ±0.17	1.59 ±0.15
10	2.00 ±0.12	1.07 ±0.16	0.50 ±0.09	0.50 ±0.09	1.31 ±0.11	1.79 ±0.11
20	3.39 ±0.69	2.05 ±0.63	0.64 ±0.10	0.64 ±0.10	1.54 ±0.12	1.93 ±0.40

Flexane

$\dot{\gamma}/10^{10}s^{-1}$	D	D_x	D_y	D_z	$D_{\parallel}/D_{\perp}$	$D\eta/pN$
	←		$/10^{-9}m^2s^{-1}$		→	
0	0.53 ±0.10	0.17 ±0.06	0.17 ±0.06	0.17 ±0.06	1.04 ±0.09	0.90 ±0.23
2	0.88 ±0.08	0.32 ±0.05	0.20 ±0.03	0.32 ±0.05	1.11 ±0.14	1.26 ±0.32
5	0.98 ±0.05	0.46 ±0.03	0.25 ±0.03	0.25 ±0.03	1.76 ±0.54	1.04 ±0.13
10	1.97 ±0.10	0.89 ±0.10	0.38 ±0.06	0.83 ±0.10	1.70 ±0.17	1.50 ±0.15
20	2.42 ±0.12	1.04 ±0.07	0.41 ±0.07	0.88 ±0.07	1.17 ±0.07	1.35 ±0.13

The data in table 6.13 is consistent with the well known experimental finding that a reduced viscosity is indicative of

the enhanced diffusion of molecules in the fluid. Although this is generally applied to the case of changes in viscosity caused by changes in temperature and/or pressure it seems also to hold for the case here of an increase in shear rate. The degree to which an inverse relationship holds between the viscosity and the diffusion can be judged from the product Dn, given in table 6.13. In hexane Dn gradually increases with shear rate but only by a small amount compared to the factor of almost ten increase in the diffusion coefficient. In flexane Dn does not show a consistent trend but is again reasonably constant considering the fivefold change in D. These results bear out the strong correlation, though perhaps not 1:1, between the fluidity, $1/n$, and the diffusion coefficient.

In hexane there is a clear tendency for the diffusion to be enhanced much more in the x-direction than in the y- or z-directions , which within errors have the same coefficient at all shear rates. In flexane the trend for D_x and D_y is the same but the behaviour of D_z appears much more erratic as it 'oscillates' between the values for D_x and D_y. This could be due to a lack of averaging but it seems likely that there maybe a different trend in flexane. From the directional structures of the fluids, given in figs.6.16 and 6.17, it might be expected that diffusion would be different in the x-direction but their is little if any indication that diffusion in the z-direction should be any different from that

in the y-direction in flexane as the density distributions are very similar.

One other point that can be drawn from table 6.13 is that the ratio $D_{\parallel}/D_{\perp}$ does not show a systematic change with shear rate in either case. As has been shown diffusion is enhanced in the x-direction under shear which coincides with that of the preferred orientation of the $\underline{r}_{16}$ vector of the molecules (sec.6.4). It would seem logical then to assume that diffusion parallel to $\underline{r}_{16}$ would also be enhanced but this appears not to be the case. There is, of course, still a distribution of orientations even at the highest shear rate (see figs.6.1Ø and 6.11) which means that there is a proportion of molecules with $\underline{r}_{16}$ far from being parallel to the x-axis. What the data in table 6.13 implies is that the diffusion of these molecules is increased more than those with their $\underline{r}_{16}$ vectors almost parallel to the x-axis. This would have to be the case for $D_{\parallel}/D_{\perp}$ to remain low whilst the degree of alignment continued to rise.

6.9 Conclusions

These results clearly demonstrate the marked effect the flexibility of the molecules can have upon the rheological properties, structure and dynamics of a fluid. It has been shown that although thermodynamically very similar at equilibrium their intramolecular dynamic properties differ significantly which in turn affects the diffusive and reorientational motion of the molecules. When sheared this effect manifests itself most notably as a difference in the zero shear rate viscosity. It is also found that the non-Newtonian behaviour of these fluids, in particular $n(\dot{\gamma})$ and $P(\dot{\gamma})$, which are of considerable practical importance, contrast quite sharply with hexane shear thinning to a larger extent and also showing more 'dilatancy'. It is also believed that for the first time the extension of molecules under shear has been demonstrated in a convincing manner.

An important aspect of the comparisons between the two fluids is the fact that in terms of the intramolecular potential flexane represents the high temperature limit of hexane So not only are the differences between two molecules of varying flexibility, at a similar state point, being probed but also the likely variation in the rheological properties of a molecule as a function of temperature. This assumes that at constant density the effect on the rheological properties of an increase in temperature is small in those molecules which

do not have barriers to internal rotation.

It was, thus, proposed that further calculations be carried out at an elevated temperature. These would reveal directly the effects on temperature on the rheological properties of molecules with internal barriers to rotation and also determine to what extent these effects are predictable from comparisons between molecules with differing flexibilities. Furthermore, as the transition rates for conformational changes were rather slow at 200K it was not possible to determine the effect of shear upon these properties, hopefully the increased temperature, and hence increased transition rates, might allow this effect to be characterised.

CHAPTER 7

HEXANE AND FLEXANE RESULTS AT 300K

7.1 Introduction

The temperature chosen of 300K was again largely arbitrary but it was realised that to see a noticeable change in the rates of conformational transitions a substantial increase in temperature was required. By increasing the temperature to 300K the barriers to internal rotation are effectively reduced by a factor of 1/3. It was also suggested that further calculations might be useful at a point close to the zero pressure isobar at a higher temperature so as to compare the effect of increasing the temperature at constant pressure and at the same time the effect of increasing the pressure at constant temperature. This was never realised, however, but the choice of temperature was made with this in mind as at a temperature of 300K and a pressure close to zero one could be reasonably confident that the model fluid would still be in a dense liquid phase. It also corresponds to the temperature regime at which most experimental data is obtained and this offered the possibility of comparisons with real n-hexane.

7.2 Details of the Simulations

Equilibrium configurations of hexane and flexane were obtained at 300K simply by taking the final configurations from the equilibrium calculations at 200K and applying the constant temperature algorithm described in sec.2.15. As no change was made in the density the pressure rose rapidly, within 0.5ps, in both systems to values ~2kbar and the relaxation of the other state variables was equally rapid. Even in hexane the dihedral angle energy rose to the level of its average equilibrium value on a similar time scale. However, to allow for any long time relaxation in the distribution of conformers and dihedral angles the first 24ps of the equilibrium run were not included in the averages of any of the properties calculated.

Having obtained equilibrium configurations at 300K shear rates of 2,5,10 and $20*10^{10}s^{-1}$ were applied to the hexane system but only one simulation was performed on flexane at a shear rate of $5*10^{10}s^{-1}$. As before equilibrium configurations were used as the starting points for the calculations at the lowest two shear rates so as to observe the attainment of a steady state. At the highest shear rates the final configuration from the simulation at $\dot{\gamma}=5*10^{10}s^{-1}$ was used to reduce the amount of time required to achieve a steady state.

7.3 Results at 300K

In table 7.1 the results are given for the mean thermodynamic functions obtained from the simulations at 300K for all the shear rates applied.

A comparison of the equilibrium data for hexane and flexane at T~300K with that at 200K (table 5.1) underlines the basic similarity of the fluids as the temperature rise increases the pressure in both systems by ~1.8kbar and the LJ 12-6 potential energy by ~2.6k$J\ mol^{-1}$. The pressure increase is much greater than that expected purely from a change in the temperature, $Nk_b\Delta T/V=80bar$, emphasising the dominance of the potential contribution. In other words the pressure increase is not caused directly by the molecules moving faster but as a consequence of the increased kinetic energy there is greater penetration of the repulsive core of the interaction sites which gives larger forces between molecules and hence a larger pressure.

In tables 7.2 and 7.3 further averages are given for the significant components of the stress/pressure tensor and the alignment tensor along with the resultant shear rate dependent viscosity

Table 7.1 The mean thermodynamic functions obtained from the constant temperature simulations on hexane and flexane at equilibrium and under shear at T~300K, ρ^*=0.33749. U=total energy, Φ=total LJ 12-6 potential energy, Φ_i=intramolecular contribution to Φ, Φ_α=total dihedral angle energy, * indicates calculated for comparison only and the figures in parentheses are the total duration of the simulation.

Hexane

$\dot{\gamma}/10^{10}s^{-1}$	U /J mol^{-1}	Φ /J mol^{-1}	Φ_i /J mol^{-1}	Φ_α /Jmol^{-1}	T/K	P/bar	Length of run /ps
0	-28870 ±210	-47660 ±90	-1460 ±10	7560 ±120	299.99 ±0.01	2370 ±20	36 (60)
2	-28820 ±130	-47630 ±50	-1450 ±10	7590 ±120	300.00 ±0.01	2409 ±30	108 (120)
5	-28900 ±160	-47540 ±70	-1440 ±10	7415 ±140	300.04 ±0.01	2520 ±50	108 (120)
10	-28910 ±90	-47340 ±60	-1450 ±20	7200 ±30	300.11 ±0.01	2700 ±40	48 (60)
20	-28870 ±160	-46760 ±90	-1410 ±10	6670 ±90	300.29 ±0.01	3180 ±40	48 (60)

Flexane

$\dot{\gamma}/10^{10}s^{-1}$	U /J mol^{-1}	Φ /Jmol^{-1}	Φ_i /Jmol^{-1}	Φ_α /Jmol^{-1}	T/K	P/bar	Length of run /ps
0	-35950 ±60	-47180 ±60	-1220 ±10	30820 ±300	300.00 ±0.02	2120 ±40	44 (44)
5	-35960 ±80	-47190 ±70	-1240 ±10	30450 ±410	300.03 ±0.02	2170 ±50	44 (55)

Table 7.2 The mean shear stress, resultant viscosity and mean normal pressure components from the steady state calculations on hexane and flexane at T~300K.

Hexane

$\dot{\gamma}/10^{10}s^{-1}$	σ_{xz}/bar	η/mPa s	P_{xx}/bar	P_{yy}/bar	P_{zz}/bar
2	264±38	1.319±0.192	2415±31	2409±49	2402±60
5	611±35	1.221±0.070	2399±70	2455±67	2719±65
10	871±30	0.871±0.030	2402±120	2674±48	3024±45
20	1278±13	0.639±0.006	2597±81	3153±98	3784±51

Flexane

$\dot{\gamma}/10^{10}s^{-1}$	σ_{xz}/bar	η/mPa s	P_{xx}/bar	P_{yy}/bar	P_{zz}/bar
5	512±62	1.024±0.123	2042±72	2244±75	2209±106

Table 7.3 The mean significant components of the alignment tensor obtained from the steady state calculations on hexane and flexane at T~300K.

Hexane

$\dot{\gamma}/10^{10}s^{-1}$	D_{xz}	$D_{xx}-1/3$	$D_{yy}-1/3$	$D_{zz}-1/3$
2	0.101±0.011	-0.012±0.021	0.013±0.016	0.001±0.014
5	0.167±0.017	0.153±0.019	-0.073±0.017	-0.080±0.012
10	0.197±0.007	0.196±0.026	-0.105±0.021	-0.090±0.011
20	0.199±0.013	0.247±0.023	-0.128±0.013	-0.118±0.016

Flexane

$\dot{\gamma}/10^{10}s^{-1}$	D_{xz}	$D_{xx}-1/3$	$D_{yy}-1/3$	$D_{zz}-1/3$
5	0.165±0.011	0.075±0.022	-0.051±0.020	-0.022±0.029

7.4 The Shear Rate Dependence of the Viscosity

A comparison of the data in table 7.2 with that in table 6.3 shows that whereas the viscosity of flexane at a shear rate of $5*10^{10} s^{-1}$ is, within error, the same at 200K and 300K there is a considerable reduction in the viscosity of hexane at the lowest two shear rates when the temperature is increased. Further interesting points to note are that the behaviour of the viscosity of hexane at 300K strongly resembles that of flexane at 200K and at the highest shear rate hexane is slightly more viscous at 300K than at 200K. These points are illustrated in figs. 7.1 and 7.2 where the viscosity data for hexane at 300K is plotted with that of hexane and flexane at 200K. The data at 300K has also been fitted to the predictions of the theories discussed in sec.3.5. The parameters for the best fits are given in table 7.4 along with the root mean square differences between the data points and the fitted curves.

Figure 7.1 $\eta(\dot{\gamma})$ vs. $\dot{\gamma}^{1/2}$, hexane T~300K (Δ) and hexane T~200K (□).

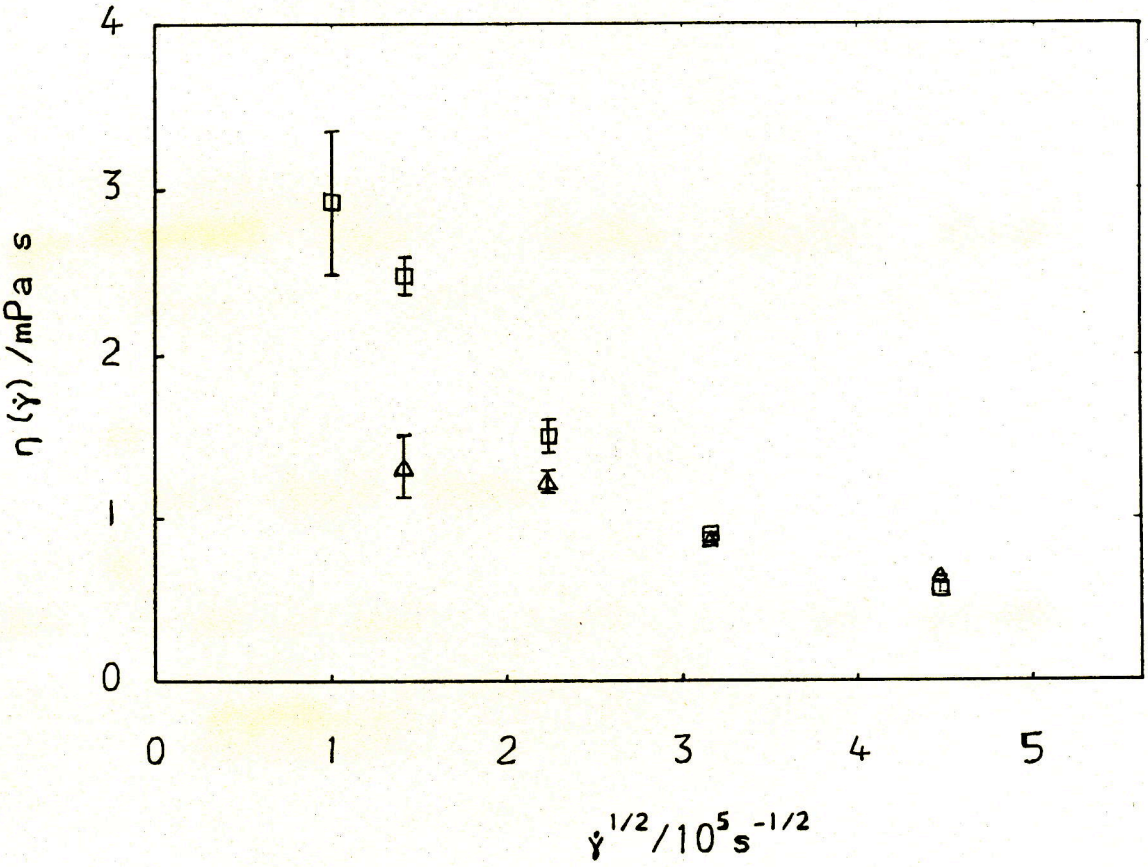

Figure 7.2 $\eta(\dot{\gamma})$ vs. $\dot{\gamma}^{1/2}$, hexane T~300K (Δ) and flexane T~200K (□).

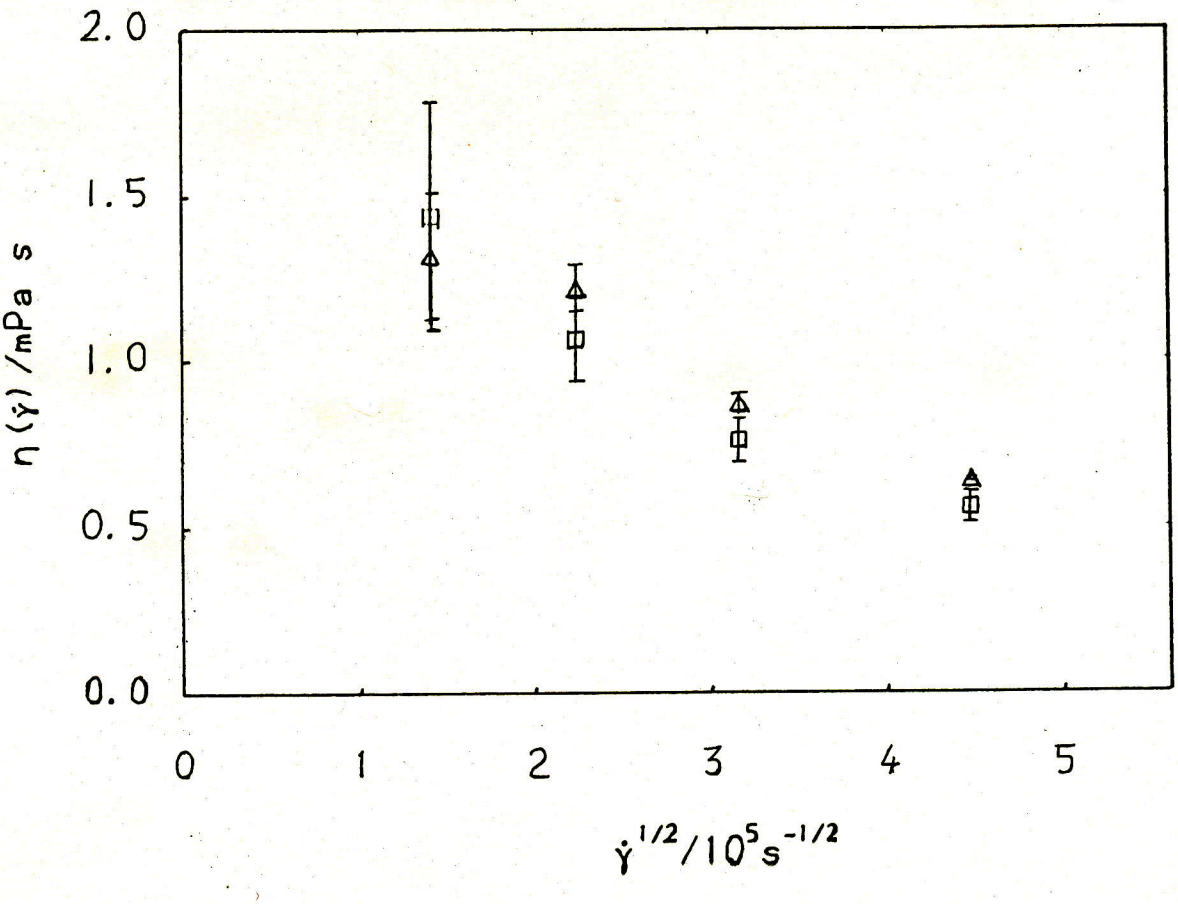

Table 7.4 The best fit parameters and root mean square differences (RMSD) for the predictions of the shear rate dependence of the viscosity from the theories of Hess, Ree-Eyring(RE) and Kawasaki-Gunton(KG) , (see sec.3.5), for the $\eta(\dot{\gamma})$ vs. $\dot{\gamma}$ data for hexane at T~300K. The best fit curves are also plotted in fig.7.3.

RE	$\eta(0)$/mPa s	1.41
	τ_e /ps	26.0
	RMSD/mPa s	0.037
Hess	$\eta(0)$/mPa s	1.38
	τ_h /ps	11.1
	k	0.632
	RMSD/mPa s	0.030
KG	$\eta(0)$/mPa s	1.68
	A /10^{-5} mPa s$^{1/2}$	0.236
	RMSD/mPa s	0.049

The ability of the various functional forms to predict the behaviour of the viscosity follows a similar pattern that has been observed before at the lower temperature for hexane and flexane and for the other systems studied. The Hess, RE and KG predictions give reasonable fits but the KG square root law shows a slight tendency to systematically deviate from the data points. From the estimates of $\eta(0)$ given in table 7.4 the zero shear rate viscosity for hexane at 300K is quoted as 1.5 ± 0.2 mPa s. This compares with the value quoted for flexane at 200K of 1.7 ± 0.3 mPa s. So if anything hexane is slightly less viscous at 300K than flexane at 200K. From the relevant constants τ_e, τ_h, k and A in tables 7.4 and 6.5 and figure 7.2

Figure 7.3 $\eta(\dot{\gamma})$ vs. $\dot{\gamma}^{1/2}$, hexane T~300K (Δ). Fits to the predictions of the theories of Hess (——), Ree-Eyring (- - -) and Kawasaki-Gunton (—·—·—).

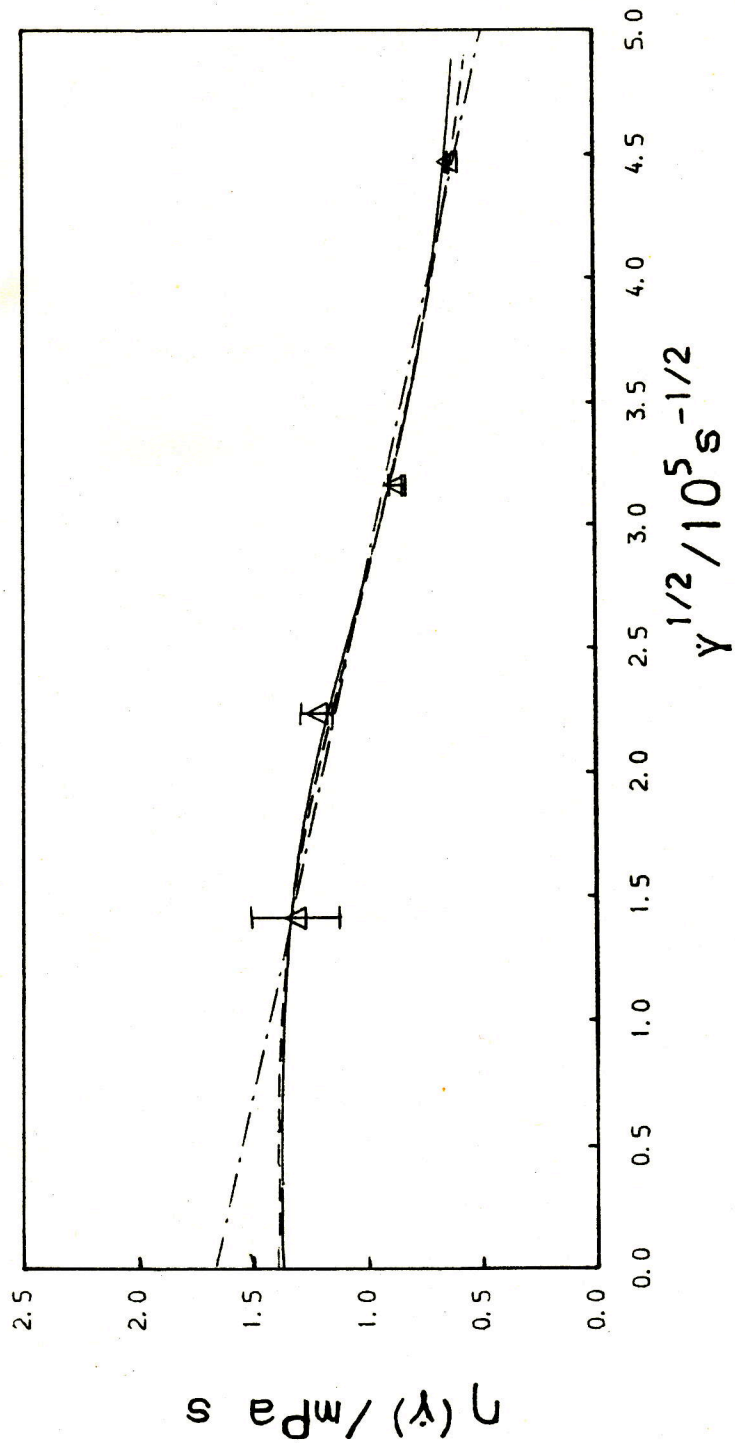

it can also be seen that hexane at 300K shear thins to a lesser extent than flexane at 200K. How this behaviour contrasts with that of flexane at 300K is difficult to say on the strength of the results at just one shear rate. However, as this point is at the lower end of the scale of shear rates used, which from the hexane results is likely to show more variation with temperature, and does not show much change from the result at 200K it would be reasonable to assume that hexane at 300K and flexane at 200K and 300K all showed very similar $n(\dot{\gamma})$ behaviour.

7.5 Shear Induced Alignment

As with the viscosity the significant components of the alignment tensor , given in table 7.3, show a shear dependence more akin to that of flexane at 200K than hexane at 200K (table 6.4). This is also the case with the values of the extinction angle, given in table 7.5, derived from the components of $\underline{\underline{D}}$ and shown in fig.7.4 with those for hexane and flexane at 200K.

Figure 7.4 The extinction angle $\theta_e(\dot{\gamma})$ vs. $\dot{\gamma}^{1/2}$, hexane T~300K (□), hexane T~200K (Δ) and flexane T~200K (∇).

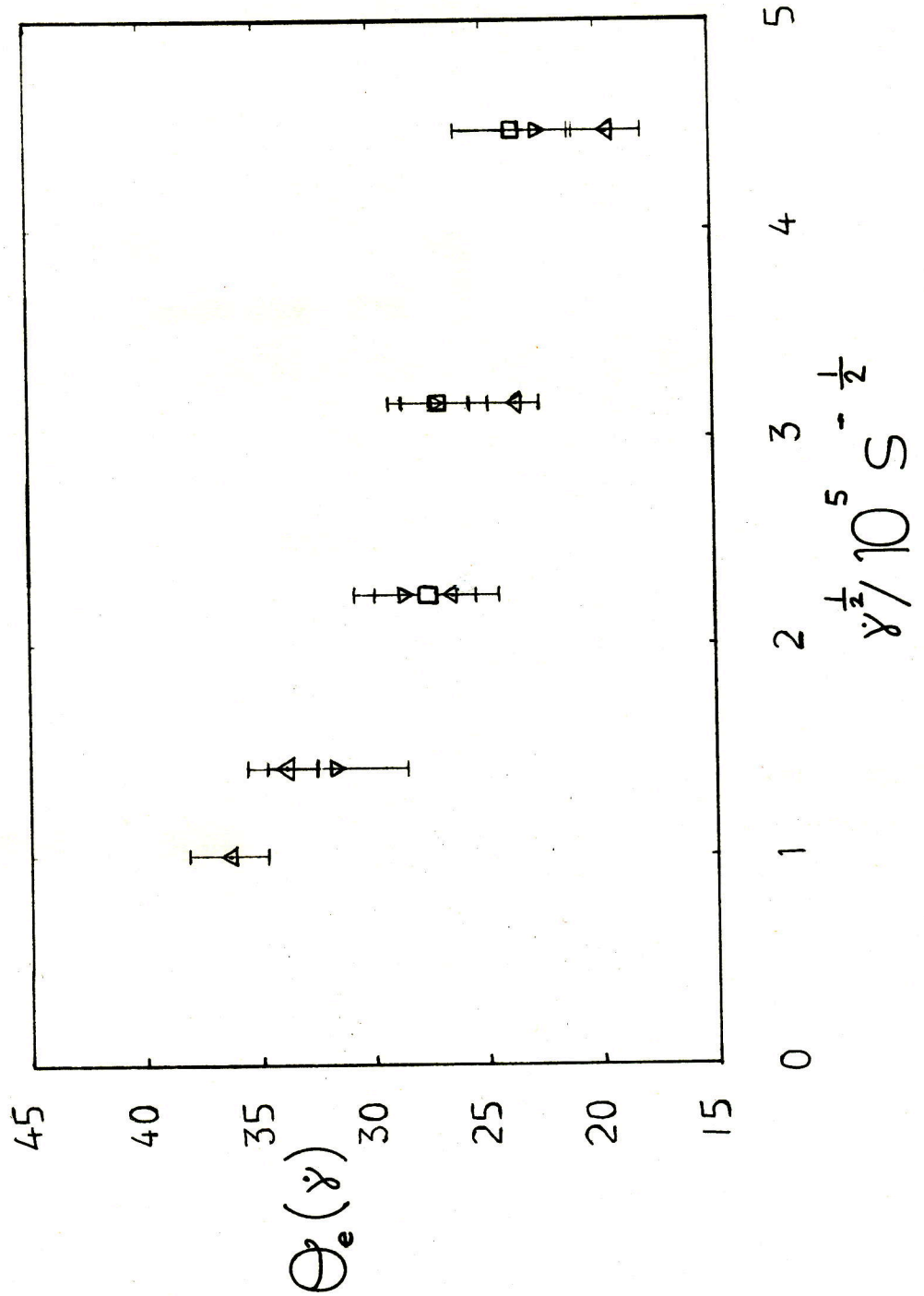

Table 7.5 The extinction angle obtained from the steady state shear calculations on hexane and flexane at T~300K.

	Hexane	Flexane
$\dot{\gamma}/10^{10}s^{-1}$	θ_e/deg	θ_e/deg
5	27.6±3.2	36.8±4.5
10	27.0±2.2	-
20	23.7±2.5	-

At the lowest shear rate studied at 300K the imprecision in the results for $\underline{\underline{D}}$ made θ_e indeterminate. For flexane at 300K and $\dot{\gamma}=5*10^{10}s^{-1}$ D_{xz} has , within error, the same value as flexane at 200K and hexane at 300K but the on diagonal components are less affected by the higher temperature and consequently the extinction angle is significantly higher in comparison.

7.6 Non-equilibrium thermodynamics

At the lower temperature the functions $\Delta U(\dot{\gamma})$, $\Delta\Phi(\dot{\gamma})$, $\Delta\Phi_\alpha(\dot{\gamma})$ and $\Delta P(\dot{\gamma})$ were calculated to show the effect of the shear flow upon the energy and the pressure of the system. As it is of interest to see the effect of temperature on these important rheological properties the same functions have been calculated from the data obtained at 300K and these are given in table 7.6.

Table 7.6 The functions $\Delta U(\dot{\gamma})$, $\Delta\Phi(\dot{\gamma})$, $\Delta\Phi_\alpha(\dot{\gamma})$ and $\Delta P(\dot{\gamma})$ obtained from the steady state shear calculations on hexane and flexane at T~300K. (* indicates calculated for comparison only.)

Hexane

$\dot{\gamma}/10^{10}s^{-1}$	$\Delta U(\dot{\gamma})/Jmol^{-1}$	$\Delta\Phi(\dot{\gamma})/Jmol^{-1}$	$\Delta\Phi_\alpha(\dot{\gamma})/Jmol^{-1}$	$\Delta P(\dot{\gamma})$/bar
2	50±240	30±100	20±170	40±40
5	-30±260	120±110	-150±180	150±50
10	-40±230	320±110	-360±130	330±50
20	10±260	900±120	-900±150	810±50

Flexane

$\dot{\gamma}/10^{10}s^{-1}$	$\Delta U(\dot{\gamma})/Jmol^{-1}$	$\Delta\Phi(\dot{\gamma})/Jmol^{-1}$	$\Delta\Phi_\alpha(\dot{\gamma})/Jmol^{-1}$	$\Delta P(\dot{\gamma})$/bar
5	-10±100	-10±100	-380±510	40±60

For hexane $\Delta U(\dot{\gamma})$ shows no systematic trend as the increase in the LJ potential energy is balanced by the decrease in the dihedral angle energy. The magnitude of the energy and pressure changes are decreased at this higher temperature so that they closely resemble those found in flexane at 200K.

In figs.7.5 and 7.6 the logarithm of $\Delta\Phi(\dot{\gamma})$ and $\Delta P(\dot{\gamma})$ are plotted against the log. of the shear rate. The data points fit well to straight lines and the adjustable parameters resulting from fits to the forms given in eqns.3.8.3 and 6.5.3 are shown in table 7.7.

Figure 7.5 $Log_{10}\Delta\Phi(\dot{\gamma})$ vs. $log_{10}\dot{\gamma}$, hexane, T~300K.

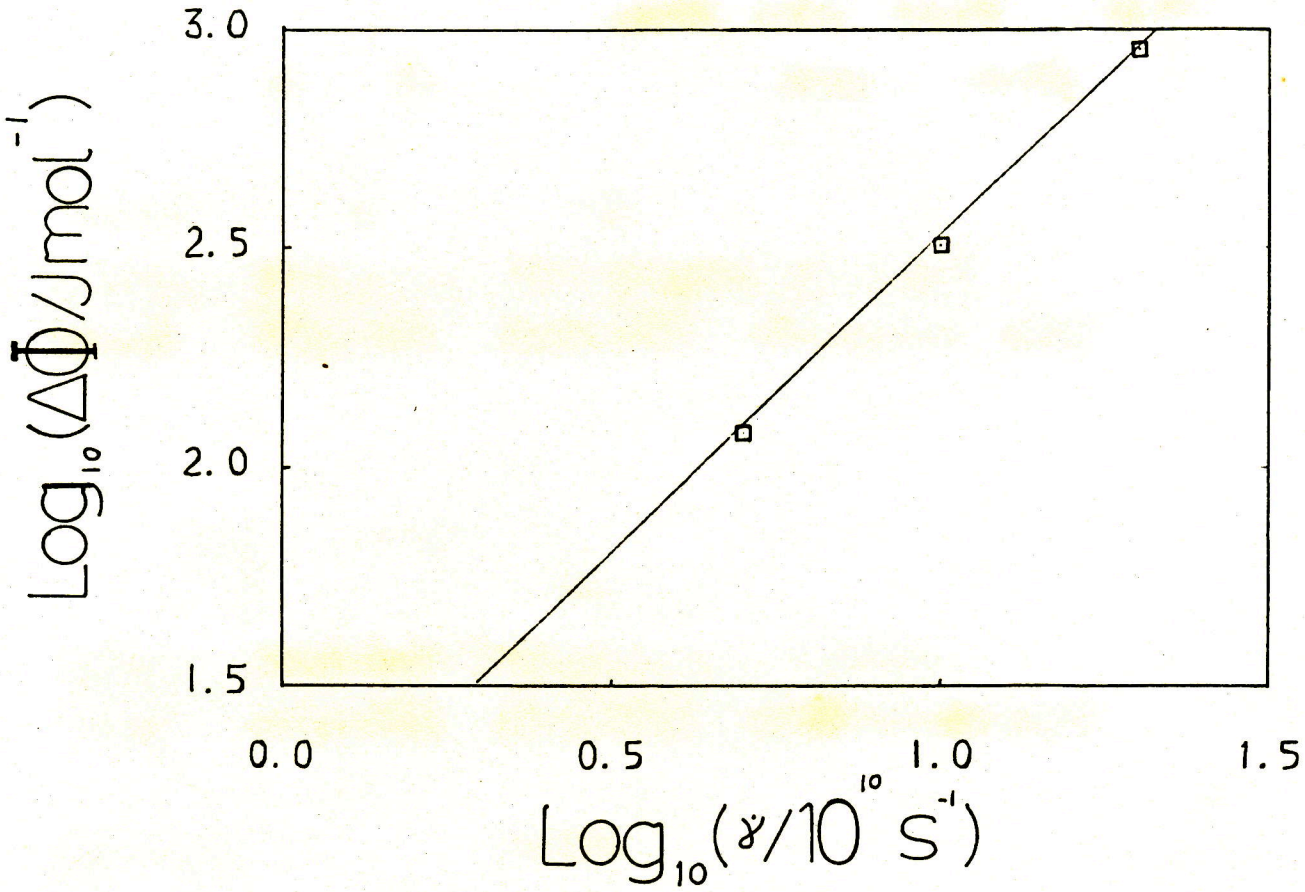

Figure 7.6 $Log_{10}\Delta P(\dot{\gamma})$ vs. $log_{10}\dot{\gamma}$, hexane, T~300K.

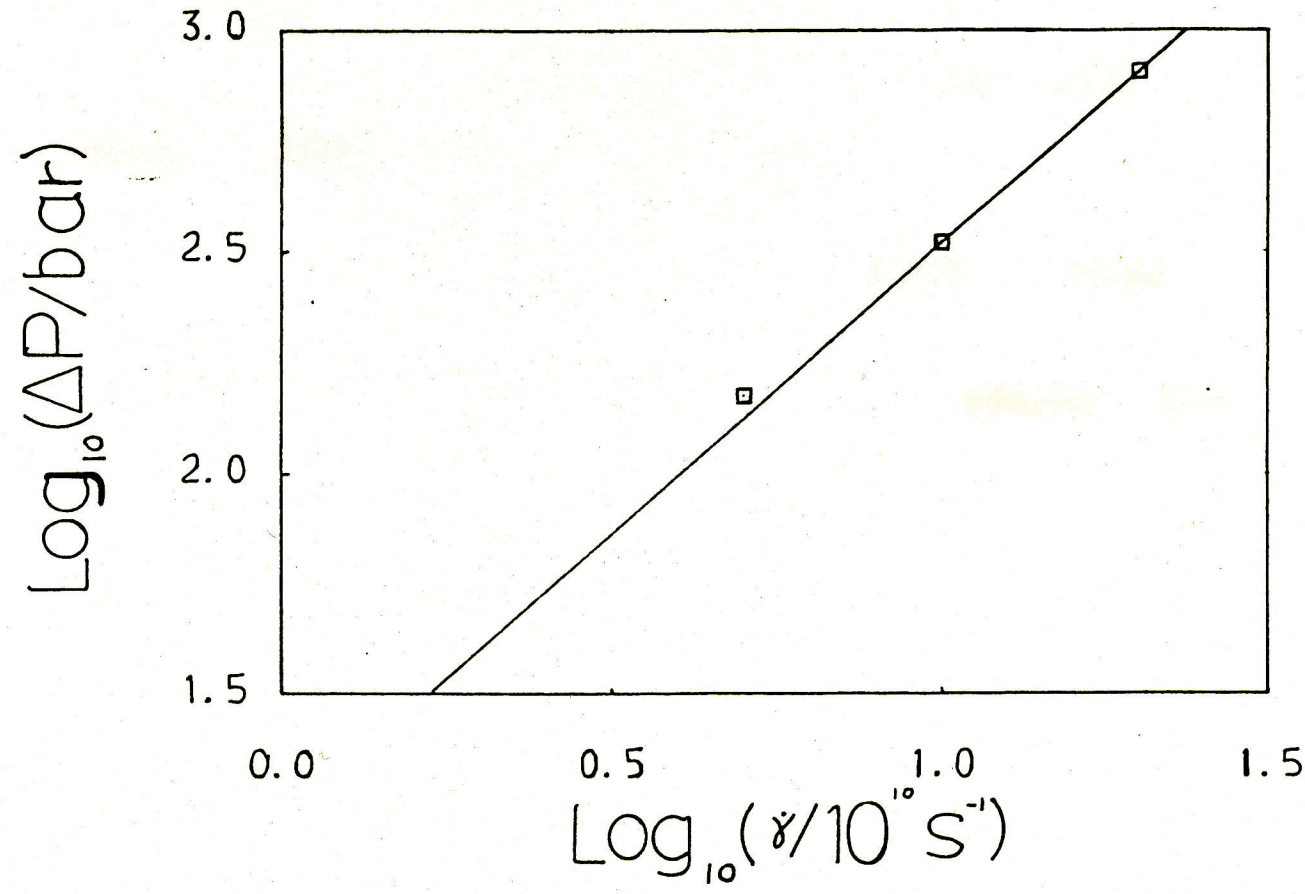

Table 7.7 The slopes (a and c) and proportionality constants (P_1 and Φ_1) for the fits of $\Delta\Phi(\dot{\gamma})$ and $\Delta P(\dot{\gamma})$ to the forms given in eqns. 3.8.3 and 6.5.3 from the steady state calculations on hexane at T~300K.

	P_1/bar	a	Φ_1/J mol^{-1}	c
Hexane	16	1.31	12	1.45

A comparison with same parameters derived from the results at 200K (table 6.8) reveals that a has increased from 0.56 to 1.31 and c has increased from 0.72 to 1.45 which is an approximate doubling of these exponents. However, the substantial decreases in the constants P_1 and Φ_1 from 224 to 16 and from 165 to 12, respectively, offsets the increases in the exponents.

These results show that the effect of shear on the energy and pressure is particularly sensitive to the temperature. As the pressure and energy are themselves more a function of density rather than temperature it is likely that the parameters given in table 7.7 will also show even larger variations with density.

The resolution of the pressure increases into the three orthogonal directions by use of the functions $\{ \Delta P_{\alpha\alpha}(\dot{\gamma}) \}$, defined in eqn.6.5.4, is shown in table 7.8

Table 7.8 The functions $\Delta P_{\alpha\alpha}(\dot{\gamma})$, as defined in eqn.6.5.4, from the steady state shear calculations on hexane and flexane at T~300K.

Hexane

$\dot{\gamma}/10^{10}s^{-1}$	$\Delta P_{xx}(\dot{\gamma})$/bar	$\Delta P_{yy}(\dot{\gamma})$/bar	$\Delta P_{zz}(\dot{\gamma})$/bar
2	10±40	0±60	-10±70
5	-130±90	-70±80	200±80
10	-300±90	-30±70	320±60
20	-580±90	-30±110	610±100

Flexane

$\dot{\gamma}/10^{10}s^{-1}$	$\Delta P_{xx}(\dot{\gamma})$/bar	$\Delta P_{yy}(\dot{\gamma})$/bar	$\Delta P_{zz}(\dot{\gamma})$/bar
5	-120±110	80±110	40±140

The trends in the $\Delta P_{\alpha\alpha}(\dot{\gamma})$'s at 300K are the same as at 200K with only a small decrease in their magnitudes. This is interesting as the actual change in $P(\dot{\gamma})$ is noticeably less at the higher temperature. So although the shear dilatancy is certainly effected by the temperature increase it appears that the normal pressure differences are relatively insensitive to this change in the conditions. The indication from this is that these two effects are more independent of each other than might be expected since they both arise from changes induced in the structure of the fluid by the shear.

7.7 Shear Induced Intermolecular Structural Changes

At 200K the changes in the intermolecular energy and the pressure were related to the distortion of certain distribution functions under shear. As the pressure and energy are affected in a similar way at the higher temperature it is reasonable to suppose that the distribution functions will also behave similarly. To check this the functions g(r), G(R), $G(\alpha)$ and $P_1(R)$, as defined previously, have been calculated.

In figs.7.7 and 7.8 the radial distribution functions for sites, g(r), and COM, G(R), are shown at a shear rate of $\dot{\gamma}=2*10^{10}s^{-1}$ along with the same function at equilibrium. Comparison with figs.6.14 and 6.15 for the same function at 200K reveal a very similar trend with g(r) showing only small changes whereas G(R) shows a general sharpening of the first and second peaks and their movement to lower values of R.

For the directional functions, $G(\alpha)$, shown in fig.7.9 at the highest shear rate, the rather poor statistics of these functions makes detailed comparison difficult but it can be seen that they are much the same as those obtained at 200K, fig.6.16. This is consistent with the similarity in the $\Delta P_{\alpha\alpha}$ at the two temperatures.

The function $P_1(R)$ is shown in fig.7.10 at the highest

Figure 7.7 g(r) vs. r, hexane,
$\dot{\gamma}=2*10^{11}s^{-1}$ (——) and $\dot{\gamma}=0$ (—·—), T~300K.

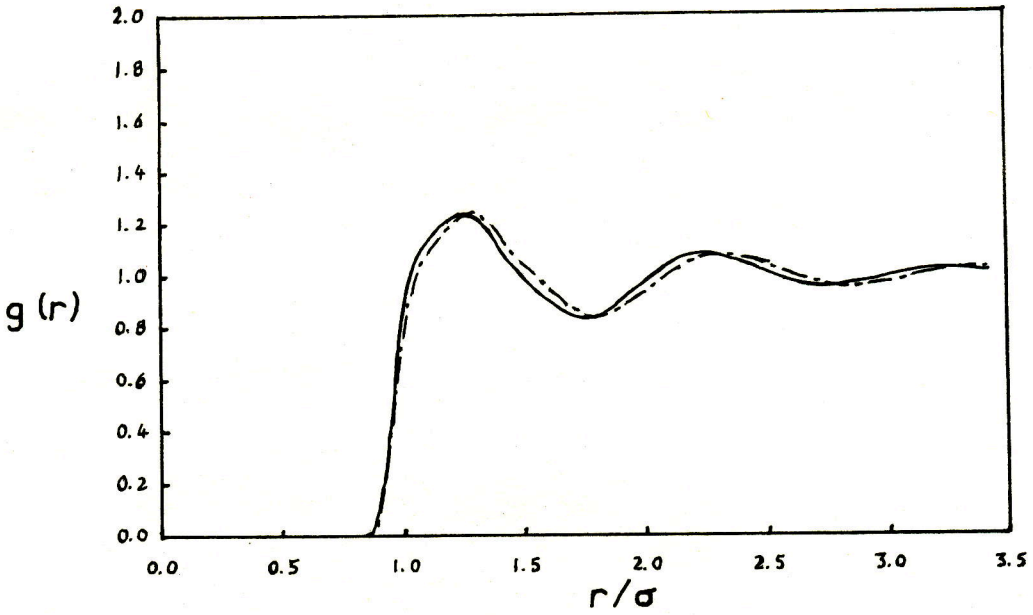

Figure 7.8 G(R) vs. R, hexane,
$\dot{\gamma}=2*10^{11}s^{-1}$ (——) and $\dot{\gamma}=0$ (—·—), T~300K.

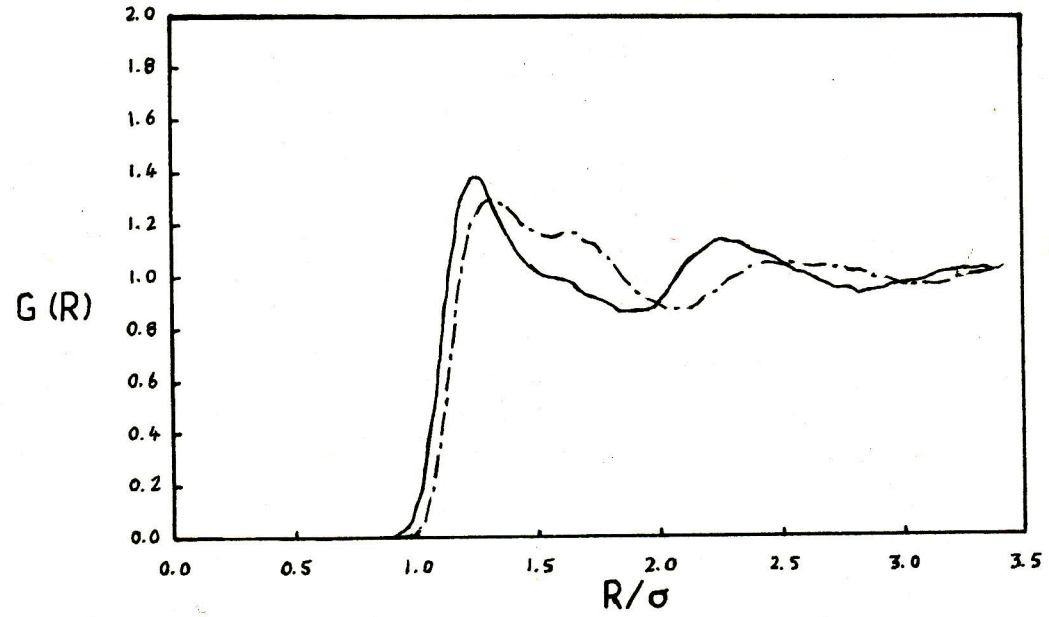

Figure 7.9 The directional distribution functions for the separations of the COM in the three orthogonal directions G(α) vs. α, for α=X (——), α=Y (—·—) and α=Z (– –), hexane $\dot{\gamma}=2*10^{11}s^{-1}$, T~300K.

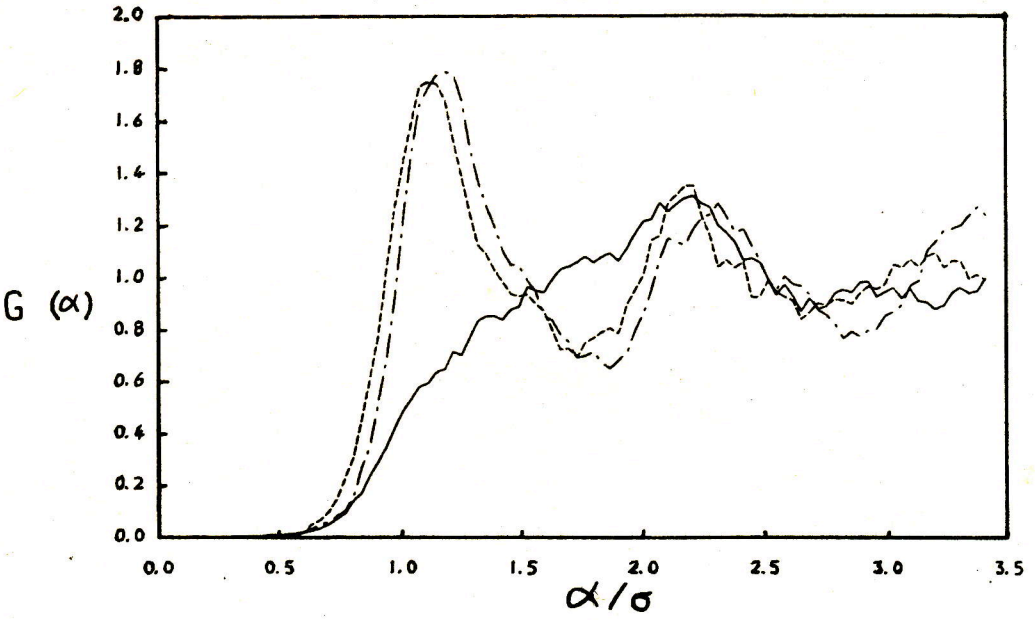

Figure 7.10 $P_1(R)$ vs. R, hexane, $\dot{\gamma}=2*10^{11}s^{-1}$ (——) and $\dot{\gamma}=0$ (—·—), T~300K.

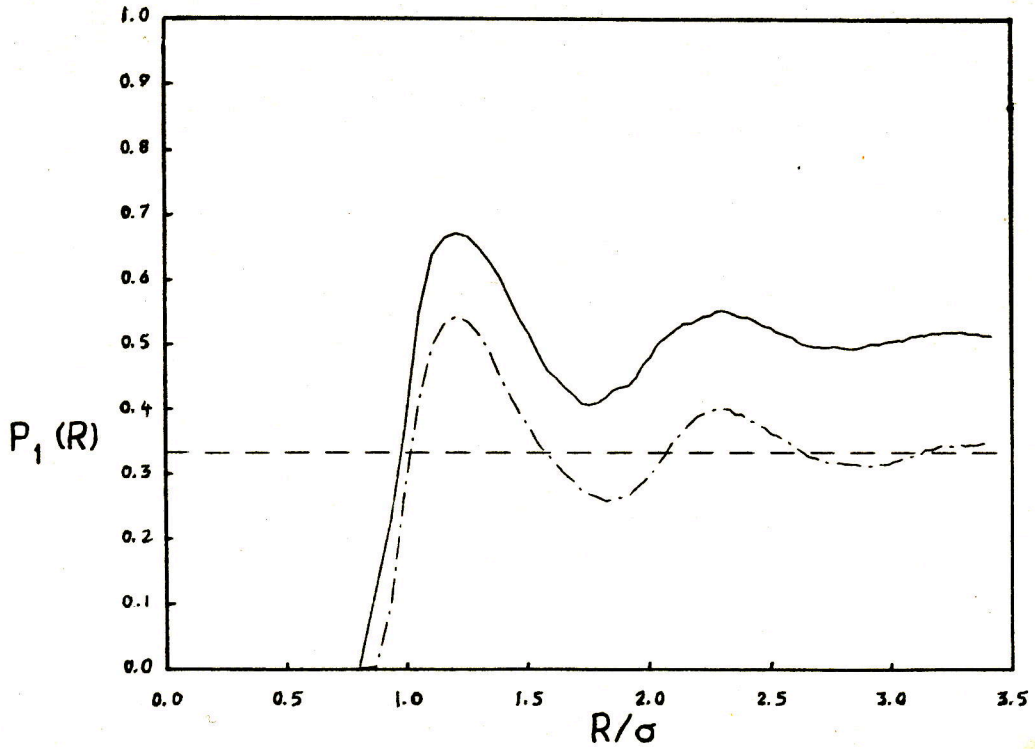

shear rate and at equilibrium. At the higher temperature the alignment tensor is not as affected by shear (table 7.3) and this is shown by a smaller increase in $P_1(\bar{R})$ compared to that at 200K, fig.6.18.

7.8 Shear Induced Intramolecular Structural Changes

At the lower temperature it was found that hexane was extended more than flexane by the shear flow. A rationale was given for this but there was some slight doubt in the results due to the general paucity of transitions in hexane. Indeed, one of the reasons for performing these calculations at a higher temperature was to check this particular result. The decrease in dihedral angle energy with increasing shear rate, noted in table 7.6, is already an indication that similar changes are taking place as at the lower temperature. To compare these further the mean intramolecular separation of sites, $d_{\alpha\beta}(\dot{\gamma})$, and the root mean square radii of gyration of sites, $s_\alpha(\dot{\gamma})$, have again been calculated and are shown in tables 7.9 and 7.10.

Table 7.9 The shear rate dependent mean intramolecular separation of sites, $d_{\alpha\beta}(\dot{\gamma})$, as defined in eqns.6.7.1→6.7.3, from the steady state calculations on hexane and flexane at T≈300K.

Hexane

$\dot{\gamma}/10^{10}s^{-1}$	$d_{14}(\dot{\gamma})$/Å	$d_{15}(\dot{\gamma})$/Å	$d_{16}(\dot{\gamma})$/Å
0	3.565±0.009	4.589±0.014	5.557±0.021
2	3.562±0.010	4.590±0.010	5.559±0.022
5	3.593±0.011	4.633±0.012	5.629±0.039
10	3.592±0.004	4.635±0.005	5.631±0.012
20	3.629±0.007	4.692±0.009	5.706±0.024

Flexane

$\dot{\gamma}/10^{10}s^{-1}$	$d_{14}(\dot{\gamma})$/Å	$d_{15}(\dot{\gamma})$/Å	$d_{16}(\dot{\gamma})$/Å
0	3.386±0.010	4.389±0.007	5.174±0.013
5	3.398±0.009	4.403±0.010	5.203±0.016

Table 7.10 The shear rate dependent root mean square radii of gyration, $s_\alpha(\dot{\gamma})$ as defined in eqns.6.7.4→6.7.6, from the equilibrium and steady state shear calculations on hexane and flexane at T~300K.

Hexane

$\dot{\gamma}/10^{10}s^{-1}$	$s_1(\dot{\gamma})$/Å	$s_2(\dot{\gamma})$/Å	$s_3(\dot{\gamma})$/Å
0	2.854±0.015	1.841±0.009	0.927±0.014
2	2.854±0.010	1.846±0.005	0.921±0.008
5	2.884±0.021	1.854±0.005	0.910±0.008
10	2.884±0.010	1.857±0.008	0.906±0.014
20	2.918±0.014	1.874±0.004	0.885±0.011

Flexane

$\dot{\gamma}/10^{10}s^{-1}$	$s_1(\dot{\gamma})$/Å	$s_2(\dot{\gamma})$/Å	$s_3(\dot{\gamma})$/Å
0	2.683±0.007	1.837±0.005	0.943±0.007
5	2.695±0.008	1.837±0.006	0.941±0.008

The equilibrium mean separations at 300K are less than those at 200K (see table 6.10) for both hexane and flexane. This is in agreement with the higher dihedral angle energies at 300K which indicate more gauche angles and hence shorter intersite distances. The $d_{\alpha\beta}$'s increase uniformly with the shear rate as at the lower temperature but not to the same extent.

The root mean square radii of gyration at equilibrium are smaller at the higher temperature for sites 1 and 2 but are greater for site 3, that closest to the COM. This is also

consistent with the existence of more gauche conformers at the higher temperature for the reasons given in sec.6.7. Under shear the tendency is for the molecules to become more linear and this results in the trends seen in the $s_\alpha(\dot{\gamma})$'s where s_1 and s_2 increase and s_3 decreases with increasing $\dot{\gamma}$.

To compare the magnitude of the increase in d_{16} with that at 200K the function $\Delta d_{16}(\dot{\gamma})$, eqn.6.7.7, has again been calculated and is given in table 7.11.

Table 7.11 The function $\Delta d_{16}(\dot{\gamma})$, as defined in eqn.6.7.7, from the steady state shear calculations on hexane and flexane at T~300K.

	Hexane	Flexane
$\dot{\gamma}/10^{10}s^{-1}$	$\Delta d_{16}(\dot{\gamma})$	$\Delta d_{16}(\dot{\gamma})$
2	0.04±0.54	-
5	1.30±0.80	0.56±0.40
10	1.33±0.43	-
20	2.68±0.57	-

For hexane there is a noticeable decrease in the amount of extension of the molecules compared to that found at 200K, table 6.12. Indeed, there is less extension in hexane at 300K than in flexane at 200K.

More detailed information concerning the change in the intramolecular structure is given by the distribution of

r_{16}'s, $\rho(r_{16})$, and dihedral angles, $\rho(\alpha)$. These functions are shown at a shear rate of $2*10^{11}s^{-1}$ and at equilibrium in figs.7.11 and 7.12.

The function $\rho(r_{16})$ clearly demonstrates the tendency for the molecules to become more linear under shear by the sharp rise in the peak at ~6.3Å corresponding to the TTT conformer. In contrast to the results at 200K the reduction in the numbers of conformers containing gauche angles is more even at 300K. At the lower temperatures the number of all trans conformers increased largely at the expense of the TTG conformers whilst the numbers of TGT molecules remained largely constant. At the higher temperature, although the situation is not entirely reversed, there is certainly a greater reduction in the peak at ~5.8Å, corresponding to the TGT conformer, than in the peak at ~5.2Å, corresponding to the TTG conformer.

The change in $\rho(\alpha)$ on shearing, fig.7.12, also shows the increased probability of trans states under shear. Compared to the changes at 200K, fig.6.22, there appears less of a reduction in the number of gauche angles. To quantify this further the percentages of dihedral angles and conformers are given in table 7.12 for hexane and also for flexane.

Figure 7.11 The probability density for the end-to-end separation $\rho(r_{16})$ vs. r_{16}, hexane, $\dot{\gamma}=2*10^{11}s^{-1}$ (——) and $\dot{\gamma}=0$ (—·—), T~300K.

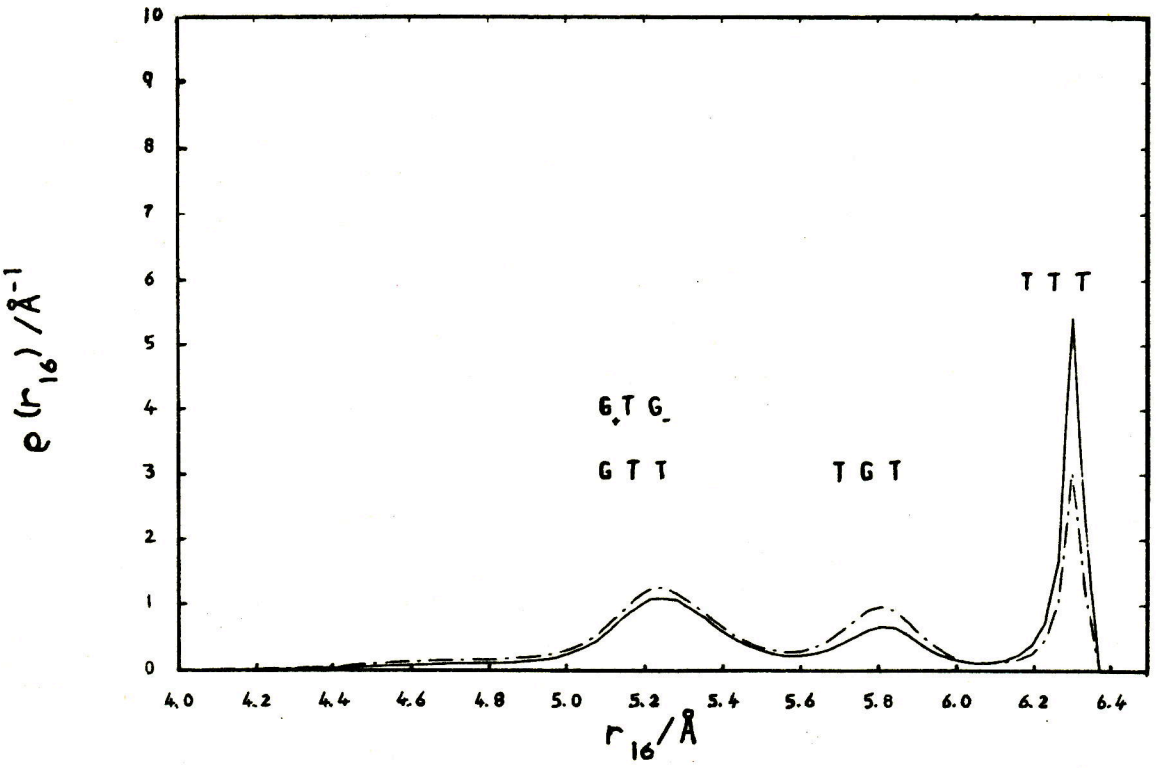

Figure 7.12 The probability density for the dihedral angle $\rho(\alpha)$ vs. α, hexane, $\dot{\gamma}=2*10^{11}s^{-1}$ (——) and $\dot{\gamma}=0$ (—·—), T~300K.

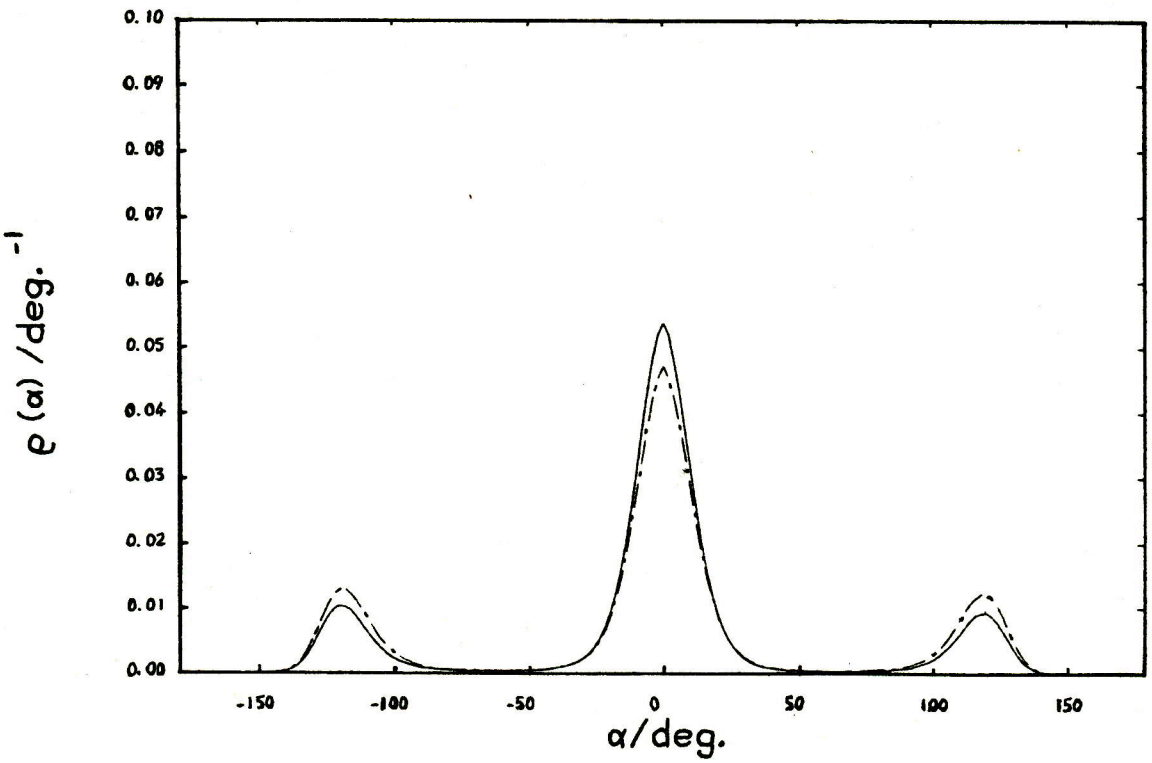

Table 7.12 The mean percentage of dihedral angles and conformers from the equilibrium and steady state shear calculations on hexane and flexane at ~300K.

% of dihedral angles

Hexane

	$\alpha_{1,3}$			α_2		
$\dot{\gamma}/10^{10}s^{-1}$	G_-	T	G_+	G_-	T	G_+
0	16.4±3.5	66.6±6.3	17.0±4.8	17.2±1.7	69.8±2.7	13.0±2.7
2	18.5±4.9	66.1±6.4	15.5±5.4	14.6±2.4	72.7±3.0	12.7±2.3
5	17.4±5.2	66.1±7.2	16.6±4.0	12.8±4.0	76.4±4.0	10.8±1.7
10	16.5±3.3	69.4±4.6	14.2±4.5	12.0±2.8	76.0±1.7	11.9±2.1
20	15.0±4.0	72.1±5.6	13.0±4.5	9.0±2.4	81.0±1.9	10.0±2.1

Flexane

	$\alpha_{1,3}$			α_2		
$\dot{\gamma}/10^{10}s^{-1}$	G_-	T	G_+	G_-	T	G_+
0	30.0±1.5	38.7±1.5	31.5±2.8	16.4±1.8	67.7±1.5	15.8±0.4
5	29.7±2.4	41.1±2.6	29.2±2.3	16.8±0.9	67.1±1.3	16.2±1.3

% of conformers

Hexane

$\dot{\gamma}/10^{10}s^{-1}$	TTT	TTG	TGT	TGG	TG_+G_-	GTG	G_+TG_-	GGG	Others
Ø	21.Ø	35.6	25.5	4.3	Ø.Ø	6.4	6.7	Ø.4	Ø.Ø
	±2.5	±2.6	±3.6	±1.9	±Ø.Ø	±2.1	±2.8	±Ø.6	±Ø.Ø
2	23.7	35.2	22.7	4.Ø	Ø.Ø	5.6	8.1	Ø.6	Ø.Ø
	±4.Ø	±3.9	±2.8	±2.Ø	±Ø.1	±1.7	±3.2	±Ø.7	±Ø.Ø
5	27.1	36.Ø	18.8	4.2	Ø.Ø	6.Ø	7.2	Ø.6	Ø.Ø
	±5.4	±5.4	±3.8	±2.3	±Ø.Ø	±2.4	±1.6	±Ø.6	±Ø.1
1Ø	29.8	34.3	21.2	2.4	Ø.Ø	4.8	7.1	Ø.3	Ø.Ø
	±2.7	±2.2	±1.9	±1.3	±Ø.2	±2.3	±2.Ø	±Ø.6	±Ø.Ø
2Ø	36.9	34.9	16.6	2.1	Ø.Ø	3.8	5.3	Ø.2	Ø.Ø
	±5.7	±5.Ø	±1.4	±1.3	±Ø.Ø	±1.3	±1.9	±Ø.4	±Ø.Ø

Flexane

$\dot{\gamma}/10^{10}s^{-1}$	TTT	TTG	TGT	TGG	TG_+G_-	GTG	G_+TG_-	GGG	Others
Ø	5.9	26.5	12.4	12.8	1.5	17.6	17.7	4.8	Ø.9
	±Ø.4	±Ø.4	±1.2	±Ø.3	±Ø.2	±Ø.8	±Ø.8	±Ø.1	±Ø.Ø
5	6.5	28.8	13.2	12.4	1.2	15.6	16.3	4.7	1.2
	±Ø.8	±1.1	±1.Ø	±Ø.7	±Ø.2	±Ø.8	±1.3	±Ø.6	±Ø.2

The figures for the percentage of conformers bear out the observations already made about $\rho(r_{is})$, fig.7.11. The approximately 15% increase in the proportion of all trans molecules on going from equilibrium to steady state shear is largely at the cost of the TGT conformers whilst the proportion of TTG molecules remains relatively constant. The rest of the difference being made up by small changes in the numbers of the less popular conformers.

7.9 Conclusions

From the results at 300K the effect of temperature on the rheological properties of these flexible molecules has been clearly demonstrated. For flexane it is reasonable to assume that even though non-equilibrium calculations were performed at one shear rate there are only small differences in the shear dependence of the viscosity , alignment, energy and pressure etc. between the two temperatures. Confirming the supposition that the density is the most important parameter in fluids composed of molecules without barriers to internal rotation. In hexane, of course, there are barriers to internal rotation which largely determine the intramolecular structure and dynamics of the molecules. As the effective height of these barriers is temperature dependent it follows that these intramolecular properties are also. What is apparent from the hexane results is that there is also a very important secondary intermolecular effect which changes the bulk rheological properties drastically. There clearly is then some interest then in establishing which properties of these fluids differ in their response to an increased temperature as it is likely that these properties are generally important in determining the rheological behaviour of fluids.

7.10 Static Properties : 200K vs. 300K

For the static intermolecular functions, such as the intermolecular potential energy and the pressure, the similarity in the changes for hexane and flexane on going from 200K to 300K have already been noted in sec.7.3. These can be related to changes in the distribution functions g(r), G(R) and $P_1(R)$ shown in figs.7.13→7.15 where the functions at 300K are compared with the results at 200K. For flexane there are only very slight changes in all the functions. The site-site r.d.f., g(r), shows the greater penetration of the repulsive core which leads to higher pressures and energies and the characteristic trend of a reduction in the order of the system, lower peaks and higher troughs in g(r), expected at elevated temperatures. G(R) and $P_1(R)$, with their poorer statistics, are virtually the same within error. For hexane it can be seen that the general trend is as it is in flexanefor g(r). G(R) and $P_1(R)$ for hexane do show some changes , however, with a loss in the distinct splitting of the first peak seen in the G(R) for hexane at 200K. This results from a reduction of the degree of alignment between molecules in this region shown very clearly in the first peak of $P_1(R)$.

The one static property that noticeably changes on increasing the temperature is the dihedral angle energy in hexane (see tables 5.1 and 7.1). This can be seen to result

Figure 7.13 g(r) vs. r, hexane (1) and flexane (2), $\dot{\gamma}$=0 T~300K (——), T~200K (—·—).

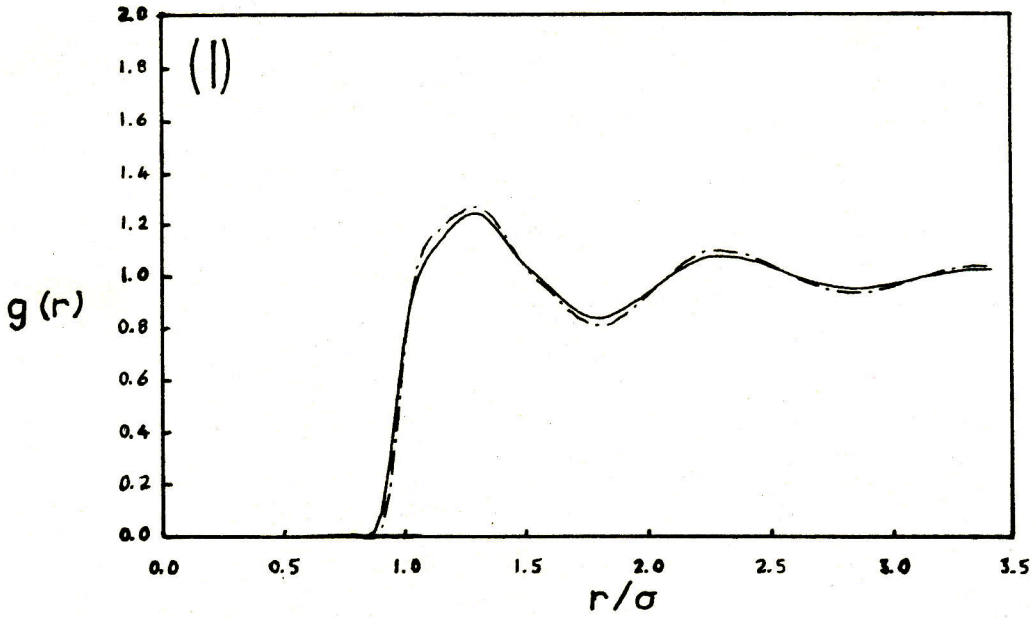

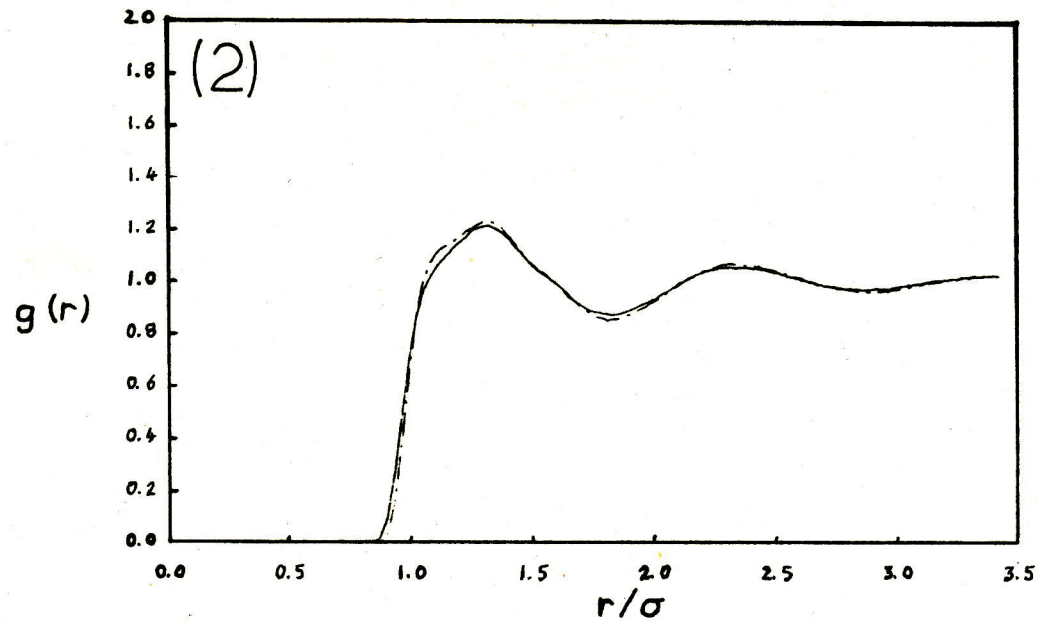

Figure 7.14 G(R) vs. R, hexane (1) and flexane (2), $\dot{\gamma}$=0 T~300K (——), T~200K (—·—).

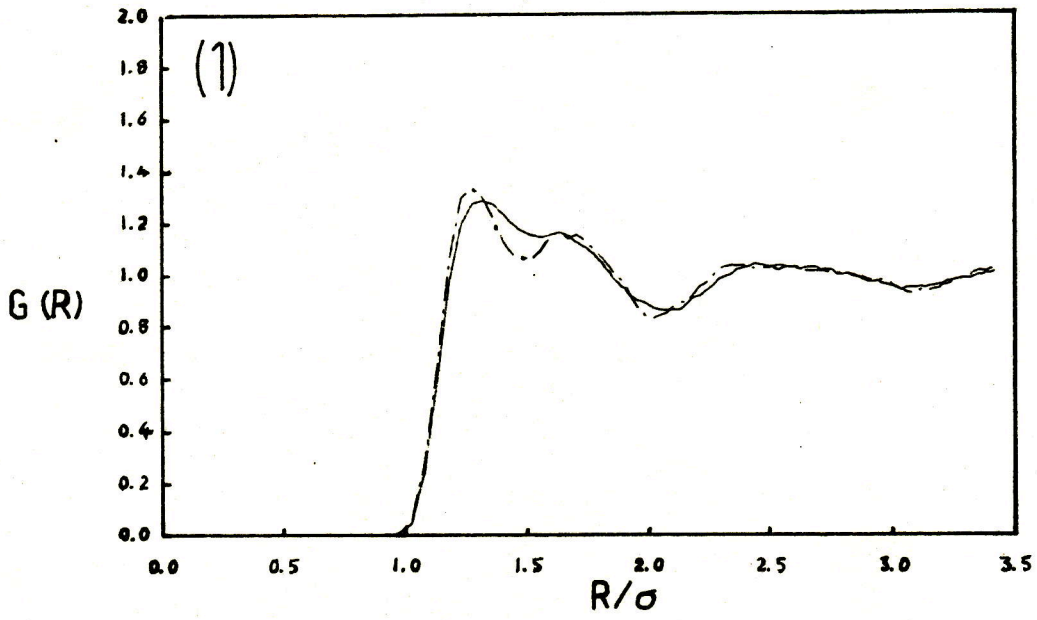

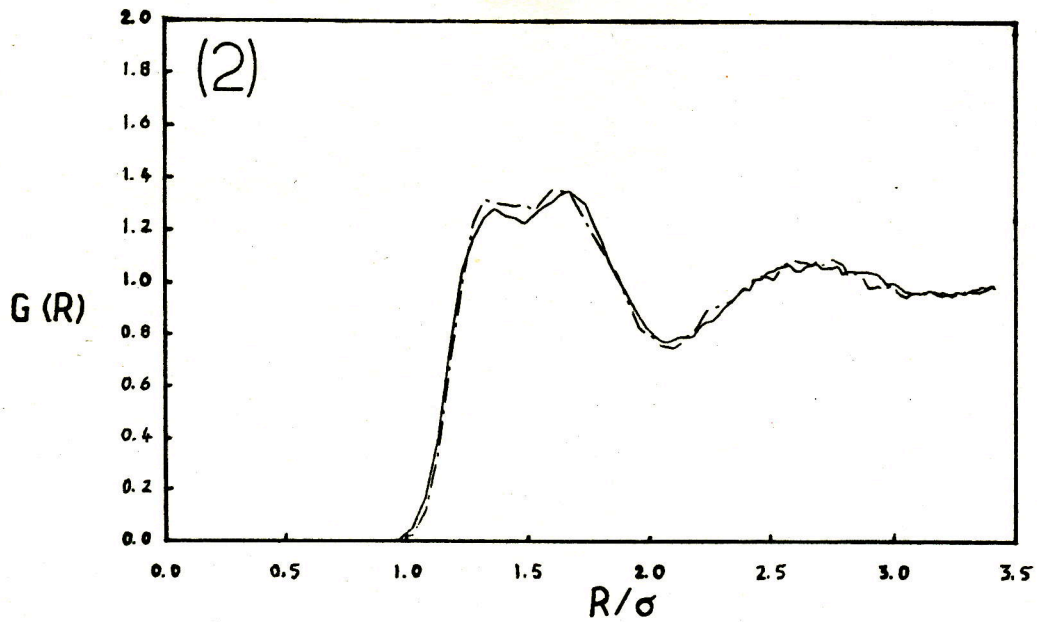

Figure 7.15 $P_1(R)$ vs. R, hexane (1) and flexane (2), $\dot{\gamma}$=0 T~300K (——), T~200K (—·—).

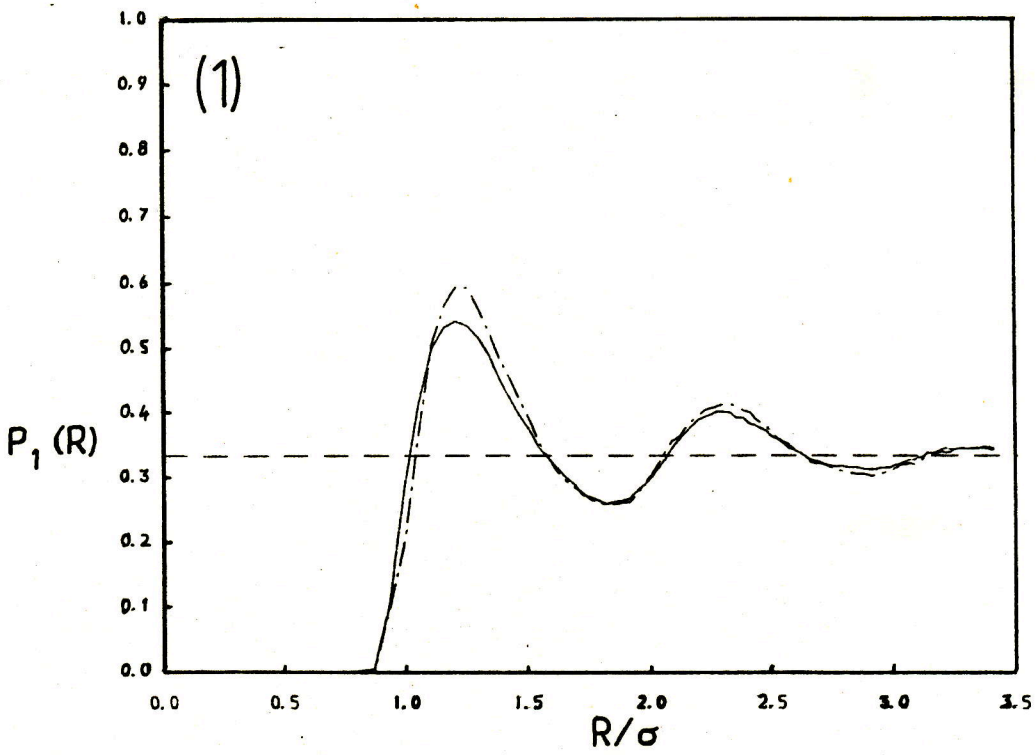

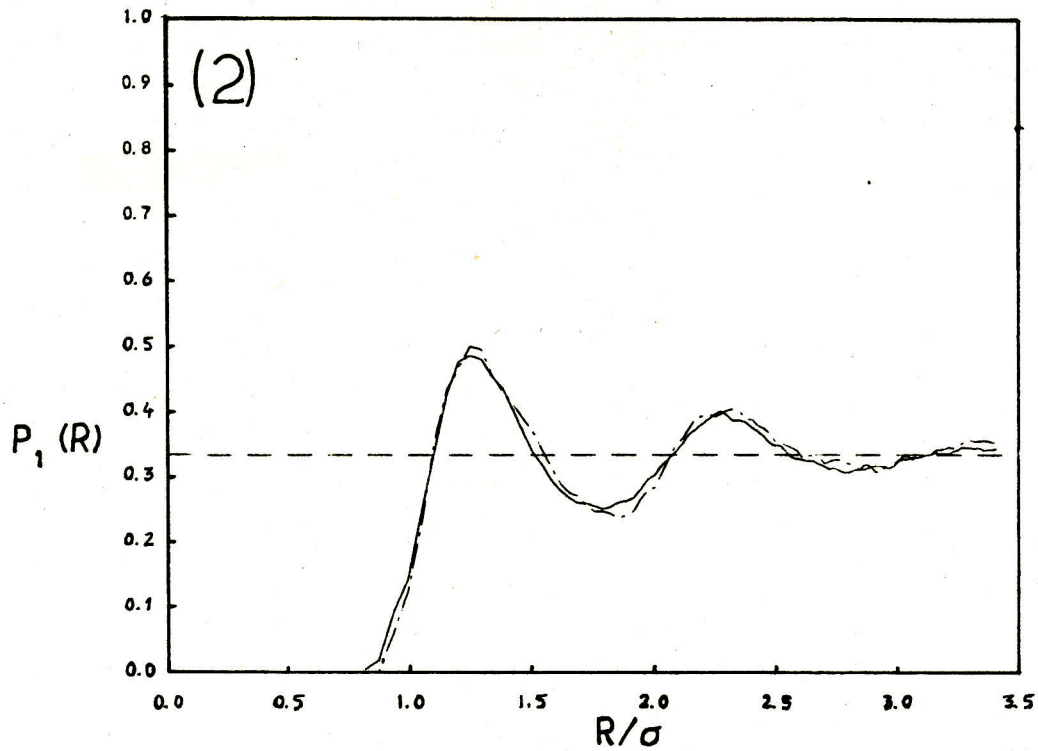

from a different distribution of dihedral angles as shown in fig.7.16. The higher temperature smoothes out the distribution reducing the height of all three peaks corresponding to the minima in the potential , $\alpha=0^{\circ}$ and $\alpha=\pm 120^{\circ}$. The net effect, however, is to reduce the number of angles in the trans state, if one uses the criteria previously described in sec.5.7, by around 6% (see tables 5.2 and 7.12). There is also a similar effect in the distribution of the end-to-end separations, fig.7.17. The actual percentages of the various conformers has already been given in tables 5.2 and 7.12. These show that the change in the TTT peak of $\rho(r_{16})$ corresponds to an approximately 11% decrease in the number of all trans conformers. The resulting increase in the numbers of gauche containing conformers is spread evenly over the available possibilities.

The functions $\rho(\alpha)$ and $\rho(r_{16})$ for flexane at the two temperatures, given in figs.7.16 and 7.17, show little difference even on the expanded scale used. This is also apparent from the percentages of conformers and dihedral angles given in tables 5.2 and 7.12.

From the initial comparisons of static properties it emerges that although the behaviour of the intramolecular structure of these two molecules as a function of temperature differs quite markedly there intermolecular structures are affected to almost the same degree giving similar changes in

Figure 7.16 $\rho(\alpha)$ vs. α, hexane (1) and flexane (2), $\dot{\gamma}=0$ T~300K (——), T~200K (—·—).

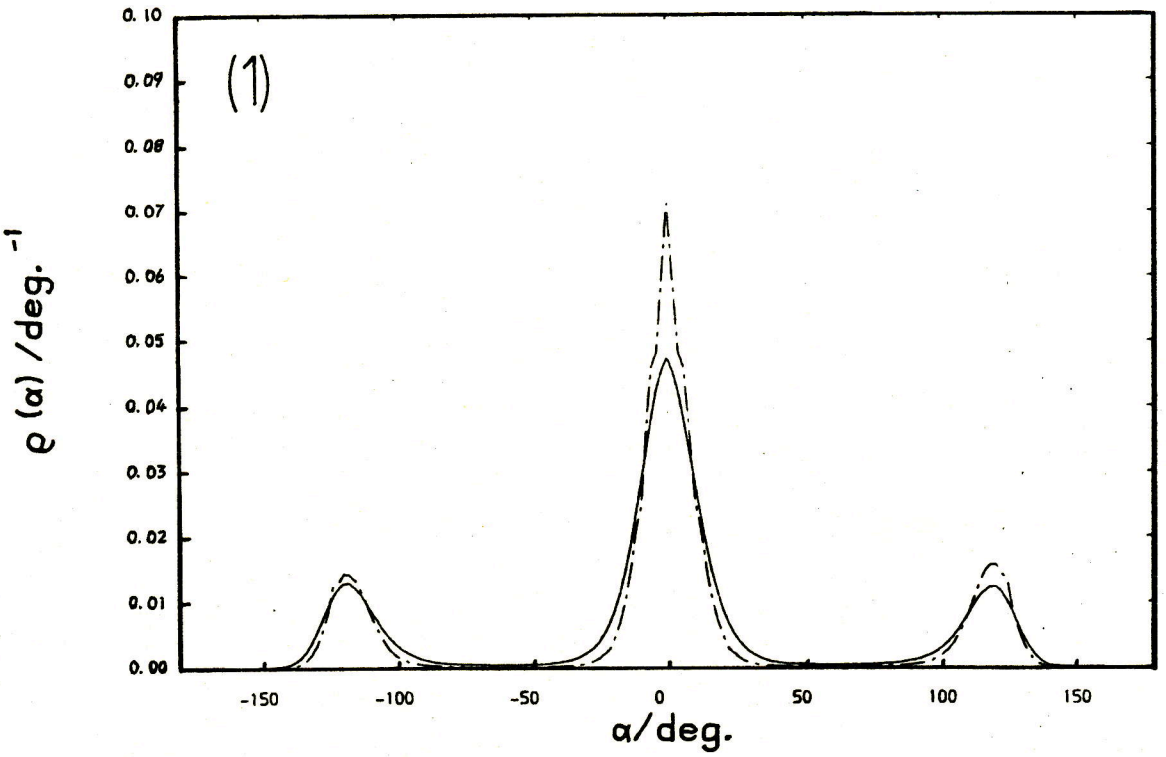

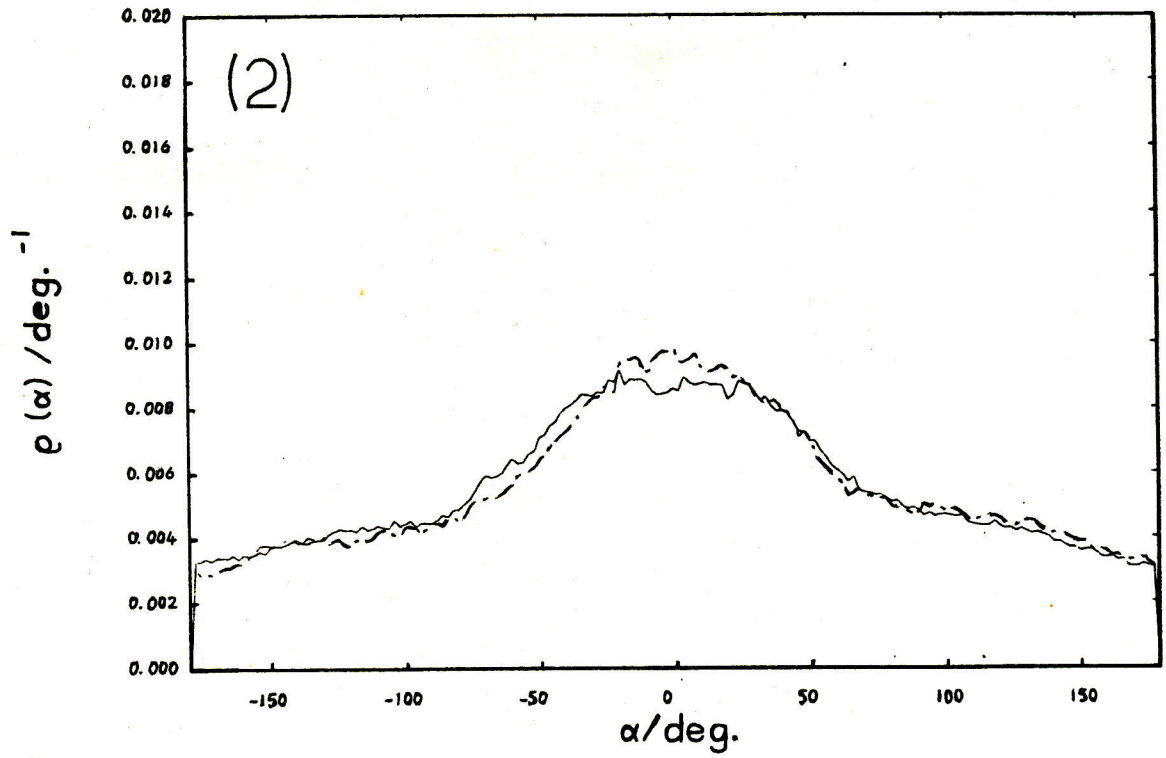

Figure 7.17 $\rho(r_{16})$ vs. r_{16}, hexane (1) and flexane (2), $\dot{\gamma}$=0 T~300K (——), T~200K (—·—).

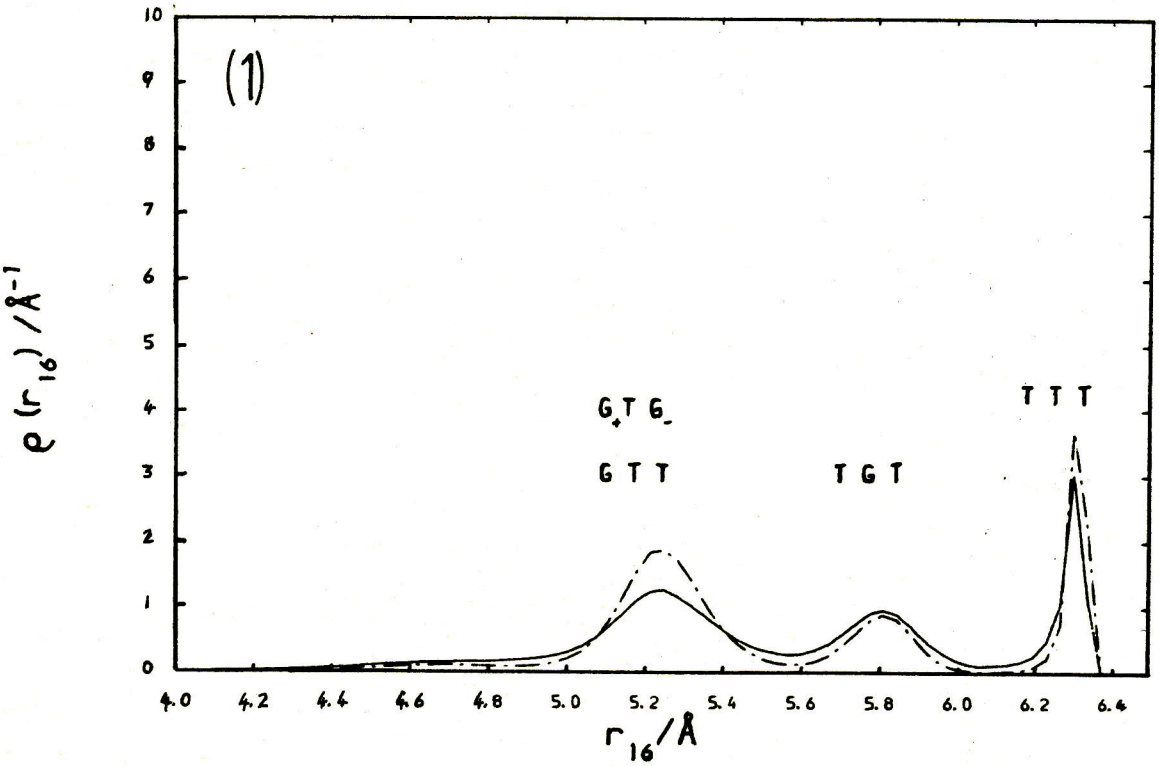

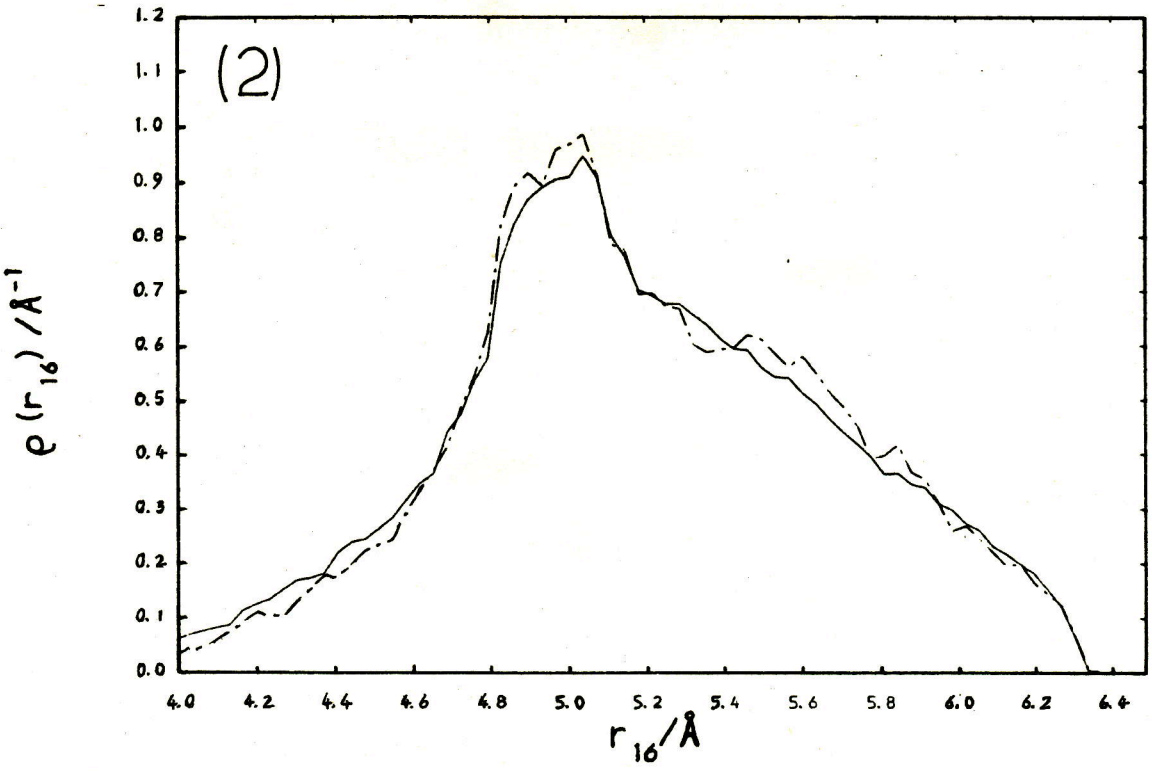

the intermolecular potential energy and the pressure. The results for flexane suggest that this change in intermolecular structure would not be enough to explain the changes in the rheological properties of hexane. It is also reasonable to assume that as the rheological properties are collective in nature the actual static intermolecular structure is in itself not an important factor. Thus, it is not possible to explain the behaviour of hexane in terms of a direct effect of the temperature upon its internal structure or through the secondary effect this has on the intermolecular structure. This leads to the conclusion that the effects seen in hexane are more a result of changes in its dynamical properties.

7.11 Dynamical Properties : 200K vs. 300K

At the lower temperature the relaxation times for the internal modes in hexane were found to be in excess of 100ps when they were determined by fitting the dihedral angle auto-correlation function, $C_\alpha(t)=\langle\alpha_i(0)\alpha_i(t)\rangle$, to the form of a single exponential,

$$\hat{C}_\alpha(t) = \exp(-t/\tau) \quad .$$

For flexane τ was found to be in the region of 0.3→0.5ps (see sec.5.8). At the higher temperature $C_\alpha(t)$ has again been calculated and fits to a single exponential have been performed. These are shown in fig.7.18 for hexane and flexane. As can be seen $C_\alpha(t)$ for hexane fits well to a single exponential form with a τ of ~17ps. The fit for

Figure 7.18 The normalised correlation function for the dihedral angle $\hat{C}_\alpha(t)$ vs. t, hexane (1) and flexane (2) with fits to single exponential, $\hat{C}_\alpha(t)=\exp(-t/\tau)$, (- - -) (1) τ=17ps, (2) τ=0.32ps.

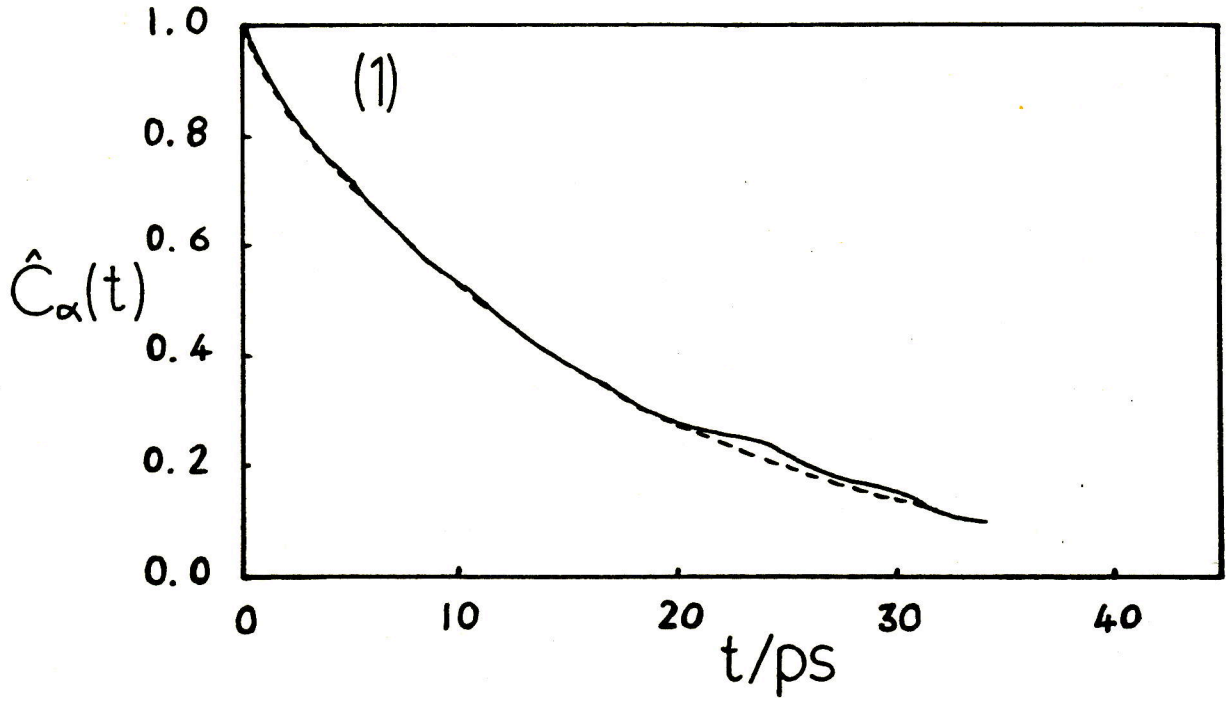

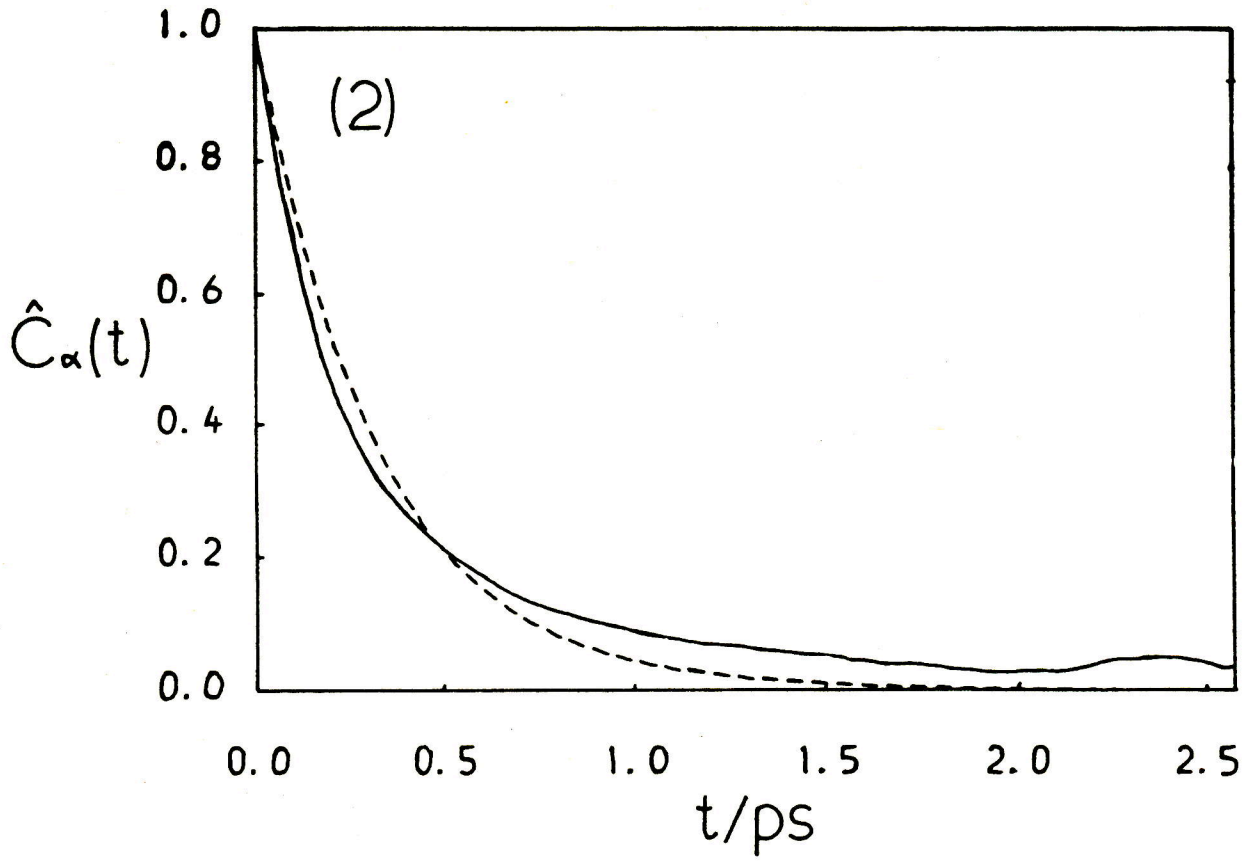

flexane is less satisfactory and it appears that there are two exponential decays present as at 200K where the correlation function for the central angle was found to have a longer relaxation time than that for the outer angles. Nevertheless, the value of τ used for the fit, 0.32ps, is virtually the same as at 200K. This is a significant result as it clearly demonstrates a major difference in the effect of temperature on the two fluids. Whereas in hexane the relaxation times for internal modes are reduced by at least a factor of six by a temperature increase of 100K the same change has virtually no effect on flexane.

To emphasise this point the mean time between transitions, τ_m, has again been calculated from the numbers of transitions in a certain time according to eqn.5.8.1. This is as described in sec.5.8 except that 300K the the number of transitions in hexane was calculated from each 500th configuration rather than every configuration. This means that there are likely to be fewer 'transitions' counted than there would have been using the original definition as an angle going from one well to another and back again within 500 steps may not be counted at all. Despite this slight inconsistency the mean transition times obtained of ~28ps and ~0.53ps for hexane and flexane respectively compared to those obtained at 200K, ~110ps and ~0.7ps, show the same effect as the dihedral angle correlation functions.

At 200K it was found that the diffusive motion was different in the two fluids with flexane having a higher diffusion coefficient and less oscillatory velocity auto-correlation function. This was qualitatively explained as being due to the fact that in flexane its much faster rates of torsional relaxation could couple more to the diffusional motion leading to 'softer' collisions and hence less 'rebound'. It might be expected then that as the increase in temperature affects the torsional relaxation of hexane much more than that of flexane it then follows that the diffusive motion of hexane should be affected more by the temperature than that of flexane. This has been checked by evaluating the velocity auto-correlation functions and the mean squared displacements and hence the diffusion coefficients. The diffusion coefficients obtained from both methods are given in table 7.13.

Table 7.13. The diffusion coefficients for hexane and flexane at 300K obtained from :-

(a) the mean squared displacements and

(b) the integral over the velocity auto correlation function.

	(a) $D/10^{-9} m^2 s^{-1}$	(b) $D/10^{-9} m^2 s^{-1}$
Hexane	0.97+0.08	0.97+0.09
Flexane	1.12+0.06	1.20+0.09

At the lower temperature it was noted that the two

methods of evaluating D gave different answers and this was attributed to truncation of the VACF. At the higher temperature this does not seem to be the case as both methods give the same values for D within the errors quoted. A comparison of the diffusion coefficients obtained using the mean square displacements approach at the two temperatures reveals that D has increased from Ø.35 to Ø.97 $*10^{-9} m^2 s^{-1}$ in hexane and from Ø.53 to 1.12 $*10^{-9} m^2 s^{-1}$ in flexane. These correspond to increases by factors of 2.8 and 2.1 respectively. Which is a significant although not spectacular difference. However, if one instead chooses to look at the short time diffusive behaviour, given by the VACF, then the difference is much more marked as D increases from Ø.49 to Ø.97 $*10^{-9} m^2 s^{-1}$ in hexane and from Ø.96 to only 1.2Ø $*10^{-9} m^2 s^{-1}$ in flexane, increases by factors of 2 and 1.25 respectively. Qualitatively this is explained by the changes in the forms of the VACFs on going from 2ØØK to 3ØØK, fig.7.19. In flexane there is some movement of the oscillations in $C_v(t)$ to shorter times, as might be expected, but only a slight decreases in their depth. In hexane there is a significant reduction in this tendency for the COM velocity to be reversed at later times compared to that at 2ØØK with the result that the short time diffusion is greatly enhanced.

It, thus, appears that there is more of a correlation between the change in the short time behaviour of the VACF and

Figure 7.19 The normalised velocity auto-correlation function $\hat{C}v_{(t)}$ vs. t, hexane (1) and flexane (2), T~300K (——) and T~200K (—·—)

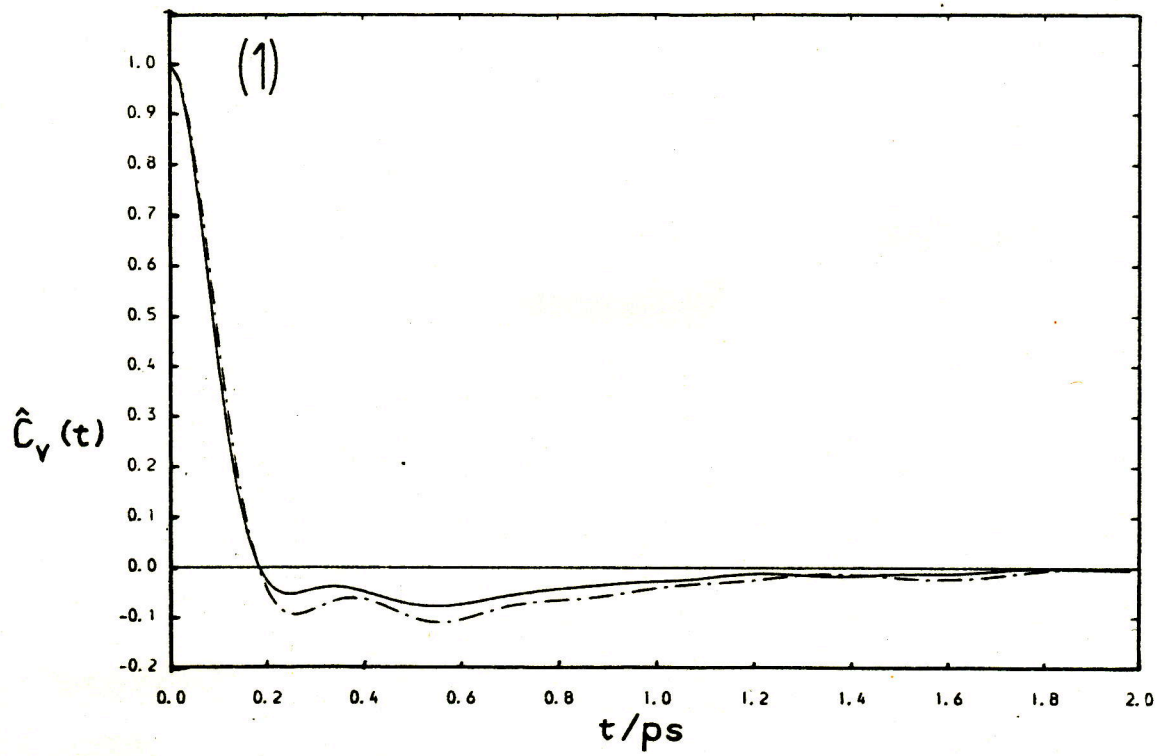

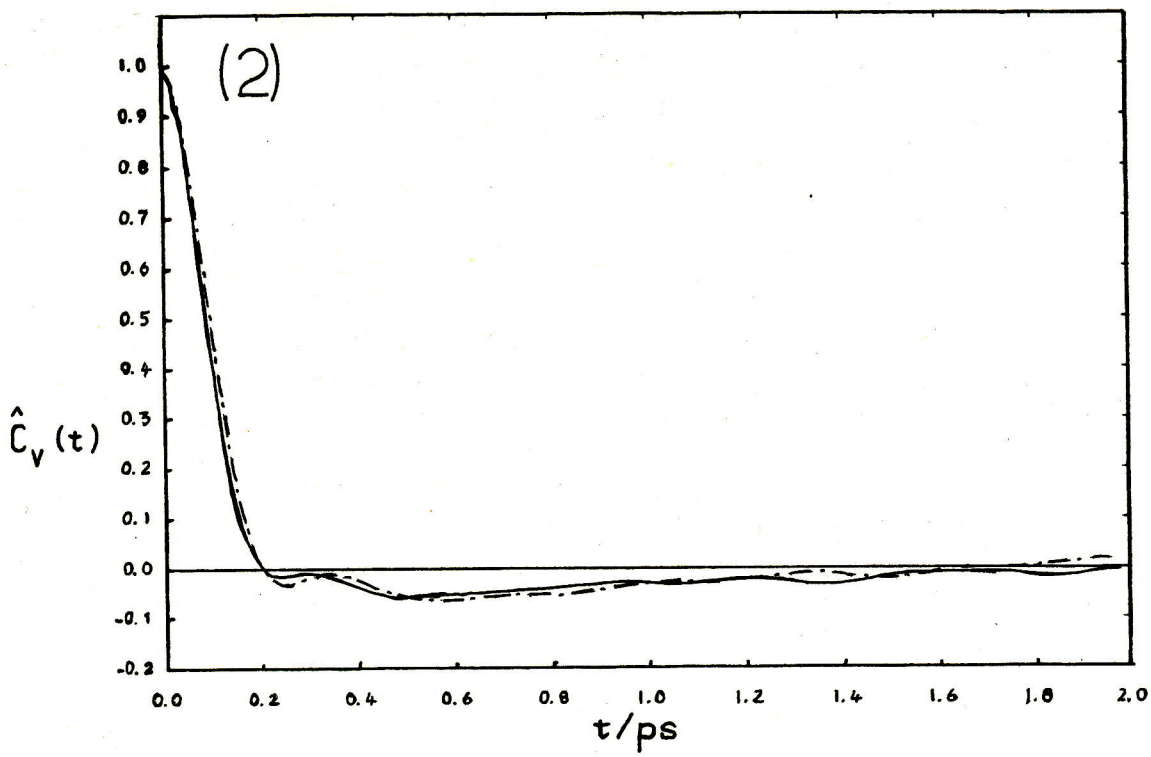

the change in the viscosity than between the diffusion coefficient and the viscosity. The lack of correlation between the viscosity and the diffusion coefficient follows from the flexane results where the increase in temperature doubles the diffusion coefficient but as far as can be ascertained hardly affects the viscosity. This means that it is not possible to explain the decrease in the viscosity of hexane in terms of the effect the internal modes have on the diffusion coefficient a more likely cause is the effect the flexibility has on the short time dynamic behaviour.

7.12 Conclusions

From the results on hexane and flexane a number of important conclusions can be drawn concerning the likely rheological behaviour of real flexible molecules. On a macroscopic scale it has been shown that the effect of the flexibility of a molecule manifests itself most noticeably in the temperature dependence of the viscosity and in the shear thinning and shear dilatant properties. The model systems used here predict that for liquids composed of molecules with differing barrier heights to internal rotation the viscosity, at constant density, will decrease more rapidly as a function of increasing temperature for that fluid containing molecules with the higher barriers. This does not necessarily mean that the temperature coefficient of viscosity will be higher as this coefficient relates the dependence of the viscosity upon

the temperature at constant pressure. The degree to which this correlation exists between the temperature coefficients will depend largely on the comparative expansivities of the two fluids. In the model calculations their would probably be a very good correlation as the fluids were designed to be as closely comparable as possible. Indeed, it was certainly found that the pressure versus temperature behaviour, at constant density , was much the same in the two fluids so it is reasonable to expect it to be also the case for the density versus temperature behaviour at constant pressure.

For fluids undergoing shear flow these model studies predict that the degree of shear thinning and shear dilatancy will be dependent upon the molecular flexibility. It has been found that less flexible molecules will shear thin to a larger extent and show a greater tendency to adjust their volume under shear. The magnitude of these effects will also decrease more rapidly with temperature in accordance with the findings for the temperature dependence of the zero shear rate viscosity.

An interesting question arises concerning the comparative mechanisms by which the viscosity falls as a function of temperature and as a function of shear rate. As the temperature is increased it appears that the viscosity decreases because the reduction in the effective barriers to rotation increase the flexibility of the molecules which in

turn alters the short time dynamic behaviour. As a function of the shear rate it is true that the shear flow can cause drastic changes in the conformation of molecules but there is not any noticeable change in the flexibility. This leads to the conclusion that the mechanism causing the shear viscosity to decrease as a function of temperature is not the same as that which causes the shear thinning. Indeed, it seems that the effect of increasing the shear rate is to reduce the importance of those properties which lead to a difference in the zero shear rate viscosity thus explaining the virtual coincidence of the high shear rate viscosity of hexane and flexane at 200K.

CHAPTER 8

GENERAL CONCLUSIONS

8.1 Diatomics

In the diatomic chlorine calculations it has been demonstrated that two molecules, differing only in their anisotropy, have quite different pressure coefficients of the viscosity. The effect is to cause the longer molecule, which is less viscous at low pressures, to become more viscous than its shorter counterpart at pressures of ~1GPa. It was found, however, that this behaviour correlated closely with the compressibilities of the two liquids, that composed of the longer molecule being the more compressible. This is an important result as in real lubrication situations pressure is the applied variable rather than density so fluids are characterised in terms of their pressure coefficients of viscosity and reasons are then sought to explain why these vary. The diatomic results suggest that a better correlation might exist for their density coefficients of viscosity and then the problem reduces to one of explaining differences in their compressibilities. Sufficient data probably exists on real lubricants to test this hypothesis, if it has not been done already.

One interesting question that remains unanswered in the diatomic systems is the degree to which the anisotropy affects

the shear thinning behaviour. If it is purely a density effect then a similar correlation would exist in their, as yet undefined, 'density coefficients of shear thinning' as for the density coefficients of the viscosity. This could be tested using HSNEMD but would require data from several more densities in addition to those studied here to get a clear picture of how the degree of shear thinning varies. It is an important question to answer as it is under the highly directional conditions found at high shear rates that the effect of the 'shape' of a molecule is most likely to manifest itself. If it transpires from these kind of model studies that the anisotropy is an important factor in determining the degree of shear thinning it would have obvious relevance to the design of real lubricant molecules.

8.2 Ethane and Propane

The results for the smaller alkanes principally demonstrate the overriding effect the interaction potential has when one considers the rheological properties in absolute terms. By simply adding an extra site to the diatomic model the resulting triatomic was demonstrably more viscous and showed greater shear thinning and shear dilatancy. It was reasoned that this was largely due to the different effective temperatures of the two liquids rather than the difference in the densities. To put the results in to context further calculations would have to be performed at different

conditions to assess the likely changes caused by geometrical factors.

8.3 Hexane and Flexane

In the hexane and flexane calculations it was possible to come closest to the desired goal of observing the effect of one parameter independently of all others, in this case the flexibility. It was found that although the two fluids differed radically in their intramolecular structure and internal dynamics, thermodynamically they were very similar. This enabled comparisons to be made between the two liquids essentially at the same state point. The results of studies at constant density and at two different temperatures revealed that the barriers to internal rotation exerted a significant influence on the rheological properties of these fluids. At the lower temperature the zero shear rate viscosity, degree of shear thinning and the shear dilatancy were all greater for the molecule with the higher internal barriers to rotation, hexane. The effect of increasing the temperature was found to be to reduce the differences between the two and it was concluded that molecules with higher internal barriers to rotation will have higher temperature coefficients of viscosity provided that their expansivities are comparable.

APPENDIX 1

Link Cells

The method of link cells [129,130] is a technique whereby large samples $N \geq 1000$, of particles interacting through short range forces can be simulated efficiently. The method works by pre-eliminating most of the $N(N-1)/2$ possible pair interactions which fall outside the interaction sphere of a particular particle. This is achieved by subdividing the main MD box into smaller cells to which the particles within them are assigned the number thereof. Particles then only interact with those in their own and neighbouring cells. To be consistent the length of a cell, CL, has to be greater than the cutoff distance of the potential and if L is the length of a side of the box L/CL must be an integer which must not be less than three. In the case used here for the diatomics the positions of the COM, which all lie between ± 1, were used to assign link cell indices. A cubic box was used in all cases of NL^3 cells, so for all sides of the MD cube L=NL*CL. Initially the indices of a particle I, say, are found from

$$IX = (XCOM(I)+1.0)/CL + 1$$

and similarly for IY and IZ. This gives the number of the cell of which I is a member as

$$IC(I) = IX + (IY-1)*NL + (IZ-1)*NL^2$$

which is stored for future reference. To join all such molecules in a certain cell together three arrays are used

LØ(NL,NL,NL), Ll(NL,NL,NL) and LINK(N). Arrays LØ and Ll are used to store the first and last members of cell IX,IY,IZ. Before the initial assignment of particles to cells LØ and Ll are zeroed. The procedure, having found the cell indices, is then to find the last member of the cell, M say, where M=Ll(IX,IY,IZ). If M=Ø, which it will do initially for all cells, then

```
      LØ(IX,IY,IZ)=I
      Ll(IX,IY,IZ)=I
```

otherwise

```
      LINK(M)=I
      Ll(IX,IY,IZ)=I.
```

This procedure performed for all N particles sets up the open chains of particles in each cell. The following procedure is then used to close the chain

```
      M=Ll(IX,IY,IZ)
      LINK(M)=LØ(IX,IY,IZ)
```

To evaluate the forces the conventional MD double loop is replaced by a loop over all cells. Having identified the indices of the subject cell, Il,Jl and Kl say, a list is generated of the indices of the molecules in that cell by

```
      IT=Ø
      I=LØ(Il,Jl,Kl)
      M=I
 9ØØ3 IT=IT+l
      INOM(IT)=I
      I=LINK(I)
      IF(I.NE.M) GOTO 9ØØ3
      ITC=IT
```

and a note is made of their number, ITC. The list, INOM, is then extended in a similar fashion to include all molecules in thirteen of the nearest neighbour cells. Only thirteen of the

possible twenty six are taken as a loop over all cells ensures that all neighbouring cells will eventually be taken together. This procedure generates in INOM a list of IT molecules the first ITC of which are in the subject cell. A simple double loop then performs the business of taking those pairs of molecules, I and J, to be interacted

```
      DO 9008 IK=1,ITC
      I=INOM(IK)
      IK1=IK+1
      :
      :
      DO 9009 JK=IK1,IT
      J=INOM(JK)
      :
      :
```

This method differs from that in [129] in that the 13 nearest neighbour cell indices only have to be generated once for each subject cell instead of once for each molecule in the subject cell.

The rest of the force routine etc. is as it is in a conventional program but as the molecules move they will eventually move out of one cell into another. To test this the number of the cell the molecule I is in now is generated from the indices and compared with IC(I). If it is the same then one passes to the next but if it has changed then its reference has to be erased from the link list of its old cell and included in that of its new cell. This occurs at the end of each time step after the implementation of the usual periodic boundary conditions.

The method is certainly very efficient in terms of store requiring at most two more N-dimensioned arrays than usual plus LØ and Ll each of dimension NL^3 and the list array INOM which will be dependent upon the maximum number of molecules to be found in a total of 14 cells. In terms of CPU time tests have shown [13Ø] that for sample numbers less than ~1ØØØ the link cell method represents a saving over conventional programming. It is slow compared to nearest neighbour table methods, however, but becomes progressively more attractive as the sample number is increased and the neighbour table method runs into memory requirement trouble and the problem that at least one very time consuming conventional double loop has to be performed periodically to update the neighbour list.

APPENDIX 2

Forces from the Dihedral Angle Potential

As the dihedral angle potential, $\Phi(\alpha)$, given in eqn. 5.2.1, is written in terms of the dihedral angle it is necessary to express α in terms of the four positions defining α to obtain the forces on these sites due to it [131]. If these sites are $\underline{r}_1$, $\underline{r}_2$, $\underline{r}_3$ and $\underline{r}_4$ then the force on site i due to the dihedral angle potential, $\underline{f}_i^{\alpha}$, is given by

$$\underline{f}_i^{\alpha} = -\frac{d\Phi(\alpha)}{d\underline{r}_i} = -\frac{d\Phi(\alpha)}{d\cos\alpha}\frac{d\cos\alpha}{d\underline{r}_i} \qquad (A2.1)$$

There is no difficulty in differentiating $\Phi(\alpha)$ with respect to $\cos\alpha$ but to perform the second part of eqn. A2.1 $\cos\alpha$ has to be expressed in terms of the positions of the sites. From fig. A2.1 it can be seen that $\cos\alpha$ is given by the dot product of the two unit vectors $\hat{\underline{m}}$ and $\hat{\underline{n}}$

$$\cos\alpha = \hat{\underline{m}}\cdot\hat{\underline{n}} \qquad (A2.2)$$

Now $\underline{m}$ is given by

$$\underline{m} = \underline{r}_{21} - \hat{\underline{r}}_{32}b_0\cos\beta = \underline{r}_{21} - \underline{r}_{32}\cos\beta \qquad (A2.3)$$

and $\underline{n}$ by

$$\underline{n} = \underline{r}_{43} - \hat{\underline{r}}_{32}b_0\cos\beta = \underline{r}_{43} - \underline{r}_{32}\cos\beta \qquad (A2.4)$$

since in the model used here the bond lengths and the bond

Figure A2.1 The dihedral angle.

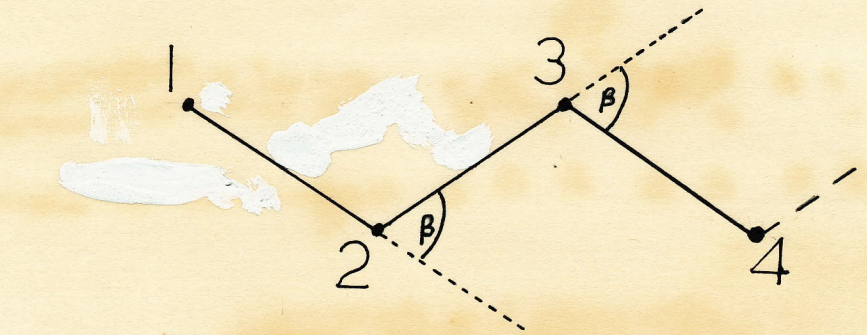

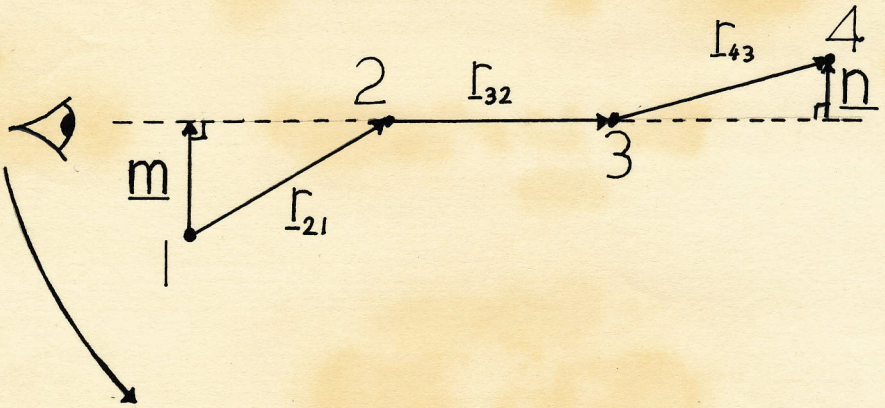

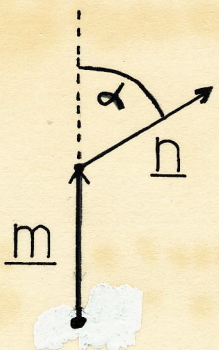

angles are rigidly fixed at the values of $b_o = 1.53\text{Å}$ and $\theta_o = 109^o28' = 180^o - \beta$. Combining eqns. A2.2, A2.3 and A2.4 gives

$$\cos\alpha = (\underline{r}_{21} - \underline{r}_{32}\cos\beta)\cdot(\underline{r}_{43} - \underline{r}_{32}\cos\beta)/b_o^2\sin^2\beta$$

$$= ((\underline{r}_{21}\cdot\underline{r}_{43}) - (\underline{r}_{32}\cdot\underline{r}_{43})\cos\beta - (\underline{r}_{21}\cdot\underline{r}_{32})\cos\beta + \underline{r}_{32}^2\cos^2\beta)/b_o^2\sin^2\beta$$

which as

$$\underline{r}_{32}\cdot\underline{r}_{43} = \underline{r}_{21}\cdot\underline{r}_{32} = b_o^2\cos\beta$$

gives

$$\cos\alpha = (r_{21}\cdot r_{43} - b_o^2\cos^2\beta)/b_o^2\sin^2\beta \quad . \qquad \text{(A2.5)}$$

Differentiating eqn. A2.5 w.r.t $\underline{r}_1$, for example, gives

$$\frac{d\cos\alpha}{d\underline{r}_1} = -\underline{r}_{43}/b_o^2\sin^2\beta$$

and combining with eqn. A2.1 gives for the force on site 1 as

$$\underline{f}_1^{\alpha} = \frac{d\Phi(\alpha)}{d\cos\alpha}\underline{r}_{43}/b_o^2\sin^2\beta$$

and similarly for the other sites.

As their are three dihedral angles per molecule sites that make up more than one angle will feel a force from each. This is simply achieved by treating each angle in turn and summing the resultant forces.

APPENDIX 3

Nearest Neighbour Tables

The method of nearest neighbour tables [102] is the predecessor to the link cell method as a means of reducing the amount of time required to access those pairs which are within each others interaction sphere. In its original form a N*N array is used to store the index of those particles which are within a certain radius, r_m, of the subject particle, I, during the course of evaluating the forces in a normal double loop. For a number of subsequent steps only those particles in the table are considered thus reducing the CPU time substantially. r_m is chosen such that $r_m - r_c$, the truncation radius, is greater than the distance that could be reasonably covered by a particle in the number of steps between updates of the table. Various improvements, refinements etc. have been suggested, e.g. [132,133,134], to try and make the process more efficient and to reduce the active memory requirements. In the method used here for the hexane/flexane program, on the CDC 7600, where for 108 molecules, i.e. 648 atoms, virtually all the small core memory was required, a simple variant of the method of neighbour tables was used requiring virtually no extra active memory space.

This was achieved by including in the conventional double loop the following alterations

```
      N1=N-1
      DO 100 I=1,N1
      XI=X(I)
      :
      :
      ITC=0
      I1=I+1
      DO 200 J=I1,N
      XD=XI-X(J)
      :
      :
      R2=XD**2+YD**2+ZD**2
      IF(R2.GE.RM2) GOTO 200
      ITC=ITC+1
      INUM(ITC)=J
      IF(R2.GE.RC2) GOTO 200
      :
      :
  200 CONTINUE
      WRITE(49)ITC,INUM
      :
      :
  100 CONTINUE
```

$(RM2 = r_m^2)$

$(RC2 = r_c^2)$

The neighbour lists are thus stored sequentially on disc, on channel 49, in machine readable form. In the case used here $r_m = r_c + 1.1\text{Å}$ and the lists were updated every 10 steps. In the alternative loop the procedure was then

```
      REWIND 49
      DO 100 I=1,N1
      XI=X(I)
      :
      READ(49)ITC,INUM
      IF(ITC.EQ.0) GOTO 100
      DO 200 JC=1,ITC
      J=INUM(JC)
      :
```

Despite the overheads incurred in writing to and reading from disc this method still represents a saving, in terms of CPU time, over the conventional MD double loop and although it is not as fast as the usual nearest neighbour method it does not have the store problems thereof requiring only one extra vector of dimension N.

REFERENCES

[1] D.M.Heyes, J.J.Kim, C.J.Montrose and T.A.Litovitz, J.Chem.Phys. 73(1980), 3987.

[2] D.M.Heyes, C.J.Montrose and T.A.Litovitz, J.C.S. Farad. Trans. II 79(1983), 611.

[3] A.W.Crook, Phil.Trans.Roy.Soc.Lond. A250(1958), 387.

[4] A.W.Crook, Phil.Trans.Roy.Soc.Lond. A254(1961, 223.

[5] A.W.Crook, Phil.Trans.Roy.Soc.Lond. A255(1963), 281.

[6] D.Dowson and G.R.Higginson, Eng.Lond. 192(1961), 158.

[7] A.Dyson, Phil.Trans.Roy.Soc.Lond. A266(1970), 1.

[8] W.Hirst and A.J.Moore, Proc.Roy.Soc.Lond. A360(1978), 403.

[9] D.M.Heyes and C.J.Montrose, ASME J.Lub.Tech. 102(1980), 459.

[10] K.L.Johnson and A.D.Roberts, Proc.Roy.Soc.Lond. A337(1974), 217.

[11] K.L.Johnson and J.L.Tevaarwerk, Proc.Roy.Soc.Lond. A356(1977), 215.

[12] W.Hirst and A.J.Moore, Proc.Roy.Soc.Lond. A344(1975), 403.

[13] J.A.Jefferis and K.L.Johnson, Proc.Instn.Mech.Engrs. 182pt.1(1967-8), 281.

[14] D.Dowson and T.C.Whomes, Proc.Instn.Mech.Engrs. 182pt.1(1967-8), 292.

[15] M.A.Plint, Proc.Instn.Mech.Engrs. 182pt.1(1967-8), 300.

[16] K.L.Johnson and R.Cameron,
Proc.Instn.Mech.Engrs. 182pt.1(1967-8), 307.

[17] J.L.Tevaarwerk and K.L.Johnson,
ASME J.Lub.Tech. 101(1979), 266.

[18] K.L.Johnson and J.L.Tevaarwerk,
Proc.Roy.Soc.Lond. A356(1977), 215.

[19] A.Dyson, Phil.Trans.Roy.Soc.Lond. A258(1965), 529.

[20] W.P.Mason, W.O.Baker, H.J.McSkimin and J.H.Heiss,
Phys.Rev. 75(1949), 936.

[21] H.J.McSkimin, J.Acoust.Soc.Am. 24(1952), 355.

[22] A.J.Barlow and J.Lamb,
Proc.Roy.Soc.Lond. A253(1959), 52.

[23] G.Harrison,
The Dynamics of Supercooled Liquids, Academic Press,
1976.

[24] J.F.Hutton, M.C.Phillips, J.Ellis, G.Powell and
E.Wyn-Jones, Proc.Leeds-Lyon Symp.Tribol.1978(publ.1979)
(5th Elastohydrodyn.Relat.Top.) p.g. 173.

[25] J.F.Hutton and M.C.Phillips,
J.Chem.Phys. 51(1969), 1065.

[26] J.F.Hutton, Proc.Roy.Soc.Lond. A304(1968), 65.

[27] A.J.Barlow, A.Erginsav and J.Lamb,
Proc.Roy.Soc.Lond. A298(1967), 481.

[28] J.Lamb, Proc.Inst.Mech.Eng. 182 Pt.3A(1967), 293.

[29] M.C.Phillips, A.J.Barlow and J.Lamb,
Proc.Roy.Soc.Lond. A329(1972), 193.

[30] A.J.Barlow, A.Erginsav and J.Lamb,
Proc.Roy.Soc.Lond. A309(1969), 473.

[31] G.Berchiesi, G.Vitali, P.Passamonti and R.Plowiec,
J.C.S.Farad.Trans. II 79(1983), 1257.

[32] D.B.Davies, A.J.Matheson and G.M.Glover,
J.C.S.Farad.Trans. II 69(1973), 305.

[33] A.J.Barlow and A.Erginsav,
J.C.S.Farad.Trans. II 69(1973), 1200.

[34] D.W.Davidson and R.H.Cole,
J.Chem.Phys. 19(1951), 1484.

[35] M.G.Kim, J.C.S.Farad.Trans. II 71(1975), 415.

[36] B.J.Alder and T.E.Wainwright,
J.Chem.Phys. 31(1959), 459.

[37] A.Rahman, Phys.Rev. 136(1964), A405.

[38] J.Barojas, D.Levesque and B.Quentrec,
Phys.Rev.A 7(1973), 1092.

[39] K.Singer, A.Taylor and J.V.L.Singer,
Mol.Phys. 33(1977), 1757.

[40] D.J.Evans and S.Murad, Mol.Phys. 34(1977), 327.

[41] G.Ciccotti, J.P.Ryckaert and H.J.C.Berendsen,
J.Comp.Phys. 23(1977), 327.

[42] M.Metropolis, A.W.Rosenbluth, M.N.Rosenbluth,
A.N.Teller and E.Teller,
J.Chem.Phys. 21(1953), 1087.

[43] M.S.Green, J.Chem.Phys. 22(1954), 398.

[44] R.Kubo, J.Phys.Soc.Japan 12(1957), 570.

[45] R.Zwanzig, Ann.Rev.Phys.Chem. 16(1965), 67.

[46] B.J.Alder, D.M.Gass and T.E.Wainwright,
J.Chem.Phys. 53(1970), 3813.

[47] E.Helfand, Phys.Rev.A 119(1960), 1.

[48] D.Levesque, L.Verlet and J.Kurkijarvi,
Phys.Rev.A 7(1963), 1960.

[49] E.M.Gosling, I.R.McDonald and K.Singer,
Mol.Phys. 26(1973), 1475.

[50] D.J.Evans and W.B.Streett,
Mol.Phys. 36(1978), 161.

[51] R.Zwanzig and R.D.Mountain,
J.Chem.Phys. 43(1965), 4464.

[52] 'Transport Phenomena in Fluids' (Dekker), 1969,
ed. H.J.M.Hanley.

[53] Theoretical Chemistry, Advances and Perspectives,
Vol. 1, ed. H.Eyring and D.Henderson (Academic Press).

[54] A.W.Lees and S.F.Edwards, J.Phys.C 5(1972), 1921.

[55] D.J.Evans, Mol.Phys. 37(1979), 1745.

[56] T.Naitoh and S.Ono, J.Chem.Phys. 70(1979), 4515.

[57] D.J.Evans and H.J.M.Hanley,
Phys.Rev.A 20(1979), 1648.

[58] D.J.Evans, Phys.Letts.A 74(1979), 229.

[59] D.J.Evans, Phys.Rev.A 22(1980), 290.

[60] D.J.Evans, Mol.Phys. 42(1981), 1355.

[61] D.J.Evans, Mol.Phys. 37(1979), 1745.

[62] W.G.Hoover, D.J.Evans, R.B.Hickman, A.J.C.Ladd,
W.T.Ashurst and B.Moran, Phys.Rev.A 22(1980), 1690.

[63] D.J.Evans, J.Chem.Phys. 78(1983), 3297.

[64] W.G.Hoover, Physica 118A(1983), 111.

[65] W.G.Hoover, A.J.C.Ladd and B.Moran,
Phys.Rev.Letts. 48(1982), 1818.

[66] D.Brown and J.H.R.Clarke,
Mol.Phys. 51(1984), 1243.

[67] K.Singer, J.V.L.Singer and D.Fincham,
Mol.Phys. 40(1980), 515.

[68] G.Ciccotti, G.Jacucci and I.R.McDonald,
J.Stat.Phys. 21(1979), 1.

[69] D.Fincham and D.M.Heyes, Chem.Phys. 78(1983), 425.

[70] M.P.Allen and D.Kivelson, Mol.Phys. 44(1981), 945.

[71] M.Whittle, Inf.Quart.MD and MC Simns. 5(1982), 14.

[72] W.T.Ashurst and W.G.Hoover,
Phys.Rev.Letts. 31(1973), 206.

[73] F.H.Ree, T.Ree and H.Eyring,
Ind.Eng.Chem. 50(1958), 1036.

[74] K.Kawasaki and J.D.Gunton, Phys.Rev.A 8(1973), 2048.

[75] W.T.Ashurst and W.G.Hoover,
Phys.Letts.A 61(1977), 175.

[76] D.J.Evans, Mol.Phys. 47(1982), 1165.

[77] B.L.Holian and D.J.Evans, J.Chem.Phys. 78(1983), 5147.

[78] A.Ram, in 'Rheology', vol.4, ed. F.Eirich,
(Academic Press, New York, 1967), ch.3.

[79] S.Hess, Z.Natursforsch 30a(1975), 728.

[80] S.Hess, Physica 86A(1977), 383.

[81] S.Hess, Physica 87A(1977), 273.

[82] S.Hess, Phys.Rev.A 25(1982), 614.

[83] B.Quentrec, Mol.Phys. 46(1982), 707.

[84] B.C.Eu, J.Chem.Phys. 79(1983), 2315.

[85] J.F.Hutton, Private communication.

[86] M.Cross, J.Colloid.Sci. 20(1965), 417.

[87] M.Cross, J.Colloid.Interface Sci. 33(1970), 30.

[88] H.Markowitz, in 'Rheology', vol.4, ed. F.Eirich, (Academic Press, New York, 1967), ch.6.

[89] W.H.Bauer and E.A.Collins, in 'Rheology', vol.4, ed. F.Eirich, (Academic Press, New York, 1967), ch.8.

[90] D.J.Evans and H.J.M.Hanley, Phys.Letts.A 79(1980), 178.

[91] D.J.Evans and H.J.M.Hanley, Phys.Letts.A 80(1980), 175.

[92] D.J.Evans and H.J.M.Hanley, Physica A 108(1981), 567.

[93] D.J.Evans, Adv.Colloid. Interface Sci. 17(1982), 51.

[94] D.J.Evans, Physica A 118(1983), 51.

[95] W.T.Ashurst and W.G.Hoover, Phys.Rev.A 11(1975), 658.

[96] D.J.Evans and R.O.Watts, Chem.Phys. 48(1980), 321.

[97] J.D.Ferry, 'Viscoelastic Properties of Polymers', (Wiley), (1980).

[98] R.B.Bird, R.C.Armstrong and O.Hassager, 'Dynamics of Polymeric Liquids ', vol. 1 : Fluid Mechanics, (Wiley), (1977).

[99] T.Weber and N.D.Annan, Mol.Phys. 46(1982), 193.

[100] I.R.McDonald and K.Singer, Mol.Phys. 23(1972), 29.

[101] D.Beeman, J.Comp.Phys. 20(1976), 130.

[102] L.Verlet, Phys.Rev. 159(1967), 98.

[103] 'Theory of Simple Liquids ', J.P.Hansen and I.R.McDonald, (Academic Press), (1976).

[104] J.P.Ryckaert, A.Bellemans and G.Ciccotti, Mol.Phys. 44(1981), 979.

[105] T.A.Weber, J.Chem.Phys. 69(1978), 2347.

[106] T.A.Weber, J.Chem.Phys. 70(1979), 4277.

[107] 'Classical Mechanics', H.Goldstein, (Addison-Wesley), (1971).

[108] P.S.Y.Cheung and J.G.Powles, Mol.Phys. 30(1975), 921.

[109] 'Numerical Initial Value Problems in Ordinary Differential Equations ', C.W.Gear, (Prentice Hall), (1971).

[110] D.J.Evans, Mol.Phys. 34(1977), 317.

[111] K.Singer, J.V.L.Singer and A.Taylor, Mol.Phys. 37(1979), 1239.

[112] D.Fincham, Inf.Quart.MD and MC Simns. 10(1983), 43.

[113] 'Elements of Linear Algebra', D.T.Finkbeiner, (Freeman), (1972).

[114] D.Fincham, Inf.Quart.MD and MC Simns., 2(1981), 6.

[115] W. van Gunsteren, subroutine SHAKE from CCP5 program HSTOCH.

[116] D.Fincham, private communication.

[117] W.Hirst and A.J.Moore, Proc.Roy.Soc.Lond. A365(1979), 537.

[118] H.C.Andersen, J.Chem.Phys. 72(1980), 2384.

[119] J.M.Haile and H.W.Graben,
J.Chem.Phys. 73(1980), 2412.

[120] D.Brown, Inf.Quart.MD and MC Simns. 4(1982), 32.

[121] J.P.Ryckaert and G.Ciccotti,
J.Chem.Phys. 78(1983), 7368.

[122] M.Doi and S.F.Edwards,
Far.Trans.Chem.Soc.II 75(1979), 918.

[123] J.P.Ryckaert and A.Bellemans,
ChemPhys.Letts. 30(1975), 123.

[124] J.P.Ryckaert and A.Bellemans,
Faraday Disc.Chem.Soc. 66(1978), 95.

[125] 'An Advanced Treatise on Physical Chemistry'
Vol II, 'The Properties of Liquids',
J.R.Partington (Longman) (1951), pg. 62.

[126] B.J.Alder and T.E.Wainwright, Phys.Rev.A 1(1970), 18.

[127] 'An Introduction to the Liquid State',
P.A.Egelstaff (Academic Press) (1967), pg. 154.

[128] 'Statistical Mechanics of Chain Molecules',
P.J.Flory, (Wiley) (1969).

[129] Link Cell program written by F.van Swol and L.V.Woodcock.

[130] D.M.Heyes, Inf.Quart.MD and MC Simns. 2(1981), 11.

[131] J.P.Ryckaert, private communication.

[132] D.Adams, Inf.Quart.MD and MC Simns. 3(1981), 32.

[133] S.M.Thompson, Inf.Quart.MD and MC Simns. 8(1983), 20.

[134] S.F.O'Shea, Inf.Quart.MD and MC Simns. 9(1983), 41.